

School of Earth and Planetary Sciences

Towards a Gravimetric Geoid Model for the Mainland India

Ropesh Goyal

**This thesis is presented for the Degree of
Doctor of Philosophy**

**as per the Joint Degree Program between
Indian Institute of Technology Kanpur
and
Curtin University of Technology**

March 2022

CERTIFICATE

It is certified that the work contained in the thesis titled **Towards a gravimetric geoid model for the mainland India** by **Ropesh Goyal** has been carried out under our supervision and that this work has not been submitted elsewhere for any other degree. The work has been carried out under the agreement for Joint Doctoral Degree Program between Indian Institute of Technology Kanpur, India and Curtin University of Technology, Australia, with IIT Kanpur as the home institution. A hard-bound copy of this thesis is being submitted to Curtin University of Technology, Australia as per the agreement for Joint Doctoral Degree Program.

Prof. Onkar Dikshit
Department of Civil Engineering
Indian Institute of Technology Kanpur
Uttar Pradesh, India

Prof. Will Featherstone
School of Earth and Planetary Sciences
Curtin University of Technology
Perth WA, Australia

Maj Gen (Dr) B. Nagarajan
Department of Civil Engineering
Indian Institute of Technology Kanpur
Uttar Pradesh, India

Dr Sten Claessens
School of Earth and Planetary Sciences
Curtin University of Technology
Perth WA, Australia

DECLARATION

This is to certify that the thesis titled **Towards a gravimetric geoid model for the mainland India** has been authored by me. It presents the research conducted by me under the supervision of:

- Prof. Onkar Dikshit and Maj Gen (Dr) B. Nagarajan, Indian Institute of Technology Kanpur, India
- Prof. Will Featherstone and Dr Sten Claessens, Curtin University of Technology, Perth, Australia,

The work has been carried out under the agreement for Joint Doctoral Degree Program between Indian Institute of Technology Kanpur, India and Curtin University of Technology, Perth, Australia, with IIT Kanpur as the home institution. A hard-bound copy of this thesis is being submitted to Curtin University of Technology, Perth, Australia as per the agreement for Joint Doctoral Degree Program.

To the best of my knowledge, it is an original work, both in terms of research content and narrative, and has not been submitted elsewhere, in part or in full, for any other degree. Further, due credit has been attributed to the relevant state-of-the-art and collaborations with appropriate citations and acknowledgements, in line with established academic norms and practices.

Ropesh Goyal

Doctoral Joint Degree Program

Department of Civil Engineering,
Indian Institute of Technology Kanpur,
Kanpur 208016, Uttar Pradesh, India

School of Earth and Planetary Sciences,
Curtin University of Technology,
Perth, WA 6845, Australia

Synopsis

Student: ROPESH GOYAL

Roll Number (IITK): 16103275

Student ID (CUT): 19553975

Degree for which submitted: Doctor of Philosophy

Department: Department of Civil Engineering, Indian Institute of Technology Kanpur, India

School of Earth and Planetary Sciences, Curtin University of Technology, Perth,
Australia

Thesis Title: Towards a gravimetric geoid model for the mainland India

Thesis Supervisors: Prof Onkar Dikshit, Maj Gen (Dr) B. Nagarajan (Indian Institute of
Technology Kanpur)

Prof Will Featherstone, Dr Sten Claessens (Curtin University of
Technology)

Thesis Committee Chairs: Prof Onkar Dikshit (Indian Institute of Technology Kanpur)

A/Prof Michael Kuhn (Curtin University of Technology)

Date of Submission: March, 2022

The geoid is the equipotential surface of the Earth's gravity field best approximated by the ocean at rest. All terrestrial geodetic and engineering surveying measurements are made after aligning the instrument's vertical axis orthogonal to an equipotential surface. The geoid, therefore, is the best candidate for a reference surface, especially for heights. Since the geoid is a physically meaningful surface, it responds to changes in the gravity field due to various geophysical and geodynamical phenomena, in turn allowing us to study them as well. A precise gravimetric geoid model is fundamental to both infrastructure development as well as for geoscientific activities.

Geoid-related studies in India have a history of more than a century, which was started with astrogeodetic geoids derived from astronomical observations. After 2005, there have been

a few gravimetric geoid-related studies over different regions of India, but all have used GRAVSOFTE subroutines with residual terrain modelling (RTM). Moreover, all these studies have been conducted only at two organisations: Survey of India and National Geophysical Research Institute, because these two organisations are the custodians of the Indian gravity data and there are national policies that restrict data sharing. Further, none of the developed geoid models for any region of India are available in the public domain.

Therefore, in this thesis we have developed the first national gravimetric geoid model of India, which will be made available in the public domain. For this thesis, the Indian terrestrial gravity data has been procured from GETECH Pty. Ltd., Leeds, UK. Unlike previous studies in India or elsewhere (to the best knowledge of the author), three different methodologies have been used to compute both gravimetric geoid and quasigeoid models for the whole of the country encapsulating a similar varied landform consisting of the Himalayas and other hill ranges, the Gangetic plains, Thar desert, plateaus and a long peninsular coastline. The three methods used herein are those developed at i) the Curtin University of Technology (CUT), Australia ii) the University of New Brunswick (UNB), Canada and iii) the Royal Institute of Technology (KTH), Sweden, all with some modifications due to the peculiarities of Indian datasets.

The major contributions in this thesis are 1) development of an efficient combined spatial-spectral method for calculating planar gravimetric terrain corrections, which can also be used in regions having slope $>45^\circ$, 2) development of a numerical method that reduces the computation time of planar gravimetric terrain correction by almost 50% as compared to the literature-recognised best method of analytical mass-prism integration, 3) introducing the dynamic integration radius for numerical global integration using the DEMs of multiple resolution, 4) providing a conceptual argument and mathematical formulation of downward continuation of height anomalies from Earth's topographical surface to ellipsoid for defining

the quasigeoid, 5) deriving exact conversion formulas for gravity, geoid undulation, dynamic height, orthometric height, normal height and ellipsoidal height among the three permanent tide systems, 6) deriving formulas for ad-hoc conversion of various ellipsoidal parameters among the three permanent tide systems of the solid Earth and providing the values of all the ellipsoidal parameters for WGS84, GRS80 and an another reference ellipsoid, in all the three permanent tide systems and 7) inter-model comparison of geoids and geoid-quasigeoid separation terms that provide new insights to the decades-long quest of a cm-precise geoid.

Other contributions include 1) development of gravimetric geoid model for the mainland India using the three methodologies that have never been tested in any region of India, 2) development of geoid calculation packages, in MATLAB, based on the CUT and the UNB methods, 3) development of local gravimetric geoid models using GRAVSOFTR subroutines (for least squares collocation) with RTM to compare the results with previous studies (available descriptive statistic) over regions of India, 4) use of the first order indirect effect for the first time in the CUT method, 5) validating geoid and quasigeoid models with the geometric geoid undulations involving normal-orthometric heights as an effort to investigate the more suitable reference surface for normal-orthometric heights in India and 6) validating Pizetti's geoid gradients with Helmert's vertical deflections noting that the curvature of the plumbline is neglected.

Before using the adopted methodologies for calculating the Indian geoid and quasigeoid models, they have been tested over Auvergne in France to calculate $\sim\pm 0.03$ m precise quasigeoid models. The precision of the developed Indian geoid model, for India is ± 0.396 m, but only from small localised dataset. However, on region-wise validation, the precision varies from a minimum of ± 0.03 m in Bangalore to a maximum of ± 0.158 m in Hyderabad. Since this study has been conducted with the available datasets of unknown quality, gravimetric geoid studies in India must continue with new precise and dense gravity, and GNSS/levelling data.

This study shows that two or more gravimetric geoid/quasigeoid models or the geoid/quasigeoid computation methodologies should not be compared for pre-eminence solely based on standard deviation of fit to GNSS/levelling or vertical deflection data. Moreover, there is no particular choice of a geoid computation methodology or a modification degree and integration radius combination that gives the smallest standard deviation (or any other descriptive statistic) for all regions of a country. Therefore, there is a need for a new geoid computation methodology that could, may be, combine several regional geoid models or different methods of geoid computation. As of today, geoid computation cannot be generalised because the geoid models with different methods can deviate up to a few metres from one another. Hence, we are yet far away from the goal of cm-precise geoid, at least in India.

Acknowledgements

This is a small effort to say thank you to all who helped me at various stages of my Ph.D.

I would like to start with sincerely thanking and communicating my deepest gratitude to my supervisors from IIT Kanpur, Prof. Onkar Dikshit and Maj Gen (Dr) B. Nagarajan for introducing me to the subject of geodesy and providing the guidance and motivation throughout my Ph.D. I thank you both for always having belief in my abilities and providing all the required academic, administrative, and emotional support.

This thesis would not have been completed without the guidance and nurturing of my supervisors from Curtin University, Prof. Will Featherstone and Dr Sten Claessens. I must mention that I cannot think of any better Ph.D. supervision than what I have received. Thank you for all the stimulating discussions, invaluable feedbacks and always lending an ear for all of my thoughts.

I would like to express my deep gratitude to Prof. Lars Sjöberg, Dr Mohammed Bagherbandi and Dr Jonas Ågren for providing me the opportunity to visit University of Gävle and KTH, Sweden. I sincerely thank Prof. Lars Sjöberg for all the invaluable discussions and motivation. I would like to extend my sincere thanks to Dr Jonas Ågren for providing me the detailed training and the discussions on the KTH method. I would also like to thank him for the short tour of Lantmäteriet and providing me the requested literature and the Geolab package. I am highly indebted to Prof. Milan Horemuz for allowing my visit to KTH and providing me all the requested invaluable geodesy reports and articles.

I am thankful to Prof. Petr Vaníček for directing my emails regarding SHGeo to the UNB group members. I express my deep appreciation to Dr Ismael Foroughi, Dr Robert Kingdon and Prof. Marcelo Santos for providing me all the requested information and sharing a subroutine that helped me understand the practical implementation of direct topographical effect in the SHGeo package.

I would like to communicate profound thanks to Prof. Dimitris Tsoulis, Dr Leyuan Wu, Dr Michael Kuhn, Dr Jack McCubbine, Dr Dai Yamazaki and Ms Olga Pimenova (Ph.D. student at UNSW) for the very useful and helpful in-depth discussions that provided me a better understanding of the topics and the underlying concepts. I also wish to thank to Prof. Christopher Jekeli, Dr Siamak Moazezi, Dr Alpay Abbak, Dr Prosper Ulotu, Dr Christian Hirt, Prof. Pavel Novák, Dr Miao Lin and Prof. Rene Forsberg for clarifying my queries including the most trivial ones and/or providing me the requested material that helped me saving several days of literature digging.

Prof. Bharat Lohani is duly thanked for imparting invaluable knowledge through coursework at IIT Kanpur. Thanks also go to Prof. Ahmed El-Mowafy, Dr Mick Filmer, Dr Jon Kirby and Prof. Joseph Awange for all the technical and/or non-technical discussions, suggestions and support during my stay at Curtin University.

Dr S.K. Singh, G&RB, Survey of India is highly acknowledged for approving my visits to

G&RB and the helpful discussions on Survey of India's effort to develop the Indian geoid model. I am also grateful to Mr Neeraj Gurjar, G&RB to allow my visit to G&RB in 2020 and would like to thank him, Mr Bhaskar Sharma, Mr Raman Verma and Mr B.S. Negi for all the discussions and their help in expediting the process of procuring the available GNSS/levelling data.

I also wish to show my appreciation to Dr V.M. Tiwari, NGRI for allowing my visit to NGRI. I gratefully acknowledge the support of Dr N. Srinivas Rao and Dr Rajeev Yadav during and after my stay at NGRI.

Special thanks to Dr Mirjam Bilker-Koivula and Ms Marita Portin from the Finnish Geodetic Institute for providing me all the requested FGI reports. I would like to acknowledge the assistance of the National Library of Sweden and the libraries of IIT Kanpur and Curtin University for arranging and providing literature requested. I would also like to extend acknowledgement to the researchers on ResearchGate who all provided me the requested literature. I thank GETECH, Leeds, UK to provide the Indian gravity data and Survey of India to provide the GNSS/levelling data.

I am sincerely grateful to the MHRD for Ph.D. fellowship and the Research office at Curtin University for CIPR and research stipend scholarships. I would also like to extend my gratitude to MHRD's SPARC scheme and the National Centre for Geodesy for providing the funds to procure gravity and GNSS/levelling data.

All the support received from the staff members: Mr R.K. Maurya, Mr Shitla Tripathi, Mr Hari Babu, Mr Rohit and Mr Arun Kumar at IIT Kanpur and Mrs Caroline Rockliff at Curtin University is highly acknowledged.

Many thanks to Dr Luyen Khac Bui for discussions on anything and everything, which was the most important constituent of my pleasant stay at Curtin. My heartfelt thanks go to my friends for all their support, love, advice, motivation, endless discussions, sleepless nights and a cheerful company: Vipul, Saurabh, Sarvesh, Jai Prakash, Sir Supreme, Maithili, Govind, Lt Col Aakash, Milaa, Sunny, Shubham, Ankul, Rajat, Prachi, Vivek and Jyotsna. My Ph.D. colleagues and seniors, Mr Jagadish Boodala, Mr Naveen, Dr Anand Mehta, Dr Ashutosh Tiwari, Mr Aswani Munnangi, Dr Anudeep Sure, Dr Avadh Bihari and Dr Divyesh Varade, are duly thanked for all the support.

Last but utmost importantly, I feel extremely blessed to have all the love and support of my parents and sister Himani throughout my life. Words cannot be enough to express my deep indebtedness to you all for keeping the belief and faith in my decisions and providing all the strength for this journey.

March 2022

Ropesh Goyal

ropeshgoyal2809@gmail.com

Dedicated to the great Geodesist and an excellent supervisor



Prof. William Edward Featherstone (Will)
1967-2022

Table of Contents

Acknowledgements.....	viii
List of Publications.....	xv
List of Figures.....	xxvii
List of Tables.....	xxiv
List of Abbreviations.....	xxvii
List of Symbols.....	xxxii
1. Introduction.....	1
1.1 Background.....	1
1.2 Height systems.....	7
1.2.1 Indian vertical datum and height system.....	11
1.3 Previous Indian gravimetric geoid models.....	18
1.4 Research gaps.....	23
1.5 Objectives.....	25
1.6 Significance of the study.....	27
1.7 Structure of the thesis.....	29
2. Datasets.....	31
2.0 Introduction.....	31
2.1 [Lack of] Freely available gravity data.....	31
2.2 GNSS/levelling.....	43
2.3 Deflection the vertical.....	45
2.4 Global geopotential models.....	48
2.5 Digital elevation models.....	53
2.6 Summary.....	57
3. Systematic effects in geoid determination.....	59
3.0 Introduction.....	59
3.1 Gravity anomalies.....	60

3.1.1	Gradient method of calculating normal gravity at any height.....	61
3.1.2	Exact method of calculating normal gravity at any height.....	63
3.2	Topographic corrections.....	68
3.2.1	CUT method.....	70
3.2.2	UNB method.....	83
3.2.3	KTH method.....	94
3.3	Atmospheric corrections.....	100
3.3.1	CUT method.....	100
3.3.2	UNB method.....	102
3.3.3	KTH method.....	105
3.4	Ellipsoidal corrections.....	109
3.4.1	CUT method.....	110
3.4.2	UNB method.....	113
3.4.3	KTH method.....	117
3.5	Downward continuation.....	118
3.5.1	CUT method.....	119
3.5.2	UNB method.....	123
3.5.3	KTH method.....	126
3.6	Zero-degree and tidal corrections.....	129
3.6.1	Zero-degree term.....	131
3.6.2	Tidal corrections to the physical Earth.....	138
3.6.3	Tidal corrections to the ellipsoidal parameters.....	144
3.6.4	Numerical test for tide-system in SHS.....	154
3.7	Summary.....	161
4.	Computation of the Indian gravimetric geoid and quasigeoid models.....	164
4.0	Introduction.....	164
4.1	Stokes's integration and kernel modification.....	164

4.1.1	Stokes's integration.....	165
4.1.2	Kernel modification.....	168
4.2	Different methods of geoid and quasigeoid calculation.....	171
4.2.1	CUT method.....	172
4.2.2	UNB method.....	177
4.2.3	KTH method.....	182
4.3	Geoid-quasigeoid separation.....	191
4.4	Hybrid geoid/quasigeoid.....	199
4.5	Summary.....	202
5.	Geoid and quasigeoid: results and validations.....	205
5.0	Introduction.....	205
5.1	Validation of the developed geoid and quasigeoid models.....	205
5.2	Indian gravimetric geoid model.....	231
5.3	Summary.....	246
6.	Conclusions and recommendations.....	248
6.0	Introduction.....	248
6.1	Summary of research.....	248
6.2	Conclusions.....	252
6.3	Scope of the future work.....	254
	References.....	257
	Appendix A – Excerpts of- Survey of India, 1950: Part III - Geodetic work.....	291
	Appendix B – Ellipsoidal parameters in different tide systems.....	293
	Appendix C – Published research papers those provide supporting information...	297

List of Publications

Papers published in peer-reviewed journals:

1. Goyal, R., Dikshit, O., Balasubramanian, N., 2019. Evaluation of different global geopotential models: A case study of India. Survey Review, 51(368), 402-412. <https://doi.org/10.1080/00396265.2018.1468537>
2. Goyal, R., Featherstone, W.E., Tsoulis, D.V., Dikshit, O., 2020. Efficient spatial-spectral computation of local planar gravimetric terrain corrections from high-resolution digital elevation models. Geophysical Journal International, 221(3), 1820-1831. <https://doi.org/10.1093/gji/ggaa107>
3. Goyal, R., Featherstone, W.E., Dikshit, O., Balasubramanian, N., 2021. Comparison and validation of satellite-derived digital elevation/surface models over India. Journal of Indian Society of Remote Sensing, 49(4), 971-986. <https://doi.org/10.1007/s12524-020-01273-7>
4. Goyal, R., Featherstone, W.E., Claessens, S.J., Dikshit, O., Balasubramanian, N., 2021. An experimental Indian gravimetric geoid model using Curtin University's approach. Terrestrial, Atmospheric and Oceanic Sciences, 32(5-II), 1-15. <https://doi.org/10.3319/TAO.2021.08.10.02>
5. Goyal, R., Ågren, J., Featherstone, W.E., Sjöberg, L.E., Dikshit, O., Balasubramanian, N., 2022. Empirical comparison between stochastic and deterministic modifiers over the French Auvergne geoid computation test-bed. Survey Review, 54(382), 57-69. <https://doi.org/10.1080/00396265.2021.1871821>
6. Featherstone, W.E., Goyal, R., 2022. Digitisation and analysis of historical deflections of the vertical in India. Accepted. Survey Review.

Conference presentations:

7. Goyal, R., Nagarajan, B., Dikshit, O., 2017. Status of precise geoid modelling in India: A review. Presented to: 37th INCA International congress on Geoinformatics for Carto-Diversity and Its Management, November 1-3, 2017. Dehradun, India.
8. Goyal, R., Devaraju, B., Featherstone, W.E., Balasubramanian, N., Claessens, S.J, Dikshit, O., 2019. A gravimetric geoid model for India: Challenges and current status. Presented to: 27th IUGG General Assembly, July 8-18, 2019. Montreal, Canada.

9. Goyal, R., Featherstone, W.E., Claessens, S.J., Devaraju, B., Balasubramanian, N., Dikshit, O., 2019. A numerical approach to the mass-prism integration for fast determination of terrain corrections. Presented to: 27th IUGG General Assembly, July 8-18, 2019. Montreal, Canada.
10. Goyal, R., Claessens, S.J., Featherstone, W.E., Dikshit, O., 2020. Subtleties in spherical harmonic synthesis of the gravity field. Presented to: European Geosciences Union General Assembly, 3-8 May 2020, Vienna, Austria. <https://doi.org/10.5194/egusphere-egu2020-59>
11. Goyal, R., Featherstone, W.E., Claessens, S.J., Dikshit, O., Balasubramanian, N., 2020. Indian gravimetric geoid modelling: data, methods, and a preliminary test using Curtin University's approach. Presented to: First Asia Pacific geoid workshop for IAG-SC2.4e (Gravity and geoid in the Asia Pacific) Taiwan.
12. Goyal, R., Featherstone, W.E., Claessens, S.J., Dikshit, O., Balasubramanian, N., 2021. Indian gravimetric geoid model: IndGG-CUT2021. Presented to: International Association of Geodesy Scientific Assembly 2021, Beijing, China.
13. Goyal, R., Featherstone, W.E., Claessens, S.J., Dikshit, O., Balasubramanian, N., 2021. Recent geoid-related studies for the whole country of India. Presented to: AGU Fall Meeting 2021. New Orleans, USA.

Awards:

1. *Rachapudi Kamakshi Memorial Gold Medal and Young Geospatial Scientist 2020* award for contribution towards developing the Indian gravimetric geoid model.

Author credit information for journal publication:

Contribution	Journal paper number					
	1	2	3	4	5	6
Devising the study	RG	RG, WF, DT	RG, WF	RG, WF	RG, WF, JÅ	WF
Calculations	RG	RG	RG	RG	RG, JÅ	WF, RG
Writing, editing and revising	RG, OD	RG, WF, DT	RG, WF	RG, WF, SC	RG, WF, JÅ, LS	WF, RG
Read, comment and approve	RG, OD, BN	RG, WF, DT, OD	RG, WF, OD, BN	RG, WF, SC, OD, BN	RG, JÅ, WF, LS, OD, BN	WF, RG

BN: Balasubramanian Nagarajan; DT: Dimitris Tsoulis; JÅ: Jonas Ågren; LS: Lars Sjöberg; OD: Onkar Dikshit; RG: Ropesh Goyal; SC: Sten Claessens; WF: Will Featherstone

List of Figures

Figure 1.2.1	Different surfaces and heights.....	8
Figure 1.2.2	Various landforms in India. Red italics shows the name of the Indian state or Union territory.....	12
Figure 1.2.3	Mean Dynamic Topography (DTU19MDT) along with tidal observatories used in IVD1909 and IVD2009.....	14
Figure 2.1.1	Error map of the Scripps v28.1 marine gravity-anomaly data (units: mGal).	38
Figure 2.1.2	Regions for the terrestrial (GETECH and EGM2008 derived) and marine gravity anomalies.....	39
Figure 2.1.3	Merged gravity anomaly data from GETECH, EGM2008 (d/o 900), and Scripps v28.1 data.....	41
Figure 2.1.4	a) Scatter plot of merged gravity anomalies and heights (linear regression fit: $y = 0.016x - 30.824$); b) Histogram of the merged gravity anomalies...	41
Figure 2.1.5	Arctangent (a) and logarithmic (b) plot of gradients of merged gravity anomaly data to attempt to identify discontinuities at the edges of the merged grids.....	42
Figure 2.2.1	GNSS/levelling data distribution.....	45
Figure 2.3.1	Deflection of vertical stations in India from Gulatee (1955).....	48
Figure 2.5.1	MERIT DEM over study area at 3"×3" resolution.....	55
Figure 3.1.1	Difference in gravity anomaly using exact solution v/s second order formula (units: mGal).....	65
Figure 3.1.2	Difference in gravity anomaly using exact solution v/s solution derived using Bruns's formula (units: mGal).....	66
Figure 3.1.3	Difference in gravity anomaly using exact solution v/s linear formula (units: mGal).....	66

Figure 3.2.1	The four integration domains. BR is the bounding radius of the whole integration area that defines the integration radius. HSR, OSR and ESR are the height dependent, optimal and exact separating radii, respectively.....	75
Figure 3.2.2	Local planar TC over India and adjacent countries at a) 3''×3'' grid, b) 0.02°×0.02° grid using spatial-spectral combined approach.....	82
Figure 3.2.3	a) Scatter plot of 0.02°×0.02° grid TCs with respect to the heights, b) histogram of 0.02°×0.02° grid TCs.....	82
Figure 3.2.4	DTE over India and adjacent regions.....	91
Figure 3.2.5	a) Scatter plot of DTE versus height; b) histogram of DTE.....	91
Figure 3.2.6	SITE over India and adjacent regions.....	92
Figure 3.2.7	a) Scatter plot of SITE versus height; b) histogram of SITE.....	92
Figure 3.2.8	PITE over India and adjacent regions.....	93
Figure 3.2.9	a) Scatter plot of PITE versus height; b) histogram of PITE.....	93
Figure 3.2.10	Total topographic effect using KTH method over India and adjacent regions.....	99
Figure 3.2.11	a) Scatter plot of combined topographic effect versus height; b) histogram of combined topographic effect.....	99
Figure 3.3.1	Atmospheric correction with different truncated degrees in Eq. (3.3.42)....	102
Figure 3.4.1	Ellipsoidal correction to (a) gravity disturbance and (b) spherical approximation as applied in the UNB method.....	117
Figure 3.5.1	Vertical gravity gradient.....	125
Figure 3.5.2	a) Scatter plot and b) Histogram of gravity gradient.....	126
Figure 3.6.1	Variation in geoid undulation for GRS80 in tide-free system and $\bar{C}_{2,0}$ of EGM2008 in different tide system.....	155

Figure 3.6.2	Difference in Ekman (1989) formula and the calculated value of geoid undulation in different tide-system (left: $k_2 = 0.3$ in Ekman (1989) and right: $k_2 = 0.30190$ in Ekman (1989)).....	155
Figure 3.6.3	Variation of the difference in degree-two geoid undulation computed using EGM2008 and GRS80 (both in same tide system).....	156
Figure 3.6.4	Variation in FAA for GRS80 in tide-free system (as is) and $\bar{C}_{2,0}$ of EGM2008 in different tide system.....	157
Figure 3.6.5	Variation of FAA when EGM2008 and GRS80 are in same tide system.....	157
Figure 3.6.6	Variation of differences in degree-two geoid undulation and free-air anomaly for EGM2008 in ZT and GRS80 (TFGRSZT- ZTGRSZT).....	159
Figure 4.2.1	Flowchart of the CUT methodology of geoid/quasigeoid computation.....	173
Figure 4.2.2	a) Faye gravity anomalies and b) residual Faye gravity anomalies as required in the CUT method.....	175
Figure 4.2.3	Residual height anomaly after Stokes integrating residual Faye gravity anomalies with FEO kernel modification ($M = 80$ and $\psi = 1.5^\circ$).....	176
Figure 4.2.4	Flowchart of the UNB methodology of geoid/quasigeoid computation.....	179
Figure 4.2.5	Residual Helmert's anomaly calculated with the DIR-RL05 GGM d/o 300.	180
Figure 4.2.6	Residual co-geoid after Stokes integrating residual Helmert's gravity anomaly with the VK kernel modification ($M = 80$ and $\psi = 1.5^\circ$).....	181
Figure 4.2.7	Flowchart of the KTH methodology of geoid followed by quasigeoid computation.....	185
Figure 4.2.8	Flowchart of the KTH methodology for quasigeoid followed by geoid computation.....	186
Figure 4.2.9	Combined atmospheric effect for the height anomalies/geoid undulations in the KTH method with LSMS kernel modification ($M = 80$ and $\psi = 1.5^\circ$).	188

Figure 4.2.10	Ellipsoidal effect for the height anomalies/geoid undulations in the KTH method with LSMS kernel modification ($M = 80$ and $\psi = 1.5^\circ$).....	189
Figure 4.2.11	Combined downward continuation effect for the height anomalies in the KTH method with LSMS kernel modification ($M = 80$ and $\psi = 1.5^\circ$).....	190
Figure 4.3.1	GQS term calculated using Flury and Rummel's (2009) method.....	196
Figure 4.3.2	GQS term calculated using Heiskanen and Moritz's (1967) method.....	197
Figure 4.3.3	Difference in the GQS term calculated using the methods given in Flury and Rummel (2009) and Heiskanen and Moritz (1967).....	198
Figure 5.1.1	Base figure to show the variation of STD or average ppm in validation results for different combinations of modification degree and integration radius (parameter sweeps).....	208
Figure 5.1.2	Standard deviation (in m) from the absolute precision assessment of geoid (blue) and quasigeoid (red) for different M and ψ combinations in the CUT method for a) India, b) UP West, c) UP East, d) Hyderabad, and e) Bangalore. The right column is for before any fitting, and the corresponding left column is for after fitting.....	210
Figure 5.1.3	Standard deviation (in m) from the absolute precision assessment of geoid (blue) and quasigeoid (red) for different M and ψ combinations in the UNB method for a) India, b) UP West, c) UP East, d) Hyderabad, and e) Bangalore. The right column is for before any fitting, and the corresponding left column is for after fitting.....	211
Figure 5.1.4	Standard deviation (in m) from the absolute precision assessment of geoid (blue) and quasigeoid (red) for different M and ψ combinations in the KTH method for a) India, b) UP West, c) UP East, d) Hyderabad, and e) Bangalore. The right column is for before any fitting, and the corresponding left column is for after fitting.....	212

- Figure 5.1.5 Standard deviation (in m) from the relative precision assessment of geoid (blue) and quasigeoid (red) for different M and ψ combinations in the CUT method for a) India, b) UP West, c) UP East, d) Hyderabad, and e) Bangalore. The right column is for before any fitting, and the corresponding left column is for after fitting..... 213
- Figure 5.1.6 Standard deviation (in m) from the relative precision assessment of geoid (blue) and quasigeoid (red) for different M and ψ combinations in the UNB method for a) India, b) UP West, c) UP East, d) Hyderabad, and e) Bangalore. The right column is for before any fitting, and the corresponding left column is for after fitting..... 214
- Figure 5.1.7 Standard deviation (in m) from the relative precision of geoid (blue) and quasigeoid (red) for different M and ψ combinations in the KTH method for a) India, b) UP West, c) UP East, d) Hyderabad, and e) Bangalore. The right column is for before any fitting, and the corresponding left column is for after fitting..... 215
- Figure 5.1.8 Average ppm (mm/km) from the relative precision assessment of geoid (blue) and quasigeoid (red) for different M and ψ combinations in the CUT method for a) India, b) UP West, c) UP East, d) Hyderabad, and e) Bangalore. The right column is for before any fitting, and the corresponding left column is for after fitting..... 216
- Figure 5.1.9 Average ppm (mm/km) from the relative precision assessment of geoid (blue) and quasigeoid (red) for different M and ψ combinations in the UNB method for a) India, b) UP West, c) UP East, d) Hyderabad, and e) Bangalore. The right column is for before any fitting, and the corresponding left column is for after fitting..... 217
- Figure 5.1.10 Average ppm (mm/km) from the relative precision assessment of geoid (blue) and quasigeoid (red) for different M and ψ combinations in the KTH method for a) India, b) UP West, c) UP East, d) Hyderabad, and e) Bangalore. The right column is for before any fitting, and the corresponding left column is for after fitting..... 218

Figure 5.1.11	Standard deviation (in arc-second) for the validation of the geoid models (computed using the three methods) with the meridional (red) and prime vertical (blue) components of the vertical deflections.....	219
Figure 5.2.1	Indian gravimetric geoid model computed using the CUT method ($M, \psi = 300, 1^\circ$).....	233
Figure 5.2.2	Indian gravimetric geoid model computed using the UNB method ($M, \psi = 300, 1^\circ$).....	234
Figure 5.2.3	Indian gravimetric geoid model computed using the KTH method ($M, \psi = 300, 1^\circ$).....	235
Figure 5.2.4	Magnitude of relative differences (blue circles) for the a) geoid (no fit) and b) geoid (4P fitting), with the CUT method ($M, \psi = 300, 1^\circ$), over 7021 GNSS-levelling baselines. Orange and yellow circles represent the maximum permissible in-field misclose for Indian high-precision ($c = 3$) and double tertiary ($c = 12$) levelling for each baseline, respectively.....	237
Figure 5.2.5	Magnitude of relative differences (blue circles) for the a. geoid (no fit) and b. geoid (4P fitting), with the UNB method ($M, \psi = 300, 1^\circ$), over 7021 GNSS-levelling baselines. Orange and yellow circles represent the maximum permissible in-field misclose for Indian high-precision ($c = 3$) and double tertiary ($c = 12$) levelling for each baseline, respectively.....	237
Figure 5.2.6	Magnitude of relative differences (blue circles) for the a. geoid (no fit) and b. geoid (4P fitting), with the KTH method ($M, \psi = 300, 1^\circ$), over 7021 GNSS-levelling baselines. Orange and yellow circles represent the maximum permissible in-field misclose for Indian high-precision ($c = 3$) and double tertiary ($c = 12$) levelling for each baseline, respectively.....	238
Figure 5.2.7	Difference between gravimetric geoid undulations computed using the CUT and the UNB methods ($M, \psi = 300, 1^\circ$).....	239

Figure 5.2.8	Scatter plot (a) and histogram (b) of the differences between gravimetric geoid undulations computed using the CUT and the UNB methods ($M, \psi = 300, 1^\circ$).....	239
Figure 5.2.9	Difference between gravimetric geoid undulations computed using the CUT and the KTH methods ($M, \psi = 300, 1^\circ$).....	240
Figure 5.2.10	Scatter plot (a) and histogram (b) of the differences between gravimetric geoid undulations computed using the CUT and the KTH methods ($M, \psi = 300, 1^\circ$).....	240
Figure 5.2.11	Difference between gravimetric geoid undulations computed using the KTH and the UNB methods ($M, \psi = 300, 1^\circ$).....	241
Figure 5.2.12	Scatter plot (a) and histogram (b) of the differences between gravimetric geoid undulations computed using the KTH and the UNB methods ($M, \psi = 300, 1^\circ$).....	241
Figure 5.2.13	Difference between gravimetric geoid undulations in UP West calculated using GEOCOL and a) CUT, b) KTH and c) UNB methods.....	242
Figure 5.2.14	Difference between gravimetric geoid undulations in UP East calculated using GEOCOL and a) CUT, b) KTH and c) UNB methods.....	242
Figure 5.2.15	Difference between gravimetric geoid models of Hyderabad calculated using GEOCOL and a) CUT, b) KTH and c) UNB methods.....	243
Figure 5.2.16	Difference between gravimetric geoid models of Bangalore calculated using GEOCOL and a) CUT, b) KTH and c) UNB methods.....	243

List of Tables

Table 1.2.1	Definition of heights.....	8
Table 1.2.2	Information about different landforms in India.....	12
Table 1.3.1	Gravimetric geoid-related studies in India.....	19
Table 2.2.1	Description of the available 119 GNSS/levelling data points.....	44
Table 2.4.1	GGM validation with GNSS/levelling points over India.....	51
Table 2.4.2	GGM validation with GNSS/levelling points over UPW and UPE.....	51
Table 2.4.3	GGM validation with GNSS/leveling points over Hyderabad and Bangalore.....	51
Table 2.4.4	GGM validation with free-air anomalies over India.....	52
Table 2.4.5	GGM validation with vertical deflections over India.....	52
Table 3.2.1	Descriptive statistics of planar TCs (in mGal) in the outer zone up to the tenth order with the separating radii of HSR = 8558 m, ESR = 4261 m and OSR = 5456 m and BR = 111320 m.....	76
Table 3.3.1	Formulas for different atmospheric effect in the KTH literature.....	106
Table 3.5.1	Three solutions for first term on the RHS of Eq. (3.5.11).....	127
Table 3.5.2	Approximate maximum values for the five terms in Eq. (3.5.15) [parametric values in the first row are from Sjöberg (2003) and in the second row are from this study; units are in m].....	128
Table 3.6.1	Values of the equipotential of the normal ellipsoid (U_0) and global geopotential (W_0).....	134
Table 3.6.2	Individual terms of Eq. (3.6.5) i.e., generalised Bruns's formula implied zero-degree term.....	135
Table 3.6.3	Defining parameters of the three normal ellipsoids.....	136

Table 3.6.4	Difference between Ekman (1989) and our conversion formula.....	144
Table 3.6.5	Conversion values of parameters for different tide-systems (for GRS80) [ZT = zero-tide; TF = tide-free; MT = mean-tide].....	151
Table 3.6.6	Difference in degree-two geoid in three tide systems. Computations are done by considering GRS80 in tide-free system and only changing $\bar{C}_{2,0}$ term of EGM2008. No changes to any parameter of GRS80 ellipsoid.....	154
Table 3.6.7	Difference in degree-two geoid undulation computed using EGM2008 and GRS80 (both in same tide system).....	156
Table 3.6.8	Difference in degree-two FAA. Computations are done by considering the GRS80 in tide-free system and only changing $\bar{C}_{2,0}$ term of EGM2008. No changes to any parameters of GRS80 ellipsoid.....	157
Table 3.6.9	Difference in degree-two FAA computed using EGM2008 and GRS80 (both in same tide system).....	157
Table 3.6.10	Difference in degree-two geoid undulations and FAA for an inconsistency in the tide-system of GRS80 (tide-system or zero-tide as per literature).....	158
Table 4.1.1	References of the three modifications to Stokes's kernel.....	169
Table 4.2.1	Examples of implementation of geoid/quasigeoid computation methodologies.....	172
Table 4.2.2	Topographical effects (in mGal) from spherical harmonic coefficients of the DEM.....	179
Table 4.3.1	Various formulas for calculating GQS term.....	193
Table 5.1.1	Descriptive statistics of absolute precision assessment of gravimetric geoid and quasigeoid models, for India and the four regions, with the three methods for a M and ψ combination that has the least standard deviation. [psi in degrees; min, max, mean and STD in m].....	220

Table 5.1.2	Descriptive statistics of relative precision assessment of gravimetric geoid and quasigeoid models, for India and the four regions, with the three methods for a M and ψ combination that has the least standard deviation. [psi in degrees; mean, STD in m; mean ppm in m/km].....	221
Table 5.1.3	Descriptive statistics of validation of gravimetric geoid models, with deflection of the vertical components, for a M, ψ combination that has the least standard deviation. [psi in degrees, min, max, mean and STD in arc-second].....	222
Table 5.1.4	Descriptive statistics of GNSS/levelling-based absolute precision assessment of the geoid and quasigeoid models calculated using GEOCOL [values in m].....	222
Table 5.1.5	Descriptive statistics of GNSS/levelling-based relative precision assessment of the geoid and quasigeoid models calculated using GEOCOL [min, max, mean, STD in m and ppm in mm/km].....	222
Table 5.2.1	Descriptive statistics of absolute precision assessment of gravimetric geoid and quasigeoid models, for India and the four regions, with the three methods for $M, \psi = 300, 1^\circ$	236
Table B.1	Ellipsoidal parameters following Moritz (2000).....	293
Table B.2	Parameters of GRS80 in all the three tide-systems. [ZT = zero-tide; TF = tide-free; MT = mean-tide].....	294
Table B.3	Parameters of WGS84 in all the three tide-systems. [ZT = zero-tide; TF = tide-free; MT = mean-tide].....	295
Table B.4	Parameters of IHRS implied possibly new normal ellipsoid (NOT OFFICIAL) in all the three tide-systems. [ZT = zero-tide; TF = tide-free; MT = mean-tide].....	296

List of Abbreviations

ASTER	Advanced Spaceborne Thermal Emission and Reflection Radiometer
BR	Bounding Radius
CIL	Coal India Limited
CUT	Curtin University of Technology
d/o	Degree and Order
DAE	Direct Atmospheric Effect
DEM	Digital Elevation Model
DSM	Digital Surface Model
DTE	Direct Topographic Effect
DTM	Digital Terrain Model
DWC	Downward Continuation
ESR	Exact Separating Radius
FEO	Featherstone Evans Olliver
FFT	Fast Fourier Transform
FOIE	First Order Indirect Effect
G&RB	Geodetic & Research Branch
GBVP	Geodetic Boundary Value Problem
GEOCOL	Gravity Field Approximations using Least Squares Collocation
GGM	Global Geopotential Model
GMSI	Gravity Map Series of India

GNSS	Global Navigation Satellite System
GOCE	Gravity Field and Steady-State Ocean Circulation Explorer
GQS	Geoid-Quasigeoid Separation
GRACE	Gravity Recovery and Climate Experiment
GRAVSOFT	Geodetic Gravity Field Modelling Programs
GRS	Geodetic Reference System
GSI	Geological Survey of India
GTS	Great Trigonometric Survey
HSR	Height-defined Separating Radius
IAG	International Association of Geodesy
ICGEM	International Centre for Global Earth Models
IGSN71	International Gravity Standardization Net 1971
IHRS	International Height Reference System
IIT	Indian Institute of Technology
INCOIS	Indian National Centre for Ocean Information Services
INGD63	Indian National Gravity Datum 1963
IUGG	International Union of Geodesy and Geophysics
IVD	Indian Vertical Datum
KTH	Royal Institute of Technology
LSC	Least Squares Collocation
LSMS	Least Squares Modification of Stokes' formula

MDT	Mean Dynamic Topography
MERIT	Multi Error Removed Improved Terrain
MSL	Mean Sea Level
MT	Mean Tide
NDMA	National Disaster Management Authority
NGRI	National Geophysical Research Institute
OIL	Oil India Limited
ONGC	Oil and Natural Gas Corporation
OSR	Optimum Separating Radius
PIAE	Primary Indirect Atmospheric Effect
PITE	Primary Indirect Topographic Effect
RCR	Remove Compute Restore
RTM	Residual Terrain Model
SHA	Spherical Harmonic Analysis
SHC	Spherical Harmonic Coefficients
SHS	Spherical Harmonic Synthesis
SIAE	Secondary Indirect Atmospheric Effect
SITE	Secondary Indirect Topographic Effect
SoI	Survey of India
SRTM	Shuttle Radar Topography Mission
STD	Standard Deviation

TC	Terrain Correction
TCM	Terrain Correction with Mass-prism analytical integration
TCS	Terrain Correction with Simpson's numerical method
TCT	Terrain Correction with Trapezoidal rule method
TF	Tide Free
TGBM	Tide Gauge Bench Mark
UNB	University of New Brunswick
UP	Uttar Pradesh
UPE	Uttar Pradesh East
UPW	Uttar Pradesh West
VK	Vaniček Kleusberg
WGS	World Geodetic System
ZT	Zero Tide

List of Symbols

a	Semi-major axis of the reference ellipsoid
b	Semi-minor axis of the reference ellipsoid
e	First eccentricity of the reference ellipsoid
f	Flattening of the reference ellipsoid
h	Ellipsoidal height (aka geodetic height)
k	Normal gravity formula constant
m	$m = (\omega^2 a^2 b) / GM$
n, m	Spherical harmonics degree and order
q	Ellipsoidal parameter (Heiskanen and Moritz, 1967 pg. 66)
r	Geocentric radius
u	Semi-minor axis of a confocal ellipsoid
x, y	Cartesian coordinates
E	Linear eccentricity of the reference ellipsoid
G	Universal gravitational constant
GM	Geocentric gravitational constant of the Earth
H	Orthometric height
J	Mean curvature of the ellipsoid
L	Maximum degree of global geopotential model
M	Modification degree of Stokes's integration
N	Geoid undulation

P	Computation point on the Earth's surface
R	Radius of the reference sphere
T	Disturbing potential
U	Normal gravity potential of the reference ellipsoid
a_E	Semi-major axis of the reference ellipsoid
a_G	Equatorial scale factor provided with global geopotential model
e'	Second eccentricity of the reference ellipsoid
\bar{g}	Mean gravity
k_2, h_2	Degree-two Love number
l_E	Euclidean distance
q_0	Ellipsoidal parameter q on the ellipsoid
r_{cp}	Geocentric radius of the computation point
s^n	Modification parameters (KTH)
$\bar{C}_{E-2n,0}$	Fully normalised zonal even degree harmonic coefficient of the reference ellipsoid
$\bar{C}_{nm}, \bar{S}_{nm}$	4π Fully normalised spherical harmonic coefficients
G_1	Molodensky's terrain term
GM_{Atm}	Geocentric gravitational constant of the Earth's atmosphere
GM	Geocentric gravitational constant of the reference ellipsoid
GM_G	Geocentric gravitational constant given in a GGM file

GM'	Geocentric gravitational constant with the Earth's atmosphere excluded
H_0	Zero-frequency tidal displacement amplitude at the poles
H^*	Normal height
H^d	Dynamic height
$J_{2,0}$	Dynamical form factor
N_0	Zero-degree term of geoid undulation
$N_{GNSS/lev}$	Geometric geoid undulation from GNSS and levelling
\hat{N}	Approximate geoid undulation (KTH)
P_n	Legendre polynomials of the first kind for degree n
\bar{P}_{nm}	4π Fully normalised associated Legendre functions of the first kind for degree n and order m
Q_n^M	Molodensky's truncation coefficient
$S(\psi)$	Stokes's kernel
$S^M(\psi)$	Modified Stokes kernel (FEO, VK and LSMS kernel modifications as used in CUT, UNB and KTH methods, respectively)
V_{atm}^{ar}	Gravitational potential of atmospheric roughness (UNB)
V_{atm}^{as}	Gravitational potential of atmospheric shell (UNB)
V_{atm}^{cr}	Gravitational potential of condensed atmospheric roughness (UNB)
V_{atm}^{cs}	Gravitational potential of condensed atmospheric shell (UNB)
V_{KTH}^a	Gravitational potential of atmosphere (KTH)

V_0^a	Zero-degree term of atmospheric gravitational potential (KTH)
V_1^a	First-degree term of atmospheric gravitational potential (KTH)
V^t	Potential of the topographical masses (UNB, KTH)
V^{ct}	Potential of the condensed topographical surface layer (UNB)
U_0	Normal potential of the reference ellipsoid
W_0	Geopotential
W_T	Tidal Potential
β	Reduced latitude
γ	Normal gravity from the reference ellipsoid
ζ	Height anomaly/ quasigeoid height
ν	Radius of curvature of the reference ellipsoid in the prime vertical direction
μ	Radius of curvature of the reference ellipsoid in the meridian direction
φ, λ	Geodetic latitude and longitude
ϕ, λ	Geocentric latitude and longitude
Φ, Λ	Astronomical latitude and longitude
ρ	Constant bulk topographic density
ψ	Spherical angular distance between two points on the sphere
ω	Angular velocity of the Earth's rotation
Θ	Total deflection of the vertical
β_γ	Difference between geodetic and geocentric latitudes

ε_n	Ellipsoidal correction to the vertical gradient of normal gravity
$\varepsilon_{\delta g}$	Ellipsoidal correction to the gravity disturbance
γ_a	Normal gravity on the reference ellipsoid at the equator
γ_b	Normal gravity on the reference ellipsoid at the poles
γ_0	Normal gravity on the reference ellipsoid
γ_{0_WGS84}	Normal gravity on the WGS84 ellipsoid
$\bar{\gamma}$	Mean normal gravity
γ_h	Normal gravity at an arbitrary height
σ_{FAA}	Estimated error of reconstructed free-air anomaly from GTECH Bouguer anomalies
η_H	East-west component (prime vertical) of Helmert's vertical deflection
ξ_H	North-south component (meridional) of Helmert's vertical deflection
η_{Pz}	East-west component (prime vertical) of Pizetti's vertical deflection
ξ_{Pz}	North-south component (meridional) of Pizetti's vertical deflection
ρ_0^a	Mean bulk density of atmosphere at sea-level
ρ_0^*	Gravitational constant times atmospheric bulk density at sea level (KTH)
ρ_{KTH}^a	Atmospheric density model (KTH)
ρ_{UNB}^a	Atmospheric density model (UNB)
σ_t	Surface density of the condensed topographical layer (UNB)

ζ_0	Approximate height anomaly (KTH)
Ω_{\oplus}	Solid spherical angle
$\delta\zeta^{Atm}$	Combined atmospheric effect on height anomaly (KTH)
$\delta\zeta^{DWC}$	Downward continuation effect on height anomaly (KTH)
$\delta\zeta^{Ell}$	Effect of ellipsoidal correction on height anomaly (KTH)
Δg_{SB}^{GETECH}	Simple Bouguer anomaly from the GETECH data
Δg^{FA}	Free-air gravity anomaly
Δg^{BA}	Planar Bouguer anomaly
δg^{NT}	Gravity disturbance in no-topography space
Δg^{BC}	Planar Bouguer correction
Δg^{RBA}	Refined planar Bouguer gravity anomaly
Δg^{SB}	Simple planar Bouguer gravity anomaly
Δg^{H^+-H}	Geoid-quasigeoid correction to the gravity anomaly (UNB)
Δg_{KTH}^a	Atmospheric gravity anomaly (KTH)
Δg_e^{GGM}	Ellipsoidal gravity anomaly from global geopotential model (CUT)
δg	Gravity disturbance
Δg_{UNB}^{ell}	Gravity anomaly with ellipsoidal correction (UNB)
Δg_{KTH}^{ell}	Gravity anomaly with ellipsoidal correction (KTH)

Δg_{KTH}^{DWC}	Downward continued gravity anomaly (KTH)
Δg_{UNB}^{DWC}	Downward continued gravity anomaly (UNB)
δG	Total ellipsoidal correction to gravity anomaly (KTH)
$\Delta g'$	Gravity anomaly on the level surface passing through the computation points (CUT, KTH)
$\Delta g'_{UNB}$	Free-air gravity anomaly on the topography (UNB)
Δg^t	Topographical gravity anomaly (KTH)
Δg^a	Atmospheric gravity anomaly (KTH)
δg_{FAC}^{GETECH}	Second-order free air correction as applied to the GETECH data
δg_{atm}^{GETECH}	Atmospheric correction as applied to the GETECH data
Δg^{NT}	Gravity anomaly in no-topography space
δN_{comb}^{atm}	Combined atmospheric effect on geoid undulation (KTH)
δN^{DWC}	Downward continuation effect on geoid undulation (KTH)
δN^{Ell}	Effect of ellipsoidal correction on geoid undulation (KTH)
δN_{comb}^T	Combined topographical effect on geoid undulation (KTH)
δN_{dir}^T	Direct topographical effect on geoid undulation (KTH)
δN_{Indir}^T	Indirect topographical effect on geoid undulation (KTH)
δV^t	Residual topographical potential (UNB)
δV^a	Residual atmospheric potential (UNB)

x	Vector of unknown parameters
v	Vector of residuals
A	Design matrix
l	Vector of observations

Chapter 1: Introduction

1.1 Background

From numerous equipotential surfaces of the Earth's gravity field, the one best approximated by the ocean at rest is the *geoid*. One should note that this is only one of the many definitions of the geoid available in the literature, which are summarised by Bašić and Varga (2018). All terrestrial geodetic and engineering survey measurements are made after aligning the instrument's vertical axis orthogonal to an equipotential surface. Hence, an equipotential surface is the best candidate for a reference surface for heights. By definition, geoid is the equipotential surface and can also be *theoretically* calculated. However, it is hardly possible to calculate a national geoid model, especially, because of the uncertainty in the plumbline curvature (discussed later). Therefore, the best approximations of the geoid, i.e., the calculated so-called geoid or quasigeoid are preferred as a vertical reference surface.

The geoid can be calculated using astrogeodetic observations, known as an astrogeodetic geoid, or using gravity observations with the Stokes (1849) and Bruns (1878) formula, known as a gravimetric geoid or using Global Navigation Satellite System (GNSS)/levelling data, known as a geometric geoid. Some have also used a combination of the astrogeodetic and gravimetric data to develop an astro-gravimetric geoid (e.g., Fryer, 1972; Marti, 1997). Astrogeodetic and gravimetric geoids have their necessities and advantages, but the former was practised long ago before development of the portable gravimeters. A geometric geoid is practically meaningful only for local regions. A gravimetric geoid is calculated with respect to a reference ellipsoid having the following three properties (e.g., as given by Heiskanen and Moritz, 1967, pg. 94; but it should be

noted that commonly used ellipsoids (e.g., GRS80) often do not have all of these properties, leading to the zero-degree term (discussed later, Section 3.6)):

- i) The potential of the reference ellipsoid (U_0) is equal to the potential of the geoid (W_0).
- ii) The ellipsoid encloses the mass numerically equal to the Earth's mass (including atmospheric mass).
- iii) The centre of the ellipsoid is coincident with the centre of mass of the Earth.

Moreover, Stokes (1849) made the assumption that the gravity anomalies for the whole world are available on the geoid and there are no external masses above the geoid. On the contrary, gravity values are observed on or above the Earth's topographical surface and are not available for the whole world. Also, there exist external masses above the geoid. Therefore, regional, national or continental geoid modelling is primarily about i) regularisation of the masses above the geoid (e.g., Helmert, 1884) and ii) applying Stokes's integral with high frequency regional gravity data, which is available only in a limited region.

The major concern in removing or shifting the masses external to the geoid is assumptions regarding the density distribution of the topographical masses (Martinec, 1993; Pagiatakis et al., 1999; Kuhn, 2001; 2003; Huang et al., 2001). Therefore, Molodensky et al. (1962) introduced the theory of the quasigeoid that is a non-equipotential surface departing not much from the geoid. They suggested use of the Earth's topographical surface as the reference surface for Stokes's integration of the gravity anomalies, i.e., gravity anomalies may now be available on the Earth's topographical surface instead of the geoid. Thus, eliminating the need for regularisation of the topographical masses between the geoid and the Earth's topographical surface.

Since i) none confirms (to our best information from the literature) that the calculated geoid is an equipotential surface (although some near-related studies have been conducted, e.g., Claessens and Filmer, 2020; Wang et al., 2021) and ii) the difference between geoid and quasigeoid is not significant (except in the mountainous regions), it has become a country's specific choice to adopt quasigeoid or geoid as the national vertical reference surface. However, calculation of both geoid and quasigeoid still needs some regularisation methods and modifications/strategies to truncate Stokes's integral to the region of interest.

In India, the first geoidal study was started more than a century ago. The detailed information is most probably provided in the archaic Survey of India (SoI) reports, which are not available in the public domain. However, we try to provide concise introductory information as gathered from different sources. The geoidal study was started in India around 1901 (SoI, 1950) based on astrogeodetic observations with respect to the Everest1830 ellipsoid. Bomford (1967) mentions that de Graaff Hunter compiled the first geoid map for India in 1922 based on astrogeodetic observations referred to an international spheroid. According to de Graaff Hunter (1932), it was published in 1923 excluding the Himalayan region (information on where it was published is not available) and published in SoI (1930) for India. The geoid map from 1923 is also provided in Daly (1969, pg. 228).

SoI (1950, pg. 146) mentions that the definitions of the geoid provided in SoI (1930) were all incorrect and hence, they rectified the definitions of the previous report. The pages with the rectified definitions in SoI (1950) are provided in Appendix A. No geoid map is provided in SoI (1950), but SoI (1951, pg. 89) provides a hard-to-read geoid map, referred to an international spheroid, for India and neighbouring countries based on the astrogeodetic data available during 1950-1951. Other than these, Fischer (1961)

mentions a more refined astrogeodetic geoid of India, with dense data, published in SoI (1957) and also themselves had developed an Indian astrogeodetic geoid (Fischer, 1968). However, neither of the two are available in the public domain.

During the 1970s to mid-1980s, a few other gravimetric and astrogeodetic geoid related studies were conducted for India (e.g., Bhattacharji, 1973; 1982; Gaur, 1981; Khosla et al., 1982; Srivastava, 1985), with respect to both Everest and GRS67 ellipsoids. The used gravity data was primarily from the geopotential coefficients (Rapp, 1977) and sometimes very coarse observed mean gravity anomaly data ($1^\circ \times 1^\circ$). None of these models is available in the public domain.

From 2007 onwards, a few more gravimetric geoid-related studies over India were available in the literature (e.g., Singh, 2007; Singh et al., 2007; Carrion et al., 2009; Srinivas et al., 2012). This was probably because the proposal for a redefined vertical datum, in 2005, mentioned adopting a gravimetric geoid model as the new Indian Vertical Datum (IVD), whenever available. After 2012, to the author's best information, there is only one gravimetric geoid study over India published, i.e., Mishra and Ghosh (2016). The results from these studies (from 2007 to 2017) are also not in the public domain.

It is important to note that the studies from 1901 to 1957 were all conducted by SoI; from 1973 to 1985 by SoI or University of Roorkee in collaboration with SoI; and from 2007 to 2017 by SoI, Indian Institute of Technology (IIT) Roorkee (previously University of Roorkee) in collaboration with SoI, National Geophysical Research Institute (NGRI) in collaboration with SoI or NGRI (but without access to GNSS/levelling data for validation, the keeper of which is SoI). This shows that until today, geoid related studies in India are somewhat governed by SoI. Hence, several stakeholders are kept deprived of any developed geoid model or the geodetic data to do geoid modelling themselves. Moreover, despite all these efforts, no Indian national gravimetric or astrogeodetic geoid

model is available in the public domain. In the present thesis, we are interested only in the gravimetric geoid model and, therefore, will keep our further discussions limited to that only, though astrogeodetic data are used for validation.

It is now over 170 years since George Gabriel Stokes published his seminal formula for geoid determination from gravity anomalies (Stokes, 1849); over 55 years since the English translation of Mikhail Sergeevich Molodensky's book was published, including the formula for quasigeoid determination from gravity anomalies (Molodensky et al., 1962); and over 50 years since Martin Hotine's monograph was published including the formula for geoid determination from gravity disturbances (Hotine, 1969). For the present thesis, we are only concerned with the geoid and quasigeoid using the gravity anomalies that require Stokes's integration.

Ideally, Stokes's integral should be implemented over the entire Earth with continuous gravity anomalies on the geoid and with the Laplace harmonicity condition ($\nabla^2 T = 0$) that there must not be any gravitating mass above it (Heiskanen and Moritz, 1967). However, in practice, the integral is reduced to a limited area, i.e., truncated because gravity anomalies over the entire Earth are not available for computations due to a multitude of reasons, e.g., inaccessible areas or national data restriction policies. Also, gravity anomalies usually exist discontinuously on or above the Earth's surface, so various types of regularisations and downward continuation have been proposed. The gaps between theoretical and practical aspects incur several kinds of errors, which geodesists have tried to reduce.

Presently, based on various ideas, philosophies and numerical approaches, there are the following four more common techniques available for geoid computation.

- i) Geoid/Quasigeoid computation methodology (GRAVSOFIT) based largely on Least Squares Collocation (LSC) developed at the University of Copenhagen, Denmark (Forsberg, 1984, 1985; Knudsen, 1987; Forsberg and Tscherning, 2008)
- ii) The Stokes-Helmert method (SHGeo) developed at the University of New Brunswick (UNB), Canada (Vaníček and Kleusberg, 1987; Vaníček and Martinec, 1994; Martinec and Vaníček, 1994a; 1994b; Vaníček et al., 1999; UNB, 2009; Tenzer et al., 2003; Ellmann and Vaníček, 2007; Vaníček et al., 2013).
- iii) Least Squares Modification of Stokes formula (LSMS) with Additive Corrections (AC) method developed at the Division of Geodesy, Royal Institute of Technology (KTH), Sweden (Sjöberg, 1984a; 1984b; 1991; 2000; 2003a; 2003b; Ågren, 2004).
- iv) Quasigeoid computation method developed at Curtin University of Technology (CUT), Australia (Featherstone, 2000; 2001; Featherstone et al., 1998; 2001; 2011; 2018; Amos and Featherstone, 2009; Claessens et al., 2011; McCubbine et al., 2018; 2021).

There are of course, other approaches such as radial basis functions (e.g., Li, 2018; Liu et al., 2020) but perhaps not yet applied as widely as the above four. Despite a long-elapsed time from the developed methodologies and numerous implementations, determination of a centimetre level precise geoid and quasigeoid still remains an ongoing quest (Sansò and Rummel, 1997; Foroughi et al., 2019; Ellmann et al., 2020). Hence, comparative studies among the different computational techniques are required to investigate, primarily, the scope of modifications to the existing methodologies or a need of precise and dense input datasets. Arguably, different approaches are necessary in different parts of the world due to, for instance, the peculiarities of the data holdings, e.g.,

Goyal et al. (2022) summarises numerous geoid/quasigeoid solutions of Auvergne in France where researchers have tested their geoid/quasigeoid calculation methods.

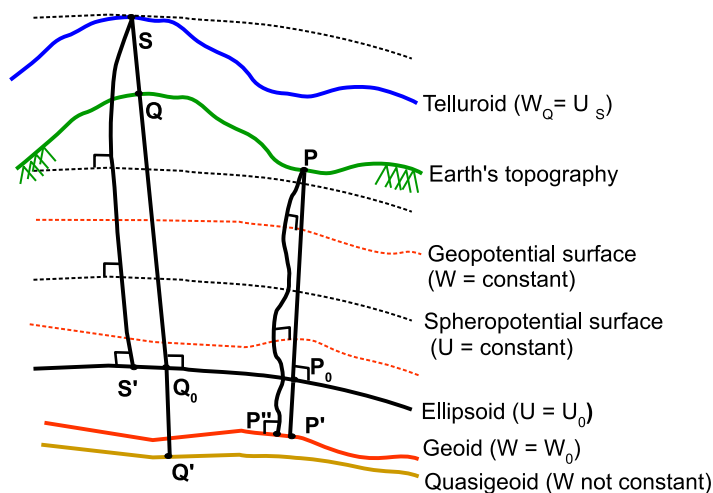
With the above background on Indian geoid-related studies, we will next discuss the IVDs and the height systems.

1.2 Height systems

Height is the vertical distance between two points. However, one could ask, what is the direction of the vertical distance? Therefore, a more precise definition of height could be, a vertical distance between two points lying on well-defined mathematical, physical or virtual surfaces along a specified direction. Scientifically, height is a coordinate that separates two points along a specified direction in a 3D space having the same 2D coordinates in a given reference frame.

In the present satellite era, 3D coordinates of our position on the Earth's surface are obtained using GNSS. There are multiple options for the height coordinate, including using GNSS itself. These options primarily depend on the direction of the vertical distance and the reference surface from where the distance is being measured. Heiskanen and Moritz (1967), Jekeli (2000), Dennis and Featherstone (2003), Featherstone and Kuhn (2006) and Amos (2007) have discussed different types of heights. Also see Tenzer et al. (2005) and Santos et al. (2006). Therefore, here we will discuss only those which are relevant to the present thesis: orthometric height, normal height, normal-orthometric height, geodetic or ellipsoidal height, geoid undulation and height anomaly.

Figure 1.2.1 shows a schematic diagram for above mentioned different heights, and Table 1.2.1 explains/defines the same.



Ellipsoidal height: P_0P and Q_0Q Orthometric height: $P''P$ (and $\sim P''P$)

Normal height: $S'S$ (and $\sim Q'Q$) Geoid undulation: P_0P'

Height anomaly: SQ and Q_0Q'

Figure 1.2.1: Different surfaces and heights

Table 1.2.1: Definition of heights

Height	Height of a point on the:	From a corresponding point on the:	Along:	Formula (Heiskanen and Moritz, 1967; Jekeli, 2000)
Orthometric	Earth's surface	Geoid	Curved and torsioned plumb line	$\frac{1}{\bar{g}} \int_0^H g dH$; $\bar{g} = \frac{1}{H} \int_0^H g dH$
Normal	Earth's surface	Quasigeoid	Curved normal plumb line	$\frac{1}{\bar{\gamma}} \int_0^{H^*} g dH^*$; $\bar{\gamma} = \frac{1}{H^*} \int_0^{H^*} \gamma dH^*$
	Telluroid	Ellipsoid	Curved normal plumb line	
Normal-orthometric	Earth's surface	Geoid or Quasigeoid*	Curved normal plumb line	$\frac{1}{\bar{\gamma}} \int_0^{H^{NO}} \gamma dH$; $\bar{\gamma} = \frac{1}{H^{NO}} \int_0^{H^{NO}} \gamma dH^{NO}$
Geodetic or Ellipsoidal	Earth's surface	Ellipsoid	Ellipsoidal surface normal	h
Geoid undulation	Geoid	Ellipsoid	Ellipsoidal normal	$\frac{T_{P'}}{\gamma_{P_0}} + \frac{U_0 - W_0}{\gamma_{P_0}}$
Height anomaly	Quasigeoid	Ellipsoid	Ellipsoidal normal	$\frac{T_Q}{\gamma_S} + \frac{U_0 - W_0}{\gamma_{P_0}}$
	Earth's surface	Telluroid	Ellipsoidal normal	

* No unique reference surface is specified for normal-orthometric height system (e.g., Filmer et al., 2010; 2014)

The definitions in Table 1.2.1 can be read as “*Column 1* height is the height of a point on *Column 2* from a corresponding point on *Column 3* along the *Column 4*,” e.g., ‘*Orthometric* height is the height of a point on the *Earth’s surface* from a corresponding point on the *geoid* along the *curved and torsioned plumb line*’. In addition to the heights explained in Table 1.2.1, there is also dynamic height. The dynamic heights are computed by dividing the geopotential number (difference between geopotential values at the geoid and point in consideration on the Earth’s topography) by some constant. The adopted constant for calculating the dynamic heights is normal gravity at 45° latitude (Heiskanen and Moritz, 1967, pp. 162-163).

From Figure 1.2.1, there exists geometrical relationship between i) geodetic height (h), orthometric height (H) and geoid undulation (N) given by Eq. (1.2.1) and ii) geodetic height, normal height (H^*) and height anomaly (ζ) given by Eq. (1.2.2). Since no unique surface is defined for normal-orthometric height (H^{NO}), H or H^* in Eqs. (1.2.1) and (1.2.2) are sometimes replaced by H^{NO} also to calculate geometric geoid undulation or geometric height anomalies, respectively.

$$N \approx h - H \quad (1.2.1)$$

$$\zeta \approx h - H^* \quad (1.2.2)$$

A ‘pure’ orthometric height is impossible to be realised practically, as this requires gravity and density information at every point on the curved and torsioned plumbline between the Earth’s surface and the geoid. Therefore, instead of using the integral mean value of Earth’s gravity along the plumbline, mean gravity is approximated using the Poincaré and Prey reduction (Heiskanen and Moritz, 1967, pg. 163), thus providing Helmert’s orthometric heights (Heiskanen and Moritz, 1967, pg. 167). Niethammer (1932)

and Mader (1954) heights, which include terrain corrections, are proved to be better than Helmert's orthometric heights (Dennis and Featherstone, 2003).

Molodensky (1945) proposed the use of normal heights, wherein the mean actual gravity is replaced by mean normal gravity between the reference ellipsoid and the telluroid (Heiskanen and Moritz, 1967). The distance between Earth's topographical surface and the telluroid is the height anomaly, and mapping of these height anomalies on the corresponding points on the ellipsoidal surface gives quasigeoid. Although not a geopotential surface, quasigeoid is a preferred choice of the vertical reference surface in many countries, including Australia and Sweden.

The main issue in the determination of orthometric heights is the computation of the integral mean gravity along the plumbline (Rapp, 1961). Tenzer et al. (2005) formulated 'rigorous' orthometric height by calculating the mean gravity along the plumbline by considering the effect of second-order correction for normal gravity, the gravitational attraction of topographical (Bouguer shell and terrain roughness) and atmospheric masses, lateral variation of topographical mass-density and the gravity disturbance due to the masses below the geoid surface. Santos et al. (2006) derived the corrections to obtain the 'rigorous' orthometric height (Tenzer et al., 2005) from Helmert's orthometric height. An effort to modernise the existing [Helmert's] orthometric height system of Canada to these 'rigorous' orthometric heights has been made by Kingdon et al. (2005).

However, despite recent advancements in the height systems, Helmert's orthometric heights (which use Poincaré and Prey reduction) are still in vogue in many countries, probably due to their relative ease of implementation. Also, there are many other countries, mainly in Eastern Europe, the former Union of Soviet Socialist Republics (USSR) and South America use normal heights.

Normal-orthometric heights are also practiced in several countries, e.g., United Kingdom (Penna et al., 2013), Australia (Featherstone and Kuhn, 2006), New Zealand (Amos, 2007), Sri Lanka (Abeyratne et al., 2010) and Uganda (Ssengendo, 2015). This height system is defined for the case when gravity observations are not available along the levelling lines and therefore, utilises spheropotential number instead of the geopotential numbers. The normal-orthometric correction (e.g., Burrard, 1910; Rapp, 1961; Bomford, 1971) is applied to the levelling height differences for calculating the normal-orthometric heights. Moreover, unlike normal or orthometric heights, there is no unique reference surface defined for normal orthometric heights, though quasigeoid is sometimes preferred (Amos, 2007; Ssengendo, 2015).

With so many height systems available, the discussion on the suitability of heights and geoid (Vaníček et al., 2012) or quasigeoid (Sjöberg, 2013) as a reference surface for heights has remained group/country specific.

1.2.1 Indian vertical datum and height system

We will start this section by depicting different major topographical landforms of India (Figure 1.2.2): the Himalayas, Aravalli and Vindhya ranges, Western and Eastern Ghats, plateaus, desert, the Gangetic plains and a long peninsular coastline of ~7500 km. To differentiate the heights of various landforms, we have used the bins of <300 m, 300 m – 600 m, 600 m – 1200 m and >1200 m, because these bins are also used in the standard school textbook (NCERT, 2006, pg. 9).

Different sources have different numbers attached to the highest peak, average elevation and length of the hill ranges in India. To provide an overview, we tabulate some information in Table 1.2.2, from not so reliable sources (Wikipedia and Encyclopedia).

Table 1.2.2: Information about different landforms in India.

Landform/coastline	Highest peak (m)	Average elevation (m)	Length/ Area
Aravalli	1722	400-600	670 km
Vindhya	752	300-650	1200 km
Western Ghats	2637	900-1500	1600 km
Eastern Ghats	1680	600	1400 km
Himalayas (India)	8586	900-4900	500,000 km ²
Thar Desert	-	150	238,254 km ²
Deccan plateau	-	600	422,000 km ²
Chota Nagpur plateau	1350	-	65,000 km ²
Gangetic plains	-	250	2,500,000 km ²
Coastline	-	-	7516 km

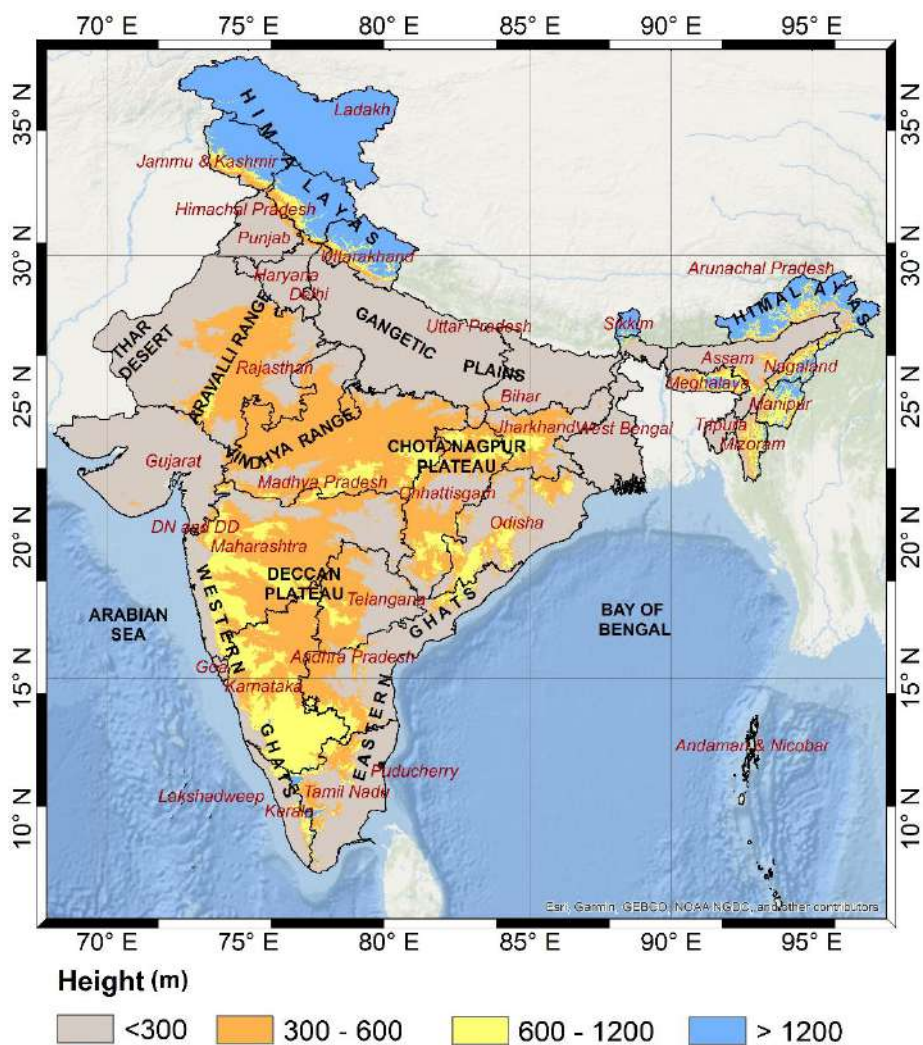


Figure 1.2.2: Various landforms in India. Red italics shows the name of the Indian state or Union territory.

The information in Table 1.2.2 and Figure 1.2.2 is provided so that readers may appreciate the painstaking job of SoI in the high precision levelling of a country like India.

Now, resuming the discussion on the vertical datums and height systems, according to Burrard (1910), the following four choices were considered and debated to establish the 'zero' surface/reference for the IVD defined in 1909 (IVD1909):

1. Any one of the benchmarks established at Delhi, Jodhpur, Raichur, Sanichari or Naubatpahar.
2. Mean Sea Level (MSL) estimate determined at one tidal observatory.
3. MSL estimates determined at all the tidal observatories.
4. MSL from a few selected tidal observatories.

After considering all the merits and limitations of the above four options, it was decided to select a few tidal observatories that would define the zero surface for the Indian levelling net or the IVD1909. To choose a set of tidal observatories from the then maintained 42 observatories by SoI, a simple rule was devised mentioning that the tidal observatory should be an open-coast station (not situated in any of the channels, estuaries, gulfs or rivers) at which successive annual determination of MSL should be consistent.

As such, only nine tidal observatories were selected, fulfilling the above-laid criteria: Karachi, Bombay (Apollo Bandar), Karwar, Beypore, Cochin, Negapatam, Madras, Vizagapatam, and False Point (Figure 1.2.3). The first five lie in the Arabian sea, while the last four in the Bay of Bengal. Thus, the precise levelling net of India consisting of 86 main lines was terminated at the Tide Gauge Bench-Marks (TGBM) of the above nine tidal observatories. The heights of these TGBMs were transferred from the tidal observatories considering that the MSL estimate at each of these nine stations is the same, i.e., zero. Thereafter, these 86 lines (including nine lines from the tidal observatory to

TGBM) were adjusted using least-squares (with the tide gauge MSL estimates constrained to zero) to define the first IVD, i.e., IVD1909 (Burrard, 1910).

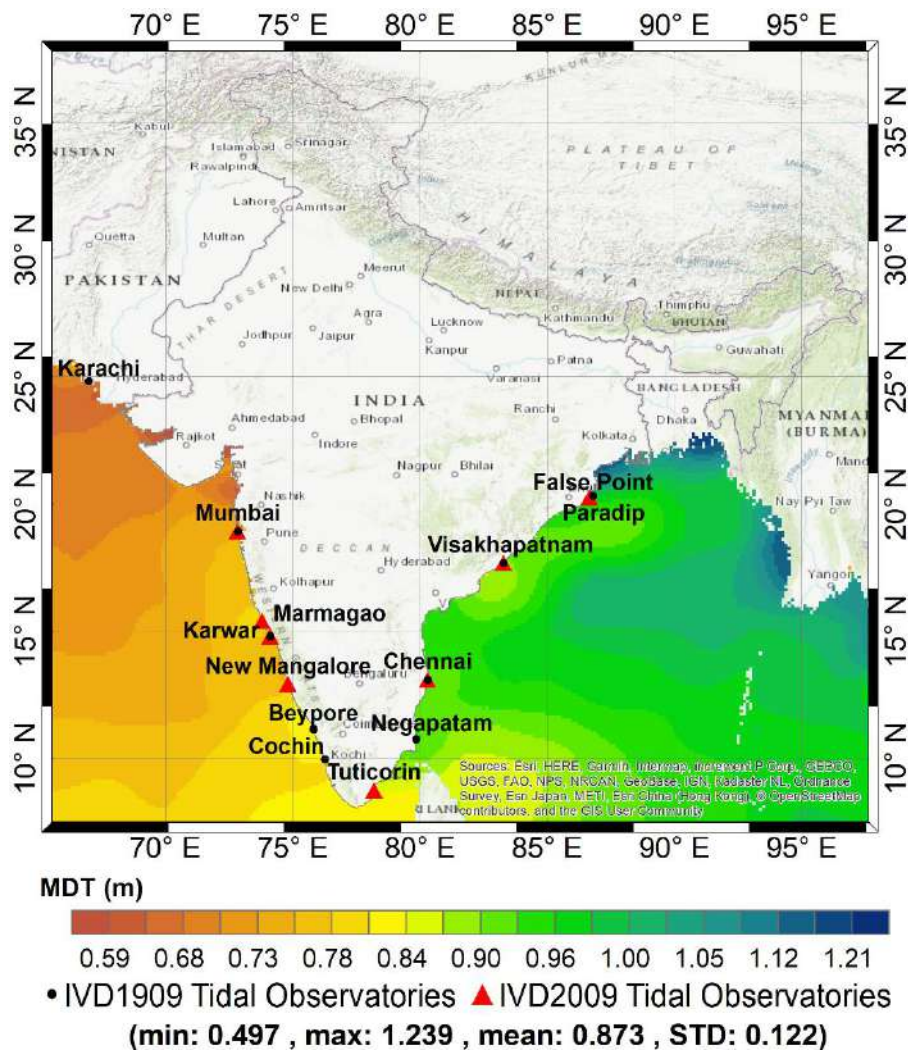


Figure 1.2.3: Mean Dynamic Topography (DTU19MDT) along with tidal observatories used in IVD1909 and IVD2009

An important fact to be mentioned here is that though the sea surface in the Bay of Bengal and Arabian sea were considered to be equal, various observations (e.g., levelling from east coast to west coast, levelling from the east coast and west coast to a centre location etc.) suggested that there might be a difference of almost one Indian foot between the two (Burrard, 1910). However, the difference (so-called error) in all the experiments was attributed to the possible levelling errors, and this difference of one foot was left for further confirmation by the future successive levelling exercises. Later, it was confirmed

by Ghildiyal and Kumar (1984; also see Shankar and Shetye, 2001) that the Bay of Bengal is on average ~320 mm higher than the Arabian sea (e.g., see difference in MDT of west and east coasts in Figure 1.2.3). It should be noted that some exercises for IVD1909 showed that even the sea surface along either east or west coast is not same, but this was also attributed to the levelling errors. There exists a similar example of discrepancies in the mean sea surface (MSS) along and across the Atlantic and Pacific coastlines in North America (Reid, 1961; Sturges, 1967; 1974). This approach of constraining the level net to multiple tide-gauges is a possible cause of a north-south tilt (Fischer, 1975; 1977; Featherstone and Filmer, 2012) that is also confirmed from our results (Chapter 5). It is possible that India may have an east-west tilt also (Figure 1.2.3), but it can't be confirmed because of the lack of GNSS/levelling data in the east-west extent (Section 2.2).

The precise levelling net for IVD1909 consisting of 86 main lines was observed during 1858 to 1909 that covered a total of ~28922 km of double-line levelling (Burrard, 1910) that was a practice of observing any given levelling line by two surveyors one after the other, immediately. A total number of 15981 benchmarks of different types (standard, embedded, inscribed, etc.) were connected by these main lines. In this half a century-long levelling exercise, 16 different levels (weighing from ~23 kg to ~12 kg) and four types of levelling staves (introduced in 1858, 1902, 1906 and 1907) were used.

The spirit levelling height differences were transformed to dynamic heights by applying a dynamic height correction using normal gravity instead of the observed gravity (Burrard, 1910, pp. 100-103) because until 1909, pendulum gravity observations were not taken at a sufficient number of benchmarks. These dynamic heights were used for the adjustment of the level net. The orthometric correction (also using normal gravity) was then applied to compute the so-called orthometric height. However, due to the use of

normal gravity in place of the observed gravity, the resultant heights from IVD1909 were actually normal-orthometric heights (Table 1.2.1; Burrard, 1910).

The IVD1909-based height information is sufficient for the needs of topographical mapping on scales of 1: 50,000 or 1: 25,000 where the contour interval is 10 m / 5 m in plain areas or 200 m / 100 m in hilly areas (as per SoI topographical maps). Now with the demand of 0.5 m to 1 m contours, the prevailing height information is not sufficient. In the past 100 years, due to developmental activities, like widening of roads and railways, construction of townships and industrial premises, most of the permanent benchmarks have been destroyed. The frequent seismic activity in various parts of the country and corresponding crustal movements have also necessitated the introduction of a new height system. Moreover, IVD1909 was defined as a suitable datum only for 50 years. It was recommended in the original report (Burrard, 1910) that the same must be revised without losing the values observed during 1858-1909 as they will be useful for various scientific studies.

Considering the fact that the height information was almost a century ago and with the availability of precise relative gravimeters, the SoI started a project in 2005 to redefine the IVD and modernise the Indian height system. There are some improvements in IVD defined in 2018 (IVD2009; G&RB, 2018) compared to IVD1909, such as using double foresight backsight levelling lines with invar staves and observed gravity values. Also, rather than fixing the MSL estimates to zero at nine tidal observatories, the average of the local geopotential value computed at eight tidal observatories was constrained in IVD2009.

The eight tidal observatories were chosen such that each has data of at least 19 years (for 18.6 years nodal tidal cycle) without significant data gaps. We could not quantify the word significant as no information is available on this. For this criterion, the following

eight tidal observatories were chosen with their data from 1976-1994: Mumbai, Marmagao, Karwar and New Mangalore on the west coast, and Paradip, Vishakhapatnam, Chennai and Tuticorin on the east coast (Figure 1.2.3). The local geopotential value at each of the eight tidal observatories was calculated as the average value of six estimates using the same tidal data (which are not available) and Mean Dynamic Topography (MDT) models but varying Global Geopotential Models (GGMs).

The difference between the chart datum and the MSS at these eight tidal observatories ranges from 0.62 m to 2.56 m for the tidal data used from 1976-1994. The average (of six) local geopotential value at these eight tidal observatories varied from $62636856.54 \text{ m}^2\text{s}^{-2}$ (at New Mangalore) to $62636861.80 \text{ m}^2\text{s}^{-2}$ (at Karwar) with the final average value (of all eight observatories) as $62636859.40 \text{ m}^2\text{s}^{-2}$, which is taken as the local geopotential value for IVD2009. Though differently but on similar lines of constraining the MSL at nine tidal observatories to zero in IVD1909, local geopotential value is now taken as the same at eight tidal observatories for IVD2009. Therefore, IVD2009 may also be prone to a north-south slope because the difference between the final geopotential value ($62636859.40 \text{ m}^2\text{s}^{-2}$) and its minimum ($62636856.54 \text{ m}^2\text{s}^{-2}$) and maximum ($62636861.80 \text{ m}^2\text{s}^{-2}$) values translates to a difference of approximately 0.29 m and -0.26 m, respectively. We cannot discuss the reasons for choosing average of the mean value for defining IVD2009 because it is not available in any publication.

The precise levelling net for IVD2009 is based on Helmert's orthometric height system that consists of 42 precise levelling lines (including eight lines between the TGBM and tidal observatories) covering a distance of 19450 linear km. The remarkable fact is that the distance of 19450 km was covered in a timeframe of three years, i.e., from 2006-2008. The levelling net was adjusted using 41 observations (one was not included as a

result of some unexplained trial and error exercises of adjustment) involving a total of 32 stations, including eight fixed TGBMs.

Not much information is available about IVD2009 in the public domain. However, in personal communication with Singh in (2021), it was concluded that IVD2009 had been defined with the best data available with SoI during that time (2017-2018), and IVD2009 also has a significant scope of improvement after further in-depth analysis. However, due to the non-availability of the data and details of the IVD2009 computation, it is difficult to further study the merits and limitations of the IVD2009.

When a redefined IVD was proposed, a long-term goal was also set to develop a precise national gravimetric geoid model to be adopted as the IVD, whenever available. Since then, officers and scientists from only either SoI or NGRI have made a few gravimetric geoid-related studies but are limited to local regions, e.g., southern India, central India, or western India. Only SoI and NGRI have put in the effort to develop regional gravimetric geoid because these two organisations are the keeper of the gravity data in India, which is deemed to be classified. Anyway, we will now discuss these regional geoid models in detail in the next section.

1.3 Previous Indian gravimetric geoid models

There have been only a few studies on gravimetric geoid modelling over India, which we have summarised in Table 1.3.1 followed by a discussion on the individual studies.

Table 1.3.1: Gravimetric geoid related studies in India

	Singh (2007)	Singh et al. (2007)	Carrion et al. (2009)	Srinivas et al. (2012)	Mishra and Ghosh (2016)	Mishra and Ghosh (2016)	Choudhary (2017)	Singh and Srivastava (2018)
Region	24° N - 29° N; 76° E - 82° E	28° N - 29° N; 76° E - 77.30° E	6° N - 14° N; 74.5° E - 80.5° E	12.5° N - 18.5° N; 75.5° E - 79.5° E	Dehradun #4 (30° 19' N, 75° 4' E)	Hyderabad #4 (17.5° N, 78.5° E)	India	20° N - 31° N, 71° E - 79° E
Software	GRAVSO FT	GRAVSO FT	GRAVSO FT	GRAVSO FT	GRAVSO FT	GRAVSO FT	NA	GRAVSO FT
Technique	FFT	FFT	Fast Collocation	LSC	LSC	LSC	NA	FFT
Type	Geoid	Geoid	Geoid	Geoid	Geoid	Geoid	Geoid	Geoid
Resolution	5'x5'	0.5 km x 0.5 km	2'x2'	NA	NA	NA	NA	15'x15'
Gravity data	SoI database	SoI database	NGRI database	NGRI database	SoI database	SoI database	SoI database	SoI database
GGM	EIGEN-GL04C	EGM96	NA	EGM2008	EGM2008	EGM2008	NA	GGM05C
0 degree	NA	NA	NA	NA	NA	NA	NA	NA
Integration radius	2	0.5	NA	NA	NA	NA	NA	NA
Kernel modification	Wong and Gore (1969)	Wong and Gore (1969)	None	None	None	None	NA	NA
Terrain treatment	TC ^{#1} and RTM	RTM ^{#2}	NA	RTM ^{#2}	RTM	RTM	NA	RTM
DEM/DSM	GLOBE 2'x2', 4'x4' and 6'x6'	Generated from 130 spot heights	NA	GTOPO30	1:50000 topo map derived	SRTM 3''x3''	NA	SRTM 30''x30''
Atmospheric correction	Constant 0.87 mGal	Yes	NA	NA	NA	NA	NA	NA
Ellipsoidal correction	NA	NA	NA	NA	NA	NA	NA	NA
No fit stats (min, max, mean, std) #0	-0.148; 0.304; 0.049; 0.089	-0.172, 0.189, -0.220, 0.083	NA	-0.360, 0.170, -0.020, 0.090	0.023, 0.266, 0.175, 0.190 ^{#5}	-0.130, 0.210, 0.070, 0.100 ^{#5}	NA	-0.346, 0.226, -0.005, 0.136
After fit stat (min, max, mean, std) #0	-0.102, 0.122, -0.001, 0.044	NA	-1.510, 1.080, 0.000, 0.220 ^{#3}	NA	NA	NA	NA	-0.064, 0.125, 0.039, 0.072

TC: Terrain Corrections

RTM: Residual Terrain Model

LSC: Least Squares Collocation

FFT: Fast Fourier Transform

DEM: Digital Elevation Model

DSM: Digital Surface Model

#0 Before and after fit statistical values (min, max, mean, STD) are given in m.

#1 In Singh (2007), planar TC have negative values that is impossible.

#2 In Singh et al. (2007), RTM is used synonymously with TC.

#3 In Carrion et al. (2009), validation is done with respect to EGM2008 derived geoid undulations.

#4 In Mishra and Ghosh (2016), only location is given in the article and not its extent.

#5 In Mishra and Ghosh (2016), root mean square error (RMSE) is provided instead of standard deviation.

Before discussing the Indian gravimetric geoid studies further, we mention two things:

- i) The free-air gravity anomalies in India, either in SoI or NGRI database, are the free-air gravity anomalies on the geoid.
- ii) If RTM is used in GRAVSOFTE, the resultant will be height anomalies for which free-air gravity anomalies are required on the Earth's topographical surface. Thereafter, GRAVSOFTE allows computation of a geoid-quasigeoid separation term to calculate the geoid undulations from height anomalies.

None of the literature from Table 1.3.1 have mentioned anything about both these aspects and have used free-air gravity anomalies on the geoid with RTM to compute geoid undulations. Though none have mentioned but to their *best* defence, we would say that a) free-air gravity anomaly on the geoid is *practically* equivalent to the free-air gravity anomaly at the Earth's topographical surface (*iff* it is assumed that the Earth's gravity gradient is equal to the normal gravity gradient, and normal height is equal to the orthometric height), and b) they have used the terms geoid-undulation and height anomaly synonymously. It should be noted that though free-air gravity anomalies at the Earth's topography and the geoid are practically equivalent, the differences can be significant in view of the cm-precise geoid, primarily, due to the mentioned assumptions. Despite considering the above discussed two points, there are certain questions that arise from the studies listed in Table 1.3.1, which are as follows:

- i) Singh (2007): The topography in the study area varies from 1 m to 6918 m. The authors have *assumed* that the atmospheric correction will not be significant and used a constant value of 0.87 mGal for the whole gravity data set, which is equal to the atmospheric correction at the sea level ($H = 0$ m; Moritz, 2000). This assumption cannot be justified at least when very simple formulations for

atmospheric correction are already available in the literature (Section 3.3). Also, it is not practically and conceptually possible to have negative planar TCs, yet the authors have achieved the same. The reported TCs vary from -3.38 mGal to 36.69 mGal with a mean and standard deviation of 0.598 mGal and 3.871 mGal, respectively. Their TC map also shows a large area with negative planar TCs.

- ii) Singh et al. (2007): The flowchart provided by the authors have shown the use of TC to compute geoid undulation. However, the formulas provided include the methodology involving RTM. They have shown in the flowchart that atmospheric correction is applied, but neither have they provided any formulation nor discussion. It becomes difficult to understand what methodology has been followed: the one shown in the flowchart or the one provided in the formulations, as these two are different. Also, the authors have prepared a DEM from spot heights, but no information is provided on the resolution or the gridding method. This information is very crucial for topographic corrections, either TC or RTM. Above all, the validation results seem intriguing because the mean value (0.220 m) is beyond the minimum (-0.172 m) and maximum (0.189 m) values. However, this might be a typographical error.
- iii) Carrion et al. (2009): We cannot comment anything on the methodology adopted because not much relevant information is provided in the article on the geoid computation.
- iv) Mishra and Ghosh (2016): It is really very hard to understand the data and methodology followed in their study.

Data used: The DEM for Dehradun region was developed using a 1:50,000 topographical map, while for Hyderabad, SRTM 3"x3" DSM is used. The authors

have not provided any rationale for this different choice of DEM in the two study areas. We can only speculate that they might have chosen to use the topographical map in and around Dehradun for the accuracy concerns of the height information because Dehradun is a relatively more undulating region than Hyderabad. However, no information is provided on either extent of the study area or the resolution of the developed DEM. Moreover, the provided coordinates of Dehradun are somewhere in the Punjab, which can only be a typographical error in longitude.

Methodology: Regarding the methodology, there are several *possibly-only-typographical* errors in the use of various GRAVSOFTE subroutines. However, the major concern is the explanation of the methodology. To provide a summary of the author's explanation: they have a set of free-air gravity anomalies that are being reduced to residual free-air anomalies by subtracting the corresponding GGM and RTM implied gravity anomaly, at the gravity data points. LSC is then used to predict the residual free-air gravity anomalies at the GNSS/levelling points to which the GGM and RTM implied gravity anomalies are restored to obtain the free-air gravity anomalies at the GNSS/levelling points. Thereafter, the geoid undulation (from GNSS/levelling data: ellipsoidal/geodetic height – normal orthometric height) and the free-air anomalies are given input in N2Zeta subroutine (of GRAVSOFTE) to obtain height anomaly and geoid-quasigeoid separation. As such, it is hard to understand what is being computed in the study. Moreover, Bouguer anomaly (and not free-air anomaly) is required to be given as input in the N2ZETA subroutine that is used to compute geoid-quasigeoid separation term.

Results: The authors talked about converting the gravity anomaly components (residual, GGM and RTM gravity anomalies) at each of the

GNSS/levelling data stations to the corresponding three height anomaly components and three geoid-quasigeoid separation terms (each for residual, GGM and RTM gravity anomalies). The corresponding terms height anomaly and geoid-quasigeoid separation terms are added to calculate final geoid undulation. However, in practice, height anomaly components are added together to calculate the height anomaly to which geoid-quasigeoid separation term calculated using the Bouguer anomalies is added for obtaining the final geoid undulations.

- v) Choudhary (2017): This is based on news coverage of the INDGEOID version 1.0 (<https://www.geospatialworld.net/videos/survey-india-launches-geoid-model-country/>) announced by the Surveyor General of India in 2017. SoI claimed to have developed INDGEOID version 1.0 as the first national gravimetric geoid model for the whole of India. However, neither the model nor any scientific article has ever been available in the public domain to verify this. Therefore, we cannot comment on the merits or limitations of the methodology adopted.
- vi) Singh and Srivastava (2018): Much relevant information pertaining to geoid modelling is missing from this article. Therefore, we cannot comment on the methodology. However, the choice of 15'x15' resolution needs a strong justification because though geoid is a smooth surface but is not smooth enough that it does not change in an area of $\sim 625 \text{ km}^2$. In fact, focal statistics tool in ArcGIS, with our calculated Indian geoid model, shows that there are certain regions in which the geoid undulation can vary up to as large as 12 m in an area of $\sim 625 \text{ km}^2$. Moreover, with the availability of high-resolution DEM, the use of SRTM 30"x30" is in contrast to the fact that high-resolution topographical representation is a must for precise computation of topographical effects.

1.4 Research gaps

The following are some key points from the discussion of the previous gravimetric geoid-related studies in India:

- i) All the studies of geoid modelling in India have been done in local areas and only using GRAVSOFTE software with RTM (including INDGEOID ver1, as per personal communication with an official at G&RB, SoI in (2018)). GRAVSOFTE, as it is available, has a limitation of handling large matrices involved in calculating RTM or matrix inversion in GEOCOL. This is a possible reason of using a coarse dataset in regional geoid-modelling studies in India.
- ii) Despite all the studies in India with GRAVSOFTE, there is no single study that reports the complete framework of the development of the gravimetric geoid model for India and its validation.
- iii) Though it has been accepted that a precise high-resolution DEM should be used for topographic effects, this has never been practiced in any geoid modelling study over India, even with the availability of freely available high-resolution global DEMs.
- iv) There is an inconsistency in reporting the methodologies and results that obstruct a fair and objective comparison of different geoid-related studies. The used data or the developed product are also never provided.
- v) India has a varying topographical landform that makes it one of the most challenging and best study areas to check the suitability of different existing algorithms or to analyse the scope of new algorithms in geoid modelling. Yet, no study has covered several landforms in one geoid calculation and discussed the results in connection with varying topography.

- vi) A gravimetric geoid model for the whole of India has remained elusive.

The research gaps identified above seem to be India specific. However, as we move forward in the thesis one may note that several other research gaps of global significance have also been addressed in this study.

1.5 Objectives

Based on the literature review and identified research gaps, we have set the following three objectives for this thesis:

- i) *Develop a gravimetric geoid model for India using all the available gravity and terrain data.*

The first high-resolution gravimetric geoid model will be calculated for the mainland India using three different approaches, which have never been applied over India in any of the regions, namely, the CUT, the KTH and the UNB methods (Chapter 5). Inconsistencies, if any, in the reported literature of the three methods (CUT, UNB and KTH) will be dealt in detail to avoid the same in future (Chapters 3 and 4). Discussions on various aspects involved in calculating the gravimetric geoid will be provided, keeping in mind the decades-long quest of geodesists for a cm-precise geoid (Chapter 3) (Sansò and Rummel, 1997; Foroughi et al., 2019).

GEOCOL with RTM method will also be used for geoid calculation but not for the whole of mainland India due to the method's limitation of large matrix inversion. Regional geoid models developed using GEOCOL will only be used for comparison and validation because one of the main motives of this study is to explore new methodologies over India that have never been tested.

- ii) *Analyse the use of high-resolution DEM in determining terrain effects.*

The major reasons for either not using or circumventing the use of high-resolution DEM for terrain effects are i) use of high-resolution DEM causes a significant increase in the computation time, e.g., it may take years for the computation of precise planar TC for India using one-arc second DEM even with a supercomputer and ii) high-resolution DEMs provide a better representation of the topography with comparatively detailed information of the undulations, therefore, certain algorithms may not provide a numerically convergent solution for terrain effects, e.g., FFT method of planar TC computation which are limited to the regions having gradients less than 45° . However, terrain effects are one of the important computations in precise geoid development, and that is only possible with the use of high-resolution DEM. So, an efficient algorithm will be developed for the fast computation of precise TC using the high-resolution DEM (Chapter 3).

- iii) *Evaluate and validate the developed gravimetric geoid and quasigeoid models.*

The reference surface for Helmert's orthometric heights is the geoid, while no unique reference surface (either geoid or quasigeoid) is specified for normal-orthometric heights. We have been provided with 119 GNSS/levelling datapoints, clustered in four regions of India, without any information on the height system. Therefore, with an assumption that the levelling heights are based on IVD1909 and normal-orthometric height system, we will validate (absolute and relative testing) our GNSS/levelling data with both geoid and quasigeoid for all the combinations of parameter sweeps in all the three methods (CUT, KTH and UNB) before and after 4-parameter fitting (Chapter 5). We will also validate Pizetti's geoid gradients with Helmert's vertical deflections noting that the curvature of the plumbline is neglected. The vertical deflections consist of 700 meridional components and 279

prime vertical components over most of India in contrast to only 119 GNSS/levelling points clustered in four regions.

We will also calculate the geoid model of four regions (Uttar Pradesh West, Uttar Pradesh East, Hyderabad and Bangalore) using GEOCOL with RTM because a few of the previous studies in India have used this approach. Since no detail work is done with GEOCOL, these geoid models have been used only for comparison with the i) geoid models developed using the other three approaches and ii) previously developed geoid models in and around these four regions. Moreover, we will also perform an inter-comparison of i) national geoid models computed using the three methods and ii) regional geoid models calculated using the four methods. It is to analyse the differences between the four methodologies in the final product (Chapter 5). The inter-comparison of geoid models will be an important analysis from the viewpoint of the quest of cm-precise geoid.

1.6 Significance of the study

A precise gravimetric geoid model is fundamental to both infrastructure developments as well as for geoscientific activities in India. The studies on gravimetric geoid for India either are not published, or those published have not provided the data and/or all the necessary computational details that restricts the repeatability of their research. Moreover, to date, no gravimetric geoid model for India is available in the public domain. Therefore, this study will be the first to provide a national gravimetric geoid model and also a strong conceptual framework using three different geoid modelling approaches (which have never been used in any part of India) that can be used by the competent authorities to develop an official geoid model using the classified gravity data.

The comparison of different geoid solutions will help in understanding any similarities or dissimilarities among different methods of geoid computation. An in-depth discussion (merits, limitations, inconsistencies) of the three methods (CUT, UNB and KTH) from the viewpoint of cm-precise geoid is provided that shall be of use to any geoid-modeller interested in developing a precise gravimetric geoid or quasigeoid model.

The IVD2009 based physically meaningful (Helmert's) orthometric heights (H), referred to the geoid, are connected with the geodetic heights obtained from GNSS positioning and referred to an ellipsoid, via the geoid undulation (Eq.(1.2.1)). An immediate consequence of this is the conversion of elevation models (e.g., national CartoDEM (NRSA, 2006)) and height observations in geodetic heights to orthometric heights effortlessly. A freely available geoid model will allow surveyors to efficiently measure physical heights with GNSS positioning by replacing the costly and laborious differential levelling (while keeping an account of accuracy required).

Recently, Indian Railways, Public Works Department and National High Speed Rail Corporation Limited have suggested using a geoid model for their infrastructural projects/developments. However, since no Indian gravimetric geoid model is available, all have mentioned using EGM2008. Therefore, all concerned organisations can now make use of our developed Indian gravimetric geoid model instead of EGM2008 or any other GGM.

Since the geoid is a physically meaningful surface, it responds to changes in the gravity field due to various geophysical and geodynamical phenomena, in turn allowing us to study them as well (e.g., Vaníček and Christou, 1993). Therefore, while benefiting a number of stakeholders: SoI, Geological Survey of India (GSI), Oil and Natural Gas Corporation (ONGC), Indian Oil Corporation Limited (IOCL), NGRI, National Disaster Management Authority (NDMA), Indian National Centre for Ocean Information Services

(INCOIS), Coal India Limited (CIL), the national gravimetric geoid model (and its intermediate results, e.g., TC) will also be invigorating sciences like geomorphometry (Coblentz et al., 2011), hydrography (Robin et al., 2016), oceanography (Ophaug et al., 2015), among many other applications (Vaníček and Christou, 1993).

1.7 Structure of the Thesis

The thesis is divided into six chapters. Chapter one provides an introduction to the previous geoid-related studies in India and their limitations. Thereafter, setting up the objectives and discussing the significance of the present thesis work.

Chapter two describes the dataset available to us: gravity, GNSS/levelling, deflections of the vertical, DEMs and GGMs.

Chapter three discusses various corrections required in gravimetric geoid or quasigeoid modelling. The corrections that are discussed are: free-air gravity correction, topographic correction, atmospheric correction, ellipsoidal correction, downward continuation, and zero-degree term and tidal corrections. Free-air gravity correction, and zero-degree and tidal corrections are described in general to any method of geoid or quasigeoid computation, while the other four are discussed as are applied in the three methods individually, i.e., the CUT, the UNB, and the KTH methods.

We have identified some inconsistencies in the formulas and tried to re-derive and resolve them. A new method of planar terrain corrections is also provided, along with a few new formulas for working in different solid Earth permanent tide systems, i.e., tide-free, zero-tide and mean-tide. With the derived algorithms and formulas, we have also provided the values of various parameters of two existing ellipsoids (WGS84 and GRS80) and a new ellipsoid (not official, but based on IHRS parameters (Poutanen and Rózsa, 2020)) in the three permanent tide-systems.

Chapter four is about the geoid and quasigeoid computation. The three methods of geoid and quasigeoid computation are discussed along with geoid-quasigeoid separation term. It should be noted that though we have used the names, the CUT, the UNB and the KTH methods, but we have not applied any method exactly in the same way as applied by the institutes who developed the methodologies. A discussion on the modifications and limitations of the methods applied as compared to the original methods is provided wherever found necessary.

In chapter five, the results of external validation with respect to GNSS/levelling dataset and deflections of the vertical are provided. Since a few previous geoid-related studies in India have utilised GEOCOL with RTM, we have also calculated geoid model of the four regions for a comparison with Indian geoid models calculated using the three methods (CUT, UNB and KTH). Further, an inter-geoid comparison of the Indian and regional geoid models is also provided.

Chapter six lists the conclusions and recommendations.

Chapter 2: Datasets

2.0 Introduction

Gravimetric geoid determination, irrespective of the methodology followed, involves three datasets, viz., gravity anomalies, Digital Elevation Model (DEM) and Global Geopotential Model (GGM). Additionally, either or both of Global Navigation Satellite System (GNSS)/levelling and deflections of vertical data are used for the validation study. Some researchers also use density models in geoid computation but is not considered in the present study because they are not available to us. Like any other study, precise datasets are favourable for precise determination of the geoid. Though all the geoid computation literature involves a brief discussion on the used datasets, many researchers have discussed the characteristics and subtleties of the datasets for their study areas, e.g., Lagios et al. (1996; Greece), Featherstone et al. (1997; Australia), Duquenne (2006; France), Borghi et al. (2007; Italy), McCubbine et al. (2017b; New Zealand) and Abd-Elmotaal et al. (2018; Africa).

In this chapter, we will discuss the availability, characteristics and hence, our choice of the datasets for the geoid modelling study over India.

2.1 [Lack of] Freely available gravity data

Gravity data are primarily used in the 1) evaluation of the GGMs (Section 2.4), 2) Stokes's integration to compute the residual geoid/quasigeoid or approximate quasigeoid (Section 4.2), and 3) computation of geoid-quasigeoid separation term (Section 4.3). Before discussing the availability of gravity data for the present study, we will briefly discuss gravimetry in India as understood from Gulatee (1948), Sundaram et al. (2009) and Tiwari et al. (2014).

Several organisations have conducted terrestrial gravity surveys over different parts of India. The gravity data comprise latitude, longitude, observed gravity, and physical height (based on the national height system). The Survey of India (SoI) began absolute gravity measurements in 1865 using brass pendulums. Five hundred and sixty-four pendulum measurements were acquired throughout the country in two separate phases, i.e., 1902-1925 and 1926-1939. After the second world war, the gravity surveys were continued for further densification using Frost and Worden gravimeters. A gravity map of India was produced at a scale of 1:12,000,000 in 1956 (Gulatee, 1956). This gravity map was drawn with a contour interval of 20 mGal using the data from around 3000 stations.

The gravity base-station for the Indian National Gravity Datum 1963 (INGD63) is situated at Dehradun. The absolute gravity value of this base station in INGD63 is 978064.0 mGal, and 978049.09 mGal based on the International Gravity Standardization Net 1971 (IGSN71; Morelli et al., 1972). Hence, a correction of ~ 14.9 mGal (which originates from an error at Potsdam, e.g., Dryden, 1942) is generally applied to data observed in the INGD63 to obtain the corresponding value in International Gravity Standardization Net 1971 (IGSN71).

During the late-1950s to the mid-1970s, other organisations, such as the Geological Survey of India (GSI) collected gravity data. The old and new data were compiled and transformed to a common datum (INGD63) to prepare the gravity map of India with a 10 mGal contour interval (GMSI, 1975). It should be noted that there is no information available on how the different data were transformed to the same datum. This map was published in 1975 at a scale of 1:5,000,000 (GMSI, 1975).

Later, due to the requirement of updated, precise gravity data, it was decided to revise the gravity map of India using the data collected by SoI, GSI, National Geophysical Research Institute (NGRI), Oil and Natural Gas Corporation (ONGC), and Oil India

Limited (OIL) under various projects. A total of 143,786 gravity data points were observed by these organisations, which were archived at GSI, Hyderabad. However, only 51,356 data points were selected to maintain a uniform coverage over the entire India. These points were re-processed to refer to IGSN71, but the reprocessing steps are not available in the literature. The final output was a revised gravity map series of India (GMSI) 2006 that comprises five sets of gravity anomaly maps, including a free-air anomaly map and Bouguer anomaly map, both at 1:2,000,000 scale (GSI-NGRI, 2006). These are the latest gravity maps computed/compiled for India.

However, pointwise observed gravity data is confidential in India. Therefore, with this predicament, we obtained a grid of Indian terrestrial gravity data from GETECH (<https://getech.com/>) that is claimed to come from the GMSI. The GETECH gravity data comprise a $0.02^\circ \times 0.02^\circ$ grid of simple Bouguer gravity anomalies over all of India (except a few regions in Jammu and Kashmir, Arunachal Pradesh, and the whole of Andaman and Nicobar and Lakshadweep) with an overall estimated precision of ± 1.5 mGal (GETECH, 2006). According to the GETECH manual for Indian gravity data, they used i) the normal gravity formula from WGS84 (NIMA, 2000),

$$\gamma_{0_WGS84} = 978032.67714 \left[\frac{1 + 0.00193185438639 \sin^2 \varphi}{\sqrt{1 - 0.00669437999013 \sin^2 \varphi}} \right] \text{mGal} \quad (2.1.1)$$

ii) a second-order free-air correction given by

$$\delta g_{FAC}^{GETECH} = (0.3083293357 + 0.0004397732 \cos^2 \varphi) h - 7.2125 \times 10^{-8} h^2 \quad (2.1.2)$$

iii) the following atmospheric correction (Ecker and Mittermayer, 1969)

$$\delta g_{atm}^{GETECH} = \begin{cases} 0.87 e^{-0.116H^{1.047}} \text{ mGal}, & H > 0 \text{ km} \\ 0.87 \text{ mGal} & , H \leq 0 \text{ km} \end{cases} \quad (2.1.3)$$

and iv) the simple planar Bouguer correction

$$\delta g_{BC}^{GETECH} = -0.04191\rho H \text{ mGal} \approx -0.1119H \text{ mGal} \quad (2.1.4)$$

where γ_{0_WGS84} is normal gravity on the WGS84 ellipsoid, δg_{FAC}^{GETECH} is the free-air correction, φ is the geodetic latitude, h is the ellipsoidal height (in m), H is the elevation (in km for Eq. (2.1.3) and in m for Eq. (2.1.4)), δg_{atm}^{GETECH} is the atmospheric correction, δg_{BC}^{GETECH} is the Bouguer correction and ρ is the constant topographical density of 2670 kgm^{-3} . We recomputed the free-air gravity anomalies (Δg) from the GETECH data using

$$\Delta g = \left. \begin{aligned} &\Delta g_{SBA}^{GETECH} + 0.1119H + \gamma_{0_WGS84} - \delta g_{FAC}^{GETECH} \\ & - \delta g_{atm}^{GETECH} - \gamma_{0_GRS80} + \delta g_{FAC}^{CUT} + \delta g_{atm}^{CUT} \end{aligned} \right\} \quad (2.1.5)$$

where from Heiskanen and Moritz (1967, pg. 78), we have

$$\delta g_{FAC}^{CUT} = \gamma_{0_GRS80} \left(\frac{2}{a} (1 + f + m - 2f \sin^2 \varphi) H - \frac{3}{a^2} H^2 \right) \quad (2.1.6)$$

$$\gamma_{0_GRS80} = \gamma_a \left(\frac{1 + k \sin^2 \varphi}{\sqrt{1 - e^2 \sin^2 \varphi}} \right) \quad (2.1.7)$$

$$\delta g_{atm}^{CUT} = \left. \begin{aligned} &0.871 - 1.0298 \times 10^{-4} H + 5.3105 \times 10^{-9} H^2 - 2.1642 \times 10^{-13} H^3 + \\ &9.5246 \times 10^{-18} H^4 - 2.2411 \times 10^{-22} H^5 \end{aligned} \right\} \quad (2.1.8)$$

For GRS80, $a = 6378137 \text{ m}$, $e^2 = 0.0066943800229$, $m = 0.0034478600308$, $f = 1/298.257222101$, $\gamma_a = 978032.67715 \text{ mGal}$ and $k = 0.001931851353$ (Moritz, 2000).

The descriptive statistics of the differences between the free-air anomalies from the GETECH data and recomputed free-air anomalies (that are mostly due to the different free air correction) are (in mGal): min = -0.001, max = 0.188, mean = 0.002, STD = ± 0.007 . It should be noted that we have used H instead of h in Eq. (2.1.2) because we believe that there might be a typographical error in the GETECH manual. The reason

being that the use of h would have provided gravity disturbances and not gravity anomalies (Hackney and Featherstone, 2003). A blanket accuracy estimate of the reconstructed free-air anomalies from the GETECH Bouguer anomalies is ± 2.4 mGal, calculated using the DEM error in the CUT reconstruction technique (Featherstone and Kirby, 2000) as per $\sigma_{FAA} = \sqrt{(1.5 \times 10^{-5})^2 + (2\pi G \rho \times 17.3)^2}$ (17.3 m is the accuracy estimate of DEM used, Section 2.5).

The atmospheric correction (Eq. (2.1.8)) was removed from the recomputed gravity anomalies because i) the GETECH data was required to be merged with other datasets, and ii) the UNB and the KTH methods have different strategies of applying the atmospheric correction (Sections 3.3.2 and 3.3.3, respectively).

We do not have gravity data from the countries neighbouring India and a well distributed sufficient data coverage is not available in the Bureau Gravimetric International (<https://bgi.obs-mip.fr/>) archives either (Country: no. of gravity data points - Pakistan: 1270, Bangladesh: 25, Sri Lanka: 48, Myanmar: 71, Afghanistan: 1649, China: 446, Nepal: 617 and Bhutan: 0). Therefore, we constructed a $0.02^\circ \times 0.02^\circ$ grid of free-air anomalies over land using EGM2008 (Pavlis et al., 2012; 2013) up to degree-order (d/o) 900 to fill-in the land gravity anomaly data in and around India where the GETECH data is not available, including Nepal, China, Pakistan, Sri Lanka, Bangladesh, Bhutan, Afghanistan, and Myanmar. The specific d/o 900 was chosen because EGM2008 uses proprietary data up to d/o 900 (Pavlis et al., 2013).

One may argue that filling-in the data using d/o 900 may provide a wrong sign in residual gravity anomalies which are computed by subtracting GGM synthesised gravity anomalies from the observed gravity anomalies. The reason being that the observed gravity anomalies contain the whole spectrum from 0 to infinity and we are using only d/o up to

900 to infill the data. Therefore, on subtracting, for the CUT method (Section 4.2.1) that uses the highest d/o GGM, gravity anomalies synthesised using d/o 2159 from i) observed gravity anomalies and ii) infill (d/o 900) gravity anomalies, sign for the two set of residual anomalies should be different.

However, we would argue that in EGM2008, proprietary gravity data has only been used up to d/o 900 (Pavlis et al., 2013) and RTM induced gravity anomalies from d/o 901 to 2159. For the CUT method (which makes use of Faye and residual Faye anomalies), we used EGM2008 d/o 900 (fill-in) and mean planar TCs on $0.02^\circ \times 0.02^\circ$ grid. Therefore, we think that subtracting EGM2008 (d/o 900) and RTM (d/o 901 to 2159) from EGM2008 (d/o 900) and TC should give same sign as subtracting EGM2008 (d/o 900) and RTM (d/o 901 to 2159) from observed gravity anomalies and TC. It should be noted that sign confusion does not arise in the use of our in-fill data with the UNB (Section 4.2.2) and the KTH (Section 4.2.3) methods because both of these use satellite-only GGMs, which has the highest d/o significantly lesser than 900.

We tested the above arguments over i) Auvergne and ii) a $5^\circ \times 5^\circ$ region in India for both of which we have the terrestrial gravity data. A comparison was made between Faye anomalies involving terrestrial gravity data and Faye anomalies involving fill-in data (EGM2008 d/o 900). Residual Faye anomalies were constructed by subtracting EGM2008 d/o 2190 free-air gravity anomalies. The results show that for both the study areas, more than 51% of the total points in the two sets of residual Faye anomalies have same sign (either positive or negative). We acknowledge that 51% is not a significant number to trust our fill-in methodology globally. However, for the present study, we work with this fill-in methodology that can be seen as one of the limitations.

Therefore, we suggest that a quantification of the errors involved due to the non-availability of data in the surrounding regions of the study area and measures to circumvent

the same (e.g., using some d/o GGM derived gravity anomalies or setting the gravity anomalies in those regions equal to zero (Featherstone et al., 2018)) should be done in future.

For the oceanic regions surrounding India, we used free-air gravity anomalies from the Scripps Institute of Oceanography, version 28.1 (Scripps v28.1, https://topex.ucsd.edu/marine_grav/mar_grav.html), which has an overall root mean square error of ± 1.23 mGal (Sandwell et al., 2021). The Scripps data is also accompanied with an error grid that we have shown for our study area in Figure 2.1.1. The data contains a 1'x1' grid that also covers the land, but we used the Scripps data only for the oceanic region because the land data, in the Scripps dataset, is from EGM2008 to avoid Gibbs fringing at the coasts. We acknowledge that there exist other versions of Scripps data along with marine gravity data from DTU, but due to the non-availability of any ship-borne gravity data for validation, we chose to work with Scripps v28.1. Figure 2.1.2 shows the regions for the three gravity anomaly datasets.

The gridding techniques for the gravity anomalies are not discussed because we already have gridded data for the present thesis work. However, it is acknowledged that gridding of the gravity anomalies is one of the most important steps in the computation of the geoid (Goos et al., 2003; Winefield, 2016; Claessens and Filmer, 2020). Since the data is generally collected along the roads and the streets (the highway effect; Colombo, 1991), gridding becomes more crucial for plateaus and the mountainous regions with rapidly undulating terrain where data is collected very sparsely. Both these landforms are present in India. Therefore, this aspect should be studied, but it will only be possible when the distributed gravity data will be available rather than already gridded data. The gridding techniques may possibly be analysed using synthetic models (Featherstone, 2002; Ågren,

2004; Kuhn and Featherstone, 2005; Vaníček et al., 2013) to have preliminary intuitive conclusions, but this is not done in the present study.

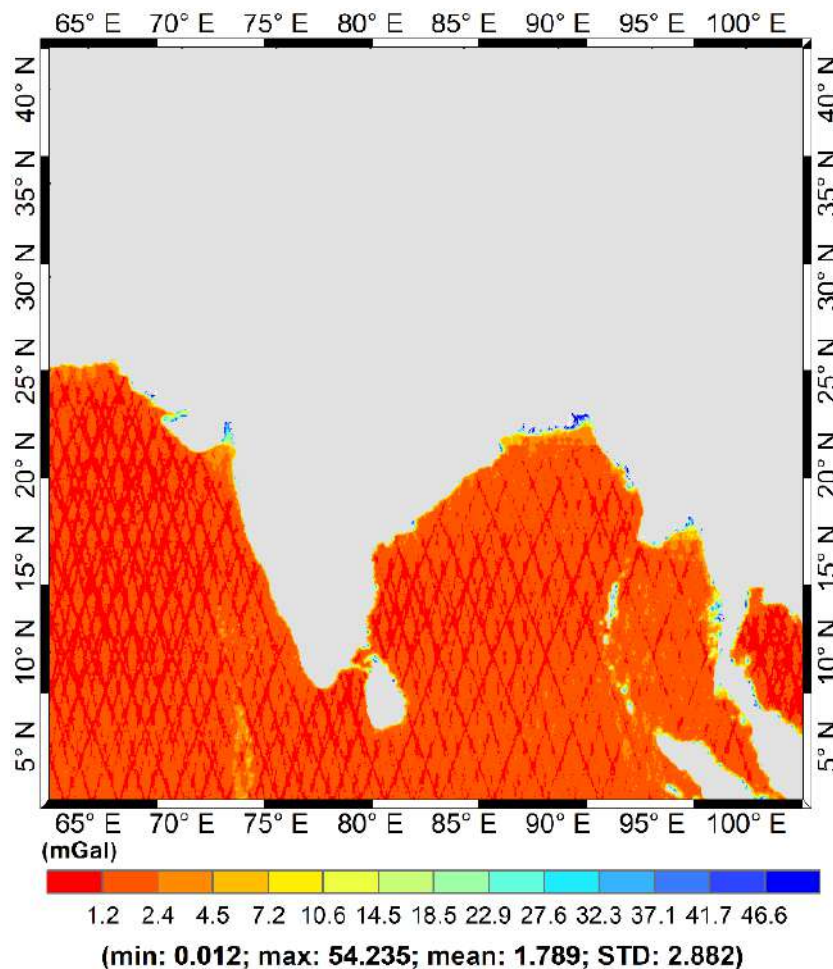


Figure 2.1.1: Error map of the Scripps v28.1 marine gravity-anomaly data (units in mGal).

For the present study, we need to merge the three available datasets to get a uniform gravity anomaly grid of $0.02^\circ \times 0.02^\circ$ interval, avoiding the Gibbs fringing of land data (both GETECH and EGM2008 individually) with the marine data.

Several sophisticated space-domain and frequency-domain methods are available for merging heterogeneous gravity anomaly datasets (e.g., Strykowski and Forsberg, 1998; Kern et al., 2003; Catalao, 2006; Olesen et al., 2002; McCubbine et al., 2018). However, we chose to work with a comparatively simpler space-domain method following Featherstone et al. (2011; 2018). The choice of this method is arbitrary because we are

working with the land gravity of unknown quality, and the strategy that we use has already been implemented in the computation of the Australian quasigeoid, which is an island nation and approximately 2.3 times larger than India. Other methods should also be tested, but it is left for the time when sufficient marine and airborne gravity data along with reliable terrestrial gravity data will be available over India.

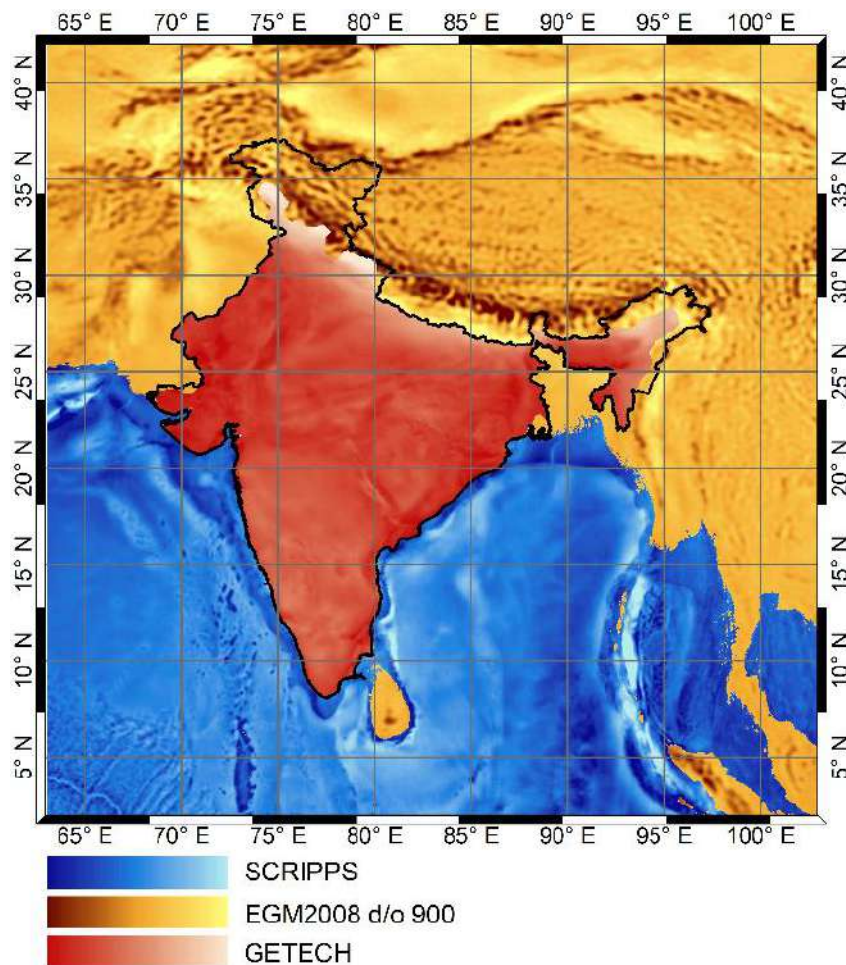


Figure 2.1.2: Regions for the terrestrial (GETECH and EGM2008 derived) and marine gravity anomalies.

In the adopted method, first, we overlaid the GETECH free-air anomaly grid over the EGM2008 (d/o 900) derived gravity anomalies. The gravity anomalies of the latter dataset at the overlapping grid nodes were replaced by the gravity anomalies from the former dataset. As a result, a $0.02^\circ \times 0.02^\circ$ grid of gravity anomalies on land are obtained.

To concatenate the land and marine gravity anomaly data, we clipped the 1'×1' gravity anomalies in the ocean from the complete Scripps dataset, i.e., on both ocean and land, using the GMT high-resolution shoreline (Wessel and Smith, 1996). It is then block averaged to the required 0.02°×0.02° grid that was overlaid with the land gravity anomaly grid. The former values were replaced by the latter at overlapping nodes to obtain the 0.02°×0.02° grid of the merged gravity anomalies.

Figure 2.1.3 shows the merged free-air gravity anomalies at 0.02°×0.02° grid. A scatter plot of gravity anomalies with respect to the topographical heights and a histogram of the gravity anomalies are shown in Figures 2.1.4a and 2.1.4b, respectively. To check for any discontinuities at the edges of the merged datasets, we computed and plotted the arctangent (Figure 2.1.4a) and logarithmic (Figure 2.1.4b) values of the gradients of the merged data. We observe no clear visual indication of any discontinuities at the boundaries of the merged data, but also partially due to the ruggedness of the dataset in our study area that can be obscuring. This grid is used for geoid/quasigeoid computation over India.

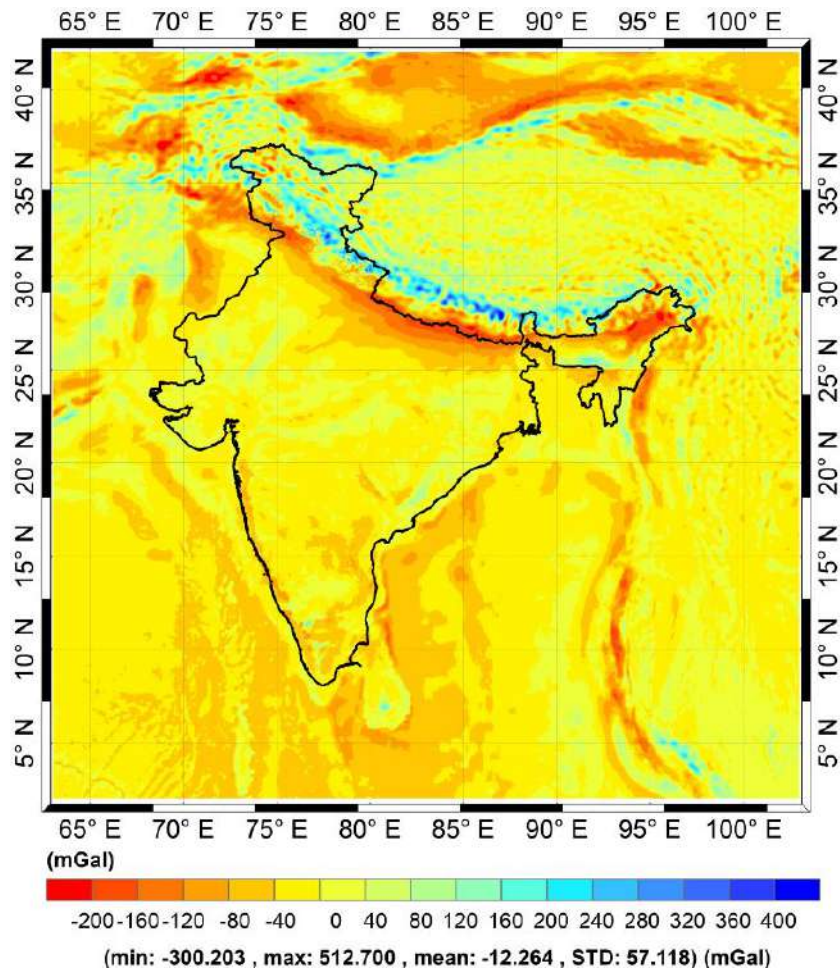


Figure 2.1.3: Merged gravity anomaly data from GETECH, EGM2008 (d/o 900), and Scripps v28.1 data.

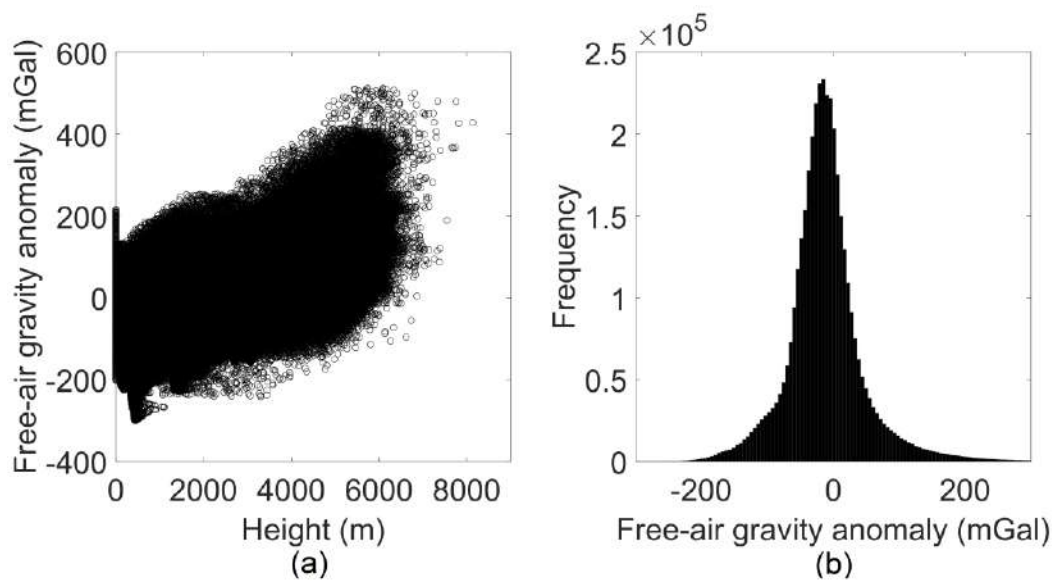


Figure 2.1.4: a) Scatter plot of merged gravity anomalies and heights (linear regression fit: $y = 0.016x - 30.824$); b) Histogram of the merged gravity anomalies.

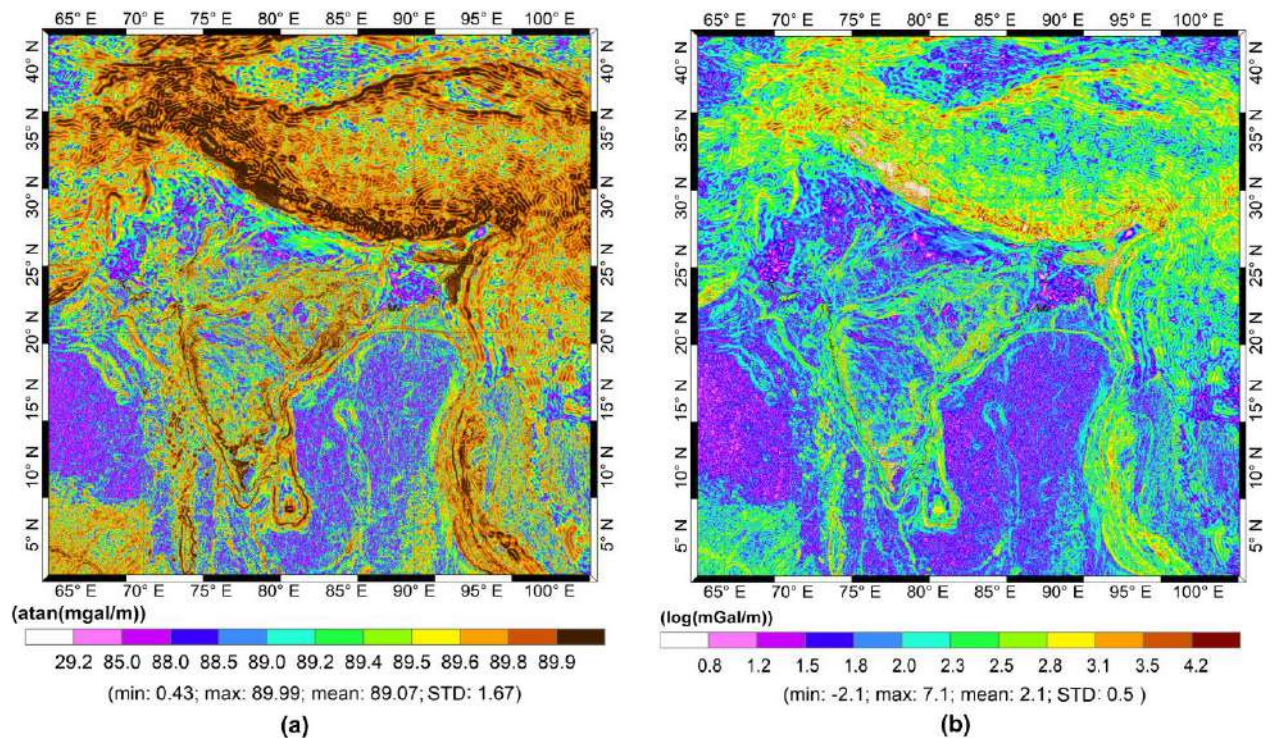


Figure 2.1.5: Arctangent (a) and logarithmic (b) plot of gradients of merged gravity anomaly data to attempt to identify discontinuities at the edges of the merged grids.

Without any atmospheric corrections, the free-air gravity anomaly in the study area varies from -300 mGal to +513 mGal, with majority of the values being in the range [-200 mGal, 200 mGal] (Figure 2.1.4b). This is the extreme range reported in the literature on geoid computation to our best knowledge, except for GGMplus (Hirt et al., 2013). The extreme positive is in the Himalayan belt in Nepal, near Mount Everest, while the extreme negative value is in the Himalayan belt in Afghanistan. From Figure 2.1.3, the free-air anomaly over mainland India varies from a minimum of -242 mGal to a maximum of +486 mGal with a mean -12 mGal and a standard deviation of ± 61 mGal. There are some unexpected rough patches of free-air anomaly observed in Figure 2.1.3 in a near-diagonal zone (parts of Uttarakhand, Himachal Pradesh and Jammu and Kashmir) of a region bounded within 29°N - 35°N latitude and 74°E - 85°E longitude. These are from the GETECH gravity dataset. For a clearer visualisation of this region, please see Figure 3.5.1

later, where we have computed the vertical gravity gradient. Though these rough patches can be due to the presence of mountainous terrain in those areas, smooth variation of free-air gravity anomaly is observed in other mountainous topographical landforms of India.

Figures 2.1.3 and 2.1.4a show that there exists some positive and negative pattern of the free-air anomalies in and around India, e.g., when moving from the Himalayas to the Gangetic Plains, parts of the Eastern Ghats ($15^{\circ}\text{N} - 20^{\circ}\text{N}$ and $80^{\circ}\text{E} - 85^{\circ}\text{E}$) and Western Ghats ($8^{\circ}\text{N} - 12^{\circ}\text{N}$ and $75^{\circ}\text{E} - 79^{\circ}\text{E}$), oceanic ridges. Geophysicists have previously studied the positive and negative patterns of the free-air anomalies over India and attributed the reason primarily to the crustal mass inequalities, i.e., isostatic compensation/under-compensation rather than any geological features (e.g., Takin, 1966; Mathur, 1969; Qureshy, 1971; Subrahmanyam and Verma, 1980; Verma, 1985; Basavaiah et al., 1991). It can be further studied in the future with the updated data.

2.2 GNSS/Levelling

GNSS/levelling data comprises points with latitude, longitude, geodetic height, and physical height (based on a national height system from differential levelling). These are required for i) the evaluation of GGMs (Section 2.4), ii) calculating hybrid geoid/quasigeoid (Section 4.4), and iii) absolute and relative validation of the computed gravimetric and hybrid geoid/quasigeoid models (Chapter 5).

A total of only 119 GNSS/levelling data points are available for the present study, again due to reasons of data restrictions. The distribution of the data points is shown in Figure 2.2.1. These data points are clustered in four regions, viz., Uttar Pradesh West (UPW), Uttar Pradesh East (UPE), Hyderabad, and Bangalore. The data in UPW (29 points) and UPE (27 points) were procured from the SoI, while the data in Hyderabad (56 points) and Bangalore (7 points) have been retrieved from Mishra (2018), who also used the SoI dataset.

No error estimates were provided by SoI for the procured GNSS/levelling data. However, Mishra (2018) mentioned that the horizontal and vertical precisions of GNSS data are within ± 12 to ± 26 mm and ± 31 to ± 53 mm, respectively. The vertical precision of the levelled heights is unknown to us, but they are from the high precision levelling net of India.

We have not been provided a clear indication on the type of physical heights, and therefore, due to this anonymity of the height system, we consider the levelling heights to be based on IVD1909 and thus, in the normal-orthometric height system (Section 1.2). Hence, we chose to validate both geoid and quasigeoid models with the available GNSS/levelling dataset to test the representativeness of the Indian heights with respect to the two surfaces. Please note that we use only the terms ‘geoid undulation’ and ‘orthometric height’ for discussing the GNSS/levelling dataset for brevity.

In India, physical heights vary from -2 m to +8586 m, and geoid undulations vary from approximately -100 m to -18 m. We acknowledge that the evaluation and validation with 119 data points can never provide a reliable estimate for the whole of India, especially when there are a variety of topographical landforms (Figure 1.2.2). Since we have no other choice but to work with the available dataset, the aforementioned evaluations and validations were done for India with 119 data points and for the four regions individually with their corresponding number of data points. The numerical description of the dataset is given in Table 2.2.1.

Table 2.2.1: Description of the available 119 GNSS/levelling data points.

		India	UPW	UPE	Hyderabad	Bangalore
h (m)	Min	-11.64	76.37	-11.64	280.67	741.48
	Max	1006.11	1006.11	371.54	430.62	826.65
	Mean	341.66	191.82	50.51	355.57	792.19
H (m)	Min	54.70	140.18	54.7	358.05	827.31
	Max	1050.74	1050.74	429.73	506.50	911.87
	Mean	272.14	248.11	114.97	432.39	877.78
$N_{GNSS/lev}$ (m)	Min	-85.86	-63.81	-68.68	-77.85	-85.85
	Max	-44.63	-44.63	-58.19	-75.84	-85.22
	Mean	-69.53	-56.29	-64.45	-76.82	-85.59
Baseline length (km)	Min	0.61	11.94	20.45	0.61	4.80
	Max	1937.37	533.88	384.32	46.75	25.16
	Mean	713.46	197.28	169.33	18.67	14.08
Datapoints	No.	119	29	27	56	7

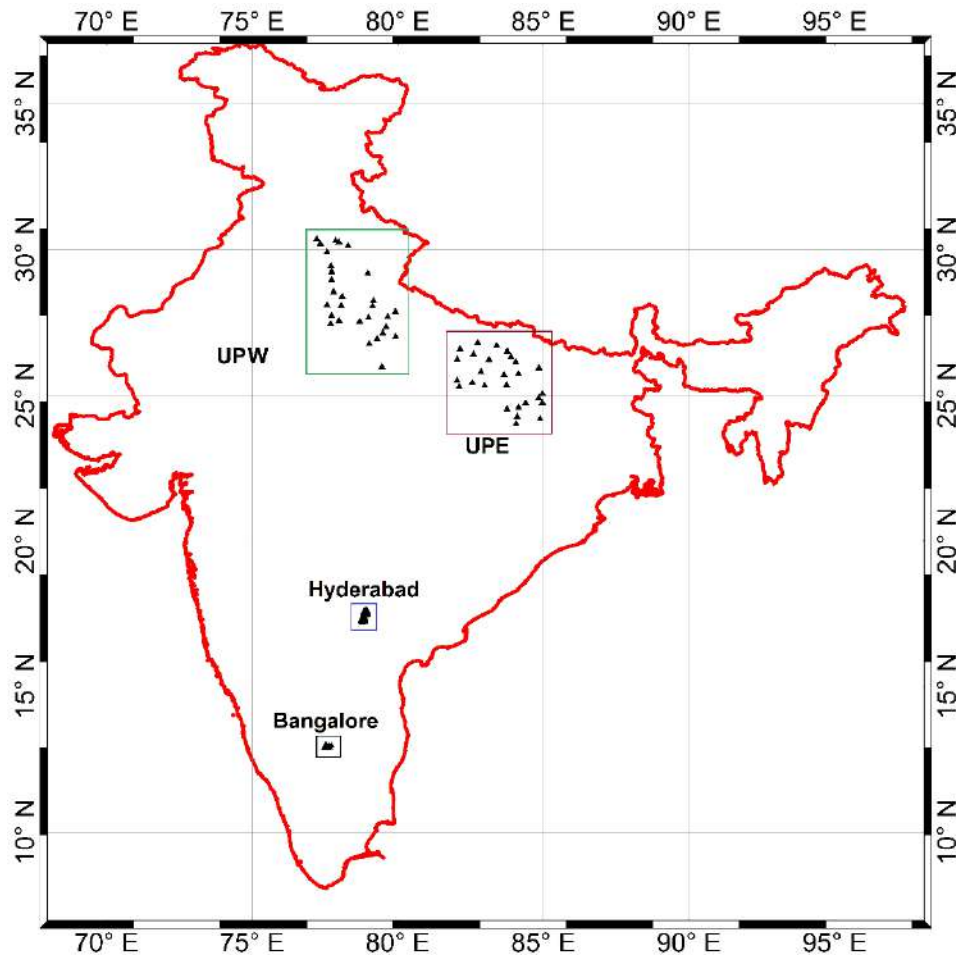


Figure 2.2.1: GNSS/levelling data distribution

From Table 2.2.1, it is observed that for 119 data points, the approximate range of $h = 1018$ m, $H = 996$ m, $N_{GNSS/lev} = 41$ m and baseline length = 1937 km. The values of $N_{GNSS/lev}$ increase as we move towards north from Bangalore to UPW. Also, the data points in Bangalore and Hyderabad are much closer than UPW and UPE.

2.3 Deflections of the Vertical

Deflections (or deviations) of the vertical data comprises data points with latitude, longitude, east-west and north-south components of the deflection of vertical. These are used for i) evaluation of the GGMs (Section 2.4) and ii) absolute validation of the computed geoid models (Chapter 5; e.g., Featherstone and Morgan, 2007; Featherstone and Lichten, 2009).

The deflection of the vertical is the angular difference between the directions of the plumbline at a point and the ellipsoidal normal at that point. From Jekeli (1999), these are termed absolute deflections when a geocentric ellipsoid is used and relative deflections when a non-geocentric, that is a regional or local, ellipsoid is used. Also, as the plumbline is curved and torsioned, the deflection varies as a function of position and height, leading to more subtle definitions such as the Pizzetti deflection at the geoid, the Helmert deflection at the Earth's surface, or the Molodensky deflection with respect to the normal plumbline, all of which are described and explained in Jekeli (1999).

The vertical deflection is usually decomposed into north-south and east-west components, principally because they are determined by comparing geodetic and astronomic coordinates (Eq. (2.3.1)). The north-south component is also termed the meridional deflection (ξ_H) and the east-west component is termed the prime vertical deflection (η_H). The equations for astronomically observed deflections are:

$$\left. \begin{aligned} \xi_H &= \Phi - \varphi \\ \eta_H &= (\Lambda - \lambda) \cos \varphi \end{aligned} \right\} \quad (2.3.1)$$

where (Φ, Λ) are the astronomical latitude and longitude and (φ, λ) are geodetic latitude and longitude.

Equation (2.3.1) is a simplified form obtained by taking small angle (in radian) approximations (i.e., $\cos x \approx 1$, $\sin x \approx x$; $\forall x \ll 1$; $x \in [\eta_H, \xi_H, (\Lambda - \lambda)]$) in Eq. (2.3.2) (Torge, 2001, pg. 220)

$$\left. \begin{aligned} \sin \varphi &= \cos \eta_H \sin(\Phi - \xi_H) \\ \sin \eta_H &= \cos \varphi \sin(\Lambda - \lambda) \end{aligned} \right\} \quad (2.3.2)$$

In the 19th century, the vertical deflections over India proved to be an important data for pursuing the idea of isostasy. Heiskanen and Vening Meinesz (1958, pg. 139) mentions: “*The existence of the isostatic compensation was established in India on the basis of deviations of the plumb line and of gravity anomalies*”. Interested readers may see Walker (1863; 1870), Danvers (1870), Key (2000) for some historical aspects regarding the Great Trigonometric Survey (GTS) of India and Pratt (1855), Crosthwait (1912), Bowie (1914), Burrard (1918; 1920) and Heiskanen and Vening Meinesz (1958, pg. 125-131) for historical development of the isostasy with the GTS observations.

The vertical deflections over India that we have access to are in the report of Gulatee (1955), which is a scanned image-only pdf. Therefore, we had to digitise them manually and perform several closed-loop checks and datum transformation, all of which are explained in detail in Featherstone and Goyal (2022; provided in Appendix C.5). It should be noted that not all stations had both deflection components. Of the 1071 stations listed, 708 points are in India (7°N to 37°N and 68°E to 98°E) of which 701 have meridional deflections but only 280 have prime vertical deflections. Figure 2.3.1 shows the distribution of the stations. The meridional deflections vary from -52.7” to +24.5”

while prime vertical deflections from $-41.1''$ to $+19.1''$ with a mean value of $-5.9''$ and $+0.1''$, respectively.

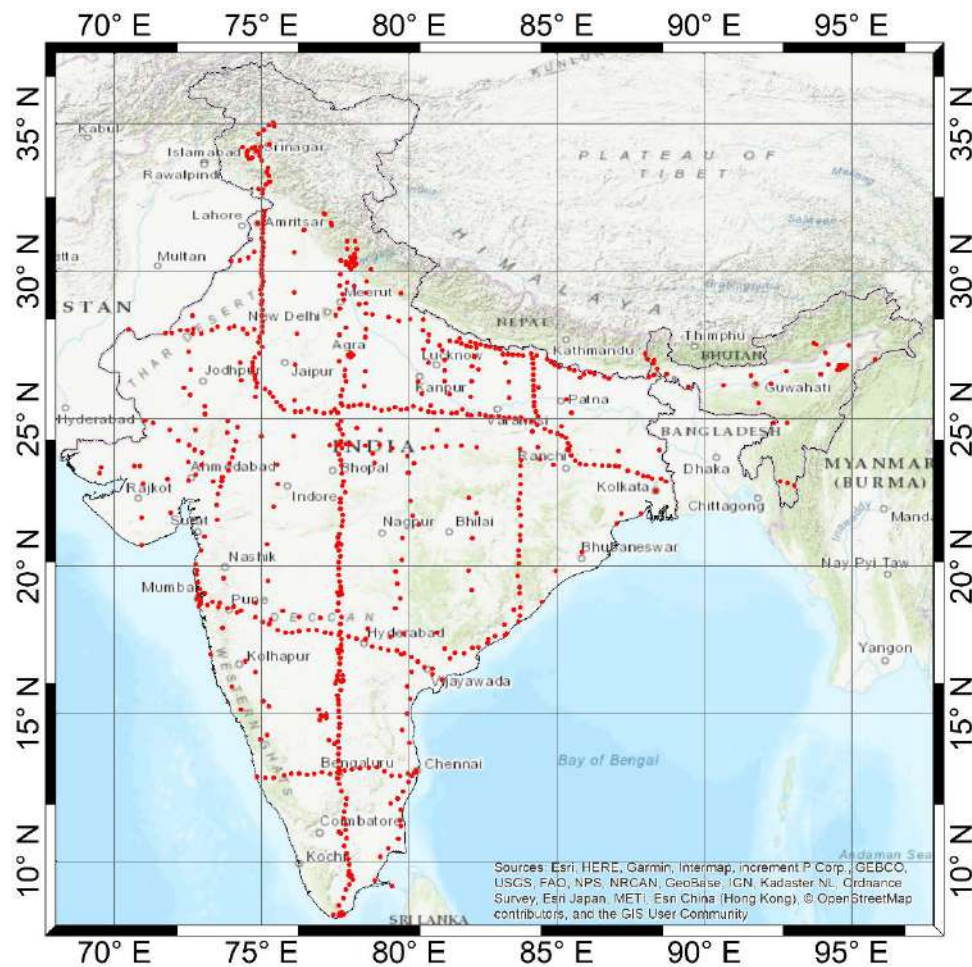


Figure 2.3.1: Deflection of vertical stations in India from Gulatee (1955)

2.4 Global Geopotential Models

Any harmonic function that satisfies Laplace's equation can be expanded into a series of spherical harmonics (e.g., Hobson, 1931). Therefore, the gravitational potential of the Earth, which is a harmonic function outside the gravitating masses, can also be expressed by a series of solid spherical harmonics (Heiskanen and Moritz, 1967, pg. 35). This involves the determination of the geopotential coefficients used in the harmonic expansion. The set of geopotential coefficients of the gravitational potential is called a GGM. These are determined either from satellite observations alone or a combination of satellite and

terrestrial observations. Accordingly, they are termed as satellite-only and combined GGMs, respectively.

Rapp (1998) provides a discussion on developments of the geopotential modelling over several decades but for pre-Gravity Recovery and Climate Experiment (GRACE; Tapley et al., 2004) and Gravity Field and Steady-State Ocean Circulation Explorer (GOCE; Drinkwater et al., 2003). Pail et al. (2011) discussed the GOCE gravity field modelling using three different approaches (direct, space-wise, time-wise) while Tapley et al. (2007), Dahle et al. (2013) and Chen et al. (2015) provided an overview of processing GRACE data for gravity field models.

The determination of the spherical harmonic coefficients (for gravitational potential or any other gravity field functional) is known as spherical harmonic analysis (SHA). The determination of the gravity field quantities or any other corresponding function using the spherical harmonic coefficients is known as spherical harmonic synthesis (SHS). Both SHA and SHS have been discussed in the literature (e.g., Kaula, 1959; Rapp, 1968; Ricardi and Burrows, 1972; Colombo, 1981; Tscherning et al., 1983; Sneeuw, 1994; Bucha and Janák, 2014; Claessens, 2016 among many others) and hence, we will not discuss the same here, instead see the cited literature and the references therein. However, we have discussed some subtleties of SHS in Section 3.6.

Briefly discussing the choice of GGM in the three methods tested (CUT, UNB, and KTH), it is observed that the CUT approach has consistently used the highest available degree of GGM, which is always a combined model. This contrasts with the KTH and the UNB methods that use a satellite-only GGM to avoid correlations in the terrestrial data when used twice (Vaníček and Sjöberg, 1991). However, it has been observed that the KTH method is sometimes being used with combined GGM but up to a lower degree-order (e.g., Ågren et al., 2009a, 2009b; Ulotu, 2009; Yildiz et al., 2012).

The [implicit] rationale for the CUT approach to use the highest available d/o GGMs is that while being fully subject to the undesirable correlation of largely the same terrestrial data being used, the use of high-degree GGM makes the residual geoid/quasigeoid smaller in magnitude. Thus, the residual geoid/quasigeoid computations are less subject to approximation errors, for e.g., ellipsoidal approximation error ($\sim 0.003N$, Heiskanen and Moritz, 1967, pg. 87) for geoid undulation of 100 m is 300 mm and the same error for (residual) geoid undulation of 1 m would be 3 mm.

There are numerous choices of satellite-only or combined GGMs with varying d/o, mostly available at International Centre for Global Earth Models (ICGEM; http://icgem.gfz-potsdam.de/tom_longtime; Ince et al., 2019). GGM testing must be done to choose the most suitable GGM for the geoid/quasigeoid computation (e.g., Amos and Featherstone, 2003). The availability of larger datasets in the future can be exploited for some more informative statistical testing also as implemented by Fotopoulos (2003) and Goyal et al. (2019a; provided in Appendix C.1) with the available data.

With our datasets discussed in Sections 2.1, 2.2 and 2.3, the GGMs were evaluated with the i) geometric geoid undulations (geodetic height minus physical height) obtained from 119 GNSS/levelling points for India (Table 2.4.1) and also region-wise (Tables 2.4.2 and 2.4.3), ii) recomputed free-air anomaly from the GETECH data at 638,625 points (Table 2.4.4) and iii) deflections of the vertical for India (Table 2.4.5)

Table 2.4.1: GGM validation with GNSS/levelling points over India (units in m)

GGM	Max d/o	min	max	mean	STD	Reference
EGM2008	2190	-1.162	0.452	-0.368	0.417	Pavlis et al. (2012; 2013)
EIGEN-6C4	2190	-1.203	0.463	-0.428	0.410	Förste et al. (2014)
GECO	2190	-1.255	0.513	-0.415	0.407	Gilardoni et al. (2016)
XGM2016	719	-1.309	0.511	-0.407	0.407	Pail et al. (2018)
DIR-R5	300	-1.711	0.563	-0.485	0.419	Bruinsma et al. (2013)
TIM-R5	280	-1.584	0.633	-0.464	0.433	Brockmann et al. (2014)
SPW-R5	330	-1.650	0.584	-0.504	0.415	Gatti et al. (2016)

Table 2.4.2: GGM validation with GNSS/levelling points over UPW and UPE

GGM	UPW (units in m)				UPE (units in m)			
	min	max	mean	STD	min	max	mean	STD
EGM2008	-1.162	-0.509	-0.824	0.192	-1.007	-0.047	-0.654	0.227
EIGEN-6C4	-1.203	-0.643	-0.870	0.105	-1.034	-0.361	-0.742	0.144
GECO	-1.255	-0.723	-0.857	0.102	-1.088	-0.418	-0.712	0.135
XGM2016	-1.309	-0.715	-0.843	0.112	-1.037	-0.453	-0.710	0.139
DIR-R5	-1.711	-0.424	-0.920	0.277	-1.120	-0.263	-0.719	0.203
TIM-R5	-1.584	-0.411	-0.904	0.258	-1.206	-0.230	-0.716	0.229
SPW-R5	-1.650	-0.480	-0.917	0.255	-1.160	-0.206	-0.739	0.234

Table 2.4.3: GGM validation with GNSS/levelling points over Hyderabad and Bangalore

GGM	Hyderabad (units in m)				Bangalore (units in m)			
	min	max	mean	STD	min	max	mean	STD
EGM2008	-0.541	0.328	-0.093	0.153	0.372	0.452	0.418	0.029
EIGEN-6C4	-0.612	0.258	-0.154	0.157	0.379	0.463	0.422	0.029
GECO	-0.611	0.260	-0.153	0.157	0.428	0.513	0.472	0.028
XGM2016	-0.632	0.250	-0.142	0.171	0.387	0.511	0.449	0.039
DIR-R5	-0.744	0.135	-0.264	0.172	0.381	0.563	0.450	0.064
TIM-R5	-0.735	0.161	-0.238	0.176	0.472	0.633	0.534	0.056
SPW-R5	-0.760	0.162	-0.299	0.166	0.401	0.584	0.477	0.065

Table 2.4.4: GGM validation with free-air anomalies over India (units in mGal)

GGM	min	max	mean	STD
EGM2008	-381.846	355.076	-0.307	15.558
EIGEN-6C4	-353.134	379.699	0.168	15.412
GECO	-348.027	374.494	0.205	15.355
XGM2016	-237.671	267.468	0.073	16.278
DIR-R5	-352.938	365.798	-0.285	22.833
TIM-R5	-345.457	368.174	-0.304	22.835
SPW-R5	-349.708	367.626	-0.263	22.821

Table 2.4.5: GGM validation with vertical deflections over India

GGM	Meridional (units in arc-second)				Prime vertical (units in arc-second)			
	min	max	mean	STD	min	max	mean	STD
EGM2008	-21.0	13.2	-0.3	2.1	-41.5	13.9	0.1	3.7
EIGEN-6C4	-19.8	12.3	-0.3	2.0	-41.3	11.4	0.0	3.7
GECO	-18.6	12.2	-0.3	2.0	-41.3	14.4	0.0	3.7
XGM2016	-16.1	16.0	-0.4	2.3	-41.6	8.4	0.0	3.8
DIR-R5	-19.7	27.4	-0.1	3.6	-40.7	15.9	0.1	4.2
TIM-R5	-19.2	28.5	-0.1	3.6	-40.4	16.0	0.1	4.2
SPW-R5	-20.2	26.3	-0.2	3.5	-40.2	15.3	0.1	4.2

In Table 2.4.5, there are only two points that have a difference value of prime vertical deflection $< -11''$ (i.e., $-41''$ and $-29''$). Removing these two points alone causes an increase of $\sim 0.3''$ in the mean values and a decrease of $\sim \pm 1.4''$ in the standard deviations of the prime vertical validation (Table 2.4.5).

Tables 2.4.1-2.4.5 do not comprehensively indicate which GGM is comparatively more suitable among combined models and satellite-alone models, individually. This is because there is no significant variation in the mean and standard deviations from different GGMs. Moreover, we do not have any authoritative accuracy estimates of our datasets. So, our choice of EIGEN-6C4 for the CUT method and DIR_R5 for the UNB and the KTH methods are arbitrary rather than based on any rigorous quantitative argument.

EGM2008 is used for filling in the gravity data (Section 2.1) and GECO and EIGEN-6C4 both include EGM2008 data in addition to other datasets. GECO and EIGEN-6C4 have provided comparable results, and we cannot claim the priority of one over the other. Therefore, the choice of EIGEN-6C4 is completely arbitrary. However, for the satellite-only models, we have chosen DIR-R5 GGM because it has been used in the literature on geoid/quasigeoid computation (e.g., Abdalla and Mogren, 2015; Işık and Erol, 2016; Foroughi et al., 2017a; 2019) as compared to other satellite-only models.

2.5 Digital Elevation Models

A DEM, sometimes known as a digital terrain model (DTM), is a bare-Earth model, i.e., it represents the solid topographic surface. We deliberately distinguish between a DEM and a Digital Surface Model (DSM) that represents the shape of the Earth's surface, which includes the height of vegetation canopy and man-made structures (e.g., Hirt, 2014). Several near-global DSMs have been produced from satellite-borne platforms from either radar, e.g., SRTM (Farr et al., 2007), or stereoscopic optical imagery, e.g., ASTER (Meyer et al., 2011). A satellite-derived DSM should be treated for speckle noise (Gallant, 2011) and stripe noise (Tarekegn and Sayama, 2013), and then it can be converted to a DEM by accounting for absolute biases (Crippen et al., 2016) and tree-height biases (O'Loughlin et al., 2016). Yamazaki et al. (2017) have treated the SRTM v2.1 DSM for all these four sources to produce a freely available 3''×3'' global DEM, i.e., the MERIT DEM.

DEMs and DSMs are used synonymously in several applications, such as mapping soil and vegetation (e.g., Dobos and Hengl, 2009; Cavazzi et al., 2013), studying natural hazards (e.g., Gruber et al., 2009; Demirkesen, 2012), catchment geomorphology and hydrology (e.g., Barnes et al., 2014; Zhao et al., 2019), watershed modelling (e.g., Park et al., 2011; Li et al., 2019), floodplain mapping (e.g., Jafarzadegan and Merwade, 2017; Nardi et al., 2019), weather and flood forecasting (e.g., Truhetz, 2010), and gravity-field forward modelling (e.g., Banerjee and Gupta, 1977; Forsberg, 1984). However, researchers have started analysing the effect of using a DSM and not the 'required' DEM for their respective applications, such as done by Yang et al. (2019) for gravity forward modelling. With the experiments involving MERIT DEM and SRTM DSM, Yang et al. (2019) suggested that DEM should always be preferred over DSM to reduce or avoid the tree-canopy effect in gravity forward modelling.

For the geoid and quasigeoid computations, we are interested in the DEMs, in both spatial and spectral forms. A precise high-resolution DEM is a crucial input primarily for calculating topographical effects (Section 3.2), atmospheric gravity corrections (Section 3.3), and analytical continuations (downward or upward) of gravimetric quantities between different surfaces/levels (Section 3.5). However, obtaining a precise DEM is still challenging, especially in the mountainous regions.

Vaniček et al. (n.d.), Varga and Bašić (2018), and Varga et al. (2019) have analysed the effect of different DEM (and DEM resolutions) on the topographic effects. It should be noted that the latter two studies included the freely available global DSMs in their computations, while Vaniček et al. (n.d.) used only DEMs. Though their study areas did not comprise a complex terrain such as that of India, all have reported significant disparities in the results with different DEMs. Thus, the choice of a precise high-resolution DEM becomes more crucial in the mountainous or rapidly undulating regions, where the problem due to the horizontal shifts among DEMs (Rodriguez et al., 2005; Denker, 2005) also becomes enormous (e.g., for India, see Goyal et al., 2021a).

Since a DEM is required for the present study, we have chosen to work with the MERIT DEM (Yamazaki et al., 2017) because this is the only DEM (to the authors best information) available over India. It should be noted that the Indian CartoDEM derived from the Cartosat mission using stereoscopic optical imagery (NRSA, 2006) is a DSM. Moreover, unlike other DSMs, it provides the geodetic heights that are referenced to the WGS84 ellipsoid (NIMA, 2000). We would like to mention that our DEM/DSM analysis (Goyal et al., 2021a; provided in Appendix C.3) has shown MERIT as the best candidate among all the tested models. The MERIT DEM for the study area is shown in Figure 2.5.1.

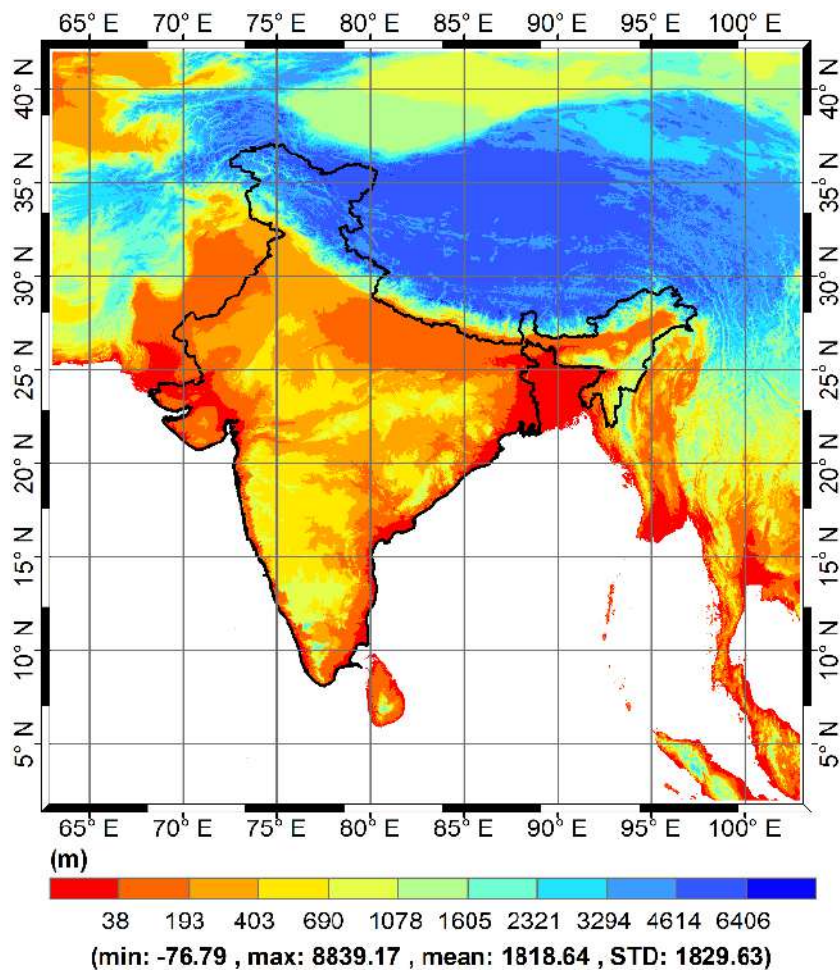


Figure 2.5.1: MERIT DEM over study area at 3'' \times 3'' resolution

The CUT method requires only the spatial form of a DEM. However, the UNB and the KTH methods also require one or all of the height, height-squared, and height-cubed spherical harmonic coefficients in addition to the spatial form of DEM. The KTH method calculates the atmospheric effects while the UNB method computes reference topographical effects using the height coefficients. Since the topographical effects in the UNB method involve global numerical integration, different resolution DEMs are required (Section 3.2). Therefore, to have consistency among the DEMs, we downloaded the whole of global 3'' \times 3'' MERIT DEM and block averaged it into grids of various resolutions, i.e., 30'' \times 30'', 5' \times 5', and 1' \times 1'.

Since we worked with the KTH method before starting with the UNB method, the global DEM was downloaded at a later stage. Therefore, we followed the KTH strategy for developing the spectral form of DEM wherein a global DEM is constructed with the block-averaged 15'×15' DTM2006 (d/o 2190) heights augmented with block-averaged 15'×15' MERIT DEM over the study area, i.e., 2°N to 42°N latitude and 63°E to 103°E longitude. Spherical harmonic coefficients for the heights to a maximum d/o of 720 are then estimated using a FORTRAN based SHA subroutine, `analyfft_grd.f` (subroutine in GEOLAB package). For height-squared and height-cubed coefficients, the heights from the constructed 15'×15' global DEM were squared and cubed, respectively, before estimating the corresponding coefficients.

Degree-order 720 has been chosen because the geoid/quasigeoid models developed using the KTH method also construct the height coefficients up to d/o 720 (Ågren, 2004; Ågren et al., 2009a, 2009b; Yildiz et al., 2012). It was also possible to construct the spherical harmonic coefficients using block-averaged global 15'×15' MERIT DEM alone, but this was not done because we already computed the harmonic coefficients following the KTH approach. We acknowledge that more in-depth quantitative testing should be done with different d/o to analyse the included effects with the height coefficients in both the UNB and the KTH method from the viewpoint of the cm-level precise geoid.

2.6 Summary

We discussed the availability and the characteristics of the five datasets over India and finalised the following to be used in Indian geoid and quasigeoid modelling:

- i) GETECH's terrestrial gravity anomaly data for India, EGM2008 (d/o 900) derived fill-in terrestrial gravity anomaly data for land areas surrounding India and oceanic gravity anomaly data from Scripps Institute of Oceanography were merged using concatenated

to construct a $0.02^\circ \times 0.02^\circ$ grid of free-air gravity anomalies for Indian geoid/quasigeoid computations. Gradient testing was performed to identify any discontinuities at the edges of the merged gravity anomaly dataset. We have not observed clear visual indication of any discontinuities at the boundaries of the merged gravity anomaly dataset.

- ii) 119 GNSS/levelling data points are available over India, distributed in four regions: Uttar Pradesh West (UPW), Uttar Pradesh East (UPE), Hyderabad, and Bangalore. No information is provided on the height system of the levelling heights. Therefore, we considered them to be based on normal-orthometric height system referring to IVD1909. Since there is no uniquely defined reference surface for normal-orthometric heights, it is decided to validate both geoid and quasigeoid models with the GNSS/levelling data.
- iii) Vertical deflections have been digitised from Gulatee (1955) that included 701 meridional deflections and 280 prime vertical deflections in India. The meridional deflections vary from $-52.7''$ to $+24.5''$ while prime vertical deflections from $-41.1''$ to $+19.1''$ with a mean value of $-5.9''$ and $+0.1''$, respectively. These are used to validate geoid models.
- iv) GGMs were evaluated with the gravity anomalies, GNSS/levelling and vertical deflections datasets. There is no clear choice of the preferred GGM from the descriptive statistics of the evaluation results. Therefore, rather based on any quantitative argument, we have arbitrarily chosen EIGEN-6C4 (max d/o 2190) for the CUT method, and DIR-RL05 (max d/o 300) for the UNB and the KTH methods. EGM2008 has been used up to d/o 900 for calculating the fill-in gravity anomaly data for the areas where we do not have access to the terrestrial gravity data. Degree-order 900 is chosen because EGM2008 uses proprietary gravity data up to d/o 900.

v) The global freely available DEM is MERIT DEM and hence, it is used in Indian geoid/quasigeoid computations. The CUT and the KTH methods use MERIT 3'' \times 3''. The UNB Method includes global integration and requires DEMs of different resolutions. Therefore, MERIT 3'' \times 3'' and block-averaged MERIT 30'' \times 30'', 5' \times 5', 1° \times 1° DEMs are used in the UNB method. Additionally, for the KTH and the UNB methods, spherical harmonic coefficients of height, height-squared and height-cubed are also constructed.

Chapter 3: Systematic effects in geoid determination

3.0 Introduction

There are various corrections and reductions that need to be applied to the datasets for the use of Stokes's formula for geoid/quasigeoid computation. These corrections, though conceptually identical, are realised using different strategies in the three methods: CUT, UNB, and KTH. Another aspect is that there have been various approximations in terms of some assumptions, truncations, and certain inconsistencies in the involved formulations that have been carried forward for decades under the umbrella of them being negligible. However, from the viewpoint of cm-level precise geoid (Sansó and Rummel, 1997), these need a revisit because any mm-level error emanating from the approximations is liable to deviate from achieving the goal significantly. That is, one-millimetre systematic error is a 10% deviation from the desired centimetre accurate geoid. Furthermore, any systematic error will not be reflected in the error propagation, thus, one may obtain centimetre or sub-centimetre precise geoid/quasigeoid but shifted by an amount equal to the systematic errors.

In this chapter, we have tried to provide our discussions on the following in view of the cm-level precise geoid/quasigeoid:

- i) Different choices for calculating normal gravity at any arbitrary height for computation of the gravity anomaly at the Earth's surface.
- ii) The topographic and the atmospheric corrections required to account for the masses above the geoid because Stokes's solution does not permit the masses above the geoid (i.e., the Laplace harmonic condition must be valid).
- iii) Ellipsoidal corrections required to compensate for the spherical approximation

used in formulating Stokes's solution.

- iv) Downward continuation of gravity anomalies from the Earth's surface to the geoid.
- v) Analytical continuation of the gravity anomalies from the Earth's surface to the computation point-level surface for quasigeoid calculation.
- vi) Consistent use of the zero-degree term.
- vii) Effect of solid Earth permanent tide systems on physical Earth and parameters of normal ellipsoid.

In the following sections, we will discuss free-air gravity anomalies only, but we use a cryptic term 'gravity anomaly' for brevity. Otherwise, we will mention specifically the type of gravity anomaly being discussed.

3.1 Gravity anomalies

Actual gravity is observed on or above the Earth's topographical surface, therefore, the computation of gravity anomaly requires either of the following:

- i) Upward continuation of normal gravity from the ellipsoid to the telluroid: For this, normal heights are required. In case normal heights are not available, they are approximated by normal orthometric heights or Helmert orthometric heights (Though it is commonly done, geoid-quasigeoid correction can be applied to avoid this approximation (Eq. 3.1.24)). By subtracting this upward continued normal gravity at the telluroid from the corresponding observed gravity at the Earth's surface, we obtain the free-air gravity anomaly at the Earth's surface (or sometimes known as Molodensky-type free-air gravity anomaly). It is conspicuous that the corresponding points on the Earth's topography and the telluroid lie along the ellipsoidal normal through the point on the Earth's topography.

- ii) Downward continuation of observed gravity from the Earth's surface to the geoid: For this, orthometric heights are required and density of the masses between the Earth's topographical surface and the geoid. The downward continuation of the Earth's gravity makes things a little complicated, but the difficulties are alleviated by using Helmert's second method of condensation (see Section 3.2). Therefore, on subtracting the normal gravity at the ellipsoid from the corresponding downward continued observed gravity at the geoid, we obtain the free-air gravity anomaly on the geoid.

As such, upward continuation of normal gravity requires normal gravity gradient while downward continuation of the Earth's gravity requires actual gravity gradient through the topography. Since the actual gravity gradient is less precisely known as compared to the normal gravity gradient (which is in fact exactly known), a common practice is to compute gravity anomalies on the Earth's surface and further process as is needed in the geoid/quasigeoid computation strategy.

Next, we discuss computing normal gravity at the telluroid (in general, at any height of interest). This involves some expressions of normal gravity gradient and a direct or exact method of computing normal gravity at any height using the concept of confocal ellipsoids (Heiskanen and Moritz, 1967, pg. 65).

3.1.1 Gradient method of calculating normal gravity at any height

Normal gravity at any height can be obtained by using a Taylor series expansion (Heiskanen and Moritz, 1967, pg. 78)

$$\gamma_h = \gamma_0 + \frac{\partial\gamma}{\partial h}h + \frac{1}{2}\frac{\partial^2\gamma}{\partial^2h}h^2 + \frac{1}{6}\frac{\partial^3\gamma}{\partial^3h}h^3 + \dots \quad (3.1.1)$$

It is observed that the above expression has been used in the literature with only the first-order term or also including a second-order term (e.g., Hackney and Featherstone, 2003).

That is, higher than second-order terms are generally neglected.

There can be different expressions for the normal gravity gradient of first- and second-order. The more conventional formulas are given as (Heiskanen and Moritz, 1967, pg. 78)

$$\frac{\partial \gamma}{\partial h} = -\frac{2\gamma_0}{a}(1 + f + m - 2f \sin^2 \varphi) \quad (3.1.2)$$

$$\frac{\partial^2 \gamma}{\partial^2 h} = \frac{6\gamma_0}{a^2} \quad (3.1.3)$$

Thus, substituting Eqs. (3.1.2) and (3.1.3) in Eq. (3.1.1), normal gravity at any geodetic height (h) can be obtained using:

$$\gamma_h = \gamma_0 \left[1 - \frac{2}{a}(1 + f + m - 2f \sin^2 \varphi)h + \frac{3}{a^2}h^2 \right] \quad (3.1.4)$$

A simple spherical approximation of Eq. (3.1.2), which is generally used in geophysics (e.g., Hackney and Featherstone, 2003) and sometimes in geodesy as well (e.g., Mishra and Ghosh, 2016) is

$$\frac{\partial \gamma}{\partial h} \approx -0.3086 \text{ mGal/m} \quad (3.1.5)$$

Another expression for the first- and second-order terms are derived using Bruns's formula (Heiskanen and Moritz, 1967, pg. 78) that gives the first-order term as

$$\frac{\partial \gamma}{\partial h} = -2\gamma_0 J - 2\omega^2 = -\gamma_0 \left(\frac{1}{\nu} + \frac{1}{\mu} \right) - 2\omega^2 \quad (3.1.6)$$

where J is the mean curvature of the ellipsoid, ω is the angular velocity of Earth's rotation, μ and ν are the principal radii of curvature in the meridian and prime vertical directions, respectively and are given as (on the reference ellipsoid)

$$\mu = \frac{a(1-e^2)}{(1-e^2 \sin^2 \varphi)^{3/2}} \quad (3.1.7)$$

$$\nu = \frac{a}{(1-e^2 \sin^2 \varphi)^{1/2}} \quad (3.1.8)$$

Substituting Eqs. (3.1.7) and (3.1.8) in Eq. (3.1.6) gives

$$\frac{\partial \gamma}{\partial h} = -\gamma_0 \left(\frac{(1-e^2 \sin^2 \varphi)^{1/2}}{a(1-e^2)} (2-e^2(1+\sin^2 \varphi)) \right) - 2\omega^2 \quad (3.1.9)$$

The second-order term is now obtained by differentiating Eq. (3.1.9) with respect to h and substituting values of μ and ν from Eqs. (3.1.7) and (3.1.8).

$$\frac{\partial^2 \gamma}{\partial^2 h} \approx \frac{\partial^2 \gamma}{\partial^2 a} = \frac{\partial}{\partial a} \left(-\gamma_0 \left(\frac{1}{\nu} + \frac{1}{\mu} \right) - 2\omega^2 \right) = -\gamma_0 \frac{\partial}{\partial a} \left(\frac{1}{\nu} + \frac{1}{\mu} \right) \quad (3.1.10)$$

$$\frac{\partial^2 \gamma}{\partial^2 h} \approx \frac{\partial^2 \gamma}{\partial^2 a} = -\gamma_0 \frac{\partial}{\partial a} \left[\frac{(a^2 - a^2 \sin^2 \varphi + b^2 \sin^2 \varphi)^{3/2} + b^2 (a^2 - a^2 \sin^2 \varphi + b^2 \sin^2 \varphi)^{1/2}}{a^2 b^2} \right] \quad (3.1.11)$$

$$\frac{\partial^2 \gamma}{\partial^2 h} \approx \frac{2\gamma_0}{b^2} \left[\frac{1}{a^2} \sqrt{(1-e^2 \sin^2 \varphi)} (a^2 (1-e^2 \sin^2 \varphi) + b^2) - \frac{1}{2} (1-\sin^2 \varphi) \left(\frac{2+e^2-3e^2 \sin^2 \varphi}{\sqrt{1-e^2 \sin^2 \varphi}} \right) \right] \quad (3.1.12)$$

Substituting Eqs. (3.1.9) and (3.1.12) in Eq. (3.1.1) gives the second expression for computing normal gravity at any height h .

3.1.2 Exact method of calculating normal gravity at any height

The exact method is based on computation of normal gravity on the surface of an ellipsoid constructed confocally and concentrically with the reference ellipsoid passing through the point at height equal to the height of interest (for our case normal height). The normal potential of any such confocal ellipsoid is given as (Heiskanen and Moritz, 1967, pg. 67):

$$U(u, \beta) = \frac{GM}{E} \tan^{-1} \frac{E}{u} + \frac{1}{2} \omega^2 a^2 \frac{q}{q_0} \left(\sin^2 \beta - \frac{1}{3} \right) + \frac{1}{2} \omega^2 (u^2 + E^2) \cos^2 \beta \quad (3.1.13)$$

where u, β are the semi-minor axis of the confocal ellipsoid and reduced latitude, respectively; E is linear eccentricity. We have omitted λ from the ellipsoidal coordinates because normal potential is independent of longitude. In Eq. (3.1.13), the other terms are

$$\left. \begin{aligned} q &= \frac{1}{2} \left[\left(1 + 3 \frac{u^2}{E^2} \right) \tan^{-1} \frac{E}{u} - 3 \frac{u}{E} \right] \\ q_0 &= \frac{1}{2} \left[\left(1 + 3 \frac{b^2}{E^2} \right) \tan^{-1} \frac{E}{b} - 3 \frac{b}{E} \right] \end{aligned} \right\} \quad (3.1.14)$$

$$\beta = \tan^{-1} \left(\frac{b}{a} \tan \varphi \right) \quad (3.1.15)$$

It should be noted that Eq. (3.1.15) holds if φ is the geodetic latitude with respect to the confocal ellipsoid through the point at altitude. For a more general relation for β and φ see Claessens (2006, Chapter 2).

$$u = \sqrt{\frac{1}{2}(r^2 - E^2) + \frac{1}{2}\sqrt{(r^2 - E^2)^2 + 4E^2 z^2}} \quad (3.1.16)$$

$$z = \left((1 - e^2)v + H \right) \sin \varphi \quad (3.1.17)$$

$$r = \sqrt{(\mu + H)^2 \cos^2 \varphi + \left((1 - e^2)v + H \right)^2 \sin^2 \varphi} \quad (3.1.18)$$

The gradient of the normal gravity potential (Eq. (3.1.13)) along the lines/directions of the ellipsoidal coordinates gives normal gravity as

$$\left. \begin{aligned} \gamma_h &= \sqrt{\gamma_u^2 + \gamma_\beta^2 + \gamma_\lambda^2} = \sqrt{\left(\frac{\partial U}{\partial s_u} \right)^2 + \left(\frac{\partial U}{\partial s_\beta} \right)^2 + \left(\frac{\partial U}{\partial s_\lambda} \right)^2} \\ &= \sqrt{\left(\frac{\partial U}{\partial u} \frac{\partial u}{\partial s_u} \right)^2 + \left(\frac{\partial U}{\partial \beta} \frac{\partial \beta}{\partial s_\beta} \right)^2 + \left(\frac{\partial U}{\partial \lambda} \frac{\partial \lambda}{\partial s_\lambda} \right)^2} \end{aligned} \right\} \quad (3.1.19)$$

where $(s_u, s_\beta, s_\lambda)$ is the triplet of the line elements of ellipsoidal coordinates. So, any arc element on the ellipsoid is calculated as (Heiskanen and Moritz, 1967, pg. 41)

$$ds^2 = \frac{u^2 + E^2 \sin^2 \beta}{u^2 + E^2} du^2 + (u^2 + E^2 \sin^2 \beta) d\beta^2 + (u^2 + E^2) \cos^2 \beta d\lambda^2 \quad (3.1.20)$$

From Eq. (3.1.13), $\frac{\partial U}{\partial \lambda} = 0$, therefore, Eq. (3.1.19) can be evaluated as

$$\gamma = \sqrt{\left(\sqrt{\frac{u^2 + E^2}{u^2 + E^2 \sin^2 \beta}} \frac{\partial U}{\partial u} \right)^2 + \left(\sqrt{\frac{1}{u^2 + E^2 \sin^2 \beta}} \frac{\partial U}{\partial \beta} \right)^2} \quad (3.1.21)$$

Equation (3.1.21) can be used to calculate the normal gravity at any height without using the gravity gradient terms of any order and that is the reason we call it the exact method.

All the above-provided formulas for normal gravity at any height are dependent on latitude and height. Hackney and Featherstone (2003) show that the difference in using Eqs. (3.1.4) and (3.1.5) can reach 5.7 mGal at the summit of Mt. Everest. We show the variation of the differences in the gravity anomaly between the conditions when normal gravity is computed using the exact formula (Eq.(3.1.21)) and i) an approximate conventional (what we call here) second-order formula (Eq. (3.1.4), Figure 3.1.1), ii) Bruns's formula (Eqs. (3.1.9) and (3.1.12), Figure 3.1.2, and iii) linear term (Eq. (3.1.5), Figure 3.1.3).

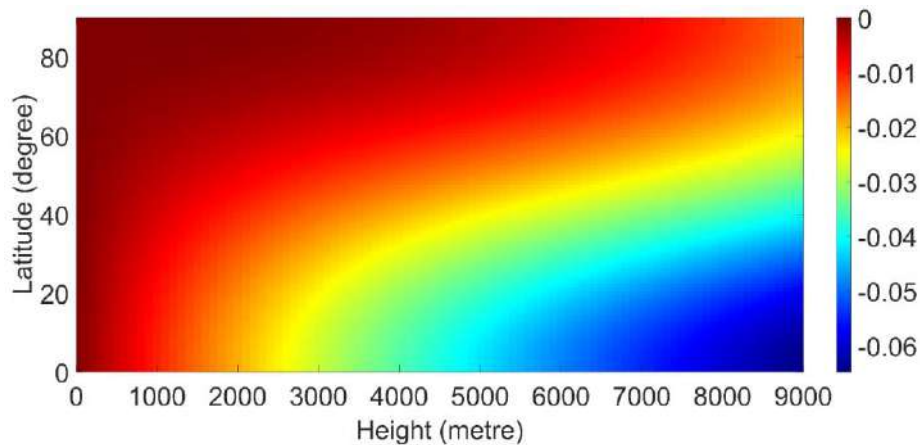


Figure 3.1.1: Difference in gravity anomaly using exact solution v/s second-order formula (mGal)

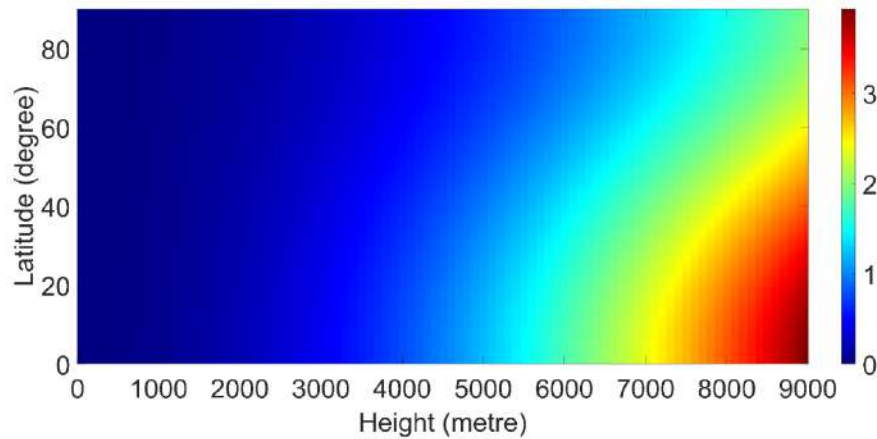


Figure 3.1.2: Difference in gravity anomaly using exact solution v/s solution derived using Brun's formula (mGal)

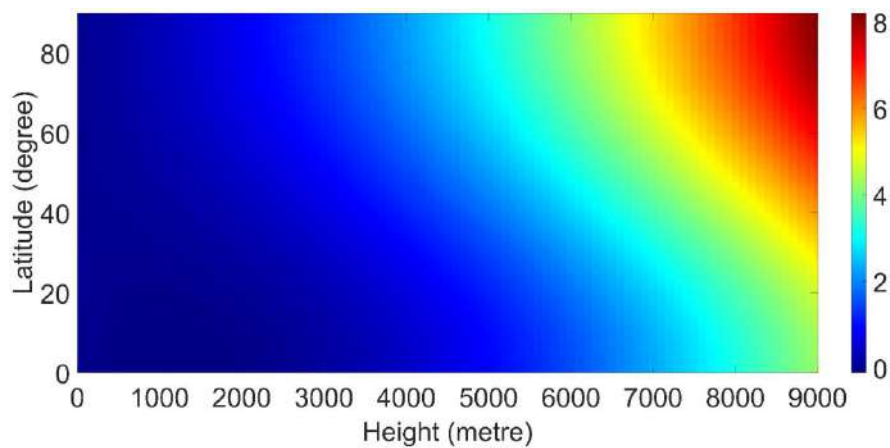


Figure 3.1.3: Difference in gravity anomaly using exact solution v/s linear formula (mGal)

Figures 3.1.1 - 3.1.3 show that, as expected, all the solutions give identical results on the ellipsoid ($h = 0$ m) and minor differences at small heights (~ 100 m) above the ellipsoid. The best approximative formula for γ_h is the conventional second-order formula. However, given the precision of present-day gravimeters (μGal), the use of exact method for γ_h is suggested. Therefore, any of the above discussed formula for γ_h can be used for computing gravity anomalies on the geoid because that require normal gravity on the ellipsoid. However, for gravity anomalies on the Earth's surface, either, preference-wise, the exact method or the conventional second-order formula must be used.

The three methods, CUT, UNB and KTH use Eq. (3.1.4) to compute normal gravity at any height and hence, the gravity anomaly at the Earth's surface. Unlike the CUT and the KTH methods, the UNB method takes it a little further. It applies a correction for using orthometric height as an approximation to the normal heights for upward continuing the normal gravity (UNB, 2009), i.e., our normal gravity is not at the, required surface, telluroid but a surface that is telluroid plus geoid-quasigeoid separation. The planar approximation of the geoid-quasigeoid separation is given as (Heiskanen and Moritz, 1967, pg. 327; Martinec, 1993)

$$H^* - H = N - \zeta \approx \frac{\Delta g^{SB}}{\gamma_0} H \quad (3.1.22)$$

where Δg^{SB} is simple planar Bouguer gravity anomaly.

Therefore, the geoid-quasigeoid correction to the gravity anomaly (Δg^{H^*-H}) is computed as

$$\Delta g^{H^*-H} = -\frac{\partial \gamma}{\partial h} \left(\frac{\Delta g^{SB}}{\gamma_0} H \right) \quad (3.1.23)$$

Equation (3.1.23) in spherical approximation can be written as

$$\Delta g^{H^*-H} \approx \frac{2H \Delta g^{SB}}{R + H} \quad (3.1.24)$$

Equation (3.1.24) never exceeds 1.67 mGal (computed for the summit of Mt. Everest i.e., $H = 8848$ m and $\Delta g^{SB} = 600$ mGal), which is a value that may cause perceptible deviation from the quest of a cm-precise geoid.

Therefore, the UNB method of computing gravity anomalies is (unless normal heights are used)

$$\Delta g'_{UNB} = \Delta g' - \left(\gamma_0 + \frac{\partial \gamma}{\partial h} H + \frac{1}{2} \frac{\partial^2 \gamma}{\partial^2 h} (H)^2 \right) + \Delta g^{H^* - H} \quad (3.1.25)$$

where $\Delta g'_{UNB}$ is the free-air gravity anomaly on topography in the UNB method and $\Delta g'$ is the free-air gravity anomaly on topography in the CUT and the KTH methods.

3.2 Topographic corrections

Stokes's formula for geoid computation requires that there be no masses outside the geoid and the gravity anomalies should refer to the geoid. However, topographical masses exist, i.e., the masses between the geoid and the Earth's topographical surface. There do exist atmospheric masses also, which will be dealt with in Section 3.3. The major argument on the limitation in the geoid computation has always been that the topographical density is less-precisely known (Heiskanen and Moritz, 1967, pg. 127). This has been attached to the problem/biases that would occur in downward continuation of the gravity values from Earth's surface to the topography. In view of this, the solution given by Molodensky et al. (1962) has been endorsed by many as an alternative to compute a quasigeoid without worrying about topographical density and the downward continuation of gravity. However, the quasigeoid is a non-equipotential surface but can always be transformed to the geoid using geoid-quasigeoid separation term (see Section 4.3).

Thus, we can say that topographic corrections are not required for the quasigeoid computation while they are mandatory for computation of the geoid (if not routed through quasigeoid). However, among different solutions to Molodensky's problem (Molodensky et al., 1962; used for quasigeoid), Moritz (1968) has shown that the involved G_I term can be approximated by the planar Terrain Correction (TC) and a term equal to the First Order Indirect Effect (FOIE).

In geoid computation, topographic masses are handled by applying three corrections (Vaníček and Kleusberg, 1987; Wang and Rapp, 1990; Heck, 1993a) before or after the gravity or gravity anomaly is downward continued to the geoid: Direct Topographical Effect (DTE) and Secondary Indirect Topographical Effect (SITE) on gravity, and Primary Indirect Topographical Effect (PITE) on the gravity potential. These three are discussed in detail in Section 3.2.2 because the UNB method strictly follows this approach.

For applying any topographic correction, the height information is the paramount information that is available from DEMs. It is known that the higher resolution DEMs provide better (detailed) information of the Earth's topography. Hence, precise DEMs of higher resolution are the key inputs for the computation of any precise topographical effect. However, with an increase in the DEM resolutions, there is an increase in the number of computation points and the attached roving points for the integration (see formulations in this Section). For a regional quantification, in an area of just $1^\circ \times 1^\circ$, the number of computation points for a $1'' \times 1''$ DEM (12,960,000) increases nine-fold compared to a $3'' \times 3''$ DEM (1,440,000) and the number of roving points will increase ~ 36 times for an integration radius of 1° . Therefore, it is important that we use the methods that are conceptually defensible and not resource-heavy. Further discussions in this section will be around this argument.

In the following three sub-sections, we will discuss about handling the topography in the CUT, the UNB and the KTH methods. A constant topographical density of $2,670 \text{ kgm}^{-3}$ is assumed in the following discussions and the formulations, although use of topographical density models is suggested (Martinec, 1993; Huang et al., 2001; Kingdon et al., 2009; Sheng et al., 2019).

3.2.1 Topographic corrections in the CUT method

The CUT method uses Molodensky's principle for the determination of the quasigeoid. The Molodensky's G_1 term is approximated by the planar TC (Moritz, 1968, 1980, McCubbine et al., 2018). However, deviating from the Moritz (1968, 1980) solution, the FOIE term is omitted in the CUT method based quasigeoid computations (Featherstone et al., 2011, 2018). The TCs are mainly used for reconstruction of Faye anomalies on the topography (Featherstone and Kirby, 2000). As of here and in general, though the CUT method makes use of the planar TC, it will not be correct to say that it applies direct or indirect topographical effect. This has been briefly revisited in Section 3.5 with a slightly different point of view. In the present section, we will discuss the method used for planar TC computation.

As discussed above, the availability of high resolution DEMs causes a drastic increase in the computation-rovig point pairs. Therefore, the use of spectral methods becomes attractive. The CUT method has always used only the FFT alone method for TC computations (e.g., Kirby and Featherstone, 1999; 2001; 2002; McCubbine et al., 2017a) in the AUSGeoid models (Featherstone et al., 2001; 2011; 2018) and New Zealand quasigeoid models (Amos and Featherstone, 2009; Claessens et al., 2011).

Spectral methods provide significant computational efficiency, but there are two principal restrictions attached to the use of discrete/fast Fourier transforms (D/FFTs). First, a convergence criterion because, use of a binomial expansion restricts D/FFT method to the regions where terrain gradients are $<45^\circ$ (cf. Sideris, 1984; Forsberg, 1985; Martinec et al., 1996; Sampietro et al., 2016). Secondly, a decision is needed on the truncation limit of the binomial expansion to obtain a convergent TC solution. Some existing strategies to address the above restrictions are summarised in Goyal et al. (2020) from where it is

observed that a guaranteed convergent TC solution had never been pursued in a satisfactory and optimal way.

We envisaged that the combined spatial-spectral approach for planar TC computation (Tsoulis, 1998; 2001) could be a reliable approach for convergent TC computation in regions with gradients $>45^\circ$. The spatial-spectral combined method uses D/FFT in the outer zone and mass-prism integration in the inner zone. Therefore, if we divide the integration domain such that the terrain having gradient $>45^\circ$ are confined to the inner zone, we can avoid using the D/FFT, i.e., avoid divergence emanating from those areas. However, there are two issues with this method when using high-resolution DEMs. First, there exists no defining rule to determine the radius that separates inner and outer zones and hence, it is decided using the “brute force” method (e.g., Tsoulis, 1998). Second, due to the increase in the computation points, mass-prism analytical integration in the inner zone (cf. Forsberg, 1984; Tsoulis, 1998; Heck and Seitz, 2007; Tsoulis et al., 2009) is still resource-heavy and time-consuming.

Therefore, as a complete solution package for local planar TC, we modified the spatial-spectral approach of Tsoulis (1998; 2001) and provided i) rules for defining the radius that separates inner and outer zones to guarantee convergence; ii) the number of terms in the binomial expansion to be used in D/FFT for including non-negligible terms (contribution $>1\mu\text{Gal}$), and iii) a new numerical approach/solution to analytical mass-prism integration. These three points are discussed below, but first, we show the source of convergence/divergence criterion mathematically.

The planar TC is given by (Forsberg 1984):

$$TC = G\rho \int_{x_1}^{x_2} \int_{y_1}^{y_2} \int_{z_1}^{z_2} \frac{z}{\left(\sqrt{x^2 + y^2 + z^2}\right)^3} dx dy dz = G\rho \iint_E \int_{z_1=0}^{z_2=H_p-H_i} \frac{z}{\left(\sqrt{x^2 + y^2 + z^2}\right)^3} dx dy dz \quad (3.2.1)$$

On integrating Eq. (3.2.1) with respect to z , we get

$$TC = G\rho \iint \left(\frac{1}{l_E} \left[1 - \left[1 + \left(\frac{z_2}{l_E} \right)^2 \right]^{-1/2} \right] \right) dydx \quad (3.2.2)$$

Where G is the universal gravitational constant, ρ is the constant bulk topographic density, $l_E = \sqrt{(x_p - x_i)^2 + (y_p - y_i)^2}$ is the horizontal Euclidean distance between the computation and the roving points; (x_p, y_p, H_p) and (x_i, y_i, H_i) are the coordinates of computation point and roving point, respectively. H_p is the height of the computation point and H_i the height of the roving point. We can write $z_2 = \Delta z = H_p - H_i$

Making use of the binomial expansion of $(1+x)^{-1/2}$ according to

$$(1+x)^{-1/2} = 1 - \frac{1}{2}x + \frac{1.3}{2.4}x^2 - \frac{1.3.5}{2.4.6}x^3 + \frac{1.3.5.7}{2.4.6.8}x^4 - \frac{1.3.5.7.9}{2.4.6.8.10}x^5 + \dots \text{ for } |x| < 1 \quad (3.2.3)$$

we expand $\left(1 + \left(\frac{\Delta z}{l} \right)^2 \right)^{-1/2}$ in Eq. (3.2.2). After rearranging the obtained terms, Eq. (3.2.2)

can be written as

$$TC \approx G\rho \int_{x_1}^{x_2} \int_{y_1}^{y_2} \left[\frac{\Delta z^2}{2l^3} - \frac{3\Delta z^4}{8l^5} + \frac{5\Delta z^6}{16l^7} - \frac{35\Delta z^8}{128l^9} + \frac{63\Delta z^{10}}{256l^{11}} - \frac{231\Delta z^{12}}{1024l^{13}} + \dots \right] dx dy \quad (3.2.4)$$

where we abbreviate each as

$$TC \approx TC_1 + TC_2 + TC_3 + TC_4 + TC_5 + TC_6 + \dots \quad (3.2.5)$$

Each term retains the appropriate sign according to Eq. (3.2.4). This formulation is a convolution, so can be solved numerically efficiently using the D/FFT (e.g., Schwarz et al., 1990).

Since Eq. (3.2.3) is valid for $|x| < 1$, the planar TC can be computed using Eq. (3.2.4) iff when the condition

$$\left| \frac{\Delta z}{l} \right| \leq 1 \quad \forall l \quad (3.2.6)$$

is met. Equation (3.2.6) is referred to as the convergence criterion. The condition $\forall l$ in Eq. (3.2.6) generally corresponds to the requirement that the slope of the terrain immediately surrounding the computation point should not exceed 45° (e.g., Forsberg, 1985; Sideris, 1985; Klose and Ilk, 1993). However, conceptually, Eq. (3.2.6) must be satisfied for each and every combination of computation and roving points in the whole integration domain, i.e., the region covered by the integration/bounding radius (BR, Figure 3.2.1), of Eq.(3.2.4).

Therefore, we need to separate our inner and outer zones such that the condition given by Eq. (3.2.6) is satisfied for all the computation-rover point pairs in the outer zone, where the D/FFT is to be used.

Now we discuss our solution of calculating planar TC using an efficient spatial-spectral combined method. This has been taken from Goyal et al. (2020), which is provided in Appendix C.2.

i) Rules for defining inner and outer zones separating radius

In the following discussion, the inner and outer zones separating radius will be interchangeably referred with the inner radius because, along with separating the study area into zones, it also defines the radius of the inner zone.

We consider three scenarios to select the radius that separates inner and outer zones (Figure 3.2.1). We term them: height-defined separating radius (HSR), exact separating radius (ESR), and optimal separating radius (OSR) as follows.

- a) HSR follows directly from Eq. (3.2.6), which is a radius equal to the magnitude of the maximum height difference in the study area, i.e.,

$$HSR = |\Delta z_{\max}| \quad (3.2.7)$$

- b) ESR is calculated from the magnitude of the maximum height difference among all the pairs of computation (P) and roving (R) points in the area bounded by a circle of radius equal to the HSR. This gives the ESR. The TC solution with any radius less than the ESR will always diverge. Computation of the ESR is time-consuming, especially when the maximum height difference is large, the size of the study area is large, and a high-resolution DEM is used. We thus define the ESR as

$$ESR = |\max(\Delta z_{PR})| \forall \left\{ \begin{array}{l} P(x_p, y_p) \subseteq (x_{\min} \leq x_p \leq x_{\max}, y_{\min} \leq y_p \leq y_{\max}) \\ \& R(x, y) : ((x - x_p)^2 + (y - y_p)^2 - \Delta z_{\max}^2 \leq 0) \end{array} \right\} \quad (3.2.8)$$

- c) OSR is the upper range in the study area. The range is computed by taking the difference between the maximum and minimum height values in an area around each cell, bounded by a circle of radius equal to the HSR. The upper range is the maximum of these range values in the entire study area. OSR can be computed faster than the ESR as

$$OSR = \max(range_c); \quad \left. \begin{array}{l} range_c = (\max(z)_c - \min(z)_c) \\ \text{where } C \equiv ((x - x_p)^2 + (y - y_p)^2 - \Delta z_{\max}^2 \leq 0) \\ \forall (x_p, y_p) \subseteq (x_{\min} \leq x_p \leq x_{\max}, y_{\min} \leq y_p \leq y_{\max}) \end{array} \right\} \quad (3.2.9)$$

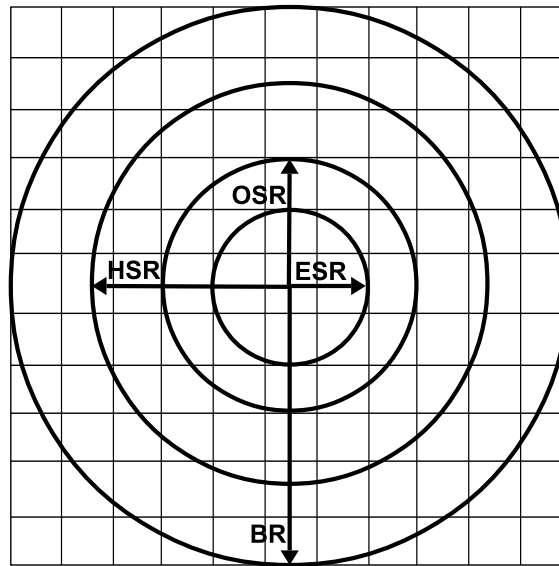


Figure 3.2.1: The four integration domains. BR is the bounding radius of the whole integration area that defines the integration radius. HSR, OSR and ESR are the height-dependent, optimal and exact separating radii, respectively.

ii) Truncation of the binomial expansion of TC solution

To test the convergence of the TC solution using the proposed choices of separating radii (HSR, ESR, OSR), we conducted the computations over five rugged topographies in the Himalayas with the SRTM 1"×1" DEM. The most rugged region was bounded within 27°N to 28°N latitude and 86°E to 87°E longitude where the height varies from 190 m to 8748 m. HSR, ESR, and OSR for this area are computed as 8558 m, 4261 m, and 5456 m, respectively. The same information about the other four study areas can be found in Goyal et al. (2020).

We used D/FFT in a tenth-order binomial expansion to compute TC with an integration radius of 111,320 m (BR) minus the three separating radii (HSR, ESR and OSR). This is done because we use D/FFT only in the outer zones. Table 3.2.1 shows the value of each TC term for the study area mentioned in the preceding paragraph.

Table 3.2.1: Descriptive statistics of planar TCs (in mGal) in the outer zone up to the tenth order with the separating radii of HSR = 8558 m, ESR = 4261 m and OSR = 5456 m and BR = 111320 m

TC term	Separating radius	Min	Max	Mean	STD
TC_1	HSR	1.237	76.047	9.195	5.393
	ESR	1.299	124.770	12.648	7.717
	OSR	1.278	107.603	11.361	6.865
TC_2	HSR	-2.45	-8.71×10^{-4}	-7.07×10^{-2}	1.00×10^{-1}
	ESR	-11.399	-8.95×10^{-4}	-2.01×10^{-1}	3.19×10^{-1}
	OSR	-7.402	-8.8×10^{-4}	-1.40×10^{-1}	2.16×10^{-1}
TC_3	HSR	1.10×10^{-6}	1.73×10^{-1}	1.74×10^{-3}	4.30×10^{-3}
	ESR	1.11×10^{-6}	2.299	1.19×10^{-2}	3.58×10^{-2}
	OSR	1.10×10^{-6}	1.128	6.15×10^{-3}	1.75×10^{-2}
TC_4	HSR	-1.69×10^{-1}	-1.84×10^{-9}	-7.84×10^{-5}	2.89×10^{-4}
	ESR	-6.50×10^{-1}	-1.85×10^{-9}	-1.32×10^{-3}	6.66×10^{-3}
	OSR	-2.27×10^{-1}	-1.84×10^{-9}	-5.00×10^{-4}	2.31×10^{-3}
TC_5	HSR	3.61×10^{-12}	1.92×10^{-3}	4.95×10^{-6}	2.54×10^{-5}
	ESR	3.58×10^{-12}	2.30×10^{-1}	2.11×10^{-4}	1.67×10^{-3}
	OSR	3.60×10^{-12}	5.32×10^{-2}	5.78×10^{-5}	4.00×10^{-4}
TC_6	HSR	-2.40×10^{-4}	-7.88×10^{-15}	-3.90×10^{-7}	2.66×10^{-6}
	ESR	-8.97×10^{-2}	1.51×10^{-13}	-4.34×10^{-5}	5.06×10^{-4}
	OSR	-1.36×10^{-2}	-4.70×10^{-15}	-8.45×10^{-6}	8.27×10^{-5}
TC_7	HSR	-7.23×10^{-18}	3.48×10^{-5}	3.60×10^{-8}	3.15×10^{-7}
	ESR	-2.52×10^{-9}	3.71×10^{-2}	1.07×10^{-5}	1.74×10^{-4}
	OSR	-5.5×10^{-11}	3.76×10^{-3}	1.46×10^{-6}	1.92×10^{-5}
TC_8	HSR	-5.31×10^{-6}	7.60×10^{-13}	-3.74×10^{-9}	4.08×10^{-8}
	ESR	-1.61×10^{-6}	9.71×10^{-8}	-3.05×10^{-6}	6.60×10^{-5}
	OSR	-1.08×10^{-3}	1.70×10^{-9}	-2.86×10^{-7}	4.88×10^{-6}
TC_9	HSR	-2.97×10^{-12}	8.45×10^{-7}	4.26×10^{-10}	5.67×10^{-9}
	ESR	-1.96×10^{-6}	7.24×10^{-3}	9.71×10^{-7}	2.66×10^{-5}
	OSR	-1.51×10^{-8}	3.28×10^{-4}	6.17×10^{-8}	1.31×10^{-6}
TC_{10}	HSR	-1.39×10^{-7}	1.19×10^{-11}	-5.24×10^{-11}	8.32×10^{-10}
	ESR	-3.33×10^{-3}	3.50×10^{-6}	-3.37×10^{-7}	1.13×10^{-5}
	OSR	-1.02×10^{-4}	1.67×10^{-7}	-1.44×10^{-8}	3.74×10^{-7}

Table 3.2.1 shows that fewer TC terms are needed to achieve convergence (of <1 μ Gal) with the HSR. However, the HSR makes the inner zone larger (cf. Figure 3.2.1), increasing the computation time for the mass-prism integration. Conversely, the ESR makes the inner zone smallest but needs the largest number of TC terms that will require more computer memory. Also, it takes a longer time to compute the ESR value. The OSR offers a compromise that balances the computation of its radius, the number of TC terms

required to achieve convergence, and computation time of the inner zone by mass prisms. We acknowledge that the exact number of TC terms required will vary depending on the study area, but we have deliberately chosen the extreme example of a 30 m DEM over Mount Everest, where convergence is achieved using six binomial terms with HSR and nine terms with OSR.

Since the above condition of the number of binomial terms is devised from the experiments in one of the most rugged topographies on the planet, it can be taken true at all times. So, we prefer and suggest working with OSR and nine terms of the binomial expansion.

iii) Numerical approach to analytical mass-prism integration

The mass-prism integration method assumes that the DEM grid cells define right-rectangular prisms with length and width given by the DEM resolution in the x and y directions, respectively. The height of the prism is defined by the height difference of the computation and roving points (Δz).

The analytical solution of Eq. (3.2.1) is

$$TC = \left[\left[\left[x \log(y+r) + y \log(x+r) - z \tan^{-1} \frac{xy}{zr} \right]_{x_1}^{x_2} \right]_{y_1}^{y_2} \right]_{z_1}^{z_2} \quad (3.2.10)$$

which is a simplified, efficient and accurate version (Banerjee and Gupta 1977; Forsberg 1984) of the solution given by Nagy (1966). Expanding Eq. (3.2.10) with respect to its limits gives

$$\begin{aligned}
TC = & \left. \begin{aligned}
& x_2 \log(y_2 + r_{222}) - x_2 \log(y_2 + r_{221}) - x_2 \log(y_1 + r_{212}) + x_2 \log(y_1 + r_{211}) - \\
& x_1 \log(y_2 + r_{122}) - x_1 \log(y_2 + r_{121}) - x_1 \log(y_1 + r_{112}) + x_1 \log(y_1 + r_{111}) + \\
& y_2 \log(x_2 + r_{222}) - y_2 \log(x_2 + r_{221}) - y_2 \log(x_1 + r_{122}) + y_2 \log(x_1 + r_{121}) - \\
& y_1 \log(x_2 + r_{212}) + y_1 \log(x_2 + r_{211}) + y_1 \log(x_1 + r_{112}) - y_1 \log(x_1 + r_{111}) - \\
& z_2 \tan^{-1} \left(\frac{x_2 y_2}{z_2 r_{222}} \right) + z_2 \tan^{-1} \left(\frac{x_2 y_1}{z_2 r_{212}} \right) + z_2 \tan^{-1} \left(\frac{x_1 y_2}{z_2 r_{122}} \right) - z_2 \tan^{-1} \left(\frac{x_1 y_1}{z_2 r_{112}} \right) + \\
& z_1 \tan^{-1} \left(\frac{x_2 y_2}{z_1 r_{221}} \right) - z_1 \tan^{-1} \left(\frac{x_2 y_1}{z_1 r_{211}} \right) - z_1 \tan^{-1} \left(\frac{x_1 y_2}{z_1 r_{121}} \right) + z_1 \tan^{-1} \left(\frac{x_1 y_1}{z_1 r_{111}} \right)
\end{aligned} \right\} \quad (3.2.11)
\end{aligned}$$

where $z_1 = 0$; $z_2 = H_p - H_i$; x_1, x_2, y_1, y_2 are the planar coordinates of a prism assuming the computation point to be at the origin of the planar coordinate system. The order of subscripts of $r = \sqrt{x^2 + y^2 + z^2}$ represents the order of coordinates (x, y, z) , and the subscript value represents the lower or upper bound of that coordinate. For example, r_{122} represents $\sqrt{x_1^2 + y_2^2 + z_2^2}$.

Rearranging the terms in Eq. (3.2.11), the analytical formula for the TC using right-rectangular mass prisms (*TCM*) is

$$\begin{aligned}
TCM = & \left. \begin{aligned}
& x_2 \left[\log \left(\frac{(y_2 + r_{222})(y_1 + r_{211})}{(y_2 + r_{221})(y_1 + r_{212})} \right) \right] - x_1 \left[\log \left(\frac{(y_2 + r_{122})(y_1 + r_{111})}{(y_2 + r_{121})(y_1 + r_{112})} \right) \right] + \\
& y_2 \left[\log \left(\frac{(x_2 + r_{222})(x_1 + r_{121})}{(x_2 + r_{221})(x_1 + r_{122})} \right) \right] - y_1 \left[\log \left(\frac{(x_2 + r_{212})(x_1 + r_{111})}{(x_2 + r_{211})(x_1 + r_{112})} \right) \right] - \\
& z_2 \left[\tan^{-1} \left(\frac{x_2 y_2}{z_2 r_{222}} \right) - \tan^{-1} \left(\frac{x_2 y_1}{z_2 r_{212}} \right) - \tan^{-1} \left(\frac{x_1 y_2}{z_2 r_{122}} \right) + \tan^{-1} \left(\frac{x_1 y_1}{z_2 r_{112}} \right) \right] + \\
& z_1 \left[\tan^{-1} \left(\frac{x_2 y_2}{z_1 r_{221}} \right) - \tan^{-1} \left(\frac{x_2 y_1}{z_1 r_{211}} \right) - \tan^{-1} \left(\frac{x_1 y_2}{z_1 r_{121}} \right) + \tan^{-1} \left(\frac{x_1 y_1}{z_1 r_{111}} \right) \right]
\end{aligned} \right\} \quad (3.2.12)
\end{aligned}$$

Solving the TC integral Eq. (3.2.1) with respect to z is convenient compared to x and y . Therefore, we extended the trapezoidal rule for single integration to double integration for solving the surface integral achieved after analytical linear integration of Eq. (3.2.1) with respect to z . According to the trapezoidal rule for single integration with $n = 2$ subintervals, we have (for any function in variable x)

$$\int_a^b f(x)dx \approx \frac{g}{2} \left[f(a) + 2f\left(\frac{a+b}{2}\right) + f(b) \right], \quad g = \frac{b-a}{n} \quad (3.2.13)$$

Extending Eq. (3.2.13) to solve double integration gives

$$\left. \begin{aligned} \int_a^b \left(\int_c^d f(x, y) dy \right) dx &\approx \int_a^b \left(\frac{d-c}{4} \left[f(x, c) + 2f\left(x, \frac{c+d}{2}\right) + f(x, d) \right] \right) dx \\ &= \int_a^b \left(\frac{d-c}{4} \right) f(x, c) dx + \int_a^b 2 \left(\frac{d-c}{4} \right) f\left(x, \frac{c+d}{2}\right) dx + \int_a^b \left(\frac{d-c}{4} \right) f(x, d) dx \end{aligned} \right\} \quad (3.2.14)$$

$$\int_a^b \left(\int_c^d f(x, y) dy \right) dx = TT1 + TT2 + TT3 \quad (3.2.15)$$

where $TT1$, $TT2$, $TT3$ represent the three integral terms in Eq. (3.2.14). By applying the trapezoidal rule for $n = 2$ to these three terms individually, we get

$$\left. \begin{aligned} TT1 &= \left(\frac{b-a}{4} \right) \left(\frac{d-c}{4} \right) \left[f(a, c) + 2f\left(a, \frac{c+d}{2}\right) + f(a, d) \right] \\ TT2 &= 2 \left(\frac{b-a}{4} \right) \left(\frac{d-c}{4} \right) \left[f\left(\frac{a+b}{2}, c\right) + 2f\left(\frac{a+b}{2}, \frac{c+d}{2}\right) + f\left(\frac{a+b}{2}, d\right) \right] \\ TT3 &= \left(\frac{b-a}{4} \right) \left(\frac{d-c}{4} \right) \left[f(b, c) + 2f\left(b, \frac{c+d}{2}\right) + f(b, d) \right] \end{aligned} \right\} \quad (3.2.16)$$

The analytical linear integral solution of the TC with respect to z is

$$TC = G\rho \left[\iiint_E \int_{z_1=0}^{z_2=h_p-h_i} \frac{z}{r^3} dz dy dx \right] = G\rho \left[\int_{x_1}^{x_2} \int_{y_1}^{y_2} \left(\frac{1}{r(x, y, z_1)} - \frac{1}{r(x, y, z_2)} \right) dy dx \right] \quad (3.2.17)$$

Using the following substitutions of Eq. (3.2.18) in Eq. (3.2.16)

$$\left. \begin{aligned} a &= x_1, \quad b = x_2, \quad c = y_1, \quad d = y_2 \\ b - a &= x_2 - x_1 = \Delta x, \quad c - d = y_2 - y_1 = \Delta y \\ z_1 &= 0, \quad z_2 = h_p - h_i = \Delta z \\ \frac{a+b}{2} &= \frac{x_1 + x_2}{2} = \bar{x}, \quad \frac{c+d}{2} = \frac{y_1 + y_2}{2} = \bar{y} \end{aligned} \right\} \quad (3.2.18)$$

and rearranging the terms, the TC with the trapezoidal rule (TCT) can be calculated using

$$TCT = G\rho \left\{ \left(\frac{\Delta x}{4} \right) \left(\frac{\Delta y}{4} \right) \left[\left(\frac{1}{r(x_1, y_1)} - \frac{1}{r(x_1, y_1, \Delta z)} \right) + 2 \left(\frac{1}{r(x_1, \bar{y})} - \frac{1}{r(x_1, \bar{y}, \Delta z)} \right) + \left(\frac{1}{r(x_1, y_2)} - \frac{1}{r(x_1, y_2, \Delta z)} \right) \right] + \right. \\ \left. 2 \left(\frac{\Delta x}{4} \right) \left(\frac{\Delta y}{4} \right) \left[\left(\frac{1}{r(\bar{x}, y_1)} - \frac{1}{r(\bar{x}, y_1, \Delta z)} \right) + 2 \left(\frac{1}{r(\bar{x}, \bar{y})} - \frac{1}{r(\bar{x}, \bar{y}, \Delta z)} \right) + \left(\frac{1}{r(\bar{x}, y_2)} - \frac{1}{r(\bar{x}, y_2, \Delta z)} \right) \right] + \right. \\ \left. \left(\frac{\Delta x}{4} \right) \left(\frac{\Delta y}{4} \right) \left[\left(\frac{1}{r(x_2, y_1)} - \frac{1}{r(x_2, y_1, \Delta z)} \right) + 2 \left(\frac{1}{r(x_2, \bar{y})} - \frac{1}{r(x_2, \bar{y}, \Delta z)} \right) + \left(\frac{1}{r(x_2, y_2)} - \frac{1}{r(x_2, y_2, \Delta z)} \right) \right] \right\} \quad (3.2.19)$$

We also derived the TC formula using the Simpson's rule (*TCS*), which is given by

$$TCS = G\rho \left\{ \left(\frac{\Delta x}{6} \right) \left(\frac{\Delta y}{6} \right) \left[\left(\frac{1}{r(x_1, y_1)} - \frac{1}{r(x_1, y_1, \Delta z)} \right) + 4 \left(\frac{1}{r(x_1, \bar{y})} - \frac{1}{r(x_1, \bar{y}, \Delta z)} \right) + \left(\frac{1}{r(x_1, y_2)} - \frac{1}{r(x_1, y_2, \Delta z)} \right) \right] + \right. \\ \left. 4 \left(\frac{\Delta x}{6} \right) \left(\frac{\Delta y}{6} \right) \left[\left(\frac{1}{r(\bar{x}, y_1)} - \frac{1}{r(\bar{x}, y_1, \Delta z)} \right) + 4 \left(\frac{1}{r(\bar{x}, \bar{y})} - \frac{1}{r(\bar{x}, \bar{y}, \Delta z)} \right) + \left(\frac{1}{r(\bar{x}, y_2)} - \frac{1}{r(\bar{x}, y_2, \Delta z)} \right) \right] + \right. \\ \left. \left(\frac{\Delta x}{6} \right) \left(\frac{\Delta y}{6} \right) \left[\left(\frac{1}{r(x_2, y_1)} - \frac{1}{r(x_2, y_1, \Delta z)} \right) + 4 \left(\frac{1}{r(x_2, \bar{y})} - \frac{1}{r(x_2, \bar{y}, \Delta z)} \right) + \left(\frac{1}{r(x_2, y_2)} - \frac{1}{r(x_2, y_2, \Delta z)} \right) \right] \right\} \quad (3.2.20)$$

Both the derived formulas (Eqs. (3.2.19) and (3.2.20)) were tested on two DEMs (1-arc-second and 3-arc-second) in three different types of topographies (plains, undulating and mountainous). These were compared with the mass-prism analytical integration solution (Eq. (3.2.12)). Both the proposed methods (*TCT* and *TCS*) decrease the computation time by ~50%. Detailed results on this comparison can be found in Goyal et al. (2019b, 2020), from where we deduce that *TCT* is comparatively equivalent to *TCM*.

In the trapezoidal and Simpson's rules of integration (*TCT* and *TCS*), the numerical results can be improved by increasing the number of subintervals, but at additional computational cost. *TCT* and *TCS* were re-derived using a combination of $n = 2$ subintervals for the inner limit and $n = 4$ for the outer limit. This was done because only an even number of subintervals can be used in Simpson's rule. On comparison, a marginal improvement was observed in the results from *TCT* and *TCS* with respect to the analytical mass-prism integration. However, the time taken for these computations became equivalent to the analytical integration, thus defeating the purpose of the new method. Hence, it is recommended to use *TCT* with $n = 2$ subintervals only, as is given in Eq. (3.2.19).

The CUT method requires a high-resolution TC grid for gridding the anomalies or so-called re-construction of the Faye anomalies (Featherstone and Kirby, 2000). Therefore, we computed the planar TC at 3'' \times 3'' resolution for India and adjacent regions using MERIT DEM (Yamazaki et al., 2017). The whole region was divided into 95 tiles each covering 8 $^{\circ}$ \times 8 $^{\circ}$ area. All these tiles have an overlap of 4 $^{\circ}$ on all the sides to avoid the windowing effect (Sideris, 1984; Bracewell, 1986). The BR or the integration radius is kept equal to 111320 m based on the change in the values of planar TC with varying BR (5500 m to 166980 m), for a few tiles. The inner and outer zones were separated using the OSR. The inner zone computations were done with *TCT* method and outer zone computations with D/FFT having nine terms of the binomial expansion. The 3'' \times 3'' and block-averaged 0.02 $^{\circ}$ \times 0.02 $^{\circ}$ planar TC maps for India and adjacent regions are shown in Figures 3.2.2 (a) and (b), respectively. The scatter plot of the 0.02 $^{\circ}$ \times 0.02 $^{\circ}$ TCs with respect to the heights is shown in Figure 3.2.3 (a), and the histogram is given in Figure 3.2.3 (b).

Figure 3.2.2 shows that larger values of TCs are obtained in the regions with high peaks and rapidly undulating terrain, as expected. In the plateau regions where we have high elevation but relatively lesser undulating terrain, TCs have smaller values. Figure 3.2.3a shows that TCs can have a long-range (\sim 1 mGal to 50 mGal) for the areas having considerable heights (\sim 4000 m to 6500 m). Thus, TC vary noticeably in the regions with the undulating terrain compared to the regions only having higher elevations.

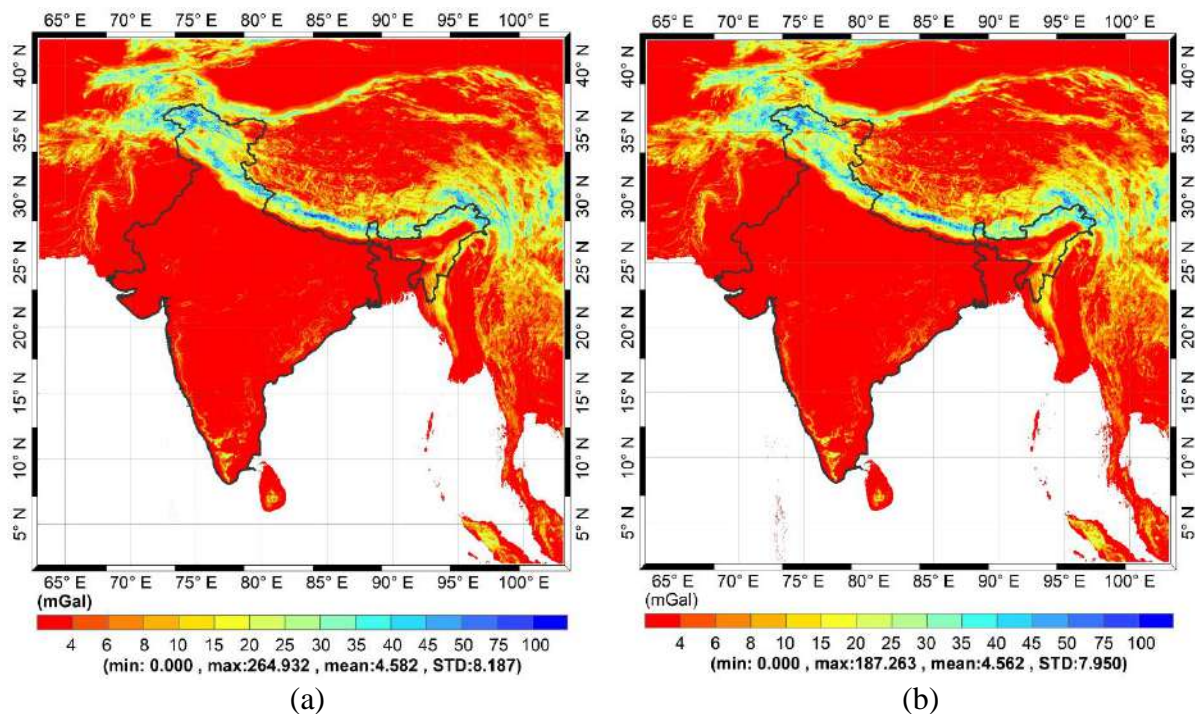


Figure 3.2.2: Local planar TC over India and adjacent countries at a) $3'' \times 3''$ grid, b) $0.02^\circ \times 0.02^\circ$ grid using spatial-spectral combined approach.

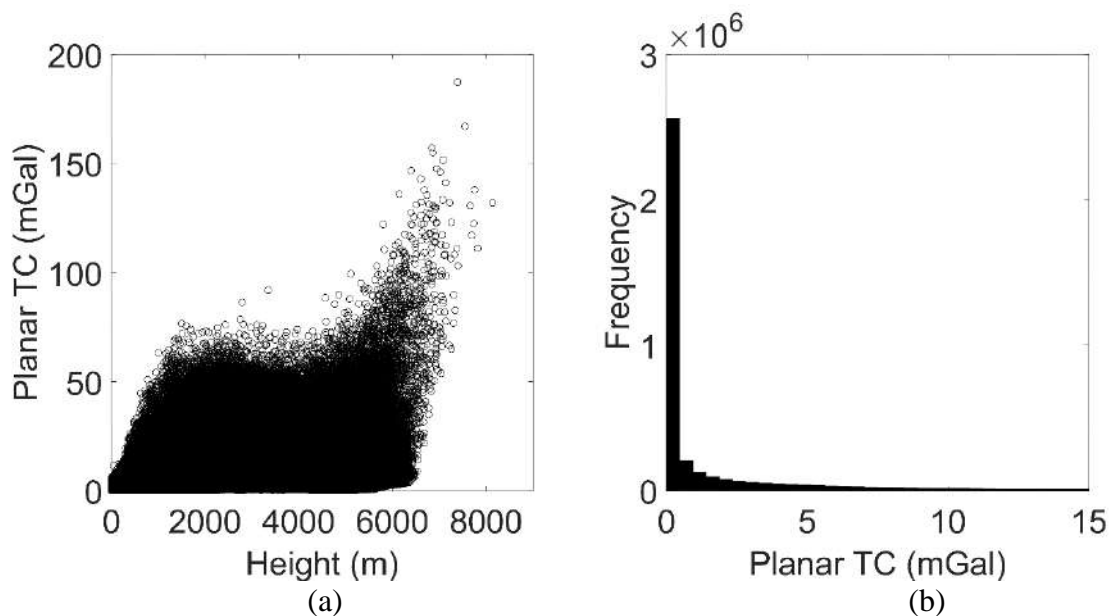


Figure 3.2.3: a) Scatter plot of $0.02^\circ \times 0.02^\circ$ grid TCs with respect to the heights, b) histogram of $0.02^\circ \times 0.02^\circ$ grid TCs.

3.2.2 Topographic corrections in the UNB method

The topographical corrections in the UNB method originate from the use of Helmert's (1884) second method of condensation, where all the topographical masses (and atmospheric masses, Section 3.3) outside the geoid are condensed as a thin layer on the geoid. The gravitational potential of the topographical masses and their corresponding condensation layer will not be exactly the same. However, it has two advantages. Firstly, condensing the topographical masses will achieve the desired harmonicity of the topographical potential above geoid (to be more precise, it should be co-geoid or compensated geoid). Secondly, instead of working with the topographical masses between the geoid and the Earth's surface that can cause a geoid undulation value as large as 1000 m (Martinec and Vaniček, 1994a), we can work with residual topographical masses. These residual topographical masses are the difference between the actual masses and the condensed layer. The gravitational potential generated from these residual topographical masses causes a substantially smaller effect on the geoid undulation values (of the order of 2 m, Martinec and Vaniček, 1994a) as compared to the topographical potential of the actual masses.

In Helmert's second method of condensation, the following three things have to be dealt with:

- i) The gravitational attraction of the residual topographic masses. In the literature, there are three names given to this: attraction change effect (Wichiencharoen, 1982), topographical attraction effect (Vaniček and Kleusberg, 1987), and the most common term, DTE (Martinec and Vaniček, 1994a).
- ii) The difference between the potentials of the actual topographical masses and the condensed topographical layer at any point on the geoid is known as residual

topographical potential. This means, with the condensed topographical masses as a surface layer, we are not computing the geoid but a different surface, known as the co-geoid (compensated geoid). Therefore, a correction term for the effect of residual topographical potential on the geoid needs to be applied. This is termed as either separation of geoid and co-geoid, or indirect effect of topography or, more precisely, the PITE.

- iii) Residual topographical potential indicates that the computation point or gravity anomaly does not correspond to the computed co-geoid but to the geoid (due to the use of orthometric heights). Thus, another correction is required that ensures that the gravity anomaly is on the co-geoid. This is realised by computing the gravitational acceleration of the masses between the co-geoid and the geoid, which is too small that there is a common practice of neglecting it. This is known as the SITE. Sjöberg (2015) discussed that the SITE could reach a maximum of -0.6 mGal with Helmert's second method of condensation and this translates to a -0.07 m effect on the geoid undulation (calculated using Featherstone and Olliver, 1997, Eq. 14). Therefore, SITE should not be neglected from the viewpoint of cm-level precise geoid.

Vaniček and Kleusberg (1987) apply the DTE and SITE on the gravity anomaly at the topographical surface. On the contrary, Wang and Rapp (1990) suggested applying the two corrections on the downward continued gravity anomaly. Here, we are dealing with the UNB's approach and hence, will discuss the DTE and SITE as applied to the gravity anomaly at the Earth's surface while PITE is applied on the geoid (~co-geoid) undulations, as per UNB.

We will now try to formulate the above discussions using some equations. Before this, we remark that there exist many dissimilarities regarding the formulation of the above

three terms. It is due to the choices of combining downward continuation with the topographic correction (Wang and Rapp, 1990) and/or the spherical (Martinec and Vaníček, 1994a; 1994b) versus a planar approximation (Wichiencharoen, 1982; Vaníček and Kleusberg, 1987). Here, we will not provide all the formulations instead, see the cited references. We will use spherical approximation in the following discussions.

Equations (3.2.21) and (3.2.22) give the potential of the topographical masses (V^t) and the condensed topographical surface layer (V^{ct}), respectively (Martinec and Vaníček, 1994a)

$$V^t(r_{cp}, \Omega) = G\rho \iint_{\Omega_{\oplus}} \int_{z=R}^{R+H(\Omega')} \frac{z^2}{(r_{cp}^2 + z^2 - 2r_{cp}z \cos \psi)^{1/2}} dz d\Omega' \quad (3.2.21)$$

$$V^{ct}(r_{cp}, \Omega) = GR^2 \iint_{\Omega_{\oplus}} \frac{\sigma_t(\Omega')}{(r_{cp}^2 + R^2 - 2r_{cp}R \cos \psi)^{1/2}} d\Omega' \quad (3.2.22)$$

where ψ is the spherical angular distance between two points on the sphere, σ_t is the surface density of the condensed topographical layer and is given by (Wichiencharoen, 1982)

$$\sigma_t(\Omega) = \frac{\rho}{R^2} \int_{z=R}^{R+H(\Omega')} z^2 dz = \rho \left(H(\Omega') + \frac{H^2(\Omega')}{R} + \frac{H^3(\Omega')}{3R^2} \right) \quad (3.2.23)$$

In this study, we use Eq. (3.2.23) that is a condensation density function with the mass-conservation scheme, i.e., the mass of the Earth is not changed. A disadvantage attached with the use of Eq. (3.2.23) is that there will be a change in the geocentre and hence, degree-one terms will come into play (Hörmander, 1976; Novák, 2000). There could be other choices of condensed density functions (Martinec, 1993; 1998), such as i) geocentre-conservation scheme or ii) more complicated mass and geocentre conservation scheme.

Both V^t and V^{ct} can be divided into a spherical shell part and its corresponding roughness part. This is something like a Bouguer correction and TC in spherical approximation (Kuhn et al., 2009). Therefore, the topographical potential (Eq. (3.2.21)) at any point is written as

$$V^t(r_{cp}, \Omega) = G\rho \left\{ \iint_{\Omega_{\oplus}} \int_{z=R}^{R+H(\Omega)} \frac{z^2}{(r_{cp}^2 + z^2 - 2r_{cp}z \cos \psi)^{1/2}} dz d\Omega' + \right. \\ \left. G\rho \iint_{\Omega_{\oplus}} \int_{z=R+H(\Omega)}^{R+H(\Omega)} \frac{z^2}{(r_{cp}^2 + z^2 - 2r_{cp}z \cos \psi)^{1/2}} dz d\Omega' \right\} \quad (3.2.24)$$

The linear integral in Eq. (3.2.24) can be computed as (Gradshteyn and Ryzhik, 1980)

$$\int_{z=z_{ll}}^{z_{ul}} \frac{z^2}{(r_{cp}^2 + z^2 - 2r_{cp}z \cos \psi)^{1/2}} dz = \left[\left(\frac{z_{ul} + 3r_{cp} \cos \psi}{2} \sqrt{r_{cp}^2 + z_{ul}^2 - 2r_{cp}z_{ul} \cos \psi} \right) - \right. \\ \left. \left(\frac{z_{ll} + 3r_{cp} \cos \psi}{2} \sqrt{r_{cp}^2 + z_{ll}^2 - 2r_{cp}z_{ll} \cos \psi} \right) + \right. \\ \left. \frac{r_{cp}^2}{2} (3 \cos^2 \psi - 1) \times \right. \\ \left. \log \left| \frac{z_{ul} - r_{cp} \cos \psi + \sqrt{r_{cp}^2 + z_{ul}^2 - 2r_{cp}z_{ul} \cos \psi}}{z_{ll} - r_{cp} \cos \psi + \sqrt{r_{cp}^2 + z_{ll}^2 - 2r_{cp}z_{ll} \cos \psi}} \right| \right] \quad (3.2.25)$$

Similarly, the gravitational potential of the condensed topographical surface layer at any point (Eq. (3.2.22)) can be written as

$$V^{ct}(r_{cp}, \Omega) = G\rho \left\{ \iint_{\Omega_{\oplus}} \frac{(R+H)^3 - R^3}{3(r_{cp}^2 + R^2 - 2r_{cp}R \cos \psi)^{1/2}} d\Omega' \right. \\ \left. + G\rho \iint_{\Omega_{\oplus}} \frac{(R+H')^3 - (R+H)^3}{3(r_{cp}^2 + R^2 - 2r_{cp}R \cos \psi)^{1/2}} d\Omega' \right\} \quad (3.2.26)$$

In Eqs. (3.2.24), (3.2.25) and (3.2.26) r_{cp} is the computation point i.e., $r_{cp} = R + H$ for computation at the Earth's surface and $r_{cp} = R$ for computation at the geoid.

Subtracting Eq. (3.2.26) from Eq. (3.2.24) the residual topographical potential

($\delta V^t = V^t - V^{ct}$) on the Earth's topography is obtained by

$$\delta V^t(R+H, \Omega) = G\rho \sum \sum \left[\left\{ \left(\frac{R+H'+3(R+H)\cos\psi}{2} \times \sqrt{(R+H)^2 + (R+H')^2 - 2(R+H)(R+H')\cos\psi} \right) - \left(\frac{R+H+3(R+H)\cos\psi}{2} \sqrt{(R+H)^2 + (R+H)^2 - 2(R+H)(R+H)\cos\psi} \right) + \frac{(R+H)^2}{2} (3\cos^2\psi - 1) \times \log \left| \frac{R+H' - (R+H)\cos\psi + \sqrt{(R+H)^2 + (R+H')^2 - 2(R+H)(R+H')\cos\psi}}{R+H - (R+H)\cos\psi + \sqrt{(R+H)^2 + (R+H)^2 - 2(R+H)(R+H)\cos\psi}} \right| \right\} - \left[\left(\frac{3R^2(H'-H) + 3R(H'^2 - H^2) + (H'^3 - H^3)}{3\sqrt{R^2 + (R+H)^2 - 2R(R+H)\cos\psi}} \right) \right] \Delta\varphi\Delta\lambda \right] \quad (3.2.27)$$

Therefore, the PITE is calculated using (Martinec and Vaníček, 1994b; Novák, 2000)

$$PITE = \frac{\delta V^t(R, \Omega)}{\gamma_0} \quad (3.2.28)$$

$$PITE = \frac{G\rho}{\gamma_0} \sum \sum \left[\left\{ -4\pi \left(\frac{H^2}{2} + \frac{H^3}{3R} \right) \right\} + \left\{ \left(\frac{R+H'+3R\cos\psi}{2} \sqrt{R^2 + (R+H')^2 - 2R(R+H')\cos\psi} \right) - \left(\frac{R+H+3R\cos\psi}{2} \sqrt{R^2 + (R+H)^2 - 2R(R+H)\cos\psi} \right) + \frac{R^2}{2} (3\cos^2\psi - 1) \times \log \left| \frac{R+H' - R\cos\psi + \sqrt{R^2 + (R+H')^2 - 2R(R+H')\cos\psi}}{R+H - R\cos\psi + \sqrt{R^2 + (R+H)^2 - 2R(R+H)\cos\psi}} \right| \right\} - \left[\left(\frac{3R^2(H'-H) + 3R(H'^2 - H^2) + (H'^3 - H^3)}{3\sqrt{R^2 + R^2 - 2RR\cos\psi}} \right) \right] \Delta\varphi\Delta\lambda \right] \quad (3.2.29)$$

and the SITE is given by (Novák, 2000)

$$SITE = \frac{2\delta V'(R+H, \Omega)}{(R+H)} \quad (3.2.30)$$

where, $\delta V'(R+H, \Omega)$ comes from Eq. (3.2.27).

The DTE is evaluated as (Martinec and Vaníček, 1994a; Novák, 2000)

$$DTE = \frac{\partial}{\partial r}(\delta V'(R+H, \Omega)) \quad (3.2.31)$$

$$DTE = G\rho \sum \sum \left\{ \left[\frac{\left(\left((R+H')^2 + 3(R+H)^2 \right) \cos\psi + (R+H)(R+H')(1-6\cos^2\psi) \right)}{\sqrt{(R+H')^2 + (R+H)^2 - 2(R+H')(R+H)\cos\psi}} - \frac{\left(\left((R+H)^2 + 3(R+H')^2 \right) \cos\psi + (R+H)(R+H')(1-6\cos^2\psi) \right)}{\sqrt{(R+H)^2 + (R+H')^2 - 2(R+H)(R+H')\cos\psi}} + (R+H)(3\cos^2\psi - 1) \right] \right. \\ \left. \log \left| \frac{(R+H') - (R+H)\cos\psi + \sqrt{(R+H')^2 + (R+H)^2 - 2(R+H')(R+H)\cos\psi}}{(R+H) - (R+H')\cos\psi + \sqrt{(R+H)^2 + (R+H')^2 - 2(R+H)(R+H')\cos\psi}} \right| - \left. \frac{\left((R\cos\psi - (R+H)) \left(3R^2(H'-H) + 3R(H'^2 - H^2) + (H'^3 - H^3) \right) \right)}{3 \left(\sqrt{R^2 + (R+H)^2 - 2R(R+H)\cos\psi} \right)^3} \right] \Delta\varphi\Delta\lambda \quad (3.2.32)$$

These topographic corrections (Eqs. (3.2.29), (3.2.30) and (3.2.32)) can be practically computed in two ways: i) global integration (brute force summation), or ii) dividing the integration area into two parts i.e., near and far zone contributions. The near-zone contribution is computed using the equations derived above and spherical harmonics are used for the far-zones (cf. Novák, 2000). In this study, we have evaluated the formulas for the topographic corrections using the global integration (summation) approach that utilises DEMs of different resolutions (e.g., Kuhn et al., 2009 for spherical Bouguer anomalies and spherical TCs).

The strategy for practical realisation of global integration is to use varying pre-decided integration radii for different (resolution) DEMs, i.e., different ‘fixed’ radii for innermost, near, far, and far-most zones. In the case of these fixed-type integration radii,

the roving point DEM cells for some computation points will overlap. Therefore, we cannot use a fixed radius for our computations. We can only speculate that the researchers might be taking this into account already, but an explicit mention of this issue is missing in the literature to the author's best knowledge. Hence, for working with cascading grids or multiple resolution DEM grids, we must use what we call a 'dynamic integration radius'.

This type of radius takes care of any overlapping/missing mass elements on moving the bounding box (integration domain) by one element of the finer resolution DEM. In simple words, dynamic integration radius for a given finer resolution DEM makes use of the 'extensions' (to the pre-defined fixed radii) that are adapted according to the relation between the location of the computation point and the resolution of the next coarser grid.

Though the overlapping of a few DEM cells (mostly in the transition boundaries of the different zones) might not affect the overall topographic correction value, this dynamic integration radius ensures that overlapping of the mass elements does not occur. The use of dynamic integration radius is essential not only in the global integration but also for the planar TCs where researchers use different resolution DEMs with pre-fixed integration radii (e.g., Gomez et al., 2013).

Another point is that the UNB method uses mean values of the computed topographic correction term. On the contrary, we think that the mean values should not be used as we are already working with the mean DEMs i.e., the coarse DEMs that are constructed by block averaging the high-resolution DEMs. Therefore, unlike the UNB strategy, we do not use, what we call, the mean of the mean values, instead the point values of the topographic correction terms computed at the gravity anomaly grid-nodes. These point values are considered to be already a mean value.

In addition to the above two modifications to the UNB strategy to compute the topographic effects, we make one more change in our computations. In the provided formulas, the radius of the geoid is approximated by the radius of the reference sphere. The UNB strategy uses a constant value of the radius, but Martinec (1993) suggests that this spherical approximation causes a maximum error of 30 mm (i.e., 0.3% ellipsoidal approximation error for $N = 100$ m) in the geoid undulation. Therefore, we use the geocentric radius to the surface of the GRS80 ellipsoid computed for each parallel of the latitude (Claessens, 2006, Chapter 6). Though not checked in this thesis, using the geocentric radius to the surface of the GRS80 ellipsoid may change the formulas for the ellipsoidal correction that are employed in the UNB method.

The DTE (Figure 3.2.4), SITE (Figure 3.2.6) and PITE (Figure 3.2.8) for India and adjacent regions are computed on a $0.02^\circ \times 0.02^\circ$ grid using MERIT $3'' \times 3''$ DEM and block averaged to $30'' \times 30''$, $5' \times 5'$ and $1^\circ \times 1^\circ$ resolutions. Figures 3.2.5, 3.2.7, and 3.2.9 show the scatter plots with respect to the heights and histograms of DTE, SITE, and PITE, respectively.

Figures 3.2.4 and 3.2.5 show that though the maximum and minimum DTE values reach -119.45 mGal and 340.66 mGal, respectively, ~99% of the total points have the value within [-50 mGal, +50 mGal] (and ~95% of the points within [-20 mGal, +20 mGal]). The DTE (Figure 3.2.5a) does not vary depending on the elevation as compared to the SITE (Figure 3.2.7a) and PITE (Figure 3.2.9a), both of which have a clear pattern of increasing absolute values with an increase in the elevation. Therefore, over India, SITE (Figure 3.2.6) and PITE (Figure 3.2.8) have larger values in the Himalayan belt followed by the Western ghats.

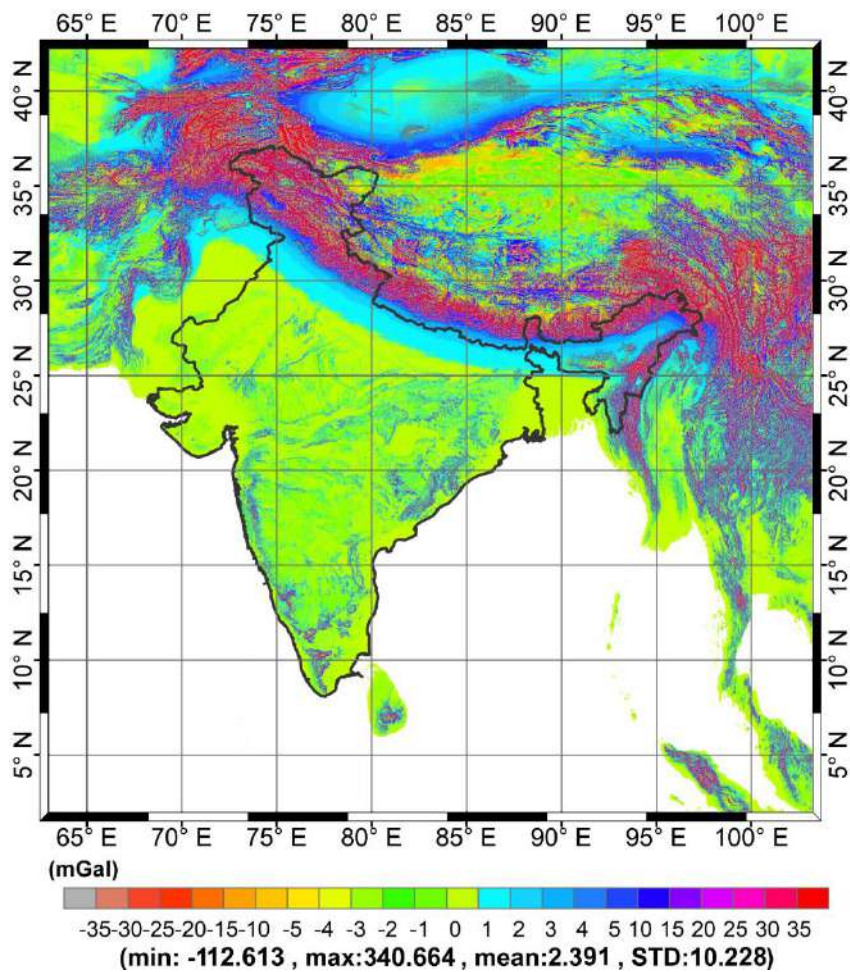


Figure 3.2.4: DTE over India and adjacent regions

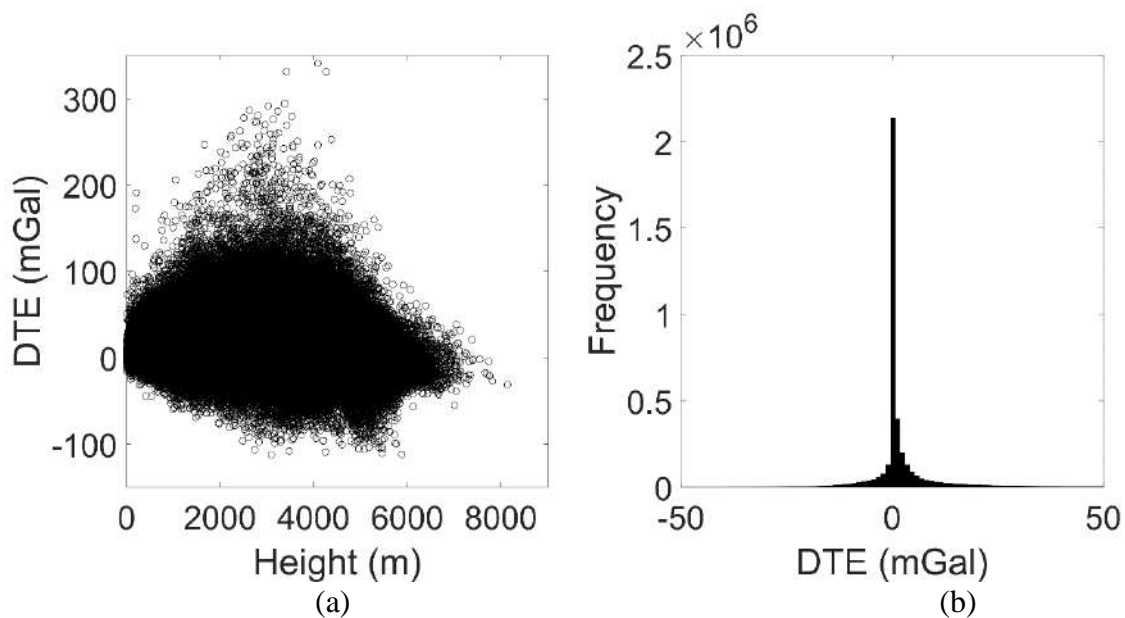


Figure 3.2.5: a) Scatter plot of DTE versus height; b) histogram of DTE

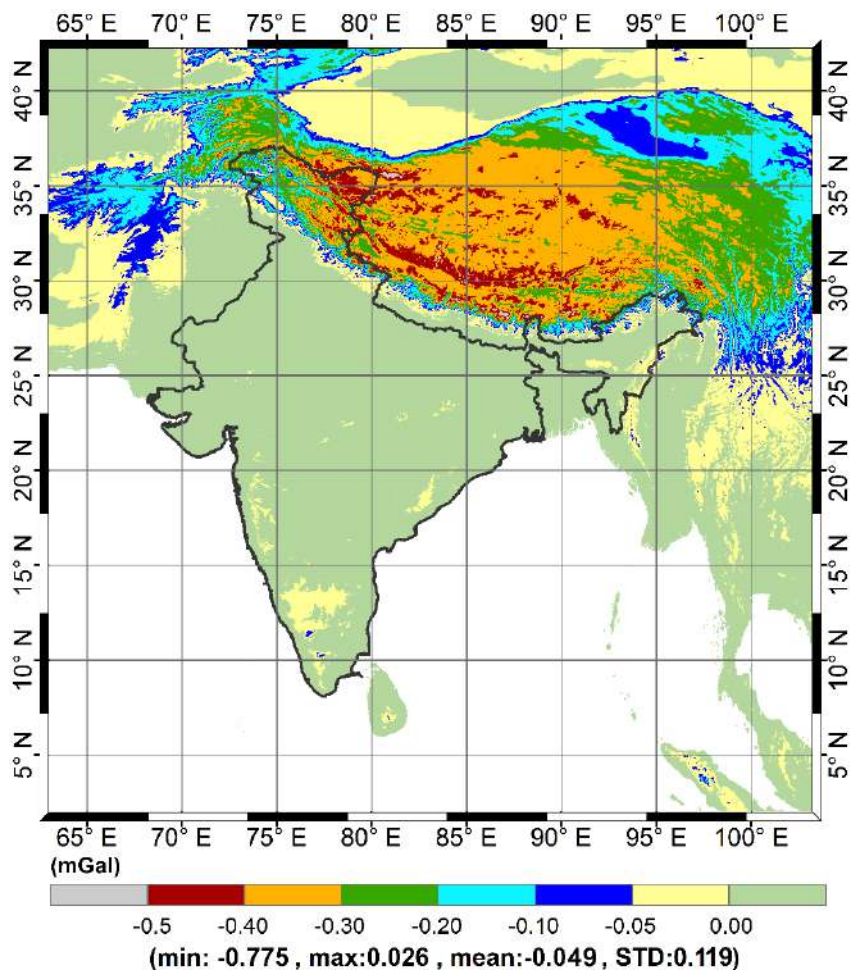


Figure 3.2.6: SITE over India and adjacent regions

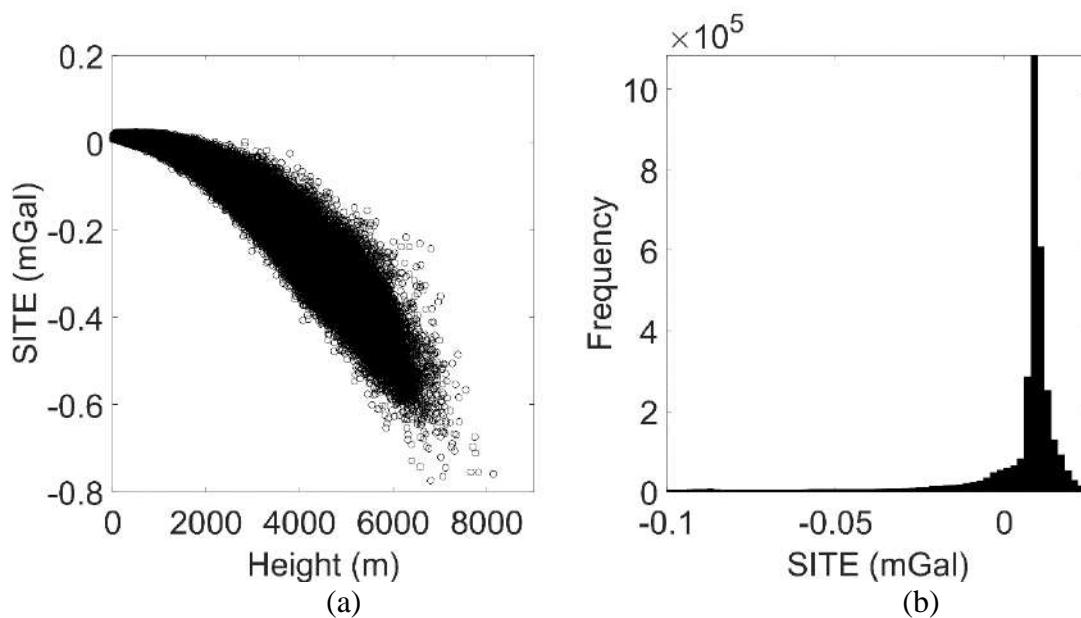


Figure 3.2.7: a) Scatter plot of SITE versus height; b) histogram of SITE

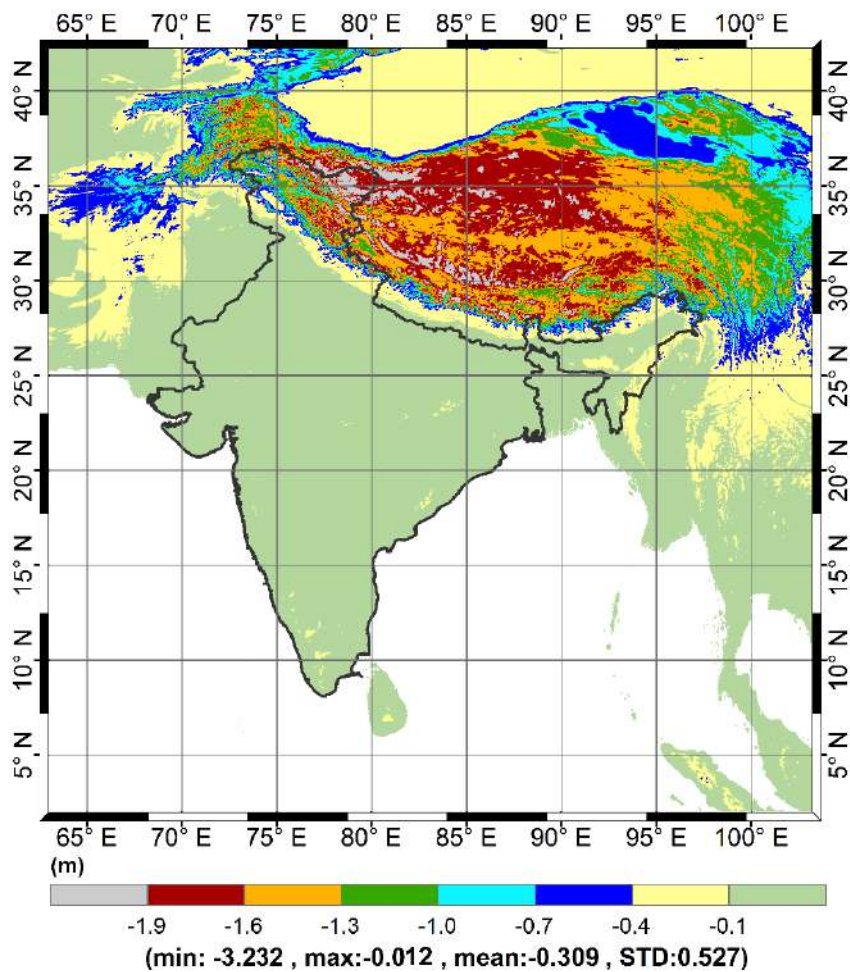


Figure 3.2.8: PITE over India and adjacent regions

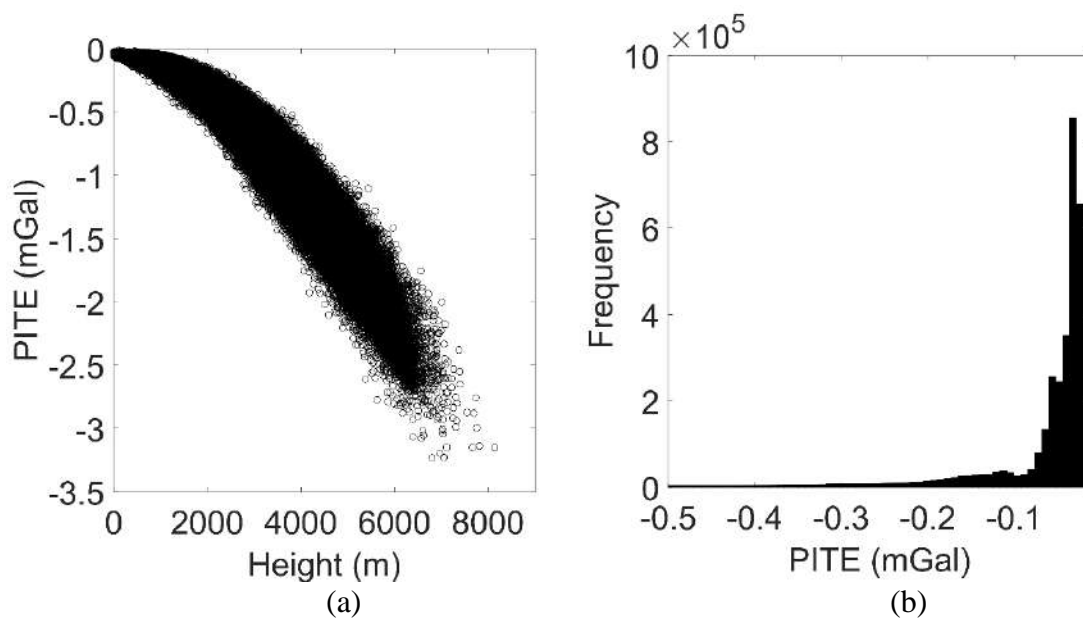


Figure 3.2.9 a) Scatter plot of PITE versus height; b) histogram of PITE

3.2.3 Topographic corrections in the KTH method

In the KTH method, SITE is not applied as a correction to account for gravity anomaly on the geoid instead of co-geoid but, it comes as a term in the derivation of topographic gravity anomaly (Sjöberg, 2014), which is termed DTE. Therefore, topographic corrections in the KTH method are divided into two effects: direct and indirect. The direct effect includes DTE and SITE, while the indirect effect is the PITE. The direct and indirect topographic effects have been studied in detail by the KTH group and hence derived several formulas (e.g., Sjöberg, 2000, 2001, Nahavandchi 1998; Nahavandchi and Sjöberg, 2001). The direct and indirect topographical effects in the KTH method are combinedly applied as the total topographical effect to the (approximate) geoid undulations.

Their strategy shows that the combined topographical effect cancels the complete gravitational attraction of the condensed topographical surface layer (Sjöberg and Bagherbandi, 2017). As such, they do not use the concept of Helmert's second method of condensation in the formulation of the topographical corrections. Instead, the reciprocal distance in the topographical potential (Eq. (3.2.21)) at the Earth's surface is expanded as an external-type series to give

$$V^t(R+H, \Omega) = G\rho R^2 \sum_{n=0}^{\infty} \left(\frac{R}{r_{cp}} \right)^{n+1} \left(\frac{1}{n+3} \iint_{\sigma} \left(\left(1 + \frac{H}{R} \right)^{n+3} - 1 \right) P_n(\cos\psi) d\sigma \right) \quad (3.2.33)$$

where n is the spherical harmonics degree and P_n is the Legendre polynomials of the first kind for degree n .

Expanding $\left(1 + \frac{H}{R} \right)^{n+3}$ in the Taylor series, they obtain

$$V'(R+H, \Omega) = G\rho R^2 \sum_{n=0}^{\infty} \left[\left(\frac{R}{r_{cp}} \right)^{n+1} \times \left(\iint_{\sigma} \left(\frac{H}{R} + \frac{n+2}{2} \left(\frac{H}{R} \right)^2 + \frac{(n+2)(n+1)}{6} \left(\frac{H}{R} \right)^3 \right) P_n(\cos\psi) d\sigma \right) \right] \quad (3.2.34)$$

Using spherical approximation of the boundary condition of physical geodesy (Heiskanen and Moritz, 1967, pg. 88) with topographical potential gives (Sjöberg, 2014, pg. 132)

$$\Delta g'(R+H, \Omega) = -\frac{\partial V'(R+H, \Omega)}{\partial r} - 2\frac{V'(R+H, \Omega)}{r} \quad (3.2.35)$$

where $\Delta g'$ is the topographical gravity anomaly (it should not be confused with free-air gravity anomaly on the topography).

Therefore, from Eqs. (3.2.34) and (3.2.35)

$$\Delta g'(R+H, \Omega) = G\rho R \sum_{n=0}^{\infty} \left[\left(\frac{R}{r_{cp}} \right)^{n+2} (n-1) \times \left(\iint_{\sigma} \left(\frac{H}{R} + \frac{n+2}{2} \left(\frac{H}{R} \right)^2 + \frac{(n+2)(n+1)}{6} \left(\frac{H}{R} \right)^3 \right) P_n(\cos\psi) d\sigma \right) \right] \quad (3.2.36)$$

Equation (3.2.35) shows that the DTE ($= -\Delta g'$) in the KTH technique is equivalent to the combination of DTE and SITE with the difference being that Eq. (3.2.35) uses the topographical potential and not the residual topographical potential.

Since the topographical effect will be added to the geoid undulation in the KTH method, we need to have the gravity anomaly (in this case topographical, Eq. (3.2.36)) on the geoid. Therefore, considering $r_{cp} \approx R$ and using Stokes's formula with Stokes's function in spectral form, the DTE on the approximate geoid (δN_{dir}^T) is given by (Sjöberg and Bagherbandi, 2017)

$$\delta N_{dir}^T = -\frac{G\rho R^2}{\gamma} \sum_{n=2}^{\infty} \left(\iint_{\sigma} \left(\frac{H}{R} + \frac{n+2}{2} \left(\frac{H}{R} \right)^2 + \frac{(n+2)(n+1)}{6} \left(\frac{H}{R} \right)^3 \right) P_n(\cos\psi) d\sigma \right) \quad (3.2.37)$$

Similarly, for computing the indirect topographical effect, the topographical potential (Eq. (3.2.21)) is expanded in surface harmonic series to obtain

$$\delta N_{indir}^T = \frac{G\rho R^2}{\gamma} \sum_{n=2}^{\infty} \left(\iint_{\sigma} \left(\frac{H}{R} - \frac{n-1}{2} \left(\frac{H}{R} \right)^2 + \frac{n(n-1)}{6} \left(\frac{H}{R} \right)^3 \right) P_n(\cos\psi) d\sigma \right) \quad (3.2.38)$$

where δN_{indir}^T is the indirect topographical effect on approximate geoid undulations.

Adding Eqs. (3.2.37) and (3.2.38) gives the combined total topographical effect

$$\delta N_{comb}^T = \delta N_{dir}^T + \delta N_{indir}^T \quad (3.2.39)$$

$$\delta N_{comb}^T = -\frac{G\rho}{\gamma} \sum_{n=2}^{\infty} \iint_{\sigma} (2n+1) \left(\frac{H_n^2}{2} + \frac{H_n^3}{3R} \right) P_n(\cos\psi) d\sigma \quad (3.2.40)$$

Unlike the UNB method, this method has not used the condensation scheme, and therefore, both zero- and first-degree terms will come into play.

Moreover, there has been no discussion on the upper limit of the degree-order of the height (height-squared or height-cubed) coefficients. Sjöberg and Bagherbandi (2017, pg. 154) show that after adding zero- and first- degree terms to Eq. (3.2.40), the combined total topographical effect is simplified to

$$\delta N_{comb}^T = -\frac{4\pi G\rho}{\gamma} \left(\frac{H^2}{2} + \frac{H^3}{3R} \right) \quad (3.2.41)$$

Following are the two observations regarding the KTH approach of computing topographical corrections:

- i) The intermediate steps of the above formulation (Eqs. (3.2.33) – (3.2.40)) cannot be realised practically with either a high-resolution DEM or with a combination of multiple resolution DEMs. It is because the spherical harmonic coefficients of

height (height-squared or height-cubed) have to be determined using a DEM only. Given the computer resources, it is not feasible to compute these height coefficients with a high-resolution global DEM. Moreover, this contrasts with the final expression of the total topographical effect (Eq. (3.2.41)) that can be evaluated using any available highest resolution DEM.

- ii) Equation (3.2.41) that gives the combined direct and indirect effect on the geoid undulation is equivalent to the first term of the PITE computed in the UNB method (Eq. (3.2.29)). However, this term in the UNB's PITE is due to the potential difference of the actual and the condensed topographical shells (with a mass-conservation condensation scheme) on the geoid, but the KTH method does not use Helmert's second condensation scheme.

One interpretation can be that the topographical correction in the KTH method is just a term from the PITE (Eq. (3.2.29)). However, there arises a few questions that need to be answered: 1) If the combined topographical effect is just a term of PITE then what is the actual topographical effect on the geoid? 2) Does the effect of DTE, SITE (effect on the geoid undulation) and *remaining* PITE term in the UNB method cancel each other out? 3) Which of the two methods (UNB or KTH) of topographic treatment is more approximate, and which one is more exact given that both exclude downward continuation and use spherical approximation in their expressions. This is important because the discrepancy in the two formulas might cause a substantial effect concerning the quest of cm-level precise geoid.

Moreover, suppose by any chance both methods are equivalent. In that case, the KTH method should be preferred over the UNB method simply because the latter is computer resource-heavy and time-consuming as compared to the former. Nahavandchi and Sjöberg (2001) have analysed the two methods and concluded that the UNB method

fits better in Sweden compared to the KTH method, but the marginally rigorous formulas as presented in this thesis were not tested. They further suggested repeating the exercise in other regions.

Figure 3.2.10 shows the total topographical effect over India and adjacent countries computed from Eq. (3.2.41) with the block averaged MERIT 3'' \times 3'' DEM to the grid resolution of the gravity anomaly data i.e., 0.02 $^{\circ}$ \times 0.02 $^{\circ}$. The corresponding scatter plot and histogram are shown in Figures 3.2.11a and 3.2.11b, respectively.

The total topographic effect in the KTH method is a function of only the computation point's height (Eq. (3.2.41)). Therefore, as shown in Figure 3.2.10, distribution of the total topographic effect follows the topography (DEM). Moreover, its scatter plot (Figure 3.2.11a) is not scattered as compared to the topographic effects in the other two methods (CUT and UNB).

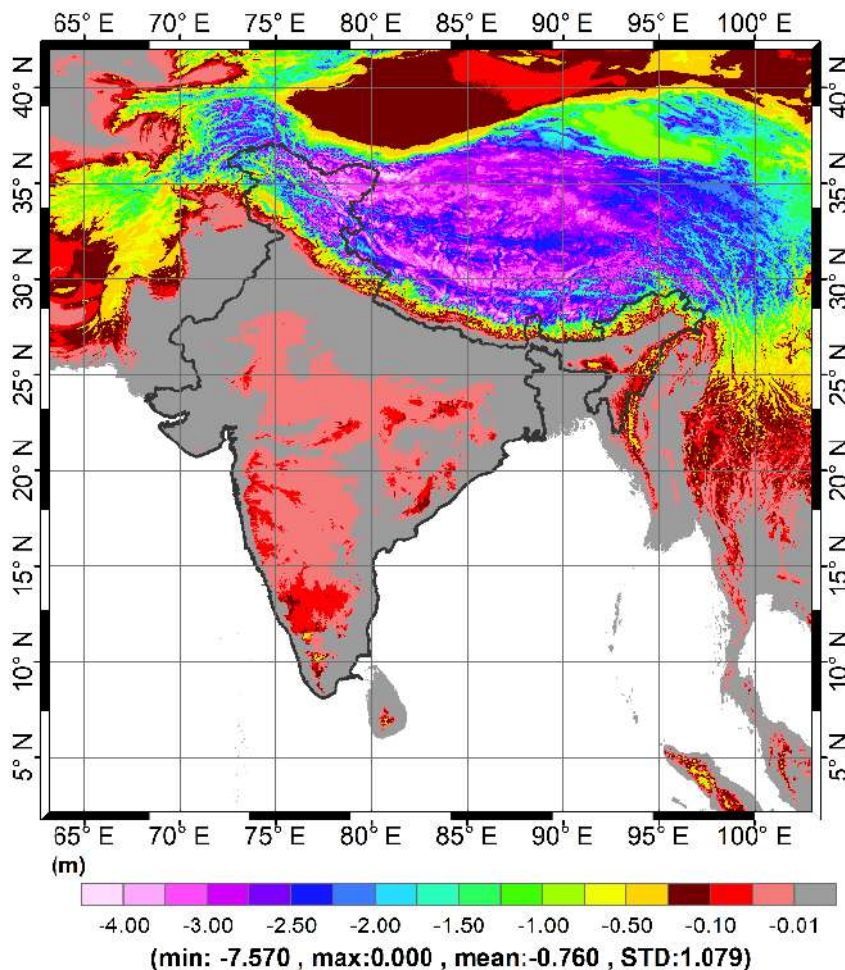


Figure 3.2.10: Total topographic effect using KTH method over India and adjacent regions.

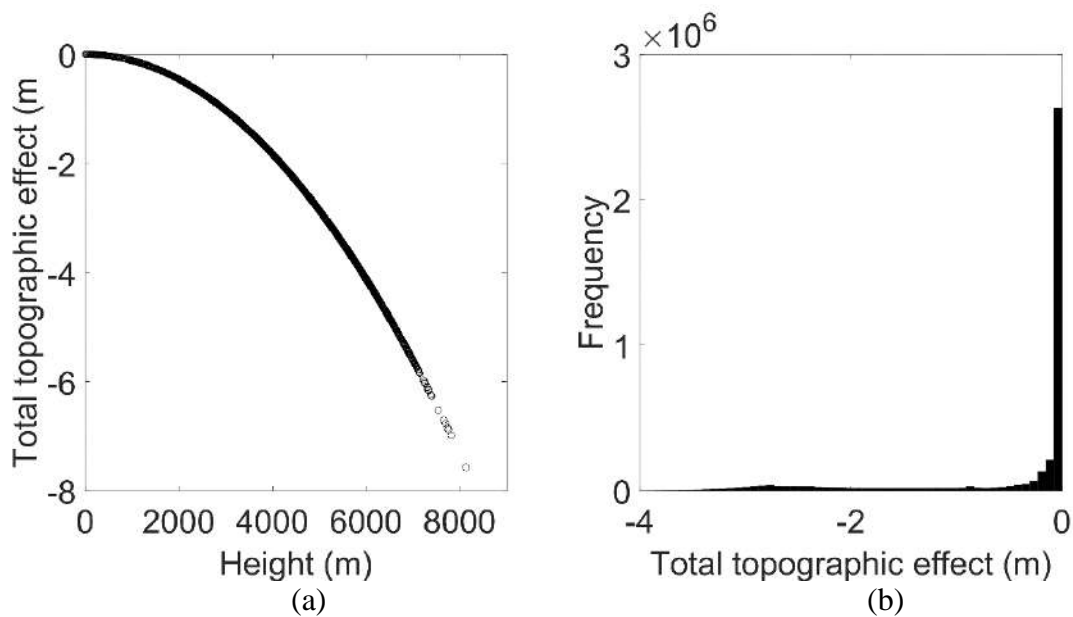


Figure 3.2.11: a) Scatter plot of total topographic effect versus height; b) histogram of total topographic effect in the KTH method.

3.3 Atmospheric Correction

The parameters used to define the normal ellipsoid come primarily from the satellite-derived geodetic data and hence, include the effect of the atmospheric masses. For WGS84 (NIMA, 2000, pg. 3-3), geocentric gravitational constant for the Earth, Earth's atmosphere and Earth with atmosphere excluded are $GM = (3986004.418) \times 10^8 \text{ m}^3\text{s}^{-2}$, $GM_{Atm} = (3.5 \pm 0.1) \times 10^8 \text{ m}^3\text{s}^{-2}$ and $GM' = (3986000.9 \pm 0.1) \times 10^8 \text{ m}^3\text{s}^{-2}$, respectively.

This implies that the even degree zonal harmonic coefficients of the normal ellipsoid include effect of the atmosphere. Moreover, as a necessary condition to use Stokes's formula atmospheric masses also must be moved inside the geoid or condensed onto it. Therefore, atmospheric correction is applied to gravity anomalies to account for i) gravitating atmospheric mass outside the geoid and ii) atmospheric mass included in the normal ellipsoid. It is applied as *always* additive correction to the observed gravity. The handling of the atmospheric correction in different geoid computation methods is discussed in the following sub-sections.

3.3.1 Atmospheric correction in the CUT method

Only the direct atmospheric effect (DAE) is applied in the CUT method on the assumption that its associated indirect effects are small. It does not make use of any atmospheric density model but uses the fifth-degree polynomial fit (Featherstone, 1992) to the values given in U.S. standard atmosphere (NOAA et al., 1976), and is given by

$$DAE = 0.871 - 1.0298 \times 10^{-4} H + 5.3105 \times 10^{-9} H^2 - 2.1642 \times 10^{-13} H^3 + \left. \begin{array}{l} 9.5246 \times 10^{-18} H^4 - 2.2411 \times 10^{-22} H^5 \end{array} \right\} \quad (3.3.42)$$

We acknowledge that there also exist other polynomial functions or other variants of Eq. (3.3.42), e.g., quadratic functions given by Wichiencharoen (1982) and Wenzel (1985; also see Ecker and Mittermayer, 1969).

It is also noted that researchers use DAE in Eq. (3.3.42) with different truncated degree polynomial (e.g., Featherstone and Dentith, 1997; Amos, 2007; Kuhn et al., 2009). Figure 3.3.1 shows the variation of the atmospheric effect with different heights and Eq. (3.3.42) truncated to different degree polynomials. Use of only degree one polynomial for atmospheric effect may cause a substantial effect to the final geoid computation in high mountainous regions. For some quantification, from Featherstone and Olliver (1997, Eq. 14) a difference of 0.2 mGal in gravity anomaly translates to 24 mm effect on the geoid. It is, therefore, recommended that the full expression with a fifth-degree polynomial fit must be used to reduce the gravity anomalies in the CUT method, unless the maximum height in the area of interest is less than 1000 m.

Moreover, we would like to emphasise that Eq. (3.3.42) is obtained after fitting a five-degree polynomial to the values and hence, it would not be conceptually strong to use any truncation in the formula. To use a truncated formula (2-, 3- or 4-degree), the corresponding degree polynomial must be fitted to the U.S. standard atmosphere values.

Sjöberg (1999; 2001) formulated that the use of Eq. (3.3.42) introduces a significant bias when used in practical Stokes's integration (i.e., truncated to a limited region). Their observations are recognised but we use Eq. (3.3.42) with the CUT method, as it has also been adopted by IAG and used in numerous CUT geoid/quasigeoid computations (e.g. Amos, 2007; Claessens et al., 2011; Featherstone et al., 2018; McCubbine et al., 2018).

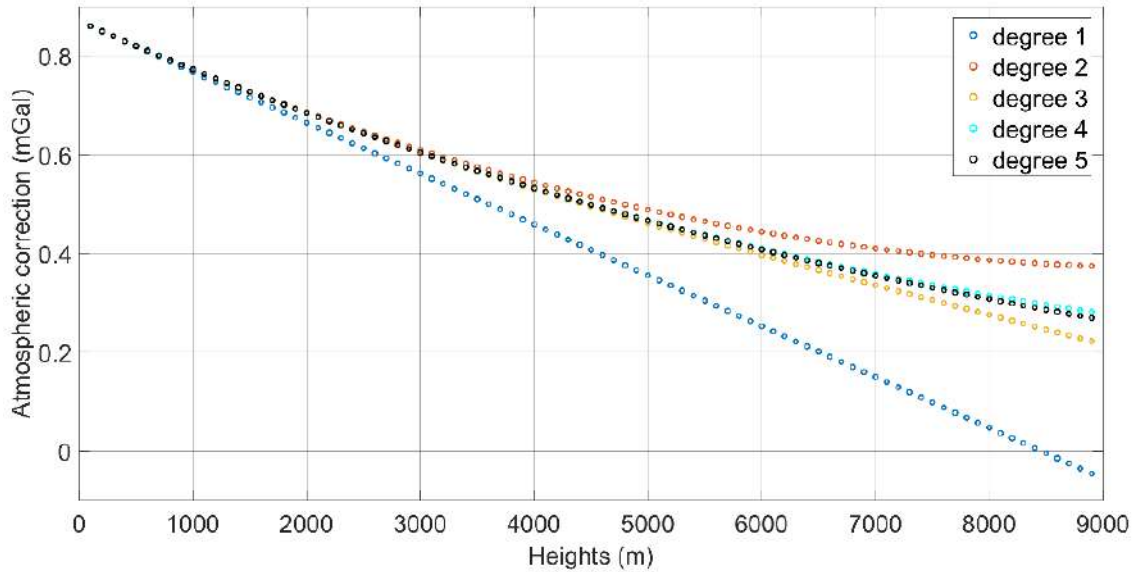


Figure 3.3.1: Atmospheric correction with different truncated degrees in Eq. (3.3.42)

3.3.2 Atmospheric correction in the UNB method

The UNB method applies DAE and Secondary Indirect Atmospheric Effect (SIAE) on gravity and Primary Indirect Atmospheric Effect (PIAE) on the geoid, similarly to the topographic effects (Section 3.2). They make use of Anderson et al. (1975) quadratic-polynomial approximation of the atmospheric density model (NOAA et al., 1976) and is given as

$$\rho_{UNB}^a(H, \Omega) = \rho_0^a + \alpha H(\Omega) + \beta H^2(\Omega) \quad (3.3.43)$$

where $\rho_0^a (= 1.2227 \text{ kgm}^{-3})$ is the mean bulk density of the atmosphere at sea level, $\alpha (= -1.1436 \times 10^{-4} \text{ kgm}^{-4})$ is the linear coefficient and $\beta (= 3.4057 \times 10^{-9} \text{ kgm}^{-5})$ is the quadratic coefficient.

Hildenbrand et al. (2002; also see Moritz, 2000) have mentioned that the atmospheric correction goes to zero at a height of ~ 34 km, however, the UNB method considers the atmosphere up to an arbitrary height of 50 km from sea-level. After the first 9 km, which is generally taken as the height of the troposphere, the remaining height is

divided into several spherical sub-shells of constant height (possibly for simplifying the computations).

Like UNB's topographical correction (Section 3.2), the building block of all the atmospheric corrections (DAE, PIAE, SIAE) is the residual atmospheric potential. This can be calculated by subtracting the potential of condensed atmospheric mass layer from the actual atmospheric masses. As such, both the actual and the condensed atmospheric masses can also be divided into their corresponding rough $(V_{atm}^{ar}, V_{atm}^{cr})$ and smooth $(V_{atm}^{as}, V_{atm}^{cs})$ parts. The residual atmospheric potential is given by (e.g., Novák 2000)

$$\delta V^a(r_{cp}, \Omega) = (V_{atm}^{ar}(r_{cp}, \Omega) + V_{atm}^{as}(r_{cp}, \Omega)) - (V_{atm}^{cr}(r_{cp}, \Omega) + V_{atm}^{cs}(r_{cp}, \Omega)) \quad (3.3.44)$$

$$\delta V^a(r_{cp}, \Omega) = \left[\begin{aligned} & G \iint_{\Omega'} \int_{r'=R+9}^{R+50} \rho_{UNB}^a(r', \Omega') \frac{1}{l(r_{cp}, \psi(\Omega, \Omega'), r')} r'^2 dr' d\Omega' + \\ & G \iint_{\Omega'} \int_{r'=R+H(\Omega')}^{R+9} \rho_{UNB}^a(r', \Omega') \frac{1}{l(r_{cp}, \psi(\Omega, \Omega'), r')} r'^2 dr' d\Omega' \end{aligned} \right] - \left[\begin{aligned} & G \iint_{\Omega'} \int_{r'=R+9}^{R+50} \rho_{UNB}^a(r', \Omega') \frac{1}{l(r_{cp}, \psi(\Omega, \Omega'), R)} r'^2 dr' d\Omega' + \\ & G \iint_{\Omega'} \int_{r'=R+H(\Omega')}^{R+9} \rho_{UNB}^a(r', \Omega') \frac{1}{l(r_{cp}, \psi(\Omega, \Omega'), R)} r'^2 dr' d\Omega' \end{aligned} \right] \quad (3.3.45)$$

The DAE and SIAE are computed at the Earth's surface, while the PIAE is computed at the co-geoid. Therefore, $r_{cp} = R + H(\Omega)$ for DAE and SIAE, and $r_{cp} = R$ for PIAE. Like the topographic corrections, DAE is the radial derivative of the residual potential of the atmospheric masses:

$$\begin{aligned}
DAE = \frac{\partial \delta V^a}{\partial r} = & \left[G \iiint_{\Omega'} \int_{r'=R+9}^{R+50} \rho_{UNB}^a(r', \Omega') \frac{\partial}{\partial r} \left(\frac{1}{l(R+H(\Omega), \psi(\Omega, \Omega'), r')} \right) r'^2 dr' d\Omega' + \right. \\
& G \iiint_{\Omega'} \int_{r'=R+H(\Omega)}^{R+9} \rho_{UNB}^a(r', \Omega') \frac{\partial}{\partial r} \left(\frac{1}{l(R+H(\Omega), \psi(\Omega, \Omega'), r')} \right) r'^2 dr' d\Omega' \left. - \right. \\
& \left[G \iiint_{\Omega'} \int_{r'=R+9}^{R+50} \rho_{UNB}^a(r', \Omega') \frac{\partial}{\partial r} \left(\frac{1}{l(R+H(\Omega), \psi(\Omega, \Omega'), R)} \right) r'^2 dr' d\Omega' + \right. \\
& \left. G \iiint_{\Omega'} \int_{r'=R+H(\Omega)}^{R+9} \rho_{UNB}^a(r', \Omega') \frac{\partial}{\partial r} \left(\frac{1}{l(R+H(\Omega), \psi(\Omega, \Omega'), R)} \right) r'^2 dr' d\Omega' \right] \quad (3.3.46)
\end{aligned}$$

It is known that the i) attraction of the atmospheric shell is zero at the inner points, i.e., first term in Eq. (3.3.46) will be zero, and ii) attraction of the condensed layer of the atmospheric shell is equal to a constant at the outer points, i.e. third term in Eq. (3.3.46) will be a constant (cf. Blakely, 1996).

A more detailed formulation on the practical evaluation of the above formula is given in Novák (2000, Section 4.4). SIAE is computed as $\frac{2}{r} \delta V^a$ and PIAE is computed as

$$\frac{\delta V^a}{\gamma_0(\Omega)}.$$

On the use of the atmospheric effect in the UNB method, some inconsistency regarding ‘signs’ has been observed in the literature. For example, Janák et al. (2017) have computed DAE over Auvergne ranging between -0.84 mGal and -0.71 mGal; also, see Klu (2015). These values would have been accepted if they are being added to the normal gravity, but they are reported to be added to the gravity anomalies in the respective studies. However, Novák (2000) reported the atmospheric correction (spherical direct effect) over Canada ranging from +0.559 mGal to +0.870 mGal. From the CUT method, we see that the effect of atmospheric masses is positive. We can only speculate about the origin of this difference in sign as the formulation done using the potential of actual masses subtracted

from the potential of the condensed atmospheric mass layer, i.e., change in sign in Eq. (3.3.44). However, DAE is added to the gravity anomaly and hence, it will introduce a bias due to the use of incorrect sign convention. We suggest using the formulas presented herein for atmospheric effects in the UNB method.

3.3.3 Atmospheric correction in the KTH method

The KTH method of atmospheric correction uses spherical harmonics with the inverse distance in the atmospheric potential formula, extended as an internal-type of series (Sjöberg and Bagherbandi, 2017). The atmospheric potential at any point on geoid is then given by

$$V_{KTH}^a(r, \Omega) = 4\pi\rho_0^*R^2 \left[\frac{1}{w-2} - \sum_{n=0}^{\infty} \frac{1}{2n+1} \left(\frac{r}{R}\right)^n \frac{H_n}{R} \right] \quad (3.3.47)$$

where $\rho_0^* = G\rho_{KTH}^a$ (gravitational constant times atmospheric bulk density at sea level), w is an arbitrary constant in the atmospheric density function used in KTH method, i.e.,

$$\rho_{KTH}^a = \rho_0^a \left(\frac{R}{r}\right)^w \quad (3.3.48)$$

Similar to the topographic gravity anomaly in the KTH method (Section 3.2.3), Eq. (3.3.47) is used in the boundary condition (spherical approximation) of physical geodesy to obtain the atmospheric gravity anomaly (Δg^a) as

$$\Delta g^a = -\left(\frac{\partial}{\partial r} + \frac{2}{r}\right)V_{KTH}^a \quad (3.3.49)$$

and therefore, direct atmospheric effect is

$$DAE = -\Delta g^a = \left(\frac{\partial}{\partial r} + \frac{2}{r}\right)V_{KTH}^a \quad (3.3.50)$$

Equation (3.3.50) is inserted in the spectral form of Stokes's formula to obtain the direct

effect of atmosphere on the geoid. Similarly, the indirect atmospheric effect on the geoid (V_{KTH}^a/γ) is also computed. The summation of the two terms provides the total atmospheric effect on the geoid.

We observe that there are somewhat different formulas reported in the literature from the KTH group and we present a few in Table 3.3.1

Table 3.3.1: Formulas for different atmospheric effect in the KTH literature.

	Direct atmospheric gravity anomaly	Direct atmospheric effect on geoid	Indirect atmospheric effect on geoid	Total atmospheric effect on geoid
Sjöberg (1999) #	$4\pi\rho_0^*\left(\frac{2R}{w-2} - \sum_{n=0}^{\infty} \frac{n+2}{2n+1} H_n^*\right)$	$\left(-\frac{V_0^a}{\gamma} - \frac{V_1^a}{\gamma}\right) - \left(\frac{4\pi\rho_0^*R}{\gamma} \times \sum_{n=2}^{\infty} \frac{n+2}{(2n+1)(n-1)} H_n^*\right)$	$\left(\frac{V_0^a}{\gamma} + \frac{V_1^a}{\gamma}\right) - \frac{4\pi\rho_0^*R}{\gamma} \sum_{n=2}^{\infty} \frac{H_n^*}{2n+1}$	$-\frac{4\pi\rho_0^*}{\gamma} \sum_{n=2}^{\infty} \frac{H_n^*}{n-1}$
Sjöberg and Nahavandchi (2000)	$4\pi\rho_0^* \sum_{n=0}^{\infty} \frac{n+2}{2n+1} H_n$	$\left(-\frac{V_0^a}{\gamma} - \frac{V_1^a}{\gamma}\right) - \left(\frac{4\pi\rho_0^*R}{\gamma} \times \sum_{n=2}^{\infty} \frac{n+2}{(2n+1)(n-1)} H_n\right)$	$\left(\frac{V_0^a}{\gamma} + \frac{V_1^a}{\gamma}\right) - \left(\frac{4\pi\rho_0^*R}{\gamma} \sum_{n=2}^{\infty} \frac{H_n}{2n+1}\right)$	$-\frac{4\pi\rho_0^*}{\gamma} \sum_{n=2}^{\infty} \frac{H_n}{n-1}$
Ellmann (2001)	$4\pi\rho_0^* \sum_{n=0}^{\infty} \frac{n+2}{2n+1} H_n$	$\left(-\frac{V_0^a}{\gamma} - \frac{V_1^a}{\gamma}\right) - \left(\frac{4\pi\rho_0^*R}{\gamma} \times \sum_{n=2}^{\infty} \frac{n+2}{(2n+1)(n-1)} H_n\right)$	$\left(\frac{V_0^a}{\gamma} + \frac{V_1^a}{\gamma}\right) - \left(\frac{4\pi\rho_0^*R}{\gamma} \sum_{n=2}^{\infty} \frac{H_n}{2n+1}\right)$	$-\frac{4\pi\rho_0^*}{\gamma} \sum_{n=2}^{\infty} \frac{H_n}{n-1}$
Sjöberg and Bagherbandi (2017) ##	$4\pi\rho_0^*\left(\frac{2R}{w-2} - \sum_{n=2}^{\infty} \frac{n+2}{2n+1} H_n\right)$	$\frac{4\pi\rho_0^*R}{\gamma} \times \left(\sum_{n=2}^{\infty} \frac{n+2}{(2n+1)(n-1)} H_n\right)$	$\frac{4\pi\rho_0^*R}{\gamma} \sum_{n=2}^{\infty} \frac{H_n}{2n+1}$	$-\frac{4\pi\rho_0^*}{\gamma} \sum_{n=2}^{\infty} \frac{H_n}{n-1} + N_{0,1}^a$

For Sjöberg (1999): $H_n^* = H_n - \frac{n+w-1}{2} \frac{H_n^2}{R}$, $V_0^a = 4\pi\rho_0^*R^2 \left(\frac{1}{v-2} - \frac{H_0}{R}\right)$ and $V_1^a = -\frac{4\pi\rho_0^*RH_1}{3}$

For Sjöberg and Bagherbandi (2017): $N_{0,1}^a = -\frac{4\pi\rho_0^*R^2}{\gamma(w-2)(w-3)}$

Following are a few observations on atmospheric effects in the KTH method:

- i) Since no atmospheric mass reduction/condensation strategy is being used in the KTH method, it will not be correct to say that Eq. (3.3.49) is a combination of direct and secondary indirect atmospheric effects. However, for the time being we assume that the first term in Eq. (3.3.50) resembles the direct effect, while second term gives the secondary indirect effect. Therefore, from Table 3.3.1 and Eq. (3.3.50), the globally accepted 0.87 mGal atmospheric effect on gravity anomaly at sea level can be interpreted as not a direct effect, but instead a combined direct and secondary indirect effect. This is because the first term in Δg^a , i.e.,

$-\left(-\frac{\partial}{\partial r} V_{KTH}^a\right)$ goes to zero at sea level ($H = 0$ m). Therefore, the contribution to

0.87 mGal at sea level originates from the second term, i.e., $-\left(-\frac{2}{r} V_{KTH}^a\right)$. We

envisage that this may not have numerical problem because the two terms are used together, but it can be worth looking in future. We would also like to mention that this observation might not hold true because it goes against the UNB method who reports a SIAE range of only -0.002 mGal to -0.001 mGal over Canada (Novák, 2000), while the major contribution is from their direct atmospheric effect.

- ii) In Table 3.3.1, while there is no change in the expression of V_0^a on substituting $n = 0$ in Eq. (3.3.47), we get a different V_1^a on substituting $n = 1$ in the same equation.

$$V_1^a = 4\pi\rho_0^*R^2 \left[\frac{1}{w-2} - \frac{1}{3} \frac{H_1}{R} \right] \quad (3.3.51)$$

It seems that the expression for V_1^a in Table 3.3.1 is obtained by neglecting the first term in Eq. (3.3.51) which further seems unguaranteed given that the first term has been retained in V_0^a (Table 3.3.1).

- iii) In the literature, we were unable to find a value for w (an arbitrary constant in the involved KTH atmospheric density function) used in Eq. (3.3.47). It is most probably because the KTH method applies the total atmospheric effect on the geoid and omits w in its final formula (Table 3.3.1). However, we computed the arbitrary value of $w=1514$ by setting $DAE = 0.87$ mGal and $H = 0$ m in Eq. (3.3.50). It is important to note here that, $w=1514$ does not provide atmospheric densities comparable to those obtained using the density function used in the UNB method (Eq. (3.3.43)). Thus, a validation study of different atmospheric density function is required. Using a trial and error approach for different values of w and comparing the graphs of UNB's and KTH's atmospheric density function with respect to heights, we estimated that the most probable value of w can range from 655 to 665. The w value in this range provides a difference between the two density functions (Eqs. (3.3.43) and (3.3.48)) not beyond $[-0.016 \text{ kgm}^{-3}, 0.016 \text{ kgm}^{-3}]$. We can only speculate that the formula for DAE in the KTH method may suffer from some approximations. We will not derive a more rigorous formula here because of the possibly better alternatives to apply atmospheric corrections (the CUT and the UNB method).
- iv) We anticipate that the use of the harmonic coefficients of heights in the atmospheric correction can be a potential cause of errors. We are working with a $0.02^\circ \times 0.02^\circ$ grid of gravity anomalies. We have developed spherical harmonic coefficients for a global DEM of $0.25^\circ \times 0.25^\circ$ resolution (Section 2.5). There can be two cases, either we do SHA on a global DEM with same working resolution (e.g., $0.02^\circ \times 0.02^\circ$ for our case) which will be computationally challenging, or we accept the, maybe, negligible errors emanating from the use of different resolutions (spatial DEM of $0.02^\circ \times 0.02^\circ$ resolution versus spectral DEM with d/o 720).

However, as mentioned in the earlier point, we have possibly better alternatives for DAE, so we will restrict ourselves from further discussion on using SHA/SHS for DAE.

3.4 Ellipsoidal Correction

Stokes's formula used to compute the geoid undulations from gravity anomalies is the solution of the fundamental equation of geodesy in spherical approximation (Heiskanen and Moritz, 1967, pg. 88):

$$\Delta g = -\frac{\partial T}{\partial r} - \frac{2}{R}T \quad (3.4.1)$$

where T is the disturbing potential.

However, the Earth is ellipsoidal in shape (flattening $\approx 1/300$). The correction applied to account for this spherical approximation is known as the ellipsoidal correction. The first term in Eq. (3.4.1) comes from the definition of the gravity disturbance (δg)

$$\delta g = -\left(\frac{\partial W}{\partial H} - \frac{\partial U}{\partial h}\right) \quad (3.4.2)$$

where W is the geopotential and U is the potential of the reference ellipsoid.

For practicality, we approximate $\frac{\partial}{\partial H} \approx \frac{\partial}{\partial h}$ to obtain

$$\delta g = -\left(\frac{\partial W}{\partial h} - \frac{\partial U}{\partial h}\right) = -\frac{\partial T}{\partial h} = -\frac{\partial T}{\partial r}$$

The error introduced due to the assumption of equivalence in the derivatives with respect to the plumbline and the ellipsoidal normal is accounted for by applying the ellipsoidal correction to the gravity disturbance ($\varepsilon_{\delta g}$); this can be written as

$$\varepsilon_{\delta g} = \frac{\partial W}{\partial H} - \frac{\partial W}{\partial h} \quad (3.4.3)$$

The second term on the R.H.S. of Eq. (3.4.1) is the spherical approximation of $\frac{1}{\gamma} \frac{\partial \gamma}{\partial h} T$ (Heiskanen and Moritz, 1967, Section 2.14). Therefore, the correction applied to account for this part of spherical approximation is known as ‘ellipsoidal correction for spherical approximation’ (ε_n) and can be written as

$$\varepsilon_n = \frac{1}{\gamma} \frac{\partial \gamma}{\partial h} T - \left(-\frac{2}{R} T \right) \quad (3.4.4)$$

Equations (3.4.3) and (3.4.4) together are termed as the ellipsoidal correction to the gravity anomalies. These two equations have been studied in detail by many, e.g., Molodensky et al. (1962), Bjerhammar (1966), Koch (1968), Moritz (1974), Jekeli (1981b), Cruz (1986), Martinec and Grafarend (1997), Martinec (1998), Fei and Sideris (2000, 2001), Brovar et al. (2001), Heck and Seitz (2003), Hipkin (2004), Najafi-Alamdari et al. (2006) among others whom are cited later in this section. Huang et al. (2003b) and Ellmann (2005a) have conducted individual comparisons of various studies on ellipsoidal corrections, and they reported that many of the methods disagree among themselves. The effect of ellipsoidal corrections in the final geoid can be of decimetre level and hence, some standardisation is required from the viewpoint of cm-level precise geoid.

Next, we will discuss the treatment/derivation or any possible improvement in the handling of the ellipsoidal correction in the three methods (CUT, UNB, KTH).

3.4.1 Ellipsoidal correction in the CUT method

The CUT method does not talk explicitly about the ellipsoidal corrections to the gravity anomalies. Ellipsoidal gravity anomalies are computed from GGM, which are subtracted from the observed gravity anomalies to obtain the residual gravity anomalies (e.g.,

Featherstone et al., 2018). Then R is replaced by the radius of the ellipsoid (Claessens, 2006, Chapter 6) in Stokes's formula, and is computed separately for each latitude parallel. As such, it is claimed that no further ellipsoidal correction is required. An important point to note here is that these ellipsoidal gravity anomalies (Eq. (3.4.5)) are computed on the topography because in the CUT method, we work with the gravity anomalies on the Earth's surface (Featherstone et al., 2018; Claessens and Filmer, 2020) as required in the Molodensky theory.

$$\Delta g_e^{GGM}(r, \Omega) = \frac{T(r, \Omega)}{\gamma(h)} \frac{\partial \gamma}{\partial h} - \frac{\partial T(r, \Omega)}{\partial h} \quad (3.4.5)$$

where Δg_e^{GGM} is the ellipsoidal gravity anomaly on the Earth's surface calculated using a GGM.

This can also be written as

$$\Delta g_e^{GGM}(r, \Omega) = \frac{T(r, \Omega)}{\gamma(h)} \frac{\partial \gamma}{\partial h} - \left(\frac{\partial r}{\partial h} \frac{\partial T(r, \Omega)}{\partial r} + \frac{\partial \theta}{\partial h} \frac{\partial T(r, \Omega)}{\partial \theta} \right) \quad (3.4.6)$$

Using the spherical approximation, we have

$$\frac{\partial T(r, \Omega)}{\partial \theta} = -r\gamma(h)\xi_H(r, \Omega) \quad (3.4.7)$$

$$\frac{\partial T(r, \Omega)}{\partial r} = -\delta g(r, \Omega) \quad (3.4.8)$$

Substituting Eqs. (3.4.7) and (3.4.8) in Eq. (3.4.6), ellipsoidal gravity anomaly on topography is

$$\Delta g_e^{GGM}(r, \Omega) = \frac{T(r, \Omega)}{\gamma(h)} \frac{\partial \gamma}{\partial h} + \left(\frac{\partial r}{\partial h} \delta g(r, \Omega) - \frac{\partial \theta}{\partial h} r\gamma(h)\xi(r, \Omega) \right) \quad (3.4.9)$$

where

$$\frac{\partial r}{\partial h} = \frac{v(1 - e^2 \sin^2 \varphi) + h}{r} \quad (3.4.10)$$

$$\frac{\partial \theta}{\partial h} = -\frac{e^2 v \cot \varphi}{(v(1 - e^2) + h)^2 + (v + h)^2 \cot^2 \varphi} \quad (3.4.11)$$

$$v = \frac{a}{\sqrt{1 - e^2 \sin^2 \varphi}} \quad (3.4.12)$$

Some important points to be noted in the practical evaluation of the above formula are:

- i) Equation (3.4.9) uses the second-order approximate normal gravity gradient, given by

$$\frac{\partial \gamma}{\partial h} \approx -\frac{2\gamma_a}{a} (1 + f + m - 2f \sin^2 \varphi) \quad (3.4.13)$$

A more rigorous formula can be derived by differentiating Eq. (3.1.21) with respect to height.

- ii) $\gamma(h)$ in Eq. (3.4.9) is the normal gravity on the Earth's topographical surface, which is computed using Eq. (3.1.4) in the CUT method (Featherstone et al., 2018, pg. 153). A more robust formula given by Eq. (3.1.21) can also be utilised.
- iii) The height involved in the computation of GGM-derived gravity anomaly at the Earth's surface must be the ellipsoidal height and should not be approximated with the orthometric height. A general way to obtain the ellipsoidal height in a regular grid is to compute geoid undulations from GGM and adding them to the block averaged DEM. The resultant will be the grid of required ellipsoidal heights. This is iterated until the difference between the current and previous ellipsoidal heights becomes imperceptible. The iteration is required because the computation of geoid

undulation from GGM itself requires ellipsoidal heights, which are approximated with orthometric heights (from DEM) in the first run (Rapp, 1997).

3.4.2 Ellipsoidal correction in the UNB method

From Vaníček et al. (1999, Eq. 11), the ellipsoidal correction to the gravity disturbance is given by

$$\varepsilon_{\delta g} = \delta g \frac{\beta_\gamma^2}{2} + g \beta_\gamma \xi + \frac{g}{2} (\xi^2 + \eta^2) \quad (3.4.14)$$

where $\beta_\gamma (= f \sin 2\phi)$ is the difference between geodetic latitude and geocentric latitude (Bomford, 1971), $\xi^2 + \eta^2 (= \Theta^2)$ is the square of the total deflection of the vertical and g is the gravity.

Vaníček et al. (1999) show that first and third terms in the R.H.S. of Eq. (3.4.14) can be neglected to obtain the ellipsoidal correction to gravity disturbance up to an accuracy of 10 μGal . Therefore, Eq. (3.4.14) is now written as

$$\varepsilon_{\delta g} = g \beta_\gamma \xi \quad (3.4.15)$$

We substitute $\beta_\gamma (= f \sin 2\phi)$ in Eq. (3.4.14) to get a comparatively more robust formula for ellipsoidal correction to the gravity disturbance

$$\varepsilon_{\delta g} = 2\delta g f^2 \sin^2 \phi \cos^2 \phi - 2g f \sin \phi \cos \phi \xi + \frac{g}{2} \Theta^2 \quad (3.4.16)$$

Further substituting $\xi = -\frac{1}{r\gamma} \frac{\partial T}{\partial \phi}$ and r in geodetic coordinates (Claessens, 2006)

$$r = r_{e_geod} = a \sqrt{\frac{1 - e^2 (2 - e^2) \sin^2 \phi}{1 - e^2 \sin^2 \phi}} \quad (3.4.17)$$

in Eq. (3.4.16), we get

$$\varepsilon_{\delta g} = 2\delta g f^2 \sin^2 \varphi \cos^2 \varphi - \left(2 \frac{g}{\gamma} \frac{f}{a} \sin \varphi \cos \varphi \sqrt{\frac{1 - e^2 \sin^2 \varphi}{1 - e^2 (2 - e^2) \sin^2 \varphi}} \right) \frac{\partial T}{\partial \varphi} + \frac{g}{2} \Theta^2 \quad (3.4.18)$$

It should be noted that e^4 term in Eq. (3.4.17) must not be omitted, as it can cause a difference of approximately 145 m in r .

To simplify Eq. (3.4.18), g/γ can be approximately taken as unity. Implementing this condition ($g/\gamma = 1$) causes a maximum error of less than 2 μGal that is five times smaller than what has been allowed in the original study ($\sim 10 \mu\text{Gal}$). Therefore, the ellipsoidal correction to the gravity disturbance up to an accuracy of 2 μGal is given as

$$\varepsilon_{\delta g} = 2\delta g f^2 \sin^2 \varphi \cos^2 \varphi - \left(2 \frac{f}{a} \sin \varphi \cos \varphi \sqrt{\frac{1 - e^2 \sin^2 \varphi}{1 - e^2 (2 - e^2) \sin^2 \varphi}} \right) \frac{\partial T}{\partial \varphi} + \frac{\gamma}{2} \Theta^2 \quad (3.4.19)$$

The first term on the R.H.S. of Eq. (3.4.19) can never get greater than 5 μGal ; hence, it can be omitted for further simplification, but we do not suggest omitting it. The third term in the R.H.S. of Eq. (3.4.19) is the deflection correction and is exactly the same as derived by Claessens (2006).

Regarding the deflection correction, Vaníček et al. (1999) reported that the maximum vertical deflection could reach a value of 30'' and as such, the maximum correction cannot exceed 10 μGal while Claessens (2006) suggested 70'' as the maximum vertical deflection and gets a maximum value of 56 μGal for the deflection correction. Both suggested neglecting the same. We can only speculate that this small value was not of much significance during those times especially when there were larger error sources to be considered. However, the maximum vertical deflections can reach $\sim 109''$ (as in GGMplus, Hirt et al., 2013) in the steep Himalayan peaks, which translates to a deflection correction of 139 μGal . Indian vertical deflections from Gulatee (1955) that were re-

processed by Featherstone and Goyal (2022) can be used in future geoid computations over India.

For some quantification, we can have a rough estimate from Vaníček et al. (1999). They computed the ellipsoidal correction to the gravity disturbance in the Canadian Rocky Mountains that ranges from -118 μGal to +157 μGal . It was reported that on Stokes's integration, this correction translates to a geoidal effect of -70 mm to +140 mm. Thus, the deflection correction (max $\sim 139 \mu\text{Gal}$), which is a term in ellipsoidal correction to the gravity disturbance (third term in the R.H.S. of Eq. (3.4.19)), must not be omitted especially when working in mountainous regions.

Next is the ellipsoidal error due to spherical approximation that is given by (fundamental equation of physical geodesy minus its spherical approximation)

$$\varepsilon_n = \left(-\frac{1}{\gamma} \frac{\partial \gamma}{\partial n} - \frac{2}{R} \right) T \quad (3.4.20)$$

The UNB method uses R as the mean radius of the Earth that can be rearranged as

$$R = (a^2 b)^{1/3} = a(1-f)^{1/3} \approx a \left(1 - \frac{f}{3} \right) \Rightarrow a = R \left(1 - \frac{f}{3} \right)^{-1} \quad (3.4.21)$$

Substituting the normal gravity gradient (Eq. 3.1.2) with a from Eq. (3.4.21) in Eq. (3.4.20) gives

$$\varepsilon_n = \left(\frac{2}{R} \left(1 - \frac{f}{3} \right) (1 + f + m - 2f \sin^2 \varphi) - \frac{2}{R} \right) T \approx \frac{2}{R} \left(f + m - 2f \sin^2 \varphi - \frac{f}{3} \right) T \quad (3.4.22)$$

This is the same equation as given in Vaníček et al. (1999).

It should be noted here that use of any other normal gravity gradient (Section 3.1) in Eq. (3.4.20) will not provide any improvement in Eq. (3.4.22). It is simply because, in

the UNB method, the ellipsoidal corrections are applied at the geoid level (e.g., Wong, 2001) and all the expressions of the normal gravity gradient will provide the same result.

There is literature from the UNB group (e.g., Vaníček and Martinec, 1994; Tenzer and Janák, 2002; Ellmann and Vaníček, 2007) that suggest using Eqs. (3.4.15) and (3.4.22) for the ellipsoidal corrections. However, in the recent manual (UNB, 2009), the following formulas have been used to apply the ellipsoidal corrections (Jekeli, 1981b; Cruz, 1986):

$$\varepsilon_{\delta g} = -\frac{e^2}{R} \sin \theta \cos \theta \frac{\partial T}{\partial \theta} \quad (3.4.23)$$

$$\varepsilon_n = -\frac{e^2}{R} (3 \cos^2 \theta - 2) T \quad (3.4.24)$$

The gravity anomalies with ellipsoidal correction (Δg_{UNB}^{ell}) are calculated using

$$\Delta g_{UNB}^{ell} = \Delta g_{UNB}^{DWC} - \frac{e^2}{R} \sin \theta \cos \theta \frac{\partial T}{\partial \theta} + \frac{e^2}{R} (3 \cos^2 \theta - 2) T \quad (3.4.25)$$

where Δg_{UNB}^{DWC} is the gravity anomaly on the geoid corrected for topographical and atmospheric masses. This follows from Jekeli (1981b, Eq. 4.21)

$$\Delta g = -\frac{\partial T}{\partial r} - \frac{2}{r} T - e^2 \sin \theta \cos \theta \frac{\partial T}{r \partial \theta} + \left(6J_2 \frac{a^2}{r^3} P_2(\cos \theta) - \frac{3\omega^2 r^2}{GM} \sin^2 \theta \right) T \quad (3.4.26)$$

where the ellipsoidal correction for the spherical approximation can be obtained by rearranging the fourth term on the R.H.S. of Eq. (3.4.26) using some approximations based on a *fortunate* similarity in the numerical values of various parameters

(e.g., $\frac{\omega^2 a^2 b}{GM} \approx \frac{e^2}{2}$). Figure 3.4.1 shows the two ellipsoidal corrections used in Eq.

(3.4.25).

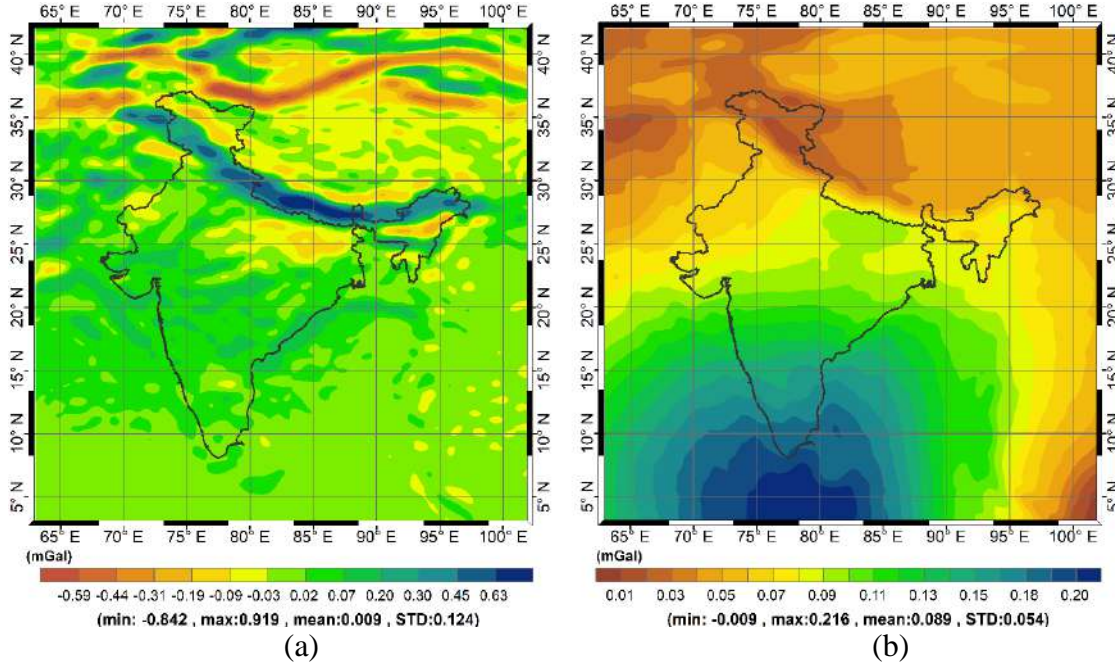


Figure 3.4.1: Ellipsoidal correction to (a) gravity disturbance and (b) spherical approximation as applied in the UNB method.

3.4.3 Ellipsoidal correction in the KTH method

The KTH method applies ellipsoidal corrections in two parts:

- i) Ellipsoidal correction due to the use of spherical boundary condition (Sjöberg, 2003c; 2004).

$$\Delta g_{ell_cor1} = \Delta g - \frac{e^2}{a} \cos \theta \sin \theta \frac{\partial T}{\partial \theta} - \frac{e^2}{a} (3 \cos^2 \theta - 2) T \quad (3.4.27)$$

Equation (3.4.27) resembles Eq. (3.4.25) used in the UNB method. However, on a closer look, there is a ‘sign’ difference between the two formulas. Following Jekeli (1981b, Section 4), the signs followed in the UNB method seem more appropriate (Eq. (3.4.26)) but needs further investigation. However, in this study with the KTH method, we use Eq. (3.4.27) as is used by the KTH group.

- ii) Upward continuation of the corrected gravity anomaly from reference ellipsoid of

radius $r_e (= a\sqrt{1-e^2 \cos^2 \theta})$ to the sphere of radius a .

$$\Delta g_{KTH}^{ell} = \Delta g_{ell_cor1} + (a - r_e) \left(\frac{\partial \Delta g_{ell_cor1}}{\partial r} \right)_{r=a} = \Delta g + \delta G \quad (3.4.28)$$

where δG is the total ellipsoidal correction that needs to be applied to the gravity anomaly and is given by (cf. Sjöberg, 2003c, Eq. 16)

$$\delta G = e^2 \left(\frac{a}{2} \cos^2 \theta \left(\frac{\partial \Delta g}{\partial r} \right)_{r=a} - \cos \theta \sin \theta \frac{\partial T}{a \partial \theta} - (3 \cos^2 \theta - 2) \frac{T}{a} \right) \quad (3.4.29)$$

Therefore, the ellipsoidal effect on geoid is (Sjöberg and Bagherbandi, 2017)

$$\delta N^{ell} = \left(\frac{a - R}{R} \right) \left(\frac{R}{4\pi\gamma} \iint_{\sigma} S(\psi) \Delta g d\sigma \right) + \frac{a}{4\pi\gamma} \iint_{\sigma} S(\psi) \delta G d\sigma - \frac{e^2 a \cos^2 \theta}{2\gamma} \left(\frac{\partial T}{\partial r} \right)_{r=a} \quad (3.4.30)$$

The first term on the R.H.S. of Eq. (3.4.30) is for geometrical scaling of the geoid undulation, while the third term is due to the change in disturbing potential between spheres with radii a and r_e .

The above formula (Eq. (3.4.30)) has also been given in terms of spherical harmonics. For details, refer to Sjöberg (2004), Sjöberg and Bagherbandi (2017).

3.5 Downward continuation

The term downward continuation is strictly meant for geoid computation using Stokes's integration, where we need the gravity anomalies on the geoid. That is, either the observed gravity or computed gravity anomalies need to be brought down from the Earth's surface to the geoid level. Please note that the geoid undulation can also be calculated using the height anomalies computed on the Earth's surface plus the geoid-quasigeoid separation term in which we do not downward continue the gravity anomalies to the geoid. This will be discussed in Section 4.3.

However, in the computation of height anomaly using the analytical continuation solution (Moritz, 1971; Pellinen, 1972) of the Molodensky's problem, we have to either upward continue or downward continue the gravity anomalies from all the points on the Earth's surface to the level of the computation point. This analytical continuation is discussed in Section 3.5.1. It should be noted here that Heiskanen and Moritz (1967, pg. 324) describe the computation of height anomalies using the downward continued gravity anomalies at the geoid/sea-level. However, this is not a usual practice to be followed as it somewhat defeats the purpose of the Molodensky's theory of determining the shape of the Earth, and hence, will not be discussed.

3.5.1 Downward continuation in the CUT method

The concept of downward continuation of gravity anomaly is also not forthright in the CUT method. Although Pellinen (1972) has shown that all the available solutions of Molodensky's problem (Molodensky et al., 1962; Brovar, 1964; Moritz, 1971) are equivalent, the CUT method makes use of the 'solution by analytical continuation', as termed by Moritz (1971). In terms of gravity anomalies, the analytical continuation method uses the Taylor series expansion to connect the gravity anomalies in the interior or exterior

of the computation point-level surface to the corresponding gravity anomaly at the computation point-level surface. This involves the use of downward or upward continuation of the gravity anomalies in the CUT method (e.g., Moritz, 1980, Section 45). To the first-order of the Taylor series, it is given by

$$\Delta g' = \Delta g_P + \Delta z \frac{\partial \Delta g}{\partial z} \quad (3.5.1)$$

where Δg_P is the gravity anomaly at any fixed point P on the Earth's surface and $\Delta g'$ is the corresponding gravity anomaly at the level surface passing through the computation point.

The second term on the R.H.S. of Eq. (3.5.1) is the gradient of the gravity anomaly times the height difference between the two point-levels. It will not be correct to call it a downward continuation because it is also used for upward continuation. As such, we will call it here an analytical continuation operator.

In spherical approximation, we have $\frac{\partial \Delta g}{\partial z} = \frac{\partial \Delta g}{\partial r} = \frac{\partial \Delta g}{\partial h}$. Thus, the gradient can

be written as (Heiskanen and Moritz, 1967, pg. 115)

$$\frac{\partial \Delta g}{\partial r} = -\frac{2\Delta g_P}{R} + \frac{R^2}{2\pi} \iint_{\sigma} \frac{\Delta g - \Delta g_P}{l^3} d\sigma \quad (3.5.2)$$

In the planar approximation, the first term on the R.H.S. of Eq. (3.5.2) is neglected, and the same is written as

$$\frac{\partial \Delta g}{\partial r} \approx \frac{R^2}{2\pi} \iint_{\sigma} \frac{\Delta g - \Delta g_P}{l^3} d\sigma \quad (3.5.3)$$

It is shown that the G_1 term in the solution of Molodensky's problem reduces to (Heiskanen and Moritz, 1967, pg. 312)

$$G_1 = -(H - H_p) \frac{\partial \Delta g}{\partial h} = -(H - H_p) \frac{\partial \Delta g}{\partial r} \quad (3.5.4)$$

We recommend the readers to see Moritz (1980, pg. 387-388) for some insights into this analytical continuation solution.

The CUT method involves the use of G_1 term (Eq. (3.5.4)), i.e., analytical continuation of gravity anomaly (downward or upward). However, it does not make use of the gradient operator (Eq. (3.5.3)) rather, approximates the G_1 term with the planar TCs (Moritz, 1980, Eq. 48-31; McCubbine et al., 2019).

$$G_1 = -(H - H_p) \frac{\partial \Delta g}{\partial h} \approx \frac{1}{2} G \rho R^2 \iint_{\sigma} \frac{(H - H_p)^2}{l^3} d\sigma \quad (3.5.5)$$

Equation (3.5.5) is derived assuming that the free-air gravity anomalies on the Earth's surface are linearly correlated with the elevation, i.e., $\Delta g - \Delta g' = 2\pi G \rho (\Delta z)$. Also see Moritz (1980, Eqs. 48-12 and 48-13), and Heiskanen and Moritz (1967, Eqs. 7-96 and 7-97).

Following are a few observations over this method that should be investigated further:

- i) The expression of G_1 (Eq.(3.5.4)) in terms of gravity gradient neglects the term $-2(H - H_p) \frac{\Delta g}{R}$ (Eq. (3.5.2)) or $-(H - H_p) \frac{\Delta g}{R}$ (Moritz, 1980, Eq. 45-29). For the Himalayan belt, where the gravity anomalies can reach 600 mGal, and height difference in an area of $1^\circ \times 1^\circ$ can reach up to 7000 m, this neglected term can reach a maximum value of ~ 1.30 mGal or ~ 0.65 mGal, depending on which formula is being used.

- ii) Following the derivation in Moritz (1980, pg. 416), we can approximate the G_1 term by the planar TC *iff* the gravity anomalies on the Earth's surface are linearly (or near linearly) correlated with the elevations. This assumption seems not to be strictly valid in various regions (e.g., Figure 2.1.5a) with varying heights. Moreover, with the use of the second-order approximate formula (Eq. 3.1.4) in the computation of free-air gravity anomalies on the Earth's surface, they should not be assumed as linearly correlated with the elevation. Therefore, it is possible that Eq. (3.5.5) might not be valid from a theoretical point of view and a numerical test should be developed to quantify the error, if any, being introduced due to this.
- iii) G_1 is not equal to but approximated by the planar TC (Eq. (3.5.5); also see Section 3.2.1; Featherstone et al., 2018; McCubbine et al., 2019). The difference between Stokes's integrated G_1 ($S(G_1)$) and Stokes's integrated TC ($S(TC)$) is equivalent to the FOIE (Moritz 1980 Eq. 48-29), i.e.,

$$S(G_1) = S(TC) - \frac{\pi G \rho H^2}{\gamma} \quad (3.5.6)$$

It should be noted that negative sign in Eq. (3.5.6) is sometimes omitted (e.g., Sjöberg, 2000; Hwang et al., 2020) and Eq. (3.5.7) is used

$$S(G_1) = S(TC) + \frac{\pi G \rho H^2}{\gamma} \quad (3.5.7)$$

We now provide a short interpretation on the quasigeoid from height anomalies that may require further speculation (also see Section 4.3). Following the CUT method, we calculate height anomalies on the Earth's surface. Therefore, the surface developed using these computed height anomalies will be telluroid and not the required quasigeoid. To obtain the quasigeoid, we think that the height anomalies should probably be downward

continued to the ellipsoid along the ellipsoidal normal. One can argue that the height anomalies are not any physical quantity but only a mathematical term and therefore, there is no need to downward continue them using the gradient of height anomaly. Instead, we can simply consider them to be on the ellipsoid.

In our support, we would like to mention that the height anomalies are computed using gravity anomalies, so they form some physical basis. Moreover, height anomaly gradients have been used for the analytical continuation of the height anomalies in the literature. For example, Eq. 8-68 in Heiskanen and Moritz (1967), but it was simplified to a more general case where the height anomaly gradient term vanishes (Heiskanen and Moritz, 1967, Eq. 8-71). Also, see Ågren (2004, Eq. 5.43), where they used height anomaly gradient in the derivation of downward continuation effect on geoid undulation. Another example comes from the spherical harmonic synthesis of geoid undulation. Rapp (1997), Hirt (2012) and Goyal et al. (2019a) upward continued the height anomaly computed on the ellipsoid to the Earth's surface for converting the height anomaly to the geoid undulation. Therefore, we reiterate that the height anomalies may be downward continued from the Earth's surface to the ellipsoid to define the quasigeoid, or there must be a convention on the interpretation of the quasigeoid.

A possible derivation for the downward continuation of height anomalies follows

differentiating $\zeta = \frac{T_P}{\gamma}$ with respect to h or r (in spherical approximation)

$$\frac{\partial \zeta}{\partial h} = \frac{1}{\gamma} \frac{\partial T}{\partial h} - \frac{T}{\gamma^2} \frac{\partial \gamma}{\partial h} = \frac{1}{\gamma} \left(\frac{\partial T}{\partial h} - \frac{T}{\gamma} \frac{\partial \gamma}{\partial h} \right) = -\frac{\Delta g_P}{\gamma} \quad (3.5.8)$$

This implies $\frac{\partial \zeta}{\partial h} = -\frac{\Delta g_P}{\gamma}$. Therefore, the height anomalies can be downward continued

using

$$\frac{\partial \zeta}{\partial h} h = -\frac{\Delta g_p}{\gamma} h \quad (3.5.9)$$

where h is the ellipsoidal height.

3.5.2 Downward continuation in the UNB method

The UNB method follows Stokes's solution that requires the gravity anomalies on the geoid. That is, the gravity anomalies on the Earth's surface need to be downward continued onto the geoid. This is done after Helmert's second condensation of the topographical and atmospheric masses (Section 3.2.2 and 3.3.2)

The UNB method predominantly uses inverse Poisson's integral for downward continuation and usually mentions a *warning* regarding its limitations in the rapidly undulating regions and/or higher than 5'×5' resolution of the computation grid (e.g., Vaníček et al., 1995). There are several papers that report on the stability and instability of inverse Poisson's integral (Martinec, 1996, 1998; Sun and Vaníček, 1998; Kingdon and Vaníček, 2011; Vaníček and Santos, 2010) and other methods (Hunegnaw, 2001; Huang, 2002; Huang et al., 2003a) for downward continuation of gravity anomalies. Despite different solutions to the inverse Poisson's integral, two common arguments that can be extracted from these studies (except Vaníček and Santos, 2010) are: i) the inverse Poisson's integral method is stable for Canadian rocky mountains and hence, it is stable for the rest of the world except perhaps for the Himalayas, and ii) the method is either unstable or convergence is slow if a grid higher than 5'×5' resolution is used.

In this study, we work in the study area having diverse topographical features varying from the Gangetic plains to the Himalayas with a computation grid of 0.02°×0.02° (=1.2'×1.2'). Thus, we have not used the inverse Poisson's integral but the analytical downward continuation (Heiskanen & Moritz, 1967, pg. 115). Though India provides the

best topography to test the extremities of any methods, an objective comparison between the two methods remains one of the limitations of the present study.

We have used the exact analytical expression as given in Heiskanen and Moritz (1967, pg. 115) without neglecting any term. To downward continue the gravity anomaly at point P on the Earth's surface, we compute the gravity gradient using Eq. (3.5.2), with

$$l_0 = 2R \sin \frac{\psi}{2}.$$

The integrand in the second term on the R.H.S. of Eq. (3.5.2) contains the inverse of distance cubed; hence, the term will not be affected significantly with the increase in distance (only after some considerable distance). We did the integration using the gravity anomaly, corrected for topographical and atmospheric masses, with an integration radius of 2°. Figure 3.5.1 shows the calculated gravity gradient used for the downward continuation of the gravity anomalies. A scatter plot and a histogram of the gravity gradients are shown in Figures 3.5.2 (a) and (b), respectively. Though most values are within [-0.03 mGal/m, +0.03 mGal/m], the large values are observed in those regions where we suspect not good quality of the GETECH gravity data, i.e., regions in Uttarakhand, Himachal Pradesh and Jammu and Kashmir, along the Himalayan belt. We suggest that a more meticulous comparison study is required for the downward continuation methodologies over the Himalayan belt with a higher than 5'×5' resolution computation grid.

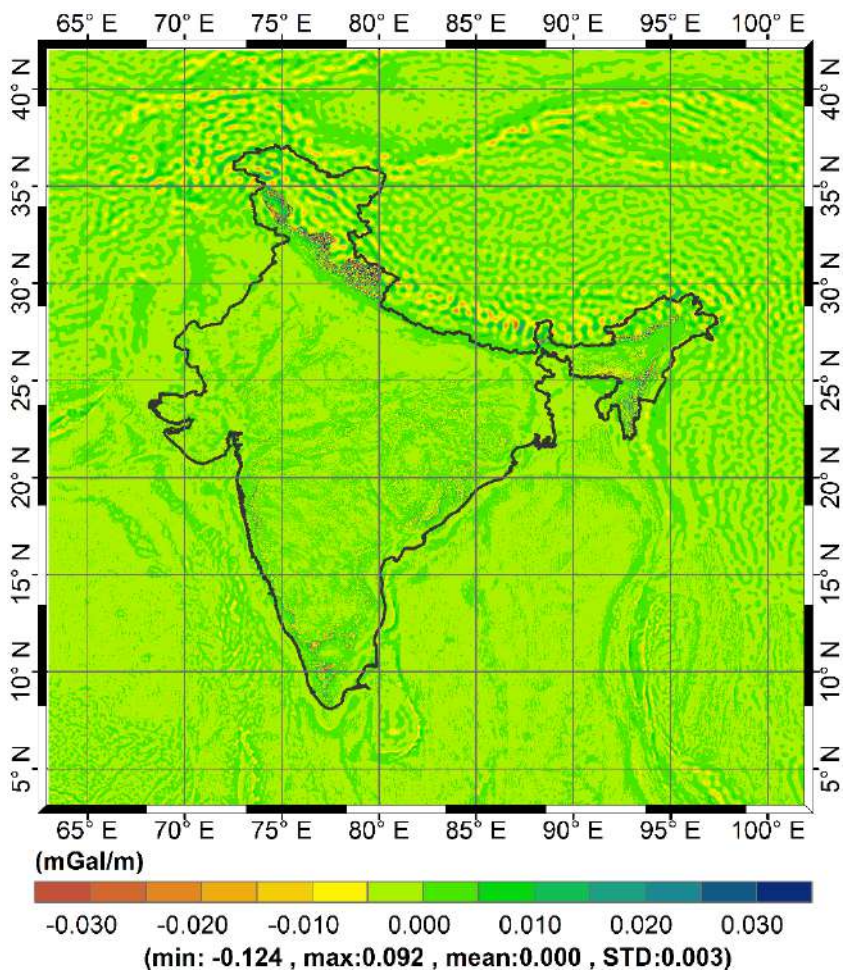


Figure 3.5.1: Vertical gravity gradient.

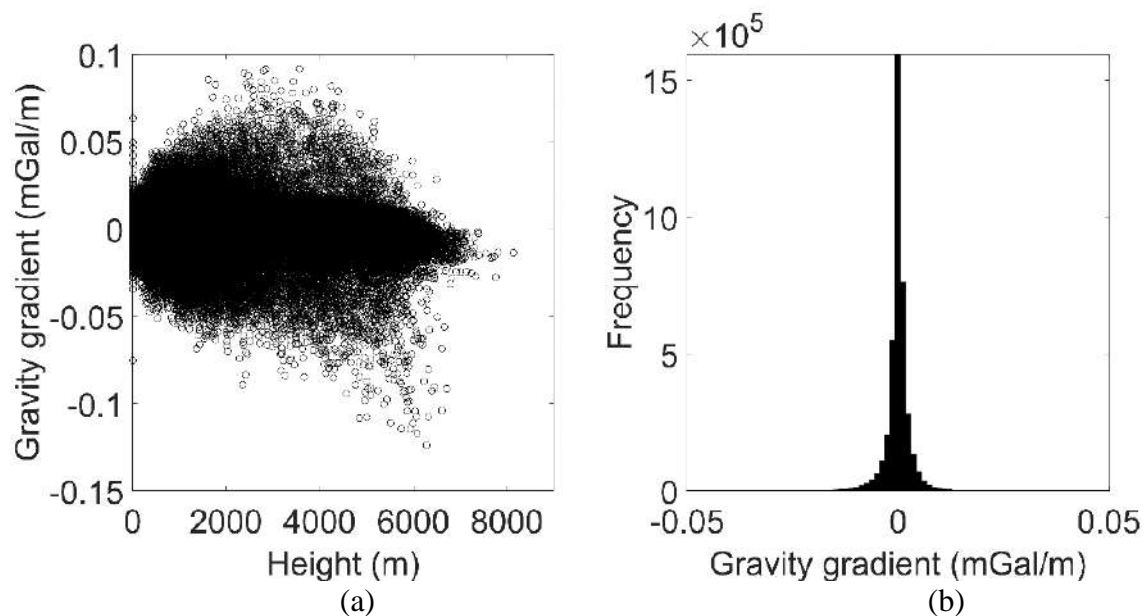


Figure 3.5.2: (a) Scatter plot and (b) Histogram of gravity gradient.

3.5.3 Downward continuation in the KTH method

The KTH method applies the effect of DWC directly on the approximate geoid undulations (δN^{DWC}) and, therefore, can be written as

$$\delta N^{DWC} = \frac{R}{4\pi\gamma_0} \iint_{\sigma} S(\psi) (\Delta g_{KTH}^{DWC} - \Delta g') d\sigma \quad (3.5.10)$$

where Δg_{KTH}^{DWC} is the downward continued gravity anomaly and $\Delta g'$ is the gravity anomaly on the Earth's topography as is required in the KTH method for (modified) Stokes's integration.

Using a concept similar to dividing the topography in the smooth shell and the rough parts, Eq. (3.5.10) can be written as

$$\delta N^{DWC} = \frac{R}{4\pi\gamma_0} \iint_{\sigma} S(\psi) \{ (\Delta g^{DWC} - \Delta g^S) + (\Delta g^S - \Delta g') \} d\sigma \quad (3.5.11)$$

$$\delta N^{DWC} = \delta N_1^{DWC} + \delta N_2^{DWC} \quad (3.5.12)$$

where Δg^S is the gravity anomaly of smooth shell.

Sjöberg (2003b), Ågren (2004), and Sjöberg and Bagherbandi (2017) in their solution to Eq. (3.5.11) gives the same expression for the second term on the R.H.S of Eq. (3.5.11)

$$\delta N_2^{DWC} = \frac{R}{4\pi\gamma_0} \iint_{\sigma} S(\psi) \frac{\partial \Delta g}{\partial r} (H(\Omega) - H(\Omega')) d\sigma \quad (3.5.13)$$

However, somewhat different expressions for the first term on the R.H.S. of Eq. (3.5.11) are observed, and are listed in Table 3.5.1.

Table 3.5.1: Three solutions for first term on the R.H.S of Eq. (3.5.11)

Reference	Solution
Sjöberg (2003b)	$\frac{H\Delta g}{\gamma} + \frac{H}{R+H}\zeta - \frac{H^2}{2\gamma} \frac{\partial \Delta g}{\partial H} - \frac{3H^2\Delta g}{\gamma(R+H)} - \frac{2H^2\zeta}{(R+H)^2} \quad (3.5.14)$
Ågren (2004)	$\frac{H\Delta g}{\gamma} + \frac{3H\zeta}{R+H} - \frac{H^2}{2\gamma} \frac{\partial \Delta g}{\partial H} + \frac{H^2\Delta g}{\gamma(R+H)} + \frac{3H^2\zeta}{(R+H)^2} \quad (3.5.15)$
Sjöberg and Bagherbandi (2017)	$\frac{H\Delta g}{\gamma} + \frac{3H\zeta}{R+H} - \frac{H^2}{2\gamma} \frac{\partial \Delta g}{\partial H} - \frac{H^2\Delta g}{\gamma(R+H)} + \frac{3H^2\zeta}{(R+H)^2} \quad (3.5.16)$

A typographical error in Eq. (3.5.14) (Sjöberg, 2003b) has already been mentioned in the other two literatures (Table 3.5.1). Our derived expression for δN_1^{DWC} is the same as Eq. (3.5.15) (Ågren, 2004). The KTH method makes use of only first three terms in Eq. (3.5.15) and ignores the last two terms in the computation of δN_1^{DWC} . A quantification of the five terms is given in Sjöberg (2003b) but we observe that the values assumed for a few quantities do not match with the observations/computations of the present study. Therefore, we recomputed the five terms in Eq. (3.5.15) with the values i) used in Sjöberg (2003b) and ii) observed (approximately) in the present study. Both are listed in Table 3.5.2, keeping the same values for height. From Table 3.5.2, along with substantial differences obtained in the first and the third terms, we believe that the fourth term cannot be ignored in mountainous regions.

Table 3.5.2: Approximate maximum values for the five terms in Eq. (3.5.15) [parametric values in the first row are from Sjöberg (2003b) and in the second row are from this study; units are in m]

	$\frac{H\Delta g}{\gamma}$	$\frac{3H\zeta}{R+H}$	$\frac{H^2}{2\gamma} \frac{\partial\Delta g}{\partial H}$	$\frac{H^2\Delta g}{\gamma(R+H)}$	$\frac{3H^2\zeta}{(R+H)^2}$
$ \zeta \leq 100 \text{ m}, \Delta g \leq 200 \text{ mGal},$ $\left \frac{\partial\Delta g}{\partial r} \right \leq 0.03 \text{ mGal/m}, H = 5000(8800) \text{ m}$	1.019 (1.794)	0.235 (0.413)	0.382 (1.184)	7.98e-4 (2.47e-3)	1.84e-4 (5.69e-4)
$ \zeta \leq 105 \text{ m}, \Delta g \leq 600 \text{ mGal},$ $\left \frac{\partial\Delta g}{\partial r} \right \leq 0.12 \text{ mGal/m}, H = 5000(8800) \text{ m}$	3.058 (5.382)	0.247 (0.434)	1.529 (4.736)	2.39e-3 (7.42e-3)	1.93e-4 (5.98e-4)

The DWC effect on height anomaly can be derived from Eq. (3.5.11) and using the analytical solution of Molodensky's problem with the involved G_1 term (Eq. (3.5.4)). Since the gravity anomalies have to be analytically continued to the computation point-level surface, the first term in Eq. (3.5.11) vanishes. Now to get the DWC effect on height anomaly, Eq. (3.5.13) is modified to be computed on the Earth's surface, i.e.,

$$\delta\zeta^{DWC} = \frac{r_{cp}}{4\pi\gamma} \iint_{\sigma} S(\psi) \frac{\partial\Delta g}{\partial r} (H(\Omega) - H(\Omega')) d\sigma \quad (3.5.17)$$

Comparing Eqs. (3.5.13) and (3.5.17), R is replaced by r_{cp} ($= R + H$) and normal gravity is now computed on the telluroid instead of on the ellipsoid. Also see Sjöberg and Bagherbandi (2017, Eq. 6.6b). From Ågren (2004, Eqs. 5.45 and 5.46), we have

$$\frac{1}{\gamma_0} = \frac{1}{\gamma} \left(1 - \frac{2H}{r_{cp}} \right) \quad (3.5.18)$$

$$\frac{1}{R} = \frac{1}{r_{cp}} \left(1 + \frac{H}{r_{cp}} \right) \quad (3.5.19)$$

Using Eqs. (3.5.18) and (3.5.19), an approximate relation between (r_{cp}, γ) and (R, γ_0) can be written as

$$\frac{r_{cp}}{\gamma} = \frac{R}{\gamma_0} \left(1 + \frac{3H}{R+H} \right) \quad (3.5.20)$$

Substituting Eq. (3.5.20) in Eq. (3.5.17), the DWC effect on height anomaly can be calculated as

$$\delta\zeta^{DWC} = \left. \begin{aligned} & \frac{R}{4\pi\gamma_0} \iint_{\sigma} S(\psi) \frac{\partial\Delta g}{\partial r} (H(\Omega) - H(\Omega')) d\sigma + \\ & \frac{3H(\Omega)}{r_{cp}} \frac{R}{4\pi\gamma_0} \iint_{\sigma} S(\psi) \frac{\partial\Delta g}{\partial r} (H(\Omega) - H(\Omega')) d\sigma \end{aligned} \right\} \quad (3.5.21)$$

Please note that the second term on the R.H.S. of Eq. (3.5.21) is not seen in KTH's DWC

literature, instead $\frac{3H\zeta_0}{r_{cp}}$ is used (e.g., Ågren, 2004; Ågren et al., 2009b). We believe

$\frac{3H\zeta_0}{r_{cp}}$ is not just the part of DWC. This term, with approximate height anomaly (ζ_0),

arises due to the use of *scaling* (Eq. (3.5.20)) that is done because for height anomalies, computations are done on the Earth's surface with normal gravity on the telluroid.

Therefore, $\frac{3H\zeta_0}{r_{cp}}$ arises from the formulation of approximate height anomaly, and similar

terms may also arise for all the additive corrections in the KTH method of height anomalies due to the scaling factor. One can always avoid this by simply using r_{cp} and normal gravity on telluroid in their formulations, i.e., by not using any scaling.

3.6 Zero-degree term and tidal corrections

Bruns's solution (*ungeneralised*; Heiskanen and Moritz, 1967, pg., 84-85) is valid based on the assumptions that i) the potential of the normal ellipsoid (U_0) and the geoid (W_0)

are same and ii) normal ellipsoid encloses the mass same as that of the Earth, i.e. $GM_{\text{Ellipsoid}} = GM_{\text{Earth}}$. There is one more assumption, i.e., the centre of the normal ellipsoid coincides with the Earth's centre of mass (this makes degree-one harmonic coefficients inadmissible). Practically, none of these assumptions are warranted. Therefore, along with Stokes's integration, one must account for any systematic bias (if any) emanating due to these three assumptions. Non-fulfilment of the first two assumptions is attached with what is known as zero-degree term while the failure of third assumption relates to the first-degree term. Here we will discuss the zero-degree term only because it has been reported inconsistently in the literature (e.g., Goyal et al., 2022).

Another important aspect is the tidal corrections for the effect of tide-generating forces of the Sun and the Moon. Here, we restrict ourselves from the discussions on the tidal potential, tidal forces, and tidal deformation (see Melchior, 1958, 1974, 1978; 1983; Vaníček, 1973; Heikkinen, 1978; among others). Instead, we discuss the effect of different permanent tide systems in relation to geoid modelling. There are *mainly* three types of permanent tide-system: tide-free, zero-tide and mean tide. Their definition, in short, is (Groten, 2004): (i) tide-free is the quantity from which all tidal effects have been removed, (ii) zero-tide includes the indirect tidal distortion, but not the direct distortion, and (iii) mean-tide includes both direct and indirect permanent tidal distortions. For more detailed definitions and distinctions among them, see, e.g., Ekman (1989), Mäkinen and Ihde (2009) or Mäkinen (2021).

In spherical harmonic synthesis (SHS) of the gravity field, the permanent tide affects the value of the dynamical form factor (J_2) and hence, the fully normalised degree-two order-zero Stokes coefficient. This further causes change in geometrical and physical parameters of the normal ellipsoid in use.

It should be noted that the changes in the normal ellipsoid due to change in the solid Earth permanent tide-system are not compulsory. It depends on how we choose to define the normal ellipsoid, i.e., a changing or an unchanging/fixed reference ellipsoid. Though it seems like the latter is the current practice, the former has also been mentioned in the literature (e.g., Vermeer and Poutanen, 1997; Smith, 1998; Lemoine et al., 1998, Section 11.1; Mäkinen, 2017; QPS, 2020). However, discussions on geodetic quantities in different tide-systems are almost always presented with respect to a fixed reference ellipsoid. Also, if there is no concern about the tide-system of an ellipsoid (i.e., for ‘the fixed ellipsoid’ case), then one can always question the use of mentioning tide-system of the ellipsoidal parameters (e.g., Moritz, 2000; Ihde et al., 2017; Drewes and Hornik, 2013; Kotsakis and Katsambalos, 2010; Angermann et al., 2016).

Therefore, in this section we discuss the change in physical Earth and also parameters of the normal ellipsoid due to change in the solid Earth permanent tide-system.

We provide numerical examples for both the cases: change and no-change in ellipsoidal parameters due to different tide-systems. It is shown that the geoid is independent of the permanent tide-system if we consider that there is a change in the ellipsoidal parameters for different tide-systems. The results recommend towards a required convention on: if we want 1. geoid undulations independent of permanent tide-system or 2. a single reference ellipsoid independent of tide-system.

Both, zero-degree term and tidal corrections are common to all the methods yet handled inconsistently in the literature on geoid computation. Like Section 3.1, we will discuss both these corrections in general rather than method-wise.

3.6.1 Zero-degree term

The geoid undulation N (without topographical biases e.g., Rapp, 1997) in spherical harmonics is given by (subscript G is for GGM and subscript E is for the normal ellipsoid)

$$N(r, \theta, \lambda) = \frac{GM_G}{r\gamma_0} \sum_{n=0}^{\infty} \left(\frac{a_G}{r} \right)^n \times \left. \sum_{m=0}^n \left[\left(\bar{C}_{G_{-nm}} - \frac{GM_E}{GM_G} \left(\frac{a_E}{a_G} \right)^n \bar{C}_{E_{-nm}} \right) \cos(m\lambda) + \bar{S}_{G_{-nm}} \sin(m\lambda) \right] \bar{P}_{nm}(\cos \theta) \right\} \quad (3.6.1)$$

$$N(r, \theta, \lambda) = \frac{GM_G}{r\gamma_0} \left(1 - \frac{GM_E}{GM_G} \right) + \left. \begin{aligned} & \frac{\sqrt{3}GM_G}{r\gamma_0} \left(\frac{a_G}{r} \right) \left[\bar{C}_{G_{-1,0}} \cos \theta + \bar{C}_{G_{-1,1}} \cos \lambda \sin \theta + \bar{S}_{G_{-1,1}} \sin \lambda \sin \theta \right] + \\ & \frac{GM_G}{r\gamma_0} \sum_{n=2}^{\infty} \left(\frac{a_G}{r} \right)^n \times \\ & \sum_{m=0}^n \left[\left(\bar{C}_{G_{-n,m}} - \frac{GM_E}{GM_G} \left(\frac{a_E}{a_G} \right)^n \bar{C}_{E_{-n,m}} \right) \cos(m\lambda) + \bar{S}_{G_{-n,m}} \sin(m\lambda) \right] \bar{P}_{n,m}(\cos \theta) \end{aligned} \right\} \quad (3.6.2)$$

$$N = N_0 + N_1 + \sum_{n=2}^{\infty} N_n \quad (3.6.3)$$

We assume that the centre of mass of the Earth is coinciding with centre of the normal ellipsoid, therefore, degree-one terms are inadmissible. Please note that this is just an assumption, which need not be true and necessary corrections are required (e.g., Heiskanen and Moritz, 1967, pg. 99; Kirby and Featherstone, 1997). Now, if the second assumption of Bruns's solution is not valid then from Eq. (3.6.2) zero-degree term comes into play. The freely available SHS software, like isGraflab (Bucha and Janák, 2014) or online services, like ICGEM (Ince et al., 2019) applies this zero-degree term (N_0) i.e.,

$$N_0 = \frac{GM_G - GM_E}{r\gamma_0} \quad (3.6.4)$$

We know that the first assumption is also not valid in real world especially when there are numerous choices of geopotential values both, local (e.g., Grafarend and Ardalan, 1997; Burša et al., 2004; Kotsakis et al., 2012; Tenzer et al., 2012; He et al., 2017) and global (e.g., Petit and Luzum, 2010; Dayoub et al., 2012; Sánchez et al., 2016; Amin et al., 2019; Poutanen and Rózsa, 2020). However, Eq. (3.6.4) does not consider difference in the values of geopotential and equipotential of the normal ellipsoid.

As such, a complete zero-degree term for the geoid can be computed using the generalised Bruns's formula that can be obtained as (Heiskanen and Moritz, 1967, Section 2-19; Smith, 1998)

$$N_0 = \frac{GM_G - GM_E}{r\gamma_0} - \frac{W_0 - U_0}{\gamma_0} \quad (3.6.5)$$

which we abbreviate as

$$N_0 = ZT_1 - ZT_2 \quad (3.6.6)$$

This zero-degree term is one of the most inconsistently reported corrections in the geoid modelling publications. Different geoid solutions in phase-1 of the Colorado geoid experiment varied substantially, and the leading cause was the inconsistent use of the zero-degree term (Wang et al., 2018; Wang and Forsberg, 2019). However, standardisation on the zero-degree term was then decided for further computations (e.g., Jiang et al., 2020; Claessens and Filmer, 2020; Wang et al., 2021).

The computations of geoid and quasigeoid over Auvergne using various approaches (e.g., Ågren et al., 2009a; Valty et al., 2012; Janák et al., 2017) and their comparison with our test computations using the CUT and the KTH methods over the same region (Goyal et al., 2022; provided in Appendix C.4) indicate that previously reported studies applied only the first term in Eq. (3.6.5). That makes ~730 mm difference in the

final geoid solutions. Further, Foroughi et al. (2019) and Ellmann et al. (2020) claim to have computed sub-centimetre geoid. However, the limited reported information on the zero-degree term is inadequate to appreciate if it is a sub-centimetre precise geoid or a sub-centimetre geoid shifted by an amount equal to the numerical value of the second term in Eq. (3.6.5). Moreover, since this forms a systematic error, its effect is not seen in error propagation.

Speaking collectively, none of the computations with the methods those we are working with (i.e., CUT, UNB and KTH) seem to have consistently reported the zero-degree term in all the computations. That is, it might be plausible that some computations might have involved the zero-degree term, while others may not. The fitting to GNSS/levelling also clouds the matter.

Now, revisiting Eq. (3.6.5) to be used with SHS of geoid undulations, the most commonly used normal ellipsoids in geoid computation are WGS84 (NIMA, 2000) and GRS80 (Moritz, 2000). Therefore, with some global W_0 values (Table 3.6.1), a quantification of Eq. (3.6.5) is provided in Table 3.6.2 using GRS80 and WGS84 ellipsoids. The value of GM_G in the computations of Table 3.6.2 is taken as $3986004.415 \times 10^8 \text{ m}^3\text{s}^{-2}$ (Ries et al., 1992), which includes atmospheric masses.

Table 3.6.1: Values of the equipotential of normal ellipsoid (U_0) and global geopotential (W_0)

Potential	Value (m^2s^{-2})	Reference
W_0	62636856.00	IERS/IAU (Petit and Luzum, 2010)
	62636855.69	Burša et al. (1999)
	62636853.40	IHRS (Sánchez et al., 2016; Poutanen and Rózsa, 2020)
U_0	62636860.8500	GRS80 (Moritz, 2000)
	62636851.7146	WGS84 (NIMA, 2000)

Table 3.6.2: Individual terms of Eq. (3.6.5) i.e., generalised Bruns's formula implied zero-degree term.

W_0	U_0		ZT_1 (m)	ZT_2 (m)	N_0 (m)
IHRS	GRS80	min	-0.9378	-0.7617	-0.1783
		max	-0.9360	-0.7577	-0.1761
EGM2008	GRS80	min	-0.9378	-0.5276	-0.4112
		max	-0.9360	-0.5248	-0.4102
IERS/IAU	GRS80	min	-0.9378	-0.4959	-0.4427
		max	-0.9360	-0.4933	-0.4419
IHRS	WGS84	min	-0.0048	0.1714	-0.1771
		max	-0.0048	0.1723	-0.1762
EGM2008	WGS84	min	-0.0048	0.4043	-0.4113
		max	-0.0048	0.4065	-0.4091
IERS/IAU	WGS84	min	-0.0048	0.4359	-0.4407
		max	-0.0048	0.4382	-0.4430

Table 3.6.2 shows a large systematic bias that can enter into the geoid solution if the zero-degree term is not handled appropriately. We further see that the overall zero-degree term (N_0) for the two different ellipsoids does not vary much compared to the significant variations in the ZT_1 and ZT_2 terms, individually. Therefore, use of both the terms in Eq. (3.6.5) is suggested. In the computation of the zero-degree term, γ_0 and r depend on latitude, so N_0 will differ by a few millimetres from equator to pole (Table 3.6.2).

It should be noted here that a few researchers (e.g., Schettino, 2015, pg. 369) provided GM_E value from WGS84 (NIMA, 2000) but U_0 value from the older version of WGS84 (Macomber, 1984), i.e., $62636860.8497 \text{ m}^2\text{s}^{-2}$. This can cause a further error/shift of $\sim 900 \text{ mm}$ in the geoid solution.

Then, there is tide-system that also enters into the computations. For example, almost all the GGMs are in the tide-free system (with a few in the zero-tide system), but there is an inconsistency in reporting the tide-system of GRS80. Rapp et al. (1991) and

Ihde et al. (2017) mentioned GRS80 to be in tide-free system, Drewes and Hornik (2013, pg. 262) report that semi-major axis and flattening of GRS80 are in zero-tide system, Kotsakis and Katsambalos (2010) use GRS80 as being defined in zero-tide system and Angermann et al. (2016, Table 3.1) mentioned that semi-major axis is in tide-free system while J_2 is in zero-tide system.

However, we interpret that the GRS80 is in the tide-free system. The rationale behind this is the explicit mention in Moritz (2000) that the dynamical form factor of GRS80 is “*excluding the permanent tidal deformation*”. Accordingly, we also interpret that the WGS84-older version (Macomber, 1984) and WGS84 (NIMA, 2000) both are in the tide-free system because they use, directly or indirectly, the same value of J_2 from GRS80.

Proof for our speculation on the similarity of WGS84 and GRS80 follows from Table 3.6.3, which tabulates their respective defining parameters.

Table 3.6.3: Defining parameters of the three normal ellipsoids.

Ellipsoid	Defining Parameters				Reference
WGS84-older version	a (m)	$\bar{C}_{2,0}$	ω (s ⁻¹)	GM (m ³ s ⁻²)	Macomber (1984)
	6378137	$-4.8416685 \times 10^{-4}$	7.292115×10^{-5}	3.986005×10^{14}	
WGS84	a (m)	$1/f$	ω (s ⁻¹)	GM (m ³ s ⁻²)	NIMA (2000)
	6378137	298.257223563	7.292115×10^{-5}	$3.986004418 \times 10^{14}$	
GRS80	a (m)	J_2	ω (s ⁻¹)	GM (m ³ s ⁻²)	Moritz (2000)
	6378137	1.08263×10^{-3}	7.292115×10^{-5}	3.986005×10^{14}	

From Table 3.6.3, the older WGS84 had the parameters exactly the same as that of the GRS80 (with $\bar{C}_{2,0}^{WGS84_old}$ truncated to eight significant digits).

$$J_2^{GRS80} = 1.08263 \times 10^{-3} = -\sqrt{5} \bar{C}_{2,0}^{GRS80} \Rightarrow \bar{C}_{2,0}^{GRS80} = -4.8416685489 \times 10^{-4} = \bar{C}_{2,0}^{WGS84_old}$$

Using $J_2 = -\sqrt{5} \bar{C}_{2,0}$, we also have $J_{2_WGS84_old} = 0.0010826299$

Using the Newton-Raphson (NR) solution for ellipsoids (see Section 3.6.3) f and U_0 are computed to be $1/f_{WGS84_old} = 298.257223563$ and $U_{0_WGS84_old} = 62636860.8497 \text{ m}^2\text{s}^{-2}$. It should be noted that the computed $1/f_{WGS84_old}$ is same as the defining parameter of WGS84 ($1/f_{WGS84}$, Table 3.6.3).

Furthermore, utilising the parameters of WGS84, we computed $J_{2_WGS84} = 0.0010826298$ and $U_{0_WGS84} = 62636851.7146 \text{ m}^2\text{s}^{-2}$. On truncating J_{2_WGS84} to eight significant digits, we have $J_{2_WGS84_old} = J_{2_WGS84} = J_{2_GRS80}$ (NIMA, 2000, pg. 7-2). The difference in the normal potential of the two versions of WGS84 ellipsoid is only due to a change in the GM value ($3.986005 \times 10^{14} \text{ m}^3\text{s}^{-2}$ versus $3.986004418 \times 10^{14} \text{ m}^3\text{s}^{-2}$). However, a difference in $1/f$ of the three ellipsoids should not have been there but is due to only truncation and rounding errors.

However, under the framework of the International Height Reference System (IHRs) it has been now suggested to use the mean-tide system for all geodetic observations, and this has been adopted as the International Association of Geodesy (IAG) convention (Poutanen and Rózsa, 2020). Therefore, if using a GGM in IHRs, there is a need to i) convert the Stokes coefficients and other ellipsoidal parameters (Section 3.6.3), among tide-systems, and ii) account for the difference between W_0 and W_0^{IHRs} .

Using the condition that U_0 and W_0 are invariant to the permanent tide systems (Burša, 1995), the zero-degree term for EGM2008 with respect to IHRs, staged *via* GRS80 (with $\gamma_0 = \gamma_a$) simplifies to

$$\left. \begin{aligned}
\Delta N_0 &= \left[\left(\frac{GM_{EGM2008} - GM_{GRS80}}{r\gamma_0} \right) - \left(\frac{W_{EGM2008} - U_{GRS80}}{\gamma_0} \right) \right] - \\
&\quad \left[\left(\frac{GM_{EGM2008} - GM_{GRS80}}{r\gamma_0} \right) - \left(\frac{W_0^{IHRs} - U_{GRS80}}{\gamma_0} \right) \right] \\
\Delta N_0 &= \left(\frac{W_0^{IHRs} - W_{EGM2008}}{\gamma_0} \right) = \frac{62636853.4 - 62636855.69}{9.78032677153479} = -0.234 \text{ m}
\end{aligned} \right\} (3.6.7)$$

If we need to transform the regional/national vertical datums to the IHRs, then local W_0 values might have to be re-computed. In the literature, we were unable to find any local W_0 value computed in the mean-tide system. The input quantities for the computation of geopotential value are dependent on the choice of tide-systems. Therefore, these W_0 values in the mean-tide system might differ (e.g., Sánchez et al., 2016) from the present values and hence, would have to be re-computed in the mean-tide system and with respect to the IAG-adopted IHRs value of W_0^{IHRs} (Sánchez et al., 2021).

3.6.2 Tidal corrections to the physical Earth

In many aspects of geodesy, conversions need to be made among different permanent tide systems (zero-tide, tide-free, mean tide) because of different conventions adopted in sub disciplines. For instance, gravimetric geoid heights are recommended to be in the zero-tide system (e.g., Vattr, 1999; IAG Resolution 16 Hamburg 1983) though several are computed in the tide-free system, GNSS positioning with respect to the International Terrestrial Reference Frame (ITRF) is in the conventional tide-free system (Poutanen et al., 1996), and levelled heights are often in the mean-tide system (Heck, 1993b; Mäkinen and Ihde, 2009; Tenzer et al., 2012), though zero-tide has been implemented in some European countries (Sacher et al., 2009).

For IGSN71 (Morelli et al., 1972) gravity network, it was suggested to use the tidal correction (Heikkinen, 1979) and Honkasalo (1964) term. This gives gravity values in

mean-tide system. However, it was followed by the suggestions from Heikkinen (1979) and Ekman (1980), which caused IAG in its resolution no. 15 adopted in IUGG General Assembly (1979) to recommend use of tide-free gravity values (Mueller, 1980; Uotila, 1980). Meanwhile, Groten (1980) and Ekman (1981) point out the problems with the use of tide-free system, and they independently suggested using zero-tide gravity observations. Following these studies, IAG in its resolution no. 9 adopted in IUGG General Assembly in Hamburg in 1983 recommended using the zero-tide system for the potential field quantities.

However, recently under the aegis of IHRIS, IAG has recommended the use of mean tide system for all the geodetic observations (Poutanen and Rózsa, 2020). Therefore, we revisit Ekman's (1989) equations (Eqs. (3.6.8) - (3.6.11)) for the conversion of gravity, geoid undulation, orthometric height and ellipsoidal height among the three tide-systems (gravity in μGal and heights in mm).

$$\begin{aligned}
 g_{MT} - g_{ZT} &= -\frac{\partial W_T}{\partial r} = -30.4 + 91.2 \sin^2 \varphi \\
 g_{ZT} - g_{TF} &= -(\delta_2 - 1) \frac{\partial W_T}{\partial r} = (\delta_2 - 1)(-30.4 + 91.2 \sin^2 \varphi) \\
 g_{MT} - g_{TF} &= -\delta_2 \frac{\partial W_T}{\partial r} = \delta_2 (-30.4 + 91.2 \sin^2 \varphi)
 \end{aligned} \tag{3.6.8}$$

$$\begin{aligned}
 N_{MT} - N_{ZT} &= \frac{W_T}{g} = 99 - 296 \sin^2 \varphi \\
 N_{ZT} - N_{TF} &= k_2 \frac{W_T}{g} = k_2 (99 - 296 \sin^2 \varphi) \\
 N_{MT} - N_{TF} &= (1 + k_2) \frac{W_T}{g} = (1 + k_2)(99 - 296 \sin^2 \varphi)
 \end{aligned} \tag{3.6.9}$$

$$\begin{aligned}
H_{MT} - H_{ZT} &= -\frac{W_T}{g} = -(99 - 296 \sin^2 \varphi) \\
H_{ZT} - H_{TF} &= -(\gamma_2 - 1) \frac{W_T}{g} = -(\gamma_2 - 1)(99 - 296 \sin^2 \varphi) \\
H_{MT} - H_{TF} &= -\gamma_2 \frac{W_T}{g} = -\gamma_2 (99 - 296 \sin^2 \varphi)
\end{aligned} \tag{3.6.10}$$

$$\begin{aligned}
h_{MT} - h_{ZT} &= 0 \\
h_{ZT} - h_{TF} &= (1 - \gamma_2 + k_2) \frac{W_T}{g} = h_2 (99 - 296 \sin^2 \varphi) \\
h_{MT} - h_{TF} &= (1 + k_2 - \gamma_2) \frac{W_T}{g} = h_2 (99 - 296 \sin^2 \varphi)
\end{aligned} \tag{3.6.11}$$

where W_T is the tidal potential, h_2 and k_2 are second-degree load Love numbers. Ekman (1988) mentions that h_2 describes the vertical tidal displacement of the crust relative to the ellipsoid and k_2 describes the additional potential due to the deformation. $\gamma_2 (= 1 + k_2 - h_2)$ and $\delta_2 \left(= 1 + h_2 - \frac{3}{2} k_2 \right)$ are the factors that come up in the derivations of vertical displacement of the geoid relative to the crust and tidal gravitation as observed on the surface of the deformed crust, respectively.

It is not clear from Ekman (1989) where these numerical values come from, which makes it difficult to understand any approximations/assumptions involved in deriving these equations and rederive the same from the viewpoint of cm-precise geoid. However, Mäkinen (2021) provides more rigorous formulations for the conversion of gravity and orthometric height among mean-tide and zero-tide systems. The building block is the tidal potential (Eq. (3.6.12)), which is transformed in terms of the geodetic coordinates (Eq. (3.6.13))

$$W_T = \frac{3}{2} H_0 \sqrt{\frac{5}{4\pi}} g_e \left(\frac{r}{R_e} \right)^2 \left(\sin^2 \phi - \frac{1}{3} \right) \tag{3.6.12}$$

$H_0 = -0.31460$ m is the zero-frequency tidal displacement amplitude, and $R_e = 6378136.55$ m is the Earth's equatorial radius and $g_e = 9.79828685$ ms⁻²

$$W_T = \left(1 + \frac{2h}{a}\right) (0.9722 - 2.8841 \sin^2 \varphi - 0.0195 \sin^4 \varphi) \quad (3.6.13)$$

Thus, the derived conversion formula for gravity and orthometric height are (Mäkinen, 2021)

$$g_{MT} - g_{ZT} = -30.49 + 90.95 \sin \varphi + 0.31 \sin^4 \varphi \quad (3.6.14)$$

$$H_{MT} - H_{ZT} = \frac{W_T(\varphi, 0)}{\gamma_0(\varphi)} = 99.40 - 295.41 \sin^2 \varphi - 0.42 \sin^4 \varphi \quad (3.6.15)$$

To our disposal, we tried to derive relatively more exact formulas for the conversion of gravity (Eq. (3.6.17)), geoid undulation (Eq. (3.6.18)), dynamic height (Eq. (3.6.19)), orthometric height (Eq. (3.6.20)), normal height (Eq. (3.6.21)) and ellipsoidal height (Eq. (3.6.22)) among different solid Earth permanent tide systems. Initially, unlike Mäkinen (2021) and Ekman (1989), we made use of exact transformation of tidal potential (Eq. (3.6.12)) in terms of geodetic coordinates (Eq. (3.6.16); Claessens, 2021)

$$W_T = A \left(1 + \frac{2h}{a}\right) \left[\frac{(2e^4 - 4e^2 + 3) \sin^2 \varphi - 1}{3(1 - e^2 \sin^2 \varphi)} \right] = \left(1 + \frac{2h}{a}\right) \left[\frac{-2.8907 \sin^2 \varphi + 0.9722}{1 - e^2 \sin^2 \varphi} \right] \quad (3.6.16)$$

where $A = -2.9166$ m²s⁻².

The derived conversion formulas are (gravity in μ Gal and heights in mm)

$$\left. \begin{aligned} g_{MT} - g_{ZT} &= -\frac{\partial W_T}{\partial h} = \frac{-30.485 + 90.644 \sin^2 \varphi}{1 - e^2 \sin^2 \varphi} \\ g_{ZT} - g_{TF} &= -(\delta_2 - 1) \frac{\partial W_T}{\partial h} = (\delta_2 - 1) \frac{-30.485 + 90.644 \sin^2 \varphi}{1 - e^2 \sin^2 \varphi} \\ g_{MT} - g_{TF} &= -\delta_2 \frac{\partial W_T}{\partial h} = \delta_2 \frac{-30.485 + 90.644 \sin^2 \varphi}{1 - e^2 \sin^2 \varphi} \end{aligned} \right\} \quad (3.6.17)$$

$$\left. \begin{aligned}
 N_{MT} - N_{ZT} &= \frac{W_T(\varphi, 0)}{\gamma_0(\varphi)} = \frac{99.4 - 295.6 \sin^2 \varphi}{(1 + k \sin^2 \varphi)(\sqrt{1 - e^2 \sin^2 \varphi})} \\
 N_{ZT} - N_{TF} &= k_2 \frac{W_T(\varphi, 0)}{\gamma_0(\varphi)} = k_2 \frac{99.4 - 295.6 \sin^2 \varphi}{(1 + k \sin^2 \varphi)(\sqrt{1 - e^2 \sin^2 \varphi})} \\
 N_{MT} - N_{TF} &= (1 + k_2) \frac{W_T(\varphi, 0)}{\gamma_0(\varphi)} = (1 + k_2) \frac{99.4 - 295.6 \sin^2 \varphi}{(1 + k \sin^2 \varphi)(\sqrt{1 - e^2 \sin^2 \varphi})}
 \end{aligned} \right\} (3.6.18)$$

$$\left. \begin{aligned}
 H_{MT}^d - H_{ZT}^d &= -\frac{W_T(\varphi, 0)}{\gamma_0(45^\circ)} = -\left(\frac{99.1 - 294.8 \sin^2 \varphi}{1 - e^2 \sin^2 \varphi} \right) \\
 H_{ZT}^d - H_{TF}^d &= -(\gamma_2 - 1) \frac{W_T(\varphi, 0)}{\gamma_0(45^\circ)} = -(\gamma_2 - 1) \left(\frac{99.1 - 294.8 \sin^2 \varphi}{1 - e^2 \sin^2 \varphi} \right) \\
 H_{MT}^d - H_{TF}^d &= -\gamma_2 \frac{W_T(\varphi, 0)}{\gamma_0(45^\circ)} = -\gamma_2 \left(\frac{99.1 - 294.8 \sin^2 \varphi}{1 - e^2 \sin^2 \varphi} \right)
 \end{aligned} \right\} (3.6.19)$$

$$\left. \begin{aligned}
 H_{MT} - H_{ZT} &= -\frac{W_T(\varphi, 0)}{\gamma_0(45^\circ)} \times \frac{\gamma_0(45^\circ)}{\bar{g}} = -\left(\frac{99.1 - 294.8 \sin^2 \varphi}{1 - e^2 \sin^2 \varphi} \right) \times \frac{\gamma_0(45^\circ)}{\bar{g}} \\
 H_{ZT} - H_{TF} &= -(\gamma_2 - 1) \frac{W_T(\varphi, 0)}{\gamma_0(45^\circ)} \times \frac{\gamma_0(45^\circ)}{\bar{g}} = -(\gamma_2 - 1) \left(\frac{99.1 - 294.8 \sin^2 \varphi}{1 - e^2 \sin^2 \varphi} \right) \times \frac{\gamma_0(45^\circ)}{\bar{g}} \\
 H_{MT} - H_{TF} &= -\gamma_2 \frac{W_T(\varphi, 0)}{\gamma_0(45^\circ)} \times \frac{\gamma_0(45^\circ)}{\bar{g}} = -\gamma_2 \left(\frac{99.1 - 294.8 \sin^2 \varphi}{1 - e^2 \sin^2 \varphi} \right) \times \frac{\gamma_0(45^\circ)}{\bar{g}}
 \end{aligned} \right\} (3.6.20)$$

$$\left. \begin{aligned}
 H_{MT}^* - H_{ZT}^* &= -\frac{W_T(\varphi, 0)}{\gamma_0(45^\circ)} \times \frac{\gamma_0(45^\circ)}{\bar{\gamma}} = -\left(\frac{99.1 - 294.8 \sin^2 \varphi}{1 - e^2 \sin^2 \varphi} \right) \times \frac{\gamma_0(45^\circ)}{\bar{\gamma}} \\
 H_{ZT}^* - H_{TF}^* &= -(\gamma_2 - 1) \frac{W_T(\varphi, 0)}{\gamma_0(45^\circ)} \times \frac{\gamma_0(45^\circ)}{\bar{\gamma}} = -(\gamma_2 - 1) \left(\frac{99.1 - 294.8 \sin^2 \varphi}{1 - e^2 \sin^2 \varphi} \right) \times \frac{\gamma_0(45^\circ)}{\bar{\gamma}} \\
 H_{MT}^* - H_{TF}^* &= -\gamma_2 \frac{W_T(\varphi, 0)}{\gamma_0(45^\circ)} \times \frac{\gamma_0(45^\circ)}{\bar{\gamma}} = -\gamma_2 \left(\frac{99.1 - 294.8 \sin^2 \varphi}{1 - e^2 \sin^2 \varphi} \right) \times \frac{\gamma_0(45^\circ)}{\bar{\gamma}}
 \end{aligned} \right\} (3.6.21)$$

$$\left. \begin{aligned} h_{MT} - h_{ZT} &= (H_{MT} - H_{ZT}) + (N_{MT} - N_{ZT}) = W_T \left(\frac{1}{\gamma_0} - \frac{1}{\bar{g}} \right) \\ h_{ZT} - h_{TF} &= (H_{ZT} - H_{TF}) + (N_{ZT} - N_{TF}) = W_T \left(\frac{k_2}{\gamma_0} - \frac{\gamma_2 - 1}{\bar{g}} \right) \\ h_{MT} - h_{TF} &= (H_{MT} - H_{TF}) + (N_{MT} - N_{TF}) = W_T \left(\frac{1 + k_2}{\gamma_0} - \frac{\gamma_2}{\bar{g}} \right) \end{aligned} \right\} \quad (3.6.22)$$

Considering $\gamma_0 \approx \bar{g}$ in Eq. (3.6.22), we get equation for conversion of the ellipsoidal height, which is comparable to Ekman (1989), i.e.,

$$\left. \begin{aligned} h_{MT} - h_{ZT} &= 0 \\ h_{ZT} - h_{TF} &= (1 + k_2 - \gamma_2) \frac{99.4 - 295.6 \sin^2 \varphi}{(1 + k \sin^2 \varphi) (\sqrt{1 - e^2 \sin^2 \varphi})} \\ h_{MT} - h_{TF} &= (1 + k_2 - \gamma_2) \frac{99.4 - 295.6 \sin^2 \varphi}{(1 + k \sin^2 \varphi) (\sqrt{1 - e^2 \sin^2 \varphi})} \end{aligned} \right\} \quad (3.6.23)$$

Table 3.6.4 provides a comparison of Ekman (1989) and our conversion formula for gravity, geoid undulation, orthometric height and ellipsoidal height over $\varphi = [0^\circ, 90^\circ]$. From Table 3.6.4, it is seen that the difference in the two formulas for heights can reach >1 mm. Hence, our equations should be used because they are relatively more exact as compared to Ekman (1989), although these differences ($>\approx 1$ mm) are mainly due to the different second-degree load Love numbers as compared to the different equations. For gravity, the difference is <1 μGal for all the conversions, and hence, as of today we can use any of the two equations but in future when portable gravimeters will be of <1 μGal precision, our formulas must be used.

Table 3.6.4: Difference between Ekman (1989) and our conversion formula

		min	max	mean	STD
Gravity	MT-ZT	-0.32	-0.09	-0.24	0.08
(μGal)	ZT-TF	-0.34	0.14	-0.11	0.17
	MT-TF	-0.58	0.06	-0.35	0.24
Geoid Undulation	MT-ZT	0.40	0.57	0.51	0.06
(mm)	ZT-TF	-0.22	0.31	0.06	0.19
	MT-TF	0.30	0.72	0.57	0.15
Orthometric*	MT-ZT	-0.55	-0.36	-0.48	0.06
(mm)	ZT-TF	-1.29	2.93	0.84	1.51
	MT-TF	-1.65	2.43	0.35	1.46
Ellipsoidal height*	MT-ZT	0.00	0.00	0.00	0.00
(mm)	ZT-TF	-0.96	2.72	0.91	1.32
	MT-TF	-0.96	2.72	0.91	1.32

* Assumed $\bar{g}(\varphi) = \gamma_0(\varphi)$ in our equations.

It is important to note here that Ekman (1989) used the second-degree load Love numbers of $k_2 = 0.3$, $h_2 = 0.62$, $\gamma_2 = 1 + k_2 - h_2 = 0.68$, $\delta_2 = 1 + h_2 - 3k_2/2 = 1.16$, and we have used $k_2 = 0.30190$, $h_2 = 0.60780$ (Petit and Luzum, 2010) $\gamma_2 = 1 + k_2 - h_2 = 0.69410$, $\delta_2 = 1 + h_2 - 3k_2/2 = 1.15495$ in our equations.

3.6.3 Tidal corrections to the ellipsoidal parameters

Before discussing the conversions of the ellipsoidal parameters in different tide systems, we distinguish among defining parameters and derived parameters (Kinoshita, 1994) in relation to the permanent tide. In principle, defining parameters of an ellipsoid are observed/calculated independently. Hence, with the change in one defining parameter (due to permanent tide) there should be no change in other defining parameters. Semi-major axis is the defining parameter of both GRS80 and WGS84. Therefore, its value should remain unaffected due to different permanent tide-system (e.g., change in J_2).

However, with the variation in J_2 the flattening must change but, if the flattening changes and the semi-major axis does not change, then we have changes only in the semi-minor axis. As such, the volume of the Earth will alter. However, the mass of the Earth

must not vary due to a different permanent tide system. So, a variation in the Earth's volume without any deviation in its mass implies a change in the Earth's density due to the different tide system, which is physically unlikely. Therefore, the Earth's volume must not change and that is possible *iff* the defining parameter- semi-major axis also changes with the change in J_2 . Hence, deviating from the meaning of the term 'defining parameter'. As such, we recommend that any new normal ellipsoid should not have semi-major axis and flattening as the defining parameters but follow the mean earth ellipsoid (Heiskanen ad Moritz, 1967, pg. 109) with defining parameters being GM , J_2 , $U_0 (=W_0)$ and ω .

Looking into the SHS of gravity field functions, we see that the effect of different permanent tide system can primarily enter in:

- i) Even-degree zonal harmonic coefficients of the ellipsoid ($\bar{C}_{E_{-2n,0}}$)

$$\bar{C}_{E_{-2n,0}} = \frac{-J_{E_{-2n}}}{\sqrt{4n+1}} \quad (3.6.24)$$

where

$$J_{E_{-2n}} = (-1)^{n+1} \frac{3e_E^{2n}}{(2n+1)(2n+3)} \left(1 - n + 5n \frac{J_{E_{-2}}}{e_E^2} \right) \quad (3.6.25)$$

Or only in terms of flattening,

$$J_{E_{-2n}} = (-1)^{n+1} \frac{3f_E^n (2-f_E)^n}{(2n+1)(2n+3)} \left(1 - n + 5n \frac{J_{E_{-2}}}{2f_E - f_E^2} \right) \quad (3.6.26)$$

- ii) The scaling of the $\bar{C}_{E_{-2n,0}}$ (Eq. (3.6.2))

$$\frac{GM_E}{GM_G} \left(\frac{a_E}{a_G} \right)^{2n} \bar{C}_{E_{-2n,0}} \quad (3.6.27)$$

iii) Normal gravity

We need to find the conversion formulas for J_2 , or the flattening for different permanent tide system because, all other parameters of an ellipsoid are a function of these two terms and, GM and ω . However, the latter two do not change with the change in the permanent tide system. We will also work on the conversion formula of semi-major axis because other studies (Heiskanen and Moritz, 1967, pg. 111; Burša, 1995; Groten, 2004) have provided formulas for it in addition to the conversion formula for flattening.

From Petit and Luzum (2010, Sections 6 and 7), we have (for brevity, we have omitted the subscript in the following discussions) for normal ellipsoid

$$\Delta\bar{C}_{2,0} = \begin{cases} \bar{C}_{2,0}^{ZI} - \bar{C}_{2,0}^{TF} = \frac{H_0}{R_e\sqrt{4\pi}}k_2 = -4.20071 \times 10^{-9} \\ \bar{C}_{20}^{MT} - \bar{C}_{20}^{ZI} = \frac{H_0}{R_e\sqrt{4\pi}} = -1.39143 \times 10^{-8} \\ \bar{C}_{20}^{MT} - \bar{C}_{20}^{TF} = \frac{H_0}{R_e\sqrt{4\pi}}(1+k_2) = -1.81150 \times 10^{-8} \end{cases} \quad (3.6.28)$$

where $k_2 = 0.30190$ is the degree-two Love number for an anelastic Earth (Petit and Luzum, 2010, pg. 83), $H_0 = -0.31460$ m is the zero-frequency tidal displacement amplitude, and $R_e = 6378136.55$ m is the Earth's equatorial radius. Normalising Eq.

(3.6.28) by $-\sqrt{5}$ gives

$$\Delta J_2 = \begin{cases} J_{2,0}^{ZI} - J_{2,0}^{TF} = -\sqrt{\frac{5}{4\pi}} \frac{H_0}{R_e} k_2 = +9.39308 \times 10^{-9} \\ J_{20}^{MT} - J_{20}^{ZI} = -\sqrt{\frac{5}{4\pi}} \frac{H_0}{R_e} = +3.11132 \times 10^{-8} \\ J_{20}^{MT} - J_{20}^{TF} = -\sqrt{\frac{5}{4\pi}} \frac{H_0}{R_e} (1+k_2) = +4.05063 \times 10^{-8} \end{cases} \quad (3.6.29)$$

Values in Eqs. (3.6.28) and (3.6.29) differ slightly from some of the values given in McCarthy and Petit (2003) and Petit and Luzum (2010), which is due to numerical rounding at each stage of their calculations. For instance, their term $A_0 = 1/(R_e \sqrt{4\pi})$ is rounded to $4.4228 \times 10^{-8} \text{ m}^{-1}$, and for EGM96 and EGM2008, the term $A_0 H_0$ is rounded to -1.391×10^{-8} , and k_2 is rounded to 0.3.

Heiskanen and Moritz (1967, pg. 111) used approximate formulas for GM , U_0 and J_2 (Heiskanen and Moritz, 1967, pgs. 77-78) to derive the formulas (in spherical approximation) for calculating the changes in the flattening (Δf) and the semi-major axis (Δa) due to the change in J_2 (ΔJ_2), which are given by

$$\Delta f = \frac{3}{2} \Delta J_2 \quad (3.6.30)$$

$$\Delta a = \frac{a}{2} \Delta J_2 \quad (3.6.31)$$

Burša (1995) and Groten (2004) derived similar formula using scale factor for length $R_0 = GM/U_0$ (Rapp, 1974), which is also considered independent of the permanent tide system (Burša, 1995). They also used the approximate formulas for GM , U_0 and J_2 , to provide Δf same as Eq. (3.6.30) but Δa as

$$\Delta a = \frac{R_0}{2} \Delta J_2 \quad (3.6.32)$$

We instead use the exact equation of J_2 from Moritz (2000) to derive the formulas for Δf and Δa

$$J_2 = \frac{e^2}{3} \left(1 - \frac{2m e'}{15q_0} \right) \quad (3.6.33)$$

where

$$m = \frac{\omega^2 a^2 b}{GM} = \frac{\omega^2 a^3 (1-f)}{GM} \quad (3.6.34)$$

Using Eq. (3.6.34) and other various geometrical relationships among the ellipsoidal parameters (Moritz, 2000), Eq. (3.6.33) is re-written as

$$J_2 = \left(\frac{2f - f^2}{3} \right) \left(1 - \frac{4\omega^2 a^3 (2f - f^2)^{3/2}}{15GM (2f^2 - 4f + 3) \tan^{-1} \left(\frac{\sqrt{2f - f^2}}{1-f} \right) - 45GM \sqrt{2f - f^2} (1-f)} \right) \quad (3.6.35)$$

The total differentiation of Eq. (3.6.34) gives

$$\Delta m = \frac{3\omega^2 a^2 (1-f)}{GM} \Delta a - \frac{\omega^2 a^3}{GM} \Delta f \quad (3.6.36)$$

Inserting the values for GRS80 and approximated values of Δf and Δa from Eqs. (3.6.30) and (3.6.31) in Eq. (3.6.36), Δm is of the order 10^{-10} , which is two orders of magnitude less than the largest ΔJ_2 in Eq. (3.6.29). Although f and m are of similar value (~ 0.003), Δf is of the order 10^{-8} and Δm is of the order 10^{-10} . Therefore, we can assume that there is no change in Δm and, therefore, from Eq. (3.6.36)

$$\Delta a = \frac{a}{3(1-f)} \Delta f \quad (3.6.37)$$

Taking the total differentiation of Eq. (3.6.35) and inserting Eq. (3.6.37) gives

$$\Delta f = \frac{1}{D_{Jf}} \Delta J_2 \quad (3.6.38)$$

$$\Delta a = \frac{a}{3D_{Jf}(1-f)} \Delta J_2 \quad (3.6.39)$$

where

$$D_{Jf} = \frac{2}{3}(1-f) - \frac{4\omega^2 a^3 (2f-f^2)^{3/2}}{45GM} \times \left[\frac{(4(1-f)^4 + 10(1-f)^2 + 1) \tan^{-1} \frac{\sqrt{2f-f^2}}{1-f} - \sqrt{2f-f^2} (8(1-f)^3 + 7(1-f))}{(1-f) \left((2(1-f)^2 + 1) \tan^{-1} \frac{\sqrt{2f-f^2}}{1-f} - 3(1-f) \sqrt{2f-f^2} \right)^2} \right] \quad (3.6.40)$$

Therefore, as required in SHS, the higher than second-degree zonal harmonic coefficients of the ellipsoid can be computed by using Eqs. (3.6.24), (3.6.26), (3.6.29) and (3.6.38) or a direct formula that we derive by taking total differentiation of Eq. (3.6.26) given by

$$\Delta C_{2n,0} = \frac{(-1)^{n+2} 3n f^{n-1} (2-f)^{n-1}}{(2n+1)(2n+3)\sqrt{4n+1}} \left[\frac{2-2f}{D_{Jf}} \left(1-n + (5n-5) \frac{J_2}{2f-f^2} \right) + 5 \right] \Delta J_2 \quad (3.6.41)$$

Burša (1995) proved that the potential is invariant to the choice of tide system, i.e., change in the J_2 , but to cross-check, we derived a formulation to compute the changes (if any) in the normal potential due to change in J_2 . We use the exact formula for normal potential of a reference ellipsoid (Heiskanen and Moritz, 1967, pg. 67)

$$U_0 = \frac{GM}{E} \tan^{-1}(e') + \frac{\omega^2 a^2}{3} \quad (3.6.42)$$

Writing Eq. (3.6.42) in terms of the semi-major axis and the flattening gives

$$U_0 = \frac{GM}{a\sqrt{2f-f^2}} \tan^{-1} \left(\frac{\sqrt{2f-f^2}}{1-f} \right) + \frac{\omega^2 a^2}{3} \quad (3.6.43)$$

Equation (3.6.43) can also be re-arranged in terms of GM as

$$GM = \frac{a\sqrt{2f-f^2} \left(U_0 - \frac{\omega^2 a^2}{3} \right)}{\tan^{-1} \left(\frac{\sqrt{2f-f^2}}{1-f} \right)} \quad (3.6.44)$$

However, taking the total differentiation of Eq. (3.6.43) gives

$$\Delta U_0 = \left\{ \begin{aligned} & \left(\frac{2\omega^2 a}{3} - \frac{GM}{a^2 \sqrt{2f-f^2}} \tan^{-1} \frac{\sqrt{2f-f^2}}{1-f} \right) \Delta a + \\ & \frac{GM}{a(2f-f^2)} \left(1 - \frac{1-f}{\sqrt{2f-f^2}} \tan^{-1} \frac{\sqrt{2f-f^2}}{1-f} \right) \Delta f \end{aligned} \right\} \quad (3.6.45)$$

and using Eqs. (3.6.38) and (3.6.39), we have

$$\Delta U_0 = \frac{D_{JU}}{D_{Jf}} \Delta J_2 \quad (3.6.46)$$

where D_{Jf} is same as Eq. (3.6.40) and

$$D_{JU} = \left(\frac{GM}{a(2f-f^2)} + \frac{2\omega^2 a^2}{9(1-f)} \right) - \frac{GM}{a} \left(\frac{1+2(1-f)^2}{3(1-f)(2f-f^2)^{3/2}} \right) \tan^{-1} \frac{\sqrt{2f-f^2}}{1-f} \quad (3.6.47)$$

Another option is to solve Eqs. (3.6.35) and (3.6.43) or (3.6.44) as system of non-linear equations using NR method with variables being a and f , keeping U_0 , GM and ω constant for each tidal J_2 (following the definition of mean Earth ellipsoid, Heiskanen and Moritz, 1967, pg. 109). We provide some quantification of the above-discussed formulas for GRS80 in Table 3.6.5

Table 3.6.5: Conversion values of parameters for different tide-systems (for GRS80) [ZT = zero-tide; TF = tide-free; MT = mean-tide]

		Burša (Eqs. (3.6.30) and (3.6.32))	Ours (Eqs. (3.6.38) and (3.6.39))	NR solution
$\Delta J_2 (\times 10^{-9})$	ZT-TF	9.39308	9.39308	9.39308
	MT-ZT	31.11320	31.11320	31.11320
	MT-TF	40.50630	40.50630	40.50630
$\Delta f (\times 10^{-8})$	ZT-TF	1.40896	1.41301	1.41301
	MT-ZT	4.66698	4.68038	4.68039
	MT-TF	6.07595	6.09339	6.09339
$\Delta a (\times 10^{-2})$ (in m)	ZT-TF	2.98872	3.01422	3.01578
	MT-ZT	9.89971	9.98417	9.98933
	MT-TF	12.88844	12.99840	13.00511
$\Delta U_0 (\times 10^{-4})^*$ (in m^2s^{-2})	ZT-TF	18.02612	1.52015	0.0000
	MT-ZT	59.70889	5.03527	0.0000
	MT-TF	77.73506	6.55543	0.0000

* Equation (3.6.45) can be used to compute ΔU_0 , but for Table 3.6.5 (all three methods) we have computed U_0 using Eq. (3.6.43) with a and f for different values of J_2 and then took the differences.

From Table 3.6.5, there are minimal differences in the existing approximate solutions and our rigorous formulas (along with NR solution). U_0 can be considered to be invariant to the choice of tide-system, but on a closer look, the approximate formula by Burša (1995) can cause an error of ~ 1 mm in the geoid solution due to the change in U_0 using their formulas. Therefore, it is suggested that to remove all the possible systematic errors in geoid computation one should use as exact as possible formulas, i.e., in this case, the best choice would be the NR's solution followed by our nearly exact formulas (Eqs. (3.6.38) and (3.6.39)).

Now, we derive the formula for conversion of normal gravity between different permanent tide-systems using normal gravity formula (Heiskanen and Moritz, 1967, pg. 77).

$$\gamma = \gamma_a \left(1 + \frac{\gamma_b - \gamma_a}{\gamma_a} \sin^2 \varphi - \frac{1}{4} \left(-\frac{1}{2} f^2 + \frac{5}{2} fm \right) \sin^2 2\varphi \right) \quad (3.6.48)$$

where

$$\gamma_a = \frac{GM}{ab} \left(1 - m - \frac{me' q'_0}{6 q_0} \right) \quad (3.6.49)$$

and

$$\gamma_b = \frac{GM}{a^2} \left(1 + \frac{me' q'_0}{3 q_0} \right) \quad (3.6.50)$$

From Eqs. (3.6.49) and (3.6.50), we derive conversion formulas for normal gravity at equator and poles

$$\left. \begin{aligned} \Delta\gamma_a &= \frac{3.15484135}{D_{Jf}} \Delta J_2 \\ \Delta\gamma_b &= -\frac{6.54767497}{D_{Jf}} \Delta J_2 \end{aligned} \right\} \quad (3.6.51)$$

Taking total differentiation of Eq. (3.6.48) and using Eqs. (3.6.51) and (3.6.38), the conversion formula for normal gravity is

$$\Delta\gamma = \frac{(3.1548 - 9.7025 \sin^2 \varphi - 0.0129 \sin^2 2\varphi)}{D_{Jf}} \Delta J_2 \quad \mu\text{Gal} \quad (3.6.52)$$

There is another constant k provided in Moritz (2000) that is given by

$$k = \frac{b}{a} \frac{\gamma_b}{\gamma_a} - 1 \quad (3.6.53)$$

for which the conversion formula becomes

$$\Delta k = \frac{-4.83346787}{D_{Jf}} \Delta J_2 \quad (3.6.54)$$

Before discussing SHS, we provide simplified conversion formulas for flattening (Eq. (3.6.55)), semi-major axis (Eq. (3.6.56)), semi-minor axis (Eq. (3.6.57)), first eccentricity (Eq. (3.6.58)), normal gravity at equator (Eq. (3.6.59)), normal gravity at poles (Eq. (3.6.60)), normal gravity on ellipsoid (Eq. (3.6.61)) and constant k (Eq. (3.6.62))

$$\left. \begin{aligned} f^{ZT} - f^{TF} &= 1.41300686 \times 10^{-8} \\ f^{MT} - f^{ZT} &= 4.68037801 \times 10^{-8} \\ f^{MT} - f^{TF} &= 6.09338788 \times 10^{-8} \end{aligned} \right\} \quad (3.6.55)$$

$$\left. \begin{aligned} a^{ZT} - a^{TF} &= 30.1 \text{ mm} \\ a^{MT} - a^{ZT} &= 99.8 \text{ mm} \\ a^{MT} - a^{TF} &= 130.0 \text{ mm} \end{aligned} \right\} \quad (3.6.56)$$

$$\left. \begin{aligned} b^{ZT} - b^{TF} &= -60.1 \text{ mm} \\ b^{MT} - b^{ZT} &= -199.0 \text{ mm} \\ b^{MT} - b^{TF} &= -259.1 \text{ mm} \end{aligned} \right\} \quad (3.6.57)$$

$$\left. \begin{aligned} e^{ZT} - e^{TF} &= 1.7212 \times 10^{-7} \\ e^{MT} - e^{ZT} &= 5.7012 \times 10^{-7} \\ e^{MT} - e^{TF} &= 7.4224 \times 10^{-7} \end{aligned} \right\} \quad (3.6.58)$$

$$\left. \begin{aligned} \gamma_a^{ZT} - \gamma_a^{TF} &= 4.4578 \text{ } \mu\text{Gal} \\ \gamma_a^{MT} - \gamma_a^{ZT} &= 14.7659 \text{ } \mu\text{Gal} \\ \gamma_a^{MT} - \gamma_a^{TF} &= 19.2237 \text{ } \mu\text{Gal} \end{aligned} \right\} \quad (3.6.59)$$

$$\left. \begin{aligned} \gamma_b^{ZT} - \gamma_b^{TF} &= -9.2519 \text{ } \mu\text{Gal} \\ \gamma_b^{MT} - \gamma_b^{ZT} &= -30.6456 \text{ } \mu\text{Gal} \\ \gamma_b^{MT} - \gamma_b^{TF} &= -39.8975 \text{ } \mu\text{Gal} \end{aligned} \right\} \quad (3.6.60)$$

$$\left. \begin{aligned} \gamma^{ZT} - \gamma^{TF} &= 4.4578 - 13.7097 \sin^2 \varphi - 0.01823 \sin^2 2\varphi \text{ } \mu\text{Gal} \\ \gamma^{MT} - \gamma^{ZT} &= 14.7657 - 45.4114 \sin^2 \varphi - 0.0604 \sin^2 2\varphi \text{ } \mu\text{Gal} \\ \gamma^{MT} - \gamma^{TF} &= 19.2234 - 59.1211 \sin^2 \varphi - 0.07860 \sin^2 2\varphi \text{ } \mu\text{Gal} \end{aligned} \right\} \quad (3.6.61)$$

$$\left. \begin{aligned} k^{ZT} - k^{TF} &= -6.8297 \times 10^{-8} \\ k^{MT} - k^{ZT} &= -22.6224 \times 10^{-8} \\ k^{MT} - k^{TF} &= -29.4522 \times 10^{-8} \end{aligned} \right\} \quad (3.6.62)$$

3.6.4 Numerical test for tide-system in SHS

We provide some numerical analysis of degree-two geoid undulation (precisely height anomaly) and free-air anomaly using SHS of EGM2008 with GRS80 ellipsoid. Table 3.6.6 and Figure 3.6.1 show the difference of height anomalies among tide-systems calculated by only converting the second-degree zonal Stokes coefficient of EGM2008 (using Eq. (3.6.28)), i.e., without touching any parameter of GRS80. Results from Ekman's (1989) geoid conversion formula are also provided in Table 3.6.6. Figure 3.6.2 provides the plot for the difference in the SHS and Ekman's (1989) values.

Table 3.6.6: Difference in degree-two geoid in three tide systems. Computations are done by considering GRS80 in tide-free system and only changing $\bar{C}_{2,0}$ term of EGM. No changes to any parameter of GRS80 ellipsoid.

		Geoid (mm)			
		min	max	mean	STD
MT-ZT	SHS	-199.763	99.405	-49.567	105.796
	Ekman (1989)	-197.000	99.000	-49.068	104.700
ZT-TF	SHS	-60.308	30.010	-14.964	31.940
	Ekman (1989)	-59.100	29.700	-14.721	31.410
MT-TF	SHS	-260.072	129.415	-64.532	137.735
	Ekman (1989)	-256.100	128.700	-63.789	136.110

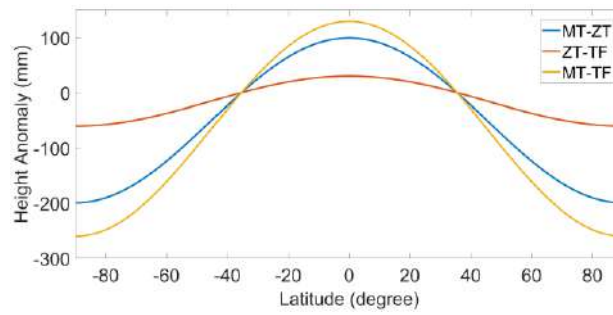


Figure 3.6.1: Variation in geoid undulation for GRS80 in tide-free system and $\bar{C}_{2,0}$ of EGM2008 in different tide system.

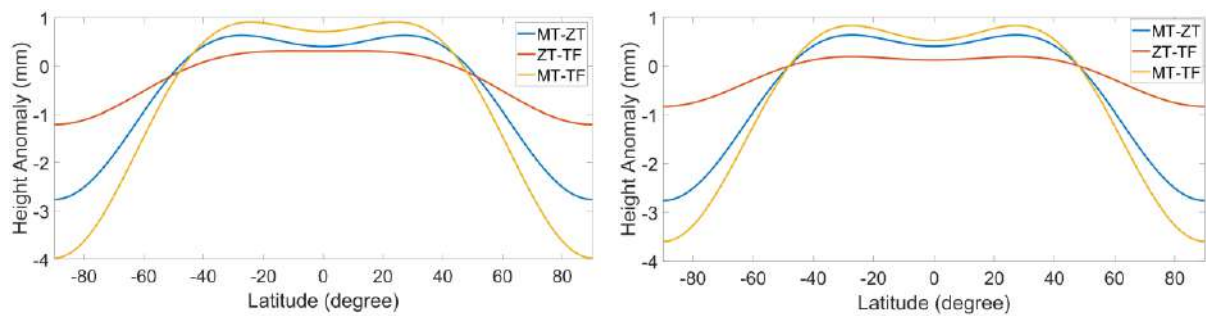


Figure 3.6.2: Difference in Ekman (1989) formula and the calculated value of geoid undulation in different tide-system. (left: $k_2 = 0.3$ in Ekman (1989) and right: $k_2 = 0.30190$ in Ekman (1989))

It should be noted that the absolute difference value of ~ 3 mm for MT-ZT in Figure 3.6.2 is in some accordance with the explanation of Mäkinen (2021, pg. 6) which suggests that an error of $+3.3$ mm can be observed if we use second-degree zonal term of the GGM converted in the mean-tide system using conversion formulas (Eq. (3.6.28)).

This type of geoid undulations that involves no change in the parameters of ellipsoid (defined in tide-free system) can be perceived as the separation between mean-tide geoid and tide-free ellipsoid or zero-tide geoid and tide-free ellipsoid or tide-free geoid and tide-free ellipsoid. We think that geoid undulation should be the separation between the geoid and ellipsoid, both in the same tide-system. Therefore, only the last choice, i.e., distance between tide-free geoid and tide-free ellipsoid provides the required geoid undulation.

To check the variation of geoid undulations between: mean-tide geoid – mean-tide ellipsoid, tide-free geoid – tide-free ellipsoid and zero-tide geoid – zero-tide ellipsoid, geoid undulations have also been computed with changed parameters of GRS80. The results are provided in Table 3.6.7 and Figure 3.6.3.

Table 3.6.7: Difference in degree-two geoid undulation computed using EGM2008 and GRS80 (both in same tide system)

	Geoid (mm)			
	min	max	mean	STD
MT-ZT	-0.056	0.108	0.027	0.057
ZT-MT	-0.017	0.033	0.008	0.017
TF-MT	-0.073	0.141	0.035	0.075

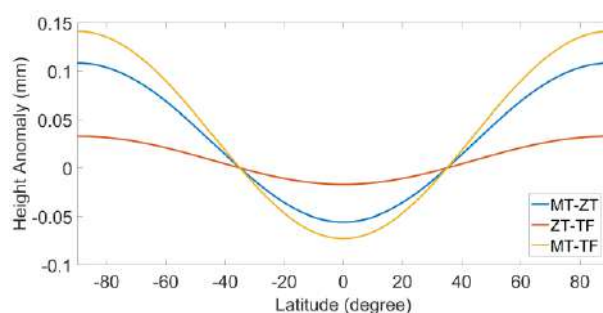


Figure 3.6.3: Variation of the difference in degree-two geoid undulation computed using EGM2008 and GRS80 (both in same tide system).

Table 3.6.7 and Figure 3.6.3 show that though geoid may deform under tidal potential (Table 3.6.6), geoid undulation is independent of the tide-system provided that geoid undulation is defined as the difference between geoid and normal ellipsoid, both in same permanent tide-system.

We also performed similar exercises for SHS of free-air gravity anomalies (FAA) using EGM2008 and GRS80. Table 3.6.8 provides the difference in FAA among three tide-systems computed only by changing the second-degree zonal term of EGM2008 and no change in GRS80 parameters. The variation of these differences is shown in Figure 3.6.4. Table 3.6.9 and Figure 3.6.5 depict the difference and their variation (among three

tide-systems) of FAA computed by considering EGM2008 and GRS80 in same tide-systems, i.e., changing the ellipsoidal parameters.

Table 3.6.8: Difference in degree-two FAA. Computations are done by considering the GRS80 in tide-free system and only changing $\bar{C}_{2,0}$ term of EGM2008. No changes to any parameter of GRS80 ellipsoid.

	FAA (μGal)			
	min	max	mean	STD
MT-ZT	-30.898	15.243	-7.683	16.317
ZT-TF	-9.328	4.602	-2.320	4.926
MT-TF	-40.226	19.845	-10.003	21.243

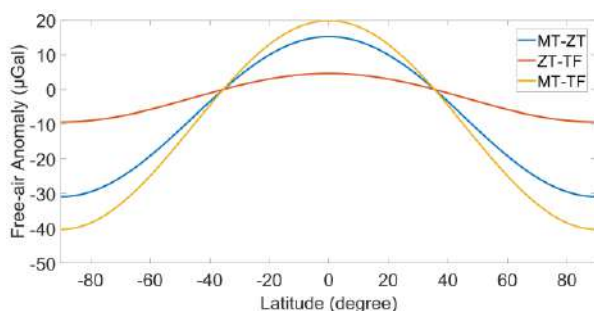


Figure 3.6.4: Variation in FAA for GRS80 in tide-free system (as is) and $\bar{C}_{2,0}$ of EGM2008 in different tide system.

Table 3.6.9: Difference in degree-two FAA with EGM2008 and GRS80 in same tide system

	FAA (μGal)			
	min	max	mean	STD
MT-ZT	-0.009	0.017	0.004	0.009
ZT-MT	-0.003	0.005	0.001	0.003
TF-MT	-0.011	0.022	0.005	0.012

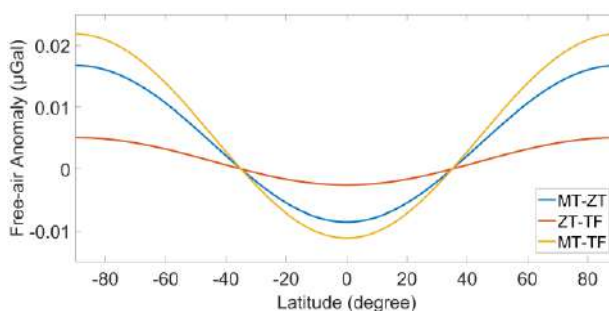


Figure 3.6.5: Variation of FAA when EGM2008 and GRS80 are in same tide system.

From Table 3.6.8, the difference values of FAA are in accordance ($<1 \mu\text{Gal}$) with the variation of normal gravity (Eq. (3.6.61)) in different tide-systems. This might be because in SHS we have used ellipsoidal parameters as defined in GRS80 (i.e., in tide-free system). Therefore, from the re-computation of the FAA with ellipsoidal parameters and EGM2008 in same tide-system, Table 3.6.9 and Figure 3.6.5 show that FAA is also acceptably independent ($<1 \mu\text{Gal}$) of the tide-system provided that EGM2008 and normal ellipsoid are in the same tide system.

As discussed in Section 3.6.2, there is some inconsistency (in the literature) on the tide-system of GRS80. Therefore, in Table 3.6.10 and Figure 3.6.6, we provide quantification of the possible error involved in SHS of geoid undulations and FAA if the tide system of GRS80 is mistaken as zero-tide instead of tide-free. In the computations, we have kept EGM2008 and GRS80 in same tide system.

Table 3.6.10: Difference in degree-two geoid undulations and FAA for an inconsistency in the tide-system of GRS80 (tide-system or zero-tide as per literature).

EGM 2008	GRS	Geoid undulation (mm)				FAA (μGal)			
		min	max	mean	STD	min	max	mean	STD
TF	TFGRSTF- ZTGRSTF*	-30.027	60.341	14.973	31.957	-4.604	9.333	2.321	4.929
ZT	TFGRSZT** - ZTGRSZT	-30.027	60.341	14.973	31.957	-4.604	9.333	2.321	4.929
MT	TFGRSMT# - ZTGRSMT###	-30.027	60.341	14.973	31.957	-4.604	9.333	2.321	4.929

* ZTGRSTF = GRS80 is in zero-tide system and converted to tide-free system

** TFGRSZT = GRS80 is in tide free system and converted to zero-tide system

ZTGRSMT = GRS80 is in zero-tide system and converted to mean-tide system

TFGRSMT = GRS80 is in tide-free system and converted to mean-tide system

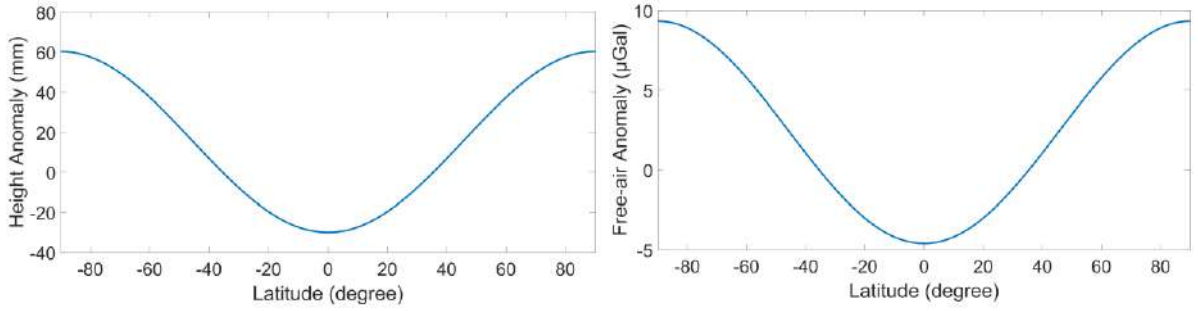


Figure 3.6.6: Variation of differences in degree-two geoid undulation and free-air anomaly for EGM2008 in ZT and GRS80 (TFGRSZT- ZTGRSZT)

Table 3.6.10 and Figure 3.6.6 show that a confusion/inconsistency in the tide-system of GRS80 ellipsoid (tide-free or zero-tide) can cause a maximum difference of ~60 mm in geoid undulation and ~9 μGal in free-air anomaly synthesised from EGM2008. This will also be true for WGS84 ellipsoid, which is also in tide-free system.

For the IAG resolution of all the geodetic quantities in mean-tide system, including coordinates, Mäkinen (2021) provides the formulas for converting geodetic latitude (Eq. (3.6.63)) and ellipsoidal height (Eq. (3.6.64)) from tide-free system to mean-tide system, derived from Petit and Luzum (2010, Section 7)

$$\varphi_{MT} - \varphi_{TF} = -0.814 \sin 2\varphi - 0.004 \sin 4\varphi \text{ mas} \quad (3.6.63)$$

$$h_{MT} - h_{TF} = 60.34 - 179.01 \sin^2 \varphi - 1.82 \sin^4 \varphi \text{ mm} \quad (3.6.64)$$

In our view, these formulas are for coordinate transformation from tide-free system to mean-tide system but with GRS80 in ‘as-is’ tide-system, i.e., tide-free system. The ellipsoidal height formula above is derived from Petit and Luzum (2010, Eq. 7.14) and is comparable with the ellipsoidal height conversion formulas derived using $(H_{MT} - H_{TF}) + (N_{MT} - N_{TF})$, i.e., Eq. (3.6.11) or Eq. (3.6.23). This is because these are also derived considering that there is no change in the tide-system of the ellipsoid. Therefore, with these conversion formulas (Eqs. (3.6.63) and (3.6.64)) mean-tide geodetic

coordinates are obtained with respect to the tide-free ellipsoid.

However, if we want mean-tide coordinates with respect to mean-tide ellipsoid, Molodensky transformation (NIMA, 2000, pg. 7-3) should be used, which are simplified to

$$\Delta\varphi'' = \frac{\sin 2\varphi}{2(\mu+h)\sin 1''} \left\{ \Delta a \left[\frac{\nu(2f-f^2)}{a} \right] + \Delta f \left[\frac{\mu}{(1-f)} + (1-f)\nu \right] \right\} \quad (3.6.65)$$

$$\Delta h = -\Delta a \left[\frac{a}{\nu} \right] + \Delta f (1-f)\nu \sin^2 \varphi \quad (3.6.66)$$

where Δa and Δf are change in semi-major axis and flattening of the ellipsoid in different tide-systems provided by Eqs. (3.6.56) and (3.6.55), respectively; ν and μ are the radius of curvature in prime vertical and meridional directions, respectively.

Therefore, there should be some consensus on the choice (conversion/no conversion) of ellipsoid parameters. The formulas given by, e.g., Ekman (1989) or Mäkinen (2021) are based on calculating the quantities in any tide-system but with respect to the tide-free ellipsoid (for GRS80 or WGS84). However, we think a better option is to also convert the ellipsoidal parameters in the working tide-system, i.e., using our formulas of conversion of ellipsoidal parameters and use them in SHS or coordinate transformation.

In case our suggestion of using GGM and normal ellipsoid in same tide-system is opted, we have computed and provided all the parameters (Table B.1) of GRS80 and WGS84 in the three-tide systems in Appendix Table B.2 and B.3, respectively. The values can be directly utilised in the SHS of the gravity field functions. The conversion formulas of various ellipsoidal parameters can also be included in the SHS subroutines. In Table B.4, we also provide the parameters of a possibly new normal ellipsoid that is consistent

with the IHR parameters (Poutanen and Rózsa, 2020, pg. 275). Please note that the values in Table B.4 are not official.

3.7 Summary

In this chapter we have discussed various corrections and reductions involved in geoid computation as handled in the three different methods viz. CUT, KTH and UNB. We also discussed about the important yet loosely handled zero-degree term and solid Earth permanent tide systems. Below are some summarising comments from the discussions in the six sub-sections of this chapter:

- i. Either for geoid or quasigeoid computation, gravity anomalies should be initially computed at the Earth's surface using the normal gravity from the exact method (Eq. (3.1.21)). If the required normal height is approximated by orthometric height or normal-orthometric height, a geoid-quasigeoid correction term (Eq. (3.1.24)) for gravity anomalies should be used.
- ii. The CUT method does not apply any topographic correction but approximates Molodensky's G_I term by the planar TC. The UNB method is theoretically the most rigorous method for handling the topography in geoid computation. However, it seems that their present approach uses an average of the mean values for the various topographic corrections due to the use of mean topographic correction values from already block-averaged DEM. We have also explicitly introduced the preferred use of dynamic integration radius instead of a fixed integration radius that may cause some overlapping of the DEM grid cells. A rigorous quantitative analysis is required to compare the formulation of topographic corrections in the KTH method and the UNB method. The effect of total topographic correction to the geoid in the KTH method is equal to a part of only indirect effect in the UNB method.

- iii. The most general method of direct atmospheric effect (DAE) is to use a polynomial function as included in the CUT method. We have shown that one should not use a truncated polynomial function to compute DAE. A similar formula has also been adopted by the International Association of Geodesy (IAG) for DAE. However, Sjöberg (1999) and Sjöberg and Nahavandchi (2000) had discussed some of its limitations. The primary parameter in the DAE is the atmospheric density function which differs among all the three methods. Moreover, only the UNB method considers the atmospheric height up to an arbitrarily chosen 50 km. Also, we discourage the use of height coefficients in DAE (as used in the KTH method) unless they are constructed using the global DEM of working resolution, i.e., resolution of the geoid ($0.02^\circ \times 0.02^\circ$ for our case). Though the DAE difference among the different methods may be negligible, some standardisation is needed.
- iv. There exist several different approaches of ellipsoidal correction which are significantly different to each other, but we had restricted the discussions to the three strategies as adopted in the CUT, UNB and KTH methods. We have given some more rigorous formulas at some junctures. There exists some discrepancy in the ‘signs’ in the formulas for ellipsoidal correction used in the UNB and the KTH methods. Although we have provided our reasons for preference to the ‘signs’ used in the UNB method, it may need some further investigation. All formulas, irrespective of the method, are realised using the Global Geopotential Model (GGM). Hence, ellipsoidal corrections will vary due to the methodology as well as the different choices of GGMs. The CUT method uses full d/o GGM to compute the residual gravity anomaly, i.e., they use the full d/o GGM for ellipsoidal correction (along with geocentric ellipsoidal radius of the computation point). The UNB and the KTH methods uses satellite-only

GGMs. Therefore, though presumably negligible, this effect needs to be quantified in the future.

- v. Downward continuation (DWC) of gravity anomalies is not applied in the CUT method because it computes the quasigeoid. However, a different viewpoint is provided where DWC is applied as the analytical continuation in the CUT method which also follows the DWC effect for calculating the height anomalies in the KTH method. A conceptual need for DWC of height anomalies from the Earth's topography to the ellipsoid is also introduced to obtain the quasigeoid. A different interpretation of the DWC effect in the quasigeoid computation of the KTH method (Eq. (3.5.17)) has been provided that may require some modifications in their additive corrections to the approximate quasigeoid.
- vi. The quantification of the significant biases introduced due to the inconsistent use of the zero-degree term has been demonstrated. Expressions/relations have been provided for the conversion of observed gravity, geoid undulation, orthometric, dynamic, normal-orthometric and ellipsoidal heights and various ellipsoidal parameters among the three permanent tide systems (tide-free, zero-tide and mean-tide). The numerical values of the defined and derived parameters of GRS80, WGS84 and an International Height Reference System (IHRM)-based possibly new normal ellipsoid have been computed in the three tide systems and are provided in Appendix A1.

Having discussed the systematic corrections, the next chapter will deal with geoid/quasigeoid computation strategies of the three methods that will also involve the order in which the above discussed corrections are applied.

Chapter 4: Computation of the Indian gravimetric geoid and quasigeoid models

4.0 Introduction

In previous chapters, we have discussed the datasets and various corrections or data handling (with some results) in the three geoid computation methodologies (CUT, UNB, KTH). In the present Chapter, we use those discussions and results to overview the geoid computation methodologies. An introduction to Stokes's integration and modification of Stokes's kernel is also provided. Since we are interested in both geoid and quasigeoid, a geoid-quasigeoid separation term is discussed to convert geoid undulations to height anomalies or *vice-versa*. Further, some parametric fitting of gravimetric geoid/quasigeoid on the geometric geoid undulation is discussed that helps in reducing the systematic biases among geodetic datums.

4.1 Stokes's integration and kernel modification

The gravimetric geoid or quasigeoid computation is basically the conversion of observed gravity values into geoid undulations or height anomalies. This is mainly achieved by using Stokes's and Bruns's formulas under two main assumptions: i) gravity data is available all around the globe on the surface of the geoid, and ii) there should be no masses above the geoid. The handling of the second assumption has been dealt with in Chapter 3. Contrary to the first assumption, the data of the entire globe is not available, and we use gravity data only for a region. Therefore, integration over the whole globe is compelled to be truncated to a limited region around the computation point. Hence, truncation error or bias is introduced in the geoid and quasigeoid (quasi/geoid) solution, but it is reduced by using a Global Geopotential Model (GGM) in a remove-compute-restore approach.

Molodensky et al. (1962) presented, for the first time, modification to the original Stokes's kernel with the main idea of reducing the truncation error. Presently, there are several kernel modifications available that can be broadly classified as either deterministic or stochastic modifiers.

In this chapter, we provide a basic overview of Stokes's integration and kernel modification without going into details, mainly due to the following two reasons:

- i) There is much literature available on these topics, and we cannot explain them any better than what is already documented.
- ii) We have not modified the existing formulas or the methodologies of Stokes's integration or kernel modifications.

Therefore, we thought it wise enough to provide only the basic equations and the most relevant references.

4.1.1 Stokes's Integration

George Gabriel Stokes, in 1849, published his formula that demonstrated for the first time the use of gravity measurements to determine the geoid (Stokes, 1849). The formula is a solution to the third geodetic boundary value problem (GBVP). In the third GBVP, gravity anomaly is modelled as a linear combination of disturbing potential and its normal derivative through the fundamental equation of physical geodesy. Also, it is given that disturbing potential is harmonic in space outside the geoid (i.e., satisfying Laplace's equation). Therefore, disturbing potential is solved on the geoid and space outside the geoid. This can be mathematically written as (e.g., Heiskanen and Moritz, 1967, pg. 86)

$$\begin{aligned}
 \text{Given: } & \begin{cases} \Delta T = 0, & \text{in space outside geoid} \\ \frac{\partial T}{\partial n} + \frac{2}{r}T = -\Delta g, & \text{on geoid} \end{cases} \quad (4.1.1) \\
 \text{Sought: } & T = ?, \text{ on geoid and in space outside geoid}
 \end{aligned}$$

Stokes (1849) derived the solution to the third GBVP (under the assumptions that $\frac{\partial}{\partial n} = \frac{\partial}{\partial r}$

and $r = R$; Heiskanen and Moritz, 1967, pg. 87-88, 92-93) as

$$T = \frac{R}{4\pi} \iint_{\sigma} S(\psi) \Delta g d\sigma \quad (4.1.2)$$

where $\iint_{\sigma} d\sigma = \int_{\alpha=0}^{2\pi} \int_{\psi=0}^{\pi} \sin(\psi) d\psi d\alpha$ in spherical polar coordinates and

$\iint_{\sigma} d\sigma = \int_{\lambda'=0}^{2\pi} \int_{\phi'=-\pi/2}^{\pi/2} \cos(\phi') d\phi' d\lambda'$ in geographical coordinates (in spherical

approximation); $S(\psi)$ is Stokes's kernel that is given in spatial and spectral forms by Eqs.

(4.1.3) and (4.1.4), respectively.

$$S(\psi) = \frac{1}{\sin\left(\frac{\psi}{2}\right)} - 6 \sin\left(\frac{\psi}{2}\right) + 1 - 5 \cos(\psi) - 3 \cos(\psi) \ln\left(\sin\left(\frac{\psi}{2}\right) + \sin^2\left(\frac{\psi}{2}\right)\right) \quad (4.1.3)$$

$$S(\psi) = \sum_{n=2}^{\infty} \frac{2n+1}{n-1} P_n(\cos \psi) \quad (4.1.4)$$

and ψ is the spherical distance given by

$$\psi = \cos^{-1}(\sin \phi \sin \phi' + \cos \phi \cos \phi' \cos(\lambda - \lambda')) \quad (4.1.5)$$

The use of Bruns's formula (Eq. (4.1.6)) in Eq. (4.1.2) gives the famous Stokes formula (Eq. (4.1.7)) that is used to calculate geoid height from gravity anomalies.

$$N = \frac{T}{\gamma_0} \quad (4.1.6)$$

$$N = \frac{R}{4\pi\gamma_0} \iint_{\sigma} S(\psi) \Delta g d\sigma \quad (4.1.7)$$

The same formula is also used to compute the height anomalies using Molodensky's problem, where geoid undulation is replaced with height anomalies. Gravity anomalies on the geoid are replaced by gravity anomalies on the Earth's surface, and normal gravity at ellipsoid is replaced by normal gravity at the telluroid. Another critical yet inconsistently reported replacement would be R by $R+H$. From Eq. (4.1.7), the use of R instead of $R+H$ can cause a difference of ~ 15 mm for a region/point with a geoid undulation value of 50 m and a height of 2000 m, but much less when remove-compute-restore is used.

Stokes's integral (Eq. (4.1.7)) can be evaluated using various methods such as 'brute force' numerical integration (Heiskanen and Moritz, 1967, pg. 117), quadrature-based numerical integration (e.g., Hirt, 2011), ring integration (Kearsley, 1986; Tsen, 1992), 1D-FFT on sphere (Haagmans et al., 1993), 2D-FFT on sphere (Strang van Hees, 1990; Forsberg and Sideris, 1993), 2D-FFT on a plane (Schwarz et al., 1990; Sideris and Li, 1993) or Least Squares Collocation (Krarup, 1969; Tscherning, 1977; Moritz and Sünkel, 1978; Moritz, 1980). Interested readers should also see Tziavos (1996) and Zhang (1997) for numerical comparisons of the spectral methods for Stokes's integration.

It is well advocated and numerically shown in the literature that solution with 1D-FFT is significantly faster than and exactly the same as numerical integration (e.g., Haagmans et al., 1993). Therefore, the use of 1D FFT in evaluating Stokes's integral is widespread in the literature on geoid computation (e.g., Ågren et al., 2009a; 2009b; Featherstone et al., 2018; Claessens and Filmer, 2020; Grigoriadis et al., 2021, among numerous others). However, Huang et al. (2000) presented a modified numerical integration that is claimed to be faster than the 1D-FFT method (e.g., Janak et al., 2017). It makes use of the symmetrical property of Stokes's and modified Stokes's kernels (Section 4.1.2) with respect to the meridian of the computation point. As such, only half

of the kernel values are required to be evaluated. This modified method is realised by shifting the ‘evaluation of kernel’ from the longitudinal loop to the latitudinal loop, which causes computation of the kernel values only once for a given latitude. Huang et al. (2000) have shown that, on their computing system (Dell Optiplex GS1p PC with 400MHz CPU), their method is ~45 times faster than the brute force numerical integration method with a modified Stokes’s kernel.

In this study, we have used this modified numerical integration (Huang et al., 2000) for evaluating Stokes’s integral, coded in MATLAB. The geoid height at any point can be obtained using the discrete version of Stokes’s integral (Eq. (4.1.8)).

$$N = \frac{R}{4\pi\gamma_0} \Delta\phi \Delta\lambda \sum_{\phi'} \sum_{\lambda'} \Delta g(\phi', \lambda') S(\psi) \cos \phi' \quad (4.1.8)$$

4.1.2 Kernel modification

Due to the availability of limited gravity anomaly data, Stokes’s integral cannot be extended over the entire Earth. Instead, it has to be truncated to a limited area (σ_0) where gravity data is available. Therefore, Stokes’s formula can be re-written as

$$\hat{N} = \frac{R}{4\pi\gamma_0} \iint_{\sigma_0} S(\psi) \Delta g d\sigma \quad (4.1.9)$$

where \hat{N} is an estimate of geoid height due to truncation of the integral. The difference between Eqs. (4.1.7) and (4.1.9) is the truncation error and is given by

$$\delta N = -\frac{R}{4\pi\gamma_0} \iint_{\sigma - \sigma_0} S(\psi) \Delta g d\sigma \quad (4.1.10)$$

$\sigma - \sigma_0$ is the area where gravity data are not available. Molodensky et al. (1962) demonstrated that the truncation error could be minimised by modifying Stokes’s kernel (minimising L_2 norm of the error kernel; Vaníček and Sjöberg, 1991).

There have been several kernel modifications that are based on reducing the truncation error (Molodensky et al., 1962; de Witte, 1967; Wong and Gore, 1969; Vaníček and Kleusberg, 1987), accelerating the convergence of the truncation error (Meissl, 1971; Heck and Grüniger, 1987), and reducing the truncation error with simultaneously accelerating its convergence (Featherstone et al., 1998). These all are categorised as deterministic modifiers. There are other modifiers that aim to reduce the errors in either one or both of the potential coefficients and terrestrial gravity data along with the truncation error using least squares solution (Sjöberg, 1984a; 1984b; 1991). These are categorized as stochastic modifiers. Other stochastic modifiers also exist, but which do not aim to reduce the truncation error, rather do the weighting of the kernel based on the errors in potential coefficients and terrestrial gravity data (Wenzel, 1981; 1983).

In this study, the geoid is computed using the three methods (CUT, UNB, KTH), therefore, only their preferred choice of modifications are discussed and used. The name and seminal references to the kernel modifications in the three methods are listed in Table 4.1.1.

Table 4.1.1: References of the three modifications to Stokes's kernel.

Method	Kernel modification	Key references
CUT	Featherstone, Evans, Olliver (FEO)	Featherstone et al. (1998)
UNB	Vaníček and Kleusberg (VK)	Vaníček and Kleusberg (1987); Vaníček and Sjöberg (1991); Vaníček et al. (1995)
KTH	Least Squares Modification of Stokes's kernel (LSMS)	Sjöberg (1980; 1981; 1984a; 1984b; 1986; 1990; 1991; 2003; 2005); Sjöberg and Hunegnaw (2000)

In addition to the references in Table 4.1.1, there have been review articles with the involved formulations on deterministic modifiers (Vaníček and Featherstone, 1998; Featherstone, 2003; 2013; Šprlák, 2010; Rahebi et al., 2012) and stochastic modifiers (Ellmann, 2005b; Rahebi, 2012; Featherstone, 2013). The detailed formulas for kernel

modifications can also be seen in various theses on geoid modelling, e.g., Novák (2000), Kern (2003), Ågren (2004), Ellmann (2004), Singh (2007), Amos (2007), Daras (2008), Abdalla (2009), Ulotu (2009) among many others. Also see Jekeli (1980, 1981a), Martinec (1993) and Sjöberg and Bagherbandi (2017).

Therefore, without duplicating the detailed derivations of each of the three modifiers, we write a general equation (Eq. (4.1.11), with $c = R/2\gamma$) for Stokes's integration that uses modified Stokes's kernel and GGM. This can take the form of remove-compute-restore (RCR) formulation as required in the CUT and the UNB methods, and also the non-RCR formulation as used in the KTH method.

$$N = \frac{c}{2\pi} \iint_{\sigma_0} S^M \Delta g^\# d\sigma + c \sum_{n=2}^L x_n \Delta g_n, \quad L \geq M \quad (4.1.11)$$

$$\Delta g^\# = \begin{cases} \Delta g - \sum_{n=2}^L \Delta g_n, & \text{for VK or FEO} \\ \Delta g, & \text{for LSMS} \end{cases} \quad (4.1.12)$$

$$\Delta g_n = \frac{GM}{r^2} \left[(n-1) \left(\frac{a}{r} \right)^n \sum_{m=0}^n (\Delta \bar{C}_{nm} \cos m\lambda + \bar{S}_{nm} \sin m\lambda) \times \bar{P}_{nm}(\cos \theta) \right] \quad (4.1.13)$$

$$x_n = \begin{cases} \frac{2}{n-1}, & \text{for VK or FEO} \\ Q_n^M + s_n, & \text{for LSMS} \end{cases} \quad (4.1.14)$$

$$S^M = \begin{cases} S(\psi) - \sum_{n=2}^M \frac{2n+1}{2} \left(\frac{2}{n-1} + t_n \right) P_n(\cos \psi), & \text{for VK} \\ S(\psi) - S(\psi_0) - \sum_{n=2}^M \frac{2n+1}{2} \left(\frac{2}{n-1} + t_n \right) (P_n(\cos \psi) - P_n(\cos \psi_0)), & \text{for FEO} \\ S(\psi) - \sum_{n=2}^M \frac{2n+1}{2} s_n P_n(\cos \psi), & \text{for LSMS} \end{cases} \quad (4.1.15)$$

Q_n^M and t_n, s_n are truncation coefficients and modification parameters, respectively, that need to be computed for determining the modified Stokes's kernel. The formulas are available in almost all the above-cited literature, also see Hagiwara (1972; 1976) and Paul (1973) for auxiliary coefficients.

4.2 Different techniques of geoid and quasigeoid calculation

The gaps between theoretical and practical aspects in quasi/geoid computation arising from the various assumptions and approximations (Chapter 3; Section 4.1) incur several errors, which geodesists have tried to reduce for the ongoing quest of cm-precise geoid (e.g., Sansó and Rummel, 1997; Tóth et al., 2000). Also, there are two choices of reference surface: geoid or quasigeoid. As such, there are several methods available for quasi/geoid computation (Goyal et al., 2022, Table A1).

A brief overview of the CUT, the UNB, and the KTH geoid computation methodologies are presented in this section. However, it is important to note here again that the methodology adopted and discussed under the names: CUT, UNB, and KTH do not strictly follow the methodology depicted in their research articles or manuals. We have mentioned a few differences between the strict and our adopted methodologies because of different aspects of the Indian data (Chapter 2).

Table 4.2.1 lists a few study areas where these three methods have been implemented, although a combination of the methods is also used and reported in the literature (e.g., Matsuo and Kuroishi, 2020). The CUT method is primarily used for quasigeoid computation. The UNB method is for geoid computation. The KTH method was initially developed to compute the geoid but later modified to calculate the quasigeoid. A geoid-quasigeoid separation term is needed to convert geoid to quasigeoid (or vice-

versa) so that both can be computed using all three methods. This separation term is dealt with in Section 4.3.

Table 4.2.1: Examples of implementation of geoid/quasigeoid computation methodologies.

Method	Region/Country	Reference
CUT	Australia New Zealand Colorado India Auvergne	Featherstone et al. (2001; 2011; 2018) Claessens et al. (2011); McCubbine et al. (2018) Claessens and Filmer (2020) Goyal et al. (2021b) Goyal et al. (2022)
UNB	Canada Brazil Iran Mexico Ghana Auvergne	Vaniček and Kleusberg (1987); Vaniček et al. (1995); Huang and Véronneau (2013) Guimarães et al. (2014) Najafi-Alamdari (2004) Hernández-Navarro (2004); Avalos Naranjo et al. (2006) Klu (2015) Foroughi et al. (2017a; b; 2019)
KTH	Sweden Baltic countries Iran Tanzania Greece Kazakhstan Sudan New Zealand Turkey Uganda Poland Malaysia Jilin province in China Auvergne	Ågren et al. (2009b) Ellmann (2004); Ellmann et al. (2020) Kiamehr (2006) Ulotu (2009) Daras et al. (2010) Inerbayeva (2010) Abdalla and Fairhead (2011) Abdalla and Tenzer (2011) Abbak et al. (2012) Ssengendo (2015) Kuczynska-Siehien et al. (2016) Pa'suya et al. (2019) Wu et al. (2020) Ågren et al. (2009a); Yildiz et al. (2012); Goyal et al. (2022)

4.2.1 CUT method of geoid/quasigeoid calculation

The CUT method uses a simplified Molodensky theory with the Moritz (1971) solution, where Molodensky's G_I term is approximated by the planar terrain correction (TC) (Moritz, 1971; 1980; McCubbine et al., 2019). A flowchart of the CUT methodology for calculating the height anomalies/geoid undulations is shown in Figure 4.2.1.

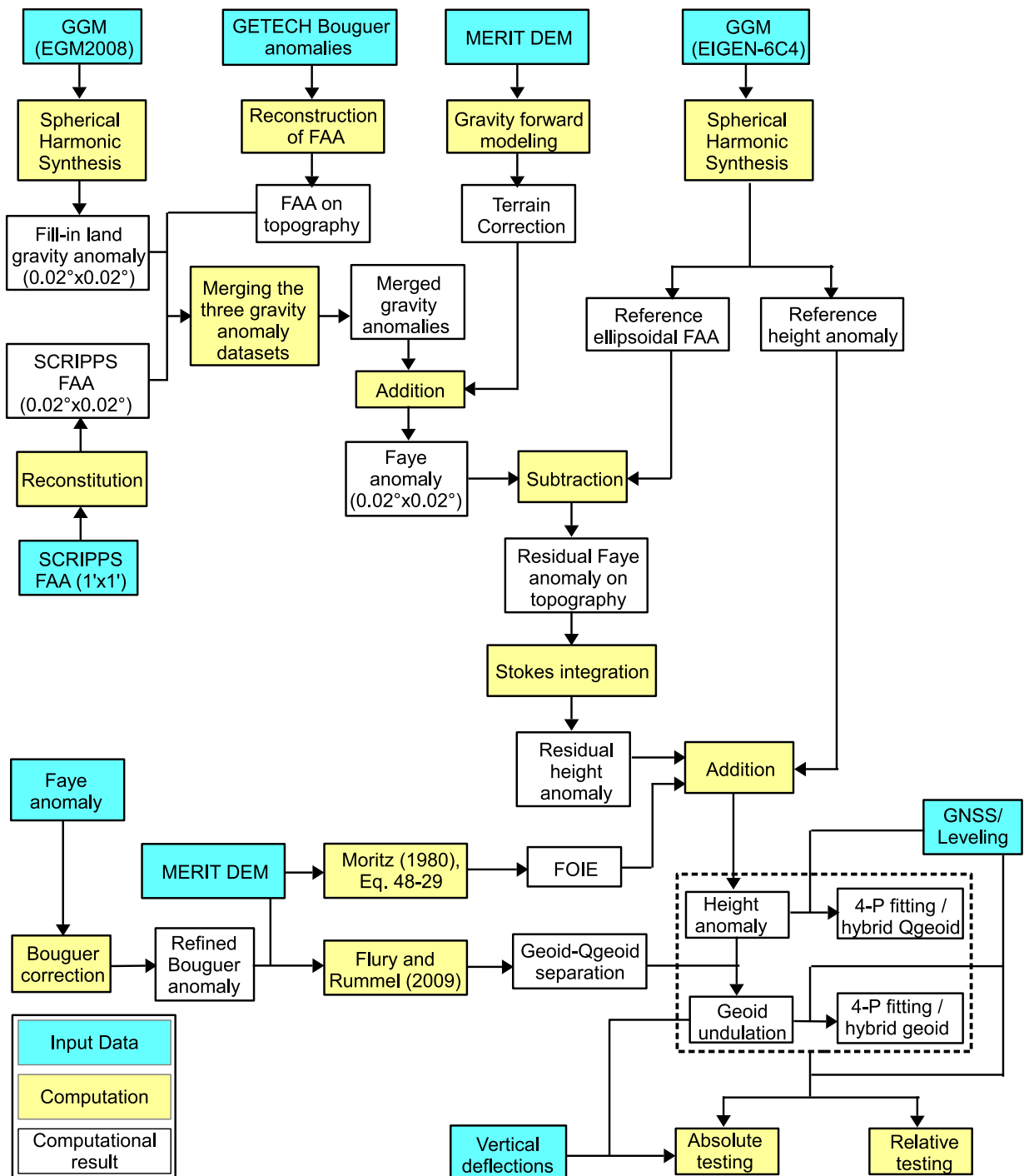


Figure 4.2.1: Flowchart of the CUT methodology of geoid/quasigeoid computation.

A brief description of Figure 4.2.1 is as follows:

With the available gravity data, free-air anomalies are calculated on the Earth's topography by subtracting normal gravity at the telluroid (Section 3.1) from the observed gravity at the Earth's surface. Atmospheric corrections (Section 3.3.1) are also added to

these free-air anomalies. TCs (Section 3.2.1) are computed using the best-available Digital Elevation Model (DEM) (Section 2.5) and block-averaged to the grid size of the gravity anomaly data. Block-averaged TCs are added to the free-air anomalies to obtain a grid of mean Faye anomalies (Figure 4.2.2a) on the Earth's topographical surface. It should be noted that if we had randomly distributed gravity data, mean Faye anomalies would have been obtained using the reconstruction technique of gridded Bouguer anomaly as discussed by Featherstone and Kirby (2000) and Goos et al. (2003).

Ellipsoidal free-air anomalies are synthesised on the topography at a grid of $3'' \times 3''$ using the highest available GGM (EIGEN-6C4 in our case), which are then block-averaged to $0.02^\circ \times 0.02^\circ$ grid to obtain the area-mean reference gravity anomalies. Residual Faye anomalies on the topography are then calculated by subtracting the mean reference gravity anomalies from the mean Faye anomalies. The residual Faye anomalies are shown in Figure 4.2.2b. These are Stokes-integrated using the FEO kernel modification (Section 4.1.2) to obtain a grid of residual height anomalies. Please recall from Section 3.4.1 that the reference radius in the Stokes integration is set equal to the ellipsoidal radius of the computation point, and this negates the need for further ellipsoidal corrections (Claessens, 2006, Chapter 6).

The residual height anomalies were computed using the following combinations (parameter sweeps) in Eq. (4.1.11): $L = 2190$, $M = 40, 80, 120, 160, 200, 240, 280, 300$, and $\psi_0 = 0.2^\circ, 0.5^\circ, 0.75^\circ, 1^\circ, 1.5^\circ, 2^\circ$. The residual height anomalies for $M = 80$ and $\psi = 1.5^\circ$ are shown in Figure 4.2.3. The reference height anomalies on the topography are computed using GGM (EIGEN-6C4) with a zero-degree term from the generalised Bruns formula (Section 3.6.1) calculated for each latitude parallel. We used normal potential $U_0 (= 62636860.85 \text{ m}^2\text{s}^{-2})$ from GRS80 and the geopotential $W_0 (= 62636853.4 \text{ m}^2\text{s}^{-2})$

from IHRS (Sánchez et al., 2016). The reference height anomalies and, unlike the CUT application, the first-order indirect effect (FOIE, Section 3.5.1) are added to the residual height anomalies to obtain the height anomalies.

The geoid-quasigeoid separation (Flury and Rummel, 2009) term is applied to the height anomalies to obtain the corresponding geoid undulations. Parametric fitting of geoid/quasigeoid is done with GNSS/levelling data to calculate the corresponding hybrid geoid/quasigeoid models. These are discussed in Sections 4.3 and 4.4, respectively. The gravimetric geoid and quasigeoid models (before and after fit) are then validated with the available GNSS/levelling data. The gravimetric geoid is also validated with Indian vertical deflections (Section 2.3).

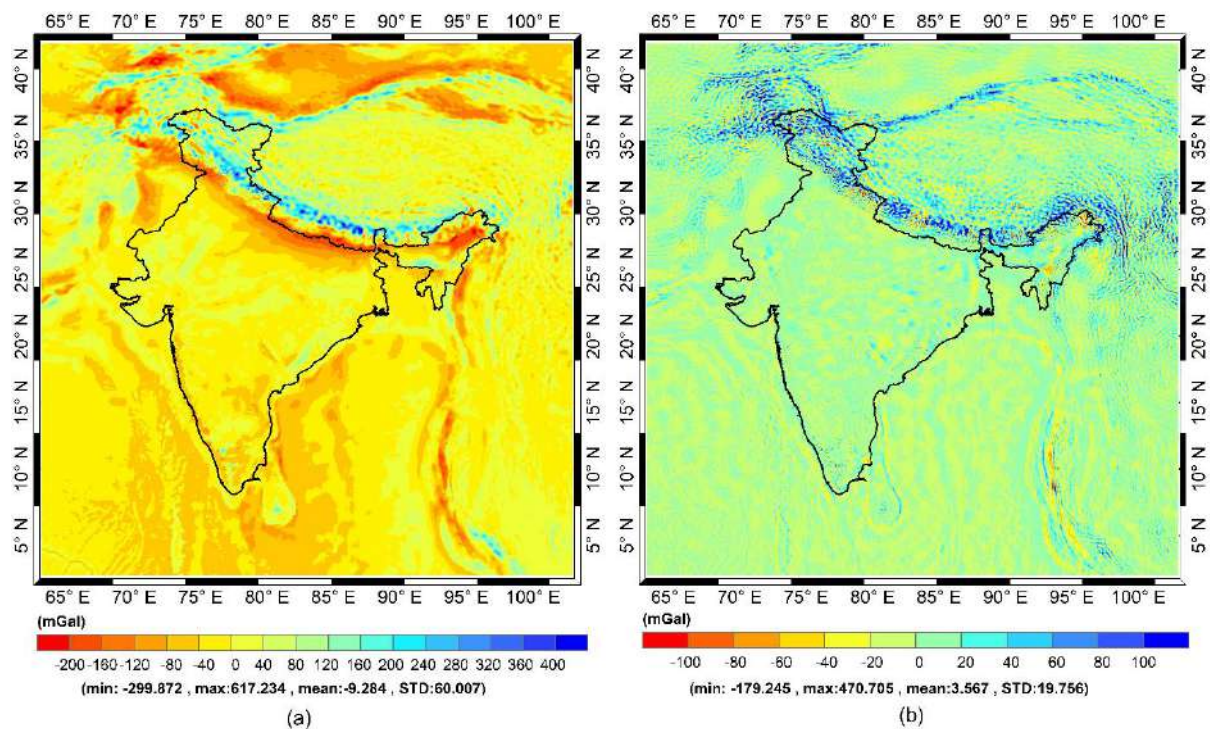


Figure 4.2.2: a) Faye gravity anomalies and b) residual Faye gravity anomalies as required in the CUT method.

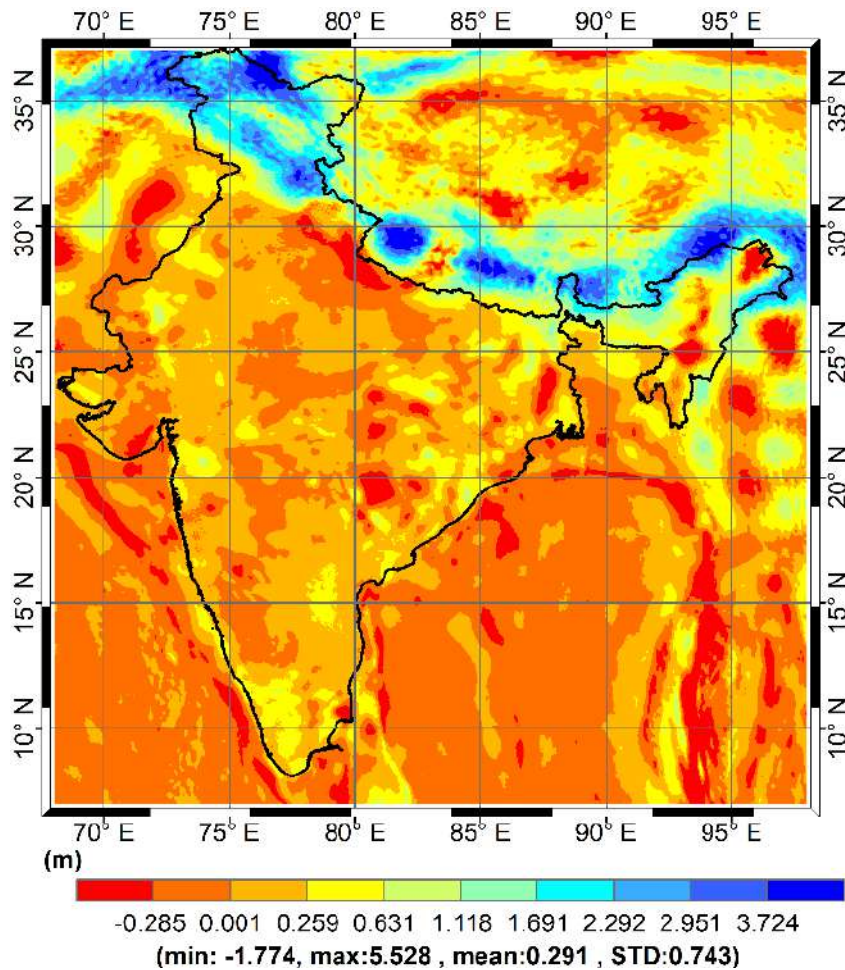


Figure 4.2.3: Residual height anomalies after Stokes integrating residual Faye gravity anomalies with FEO kernel modification ($M = 80$ and $\psi = 1.5^\circ$)

The following are the major differences from the original CUT method:

- i) Due to the availability of already gridded Bouguer anomalies data, a different approach is used to calculate Faye anomalies on the Earth's topographical surface.
- ii) A different method is used to compute the planar TC (Section 3.2.1).
- iii) FOIE is applied in this study.
- iv) The zero-degree term based on generalised Bruns's formula is used and explicitly mentioned.
- v) The geoid-quasigeoid separation term is computed using the Flury and Rummel (2009) method.

- vi) The numerical method (Huang et al., 2000) has been used instead of 1D-FFT (Haagmans et al., 1993) for Stokes's integration.

4.2.2 UNB method of geoid/quasigeoid calculation

The UNB method generally talks about two spaces, i.e., the real space and Helmert's space. The difference between the two is that in Helmert's space, all the masses above the geoid (topographic and atmospheric), present in the real space, are condensed as a thin surface layer on the geoid (Helmert's second condensation). This makes the space between the geoid and the Earth's surface harmonic (Martinec, 1993), i.e., it satisfies Laplace's equation.

The method starts with formulating the spherical fundamental equation of physical geodesy on the Earth's surface and thus calculating the free-air anomaly on the topography in the real space (Section 2.1). However, for geoid determination, gravity anomalies are desired on the geoid. Since there are masses above the geoid, the gravity anomalies are transformed from the real space to Helmert's space, but still referring to the Earth's surface. This transformation is done by applying direct (DTE) and secondary indirect (SITE) topographical (Section 3.2.2) and direct (DAE) and secondary indirect (SIAE) atmospheric effects (Section 3.3.2).

These Helmert's gravity anomalies are downward-continued (DWC; Section 3.5.2) from the Earth's surface to the geoid, or more precisely the Helmert co-geoid. Ellipsoidal corrections are then applied to Helmert's gravity anomalies at the geoid level (Section 3.4.2).

The so-obtained Helmert's gravity anomalies on the geoid in the UNB approach are decomposed into the low- and high-frequency of the gravity field. The latter is achieved by removing reference Helmert's gravity anomaly, i.e., reference gravity anomaly (GGM

derived, DIR-RL05 in this case) along with reference topographical effects (DEM SHC d/o 300 derived; Novák, 2000, pgs. 51-56; Table 4.2.2). The result is residual (high-frequency) Helmert's gravity anomalies (Figure 4.2.5) that are Stokes-integrated using the VK kernel modification (Section 4.1.2) to obtain residual (high-frequency) co-geoid.

The residual co-geoid is computed using the following combinations (parameter sweeps) in Eq. (4.1.11): $L = 300$, $M = 0, 40, 80, 120, 160, 200, 240, 280, 300$, and $\psi_0 = 0.2^\circ, 0.5^\circ, 0.75^\circ, 1^\circ, 1.5^\circ, 2^\circ$. The residual height anomalies for $M = 80$ and $\psi = 1.5^\circ$ is shown in Figure 4.2.6. The reference spheroid (GGM (DIR-RL05) derived geoid undulations and reference primary indirect topographic effect (PITE)) are added to the residual co-geoid. GGM-derived geoid undulations are computed with a zero-degree term from the generalised Bruns's formula (Section 3.6.1) calculated for each latitude parallel. We used normal potential $U_0 (= 62636860.85 \text{ m}^2\text{s}^{-2})$ from GRS80 and the geopotential $W_0 (= 62636853.4 \text{ m}^2\text{s}^{-2})$ from IHRS (Sánchez et al., 2016). Finally, the geoid from Helmert's space (co-geoid) is transformed to the required geoid in the real space by applying PITE and primary indirect atmospheric effects (PIAE).

The geoid-quasigeoid separation term (Flury and Rummel, 2009) is applied to the geoid undulations to obtain the corresponding height anomalies. Parametric fitting of geoid/quasigeoid is done with GNSS/levelling data to calculate the corresponding hybrid geoid/quasigeoid models. These are discussed in Sections 4.3 and 4.4, respectively. The gravimetric geoid and quasigeoid models (before and after fit) are then validated with the available GNSS/levelling data. The gravimetric geoid is also validated with vertical deflections (Section 2.3).

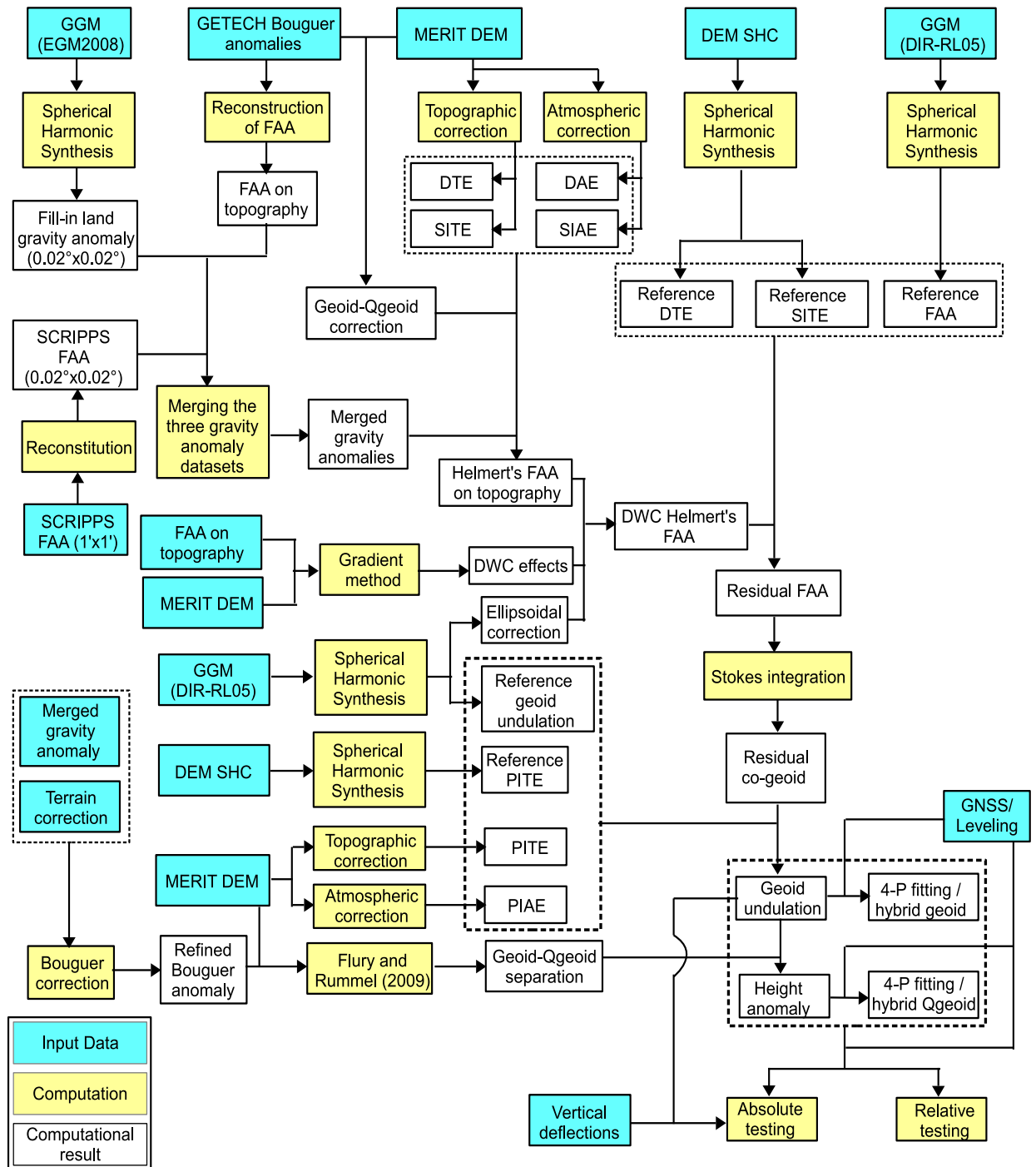


Figure 4.2.4: Flowchart of the UNB methodology of geoid/quasigeoid computation.

Table 4.2.2: Topographical effects (in mGal) from spherical harmonic coefficients of the DEM.

	d/o	min	max	mean	STD
DTE	160	-13.557	9.627	-0.168	±2.289
	300	-25.733	23.174	-0.161	±3.344
SITE	160	-0.554	0.084	-0.056	±0.136
	300	-0.617	0.082	-0.056	±0.137

Though we have used d/o 300 for our computations, corresponding values calculated with d/o 160 are also depicted in Table 4.2.2 only to emphasise that there can be substantial absolute differences (~ 10 mGal to ~ 15 mGal) in the reference topographical effects. These differences will have equivalent effect (~ 10 mGal to ~ 15 mGal) on Helmert's residual gravity anomalies, affecting the final geoid solution. Therefore, from the viewpoint of cm-precise geoid model, we suggest to study the effects of different d/o of DEM for calculating Helmert's residual gravity anomaly.

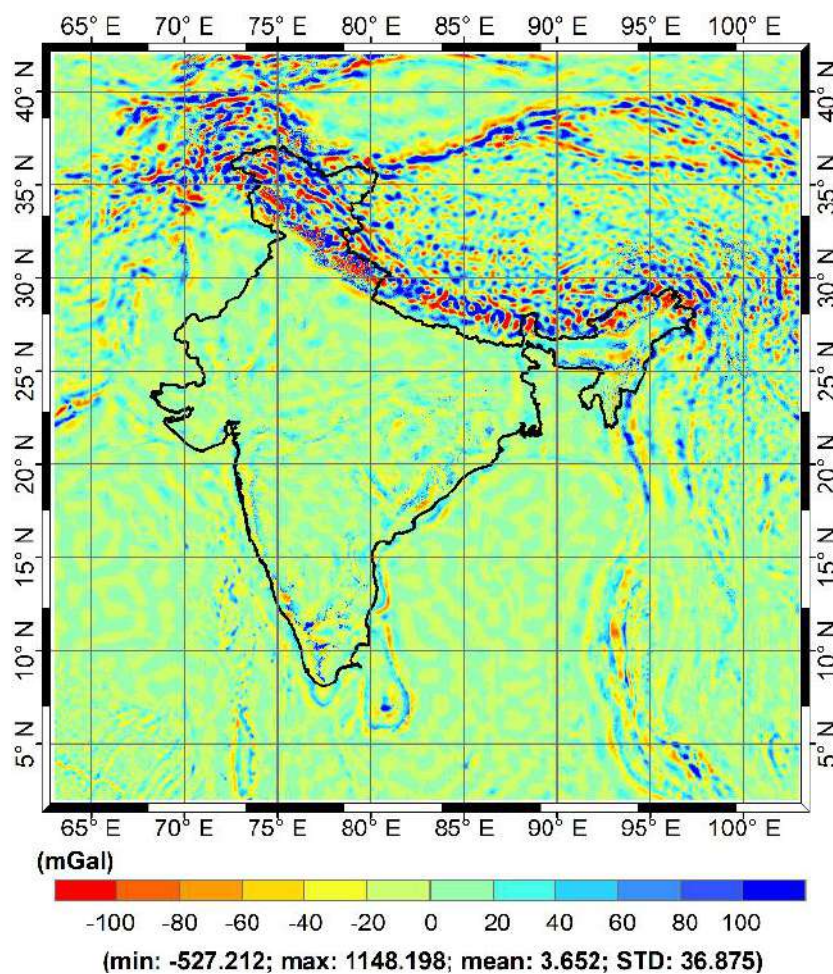


Figure 4.2.5: Residual Helmert's anomaly calculated with the DIR-RL05 GGM d/o 300.

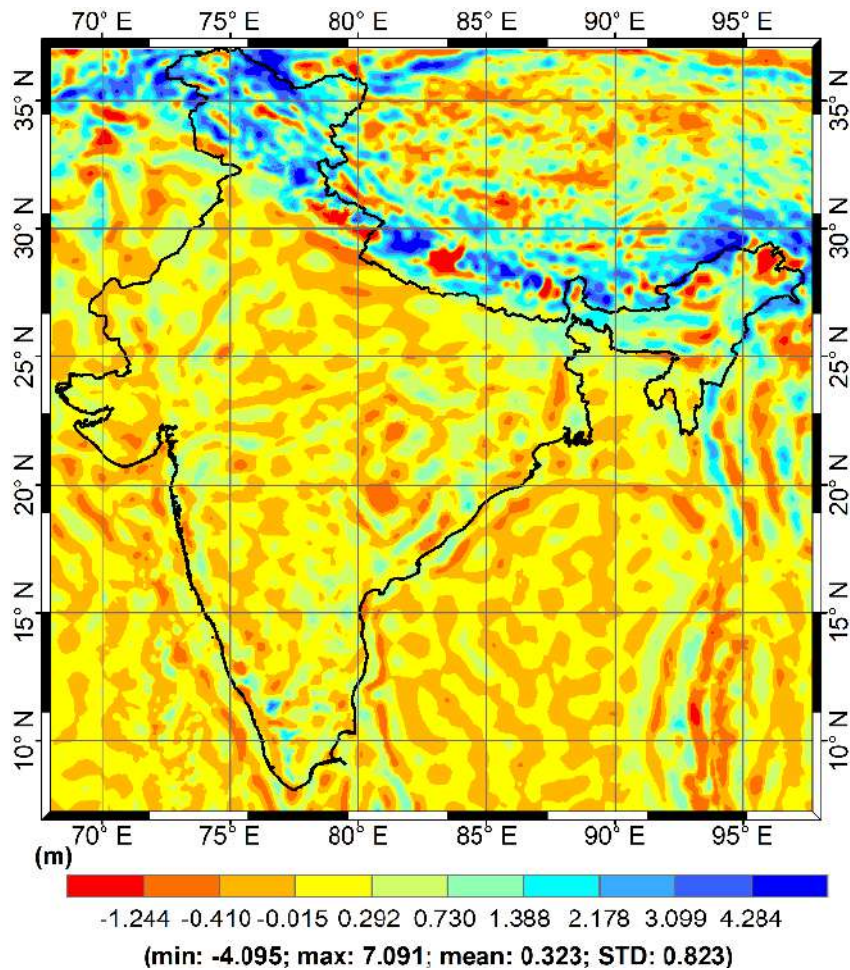


Figure 4.2.6: Residual co-geoid after Stokes-integrating residual Helmert's gravity anomaly with the VK kernel modification ($M = 80$ and $\psi = 1.5^\circ$)

The large residual Helmert's gravity anomalies (Figure 4.2.5) are possibly due to the large gravity gradients (Figure 3.5.1) in the regions where we suspect poor quality of the GETECH gravity data (Section 2.1).

The following are the major differences from the original UNB method:

- i) The computed topographic effects are considered as the mean value, which contrasts with the UNB method, where the mean value is calculated by averaging the topographic effect computed using DEMs with different resolutions (Section 3.2.2).

- ii) For the present study, we have not used the formulas used in the UNB method for atmospheric effects. We have only applied direct atmospheric effect as discussed in Section (3.3.1) and do not apply primary and secondary indirect atmospheric effect, and reference atmospheric effects. As discussed in Section 3.3, though atmospheric correction may not be significant but needs to be studied meticulously to have some consensus on the same among different methods.
- iii) For DWC, we have used the gravity gradient method instead of inverse Poisson's integration (Section 3.5.2).
- iv) We have not used the 'distant zone contribution' (Novák, 2000, pg. 62) in the final geoid solution and have utilised GGM with d/o 300 to remove the reference gravity anomalies and restore the reference geoid undulations. This contrasts with the idea of a satellite-only reference spheroid in the UNB method (e.g., Vaníček and Martinec, 1994; Vaníček et al., 1995).
- v) The zero-degree term based on the generalised Bruns formula is used and explicitly mentioned.
- vi) The geoid-quasigeoid separation term is computed using the Flury and Rummel (2009) method.

4.2.3 KTH method of geoid/quasigeoid calculation

The primary uniqueness of the KTH method lies in the stochastic modification of Stokes's kernel and additive corrections to the gravity data. Unlike the other methods tested (CUT, UNB, LSC), the direct and indirect effects needed to make the observations accordant with the geodetic boundary value problem are added as separate combined corrections to the approximate geoid estimates obtained using Stokes's integration with un-reduced gridded terrestrial gravity data.

Firstly, in the KTH method, approximate values of geoid undulations are computed from the un-reduced gridded gravity anomalies and GGM using the unbiased least-squares geoid estimator (Eq. (4.1.11), with $L = M$). One of the most important steps in calculating approximate geoid is determining *a priori* estimates of signal and error degree variances. These are necessary to compute a better choice of modification parameters to be used in the least-squares modification method (Ågren, 2004; Ågren et al., 2009b).

We have used KTH's preferred Tscherning and Rapp (1974) model to compute the gravity signal degree variance. The error degree variance of the GGM gravity is computed from the published error estimates that accompany the GGM coefficients (Rapp and Pavlis, 1990). The error degree variance of terrestrial gravity anomalies is assumed to be a combination of white noise and a reciprocal distance covariance model (Ågren, 2004; Ågren and Sjöberg, 2014). The signal and the GGM error degree variances are further rescaled by an empirically determined factor to best depict the 'reality' of the study area.

Next are the additive corrections. The basic equation for geoid modelling using the KTH method is

$$N = \hat{N} + \delta N_{comb}^T + \delta N^{DWC} + \delta N_{comb}^{atm} + \delta N^{Ell} \quad (4.2.1)$$

The various additive corrections (atmospheric, ellipsoidal, and downward continuation) discussed in Chapter 3 are reformulated using the modified Stokes kernel for practical geoid computation. Only the combined topographic effect remains the same (Eq. (3.2.41)) (Sjöberg, 2000; Ågren, 2004). However, we would mention that there exists some discrepancy in the expression of combined topographical effect on geoid emanating from the use of R (e.g., Sjöberg and Bagherbandi, 2017) versus $R + H_p$ (e.g., Ågren et al., 2009b) in the second term of Eq. (3.2.41).

In addition to the total combined topographical effects, other three corrections in Eq. (4.2.1) are given as:

- i) Downward continuation effect on geoid (δN^{DWC}) (Sjöberg, 2003b)

$$\delta N^{DWC} = \frac{\Delta g}{\gamma} H_p + 3 \frac{\zeta_0}{R + H_p} H_p - \frac{1}{2\gamma} \frac{\partial \Delta g}{\partial r} H_p^2 + \left[\frac{R}{2\pi} \sum_{n=2}^M (Q_n^M + s_n) \times \left(\left(\frac{R}{R + H_p} \right)^{n+2} - 1 \right) \Delta g_n \right] + \frac{R}{4\pi\gamma} \iint_{\sigma_0} S^M(\psi) \left(\frac{\partial \Delta g}{\partial r} (H_p - H_Q) \right) d\sigma \quad (4.2.2)$$

- ii) Atmospheric correction (Sjöberg, 1999; 2001; Sjöberg and Nahavandchi, 2000)

$$\delta N_{comb}^{atm} = \frac{\delta V_0^{atm}}{\gamma} - \frac{2\pi R \rho_{atm}}{\gamma} \sum_{n=2}^M \left(\frac{2}{n-1} - Q_n^M - s_n \right) H_n - \left. \frac{2\pi R \rho_{atm}}{\gamma} \sum_{n=M+1}^{\infty} \left(\frac{2}{n-1} - \frac{n+2}{2n+1} Q_n^M \right) H_n \right\} \quad (4.2.3)$$

- iii) Ellipsoidal correction to the geoid height (Sjöberg, 2003c; 2004)

$$\delta N^{Ell} = \frac{R}{2\gamma} \sum_{n=2}^{\infty} \left(\frac{2}{n-1} - s_n^* - Q_n^M \right) \left(\frac{a-R}{R} \Delta g_n + \frac{e^2}{2R} \sum_{m=-n}^n \left[(3-(n+2)F_{nm})T_{nm} - (n+1)G_{nm}T_{n-2,m} - (n+7)E_{nm}T_{n+2,m} \right] Y_{nm} \right) \quad (4.2.4)$$

where $s_n^* = \begin{cases} s_n, & \text{if } 2 \leq n \leq M \\ 0, & \text{otherwise} \end{cases}$

T_{nm} are spherical harmonic coefficients of disturbing potential and E_{nm}, F_{nm} , and G_{nm} are ellipsoidal coefficients arising in the derivations (e.g., Sjöberg, 2003a; 2003d).

We have not duplicated the derivations because they are provided in detail in the cited references, almost all doctoral and master dissertations from the KTH on geoid modelling, and the book by Sjöberg and Bagherbandi (2017).

The above four corrections are collectively known as additive corrections, and these are applied to the approximate geoid height to obtain the final geoid height. The geoid-quasigeoid separation term is applied to convert the geoid height to the height anomalies (Section 4.3). This procedure is shown as a flowchart in Figure 4.2.7.

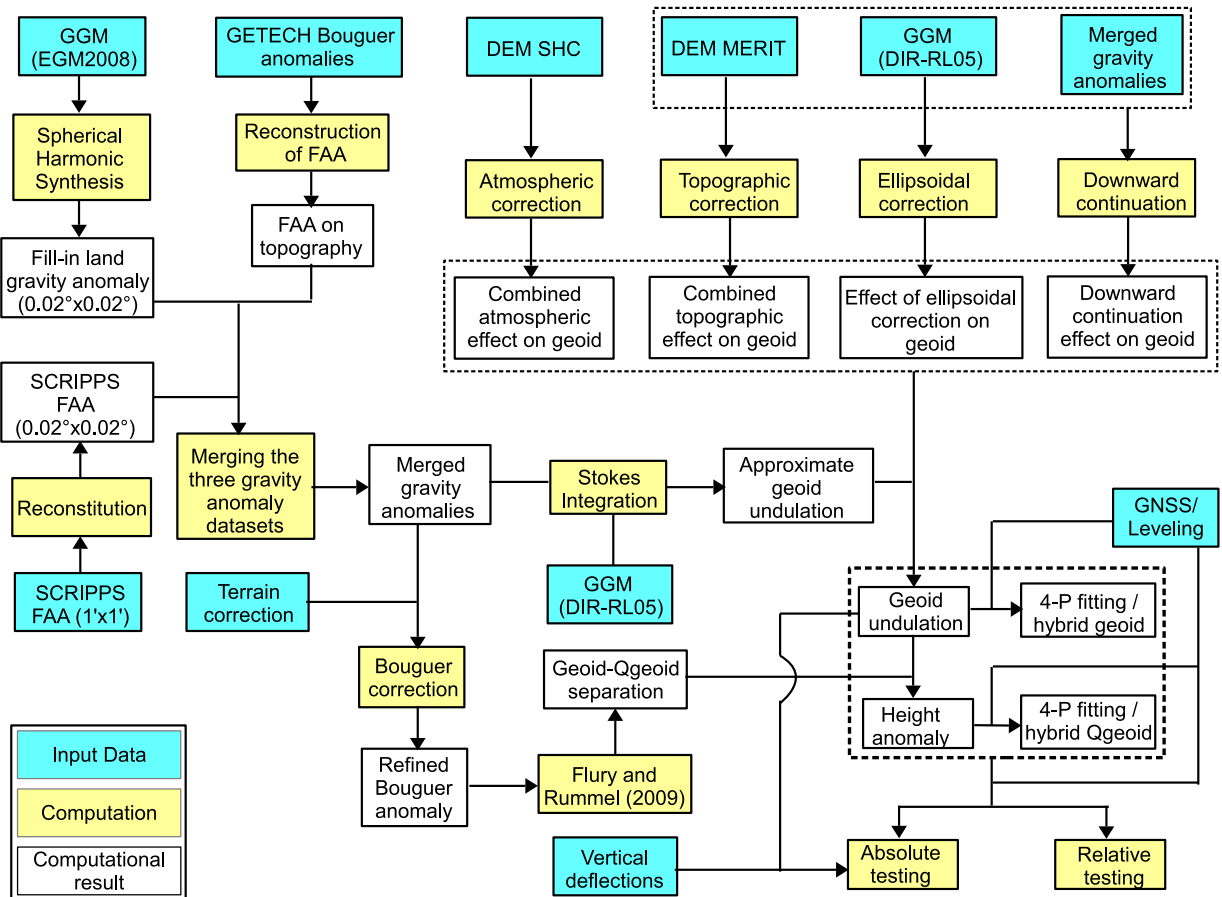


Figure 4.2.7: Flowchart of the KTH methodology of geoid followed by quasigeoid computation.

The KTH method has been designed primarily to compute a gravimetric geoid, which is then converted to quasigeoid by adding the geoid-quasigeoid separation term. However, Sjöberg (2000) and Ågren et al. (2009b) show that if the combined topographic effects are not applied in the computations using the KTH method and if the downward continuation is also adjusted accordingly, the result will be a quasigeoid. The modification to the downward continuation is based on the analytical continuation solution using

Molodensky’s G_I term. This eliminates the need for computing the topographic effects and further correction terms to convert the geoid to quasigeoid. It has been discussed in Section 3.5.3. For practical computations, the stochastically modified Stokes’s kernel is used in the modified DWC effect for quasigeoid, which is then given by

$$\delta\zeta^{DWC} = 3 \frac{\zeta_0}{R + H_p} H_p + \frac{R}{2\pi} \sum_{n=2}^M (Q_n^M + S_n) \left(\left(\frac{R}{R + H_p} \right)^{n+2} - 1 \right) \Delta g_n + \left. \frac{R}{4\pi\gamma_{\sigma_0}} \iint S^M(\psi) \left(\frac{\partial \Delta g}{\partial r} (H_p - H_Q) \right) d\sigma \right\} \quad (4.2.5)$$

Atmospheric and ellipsoidal corrections remain the same i.e., $\delta\zeta_{comb}^{atm} = \delta N_{comb}^{atm}$ and $\delta\zeta^{Ell} = \delta N^{Ell}$ (Ågren et al., 2009b). An overview of the direct quasigeoid computation using the KTH method is given in Figure 4.2.8.

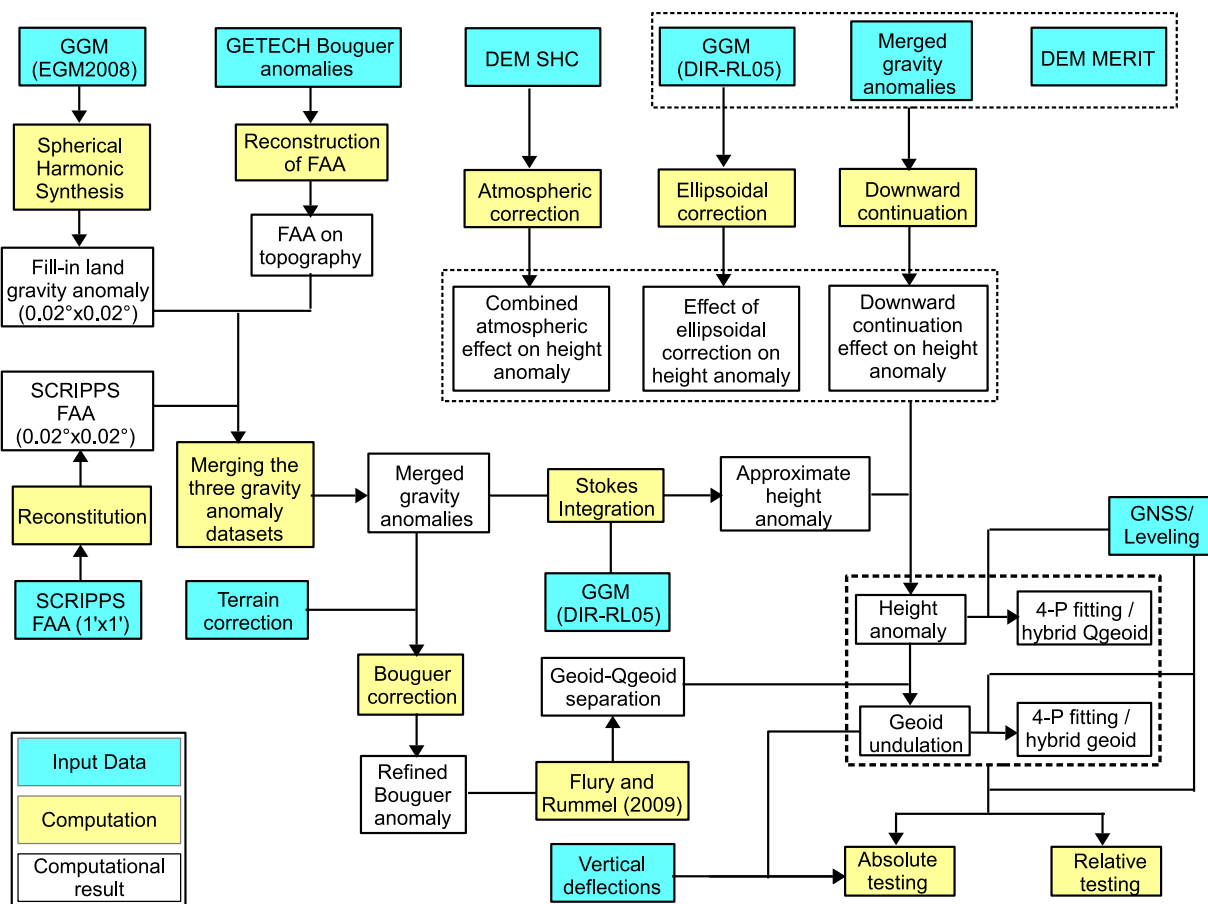


Figure 4.2.8: Flowchart of the KTH methodology for quasigeoid followed by geoid computation.

For our computations with the KTH method, we used the latter method with DIR-RL05 GGM and following combinations (parameter sweeps): $L = M = 40, 80, 120, 160, 200, 240, 280, 300$, and $\psi_0 = 0.2^\circ, 0.5^\circ, 0.75^\circ, 1^\circ, 1.5^\circ, 2^\circ$ in Eq. (4.1.11). The reference height anomalies on the topography are computed using GGM with a zero-degree term from the generalised Bruns's formula (Section 3.6.1) calculated for each latitude parallel. We used normal potential $U_0 (= 62636860.85 \text{ m}^2\text{s}^{-2})$ from GRS80 and the geopotential $W_0 (= 62636853.4 \text{ m}^2\text{s}^{-2})$ from IHRS (Sánchez et al., 2016).

The geoid-quasigeoid separation (Flury and Rummel, 2009) term is applied to the height anomalies to obtain the corresponding geoid undulations. Parametric fitting of geoid/quasigeoid is done with GNSS/levelling data to calculate the corresponding hybrid geoid/quasigeoid models. These are discussed in Sections 4.3 and 4.4, respectively. The gravimetric geoid and quasigeoid models (before and after fit) are then validated with the available GNSS/levelling data. The gravimetric geoid is also validated with vertical deflections (Section 3.3).

Only for illustration purposes, the atmospheric, ellipsoidal, and the DWC effect are shown in Figures 4.2.9, 4.2.10, and 4.2.11, respectively, computed with LSMS kernel modification ($M = 80$ and $\psi = 1.5^\circ$).

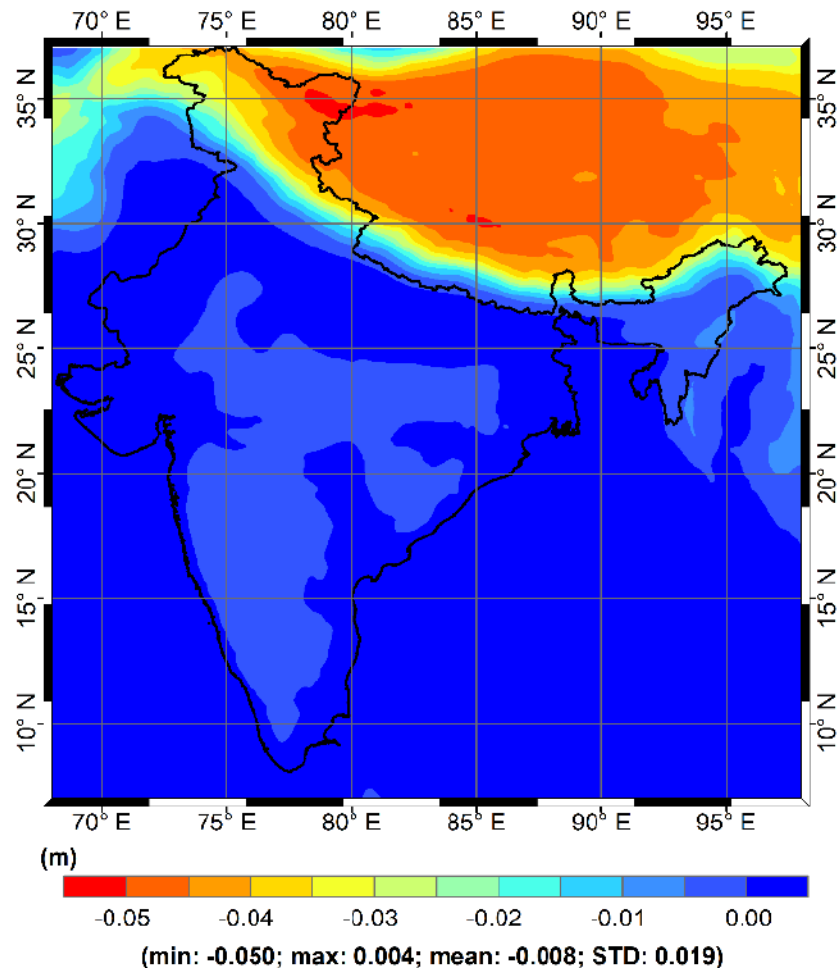


Figure 4.2.9: Combined atmospheric effect for the height anomalies/geoid undulations in the KTH method with LSMS kernel modification ($M = 80$ and $\psi = 1.5^\circ$)

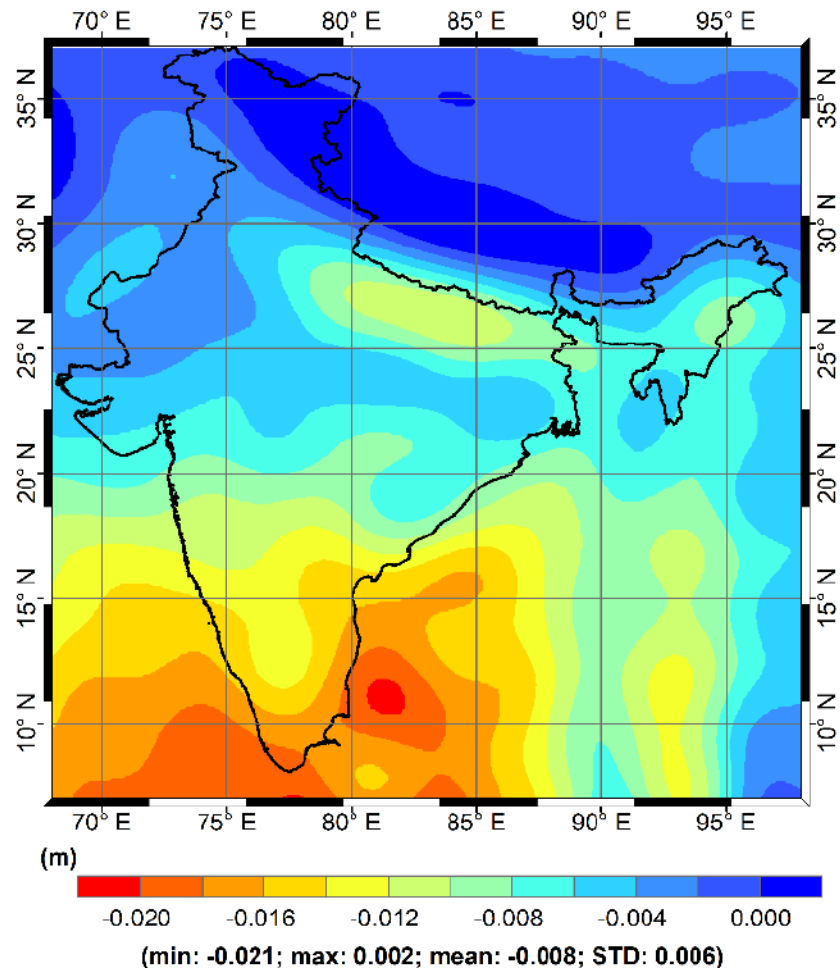


Figure 4.2.10: Ellipsoidal effect for the height anomalies/geoid undulations in the KTH method with LSMS kernel modification ($M = 80$ and $\psi = 1.5^\circ$)

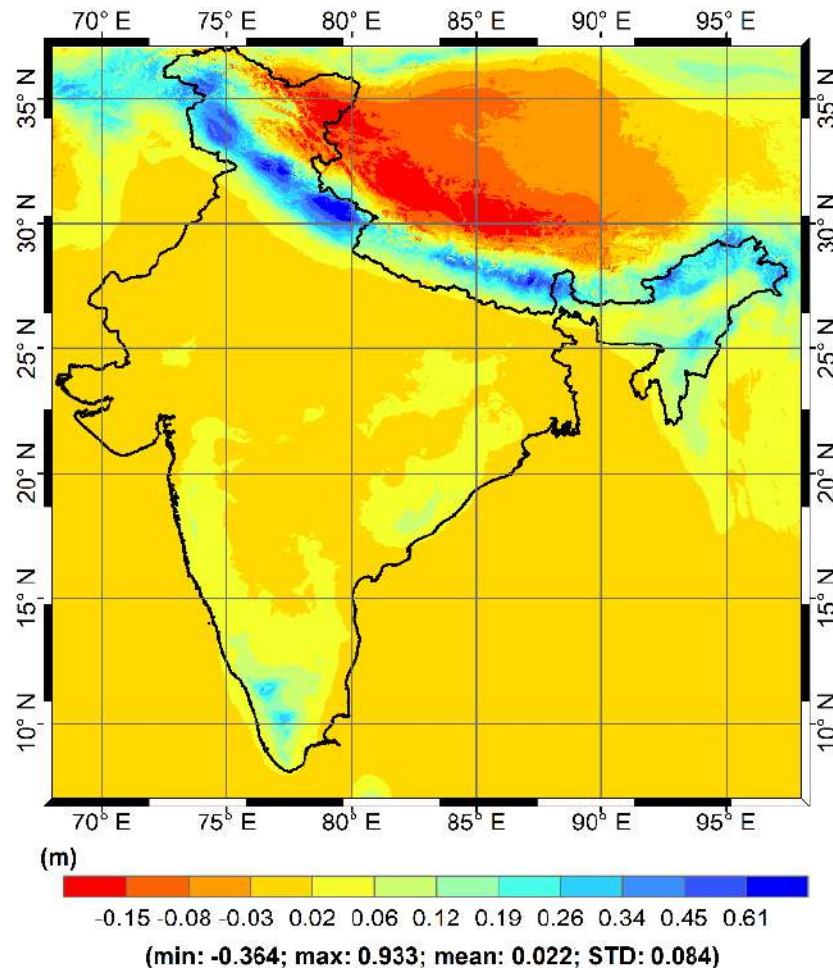


Figure 4.2.11: Combined downward continuation effect for the height anomalies in the KTH method with LSMS kernel modification ($M = 80$ and $\psi = 1.5^\circ$)

The following are the major differences from the original KTH method:

- i) We could not follow the remove-compute-restore method for gridding the gravity anomalies because we already had the gridded gravity anomalies.
- ii) The zero-degree term based on generalised Bruns's formula is used and explicitly mentioned.
- iii) The geoid-quasigeoid separation term is computed using the Flury and Rummel (2009) method.

4.3 Geoid-quasigeoid separation

Primarily there are three choices of height systems (Featherstone and Kuhn, 2006): orthometric heights (either Helmert (1884) or rigorous (Tenzer et al., 2005; Santos et al., 2006)) referred to the geoid, normal heights referred to the quasigeoid (Molodensky et al., 1962), and normal-orthometric heights referred to a non-explicitly mentioned surface (Filmer et al., 2010; 2014). There have been discussions on the choice of geoid vs. quasigeoid (Vaníček et al., 2012; Sjöberg, 2013; 2018; Penna et al., 2013; Foroughi et al., 2017b; Popadyev, 2019; Santos et al., 2021) as a reference surface for physical heights. Since both have their respective advantages and disadvantages, no consensus has been attained. Therefore, different countries have their individual preference of one surface over the other. A ‘bridge’ term connecting the two surfaces without an intensive independent/separate computation of geoid and quasigeoid is the geoid-quasigeoid separation (GQS) term.

The major motivations for pursuing GQS term are:

- i) Avoiding the re-computations for the countries that are shifting from one height system to another.
- ii) Use of consistent height system in the whole of the country or adjacent countries.
- iii) Investigate the suitable representative surface for the normal-orthometric height system and thereafter calculate hybrid geoid or hybrid quasigeoid.
- iv) An aid to geophysical studies (e.g., Mehramuz et al., 2011)

The third point is the motivation to calculate GQS term for the present study. The CUT and the KTH methods provide height anomalies (KTH method can also provide geoid undulations, Section 4.2.3), while the UNB method provides geoid undulations. Therefore, to convert among geoid undulations and height anomalies, the GQS term is

required.

The background for GQS term is the relation between geodetic height and i) orthometric height and geoid undulation (Eq. (4.3.1)), and ii) normal height and height anomaly (Eq. (4.3.2))

$$h \approx H + N \quad (4.3.1)$$

$$h \approx H^* + \zeta \quad (4.3.2)$$

From Eqs. (4.3.1) and (4.3.2),

$$H + N \approx H^* + \zeta \Rightarrow N - \zeta \approx H^* - H \quad (4.3.3)$$

From the relations of H and H^* with the geopotential number (C), i.e., $H = \frac{C}{\bar{g}}$ and

$H^* = \frac{C}{\bar{\gamma}}$ we have

$$H^* - H \approx \frac{\bar{g} - \bar{\gamma}}{\bar{\gamma}} H \quad (4.3.4)$$

Therefore, substituting Eq. (4.3.4) in Eq. (4.3.3), the relation between geoid undulation and height anomaly is given by

$$N - \zeta \approx \frac{\bar{g} - \bar{\gamma}}{\bar{\gamma}} H \quad (4.3.5)$$

where \bar{g} is the mean gravity along the curved and torsioned plumb line and $\bar{\gamma}$ is the mean normal gravity along the curved normal plumb line. If we consider ζ as the separation between the ellipsoid and the quasigeoid, Eq. (4.3.5) can also be regarded as the GQS.

Therefore, the problem of GQS has now reduced mainly to the determination of mean gravity \bar{g} along the curved and torsioned plumb line. The treatment of \bar{g} is the

principal source of various available formulas for GQS term. Table 4.3.1 lists a few of the GQS term formulas available in the literature. We have not discussed their detailed methodology, instead see the literature cited.

Table 4.3.1: Various formulas for calculating GQS term.

Reference	GQS term
Heiskanen and Moritz (1967, pg. 327)	$\frac{\Delta g^{BA}}{\bar{\gamma}} H \quad (4.3.6)$
Heiskanen and Moritz (1967, pg. 328)	$\left(\Delta g^{BA}\right)_{in\ Gals} \left(H\right)_{in\ km} \quad (4.3.7)$
Ågren (2004)	$\frac{\Delta g^{BA}}{\gamma} H - \frac{H^2}{2\gamma} \frac{\partial \Delta g}{\partial r} \quad (4.3.8)$
Sadiq et al. (2009)	$\frac{\Delta g^{BA}}{\bar{\gamma}} H + \frac{H^2}{2\gamma} \frac{\partial \Delta g}{\partial H} \quad (4.3.9)$
Flury and Rummel (2009)	$\frac{\Delta g^{BA}}{\bar{\gamma}} H + \frac{V_R^t - V_{R+H}^t}{\bar{\gamma}} \quad (4.3.10)$
Sjöberg (2010)	$\frac{\Delta g^{BA}}{\bar{\gamma}} H + \frac{V_R^t - V_{R+H}^t}{\bar{\gamma}} \left(1 - \frac{H}{R}\right) - \frac{H^2}{2\gamma_{R+H}} \frac{\partial \Delta g^{mt}}{\partial h} \quad (4.3.11)$
Chijun et al. (2011)	$\frac{\Delta g^{BA}}{\bar{\gamma}} H - \frac{H^2}{2\gamma} \frac{\partial \delta g}{\partial h} \quad (4.3.12)$
Schwabe et al. (2016)	$\frac{\delta g^{mt}}{\gamma_0} H + \frac{V_R^t - V_{R+H}^t}{\gamma_0} - \frac{H^2}{2\gamma_0} \frac{\partial \delta g^{mt}}{\partial h} + \zeta \left(\frac{\gamma_{R+H^*}}{\gamma_0} - 1 \right) \quad (4.3.13)$

There also exist formulas for GQS that include density contribution (e.g., Tenzer et al., 2006; 2015; Foroughi and Tenzer, 2017) but are not provided here because no national Digital Density Model (DDM) is available for India.

The formulas presented by Flury and Rummel (2009) and Sjöberg (2010) do not vary more than a centimetre anywhere on the Earth (Sjöberg, 2010; Flury and Rummel, 2011). In addition to the several available GQS formulas, there has been a mild inconsistency in the use of simple or refined Bouguer anomalies in the formulas in Table 4.3.1. Heiskanen and Moritz (1967) and Ågren (2004) use simple planar Bouguer anomalies, while others (in Table 4.3.1) have used refined Bouguer anomalies. Ádám

(1999), Lasagna (2017) and Wang et al. (2020) preferred using simple Bouguer anomalies, while Hwang et al. (2020) have worked with refined Bouguer anomalies with the formulas in Heiskanen and Moritz (1967, pg. 327). From the derivations in the cited literature, it can be observed that the use of simple versus refined Bouguer anomalies is dependent on the choice of formulating \bar{g} (e.g., Rapp, 1961, pg. 39-69; Heiskanen and Moritz, 1967, pg. 166-167).

We now provide our interpretation of GQS (without density considerations). Recalling from Section 3.5.1, height anomaly calculated by formulating the boundary condition at the Earth's surface will provide the telluroid. Therefore, height anomalies should be downward continued to the ellipsoid to construct the quasigeoid. As such, the difference between geoid undulations and downward continued height anomalies should be called GQS. Hence, the difference between geoid undulation and height anomaly should not be stated as equal to the difference between geoid and quasigeoid.

We acknowledge that quasigeoid is interpreted and defined as a surface generated by plotting the computed height anomalies (at Earth's topography) on the reference ellipsoid. We also recall sentences regarding quasigeoid by 1. Vaníček (1974): "*The height anomaly can be – and very often is – interpreted as height above the reference ellipsoid. The locus of such interpreted height anomalies is surface known as quasigeoid*" and 2. Moritz (2011): "*The height anomalies are similar in magnitude to the geoid height, but have quite a different geometric interpretation....Molodensky introduced an artificial "quasigeoid" by plotting the height anomaly above the ellipsoid.*" In such a case, if height anomalies are downward continued to the ellipsoid, the height of a point above the quasigeoid should not be a normal height. However, next we provide a mathematical formulation involving downward continuation of height anomalies to the ellipsoid that recommend towards a convention for defining/interpreting quasigeoid.

Since the major difference in the computational theory of geoid and quasigeoid is the required treatment of topographical effects in the former surface, the GQS should comprise the terms related to topographical effects. Therefore, GQS can be given by

$$N - \left(\zeta_P - \left(-\frac{\Delta g^{FA}}{\gamma_Q} h \right) \right) \approx \frac{\Delta g^{BC}}{\gamma_Q} h + \frac{TC}{\gamma_Q} h + PITE \quad (4.3.14)$$

The third term on the L.H.S. of Eq. (4.3.14) is the gradient of height anomalies $\left(\frac{\partial \zeta}{\partial h} \right)$

(Section 3.5.1). Eq. (4.3.14) can be rearranged to a more general term that is given as

$$N - \zeta_P \approx \frac{\Delta g^{FA} + \Delta g^{BC} + TC}{\gamma_Q} h + PITE = \frac{\Delta g^{RBA}}{\gamma_Q} h + PITE \quad (4.3.15)$$

where Δg^{BC} and Δg^{RBA} are the planar Bouguer correction and refined planar Bouguer anomalies, respectively.

We have used h because the height anomalies are downward-continued from the Earth's topography to the ellipsoid. Our Eq. (4.3.15) is comparable with Flury and Rummel's (2009) formula (Table 4.3.1). Therefore, our interpretation of GQS as the separation between geoid undulations and downward-continued height anomalies is valid. However, for the present study, we have computed the GQS term using Flury and Rummel's (2009) formula, which is shown in Figure 4.3.1. We also calculated the GQS term using Heiskanen and Moritz's (1967, pg. 327) formula (Figure 4.3.2) to compare the values obtained using the two formulas. The differences in the GQS term with the two formulas are shown in Figure 4.3.3. It should be noted that the refined planar Bouguer anomalies have been used in implementing both formulas.

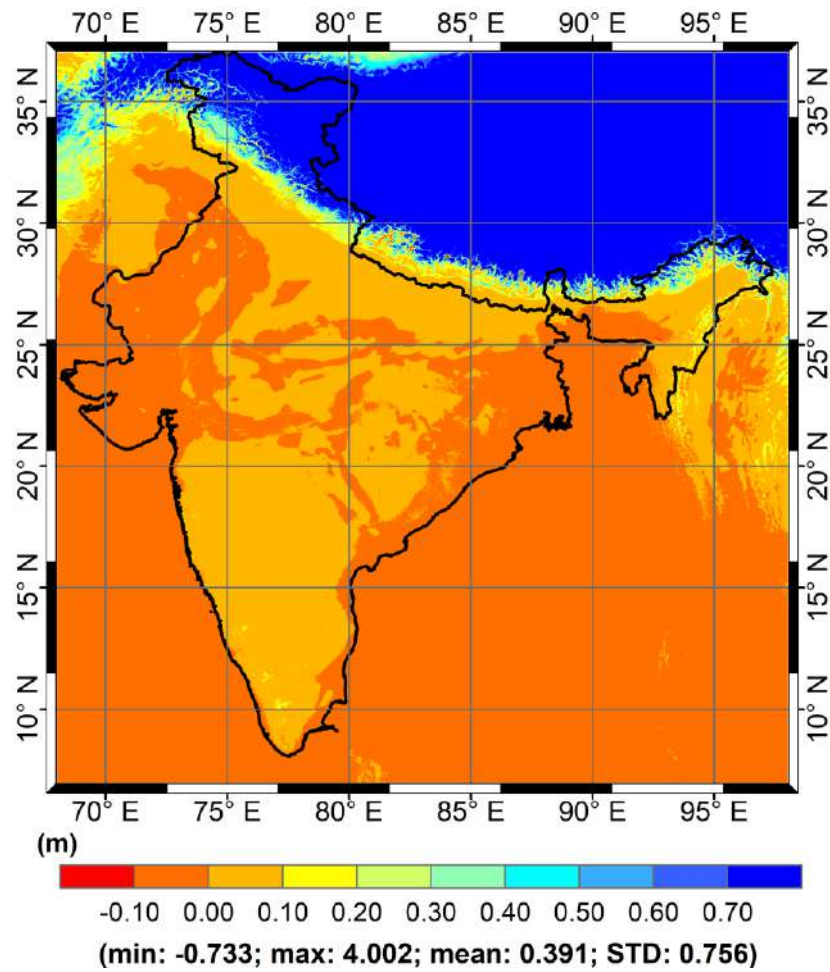


Figure 4.3.1: GQS term calculated using Flury and Rummel's (2009) method.

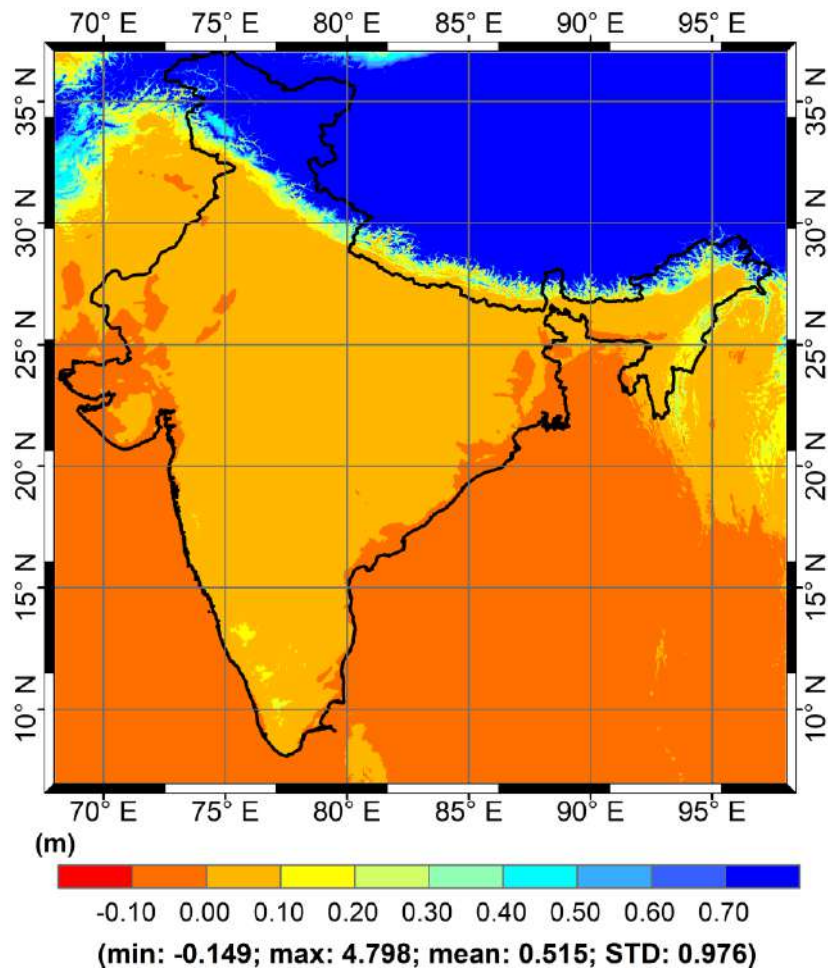


Figure 4.3.2: GQS term calculated using Heiskanen and Moritz's (1967) method.

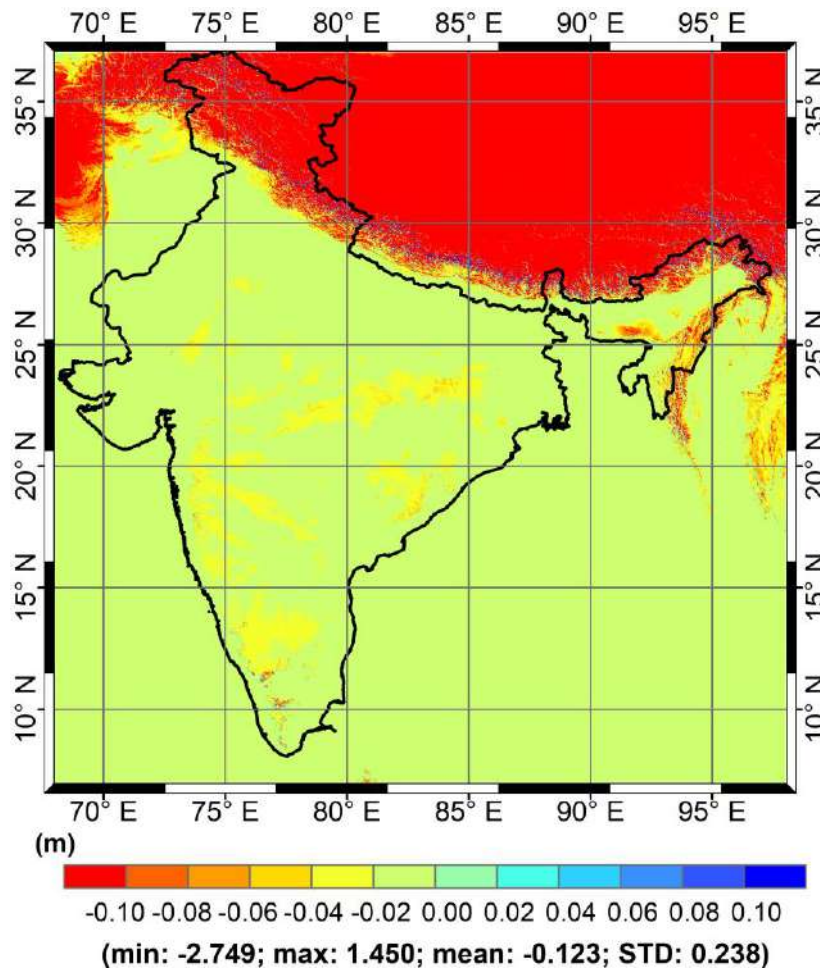


Figure 4.3.3: Difference in the GQS term calculated using the methods given in Flury and Rummel (2009) and Heiskanen and Moritz (1967).

Large values (>4 m) of the GQS term are achieved using different methods (Figures 4.3.1 and 4.3.2). For our study area, there is a significant difference (Figure 4.3.3) in the GQS term calculated using the Flury and Rummel (2009) and Heiskanen and Moritz (1967) methods. The differences in the GQS term from the two methods vary from -2.75 m to $+1.45$ m with a mean of -0.12 m and standard deviation of ± 0.24 m. These large differences among GQS terms with different methods are a caution for geoid modellers who seek either a cm-precise geoid calculated using the quasigeoid and the GQS term or cm-precise quasigeoid calculated using the geoid and the GQS term.

Furthermore, we have computed the GQS term at a grid spacing of $0.02^\circ \times 0.02^\circ$ that may possibly omit some values in regions within/between these nodes. For example,

Jiang et al. (2021) show a value of GQS as -1.30 m calculated using the Flury and Rummel (2009) method for the summit of Mt. Everest.

4.4 Hybrid geoid/quasigeoid

Ideally, the following geometrical relation between the geodetic height, orthometric height and geoid undulation must hold true.

$$h - H - N = 0 \quad (4.4.1)$$

However, due to, primarily, following factors Eq. (4.4.1) is never satisfied (Rummel and Teunissen, 1988; Kearsley et al., 1993; Featherstone, 1998; Kotsakis and Sideris, 1999, among many others):

- i) The reference surfaces for the three heights are entirely different: ellipsoid for h , tide gauge station(s) based local vertical datum for H , and gravity and GGM-based reference surface for N .
- ii) There are numerous datum inconsistencies (e.g., different permanent tide systems, long-wavelength errors in N , over-constrained adjustment of levelling networks, zero-degree term offsets in local vertical datums), theoretical approximations and assumptions in calculating H , N or vertical deflections (e.g., use of approximate formulas and negligence of density, sea surface topography, curved and torsioned plumb line at each point is along a different path, etc.)
- iii) Observations at different epochs, non-consideration of vertical land motion and/or use of different GNSS data processing softwares (e.g., Featherstone et al., 2019).
- iv) Eq. (4.4.1) does also not hold for a theoretical reason, that is, h is measured along the ellipsoidal normal, while H is measured along the curved and torsioned plumb line.

The requirement and methods of fitting a gravimetric geoid to the GNSS/levelling dataset have been studied by many (e.g., Jiang and Duquenne, 1996; Kotsakis and Sideris, 1999; Denker et al., 2000; Fotopoulos, 2003, among many others). A geoid model obtained after fitting to the GNSS/levelling data is often known as hybrid geoid. Several researchers have computed the national hybrid geoid/quasigeoid models (e.g., Erol and Erol, 2013; Lee et al., 2013; Miyahara et al., 2014; Brown et al., 2018; Roman and Ahlgren, 2019; Borghi et al., 2020; Yildiz et al., 2020; Hwang et al., 2020).

There are two common approaches of constructing a hybrid geoid: i) finding the offsets between the gravimetric (N) and geometric ($h - H$) undulations, which are then interpolated on a regular grid to be added to the gravimetric geoid model, and ii) least-squares fitting of gravimetric and geometric undulations using some parametric model, thereby reducing the offsets for some biases and tilts in different reference surfaces, which are then interpolated to be added to the geoid model. The interpolation methods include polynomial surfaces (Featherstone, 2000; Fotopoulos et al., 2002) and least-squares collocation (e.g., Moritz, 1980, Fukuda et al., 1997; Featherstone, 2000; Featherstone and Sproule, 2006; Miyahara et al., 2014; Al-Kherayef et al., 2020).

The basic model to compute geoid offset along with minimising the effect of vertical datum inconsistencies using parametric equations is (Heiskanen and Moritz, 1967, pg. 206)

$$\Delta N = N_{GNSS/lev} - N = h_i - H_i - N_i = \mathbf{a}^T \mathbf{x} + \mathbf{v}_i \quad (4.4.2)$$

where \mathbf{x} is a $m \times 1$ vector of unknown parameters in the parametric model, \mathbf{a} is a $m \times 1$ vector of known coefficients and \mathbf{v} is a $n \times 1$ vector of residuals, n is the number of observations, and m is the number of parameters in the model. All the possible datum inconsistencies and systematic bias in the data are described by the parametric part $\mathbf{a}^T \mathbf{x}$.

The choices of multi-parametric models (Heiskanen and Moritz, 1967; Kotsakis et al., 2001; Sjöberg and Bagherbandi, 2017) viz. three-, four-, five- and seven-parameter transformation models are given by

$$\left. \begin{aligned}
 \text{3-parameter: } \Delta N &= (\cos \phi \cos \lambda) x_1 + (\cos \phi \sin \lambda) x_2 + (\sin \phi) x_3 + \mathbf{v} \\
 \text{4-parameter: } \Delta N &= (\cos \phi \cos \lambda) x_1 + (\cos \phi \sin \lambda) x_2 + (\sin \phi) x_3 + x_4 + \mathbf{v} \\
 \text{5-parameter: } \Delta N &= (\cos \phi \cos \lambda) x_1 + (\cos \phi \sin \lambda) x_2 + (\sin \phi) x_3 + (\sin^2 \phi) x_4 + x_5 + \mathbf{v} \\
 \text{7-parameter: } \Delta N &= (\cos \phi \cos \lambda) x_1 + (\cos \phi \sin \lambda) x_2 + (\sin \phi) x_3 + \left(\frac{\cos \phi \sin \phi \sin \lambda}{\sqrt{1-e^2 \sin^2 \phi}} \right) x_4 + \\
 &\quad \left(\frac{\cos \phi \sin \phi \cos \lambda}{\sqrt{1-e^2 \sin^2 \phi}} \right) x_5 + \left(\frac{1-f^2 \sin^2 \phi}{\sqrt{1-e^2 \sin^2 \phi}} \right) x_6 + \left(\frac{\sin^2 \phi}{\sqrt{1-e^2 \sin^2 \phi}} \right) x_7 + \mathbf{v}
 \end{aligned} \right\} (4.4.3)$$

As an example, for a four-parameter model and one observation $(h-H-N)$, vectors \mathbf{a} and \mathbf{x} are given by

$$\mathbf{a} = \begin{pmatrix} \cos \phi \cos \lambda \\ \cos \phi \sin \lambda \\ \sin \phi \\ 1 \end{pmatrix} \text{ and } \mathbf{x} = \begin{pmatrix} x_1 \\ x_2 \\ x_3 \\ x_4 \end{pmatrix} \quad (4.4.4)$$

where \mathbf{x} can be solved using

$$\mathbf{x} = (\mathbf{A}^T \mathbf{A})^{-1} (\mathbf{A}^T \mathbf{l}) \quad (4.4.5)$$

with \mathbf{A} being the design matrix of size $n \times m$, \mathbf{A}^T is the transpose of matrix \mathbf{A} and \mathbf{l} is a $n \times 1$ vector of the observations obtained using Eq. (4.4.2).

Thereafter, adjusted ΔN (ΔN_a) can be obtained, which represents the gravimetric-geometric geoid offset treated for biases, tilts, or any other type of systematic differences between the two data sets (N and $N_{GNSS/lev}$). These ΔN_a values are interpolated at a grid

of the size and resolution of the gravimetric geoid using some interpolation technique, which is then applied to the gravimetric geoid.

Due to the availability of several parametric models, the choice of one over others is sometimes based on i) arbitrary choice, ii) least standard deviation on validation with the GNSS/levelling data or iii) some other statistical testing (e.g., k -fold cross validation (Stone, 1974; 1977; Shao, 1993)). With the seven-parameter model, we almost always get the results with the smallest standard deviation (e.g., Abdalla, 2009; Goyal et al., 2019a). Still, under certain conditions, it is possible that the seven-parameter model cannot be used (e.g., not sufficient datapoints) or suffer from over-parametrisation. Therefore, a meticulous statistical study is required in this direction. Though not covered in this thesis, we would like to direct towards a starting point where i) Fotopoulos (2003) has used descriptive statistics, goodness of fit and adjusted goodness of fit, cross-validation, and three tests for parameter significance (forward elimination, backward elimination, stepwise procedure), and ii) Goyal et al. (2019a) demonstrated the use of Akaike's information criterion (Akaike, 1974) and Bayesian information criterion (Schwarz, 1978) for testing parameter significance. It should be noted that there is a typographical error in Eqn. 9 of Goyal et al. (2019a); the denominator should read r^2 instead of γr .

4.5 Summary

In this chapter, we discussed the three methodologies (CUT, UNB and KTH) of calculating geoid and quasigeoid models. The three methods are significantly different from each other. The CUT method uses Moritz's analytical solution of the Molodensky's problem to calculate the height anomalies. The UNB method uses Helmert's second condensation scheme to account for the gravitating masses above the geoid for the calculation of geoid undulations. The CUT and the UNB methods apply the Stokes integration on residual

gravity anomalies with deterministically modified (but different) Stokes's kernel. The KTH method applies the Stokes integration on the un-reduced gravity anomalies with stochastically modified Stokes's kernel. The KTH method uses least squares modification of Stokes's kernel with additive corrections to the approximate height anomalies for calculating the height anomalies.

We have explicitly mentioned the differences between the methodologies strictly followed by the respective developers of the three methods and our application due to the unique aspects of the Indian data.

Since the CUT and the KTH methods provide height anomalies and the UNB method provides geoid undulation, a discussion on the geoid-quasigeoid separation (GQS) term is provided that is used to calculate geoid undulations from height anomalies or *vice-versa*. This is important because we aim to compare our GNSS/levelling data with both geoid and quasigeoid.

We have provided a list of different formulas available in the literature for GQS term. It is shown that the difference in the GQS term calculated with two more commonly used formulas (Heiskanen and Moritz, 1967; Flury and Rummel, 2009) can range from -2.75 m to +1.45 m, which is substantial from the viewpoint of cm-precise geoid calculated using quasigeoid modelling technique and the GQS term or cm-precise quasigeoid calculated using geoid modelling technique and the GQS term.

A discussion is provided that the difference between the geoid undulations and the height anomalies should not be called GQS. However, GQS should be defined as the difference between the geoid undulations and the downward-continued height anomalies. A mathematical proof has also been provided for the latter definition, which is comparable to the GQS formula derived by Flury and Rummel (2009).

Finally, we have presented the method of calculating hybrid geoid and hybrid quasigeoid models using three-, four-, five-, and seven-parameter fitting, which are generally used to account (remove) for tilts and biases in the vertical datum.

Chapter 5: Geoid and quasigeoid: results and validations

5.0 Introduction

This chapter presents the results of the geoid and quasigeoid models of i) the whole of mainland India calculated using the three methods as discussed in Sections 4.2.1, 4.2.2, and 4.2.3 and ii) four regions (UP West, UP East, Hyderabad and Bangalore) calculated using GRAVSOFIT with LSC (GEOCOL) and RTM as described in Forsberg and Tscherning (2008). The geoid and quasigeoid models are validated with the available GNSS/levelling data in an absolute and relative sense. Since we do not have a well-distributed dataset, the validation has been done using the whole of GNSS/levelling data (for India) and using the datasets from the four clusters/regions (UP West, UP East, Hyderabad and Bangalore, Figure 2.2.1). Moreover, we have validated the gravimetric geoid models with the north-south and east-west components of the vertical deflections. Since the quasigeoid is not an equipotential surface, the quasigeoid models are not validated with the vertical deflections. The gravimetric geoid models of India based on the CUT, the UNB and the KTH methods and an inter-model comparison are also provided in this chapter.

5.1 Validation of the developed geoid and quasigeoid models

The absolute testing is realised through point-wise subtraction of gravimetric geoid undulations (or height anomalies) obtained using Stokes's integration (N or ζ) and the geometrical geoid undulation ($h - H$) or height anomaly obtained using GNSS/levelling data (Eq. (5.1.1)).

$$\mathcal{E}_i^{abs} = N_i^{grav} - N_i^{GNSS/lev} = N_i^{grav} - (h_i - H_i) \quad \forall i = 1, 2, 3, \dots, n \quad (5.1.1)$$

where n is the total number of discrete GNSS/levelling data points. However, it should be again noted that the height system of the available levelling data (in this study; Section 2.2) is unknown and we have assumed it to be based on IVD1909, which is in the normal-orthometric height system. Though absolute precision assessment is practiced by the ‘subtraction’ of data points, it is important to acknowledge that absolute precision is only an assumption. This is principally because the levelled heights that refer to the local vertical datum are not necessarily coincident with the geoid (Featherstone, 2001). Without going into further details, we have also used ‘subtraction’ of gravimetric and geometric geoid undulations after a 4-parameter fit for absolute precision assessment.

The test for the relative fit of geoid and quasigeoid is an analysis tool to investigate the geoid/quasigeoid gradients. This type of analysis (Eq. (5.1.2)) is of more interest to land surveyors who use relative GNSS baselines and geoid/quasigeoid gradients as a replacement for the time-consuming differential levelling.

$$\varepsilon_{ij}^{rel} = \Delta N_{ij}^{grav} - \Delta N_{ij}^{GNSS/lev} = \Delta N_{ij}^{grav} - (\Delta h_{ij} - \Delta H_{ij}) \quad \forall i, j = 1, 2, 3, \dots, n; i \neq j \quad (5.1.2)$$

We have computed (for ε_{ij}^{rel}) minimum, maximum, mean, standard deviation, and the ratio of mean differences to the mean baseline length in parts per million (average ppm in mm/km) for geoid and quasigeoid, before and after a 4-parameter fitting. Featherstone (2001) has also discussed the relative precision assessment of geoid/quasigeoid.

Helmert’s vertical deflections (obtained by astrogeodetic observations) are compared with Pizetti’s vertical deflections (obtained from the horizontal gradients of the geoid models). Pizetti’s vertical deflections can also be obtained using Vening-Meinesz’s integral (Heiskanen and Moritz, 1967) but this is not used here. Instead, we used the horizontal gradients of the developed geoid models using the three methods (CUT, UNB and KTH) with all the tested combinations (parameter sweeps) of modification degree and

integration radius. Pizetti's north-south (ξ_{Pz}) and east-west (η_{Pz}) vertical deflection's components are calculated using Eqs. (5.1.3) and (5.1.4), respectively (Featherstone and Lichti, 2008)

$$\xi_{Pz} = \frac{-\Delta N_{\Delta\varphi}}{\mu \Delta\varphi} \quad (5.1.3)$$

$$\eta_{Pz} = \frac{-\Delta N_{\Delta\lambda}}{\nu \Delta\lambda \cos\varphi} \quad (5.1.4)$$

where $\Delta N_{\Delta\varphi}$ and $\Delta N_{\Delta\lambda}$ are the changes in the geoid undulation at the grid nodes defining $\Delta\varphi$ and $\Delta\lambda$, respectively. μ and ν are the radii of curvature in meridional and prime-vertical, respectively.

As a recall from Chapter 2, for validation we have 119 GNSS/levelling data points, and 701 meridional components and 280 prime vertical components of the vertical deflections. Figure 5.1.1 shows the base figure, i.e., following which the results of parameter sweeps have been depicted in Figures 5.1.2 to 5.1.11. We provide this base figure as an explanation because, in the literature, parameter sweeps are depicted in a different way (e.g., Featherstone et al., 2018; Claessens and Filmer, 2020). This way of plotting the results of parameter sweeps was chosen so that the plots for geoid (blue) and quasigeoid (red) can be shown on the same graph for a better comparison. There are eight columns in Figure 5.1.1, each of which is assigned to a modification degree (40, 80, 120, 160, 200, 240, 280 and 300). Each circle in a column represents a combination of M and ψ starting with $M = 40$, $\psi = 0.2^\circ$ to $M = 40$, $\psi = 2^\circ$ in the first column, then $M = 80$, $\psi = 0.2^\circ$ to $M = 80$, $\psi = 2^\circ$ in the second column up to $M = 300$, $\psi = 0.2^\circ$ to $M = 300$, $\psi = 2^\circ$ in the last column. y-axis shows the statistic (standard deviation or average ppm) for all the combinations of M and ψ .

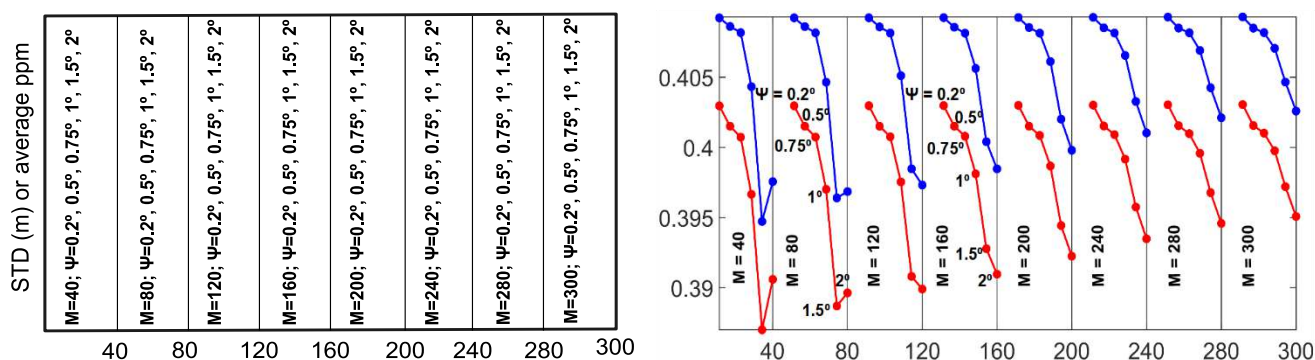


Figure 5.1.1: Base figure to show the variation of STD or average ppm in validation results for different combinations of modification degree and integration radius (parameter sweeps).

The results are arranged as follows:

Figures 5.1.2, 5.1.3, and 5.1.4 show the variation of standard deviation (for absolute precision assessment with respect to GNSS/levelling) in the geoid and quasigeoid for different combinations of modification degree (40, 80, 120, 160, 200, 240, 280, 300) and integration radius ($0.2^\circ, 0.5^\circ, 0.75^\circ, 1^\circ, 1.5^\circ, 2^\circ$) for India and four local regions using the CUT, the UNB, and the KTH methods, respectively.

Figures 5.1.5, 5.1.6, and 5.1.7 depict the variation of standard deviation (for relative precision assessment with respect to GNSS/levelling) in the geoid and quasigeoid for different combinations of modification degree (40, 80, 120, 160, 200, 240, 280, 300) and integration radius ($0.2^\circ, 0.5^\circ, 0.75^\circ, 1^\circ, 1.5^\circ, 2^\circ$) for India and four local regions using the CUT, the UNB, and the KTH methods, respectively.

Figures 5.1.8, 5.1.9, and 5.1.10 depict the variation of average ppm (for relative precision assessment with respect to GNSS/levelling) in the geoid and quasigeoid for different combinations of modification degree (40, 80, 120, 160, 200, 240, 280, 300) and integration radius ($0.2^\circ, 0.5^\circ, 0.75^\circ, 1^\circ, 1.5^\circ, 2^\circ$) for India and four local regions using the CUT, the UNB, and the KTH methods, respectively.

Figure 5.1.11 depicts the variation of the standard deviation for geoid validation with the vertical deflection's components. The results are presented for India geoid models developed using the three methods with different combinations of modification degree (40, 80, 120, 160, 200, 240, 280, 300) and integration radius (0.2° , 0.5° , 0.75° , 1° , 1.5° , 2°).

Table 5.1.1 provides the minimum, maximum, mean, and standard deviation of the absolute precision assessment of geoid and quasigeoid, before and after fit, computed using the CUT, UNB and KTH methods. The values are provided for the combination of modification degree and integration radius providing the minimum standard deviation among all combinations for India and four local regions.

Table 5.1.2 provides the mean, standard deviation, and average ppm for the relative precision assessment of geoid and quasigeoid, before and after fit, computed using the CUT, UNB and KTH methods. The values are provided for the combination of modification degree and integration radius providing the minimum standard deviation among all combinations for India and four local regions.

Table 5.1.3 provides the minimum, maximum, mean, and standard deviation of the geoid validated with the meridional and prime vertical components of vertical deflections. The values are provided for the combination of modification degree and integration radius providing the minimum standard deviation among all combinations.

Tables 5.1.4 and 5.1.5 provide the results of the absolute and relative precision assessment, respectively, of geoid and quasigeoid, before and after fit, computed using the GEOCOL with RTM.

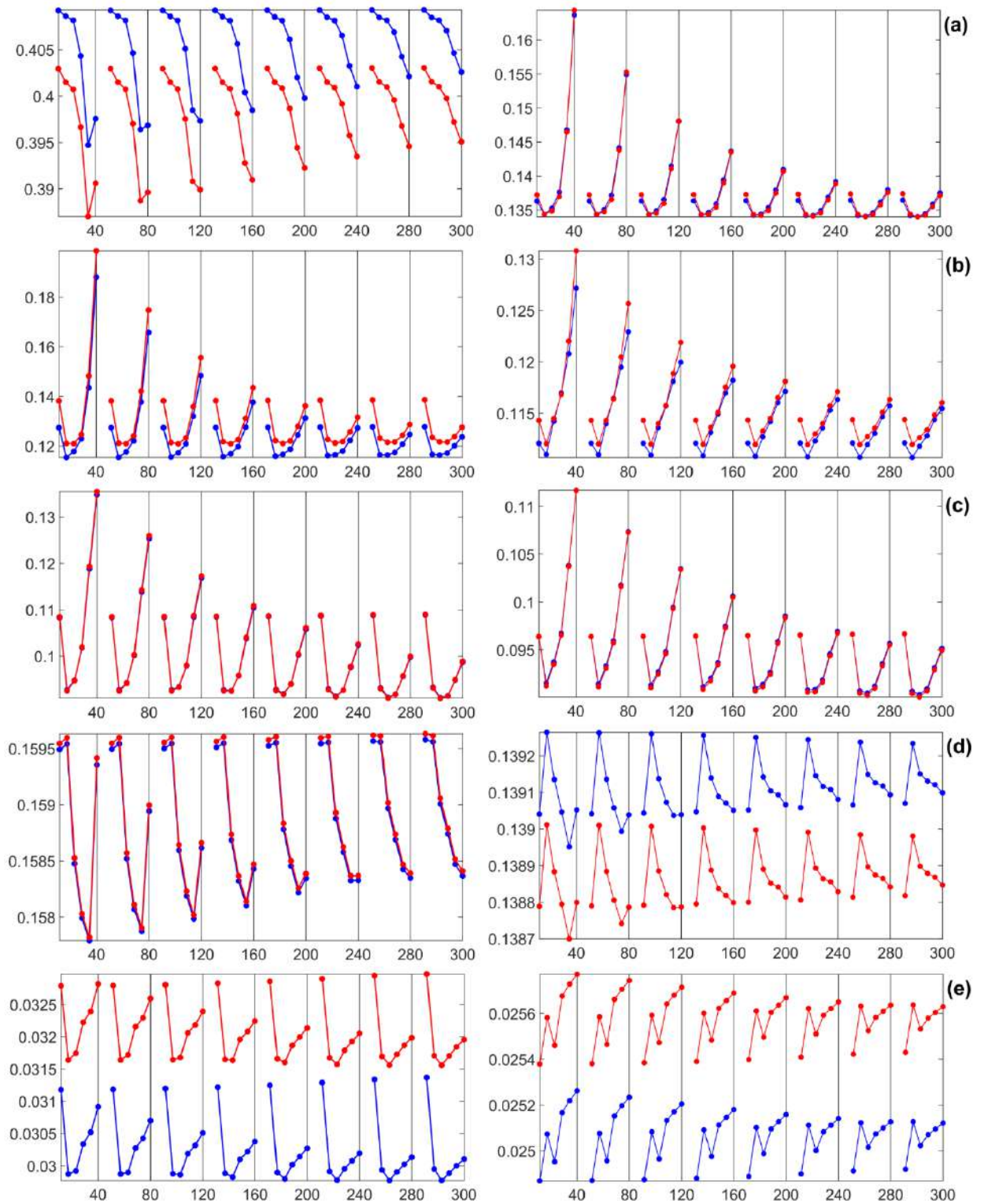


Figure 5.1.2: Standard deviation (in m) from the absolute precision assessment of geoid (blue) and quasigeoid (red) for different M and ψ combinations in the CUT method for a) India, b) UP West, c) UP East, d) Hyderabad, and e) Bangalore. The left column is for before any fitting, and the corresponding right column is for after fitting.

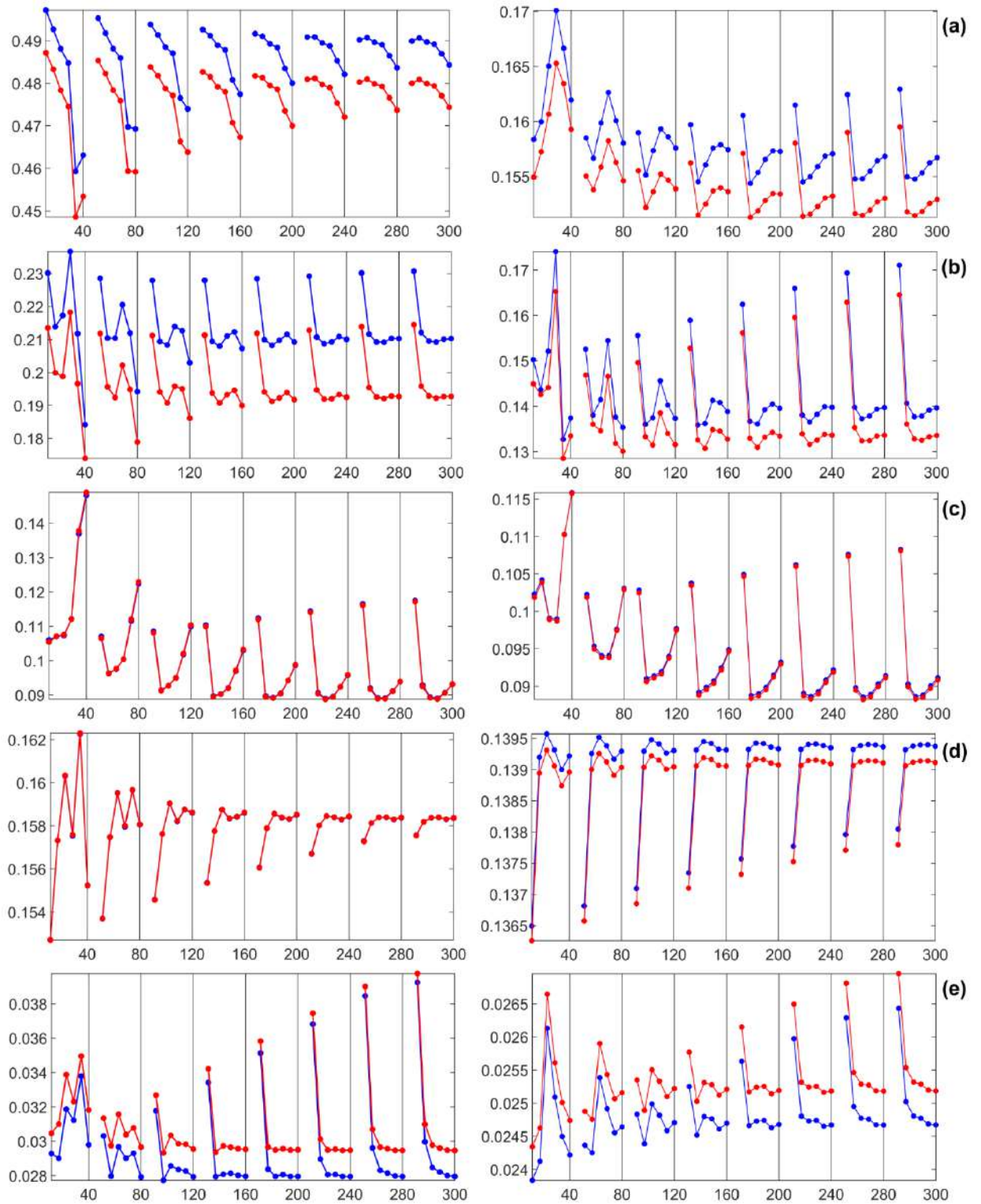


Figure 5.1.3: Standard deviation (in m) from the absolute precision assessment of geoid (blue) and quasigeoid (red) for different M and ψ combinations in the UNB method for a) India, b) UP West, c) UP East, d) Hyderabad, and e) Bangalore. The left column is for before any fitting, and the corresponding right column is for after fitting.

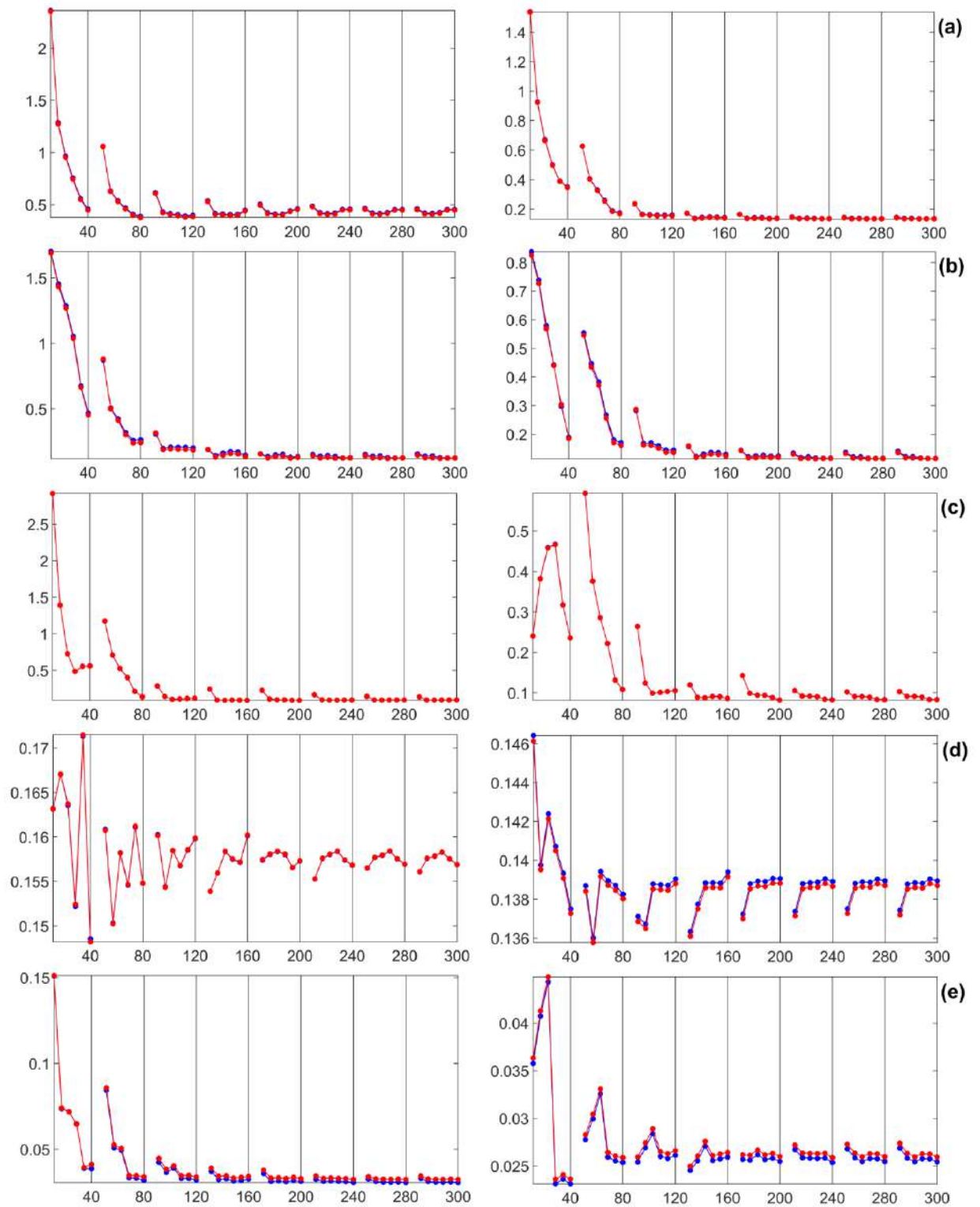


Figure 5.1.4: Standard deviation (in m) from the absolute precision assessment of geoid (blue) and quasigeoid (red) for different M and ψ combinations in the KTH method for a) India, b) UP West, c) UP East, d) Hyderabad, and e) Bangalore. The left column is for before any fitting, and the corresponding right column is for after fitting.

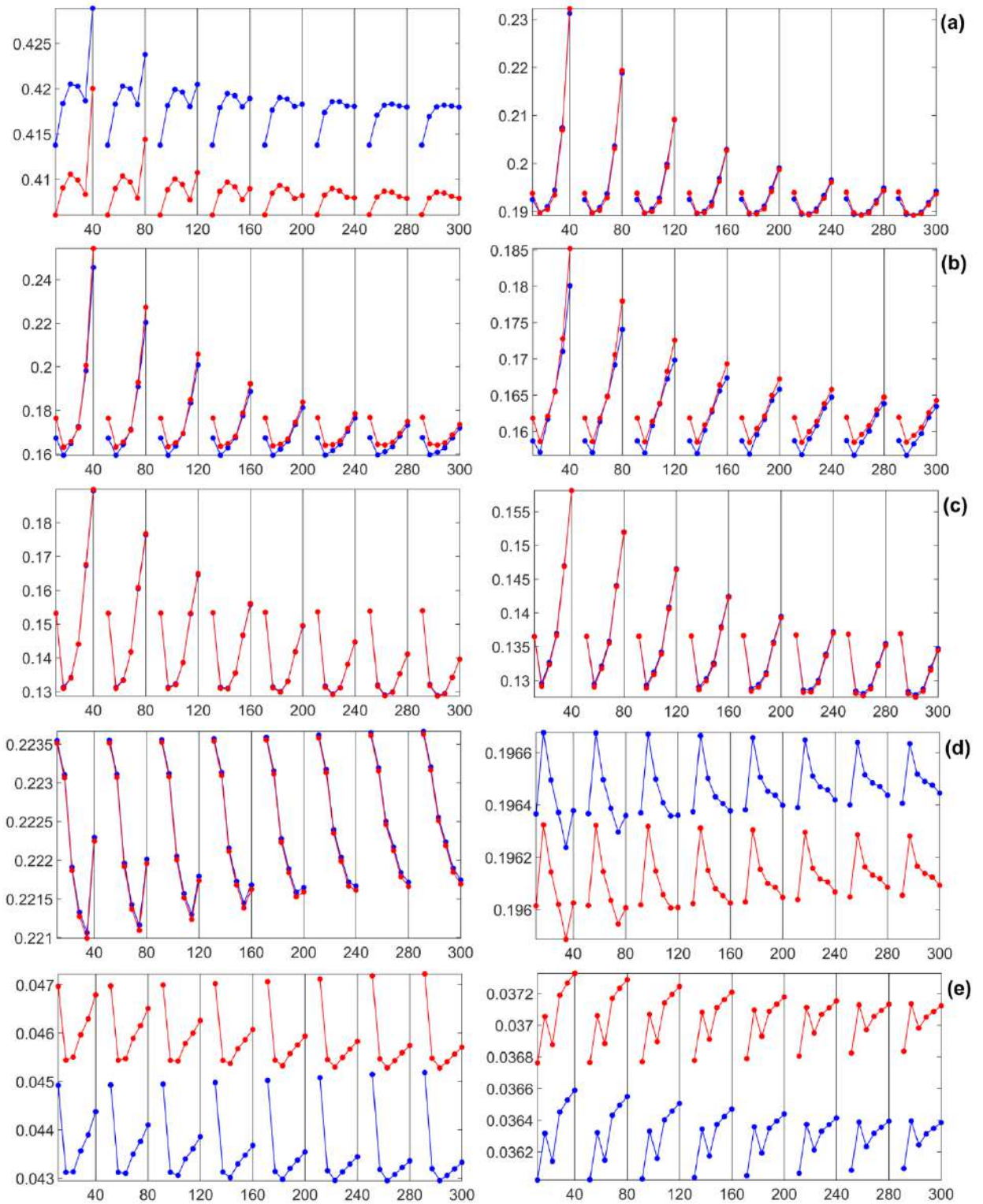


Figure 5.1.5: Standard deviation (in m) from the relative precision assessment of geoid (blue) and quasigeoid (red) for different M and ψ combinations in the CUT method for a) India, b) UP West, c) UP East, d) Hyderabad, and e) Bangalore. The right column is for before any fitting, and the corresponding left column is for after fitting.

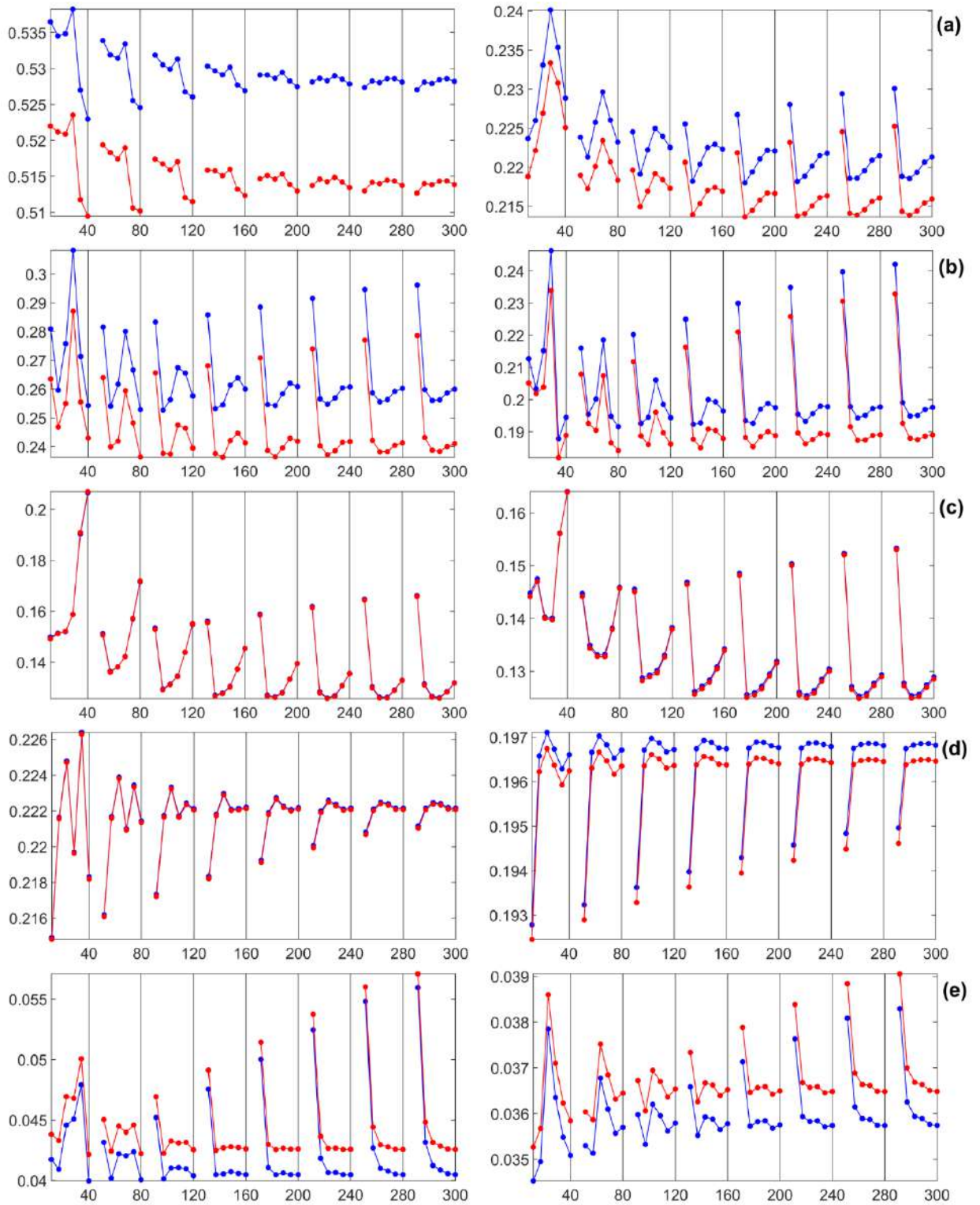


Figure 5.1.6: Standard deviation (in m) from the relative precision assessment of geoid (blue) and quasigeoid (red) for different M and ψ combinations in the UNB method for a) India, b) UP West, c) UP East, d) Hyderabad, and e) Bangalore. The left column is for before any fitting, and the corresponding right column is for after fitting.

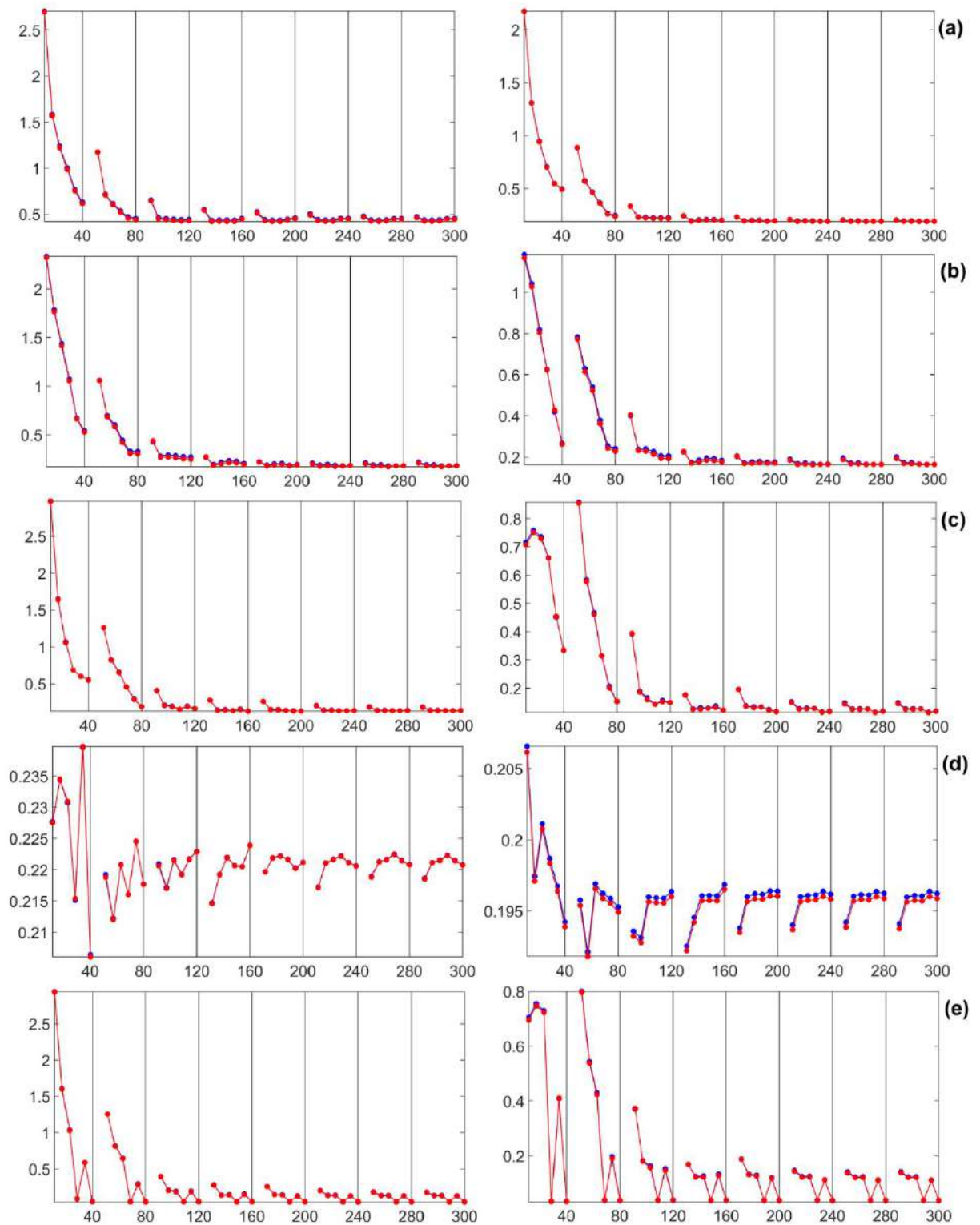


Figure 5.1.7: Standard deviation (in m) from the relative precision of geoid (blue) and quasigeoid (red) for different M and ψ combinations in the KTH method for a) India, b) UP West, c) UP East, d) Hyderabad, and e) Bangalore. The left column is for before any fitting, and the corresponding right column is for after fitting.

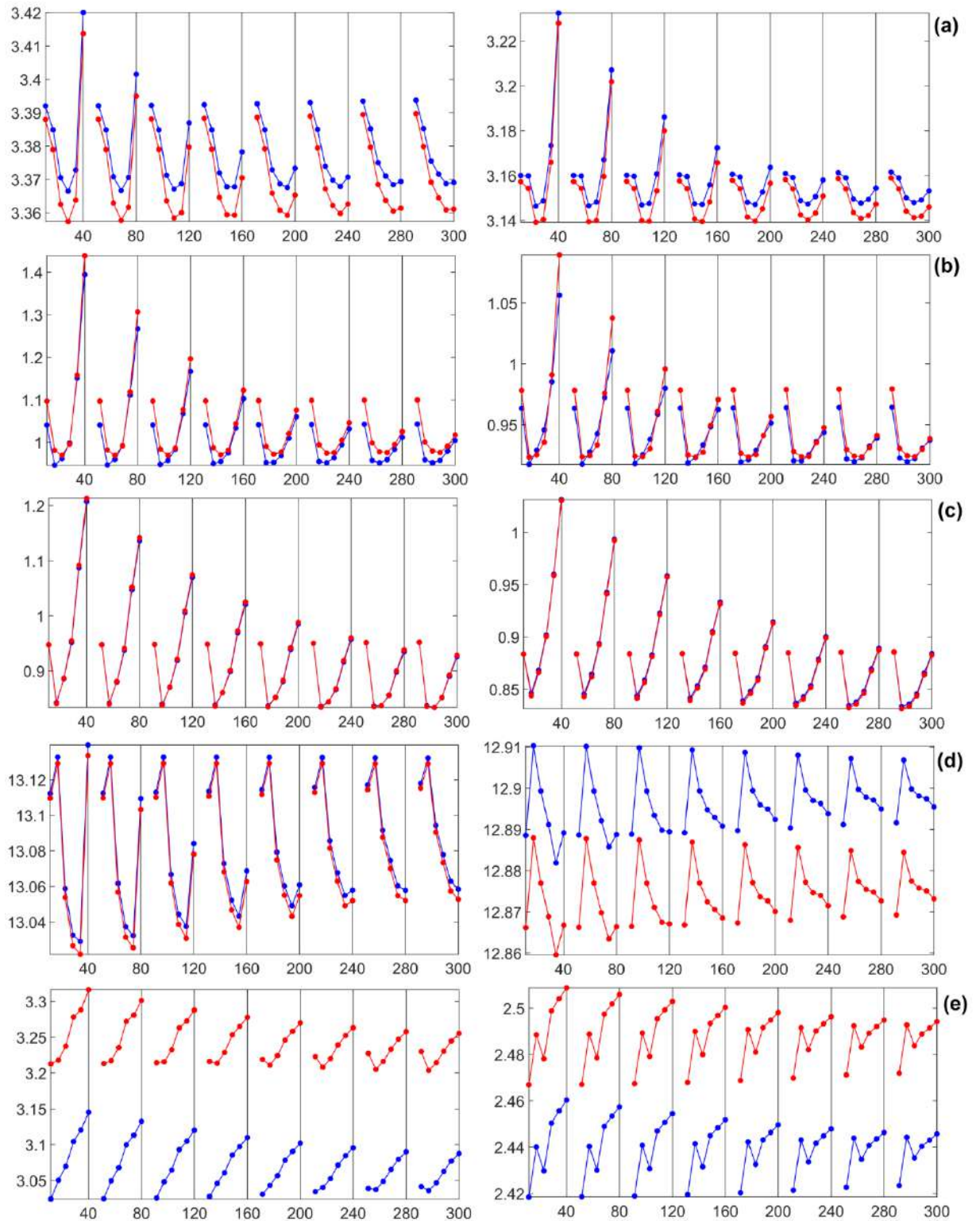


Figure 5.1.8: Average ppm (mm/km) from the relative precision assessment of geoid (blue) and quasigeoid (red) for different M and ψ combinations in the CUT method for a) India, b) UP West, c) UP East, d) Hyderabad, and e) Bangalore. The right column is for before any fitting, and the corresponding left column is for after fitting.

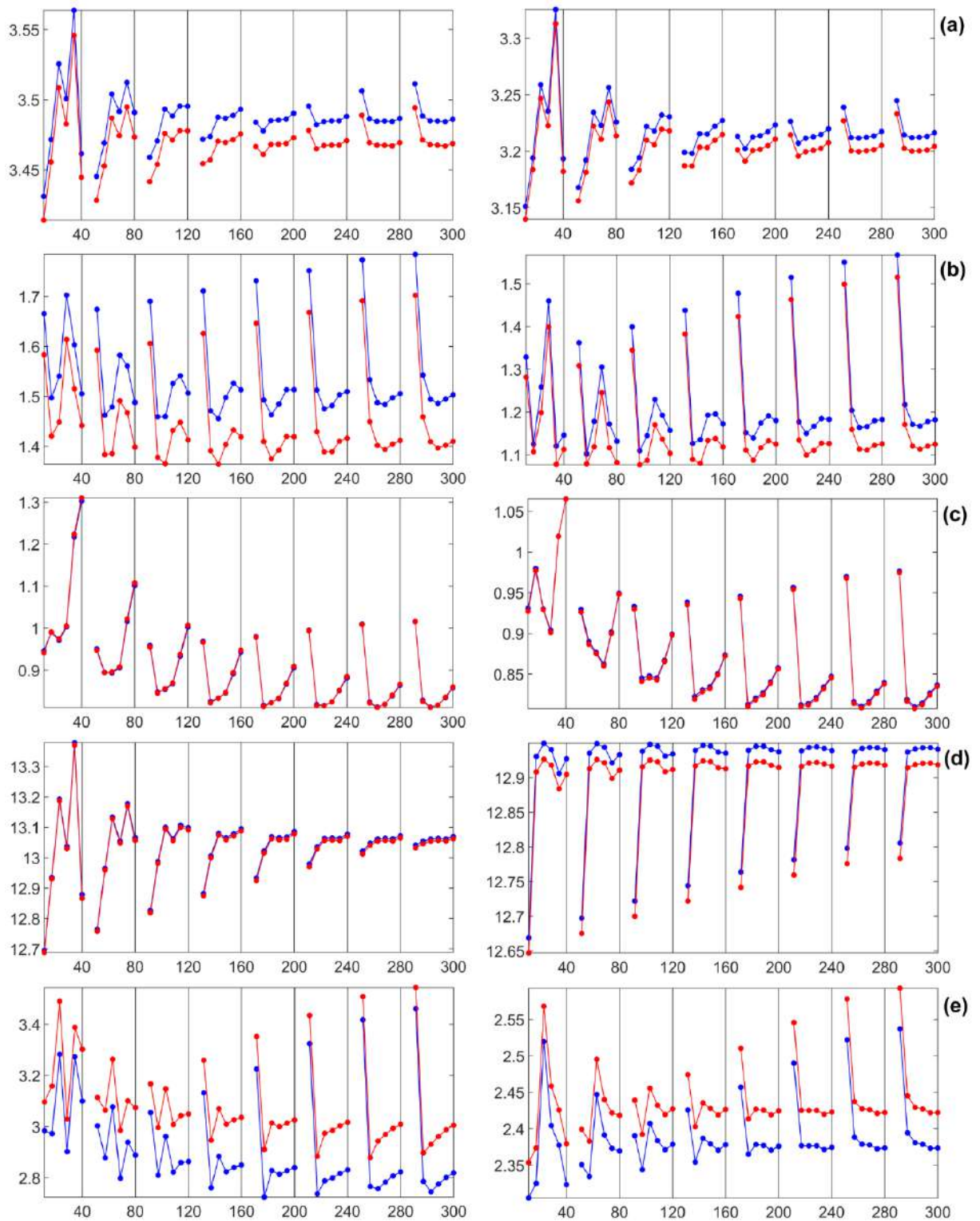


Figure 5.1.9: Average ppm (mm/km) from the relative precision assessment of geoid (blue) and quasigeoid (red) for different M and ψ combinations in the UNB method for a) India, b) UP West, c) UP East, d) Hyderabad, and e) Bangalore. The left column is for before any fitting, and the corresponding right column is for after fitting.

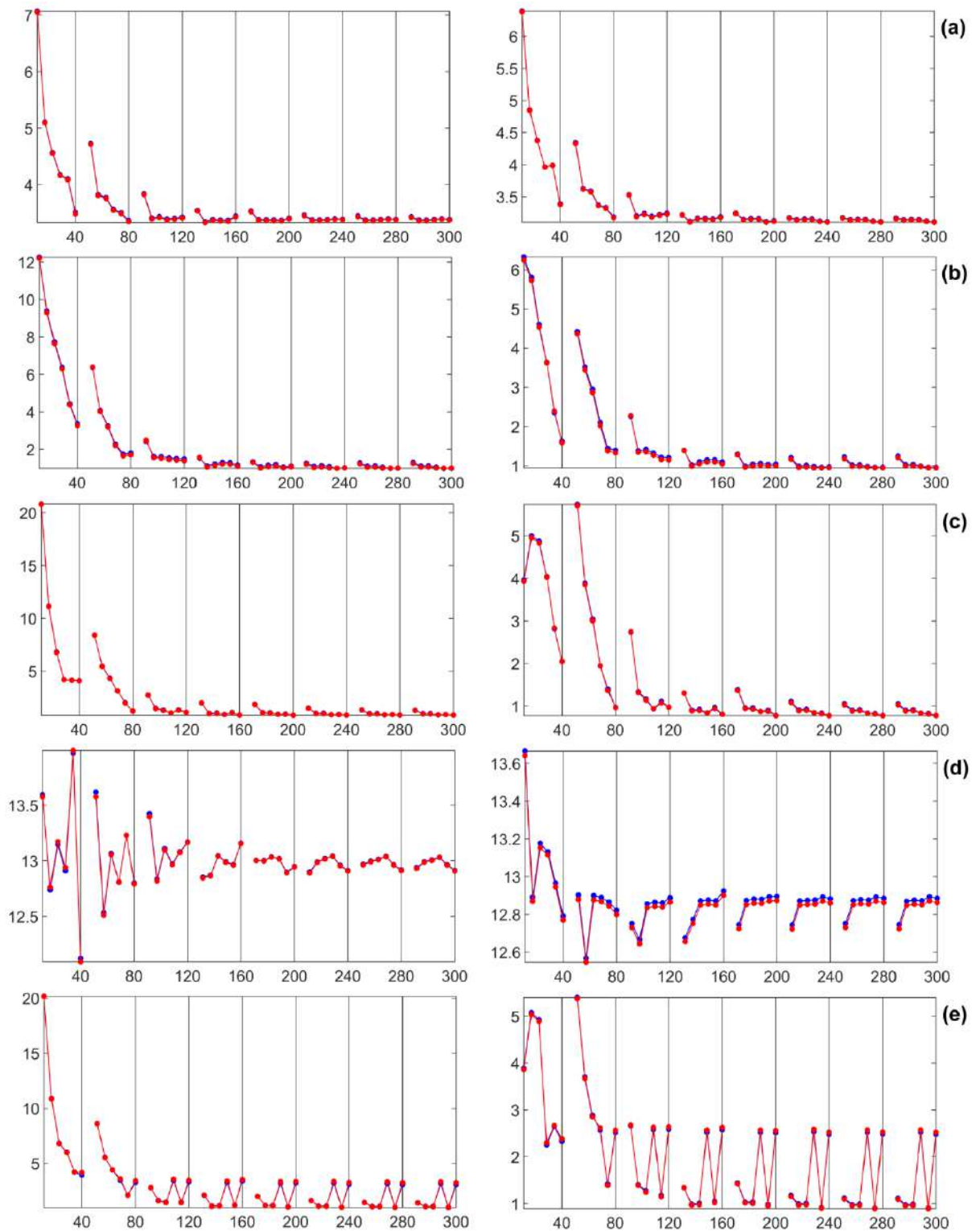


Figure 5.1.10: Average ppm (mm/km) from the relative precision assessment of geoid (blue) and quasigeoid (red) for different M and ψ combinations in the KTH method for a) India, b) UP West, c) UP East, d) Hyderabad, and e) Bangalore. The left column is for before any fitting, and the corresponding right column is for after fitting.

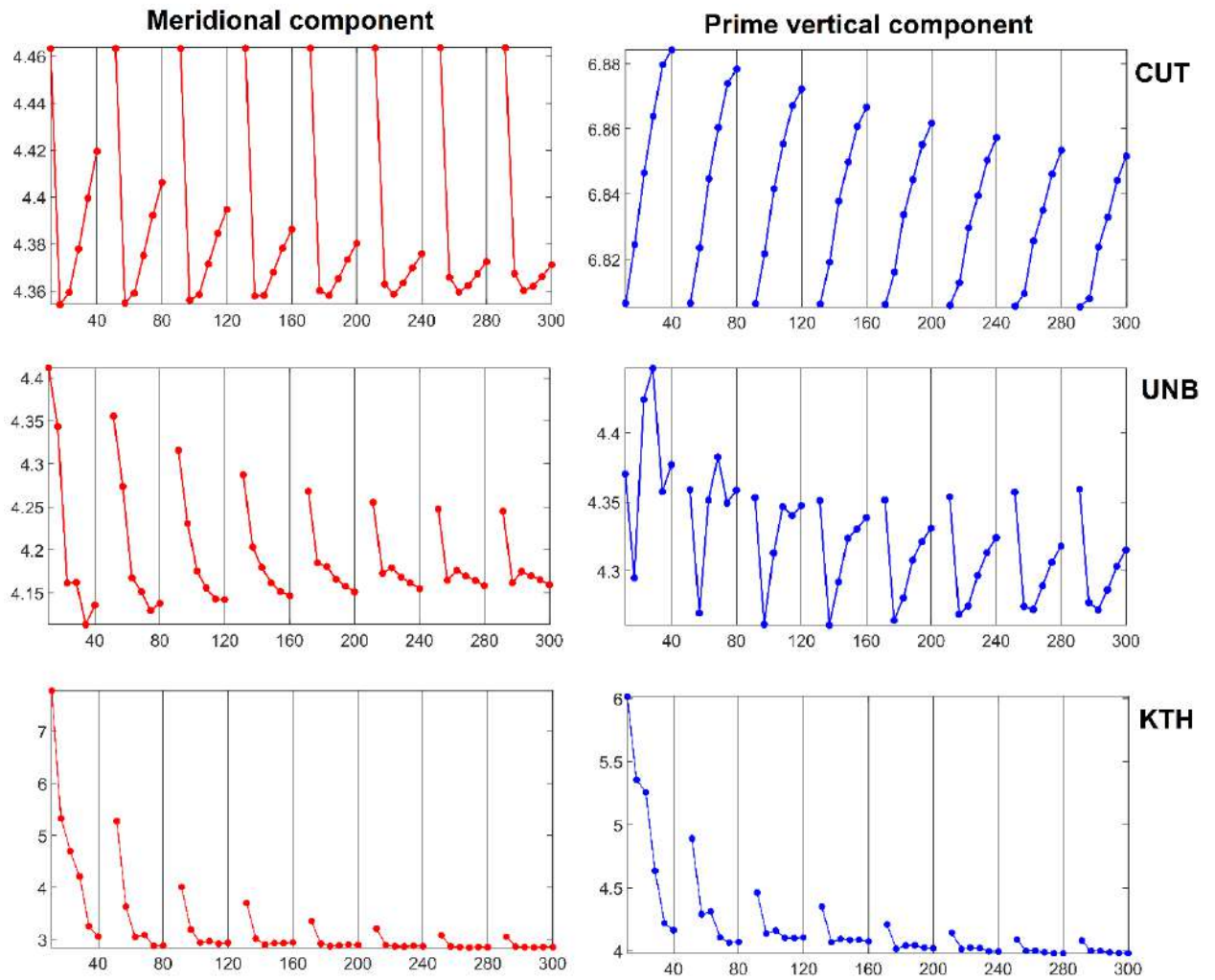


Figure 5.1.11: Standard deviation (in arc-second) for the validation of the geoid models (computed using the three methods) with the meridional (red) and prime vertical (blue) components of the vertical deflections.

Table 5.1.1: Descriptive statistics of absolute precision assessment of gravimetric geoid and quasigeoid models, for India and the four regions, with the three methods for a M and ψ combination that has the least standard deviation. [psi in degrees, min, max, mean and STD in m]

			Geoid					Quasigeoid				
			mod(psi)	min	max	mean	STD	mod(psi)	min	max	mean	STD
India	CUT	no fit	40(1.5)	-0.881	0.783	-0.176	0.395	40(1.5)	-0.890	0.721	-0.191	0.387
		4pfit	300(0.75)	-0.475	0.408	0.000	0.134	300(0.75)	-0.477	0.409	0.000	0.134
	UNB	no fit	40(1.5)	-1.186	0.696	-0.419	0.459	40(1.5)	-1.193	0.635	-0.434	0.449
		4pfit	200(0.5)	-0.509	0.435	0.000	0.154	200(0.5)	-0.506	0.436	0.000	0.151
	KTH	no fit	80(2)	-0.827	0.816	-0.086	0.388	80(2)	-0.836	0.754	-0.100	0.377
		4pfit	300(2)	-0.518	0.433	0.000	0.134	280(1)	-0.463	0.427	0.000	0.133
UP West	CUT	no fit	40(0.5)	-0.981	-0.327	-0.577	0.115	120(0.75)	-0.985	-0.295	-0.578	0.121
		4pfit	300(0.5)	-0.417	0.207	0.000	0.111	240(0.5)	-0.415	0.222	0.000	0.112
	UNB	no fit	40(2)	-1.123	-0.322	-0.723	0.184	40(2)	-1.132	-0.352	-0.739	0.174
		4pfit	40(1.5)	-0.471	0.245	0.000	0.133	40(1.5)	-0.467	0.247	0.000	0.129
	KTH	no fit	300(1.5)	-1.156	-0.460	-0.647	0.126	280(1)	-1.051	-0.375	-0.588	0.121
		4pfit	300(2)	-0.441	0.220	0.000	0.116	240(1)	-0.439	0.215	0.000	0.114
UP East	CUT	no fit	300(0.75)	-0.708	-0.305	-0.470	0.091	300(0.75)	-0.707	-0.306	-0.473	0.091
		4pfit	300(0.75)	-0.220	0.158	0.000	0.090	300(0.75)	-0.219	0.157	0.000	0.090
	UNB	no fit	240(0.75)	-1.074	-0.700	-0.838	0.089	240(0.75)	-1.073	-0.702	-0.840	0.089
		4pfit	280(0.75)	-0.229	0.126	0.000	0.089	280(0.75)	-0.227	0.130	0.000	0.088
	KTH	no fit	160(2)	-0.698	-0.326	-0.466	0.090	160(2)	-0.697	-0.327	-0.468	0.091
		4pfit	200(2)	-0.193	0.128	0.000	0.082	200(2)	-0.192	0.127	0.000	0.082
Hyderabad	CUT	no fit	80(1.5)	-0.385	0.501	0.070	0.158	80(1.5)	-0.400	0.488	0.057	0.158
		4pfit	80(1.5)	-0.369	0.408	0.000	0.139	80(1.5)	-0.368	0.407	0.000	0.139
	UNB	no fit	40(0.2)	-0.438	0.427	-0.004	0.153	40(0.2)	-0.453	0.414	-0.017	0.153
		4pfit	40(0.2)	-0.359	0.402	0.000	0.136	40(0.2)	-0.358	0.401	0.000	0.136
	KTH	no fit	40(2)	-0.350	0.522	0.034	0.149	40(2)	-0.365	0.509	0.021	0.148
		4pfit	80(0.5)	-0.362	0.410	0.000	0.136	80(0.5)	-0.361	0.409	0.000	0.136
Bangalore	CUT	no fit	280(0.75)	0.727	0.810	0.769	0.030	300(0.75)	0.662	0.748	0.707	0.032
		4pfit	40(0.2)	-0.023	0.047	0.000	0.025	40(0.2)	-0.023	0.048	0.000	0.025
	UNB	no fit	120(0.5)	0.687	0.769	0.726	0.028	120(0.5)	0.622	0.708	0.665	0.029
		4pfit	40(0.2)	-0.022	0.045	0.000	0.024	40(0.2)	-0.022	0.046	0.000	0.024
	KTH	no fit	300(2)	0.724	0.811	0.764	0.031	300(2)	0.659	0.749	0.704	0.032
		4pfit	40(2)	-0.022	0.042	0.000	0.023	40(1)	-0.023	0.044	0.000	0.024

Table 5.1.2: Descriptive statistics of relative precision assessment of gravimetric geoid and quasigeoid models, for India and the four regions, with the three methods for a M and ψ combination that has the least standard deviation. [psi in degrees; mean, STD in m; mean ppm in mm/km]

			Geoid				Quasigeoid			
			mod(psi)	mean	STD	ppm	mod(psi)	mean	STD	ppm
India	CUT	no fit	40(0.2)	0.405	0.414	3.392	40(0.2)	0.400	0.406	3.388
		4pfit	300(0.75)	-0.011	0.189	3.150	300(0.75)	-0.011	0.189	3.144
	UNB	no fit	40(2)	0.394	0.523	3.462	40(2)	0.389	0.509	3.447
		4pfit	200(0.5)	-0.012	0.218	3.202	200(0.5)	-0.012	0.214	3.191
	KTH	no fit	160(0.5)	0.399	0.431	3.346	160(0.5)	0.395	0.419	3.332
		4pfit	300(2)	-0.009	0.190	3.107	280(1)	-0.010	0.188	3.138
UP West	CUT	no fit	160(0.5)	0.037	0.159	0.950	40(0.5)	0.052	0.163	0.981
		4pfit	300(0.5)	0.001	0.157	0.923	240(0.5)	0.001	0.159	0.928
	UNB	no fit	120(0.5)	-0.155	0.253	1.459	160(0.75)	-0.131	0.236	1.364
		4pfit	40(1.5)	0.004	0.188	1.121	40(1.5)	0.004	0.182	1.078
	KTH	no fit	280(1)	-0.043	0.177	1.044	280(1)	-0.026	0.170	0.988
		4pfit	300(2)	0.002	0.164	0.954	240(1)	0.003	0.162	0.939
UP East	CUT	no fit	300(0.75)	0.001	0.129	0.834	300(0.75)	0.004	0.129	0.834
		4pfit	300(0.75)	-0.003	0.128	0.835	300(0.75)	-0.003	0.128	0.834
	UNB	no fit	240(0.75)	0.000	0.126	0.816	240(0.75)	0.003	0.126	0.815
		4pfit	280(0.75)	-0.005	0.125	0.810	280(0.75)	-0.004	0.125	0.808
	KTH	no fit	160(2)	0.023	0.126	0.832	160(2)	0.027	0.126	0.835
		4pfit	300(1.5)	-0.004	0.114	0.823	300(1.5)	-0.004	0.114	0.811
Hyderabad	CUT	no fit	40(1.5)	-0.031	0.221	13.029	40(1.5)	-0.032	0.221	13.022
		4pfit	40(1.5)	0.011	0.196	12.882	40(1.5)	0.011	0.196	12.860
	UNB	no fit	40(0.2)	-0.022	0.215	12.827	40(0.2)	-0.023	0.215	12.688
		4pfit	40(0.2)	0.011	0.193	12.669	40(0.2)	0.011	0.192	12.647
	KTH	no fit	40(2)	0.040	0.206	12.122	40(2)	0.039	0.206	12.091
		4pfit	80(0.5)	0.010	0.192	12.567	80(0.5)	0.010	0.192	12.546
Bangalore	CUT	no fit	280(0.75)	-0.004	0.043	3.049	300(0.75)	-0.006	0.045	3.215
		4pfit	40(0.2)	-0.001	0.036	2.418	40(0.2)	-0.001	0.037	2.467
	UNB	no fit	40(2)	-0.016	0.040	3.100	40(2)	-0.018	0.042	3.303
		4pfit	40(0.2)	-0.001	0.035	2.305	40(0.2)	-0.001	0.035	2.354
	KTH	no fit	40(1.5)	-0.006	0.044	3.054	300(2)	-0.008	0.046	3.236
		4pfit	40(2)	-0.001	0.033	2.336	40(1)	-0.001	0.034	2.303

Table 5.1.3: Descriptive statistics of validation of gravimetric geoid models, with deflection of the vertical's components, for a M, ψ combination that has the least standard deviation. [psi in degrees, min, max, mean and STD in arc-second]

	Meridional					Prime vertical				
	mod(psi)	min	max	mean	STD	mod(psi)	min	max	mean	STD
CUT	40(0.5)	-38.230	31.270	-0.675	4.354	300 (0.2)	-75.869	35.542	-2.163	6.805
UNB	40(1.5)	-28.231	67.084	-0.338	4.113	160(0.5)	-41.783	17.996	0.200	4.261
KTH	280(1)	-25.576	32.096	-0.308	2.848	280(2)	-41.717	10.258	0.123	3.981

Table 5.1.4: Descriptive statistics of GNSS/levelling-based absolute precision assessment of the geoid and quasigeoid models calculated using GEOCOL [values in m].

		Geoid (m)				Quasigeoid (m)			
		min	max	mean	STD	min	max	mean	STD
India	no fit	-0.325	0.408	0.006	0.114	-0.340	0.395	-0.007	0.110
	4pfit	-0.325	0.356	0.000	0.103	-0.325	0.356	0.000	0.101
UP West	no fit	-0.253	0.394	0.000	0.109	-0.262	0.282	-0.017	0.093
	4pfit	-0.222	0.286	0.000	0.086	-0.217	0.224	0.000	0.079
UP East	no fit	-0.317	0.211	-0.012	0.112	-0.316	0.211	-0.014	0.113
	4pfit	-0.196	0.155	0.000	0.093	-0.194	0.152	0.000	0.093
Hyderabad	no fit	-0.325	0.408	0.015	0.124	-0.340	0.395	0.001	0.124
	4pfit	-0.325	0.356	0.000	0.122	-0.325	0.356	0.000	0.121
Bangalore	no fit	-0.033	0.063	0.023	0.037	-0.074	0.030	-0.015	0.037
	4pfit	-0.026	0.051	0.000	0.027	-0.026	0.052	0.000	0.028

Table 5.1.5: Descriptive statistics of GNSS/levelling-based relative precision assessment of the geoid and quasigeoid models calculated using GEOCOL [min, max, mean, STD in m and ppm in mm/km].

		Geoid					Quasigeoid				
		min	max	mean	STD	ppm	min	max	mean	STD	ppm
India	no fit	-0.725	0.733	-0.009	0.160	2.607	-0.578	0.682	0.001	0.145	2.640
	4p fit	-0.711	0.735	-0.004	0.155	2.598	-0.573	0.681	0.001	0.143	2.634
UP West	no fit	-0.647	0.418	-0.050	0.146	0.789	-0.545	0.363	-0.032	0.127	0.727
	4p fit	-0.508	0.435	0.003	0.121	0.698	-0.442	0.378	0.003	0.111	0.666
UP East	no fit	-0.456	0.528	0.023	0.158	0.949	-0.452	0.527	0.027	0.157	0.945
	4p fit	-0.306	0.350	-0.001	0.132	0.837	-0.305	0.346	-0.001	0.131	0.832
Hyderabad	no fit	-0.565	0.733	0.014	0.174	11.027	-0.568	0.735	0.013	0.174	11.012
	4p fit	-0.563	0.682	0.005	0.172	11.282	-0.563	0.681	0.004	0.172	11.271
Bangalore	no fit	-0.069	0.095	0.009	0.052	3.711	-0.074	0.104	0.008	0.052	3.764
	4p fit	-0.077	0.076	-0.001	0.039	2.604	-0.076	0.078	-0.001	0.040	2.671

Following are the observations from the above results:

1. From Figures 5.1.2 - 5.1.3, no clear pattern is observed for the increase or decrease of the standard deviation of either geoid or quasigeoid with any method and any region. The FEO and VK kernels are claimed to be unstable (Featherstone, 2001; Li and Wang, 2011) for higher modification degrees and larger integration radius. However, we have not observed any instability in Figures 5.1.2 and 5.1.3, most possibly only because of our lower/restricted choice of parameter sweeps (e.g., McCubbine et al., 2021) and limited dataset for validation.
2. For the CUT and UNB methods, variation in the standard deviation for all the combinations of M and ψ do not exceed ~ 60 mm and ~ 40 mm for the before fit and after fit cases, respectively. The maximum variation is in UP West, followed by UP East. The variation in standard deviation for Hyderabad and Bangalore is within 10 mm. The probable causes can be that UP West and UP East have different landforms, and also, the data points in these regions are distributed over a larger area and more variable terrain. However, for the KTH method, a large variation is observed that reaches beyond 1.5 m for UP West and UP East. This is also reflected in the standard deviation for India with the KTH method. These large variations are mainly observed for lower modification degrees, i.e., $M = 40$ and 80 . The large values can be due to the omission of the medium wavelengths from the geoid/quasigeoid solution using the KTH method because of $L = M = 40$ and 80 , unlike the CUT or the UNB method where $L = 2190$ and 300 , respectively. For $L = M > 80$, the KTH method also provided a range of standard deviation within 10 mm for Hyderabad and Bangalore.
3. For all three methods and all regions, the difference in the standard deviation of the geoid and quasigeoid solutions is less than 20 mm. However, for the UNB and the KTH methods, the variation in the maximum value of the difference between absolute

precision assessment of geoid and quasigeoid reaches 100 mm for UP West, while with the CUT method the maximum variation is never beyond 20 mm. This can be because the CUT method provides a smaller standard deviation of geoid and quasigeoid for UP West as compared to the UNB and the KTH methods. It should be noted that this observation does not show that the CUT method is superior to other methods because it might be due to the use of the highest available degree-order GGM into which, probably, GETECH data might already have been incorporated and hence comparably better results.

4. The standard deviation of the absolute precision assessment in the four regions, individually, is smaller as compared to the standard deviation for India. This indicates a large variation in the mean values of the four regions (Table 5.1.1). The average of the mean values for different combinations of M and ψ in the four regions (UP West, UP East, Hyderabad, and Bangalore) with i) the CUT method are: -570 mm, -480 mm, 100 mm, and 760 mm, respectively; ii) the UNB method: -730 mm, -860 mm, -20 mm, and 710 mm, respectively; iii) the KTH method: -680 mm, -650 m, 100 mm, and 810 mm, respectively. The mean values and the locations of the four regions (Figure 2.2.1) indicate a north-south tilt in the Indian vertical datum.

The variation of the standard deviation of UP East with the CUT and the UNB methods is within 2 mm, but the mean value differs by ~400 mm (also see Figures 5.2.7, 5.2.9 and 5.2.11, later). Also, the standard deviation of Hyderabad for different M and ψ combinations agree within 30 mm for the three methods, but the mean value with the UNB method is -20 mm while with the other two methods is 100 mm. Therefore, comparing the geoid models (or methods) based on only standard deviation may not provide an objective comparison. However, in the present study, we do not have sufficient datapoints to explore other statistical parameters for the methodology

comparison, and therefore, we will unwillingly provide discussions solely around standard deviations.

5. The increasing minimum, maximum, and mean values (Table 5.1.1) while moving from a northern region to the southern region (UP West→UP East→Hyderabad→Bangalore) indicates a north-south tilt (Fischer, 1975; 1977) in the Indian vertical datum. This is probably because IVD1909 was based on constraining the spirit levelling of the nine tide gauges along the Indian coast at zero heights (Burrard, 1910), and for IVD2009 (G&RB, 2019), local geopotential values at eight tide gauges are constrained to the same value. Hence, a tilt in the datum is possible due to the ocean's time-mean dynamic topography (e.g., Featherstone and Filmer, 2012)
6. The plots of standard deviation for the relative precision assessment follows the same pattern as that of standard deviation plots of absolute precision assessment for all the three methods in all the regions, except for i) India with the CUT and the UNB methods, and ii) Bangalore with the KTH method. Also, the standard deviations for relative testing are always larger as compared to absolute testing.
7. The average ppm (mm/km) for India (7021 baselines) varies from 3.37 to 3.42 and 3.43 to 3.56 with the CUT and the UNB methods, respectively, for different M and ψ combinations. For the KTH method with M greater than 80, the average ppm varies from 3.35 to 3.84. The KTH method in all the regions except Hyderabad shows higher average ppm values for $M < 80$ with exceptions of larger integration radius ($\psi > 1^\circ$). A relatively larger difference in the average ppm of geoid and quasigeoid is observed with i) most of the M and ψ combinations in the UNB method for Bangalore (~0.2), and UP West (~0.1), the CUT method for Bangalore (~0.15) and ii) only a few M and ψ combinations in the KTH method for Bangalore (~0.15). However, the differences

for the average ppm (for both geoid and quasigeoid) in all the three methods (the KTH method with M larger than 80) for all the regions may not be statistically significant for local areas (< 10 km).

8. Table 5.1.1 shows that there is no particular choice of M and ψ combination that provides a minimum standard deviation in all four regions and India. Table 5.1.1 further depicts that the minimum standard deviation before and after fit is achieved with different M and ψ combinations. Based on standard deviation alone, we cannot comment on the use of a lower or higher degree of modification for any method because, for e.g., with the CUT method, combination of $M, \psi = 40, 0.5^\circ$ gives minimum standard deviation in UP West while $M, \psi = 300, 0.75^\circ$ gives minimum standard deviation in UP East. With the available datasets, this is true for geoid and quasigeoid, before and after fit, and for all methods. Therefore, it also backs up our argument of point 4 that the *numerical value* of standard deviation alone should not be the deciding factor of pre-eminence of one method and/or one M and ψ combination over the other.
9. EIGEN-6C4 is used with the CUT method and DIR-RL05 with the UNB and the KTH methods. On comparison of Table 5.1.1 with the validation of EIGEN-6C4 (Tables 2.3.1 - 2.3.3), it is observed that for the CUT method, though the overall mean values are improved for all the regions except Bangalore, an improvement in the standard deviation beyond 10 mm is observed only for UP East. However, the standard deviation of gravimetric geoid in UP West is degraded by 10 mm as compared to the EIGEN-6C4. A degradation in standard deviation of gravimetric geoid is also observed in Featherstone and Sideris (1998) and Forsberg and Featherstone (1998). This was,

and similarly is, attributed to errors in either one, more or all of the terrestrial gravity data, GGMs, and the GNSS/levelling data.

On comparison of Table 5.1.1 with the validation of DIR-RL05 (Tables 2.3.1 - 2.3.3), it is observed that with the UNB and the KTH methods there is an improvement in the mean values of all the regions except for Bangalore and UP East (with the UNB method). Moreover, an improvement in the standard deviation is observed for all the regions except for the whole of India with the UNB method. The improvement in the standard deviation reached more than or equal to 100 mm for UP West and UP East regions with both the methods.

However, it should be noted that though there is more improvement, with respect to GGMs, on the inclusion of the terrestrial gravity data in the UNB and the KTH methods as compared to the CUT method, the standard deviations with the three methods are almost equivalent except for the whole of India and UP West with the UNB method.

Therefore, no method can be suggested as more preferred because each of the three methods has provided the least standard deviation (numerically and may not be statistically) at least in one of the regions, e.g., the CUT method in UP West, the UNB method in UP East and Bangalore, and the KTH method in Hyderabad. Moreover, a M and ψ combination providing the least standard deviation does not necessarily have the least mean value. For example, $M, \psi = 40, 1.5^\circ$ in the UNB method for India gives the least standard deviation of 459 mm and a mean value of -419 mm, but the least mean value for India with the UNB method is achieved for a combination of $M, \psi = 40, 0.5^\circ$ with the values being: standard deviation = 493 mm and mean value = -315 mm.

10. The standard deviation is minimally smaller (~ 10 mm) for quasigeoid compared to geoid for India. However, for all four regions individually, the standard deviation is smaller or equal for geoid compared to quasigeoid with a maximum difference of ~ 10 mm for UP West with the UNB method. The larger standard deviation of geoid for India can be attributable to the larger mean of geoid compared to quasigeoid for Bangalore (difference ~ 60 mm) and Hyderabad (difference ~ 10 mm) regions.
11. Similar to Table 5.1.1, there is no clear indication about the choice of the M and ψ combination from Table 5.1.2 because the three methods provide the least standard deviation for different M and ψ combinations for different regions. Also, the difference between ppm of geoid and quasigeoid for all the regions and India are within ± 0.2 mm/km for all the methods, before and after fit.
12. From Table 5.1.2, there is an improvement of less than 100 mm in standard deviation for all the four regions after fitting as compared to without any fitting. However, there is an improvement of ~ 300 mm in standard deviation for India, with all three methods, for geoid and quasigeoid both. This indicates that after fitting, there is more improvement for inter-region baselines as compared to intra-region baselines. The larger average ppm (mm/km) values for India (~ 3.4) are attributable to the larger values of ppm for baselines in Bangalore (~ 3) and significantly larger values for baselines in Hyderabad (~ 12.7). These are further attributable to the relatively smaller baseline lengths in the two regions ([0.61 km, 46.75 km] for Hyderabad and [4.80 km, 25.16 km] for Bangalore). For our tests, the standard deviation always reduced after fitting. However, for the KTH method with $M \leq 80$ and any ψ , though there is a reduction in standard deviation, the average ppm value increased. Therefore, it can be said that a reduction in standard deviation need not always indicate a reduction in the average ppm value.

13. The KTH method with larger modification degree and integration radius provides better results (minimum standard deviation) as compared to the UNB and the CUT methods on validation with the vertical deflections. However, similar to the GNSS/levelling-based validation, the KTH method has not provided better results on validation with vertical deflections for smaller modification degrees ($M \leq 80$). Though the CUT method provides comparable descriptive statistical values for the meridional component, the mean and standard deviation for the prime vertical are $\sim 2''$ larger than the other two methods. Also, the minimum and maximum values of prime vertical validation are almost 2 times larger with the CUT method. Though, maximum, mean and standard deviation of the meridional component-based validation of the geoid model with the UNB method are comparable with the other methods, the maximum value ($67.1''$) is larger than double as compared to the CUT ($31.3''$) and the KTH ($32.1''$) methods.
14. GRAVSOFIT with GEOCOL and RTM have the limitation of using large data set especially due to involved inversion of matrix with a dimension equal to the number of data points. Therefore, GEOCOL is generally used with sparse gravity data or block-wise over smaller areas (with overlap between blocks) else, thinning of the gravity data is required. Hence, it can be interpreted that the use of coarse gravity and DEM grids in previous geoid modelling studies in India (Table 1.3.1) is possibly because GRAVSOFIT has a limitation of using large matrices. Moreover, from Tables 5.1.4 and 5.1.5, no tilt in the datum is observed, which is in contrast with the results of other three methods (CUT, UNB, KTH; Table 5.1.1). This is because LSC removes the trends a-priori to make the residual field stationary in the stochastic sense (Moritz, 1980; Darbeheshti, 2009).

The descriptive statistic values in Table 5.1.4 are comparable with previous studies over regions of India using LSC (Table 1.3.1) except for the Dehradun region (lies in UP West) in Mishra and Ghosh (2016). However, results of UP West are comparable to other studies in and around same region (Singh, 2007; Singh and Srivastava, 2018) using GRAVSOFIT but with FFT subroutines and Stokes's integration. The results are thus reassuring that the previous studies (and their limitations) over Indian regions are realistic. The difference in the results of previous studies and our GEOCOL experiment are due to one, more or all of the different GGMs, use of gravity anomaly data grids or points, different DEM, resolution of computation (i.e., grid size of final geoid/quasigeoid model) and most importantly different gravity database.

15. It is observed that GEOCOL does not apply the full zero -degree term (Eq. (3.6.5)), instead it uses only the first term (Eq. (3.6.4)). In the LSC solutions (only) we have also not applied the full zero-degree term because the main motive of using LSC was to assess the calculations of previous studies and none of those studies mentioned using the zero-degree term. Moreover, comparable results with respect to the previous studies have been obtained without addition of the second term of Eq. (3.6.5) in the LSC solutions. Though the second term in Eq. (3.6.5) is constant ($= -0.76$ m for W_0 of IHR5 and U_0 of GRS80) and can be added to the geoid undulations calculated using the LSC method, it may cause significant differences with respect to the other three methods.

Therefore, the smaller values of minimum, maximum and mean with the LSC solution (Table 5.1.4) as compared to CUT, UNB and KTH methods (Table 5.1.1) are most probably because i) GEOCOL does not use the generalised Bruns's formula, ii) GEOCOL makes use of residual gravity and residual GNSS/levelling datasets to

calculate residual height anomalies, and iii) GEOCOL remove trends a-priori, which can also be seen as 1-parameter fit during the geoid/quasigeoid computation itself.

5.2 Indian gravimetric geoid model

In this section, we provide the final geoid model for India calculated using the three methods. As discussed in the previous section, we do not have a clear indication of the more preferred choice of M and ψ combination for any method. However, we do have a certain idea about the M and ψ combinations for any particular method that should not be used, e.g., $M \leq 80, \forall \psi$ for the KTH method. Therefore, we have chosen to show the gravimetric geoid model for $M, \psi = 300, 1^\circ$ with all three methods, namely, the CUT, the UNB, and the KTH.

The difference between mean absolute error and standard deviation with $M, \psi = 300, 1^\circ$ for India with all the three methods does not exceed 50 mm as compared to their respective M and ψ combination providing the minimum standard deviation (Table 5.1.1). Mean absolute difference and standard deviation for M and ψ combination giving minimum standard deviation versus $M, \psi = 300, 1^\circ$ is, all in mm, $(360 \pm 400$ vs. $370 \pm 410)$, $(510 \pm 460$ vs. $470 \pm 490)$, and $(330 \pm 390$ vs. $380 \pm 420)$ for the CUT, the UNB, and the KTH methods, respectively.

Figures 5.2.1, 5.2.2, and 5.2.3 show the gravimetric geoid models for India calculated using the CUT, the UNB, and the KTH methods, respectively for $M, \psi = 300, 1^\circ$. We have not shown quasigeoid because they are within 50 mm of standard deviation as compared to the geoid model for our chosen M, ψ combination. Moreover, SoI has decided to compute geoid over quasigeoid. The descriptive statistics of the three geoid models are depicted in Table 5.2.1. Figures 5.2.4, 5.2.5, and 5.2.6 show the scatter plots of the relative difference (magnitudes) of the geoid models for the CUT, the UNB, and the

KTH methods, respectively. The curved lines in each figure depict the maximum allowable in-field misclose for Indian high precision (lower curve) and double tertiary (upper curve) levelling for all the 7071 baselines computed using Eq. (5.2.1) with c equal to 3 and 12, respectively.

$$r = c\sqrt{d} \quad (5.2.1)$$

where r = allowable misclose, in mm; c = empirically derived factor for a given ‘type of levelling’; d = distance between stations, in km.

The pixel-wise difference maps for India are shown in Figures 5.2.7, 5.2.9 and 5.2.11 for the pairs of geoid model calculated using i) CUT and UNB, ii) CUT and KTH, and iii) KTH and UNB methods, respectively. The corresponding scatter plots and histograms for the three difference maps are shown in Figures 5.2.8, 5.2.10 and 5.2.12, respectively. The regional geoid models have been computed for UP West, UP East, Hyderabad and Bangalore, individually using GEOCOL with RTM. Figures 5.2.13, 5.2.14, 5.2.15 and 5.2.16 show the regional difference maps of GEOCOL-based geoid models of UP West, UP East, Hyderabad and Bangalore, respectively, with respect to the geoid models calculated using the CUT, UNB and KTH methods.

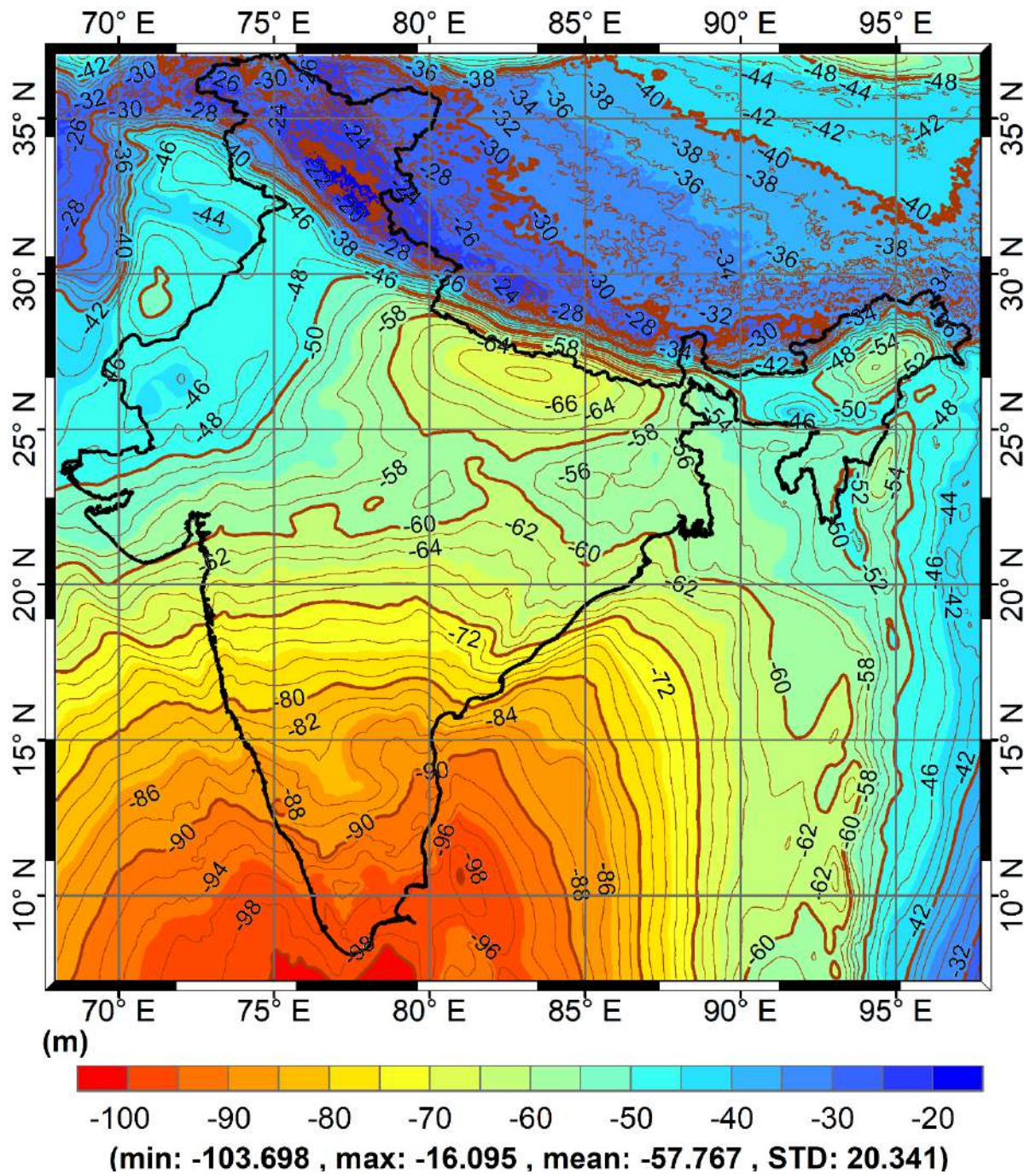


Figure 5.2.1: Indian gravimetric geoid model computed using the CUT method ($M, \psi = 300, 1^\circ$).

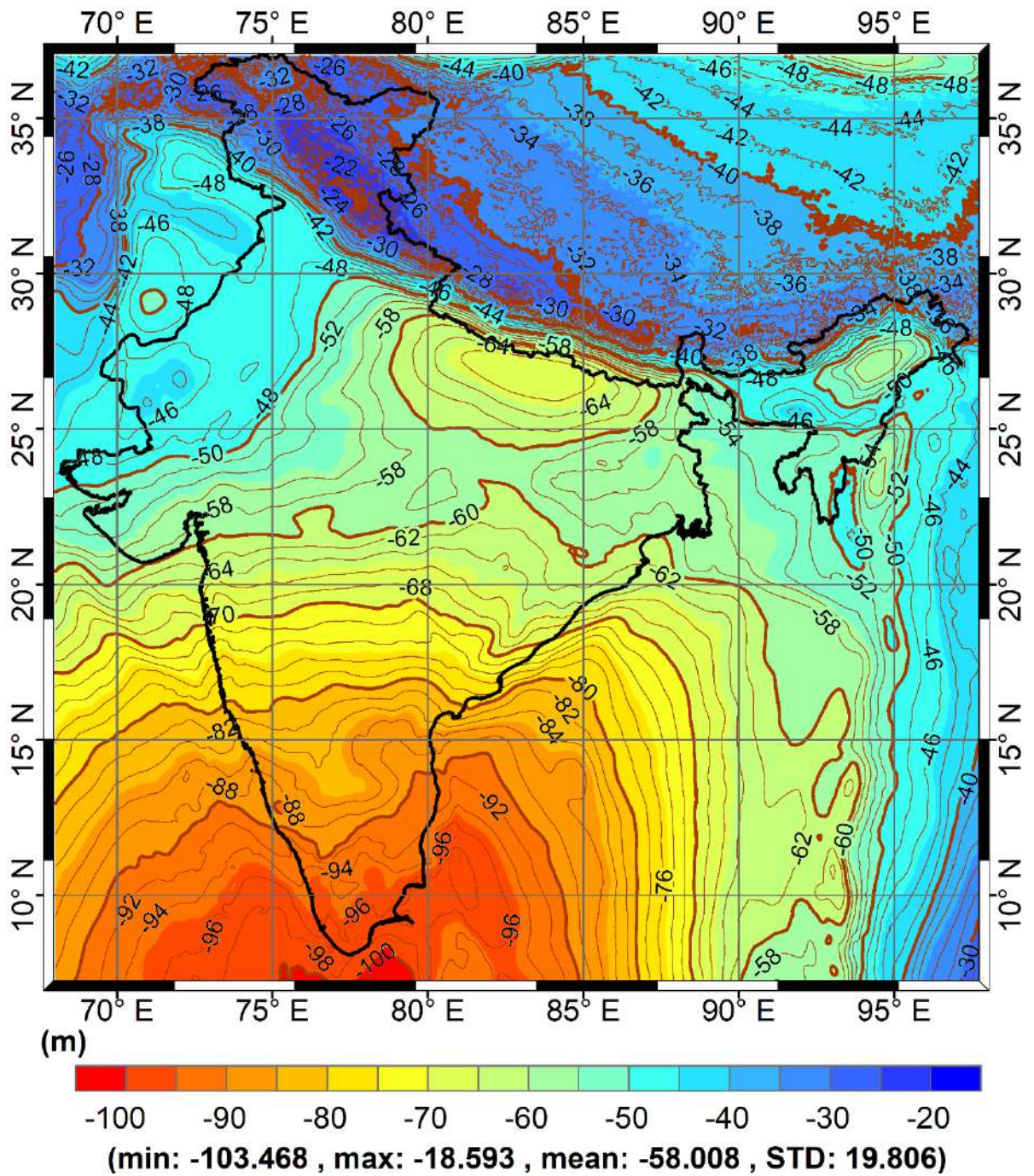


Figure 5.2.2: Indian gravimetric geoid model computed using the UNB method ($M, \psi = 300, 1^\circ$).

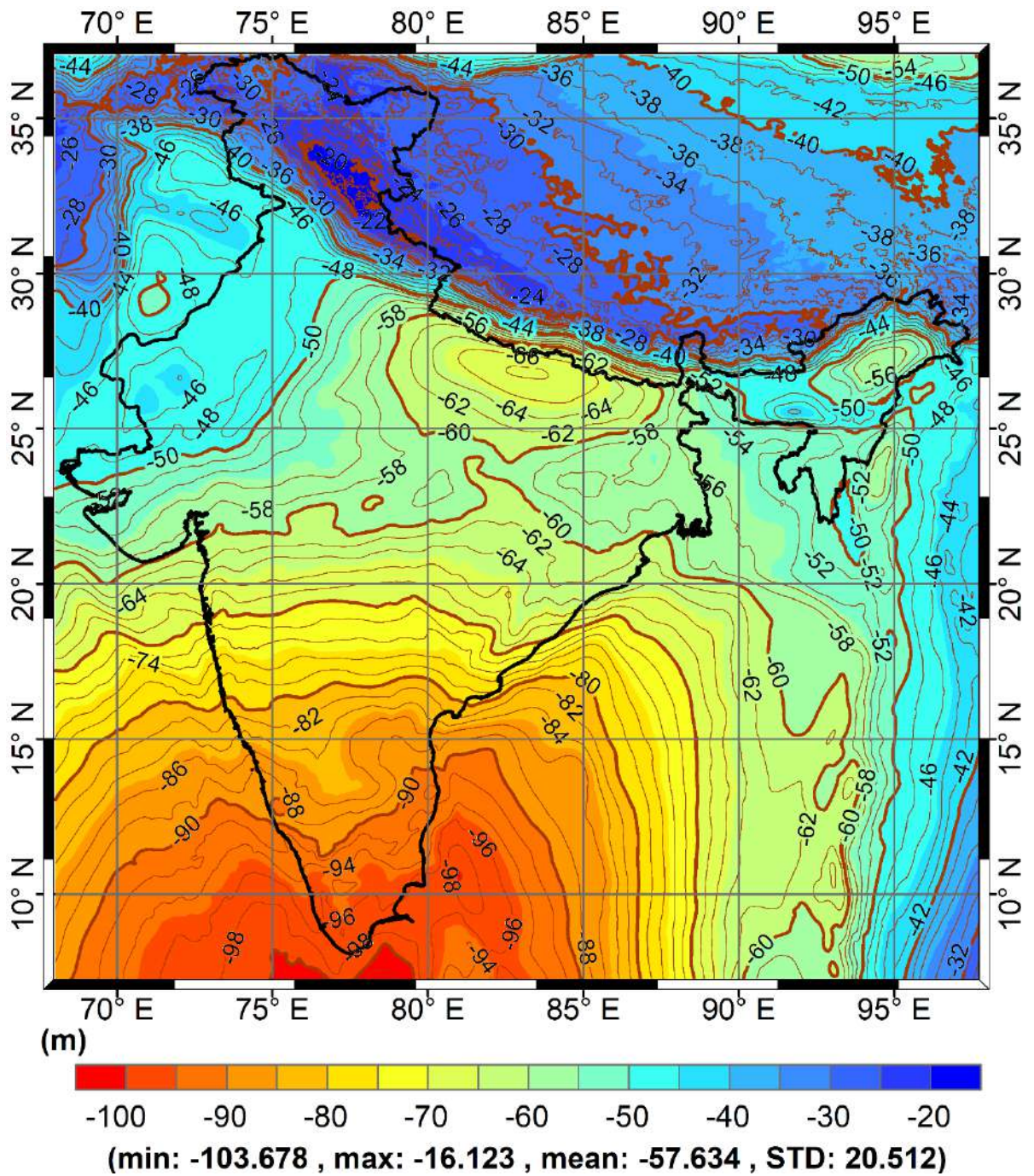


Figure 5.2.3: Indian gravimetric geoid model computed using the KTH method ($M, \psi = 300, 1^\circ$).

Table 5.2.1: Descriptive statistics of absolute precision assessment of gravimetric geoid and quasigeoid models, for India and the four regions, with the CUT, UNB and KTH methods for $M, \psi = 300, 1^\circ$.

			Geoid				Quasigeoid			
			min	max	mean	STD	min	max	mean	STD
India	CUT	no fit	-0.973	0.809	-0.149	0.407	-0.982	0.747	-0.163	0.400
		4pfit	-0.475	0.408	0.000	0.134	-0.477	0.409	0.000	0.134
	UNB	no fit	-1.266	0.769	-0.328	0.489	-1.275	0.707	-0.342	0.479
		4pfit	-0.503	0.434	0.000	0.155	-0.500	0.435	0.000	0.152
	KTH	no fit	-1.050	0.839	-0.140	0.425	-1.059	0.777	-0.154	0.417
		4pfit	-0.464	0.426	0.000	0.135	-0.462	0.427	0.000	0.134
UP West	CUT	no fit	-0.973	-0.293	-0.565	0.117	-0.982	-0.303	-0.581	0.122
		4pfit	-0.434	0.225	0.000	0.113	-0.430	0.237	0.000	0.113
	UNB	no fit	-1.266	-0.280	-0.732	0.209	-1.275	-0.372	-0.748	0.192
		4pfit	-0.483	0.187	0.000	0.138	-0.479	0.184	0.000	0.133
	KTH	no fit	-1.050	-0.368	-0.577	0.128	-1.059	-0.378	-0.593	0.122
		4pfit	-0.431	0.226	0.000	0.117	-0.427	0.238	0.000	0.116
UP East	CUT	no fit	-0.702	-0.311	-0.476	0.091	-0.701	-0.313	-0.478	0.091
		4pfit	-0.226	0.151	0.000	0.091	-0.224	0.150	0.000	0.091
	UNB	no fit	-1.074	-0.702	-0.840	0.089	-1.073	-0.704	-0.842	0.089
		4pfit	-0.229	0.129	0.000	0.089	-0.227	0.131	0.000	0.088
	KTH	no fit	-0.764	-0.326	-0.488	0.096	-0.763	-0.328	-0.490	0.097
		4pfit	-0.232	0.118	0.000	0.090	-0.231	0.117	0.000	0.089
Hyderabad	CUT	no fit	-0.349	0.542	0.110	0.159	-0.364	0.529	0.096	0.159
		4pfit	-0.369	0.408	0.000	0.139	-0.368	0.408	0.000	0.139
	UNB	no fit	-0.457	0.433	-0.002	0.158	-0.473	0.420	-0.016	0.158
		4pfit	-0.370	0.407	0.000	0.139	-0.369	0.406	0.000	0.139
	KTH	no fit	-0.318	0.577	0.137	0.158	-0.333	0.564	0.124	0.158
		4pfit	-0.368	0.407	0.000	0.139	-0.368	0.406	0.000	0.139
Bangalore	CUT	no fit	0.726	0.809	0.768	0.030	0.662	0.747	0.707	0.032
		4pfit	-0.023	0.047	0.000	0.025	-0.023	0.048	0.000	0.026
	UNB	no fit	0.680	0.769	0.720	0.028	0.616	0.707	0.659	0.030
		4pfit	-0.023	0.047	0.000	0.025	-0.023	0.047	0.000	0.025
	KTH	no fit	0.751	0.839	0.794	0.031	0.687	0.777	0.733	0.033
		4pfit	-0.025	0.048	0.000	0.026	-0.024	0.049	0.000	0.026

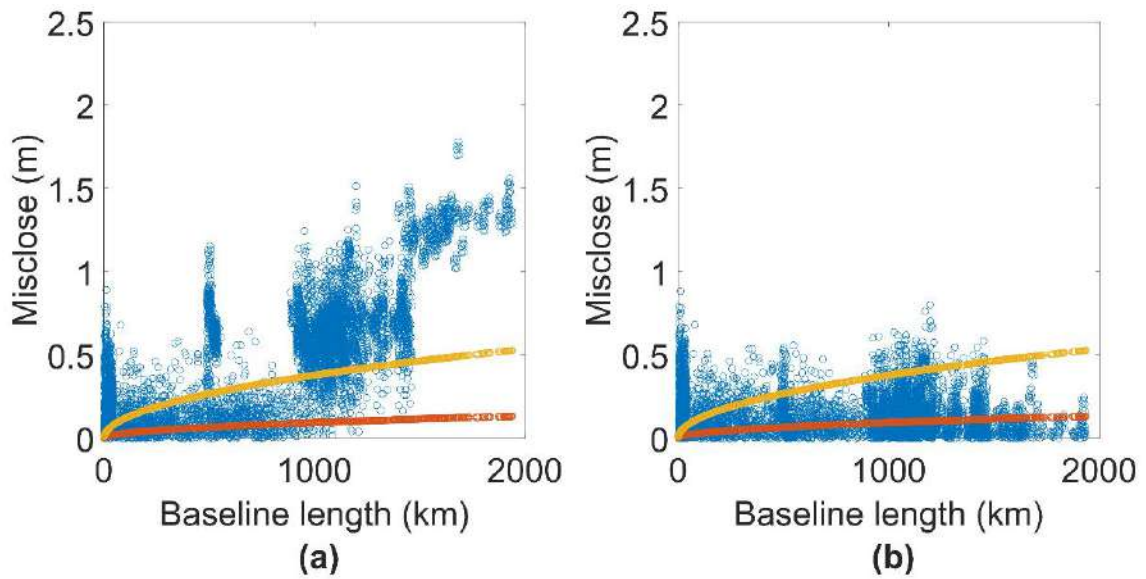


Figure 5.2.4: Magnitude of relative differences (blue circles) for the a. geoid (no fit) and b. geoid (4P fitting), with the CUT method ($M, \psi = 300, 1^\circ$), over 7021 GNSS-levelling baselines. Orange and yellow circles represent the maximum permissible in-field misclose for Indian high-precision ($c = 3$) and double tertiary ($c = 12$) levelling for each baseline, respectively.

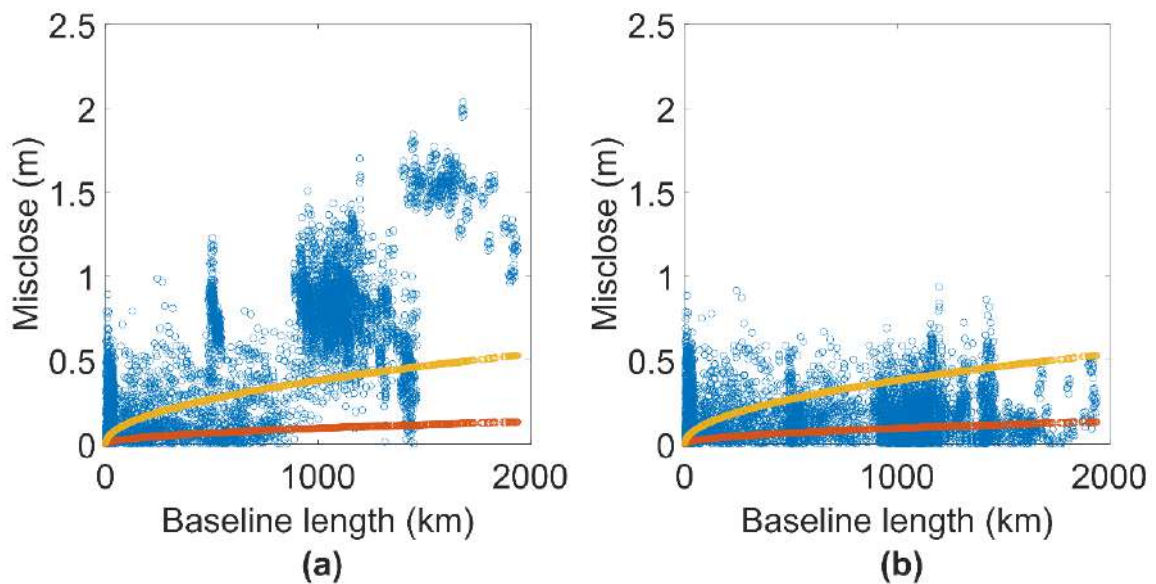


Figure 5.2.5: Magnitude of relative differences (blue circles) for the a. geoid (no fit) and b. geoid (4P fitting), with the UNB method ($M, \psi = 300, 1^\circ$), over 7021 GNSS-levelling baselines. Orange and yellow circles represent the maximum permissible in-field misclose for Indian high-precision ($c = 3$) and double tertiary ($c = 12$) levelling for each baseline, respectively.

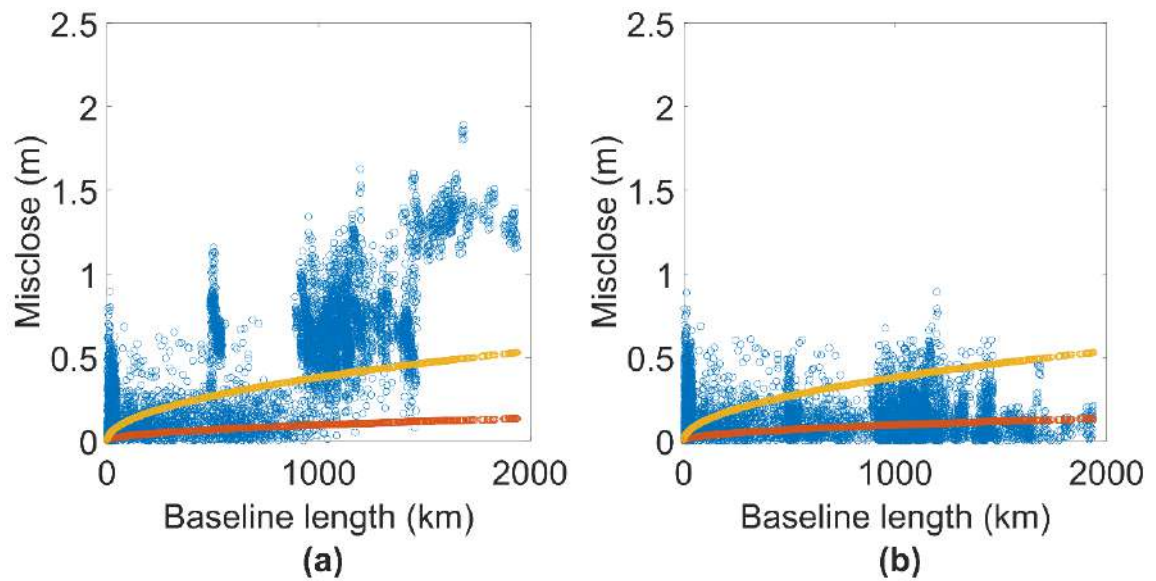


Figure 5.2.6: Magnitude of relative differences (blue circles) for the a. geoid (no fit) and b. geoid (4P fitting), with the KTH method ($M, \psi = 300, 1^\circ$), over 7021 GNSS-levelling baselines. Orange and yellow circles represent the maximum permissible in-field misclose for Indian high-precision ($c = 3$) and double tertiary ($c = 12$) levelling for each baseline, respectively.

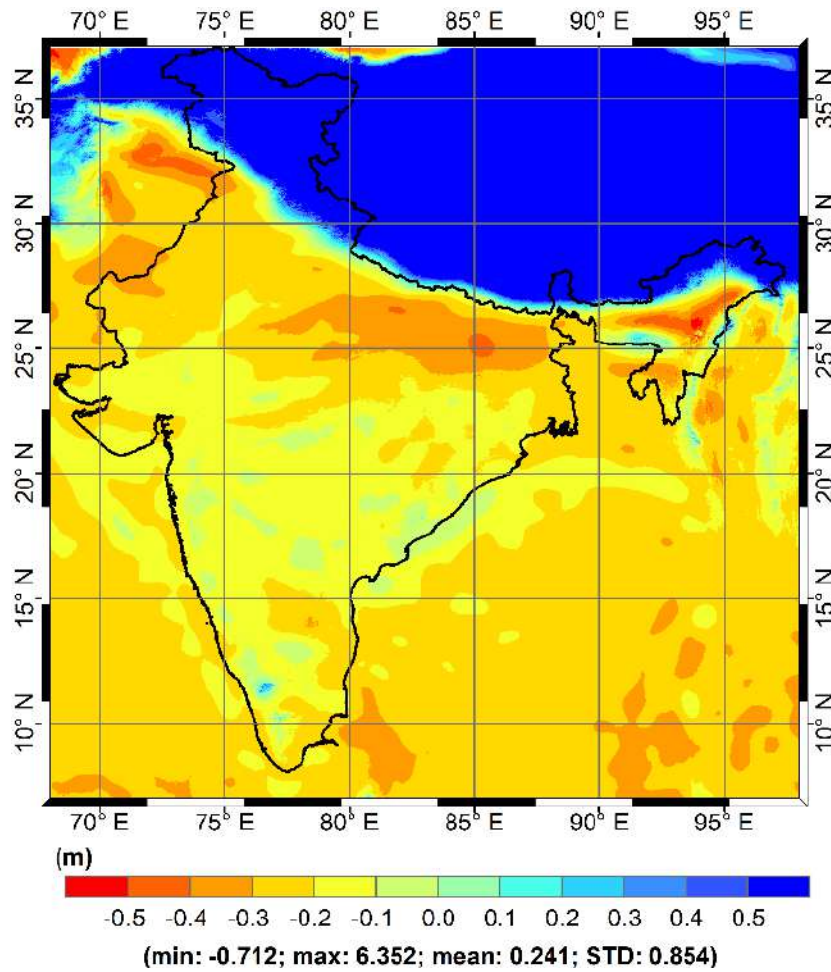


Figure 5.2.7: Difference between gravimetric geoid undulations computed using the CUT and the UNB methods ($M, \psi = 300, 1^\circ$).

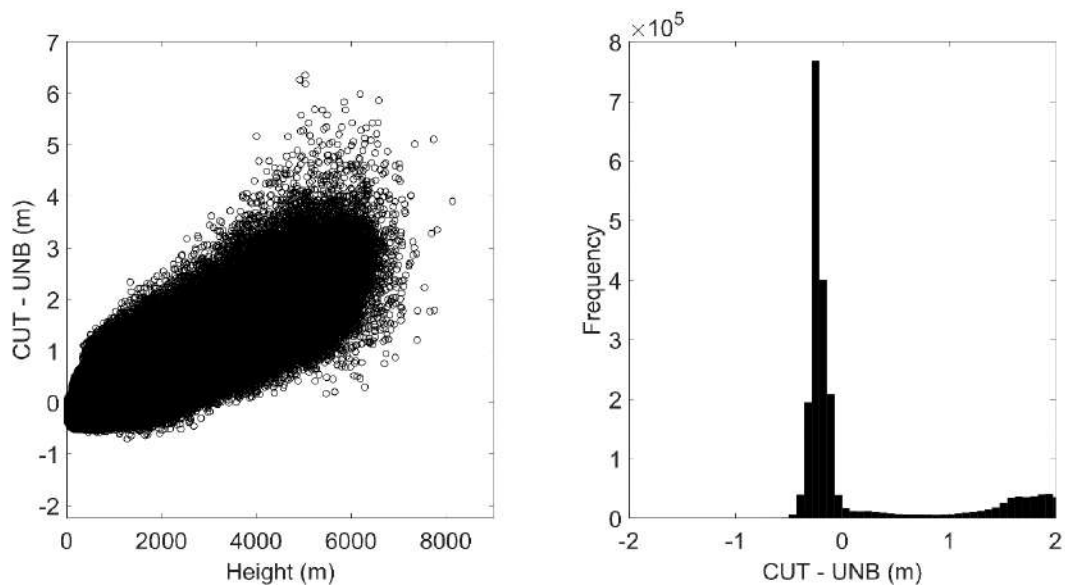


Figure 5.2.8: Scatter plot (a) and histogram (b) of the differences between gravimetric geoid undulations computed using the CUT and the UNB methods ($M, \psi = 300, 1^\circ$).

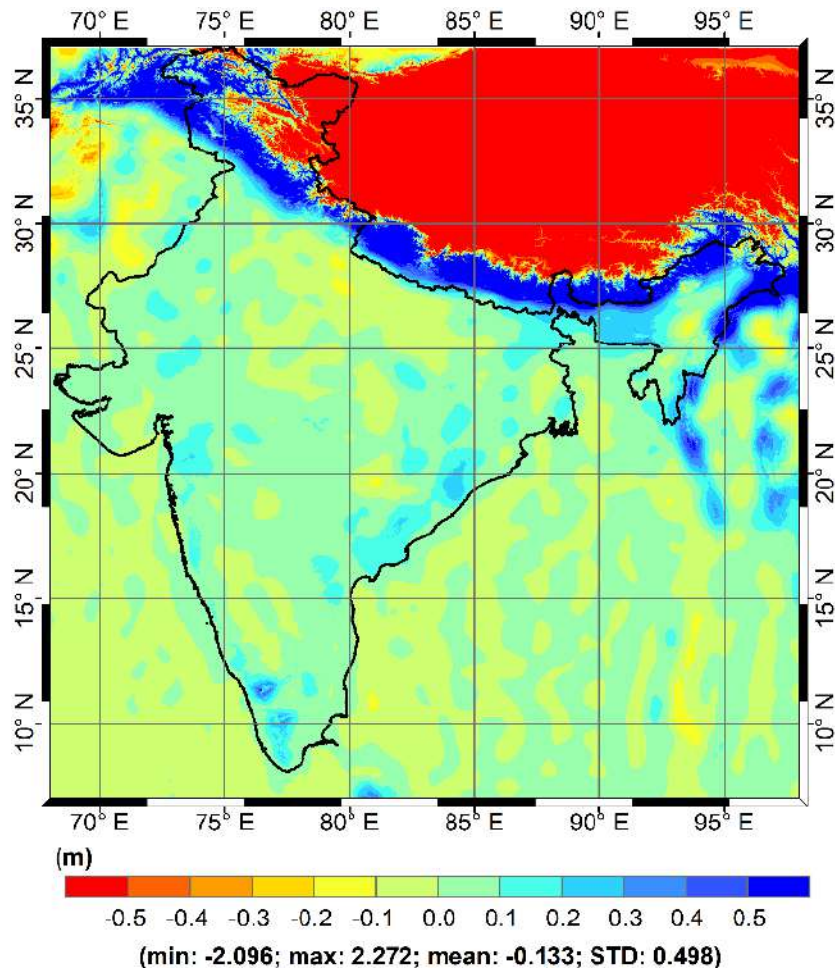


Figure 5.2.9: Difference between gravimetric geoid undulations computed using the CUT and the KTH methods ($M, \psi = 300, 1^\circ$).

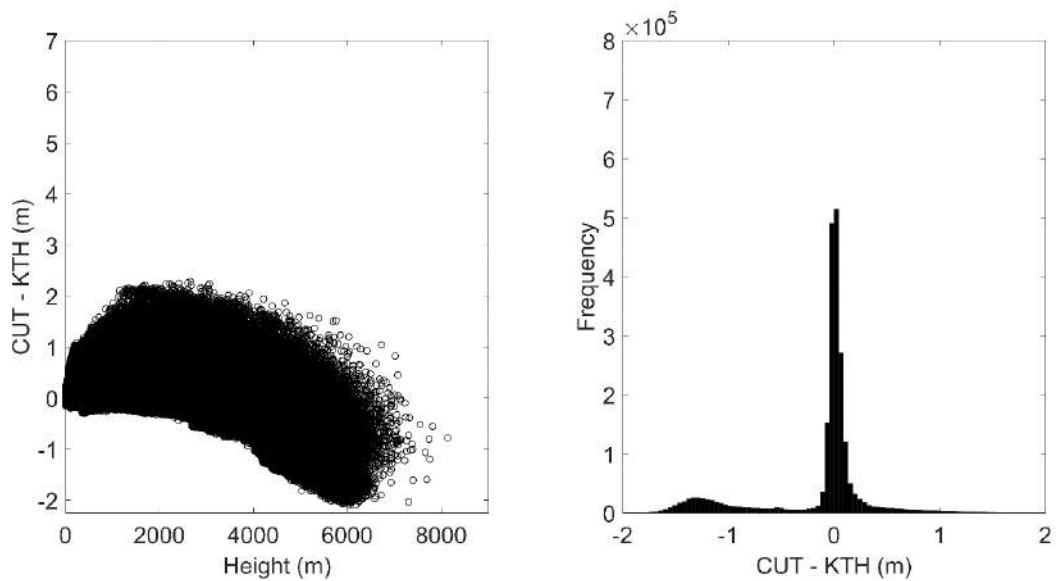


Figure 5.2.10: Scatter plot (a) and histogram (b) of the differences between gravimetric geoid undulations computed using the CUT and the KTH methods ($M, \psi = 300, 1^\circ$).

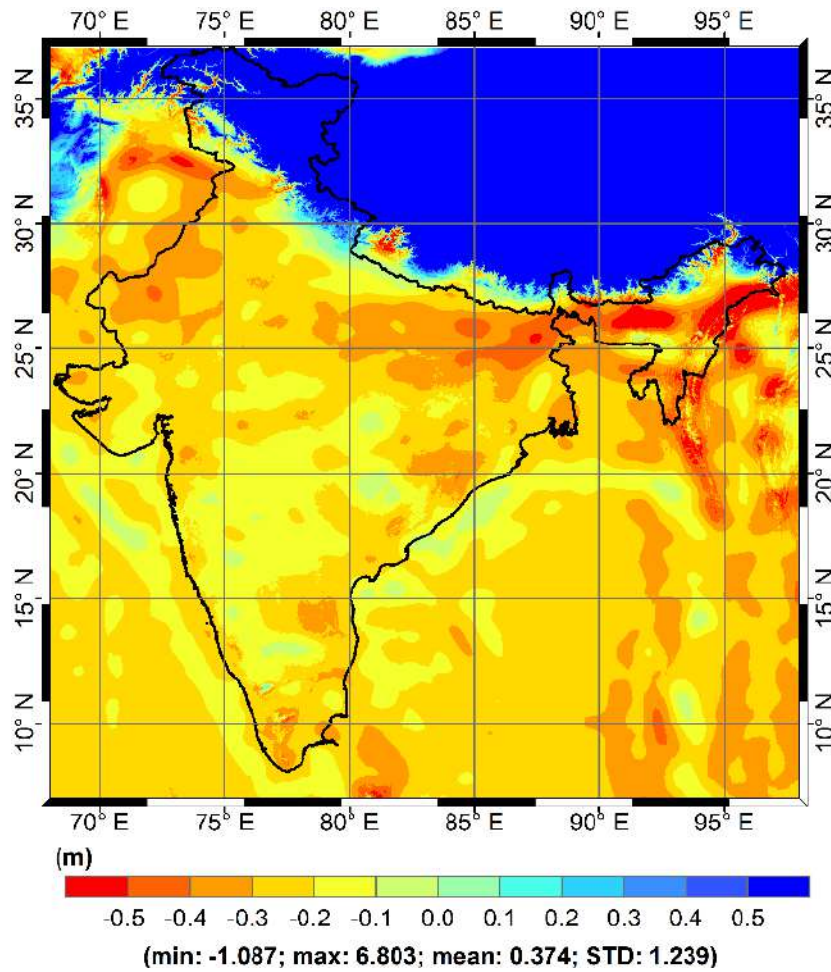


Figure 5.2.11: Difference between gravimetric geoid undulations computed using the KTH and the UNB methods ($M, \psi = 300, 1^\circ$).

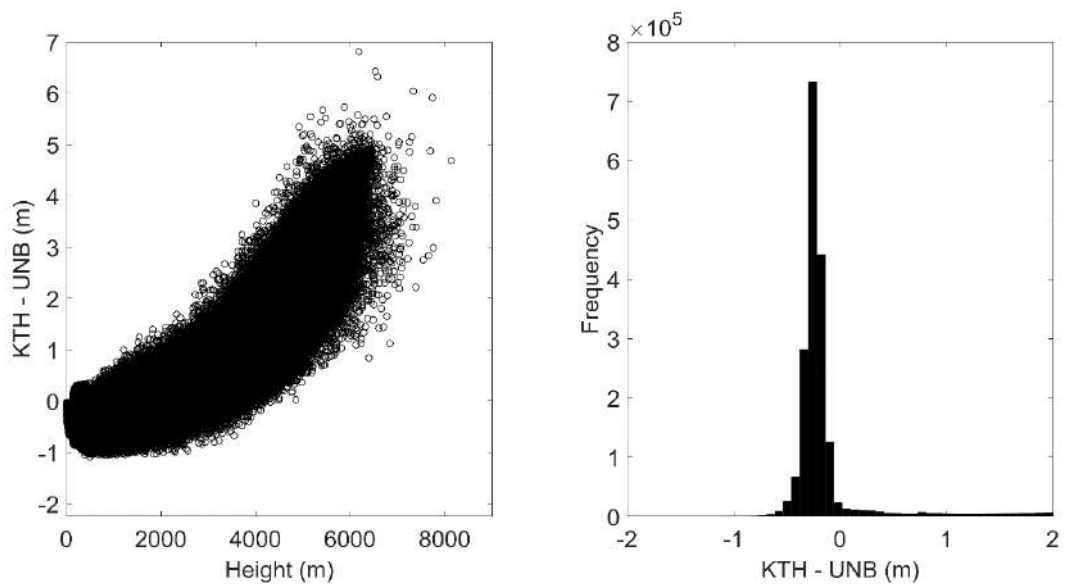


Figure 5.2.12: Scatter plot (a) and histogram (b) of the differences between gravimetric geoid undulations computed using the KTH and the UNB methods ($M, \psi = 300, 1^\circ$).

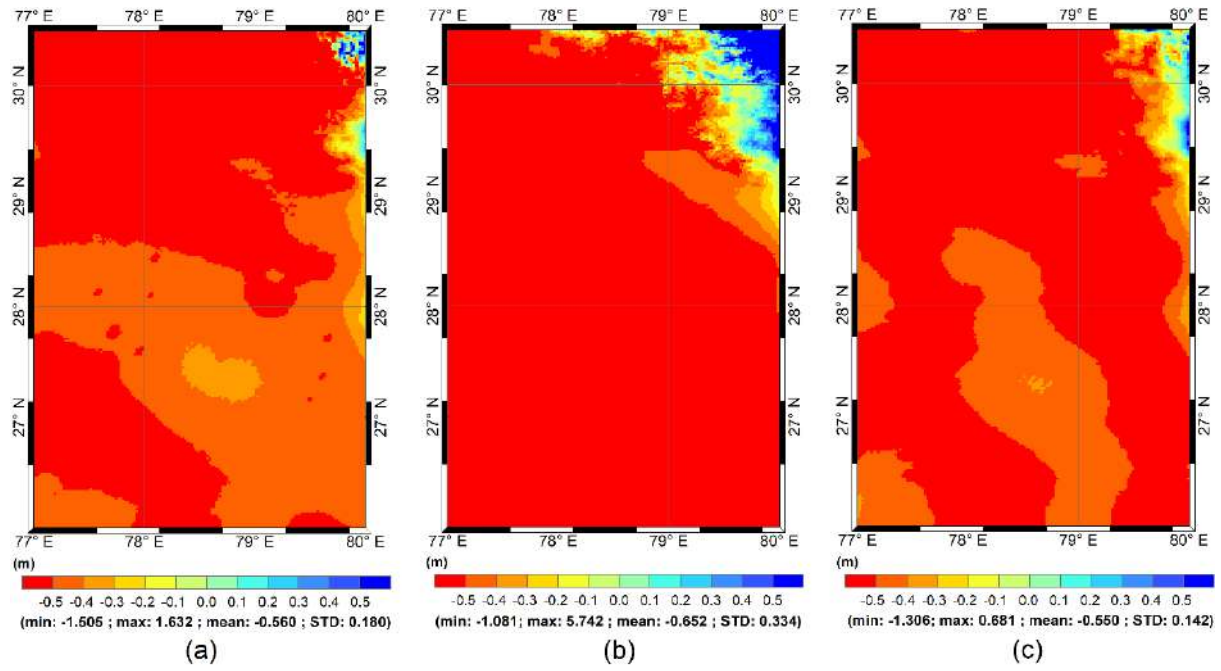


Figure 5.2.13: Difference between gravimetric geoid undulations in UP West calculated using GEOCOL and a) CUT, b) UNB and c) KTH methods

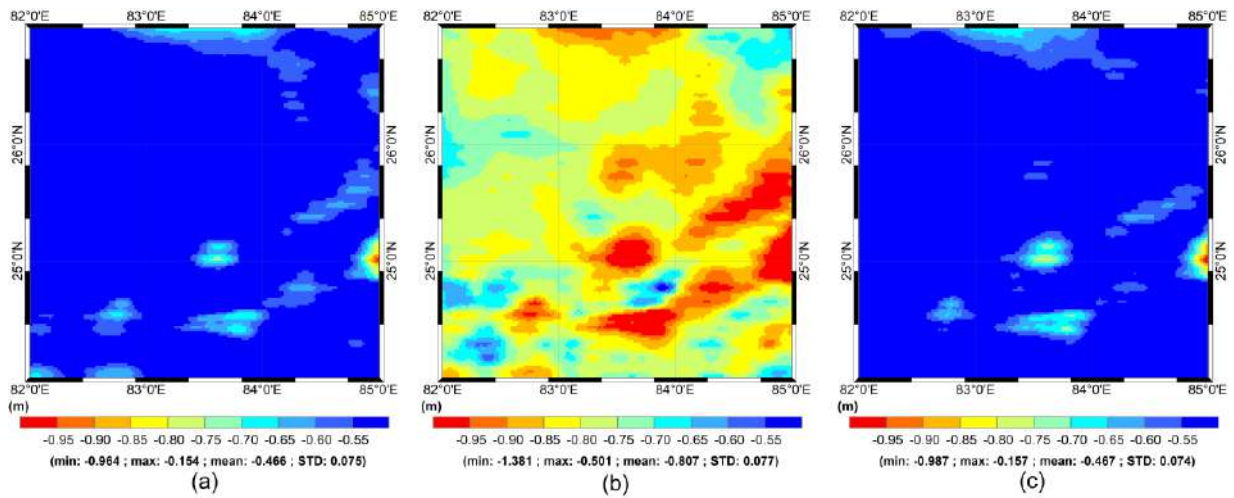


Figure 5.2.14: Difference between geoid models of UP East calculated using GEOCOL and a) CUT, b) UNB and c) KTH methods

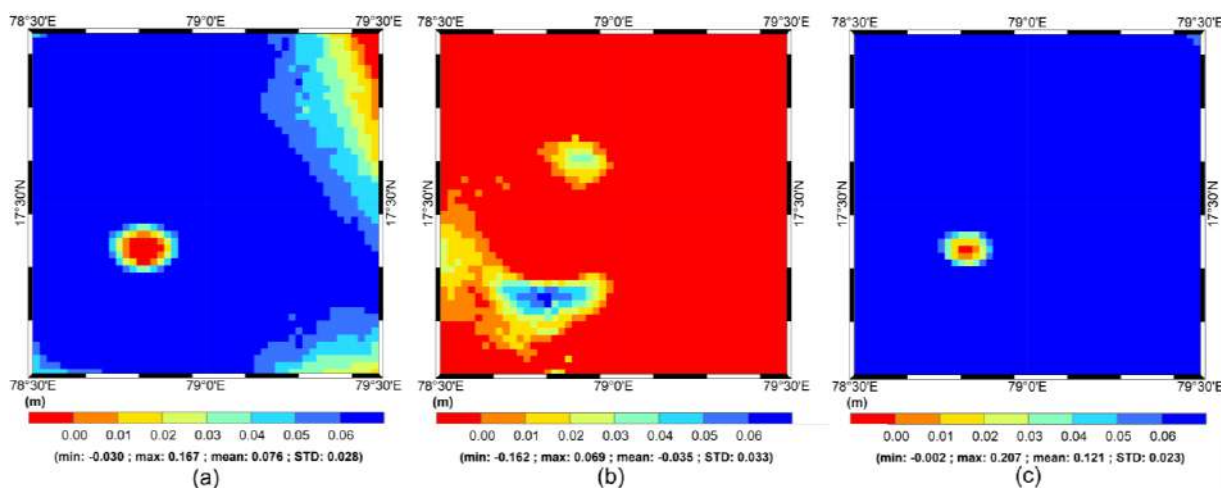


Figure 5.2.15: Difference between geoid models of Hyderabad calculated using GEOCOL and a) CUT, b) UNB and c) KTH methods

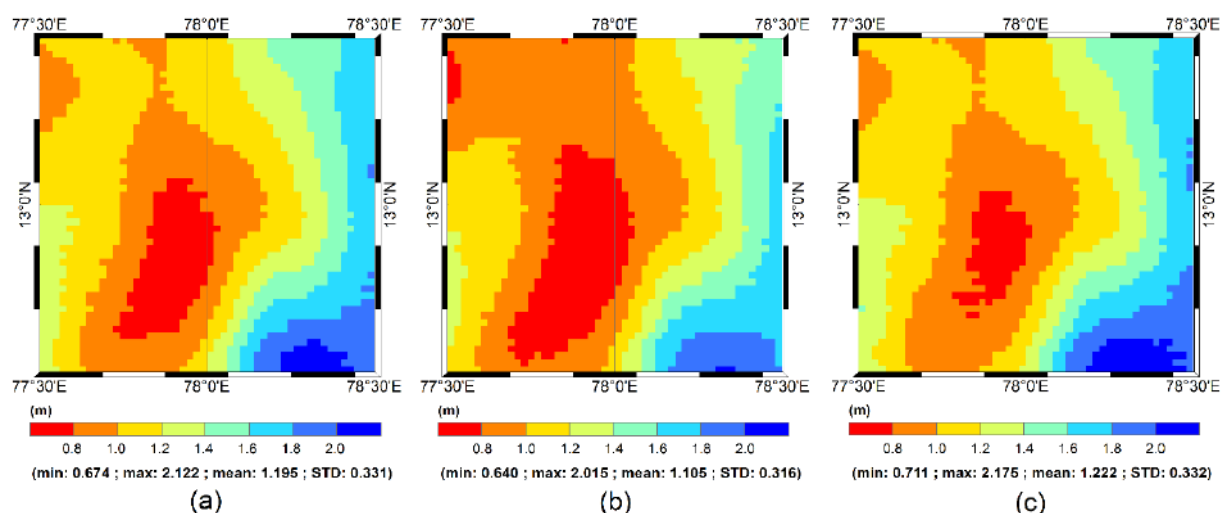


Figure 5.2.16: Difference between geoid models of Bangalore calculated using GEOCOL and a) CUT, b) UNB and c) KTH methods

Following are the main observations:

1. Though the Indian gravimetric geoid models computed using the three methods (Figure 5.2.1 – 5.2.3) differ from each other (Figures 5.2.7, 5.2.9, 5.2.11), all three somewhat depict the separation line of the Indian and the Eurasian plate. Thus, a gravimetric geoid can be important for some lithospheric studies over India. The contour pattern around the location of 24°N and 82°E seems intriguing for some

gravimetric studies in that region. It should be noted that the area comprises a diamond mine and one of the largest coalfields of India with the thickest and different varieties of coal seams.

2. Though the maximum standard deviation does not exceed 0.46 m (Table 5.1.1) on validation of the three geoid models with GNSS-levelling datapoints for India, a large standard deviation is observed for inter-model differences (Figures 5.2.7, 5.2.9, 5.2.11) among the three methods: CUT-UNB = 0.854 m, CUT-KTH = 0.498 m and KTH-UNB = 1.239 m.
3. At the first instance, based on standard deviation, the UNB method can be interpreted to provide less precise results for UP West and for the whole country. However, the larger standard deviation in UP West can be only due to the erroneous GETECH data in the region that causes more significant vertical gravity gradients (Section 3.5.2) and hence, enormous residual Helmert's gravity anomalies (used in the UNB method) for Stokes's integration.
4. The largest misclosures in Figures 5.2.4 - 5.2.6 are most probably due to the tilt in the Indian height datum and the relative closeness of the datapoints in Hyderabad and Bangalore. Sudden spikes in Figures 5.2.4a, 5.2.5a, and 5.2.6a at distances of approximately [0-50] km, [450-550] km, [900-1200] km, and [1200-1900] km are due to the errors and differences (north-south tilt) in the baselines for [Bangalore and Hyderabad, individually], [Bangalore to Hyderabad], [UP West, UP East to Hyderabad], and [UP West, UP East to Bangalore], respectively. From Figures 5.2.4b, 5.2.5b, and 5.2.6b, after fitting, the misclosures for large baselines are diminished significantly, but the misclosures in Hyderabad and Bangalore are diminished less than those in UP because the points are closer together in former two regions. This also explains the larger ppm values found in those regions (Table 5.1.2).

5. The major differences between the geoid models using the three methods (CUT, UNB, KTH) are observed in the high mountains (Figures 5.2.7 - 5.2.12). There is a clear correlation between the geoid undulation differences and topographic heights (Figures 5.2.8 and 5.2.12). The differences between geoid models using the CUT and the KTH methods are smaller as compared to the differences using the UNB and the other two methods. This is possibly because the topographical effects are numerically larger in the mountainous undulating terrains and the UNB method treats the topography more rigorously as compared to the other two methods (Section 3.2).
6. Large differences (> 5 m) are observed in the Indian geoid models calculated using the CUT and the KTH methods with respect to the UNB method (Figures 5.2.7 and 5.2.11). Similar large differences (max = 5.742 m) are also observed in the difference map of geoid undulations with GEOCOL and UNB methods for UP West (Figure 5.2.13c). We reiterate here that a constant of -0.76 m (arising from generalised Bruns's formula) is not applied in the GEOCOL solutions and therefore, an equivalent difference value is expected in the difference maps with respect to the CUT, UNB and KTH methods in all the four regions (Figures 5.2.13 - 5.2.16). Mean values ranging within [-0.652 m, -0.550 m] and [-0.807 m, -0.466 m] have been observed for UP West (Figure 5.2.13) and UP East (Figure 5.2.14), respectively. However, mean values of [-0.035 m, 0.0121 m] for Hyderabad (Figure 5.2.15) and [1.105 m, 1.222 m] for Bangalore (Figure 5.2.16) are concerning enough to further investigate the GEOCOL solutions because these values deviate more than 0.30 m of what is expected (i.e., ~ 0.76 m due to zero-degree term).

5.3 Summary

In this chapter, we presented the validation results of the developed Indian geoid and quasigeoid models using the three methods, i.e., CUT, UNB and KTH. The validations are performed with respect to the GNSS/levelling data for India and the four regions individually (UP west, UP east, Hyderabad, and Bangalore).

With the available GNSS/levelling data, the smallest standard deviation for Indian geoid model is ± 0.39 m with the KTH method. However, region-wise, smallest standard deviation for UP west is ± 0.12 m, UP east: ± 0.09 m, Hyderabad: ± 0.15 m and Bangalore: ± 0.03 m, with CUT, UNB, KTH and UNB methods, respectively. For any given method (CUT, UNB or KTH), there is no particular combination of modification degree and integration radius that provides the smallest standard deviation in the validation of geoid and quasigeoid models of all the four regions. Therefore, it is not possible to comment on the pre-eminence of any one geoid/quasigeoid computation methodology over other.

Difference between the smallest standard deviation obtained from GNSS/levelling-based validations of geoid model and corresponding quasigeoid model does not exceed ± 0.01 m for all three methods in all four regions and India. Therefore, with the available validation data, we can also not comment on the suitability of geoid or quasigeoid model as a preferable reference surface for the Indian normal-orthometric heights.

With the available data, a north-south tilt is observed in the Indian vertical datum. An east-west slope may also be present in the Indian vertical datum due to the location of its tide-gauge stations. However, we could not identify this because of the lack of validation data.

An additional validation of the developed geoid models has been performed that include components of vertical deflections. The geoid gradients (Pizetti's vertical

deflection) have been validated with the Helmert's vertical deflections. In this validation, the KTH method proves to perform better (based on the smallest mean \pm standard deviation) as compared to the other two methods (CUT and UNB).

Gravimetric geoid and quasigeoid models for the four regions have also been computed using GEOCOL. The validation with GNSS/levelling shows that the standard deviation, for the four regions, varies no more than ± 0.02 m as compared to the smallest standard deviations in those regions with either of the CUT, UNB or KTH methods (mentioned above). There is a significant improvement in standard deviation with the complete GNSS/levelling data, i.e., ± 0.11 m (using GEOCOL) compared to ± 0.39 m (using KTH method). However, it should be noted that the GEOCOL calculations does not include the zero-degree term calculated from the generalised Bruns's formula. Though it will not cause any change in the standard deviation values (because it will be a constant term), zero-degree term will cause significant changes (~ 0.75 m) in other descriptive statistic (minimum, maximum, mean).

An inter-model comparison of geoid models has also been presented for 1. India for the following pairs: CUT-UNB, CUT-KTH and KTH-UNB, and 2. the four regions for the pairs: GEOCOL-CUT, GEOCOL-KTH and GEOCOL-UNB. The analysis shows that difference between the geoid models with different methods can vary >1 m, which is significant in the quest for cm-precise geoid. The major differences in the geoid computation methods are in the mountainous regions. Therefore, it has been suggested that a study is required for either merging precise regional geoid models to develop a nationwide geoid model or merging different geoid computation methodologies.

Chapter 6: Conclusions and future recommendations

6.0 Introduction

This chapter provides the final remarks on this study and is divided into three sections. First, a summary of the complete research has been provided. It consists of the key points that emerged from various tests, results, validations and discussions in the first five chapters. Second, conclusions of the study are given with respect to each of the three objectives of the thesis. Finally, due to the limitations of the present study, primarily because of the datasets, a few recommendations for future work are provided.

6.1 Summary of research

The study aimed to develop gravimetric geoid models for mainland India using three methods (CUT, UNB and KTH) and discuss the involved systematic effects from the viewpoint of the cm-precise geoid.

In chapter one, the background on the geoid-related studies over India has been presented. The discussion on the studies has revealed that despite a few studies, a national gravimetric geoid model for India or a detailed computation methodology for the Indian geoid model has never been available in the public domain.

The geodetic data in India has been imposed with numerous restrictions that make it almost impossible to procure the data from the national surveying organisation. Therefore, in chapter two, a discussion on the limitations of this study in terms of the datasets is provided. We discussed the following datasets that have been used in this study: gravity, GNSS/levelling, vertical deflections, GGMs and DEM. Unlike any previous geoid-related study over India, a DEM has been used in the present study instead of DSM

and vertical deflections have been used in addition to the GNSS/levelling data to validate the developed geoid models.

Chapter three discussed the following systematic effects as applied in the three methods (CUT, UNB and KTH) individually: topographic correction, atmospheric correction, ellipsoidal correction and downward continuation. In addition to these four, the following three effects have also been discussed irrespective of the geoid computation methodology: i) different formulas for calculating normal gravity at any arbitrary ellipsoidal height, ii) consistent use of the zero-degree term and iii) conversion formulas for gravity, geoid undulation, orthometric height, normal height, dynamic height, geodetic height and ellipsoidal parameters among the solid Earth permanent tide systems (tide-free, zero-degree and mean-tide).

Three methods for calculating normal gravity using the normal gravity gradient method and one exact method based on confocal ellipsoid has been discussed with a suggestion to use the exact method wherever possible. A new method for calculating local planar TCs has been formulated to be used in the CUT method. For the UNB method, a discussion is provided to use the point values of the topographical effects calculated using the cascading grids instead of the block mean value. The combined topographical effect in the KTH method is explored to be a part of the primary indirect topographical effect in the UNB method.

It has been shown that the formula used for the atmospheric correction in the CUT method should be used as it is, i.e., without truncating/neglecting any term, at least when the maximum height in the study area is >1000 m. A discussion is provided where it is discouraged to use spherical harmonic coefficients for DEM to compute the atmospheric effect. Though the atmospheric correction is lesser than other corrections, the difference needs to be quantified from the viewpoint of the cm-precise geoid.

The CUT method uses ellipsoidal reference gravity anomalies (to calculate residual Faye anomalies) and ellipsoidal radius computed at each latitudinal parallel in Stokes's integration, negating the use of the ellipsoidal correction. The UNB and the KTH methods have similar formulas for the ellipsoidal correction, but the two formulas have a sign inconsistency. It has been discussed that the deflection correction (a term arising in the derivation of the ellipsoidal correction to the gravity disturbance) should also be applied because it can reach up to 139 μGal , which is significant with respect to the present day 1 μGal precise gravimeters. The UNB's formula for the ellipsoidal correction to the gravity disturbance that was precise up to 10 μGal has been modified to a precision level of 2 μGal .

Unlike the UNB and the KTH (of direct geoid computation) methods, the CUT and the KTH (of quasigeoid computation) methods do not require downward continuation. Instead, the latter two use analytical continuation that can be either downward or upward continuation. The CUT method uses the planar TCs as an approximation to the analytical continuation of gravity anomalies. We also presented an argument for the possible downward continuation of the height anomalies from the topographical surface to the ellipsoid to define the quasigeoid. Gravity gradients have been calculated to downward continue the gravity anomalies to the geoid in the UNB method. The downward continuation formula in the KTH method comprises five terms, of which only the first three are used, and the last two are neglected. It has been shown that though we can ignore the fifth term, the fourth term should be included in the calculations because its value can reach $\sim 7 \mu\text{Gal}$, which is seven times the precision of the present-day gravimeters.

The error that can be introduced due to the zero-degree term in Bruns's formula instead of generalised Bruns's formula has been quantified with a suggestion to always use generalised Bruns's formula. It has been shown that geoid undulations and free-air

gravity anomalies do not depend on the solid Earth permanent tide-system, i.e., if the GGM and the ellipsoidal parameters are in the same tide-system there will be no perceptible changes in either of the two for different tide-systems. However, a misinterpretation in tide-system of J_2 of GRS80 (zero-tide instead of tide-free) can cause an error of the order 60 mm in geoid undulations and 10 μGal in free-air anomalies. Several formulas have also been given for the ad-hoc transformation of the ellipsoidal parameters among different tide-systems. It is clearly acknowledged that the change in the ellipsoidal parameters due to different permanent tide systems are not compulsory. Change in the ellipsoidal parameters and the above-mentioned errors of 60 mm in geoid undulation and 10 μGal in free-air anomalies will arise *iff* we do not define our reference ellipsoid as *fixed* or *unchanging*. Hence, we have recommended the need for a convention on the choice of reference ellipsoid (changing or unchanging) while dealing with the solid Earth permanent tide systems.

Chapter 4 discussed the CUT, the UNB and the KTH methods of geoid and quasigeoid computation and the changes that we made to the original methods due to the peculiarities of our dataset. Methods of calculating the geoid-quasigeoid separation (GQS) term and hybrid geoid/quasigeoid have also been presented. It has been shown that the GQS term needs further investigation as different methods can deviate up to ~ 2.5 m, which is significant in the quest of a cm-precise geoid. This is important for the geoid modellers who calculate geoid from quasigeoid and GQS term or quasigeoid from geoid and GQS term. Furthermore, an interpretation with a formulation has been provided that suggests the difference between geoid undulations and height anomalies (as computed on the Earth's topographical surface) may not be called GQS; instead, height anomalies may be first downward continued to the ellipsoid. However, we have acknowledged that

downward continuation of height anomalies may not result in normal heights and therefore, further study or a convention is required for the interpretation of quasigeoid.

The gravimetric geoid models for India and their validation results have been presented in chapter 5. Validation has been done with the GNSS/levelling dataset for India and region-wise because the data were clustered in four regions: Uttar Pradesh West, Uttar Pradesh East, Hyderabad and Bangalore. Pizetti's vertical deflection components have been computed using the horizontal gradients of the geoid models, which were validated with Helmert's vertical deflection components. Regional gravimetric geoid models have also been computed using GEOCOL with residual terrain modelling (RTM). No detailed work is done with GEOCOL in this thesis, and the developed regional models are used only for comparison study with respect to the models developed in this study using other methods (CUT, UNB and KTH) and previously developed regional geoid models available in literature. An inter-model comparison of geoid models for India (calculated using CUT, UNB and KTH methods) has also been presented. The results suggest that, as of now, we cannot generalise the geoid computation methodology because i) they deviate up to a few metres among themselves and ii) each of the three methods provides the least standard deviation in some region of India on validation with GNSS/levelling data.

6.2 Conclusions

Following are the conclusions of this study with respect to each of the three objectives:

- i) *Develop a gravimetric geoid model for India using all the available gravity and terrain data.*

Gravimetric geoid models for the whole of mainland India have been developed using the CUT, the UNB and the KTH methods at a grid of $0.02^\circ \times 0.02^\circ$. The geoid model computed using the CUT method (Goyal et al., 2021, provided in Appendix C.6) will be available

from the International Service for the Geoid (ISG) website (<https://www.isgeoid.polimi.it/>). The precision of this model, for India, as computed with the available 119 GNSS/levelling data is ± 0.396 m. However, region-wise, the precision varies from a minimum of ± 0.03 m in Bangalore to a maximum of ± 0.158 m in Hyderabad. Other geoid models can be shared on individual requests. Therefore, in this study, the first gravimetric geoid model for India has been developed that will also be available in the public domain. However, the cm-precise geoid is not possible with the present data. Hence, the gravimetric geoid studies in India must be continued with new precise and dense gravity and GNSS/levelling data.

ii) *Analyse the use of high-resolution DEM in determining terrain effects.*

We have developed an efficient spatial-spectral combined method for calculating planar TCs using high-resolution DEMs (Goyal et al., 2020). The developed method has no implementing restrictions on the type of topography. Moreover, the developed numerical method is sufficiently accurate with respect to the analytical solution and reduces the computation time by almost 50%. Local planar TCs have been computed on a grid of $3'' \times 3''$ for a region of $40^\circ \times 40^\circ$ in and around India using MERIT DEM. This is the first planar TC computation that i) has been conducted in a study area encapsulating typical landforms, e.g., the Himalayas, Gangetic plains, Thar desert, plateaus and other hill ranges, ii) uses a single high-resolution DEM and without removing the DEM points to circumvent the divergence issue and iii) provides convergent solution down to $< 1 \mu\text{Gal}$.

iii) *Evaluate and validate developed gravimetric geoid and quasigeoid models.*

The study suggests that the gravimetric geoid or quasigeoid models should be validated after clustering the GNSS/levelling data in groups (maybe based on region or topography) in addition to the validation with the complete dataset. Moreover, two or more gravimetric

geoid/quasigeoid models or the geoid/quasigeoid computation methodologies should not be compared for pre-eminence solely based on standard deviation. There is no particular choice of a geoid computation methodology or a modification degree and integration radius combination that would give the least standard deviation (or any descriptive statistical value) for a country if validated region-wise. Therefore, there is a need for a new geoid computation methodology that could combine several regional geoid models or different methods of geoid computation. The vertical deflection components, if available, should also be used for geoid validation. As of today, the geoid computation cannot be generalised because the geoid models with different methods can deviate up to a few metres from one another. Therefore, we are yet far away from the goal of the cm-precise geoid.

6.3 Scope of the future work

The suggestions for future work have been discussed in several sections of this thesis and are summarised as follows:

- i) There must be some work done towards improved availability of point-wise gravity data in India.
- ii) Generally, the gravity data is limited to the study area but is also required in the regions surrounding the study area. Therefore, different methods for filling the gravity (or gravity anomaly) data in the surrounding regions of the study area should be analysed and quantified.
- iii) There are large variations of the gravity anomalies in the mountainous regions. Sometimes, they are presented in the horizontal layers of positive and negative anomalies while transiting different landforms. Moreover, we have multiple gravity datasets, e.g., terrestrial, airborne and marine gravity data, with very little

data coverage in the mountainous regions due to the highway effect. Therefore, with the precise and dense observed gravity data or synthesised gravity data, various gravity merging and interpolation techniques should be analysed over different landforms and the whole of a country.

- iv) A few modified formulas, which are derived and discussed in Sections 3.1 to 3.5, must be analysed with precise gravity data. The associated errors or differences between the existing and modified formulas must be quantified in calculating geoid undulations or height anomalies.
- v) The effect of the topographical corrections to the geoid in the KTH and the UNB method must be rigorously analysed because the combined topographic effect in the KTH method is equivalent to a part only of the primary indirect topographic effect of the UNB method. Moreover, ellipsoidal correction formulas in the UNB and the KTH methods must be analysed for the sign inconsistency.
- vi) Downward continuation of the height anomalies from the Earth's topographical surface to the ellipsoid for defining the quasigeoid can be studied further, along with formulating our interpretation of the geoid-quasigeoid separation term. A starting point can be quantifying the difference between the ellipsoidal normal and the curved normal plumb line.
- vii) It is common to test the geoid models or methodologies based on standard deviation. However, it should be noted that standard deviation is a measure of precision and not accuracy. Also, the GNSS/levelling-based validations are highly dependent on the quality of the GNSS and levelling data and on any outliers in the data. Therefore, it is possible that one may obtain a high-precise geoid but with an offset. A statistical study is required to compare geoid models or methods more objectively.

- viii) More validation studies are required to comment on the suitability of the geoid or quasigeoid model as a reference surface for the normal-orthometric height system. However, the geoid must be validated with orthometric (Helmert's or rigorous) height and quasigeoid with normal heights. Therefore, the physical heights in the GNSS/levelling dataset must be converted to the required height system before validating the geoid or quasigeoid.
- ix) The geoid models from different methods can significantly deviate from each other. According to this study with limited datasets, there is no geoid/quasigeoid computation method that gives consistent results in the country, i.e., different methods can be suitable for different types of landforms/topography. Therefore, a new method is required to compute the national gravimetric geoid model. A starting point could be devising an algorithm for merging several regional geoid models. However, before working on a new method, perhaps, the methods need to be compared in different areas with higher quality data than that available in India. A cluster-wise validation and inter-model analysis may be performed on the Colorado geoid models (https://www.isgeoid.polimi.it/Projects/colorado_experiment.html) or Auvergne geoid models (https://www.isgeoid.polimi.it/Projects/Auvergne_test.html).

References

- Abbak, R.A., Erol, B., Ustun, A., 2012. Comparison of the KTH and remove–compute–restore techniques to geoid modelling in a mountainous area. *Computers & Geosciences*, 48, 31–40. <https://doi.org/10.1016/j.cageo.2012.05.019>
- Abdalla, A., 2009. Determination of a gravimetric geoid model of Sudan using the KTH method. M.Sc. Thesis, Royal Institute of Technology (KTH), Stockholm, Sweden. <https://www.diva-portal.org/smash/get/diva2:1064844/FULLTEXT01.pdf>
- Abdalla, A., Fairhead, D., 2011. A new gravimetric geoid model for Sudan using the KTH method. *Journal of African Earth Sciences*, 60(4), 213–221. <https://doi.org/10.1016/j.jafrearsci.2011.02.012>
- Abdalla, A., Mogren, S., 2015. Implementation of a rigorous least-squares modification of Stokes' formula to compute a gravimetric geoid model over Saudi Arabia (SAGEO13). *Canadian Journal of Earth Sciences*, 52(10), 823–832. <https://doi.org/10.1139/cjes-2014-0192>
- Abdalla, A., Tenzer, R., 2011. The evaluation of the New Zealand's geoid model using the KTH method. *Geodesy and Cartography*, 37(1), 5–14. <https://doi.org/10.3846/13921541.2011.558326>
- Abd-Elmotaal, H.A., Seitz, K., Kühtreiber, N., Heck, B., 2018. AFRGDB_V2.0: The Gravity Database for the Geoid Determination in Africa. In: Freymueller J., Sánchez, L., (eds.) *International Symposium on Advancing Geodesy in a Changing World*. International Association of Geodesy Symposia, vol 149, pp. 61-70. Springer. https://doi.org/10.1007/1345_2018_29
- Abeyratne, P.G.V., Featherstone, W.E., Tantrigoda, D.A., 2010. On the geodetic datums in Sri Lanka. *Survey Review*, 42(317), 229–239. <https://doi.org/10.1179/003962610X12572516251880>
- Ádám, J., 1999. Difference between geoid undulation and quasigeoid height in Hungary. *Bollettino Di Geofisica Teorica Ed Applicata*, 40(3–4), 571–575.
- Ågren, J., 2004. Regional geoid model determination methods for the era of satellite gravimetry (Numerical investigations using synthetic earth gravity models). Ph.D. Thesis, Royal Institute of Technology (KTH), Stockholm, Sweden. <https://www.diva-portal.org/smash/get/diva2:14396/FULLTEXT01.pdf>
- Ågren, J., Barzaghi, R., Carrion, D., Denker, H., Grigoriadis, V.N., Kiamehr, R., Sona, G., Tscherning, C.C., Tziavos, I.N., 2009a. Different geoid computation methods applied on a test dataset: results and considerations. In: Poster presented at VII Hotine-Marussi Symposium on Mathematical Geodesy, Rome, Italy.
- Ågren, J., Sjöberg, L.E., 2014. Investigation of gravity data requirements for a 5 mm-quasigeoid model over Sweden. In: Marti, U., (eds.) *Gravity, Geoid and Height Systems*. International Association of Geodesy Symposia, vol 141, pp. 143-150. Springer. https://doi.org/10.1007/978-3-319-10837-7_18
- Ågren, J., Sjöberg, L.E., Kiamehr, R., 2009b. The new gravimetric quasigeoid model KTH08 over Sweden. *Journal of Applied Geodesy*, 3(3), 143–153. <https://doi.org/10.1515/JAG.2009.015>
- Akaike, H., 1974. A new look at the statistical model identification. *IEEE Transactions on Automatic Control*, 19(6), 716–723. <https://doi.org/10.1109/TAC.1974.1100705>

- Al-Kherayef, O., Golubinka, I., Al-Shahrani, S., Grebenitcharsky, R., 2020. An improved hybrid geoid model over Kingdom of Saudi Arabia utilizing new GNSS ellipsoidal heights on benchmarks of KSA national vertical network. In: FIG working week, 2020, Amsterdam, The Netherlands.
https://fig.net/resources/proceedings/fig_proceedings/fig2020/papers/ts04g/TS04G_al-kherayef_zayats_et_al_10445.pdf
- Amin, H., Sjöberg, L.E., Bagherbandi, M., 2019. A global vertical datum defined by the conventional geoid potential and the Earth ellipsoid parameters. *Journal of Geodesy*, 93(10), 1943-1961. <https://doi.org/10.1007/s00190-019-01293-3>
- Amos, M., Featherstone, W.E., 2003. Comparisons of recent global geopotential models with terrestrial gravity field observations over New Zealand and Australia. *Geomatics Research Australasia*, 79, 1–20.
- Amos, M.J., 2007. Quasigeoid modelling in New Zealand to unify multiple local vertical datums. Ph.D. Thesis, Curtin University of Technology, Perth, Australia.
<https://espace.curtin.edu.au/handle/20.500.11937/1949>
- Amos, M.J., Featherstone, W.E., 2009. Unification of New Zealand's local vertical datums: Iterative gravimetric quasigeoid computations. *Journal of Geodesy*, 83(1), 57–68.
<https://doi.org/10.1007/s00190-008-0232-y>
- Anderson, E.G., Rizos, C., Mather, R.S., 1975. Atmospheric effects in physical geodesy. UNISURV Report G23. University of New South Wales, Kensington, Australia.
- Angermann, D., Gruber, T., Gerstl, M., Heinkelmann, R., Hugentobler, U., Sánchez, L., Steigenberger, P., 2016. GGOS bureau of products and standards: inventory of standards and conventions used for the generation of IAG products. *Journal of Geodesy*, 90(10), 1095-1156.
<https://doi.org/10.1007/s00190-016-0948-z>
- Avalos Naranjo, D., Hernández-Navarro, A., Muñoz-Abundes, R., Sosa-Gaytán, M., 2006. The Mexican gravimetric geoid: GGM06. V. 1.0. GFZ Data Services.
<https://doi.org/10.5880/isg.2006.001>
- Banerjee, B., Gupta, S.P.D., 1977. Gravitational attraction of a rectangular parallelepiped. *Geophysics*, 42(5), 1053–1055. <https://doi.org/10.1190/1.1440766>
- Barnes, R., Lehman, C., Mulla, D., 2014. An efficient assignment of drainage direction over flat surfaces in raster digital elevation models. *Computers & Geosciences*, 62, 128–135.
<https://doi.org/10.1016/j.cageo.2013.01.009>
- Basavaiah, N., Singh, B.P., Radhakrishna Murthy, I.V., 1991. The Himalayan riddle of the free-air satellite gravity and a possible solution. *Physics of the Earth and Planetary Interiors*, 69(1–2), 14–19. [https://doi.org/10.1016/0031-9201\(91\)90150-G](https://doi.org/10.1016/0031-9201(91)90150-G)
- Bašić, T., Varga, M., 2018. A brief (historical) review on definitions and applications of the geoid. In: IX Hotine-Marussi Symposium, Rome, Italy, June 18-22, 2018.
- Bhattacharji, J.C., 1973. Geoid, isostatic geoid, isostatic co-geoid and indirect effect of gravity in India. In: Proceedings of symposium on Earth's gravitational field and secular variations in position, Sydney, Australia, pp. 227-239. University of New South Wales, Australia.
https://www.sage.unsw.edu.au/sites/sage/files/SAGE_collection/SpecialSeries/s11D.pdf

- Bhattacharji, J.C., 1982. Absolute GRS67 geoid and deflections of the vertical in India. *Indian Journal of Earth Sciences*, 9(1), 67-71.
- Bjerhammar, A., 1966. On the determination of the shape of the geoid and the shape of the earth from an ellipsoidal surface of reference. *Bulletin Géodésique*, 81(1), 235–265. <https://doi.org/10.1007/BF02527013>
- Blakely, R.J., 1996. *Potential theory in gravity and magnetic applications*. Cambridge University Press, Cambridge, UK.
- Bomford G., 1967. James de Graaff-Hunter, 1881-1967. *Biographical Memoirs of Fellows of the Royal Society*, 13, 78–88. <http://doi.org/10.1098/rsbm.1967.0004>
- Bomford, G., 1971. *Geodesy*, 3rd edition. Oxford University Press, London.
- Borghi, A., Barzaghi, R., Al-Bayari, O., Al Madani, S., 2020. Centimeter precision geoid model for Jeddah Region (Saudi Arabia). *Remote Sensing*, 12(12), 2066. <https://doi.org/10.3390/rs12122066>
- Borghi, A., Carrion, D., Sona, G., 2007. Validation and fusion of different databases in preparation of high-resolution geoid determination. *Geophysical Journal International*, 171(2), 539–549. <https://doi.org/10.1111/j.1365-246X.2007.03541.x>
- Bowie, W., 1914. Isostasy in India. *Journal of the Washington Academy of Sciences*, IV(10), 245-249. <https://www.jstor.org/stable/24520967>
- Bracewell, R., 1986. *The Fourier transform and its applications*. McGraw Hill, New York.
- Brockmann, J.M., Zehentner, N., Höck, E., Pail, R., Loth, I., Mayer-Gürr, T., Schuh, W.-D., 2014. EGM_TIM_RL05: An independent geoid with centimeter accuracy purely based on the GOCE mission. *Geophysical Research Letters*, 41(22), 8089–8099. <https://doi.org/10.1002/2014GL061904>
- Brovar, V.V., 1964. On the solution of Molodensky's boundary value problem. *Bulletin Géodésique*, 72, 167-173. <https://doi.org/10.1007/BF02526971>
- Brovar, V.V., Kopeikina, Z.S., Pavlova, M.V., 2001. Solution of the Dirichlet and Stokes exterior boundary problems for the Earth's ellipsoid. *Journal of Geodesy*, 74(11–12), 767–772. <https://doi.org/10.1007/s001900000100>
- Brown, N.J., McCubbine, J.C., Featherstone, W.E., Gowans, N., Woods, A., Baran, I., 2018. AUSGeoid2020 combined gravimetric–geometric model: Location-specific uncertainties and baseline-length-dependent error decorrelation. *Journal of Geodesy*, 92(12), 1457–1465. <https://doi.org/10.1007/s00190-018-1202-7>
- Bruinsma, S.L., Förste, C., Abrikosov, O., Marty, J.-C., Rio, M.-H., Mulet, S., Bonvalot, S., 2013. The new ESA satellite-only gravity field model via the direct approach. *Geophysical Research Letters*, 40(14), 3607–3612. <https://doi.org/10.1002/grl.50716>
- Bruns, H., 1878. *Die figur der Erde (The figure of the Earth)*. Publication of the Royal Prussian Geodetic Institute, Berlin.
- Bucha, B., Janák, J., 2014. A MATLAB-based graphical user interface program for computing functionals of the geopotential up to ultra-high degrees and orders: Efficient computation at

- irregular surfaces. *Computers & Geosciences*, 66, 219–227. <https://doi.org/10.1016/j.cageo.2014.02.005>
- Burrard, S.G., 1910. Levelling of precision in India, vol. XIX. The Office of the Trigonometrical Survey of India, Dehradun, India.
- Burrard, S.G., 1918. Investigations of isostasy in Himalayan and neighbouring regions. Professional paper No. 17, Survey of India, Dehradun, India.
- Burrard, S.G., 1920. A brief review of the evidence upon which the theory of isostasy has been based. *The Geographical Journal*, 56(1), 47–52. <https://doi.org/10.2307/1781294>
- Burša, M., 1995. Geoidal potential free of zero-frequency tidal distortion. *Earth, Moon, and Planets*, 71(1-2), 59-64. <https://doi.org/10.1007/BF00612869>
- Burša, M., Kenyon, S., Kouba, J., Šíma, Z., Vátrt, V., Vojtíšková, M., 2004. A global vertical reference frame based on four regional vertical datums. *Studia Geophysica et Geodaetica*, 48(3), 493–502. <https://doi.org/10.1023/B:SGEG.0000037468.48585.e6>
- Burša, M., Kouba J., Kumar M., Müller, A., Raděj, K., True, S.C., Vátrt V., Vojtíšková, M., 1999. Geoidal geopotential and world height system. *Studia Geophysica et Geodaetica*, 43(4), 327-337. <https://doi.org/10.1023/A:1023273416512>
- Carrion, D., Kumar, N., Barzaghi, R., Singh, A.P., Singh, B., 2009. Gravity and geoid estimate in south India and their comparison with EGM2008. *Newton's Bulletin*, 4, 275–283.
- Catalao, J., 2006. Iberia-Azores Gravity Model (IAGRM) using multi-source gravity data. *Earth, Planets and Space*, 58(3), 277–286. <https://doi.org/10.1186/BF03351924>
- Cavazzi, S., Corstanje, R., Mayr, T., Hannam, J., Fealy, R., 2013. Are fine resolution digital elevation models always the best choice in digital soil mapping? *Geoderma*, 195–196, 111–121. <https://doi.org/10.1016/j.geoderma.2012.11.020>.
- Chen, Q., Shen, Y., Zhang, X., Chen, W., Hsu, H., 2015. Tongji-GRACE01: A GRACE-only static gravity field model recovered from GRACE Level-1B data using modified short arc approach. *Advances in Space Research*, 56(5), 941–951. <https://doi.org/10.1016/j.asr.2015.05.034>
- Chijun, Z., Shaofeng, B., Zhouyun, Y., Lingtao, L., Jian, F., 2011. Refining geoid and vertical gradient of gravity anomaly. *Geodesy and Geodynamics*, 2(4), 1–9. <https://doi.org/10.3724/SP.J.1246.2011.00009>
- Choudhary, M., 2017. Survey of India launches geoid model of India-INDGEOID Ver.1.0. <https://www.geospatialworld.net/videos/survey-india-launches-geoid-model-country/>
- Claessens, S., 2021. The tide-generating potential in geodetic coordinates. Unpublished.
- Claessens, S.J., 2006. Solutions to ellipsoidal boundary value problems for gravity field modelling. Ph.D. Thesis, Curtin University of Technology, Perth, Australia. <https://espace.curtin.edu.au/handle/20.500.11937/1637>
- Claessens, S.J., 2016. Spherical harmonic analysis of a harmonic function given on a spheroid. *Geophysical Journal International*, 206(1), 142–151. <https://doi.org/10.1093/gji/ggw126>

- Claessens, S.J., Filmer, M.S., 2020. Towards an International Height Reference System: Insights from the Colorado geoid experiment using AUSGeoid computation methods. *Journal of Geodesy*, 94(5), 52. <https://doi.org/10.1007/s00190-020-01379-3>
- Claessens, S.J., Hirt, C., Amos, M.J., Featherstone, W.E., Kirby, J.F., 2011. The NZGeoid09 model of New Zealand. *Survey Review*, 43(319), 2–5. <https://doi.org/10.1179/003962610X12747001420780>
- Colombo, O.L., 1981. Numerical methods for harmonic analysis on the sphere. Department of Geodetic Science Report No. 310. The Ohio State University, Columbus, USA. <https://earthsciences.osu.edu/sites/earthsciences.osu.edu/files/report-310.pdf>
- Colombo, O.L., 1991. The role of GPS/INS in mapping the Earth's gravity field in the 1990's. In: Schwarz, K.-P., Lachapelle, G., (ed.) *Kinematic systems in geodesy, surveying, and remote sensing*. International Association of Geodesy Symposium, vol 107, pp. 463-476. Springer. https://doi.org/10.1007/978-1-4612-3102-8_42
- Crippen, R., Buckley, S., Agram, P., Belz, E., Gurrola, E., Hensley, S., Kobrick, M., Lavallo, M., Martin, J., Neumann, M., Nguyen, Q., Rosen, P., Shimada, J., Simard, M., Tung, W., 2016. NASADEM global elevation model: methods and progress. *ISPRS - International Archives of the Photogrammetry, Remote Sensing and Spatial Information Sciences*, XLI-B4, 125–128. <https://doi.org/10.5194/isprsarchives-XLI-B4-125-2016>
- Crosthwait, H.L., 1912. Investigation of the theory of isostasy in India. Professional paper No. 13. Survey of India, Dehradun, India.
- Cruz, J.Y., 1986. Ellipsoidal corrections to potential coefficients obtained from gravity anomaly data on the ellipsoid. Department of Geodetic Science and Surveying Report No. 371. The Ohio State University, Columbus, USA.
- Dahle, C., Flechtner, F., Gruber, C., König, D., König, R., Michalak, G., Neumayer, K.-H., 2013. GFZ GRACE level-2 processing standards document for level-2 product release 0005: revised edition, January 2013. Scientific Technical Report STR - Data12/02 rev. ed., Deutsches GeoForschungs Zentrum GFZ, Potsdam. <https://doi.org/10.2312/GFZ.b103-1202-25>
- Daly, R.A., 1969. *Strength and structure of the Earth*. Hafner publishing Co., New York and London.
- Danvers, F.C., 1870. The surveys of India, II. The trigonometrical survey. *Quarterly Journal of Science*, XXVIII, 448-458.
- Daras, I., 2008. Determination of a gravimetric geoid model of Greece using the KTH method. M.Sc. Thesis, Royal Institute of Technology (KTH), Stockholm, Sweden. <https://www.diva-portal.org/smash/get/diva2:1064985/FULLTEXT01.pdf>
- Daras, I., Fan, H., Papazissi, K., Fairhead, J.D., 2010. Determination of a gravimetric geoid model of Greece using the method of KTH. In: Mertikas, S., (eds.) *Gravity, Geoid and Earth Observation*. International Association of Geodesy Symposia, vol. 135, pp. 401-413. Springer. https://doi.org/10.1007/978-3-642-10634-7_54
- Darbeheshti, N., 2009. Modification of the least-squares collocation method for non-stationary gravity field modelling. Ph.D. Thesis, Curtin University of Technology, Perth, Australia. <https://espace.curtin.edu.au/handle/20.500.11937/2228>

- Dayoub, N., Edwards, S.J., Moore, P., 2012. The Gauss-Listing potential value W_0 and its rate from altimetric mean sea level and GRACE. *Journal of Geodesy*, 86(9), 681-694. <http://doi.org/10.1007/s00190-012-1547-6>
- de Witte, L., 1967. Truncation errors in the Stokes and Vening Meinesz formulae for different order spherical harmonic gravity terms. *Geophysical Journal International*, 12(5), 449-464. <https://doi.org/10.1111/j.1365-246X.1967.tb03125.x>
- Demirkesen, A.C., 2012. Multi-risk interpretation of natural hazards for settlements of the Hatay province in the east Mediterranean region, Turkey using SRTM DEM. *Environmental Earth Sciences*, 65(6), 1895-1907. <https://doi.org/10.1007/s12665-011-1171-0>.
- Denker, H., 2005. Evaluation of SRTM3 and GTOPO30 terrain data in Germany. In: Jekeli, C., Bastos, L., Fernandes, J. (eds.), *Gravity, Geoid and Space Missions*. International Association of Geodesy Symposium, vol. 129, pp. 218-223. Springer. https://doi.org/10.1007/3-540-26932-0_38.
- Denker, H., Torge, W., Wenzel, G., Ihde, J., Schirmer, U., 2000. Investigation of different methods for the combination of gravity and GPS/levelling data. In: Schwarz, K.P., (eds.) *Geodesy Beyond 2000*. International Association of Geodesy Symposia, vol. 121, pp. 137-142. Springer. https://doi.org/10.1007/978-3-642-59742-8_23
- Dennis, M.L. Featherstone, W.E., 2003. Evaluation of orthometric and related height systems using a simulated mountain gravity field. In: Tziavos, I.N., (ed.) *Gravity and Geoid 2002*, pp. 389-394. Department of Surveying and Geodesy, Aristotle University of Thessaloniki, Greece.
- Dobos, E., Hengl, T., 2009. Soil mapping applications. In: Hengl, T., Reuter, H.I., (eds.), *Geomorphometry: concepts, software, applications*. Developments in soil science, vol. 33, pp. 461-480. Elsevier.
- Drewes, H., Hornik, H., (eds.), 2013. *International Association of Geodesy Travaux* vol. 38, Reports 2011-2013. https://iag.dgfi.tum.de/fileadmin/IAG-docs/Travaux_2011-2013.pdf
- Drinkwater, M.R., Floberghagen, R., Haagmans, R., Muzi, D., Popescu, A., 2003. GOCE: ESA's first Earth explorer core mission. *Space Science Reviews*, 108, 419-432. <https://doi.org/10.1023/A:1026104216284>
- Dryden, H.L., 1942. A re-examination of the Potsdam absolute determination of gravity. *Journal of Research of the National Bureau of Standards*, 29, 303-314.
- Duquenne, H., 2006. A data set to test geoid computation methods. In: *Proceedings of the 1st International Symposium of the International Gravity Field Service*, pp. 61-65. Istanbul, Turkey.
- Ecker, E., Mittermayer, E., 1969. Gravity corrections for the influence of the atmosphere. *Bulletin of Theoretical and Applied Geophysics*, 11, 70-80.
- Ekman, M., 1980. On the error introduced into Stokes' formula by applying the Honkasalo tidal gravity term: Remarks on *Bulletin Géodésique*, vol. 53, no. 3, pp. 239-245, by M. Heikkinen. *Bulletin Géodésique*, 54(4), 528-530. <https://doi.org/10.1007/BF02530710>
- Ekman, M., 1981. On the definition of gravity. *Journal of Geodesy*, 55(2), 167-168. <https://doi.org/10.1007/BF02530838>

- Ekman, M., 1988. The impact of geodynamic phenomena on systems for height and gravity. Professional papers No. 26. Nordic Geodetic Commission, Ebeltoft, Denmark.
- Ekman, M., 1989. Impacts of geodynamic phenomena on systems for height and gravity. *Bulletin Géodésique*, 63(3), 281–296. <https://doi.org/10.1007/BF02520477>
- Ellmann, A., 2001. Least squares modification of Stokes formula with applications to the Estonian geoid. Licentiate Thesis, Royal Institute of Technology (KTH), Stockholm, Sweden.
- Ellmann, A., 2004. The geoid for the Baltic countries determined by the least squares modification of Stokes' formula. Ph.D. Thesis, Royal Institute of Technology (KTH), Stockholm, Sweden. <http://kth.diva-portal.org/smash/get/diva2:9592/FULLTEXT01.pdf>
- Ellmann, A., 2005a. A numerical comparison of different ellipsoidal corrections to Stokes' formula. In: Sansò, F., (eds.) *A Window on the Future of Geodesy*. International Association of Geodesy Symposia, vol. 128, pp. 409–414. Springer. https://doi.org/10.1007/3-540-27432-4_70
- Ellmann, A., 2005b. Computation of three stochastic modifications of Stokes's formula for regional geoid determination. *Computers & Geosciences*, 31(6), 742–755. <https://doi.org/10.1016/j.cageo.2005.01.008>
- Ellmann, A., Märdla, S., Oja, T., 2020. The 5 mm geoid model for Estonia computed by the least squares modified Stokes's formula. *Survey Review*, 52(373), 352–372. <https://doi.org/10.1080/00396265.2019.1583848>
- Ellmann, A., Vaníček, P., 2007. UNB application of Stokes–Helmert's approach to geoid computation. *Journal of Geodynamics*, 43(2), 200–213. <https://doi.org/10.1016/j.jog.2006.09.019>
- Erol, B., Erol, S., 2013. Learning-based computing techniques in geoid modeling for precise height transformation. *Computers & Geosciences*, 52, 95–107. <https://doi.org/10.1016/j.cageo.2012.09.010>
- Farr, T.G., Rosen, P.A., Caro, E., Crippen, R., Duren, R., Hensley, S., Kobrick, M., Paller, M., Rodriguez, E., Roth, L., Seal, D., Shaffer, S., Shimada, J., Umland, J., Werner, M., Oskin, M., Burbank, D., Alsdorf, D., 2007. The Shuttle Radar Topography Mission. *Reviews of Geophysics*, 45(2), RG2004. <https://doi.org/10.1029/2005RG000183>
- Featherstone W.E., 2002. Tests of two forms of Stokes's integral using a synthetic gravity field based on spherical harmonics. In: Grafarend E.W., Krumm F.W., Schwarze V.S., (eds.) *Geodesy-The Challenge of the 3rd Millennium*, pp. 163–171. Springer. https://doi.org/10.1007/978-3-662-05296-9_17
- Featherstone, W., 1998. Do we need a gravimetric geoid or a model of the Australian height datum to transform GPS Heights in Australia? *The Australian Surveyor*, 43(4), 273–280.
- Featherstone, W.E., 1992. A GPS controlled gravimetric determination of the geoid of the British Isles. Ph.D. Thesis, Oxford University, United Kingdom.
- Featherstone, W.E., 2000. Refinement of gravimetric geoid using GPS and leveling data. *Journal of Surveying Engineering*, 126(2), 27–56. [https://doi.org/10.1061/\(ASCE\)0733-9453\(2000\)126:2\(27\)](https://doi.org/10.1061/(ASCE)0733-9453(2000)126:2(27))

- Featherstone, W.E., 2001. Absolute and relative testing of gravimetric geoid models using Global Positioning System and orthometric height data. *Computers & Geosciences*, 27(7), 807–814. [https://doi.org/10.1016/S0098-3004\(00\)00169-2](https://doi.org/10.1016/S0098-3004(00)00169-2)
- Featherstone, W.E., 2003. Software for computing five existing types of deterministically modified integration kernel for gravimetric geoid determination. *Computers & Geosciences*, 29(2), 183–193. [https://doi.org/10.1016/S0098-3004\(02\)00074-2](https://doi.org/10.1016/S0098-3004(02)00074-2)
- Featherstone, W.E., 2013. Deterministic, stochastic, hybrid and band-limited modifications of Hotine's integral. *Journal of Geodesy*, 87(5), 487–500. <https://doi.org/10.1007/s00190-013-0612-9>
- Featherstone, W.E., Dentith, M.C., 1997. A geodetic approach to gravity data reduction for geophysics. *Computers & Geosciences*, 23(10), 1063–1070. [https://doi.org/10.1016/S0098-3004\(97\)00092-7](https://doi.org/10.1016/S0098-3004(97)00092-7)
- Featherstone, W.E., Filmer, M.S., 2012. The north-south tilt in the Australian Height Datum is explained by the ocean's mean dynamic topography. *Journal of Geophysical Research: Oceans*, 117(C8), C08035. <https://doi.org/10.1029/2012JC007974>
- Featherstone, W.E., Goyal, R., 2022. Digitisation and analysis of historical deflections of the vertical in India. Accepted. *Survey Review*. <https://doi.org/10.1080/00396265.2022.2088016>
- Featherstone, W.E., Kirby, J.F., 2000. The reduction of aliasing in gravity anomalies and geoid heights using digital terrain data. *Geophysical Journal International*, 141(1), 204–212. <https://doi.org/10.1046/j.1365-246X.2000.00082.x>
- Featherstone, W.E., Kuhn, M., 2006. Height systems and vertical datums: A review in the Australian context. *Journal of Spatial Science*, 51(1), 21–41. <https://doi.org/10.1080/14498596.2006.9635062>
- Featherstone, W.E., Lichti, D.D., 2009. Fitting gravimetric geoid models to vertical deflections. *Journal of Geodesy*, 83(6), 583–589. <https://doi.org/10.1007/s00190-008-0263-4>
- Featherstone, W.E., Morgan, L., 2007. Validation of the AUSGeoid98 model in Western Australia using historic astrogeodetically observed deviations of the vertical. *Journal of the Royal Society of Western Australia*, 90(3), 143–150.
- Featherstone, W.E., Olliver, J.G., 1997. A method to validate gravimetric-geoid computation software based on Stokes's integral formula. *Journal of Geodesy*, 71(9), 571–576. <https://doi.org/10.1007/s001900050125>
- Featherstone, W.E., Sideris, M.G., 1998. Modified Kernels in Spectral Geoid Determination: First Results from Western Australia. In: Forsberg, R., Feissel, M., Dietrich, R., (eds.) *Geodesy on the Move*. International Association of Geodesy Symposia, vol. 119, pp. 188-193. Springer. https://doi.org/10.1007/978-3-642-72245-5_26
- Featherstone, W.E., Sproule, D.M., 2006. Fitting AUSGeoid98 to the Australian height datum using GPS-levelling and least squares collocation: Application of a cross-validation technique. *Survey Review*, 38(301), 573–582. <https://doi.org/10.1179/sre.2006.38.301.573>
- Featherstone, W.E., Evans, J.D., Olliver, J.G., 1998. A Meissl-modified Vaníček and Kleusberg kernel to reduce the truncation error in gravimetric geoid computations. *Journal of Geodesy*, 72(3), 154–160. <https://doi.org/10.1007/s001900050157>

- Featherstone, W.E., Kearsley, A.H.W., Gilliland, J.R., 1997. Data preparations for a new Australian gravimetric geoid. *Australian Surveyor*, 42(1), 33–44. <https://doi.org/10.1080/00050342.1997.10558664>
- Featherstone, W.E., Lyon, T.J., McCubbine, J.C., 2019. Potentially misleading GPS leveling–based assessment of gravimetric geoid or quasigeoid models due to vertical land motion and different GPS processing software. *Journal of Surveying Engineering*, 145(4), 04019015. [https://doi.org/10.1061/\(ASCE\)SU.1943-5428.0000293](https://doi.org/10.1061/(ASCE)SU.1943-5428.0000293)
- Featherstone, W.E., Kirby, J.F., Hirt, C., Filmer, M.S., Claessens, S.J., Brown, N.J., Hu, G., Johnston, G.M., 2011. The AUSGeoid09 model of the Australian height datum. *Journal of Geodesy*, 85(3), 133–150. <https://doi.org/10.1007/s00190-010-0422-2>
- Featherstone, W.E., Kirby, J.F., Kearsley, A.H.W., Gilliland, J.R., Johnston, G.M., Steed, J., Forsberg, R., Sideris, M.G., 2001. The AUSGeoid98 geoid model of Australia: data treatment, computations and comparisons with GPS–levelling data. *Journal of Geodesy*, 75(5–6), 313–330. <https://doi.org/10.1007/s001900100177>
- Featherstone, W.E., McCubbine, J.C., Brown, N.J., Claessens, S.J., Filmer, M.S., Kirby, J.F., 2018. The first Australian gravimetric quasigeoid model with location-specific uncertainty estimates. *Journal of Geodesy*, 92(2), 149–168. <https://doi.org/10.1007/s00190-017-1053-7>
- Fei, Z.L., Sideris, M.G., 2000. A new method for computing the ellipsoidal correction for Stokes’s formula. *Journal of Geodesy*, 74(2), 223–231. <https://doi.org/10.1007/s001900050280>
- Fei, Z.L., Sideris, M.G., 2001. Corrections to “A new method for computing the ellipsoidal correction for Stokes’s formula”. *Journal of Geodesy*, 74(9), 671. <https://doi.org/10.1007/s001900000131>
- Filmer, M.S., Featherstone, W.E., Kuhn, M., 2010. The effect of EGM2008-based normal, normal-orthometric and Helmert orthometric height systems on the Australian levelling network. *Journal of Geodesy*, 84(8), 501–513. <https://doi.org/10.1007/s00190-010-0388-0>
- Filmer, M.S., Featherstone, W.E., Kuhn, M., 2014. Erratum to: The effect of EGM2008-based normal, normal-orthometric and Helmert orthometric height systems on the Australian levelling network. *Journal of Geodesy*, 88(1), 93–93. <https://doi.org/10.1007/s00190-013-0666-8>
- Fischer, I., 1961. The present extent of the astro-geodetic geoid and the geodetic world datum derived from it. *Bulletin Géodésique*, 61(1), 245–264. <https://doi.org/10.1007/BF02854151>
- Fischer, I., 1968. A Modification of the Mercury datum. Technical Report, 67, Army Topographic Command. USA.
- Fischer, I., 1975. Does mean sea level slope up or down toward north?. *Bulletin Géodésique*, 115, 17–26. <https://doi.org/10.1007/BF02523939>
- Fischer, I., 1977. Mean sea level and the marine geoid—An analysis of concepts. *Marine Geodesy*, 1(1), 37–59. <https://doi.org/10.1080/01490417709387950>
- Flury, J., Rummel, R., 2009. On the geoid–quasigeoid separation in mountain areas. *Journal of Geodesy*, 83(9), 829–847. <https://doi.org/10.1007/s00190-009-0302-9>

- Flury, J., Rummel, R., 2011. On the computation of the geoid–quasigeoid separation: Response to “A strict formula for geoid-to-quasigeoid separation” by Lars Sjöberg. *Journal of Geodesy*, 85(3), 185–186. <https://doi.org/10.1007/s00190-011-0447-1>
- Foroughi, I., Tenzer, R., 2017. Comparison of different methods for estimating the geoid-to-quasigeoid separation. *Geophysical Journal International*, 210(2), 1001–1020. <https://doi.org/10.1093/gji/ggx221>
- Foroughi, I., Vaníček, P., Kingdon, R.W., Goli, M., Sheng, M., Afrasteh, Y., Novák, P., Santos, M.C., 2019. Sub-centimetre geoid. *Journal of Geodesy*, 93(6), 849–868. <https://doi.org/10.1007/s00190-018-1208-1>
- Foroughi, I., Vaníček, P., Novák, P., Kingdon, R.W., Sheng, M., Santos, M.C., 2017a. Optimal Combination of Satellite and Terrestrial Gravity Data for Regional Geoid Determination Using Stokes-Helmert’s Method, the Auvergne Test Case. In: Vergos, G., Pail, R., Barzaghi, R., (eds.) *International Symposium on Gravity, Geoid and Height Systems 2016*. International Association of Geodesy Symposia, vol. 148, pp. 37-43. Springer. https://doi.org/10.1007/1345_2017_22
- Foroughi, I., Vaníček, P., Sheng, M., Kingdon, R.W., Santos, M.C., 2017b. In defense of the classical height system. *Geophysical Journal International*, 211(2), 1154–1161. <https://doi.org/10.1093/gji/ggx366>
- Forsberg, R., 1984. Study of terrain reductions, density anomalies and geophysical inversion methods in gravity field modelling. Department of Geodetic Science and Surveying Report No. 355. The Ohio State University, Columbus, USA. <https://earthsciences.osu.edu/sites/earthsciences.osu.edu/files/report-355.pdf>
- Forsberg, R., 1985. Gravity field terrain effect computations by FFT. *Bulletin Géodésique*, 59(4), 342–360. <https://doi.org/10.1007/BF02521068>
- Forsberg, R., Featherstone, W., 1998. Geoids and cap sizes. In: Forsberg, R., Feissel, M., Dietrich, R., (eds.) *Geodesy on the Move*. International Association of Geodesy Symposia, vol. 119, pp. 194-200. Springer. https://doi.org/10.1007/978-3-642-72245-5_27
- Forsberg, R., Sideris, M.G., 1993. Geoid computations by the multi-band spherical FFT approach. *manuscripta geodaetica*, 18(2), 82-90.
- Forsberg, R., Tscherning, C.C., 2008. An overview manual for the GRAVSOFTE geodetic gravity field modelling programs. https://ftp.space.dtu.dk/pub/RF/gravsoft_manual2014.pdf
- Förste, C., Bruinsma, S.L., Abrikosov, O., Lemoine, J.-M., Schaller, T., Götze, H.-J., Ebbing, J., Marty, J.C., Flechtner, F., Balmino, G., Biancale, R., 2014. EIGEN-6C4: The latest combined global gravity field model including GOCE data up to degree and order 2190 of GFZ Potsdam and GRGS Toulouse. GFZ Data Services. <https://doi.org/10.5880/icgem.2015.1>
- Fotopoulos, G., 2003. An analysis on the optimal combination of geoid, orthometric and ellipsoidal height data. Ph.D. Thesis, University of Calgary, Alberta, Canada. https://www.ucalgary.ca/engo_webdocs/MGS/03.20185.GFotopoulos.pdf
- Fotopoulos, G., Featherstone, W.E., Sideris, M.G., 2002. Fitting a gravimetric geoid model to the Australian height datum via GPS data. In: Tziavos, I.N., (ed.) *Proceedings of the 3rd Meeting of the International Gravity and Geoid Commission*, pp. 173-178. Thessaloniki, Greece

- Fryer, J.G., 1972. The Australian geoid. *Australian Surveyor*, 24(4), 203-214. <https://doi.org/10.1080/00050326.1972.10440630>
- Fukuda, Y., Kuroda, J., Takabatake, Y., Itoh, J., Murakami, M., 1997. Improvement of JGEOID 93 by the geoidal heights derived from GPS/Leveling survey. In: Segawa, J., Fujimoto, H., Okubo, S., (eds.) *Gravity, Geoid and Marine Geodesy*. International Association of Geodesy Symposia, vol. 117, pp. 589-596. Springer. https://doi.org/10.1007/978-3-662-03482-8_78
- G&RB – Geodetic & Research Branch, 2018. Report on redefinition of Indian Vertical Datum IVD2009. Geodetic and Research Branch, Survey of India, Dehradun, India.
- Gallant, J., 2011. Adaptive smoothing for noise DEMs. In: Hengl, T., (ed.) *Proceedings of Geomorphometry 2011*, pp. 37-40. Redlands, California.
- Gatti, A., Reguzzoni, M., Migliaccio, F., Sansò, F., 2016. Computation and assessment of the fifth release of the GOCE-only space-wise solution. In: 1st Joint Commission 2 and IGFS Meeting, 19-23 September 2016. Thessaloníki, Greece.
- Gaur, V. K., 1981. Determination of partial geoidal parameters over the Indian sub-continent. *Journal of Earth System Science*, 90(2), 147–153. <https://doi.org/10.1007/BF02880259>
- GETECH, 2006. Gravity data compilation of India. Report No. G0610. University of Leeds, United Kingdom.
- Ghildyal, H.S., Kumar, A., 1984. Global mean sea level investigations: Discrepancy between the local mean sea level of the Bay of Bengal and the local mean sea level of the Arabian Sea, Technical Paper, Survey of India, Dehradun, India.
- Gilardoni, M., Reguzzoni, M., Sampietro, D., 2016. GECO: A global gravity model by locally combining GOCE data and EGM2008. *Studia Geophysica et Geodaetica*, 60(2), 228–247. <https://doi.org/10.1007/s11200-015-1114-4>
- GMSI, 1975. Gravity map series of India on 1:5 million scale with 10 mGal contour interval (GPH 1-4). National Geophysical Research Institute, Hyderabad, India.
- Gomez, M.E., Bagu, D.R., Del Cogliano, D., Perdomo, R.A., 2013. Evaluation of terrain corrections through FFT and classical integration in two selected areas of the Andes and their impact on geoidal heights. *Boletim de Ciências Geodésicas*, 19(3), 407–419. <https://doi.org/10.1590/S1982-21702013000300004>
- Goos, J.M., Featherstone, W.E., Kirby, J.F., Holmes, S.A., 2003. Experiments with two different approaches to gridding terrestrial gravity anomalies and their effect on regional geoid computation. *Survey Review*, 37(288), 92–112. <https://doi.org/10.1179/sre.2003.37.288.92>
- Goyal, R., Ågren, J., Featherstone, W.E., Sjöberg, L.E., Dikshit, O., Balasubramanian, N., 2022. Empirical comparison between stochastic and deterministic modifiers over the French Auvergne geoid computation test-bed. *Survey Review*, 54(382), 57-69. <https://doi.org/10.1080/00396265.2021.1871821>
- Goyal, R., Dikshit, O., Balasubramania, N., 2019a. Evaluation of global geopotential models: A case study for India. *Survey Review*, 51(368), 402–412. <https://doi.org/10.1080/00396265.2018.1468537>

- Goyal, R., Featherstone, W.E., Dikshit, O., Balasubramanian, N., 2021a. Comparison and validation of satellite-derived digital surface/elevation models over India. *Journal of the Indian Society of Remote Sensing*, 49(4), 971–986. <https://doi.org/10.1007/s12524-020-01273-7>
- Goyal, R., Featherstone, W.E., Claessens, S.J., Devaraju, B., Balasubramanian, N., Dikshit, O., 2019b. A numerical approach to the mass-prism integration for fast determination of terrain corrections. In: 27th IUGG General Assembly, Montréal, Québec, Canada.
- Goyal, R., Featherstone, W.E., Claessens, S.J., Dikshit, O., Balasubramanian, N., 2021b. An experimental Indian gravimetric geoid model using Curtin University's approach. *Terrestrial, Atmospheric and Oceanic Sciences*, online first. <https://doi.org/10.3319/TAO.2021.08.10.02>
- Goyal, R., Featherstone, W.E., Tsoulis, D., Dikshit, O., 2020. Efficient spatial-spectral computation of local planar gravimetric terrain corrections from high-resolution digital elevation models. *Geophysical Journal International*, 221(3), 1820–1831. <https://doi.org/10.1093/gji/ggaa107>
- Gradshteyn, I.S., Ryzhik, I.M., 1980. *Tables of integrals, series and products*. Academic Press, New York, USA.
- Grafarend, E.W., Ardalan, A.A., 1997. W_0 : an estimate in the Finnish height datum N60, epoch 1993.4, from twenty-five GPS points of the Baltic sea level project. *Journal of Geodesy*, 71(11), 673–679. <https://doi.org/10.1007/s001900050134>
- Grigoriadis, V.N., Vergos, G.S., Barzaghi, R., Carrion, D., Koç, Ö., 2021. Collocation and FFT-based geoid estimation within the Colorado 1 cm geoid experiment. *Journal of Geodesy*, 95(5), 52. <https://doi.org/10.1007/s00190-021-01507-7>
- Groten, E., 1980. A remark on M. Heikkinen's paper "On the Honkasalo term in tidal corrections to gravimetric observations", *B.G.* 53, 3, 239–245. *Bulletin Géodésique*, 54(2), 221–222. <https://doi.org/10.1007/BF02521250>
- Groten, E., 2004. Fundamental parameters and current (2004) best estimates of the parameters of common relevance to astronomy, geodesy, and geodynamics by Erwin Groten, IPGD, Darmstadt. *Journal of Geodesy*, 77(10-11), 724–797. <https://doi.org/10.1007/s00190-003-0373-y>
- Gruber, S., Huggel, C., Pike, R., 2009. Modelling mass movements and landslide susceptibility. in: Hengl, T., Reuter, H.I., (eds.), *Geomorphometry: concepts, software, applications*. *Developments in Soil Science*, vol. 33, pp. 527–550. Elsevier.
- GSI-NGRI, 2006. Gravity map series of India on 1:2,000,000 scale with 5mGal contour interval. Geological Survey of India & National Geophysical Research Institute, India.
- Guimarães, G.do-N., Blitzkow, D., Barzaghi, R., de Matos, A.C.O.C., 2014. The computation of the geoid model in the state of São Paulo using two methodologies and GOCE models. *Boletim de Ciências Geodésicas*, 20(1), 183–203. <https://doi.org/10.1590/s1982-21702014000100012>
- Gulatee, B.L., 1948. Value of gravity at Dehra Dun. Survey of India Technical report No. 2. Survey of India, Dehradun, India.
- Gulatee, B.L., 1955. Deviation of the vertical in India. Survey of India Technical paper No. 9. Survey of India, Dehradun, India.

- Gulatee, B.L., 1956. Gravity data in India. Survey of India Technical Paper No. 10. Survey of India, Dehradun, India.
- Haagmans, R.R.N., de Min, E., van Geldren, M., 1993. Fast evaluation of convolution integrals on the sphere using 1DFFT, and a comparison with existing methods for Stokes's integral. *manuscripta geodaetica*, 18, 227–241.
- Hackney, R.I., Featherstone, W.E., 2003. Geodetic versus geophysical perspectives of the 'gravity anomaly.' *Geophysical Journal International*, 154(1), 35–43. <https://doi.org/10.1046/j.1365-246X.2003.01941.x>
- Hagiwara, Y., 1972. Truncation error formulas for the geoidal height and the deflection of the vertical. *Bulletin Géodésique*, 106(1), 453–466. <https://doi.org/10.1007/BF02522052>
- Hagiwara, Y., 1976. A new formula for evaluating the truncation error coefficient. *Bulletin Géodésique*, 50(2), 131–135. <https://doi.org/10.1007/BF02522312>
- He, L., Chu, Y., Yu, N., 2017. Evaluation of the geopotential value W_0^{LVD} of China. *Geodesy and Geodynamics*, 8(6), 408–412. <https://doi.org/10.1016/j.geog.2017.05.004>
- Heck B., Seitz K., 2007. A comparison of the tesseroid, prism and point-mass approaches for mass reductions in gravity field modelling. *Journal of Geodesy*, 81(2), 121–136. <https://doi.org/10.1007/s00190-006-0094-0>
- Heck, B., 1993a. A revision of Helmert's second method of condensation in geoid and quasigeoid determination. In: Montag, H., Reigber, C., (eds.) *Geodesy and Physics of the Earth. International Association of Geodesy Symposia*, vol 112., pp. 246-251. Springer. https://doi.org/10.1007/978-3-642-78149-0_58
- Heck, B., 1993b. Tidal corrections in geodetic height determination. In: Linkwitz, K., Eisele, V., Mönicke, H.J., (eds.) *Applications of Geodesy to Engineering. International Association of Geodesy Symposia*, vol 108, pp. 11-24. Springer. https://doi.org/10.1007/978-3-642-77958-9_2
- Heck, B., Grüniger, W., 1987. Modification of Stokes's integral formula by combining two classical approaches. In: *Proceedings of the XIX General Assembly of the International Union of Geodesy and Geophysics*, vol 2., pp. 309–337. Vancouver, Canada.
- Heck, B., Seitz, K., 2003. Solutions of the linearized geodetic boundary value problem for an ellipsoidal boundary to order e^3 . *Journal of Geodesy*, 77(3–4), 182–192. <https://doi.org/10.1007/s00190-002-0309-y>
- Heikkinen, M., 1979. On the Honkasalo term in tidal corrections to gravimetric observations. *Bulletin Géodésique*, 53(3), 239–245. <https://doi.org/10.1007/BF02523955>
- Heikkinen, M., 1978. On the tide-generating forces. Publication of the Finnish Geodetic Institute No. 85. Helsinki, Finland.
- Heiskanen, W.A., Moritz, H., 1967. *Physical geodesy*. W H Freeman and Co., San Francisco and London.
- Heiskanen W.A., Vening Meinesz F.A., 1958. *The Earth and its gravity field*. McGraw-Hill, New York.

- Helmert, F.R., 1884. *Mathematical and physical theories of higher geodesy, Part-II: The physical theories.* (English translation). B.G. Teubner, Printing and publishing company, Leipzig, Germany.
- Hernández-Navarro, A., 2004. The submetric geoid of Mexico. In: FIG working week, Athens, Greece.
http://www2.unb.ca/gge/Research/GRL/GeodesyGroup/SHGeo/8_Results/2004_Hernandez-Navarro.pdf
- Hildenbrand, T.G., Briesacher, A., Flanagan, G., Hinze, W.J., Hittelman, A.M., Keller, G.R., Kucks, R.P., Plouff, D., Roest, W., Seeley, J., Smith, D.A., Webring, M., 2002. Rationale and operational plan to upgrade the U.S. gravity database. Open-File Report 02-463, USGS publications. <https://doi.org/10.3133/ofr02463>
- Hipkin, R.G., 2004. Ellipsoidal geoid computation. *Journal of Geodesy*, 78(3), 167–179.
<https://doi.org/10.1007/s00190-004-0389-y>
- Hirt, C., 2011. Mean kernels to improve gravimetric geoid determination based on modified Stokes's integration. *Computers & Geosciences*, 37(11), 1836–1842.
<https://doi.org/10.1016/j.cageo.2011.01.005>
- Hirt, C., 2012. Efficient and accurate high-degree spherical harmonic synthesis of gravity field functionals at the Earth's surface using the gradient approach. *Journal of Geodesy*, 86(9), 729–744. <https://doi.org/10.1007/s00190-012-0550-y>
- Hirt, C., 2014. Digital Terrain Models. In: Grafarend, E., (ed.) *Encyclopedia of Geodesy*, pp. 1–6.
https://doi.org/10.1007/978-3-319-02370-0_31-1.
- Hirt, C., Claessens, S., Fecher, T., Kuhn, M., Pail, R., Rexer, M., 2013. New ultrahigh-resolution picture of Earth's gravity field. *Geophysical Research Letters*, 40(16), 4279–4283.
<https://doi.org/10.1002/grl.50838>
- Hobson, E.W., 1931. *The theory of spherical and ellipsoidal harmonics.* Cambridge University Press, England.
- Honkasalo, T., 1964. On the tidal gravity correction. *Bolletino di Geofisica teorica ed applicate*, VI:21, 32–36.
- Hörmander, L., 1976. The boundary problems of physical geodesy. *Archive for Rational Mechanics and Analysis*, 62(1), 1–52. <https://doi.org/10.1007/BF00251855>
- Hotine, M., 1969. *Mathematical Geodesy.* ESSA Monograph 2, Department of Commerce, Washington, USA.
- Huang, J., 2002. Computational methods for the discrete downward continuation of the Earth gravity and effects of lateral topographic mass density variation of gravity and the geoid. Ph.D. Thesis, University of New Brunswick, Fredericton, Canada.
<http://www2.unb.ca/gge/Pubs/TR216.pdf>
- Huang, J., Sideris, M.G., Vaníček, P., Tziavos, I.N., 2003a. Numerical investigation of downward continuation techniques for gravity anomalies. *Bollettino di Geofisica Teorica ed Applicata*, LXII(1), 34–48.

- Huang, J., Vaníček, P., Novák, P., 2000. An alternative algorithm to FFT for the numerical evaluation of Stokes's integral. *Studia Geophysica et Geodaetica*, 44(3), 374–380. <https://doi.org/10.1023/A:1022160504156>
- Huang, J., Vaníček, P., Pagiatakis, S.D., Brink, W., 2001. Effect of topographical density on geoid in the Canadian Rocky mountains. *Journal of Geodesy*, 74(11), 805–815. <https://doi.org/10.1007/s001900000145>
- Huang, J., Véronneau, M., 2013. Canadian gravimetric geoid model 2010. *Journal of Geodesy*, 87(8), 771–790. <https://doi.org/10.1007/s00190-013-0645-0>
- Huang, J., Véronneau, M., Pagiatakis, S.D., 2003b. On the ellipsoidal correction to the spherical Stokes solution of the gravimetric geoid. *Journal of Geodesy*, 77(3–4), 171–181. <https://doi.org/10.1007/s00190-003-0317-6>
- Hunegnaw, A., 2001. Geoid determination over Ethiopia with emphasis on downward continuation of gravity anomalies. Ph.D. Thesis, Royal Institute of Technology (KTH), Stockholm, Sweden.
- de Graaff Hunter, J., 1932. The hypothesis of isostasy. *Geophysical Supplements to the Monthly Notices of the Royal Astronomical Society*, 3(1), 42–51. <https://doi.org/10.1111/j.1365-246X.1932.tb03657.x>
- Hwang, C., Hsu, H.-J., Featherstone, W.E., Cheng, C.-C., Yang, M., Huang, W., Wang, C.-Y., Huang, J.-F., Chen, K.-H., Huang, C.-H., Chen, H., Su, W.-Y., 2020. New gravimetric-only and hybrid geoid models of Taiwan for height modernisation, cross-island datum connection and airborne LiDAR mapping. *Journal of Geodesy*, 94(9), 83. <https://doi.org/10.1007/s00190-020-01412-5>
- Ihde, J., Sánchez, L., Barzaghi, R., Drewes, H., Förste, C., Gruber, T., Liebsch, G., Marti, U., Pail, R., Sideris, M., 2017. Definition and proposed realization of the International Height Reference System (IHRs). *Surveys in Geophysics*, 38(3), 549–570. <https://doi.org/10.1007/s10712-017-9409-3>
- Ince, E.S., Barthelmes, F., Reißland, S., Elger, K., Förste, C., Flechtner, F., Schuh, H., 2019. ICGEM – 15 years of successful collection and distribution of global gravitational models, associated services, and future plans. *Earth System Science Data*, 11(2), 647–674. <https://doi.org/10.5194/essd-11-647-2019>
- Inerbayeva, D., 2010. Determination of a gravimetric geoid model Kazakhstan using the KTH method. M.Sc. Thesis, Royal Institute of Technology (KTH), Stockholm, Sweden. <http://kth.diva-portal.org/smash/get/diva2:465930/FULLTEXT01.pdf>
- Işık, M.S., Erol, B., 2016. Geoid determination using GOCE-based models in Turkey. In: European Geosciences Union General Assembly 2016. Vienna, Austria.
- Jafarzaghan, K., Merwade, V., 2017. A DEM-based approach for large-scale floodplain mapping in ungauged watersheds. *Journal of Hydrology*, 550, 650–662. <https://doi.org/10.1016/j.jhydrol.2017.04.053>.
- Janák, J., Vaníček, P., Foroughi, I., Kingdon, R., Sheng, M.B., Santos, M.C., 2017. Computation of precise geoid model of Auvergne using current UNB Stokes-Helmert's approach. *Contributions to Geophysics and Geodesy*, 47(3), 201–229. <https://doi.org/10.1515/congeo-2017-0011>

- Jekeli, C., 1980. Reducing the error in geoid undulation computations by modifying Stokes's function. Department of Geodetic Science and Surveying Report No. 301. The Ohio State University, Columbus, USA. <https://earthsciences.osu.edu/sites/earthsciences.osu.edu/files/report-301.pdf>
- Jekeli, C., 1981a. Modifying Stokes' function to reduce the error of geoid undulation computations. *Journal of Geophysical Research*, 86(B8), 6985. <https://doi.org/10.1029/JB086iB08p06985>
- Jekeli, C., 1981b. The downward continuation to the Earth's surface of truncated spherical and ellipsoidal harmonic series of the gravity and height anomalies. Department of Geodetic Science and Surveying Report No. 323. The Ohio State University, Columbus, USA. <https://earthsciences.osu.edu/sites/earthsciences.osu.edu/files/report-323.pdf>
- Jekeli, C., 1999. An analysis of vertical deflections derived from high-degree spherical harmonic models. *Journal of Geodesy*, 73(1), 10–22. <https://doi.org/10.1007/s001900050213>
- Jekeli, C., 2000. Heights, the geopotential, and vertical datums. Department of Geodetic Science and Surveying Report No. 459. The Ohio State University, Columbus, USA. <https://earthsciences.osu.edu/sites/earthsciences.osu.edu/files/report-459.pdf>
- Jiang, T., Dang, Y., Guo, C., Zhang, C., 2021. Realization of the international height reference system in the region of Mount Qomolangma (Everest). In: International Association of Geodesy Scientific Assembly 2021. Beijing, China.
- Jiang, T., Dang, Y., Zhang, C., 2020. Gravimetric geoid modeling from the combination of satellite gravity model, terrestrial and airborne gravity data: A case study in the mountainous area, Colorado. *Earth, Planets and Space*, 72(1), 189. <https://doi.org/10.1186/s40623-020-01287-y>
- Jiang, Z., Duquenne, H., 1996. On the combined adjustment of a gravimetrically determined geoid and GPS levelling stations. *Journal of Geodesy*, 70(8), 505–514. <https://doi.org/10.1007/BF00863623>
- Kaula, W.M., 1959. Statistical and harmonic analysis of gravity. *Journal of Geophysical Research*, 64(12), 2401–2421. <https://doi.org/10.1029/JZ064i012p02401>
- Kearsley, A.H.W., 1986. The determination of precise geoid height differences using ring integration. *Bollettino di Geodesia e Scienze Affini*, XLV(2), 151-174.
- Kearsley, A.H.W., Ahmad, Z., Chan, A., 1993. National height datums, levelling, GPS heights and geoids. *Australian Journal of Geodesy, Photogrammetry, and Surveying*, 59, 53-88.
- Keay, J., 2000. *The great arc: the dramatic tale of how India was mapped and Everest was named.* HarperCollins publisher, New York, USA.
- Kern, M., 2003. An analysis of the combination and downward continuation of satellite, airborne and terrestrial gravity data. Ph.D. Thesis, University of Calgary, Alberta, Canada. https://www.ucalgary.ca/engo_webdocs/KPS/03.20172.MKern.pdf
- Kern, M., Schwarz, K.K.P.P., Sneeuw, N., 2003. A study on the combination of satellite, airborne, and terrestrial gravity data. *Journal of Geodesy*, 77(3–4), 217–225. <https://doi.org/10.1007/s00190-003-0313-x>

- Khosla, K.L., Arur, M.G., Bains, P.S., 1982. Gravimetric and astro-geodetic geoids and mean free-air anomalies in India. *Bulletin Géodésique*, 56(3), 196–208. <https://doi.org/10.1007/BF02525581>
- Kiamehr, R., 2006. Precise gravimetric geoid model for Iran based on GRACE and SRTM data and the least-squares modification of Stokes' formula: with some geodynamic interpretations. Ph.D. Thesis, Royal Institute of Technology (KTH). Stockholm, Sweden. <https://www.diva-portal.org/smash/get/diva2:10840/FULLTEXT01.pdf>
- Kingdon, R., Vaníček, P., 2011. Poisson downward continuation solution by the Jacobi method. *Journal of Geodetic Science*, 1(1), 74–81. <https://doi.org/10.2478/v10156-010-0009-0>
- Kingdon, R., Vaníček, P., Santos, M., 2009. Modeling topographical density for geoid determination. *Canadian Journal of Earth Sciences*, 46(8), 571–585. <https://doi.org/10.1139/E09-018>
- Kingdon, R., Vaníček, P., Santos, M., Ellmann, A., Tenzer, R., 2005. Toward improved orthometric height system for Canada. *Geomatica*, 59(3), 241–249. <https://doi.org/10.5623/geomat-2005-0033>
- Kinoshita, H., 1994. Is the equatorial radius of the Earth a primary constant, a derived constant, or a defining constant? *Studia Geophysica et Geodaetica*, 38(2), 109–116. <https://doi.org/10.1007/BF02295907>
- Kirby, J.F., Featherstone, W.E., 1997. A study of zero- and first-degree terms in geopotential models over Australia. *Geomatics Research Australasia*, 66, 93–108.
- Kirby, J.F., Featherstone, W.E., 1999. Terrain correcting Australian gravity observations using the national digital elevation model and the fast Fourier transform. *Australian Journal of Earth Sciences*, 46(4), 555–562. <https://doi.org/10.1046/j.1440-0952.1999.00731.x>
- Kirby, J.F., Featherstone, W.E., 2001. Anomalously large gradients in Version 1 of the “GEODATA 9 SECOND” digital elevation model of Australia, and their effects on gravimetric terrain corrections. *Cartography*, 30(1), 1–10. <https://doi.org/10.1080/00690805.2001.9714131>
- Kirby, J.F., Featherstone, W.E., 2002. High-resolution grids of gravimetric terrain correction and complete Bouguer corrections over Australia. *Exploration Geophysics*, 33(4), 161. <https://doi.org/10.1071/EG02161>
- Klose, U., Ilk, K., 1993. A solution to the singularity problem occurring in the terrain correction formula. *manuscripta geodaetica*, 18(5), 263–279.
- Klu, A.M., 2015. Determination of a geoid model for Ghana using the Stokes-Helmert method. M.Sc. Thesis, University of New Brunswick, Fredericton, Canada. <http://www2.unb.ca/gge/Pubs/TR298.pdf>
- Knudsen, P., 1987. Estimation and modelling of the local empirical covariance function using gravity and satellite altimeter data. *Bulletin Géodésique*, 61(2), 145–160. <https://doi.org/10.1007/BF02521264>
- Koch, K.-R., 1968. Solution of the geodetic boundary value problem in case of a reference ellipsoid. Department of Geodetic Science and Surveying Report No. 104. The Ohio State University, Columbus, USA.

- Kotsakis, C., Fotopoulos, G., Sideris, M.G., 2001. Optimal fitting of gravimetric geoid undulations to GPS/levelling data using an extended similarity transformation model. In: The 27th Annual meeting joint with the 58th Eastern snow conference of the Canadian Geophysical Union, May 14-17. Ottawa, Canada.
- Kotsakis, C., Katsambalos, K., 2010. Quality analysis of global geopotential models at 1542 GPS/levelling benchmarks over the Hellenic mainland. *Survey Review*, 42(318), 327–344. <https://doi.org/10.1179/003962610X12747001420500>
- Kotsakis, C., Katsambalos, K., Ampatzidis, D., 2012 Estimation of the zero-height geopotential level W_0^{LVD} in a local vertical datum from inversion of co-located GPS, leveling and geoid heights: a case study in the Hellenic islands. *Journal of Geodesy*, 86(6), 423-439. <https://doi.org/10.1007/s00190-011-0530-7>
- Kotsakis, C., Sideris, M.G., 1999. On the adjustment of combined GPS/levelling/geoid networks. *Journal of Geodesy*, 73(8), 412–421. <https://doi.org/10.1007/s001900050261>
- Krarup, T., 1969. A contribution to the mathematical foundation of physical geodesy. Geodaetisk Institut, Meddelelse No. 44. Copenhagen, Denmark.
- Kuczynska-Siehien, J., Lyszkowicz, A., Birylo, M., 2016. Geoid determination for the area of Poland by the least squares modification of Stokes' formula. *Acta Geodynamica et Geomaterialia*, 13(1), 19–26. <https://doi.org/10.13168/AGG.2015.0041>
- Kuhn, M., 2001. Density modelling for geoid determination. In: Sideris, M.G., (ed.) *Gravity, Geoid and Geodynamics 2000*. International Association of Geodesy Symposia, vol. 123, pp. 271–276. Springer. https://doi.org/10.1007/978-3-662-04827-6_46
- Kuhn, M., 2003. Geoid determination with density hypotheses from isostatic models and geological information. *Journal of Geodesy*, 77(1–2), 50–65. <https://doi.org/10.1007/s00190-002-0297-y>
- Kuhn, M., Featherstone, W.E., 2005. Construction of a synthetic earth gravity model by forward gravity modelling. In: Sansò, F., (ed.) *A Window on the Future of Geodesy*. International Association of Geodesy Symposia, vol. 128, pp. 350–355. Springer. https://doi.org/10.1007/3-540-27432-4_60
- Kuhn, M., Featherstone, W.E., Kirby, J.F., 2009. Complete spherical Bouguer gravity anomalies over Australia. *Australian Journal of Earth Sciences*, 56(2), 213–223. <https://doi.org/10.1080/08120090802547041>
- Lagios, E., Chailas, S., Hipkin, R.G., 1996. Newly compiled gravity and topographic data banks of Greece. *Geophysical Journal International*, 126(1), 287–290. <https://doi.org/10.1111/j.1365-246X.1996.tb05287.x>
- Lasagna, P., 2017. Geoid modelling in the Sultanate of Oman. M.Sc. Thesis. The York University, Ontario, Canada. <http://hdl.handle.net/10315/33619>
- Lee, D.H., Yun, H.S., Jung, H.I., Cho, J.M., Cho, J.H., Jung, W.C., Hwang, J.S., 2013. Transformation of vertical datum surface in the coastal area using hybrid geoid models. *Journal of Coastal Research*, 2(65), 1427-1432. <https://doi.org/10.2112/SI65-241.1>
- Lemoine, F.G., Kenyon, S.C., Factor, J.K., Trimmer, R.G., Pavlis, N.K., Chinn, D.S., Cox, C.M., Klosko, S.M., Luthcke, S.B., Torrence, M.H., Wang, Y.M., Williamson, R.G., Pavlis, E.C., Rapp, R.H., Olson, T.R., 1998. The development of the joint NASA GSFC and NIMA

- geopotential model EGM96. NASA Technical Publication 1998-206861. GSFC, Maryland, USA.
- Li, C., Wang, Y., Ye, C., Wei, W., Zheng, B., Xu, B., 2019. A proposed delineation method for lake buffer zones in watersheds dominated by non-point source pollution. *Science of The Total Environment*, 660, 32–39. <https://doi.org/10.1016/j.scitotenv.2018.12.468>.
- Li, X., 2018. Using radial basis functions in airborne gravimetry for local geoid improvement. *Journal of Geodesy*, 92(5), 471–485. <https://doi.org/10.1007/s00190-017-1074-2>
- Li, X., Wang, Y., 2011. Comparisons of geoid models over Alaska computed with different Stokes' kernel modifications. *Journal of Geodetic Science*, 1(2), 136–142. <https://doi.org/10.2478/v10156-010-0016-1>
- Liu, Q., Schmidt, M., Sánchez, L., Willberg, M., 2020. Regional gravity field refinement for (quasi-) geoid determination based on spherical radial basis functions in Colorado. *Journal of Geodesy*, 94(10), 99. <https://doi.org/10.1007/s00190-020-01431-2>
- Macomber, M.M., 1984. World Geodetic System 1984. Defense Mapping Agency, Washington D.C., USA. <https://apps.dtic.mil/sti/pdfs/ADA147409.pdf>
- Mader, K., 1954. Die orthometrische schwerekorrektion des präzisions-nivellements in den hohen tauern (The orthometric weight correction of precision levelling in high terrain). *Österreichische Zeitschrift für Vermessungswesen, Sonderheft 15*, Vienna.
- Mäkinen, J., 2017. The permanent tide and the International Height Reference System IHRS. In: IAG-IASPEI Joint Scientific Assembly, July 30 - August 4. Kobe, Japan. https://ihrs.dgfi.tum.de/fileadmin/JWG_2015/04_5_SplinterMeeting_JWG012_Kobe_2017_TideSystem_IHRS_Maekinen.pdf
- Mäkinen, J., 2021. The permanent tide and the International Height Reference Frame IHRF. *Journal of Geodesy*, 95(9), 106. <https://doi.org/10.1007/s00190-021-01541-5>
- Mäkinen, J., Ihde, J., 2009. The permanent tide in height systems. In: Sideris, M.G., (eds.) *Observing our Changing Earth. International Association of Geodesy Symposia*, vol. 133, pp. 81-87. Springer. https://doi.org/10.1007/978-3-540-85426-5_10
- Marti, U., 1997. Geoid der Schweiz 1997. Geodätisch geophysikalische Arbeiten in der Schweiz No. 56. Schweizerische Geodätische Kommission, Zürich, Switzerland.
- Martinec, Z., 1993. Effect of lateral density variations of topographical masses in view of improving geoid model accuracy over Canada. Final report under DSS contract No. 23244-2-4356/01-SS. Geodetic Survey of Canada, Ottawa, Canada.
- Martinec, Z., 1996. Stability investigations of a discrete downward continuation problem for geoid determination in the Canadian Rocky Mountains. *Journal of Geodesy*, 70(11), 805–828. <https://doi.org/10.1007/BF00867158>
- Martinec, Z., 1998. Boundary-value problems for gravimetric determination of a precise geoid. Springer. <https://doi.org/10.1007/BFb0010337>
- Martinec, Z., Grafarend, E.W., 1997. Solution to the Stokes boundary-value problem on an ellipsoid of revolution. *Journal of Geodesy*, 41(2), 103–129. <https://doi.org/10.1023/A:1023380427166>

- Martinec, Z., Vaníček, P., 1994a. Direct topographical effect of Helmert's condensation for a spherical approximation of the geoid. *manuscripta geodaetica*, 19, 257-268.
- Martinec, Z., Vaníček, P., 1994b. Indirect effect of topography in the Stokes-Helmert technique for a spherical approximation of the geoid. *manuscripta geodaetica*, 19, 213-219.
- Martinec, Z., Vaníček, P., Mainville, A., Véronneau, M., 1996. Evaluation of topographical effects in precise geoid computation from densely sampled heights. *Journal of Geodesy*, 70(11), 746–754. <https://doi.org/10.1007/BF00867153>
- Mathur, S.P., 1969. Standardization of gravity and Bouguer anomalies in India. Ph.D. Thesis, University of Hawaii, Manoa, USA.
- Matsuo, K., Kuroishi, Y., 2020. Refinement of a gravimetric geoid model for Japan using GOCE and an updated regional gravity field model. *Earth, Planets and Space*, 72(1), 33. <https://doi.org/10.1186/s40623-020-01158-6>
- McCarthy, D.D., Petit, G., 2003. IERS Conventions (2003). International Earth Rotation and Reference Systems Service Central Bureau Bundesamt für Kartographie und Geodäsie Richard-Strauss-Allee, Frankfurt am Main Germany. IERS Technical Note, No. 32. <https://www.iers.org/SharedDocs/Publikationen/EN/IERS/Publications/tn/TechnNote32/>
- McCubbine, J.C., Amos, M.J., Tontini, F.C., Smith, E., Winefield, R., Stagpoole, V., Featherstone, W.E., 2018. The New Zealand gravimetric quasigeoid model 2017 that incorporates nationwide airborne gravimetry. *Journal of Geodesy*, 92(8), 923–937. <https://doi.org/10.1007/s00190-017-1103-1>
- McCubbine, J.C., Featherstone, W.E., Brown, N.J., 2019. Error propagation for the Molodensky G_1 term. *Journal of Geodesy*, 93, 889–898. <https://doi.org/10.1007/s00190-018-1211-6>
- McCubbine, J.C., Featherstone, W.E., Brown, N.J., 2021. Australian quasigeoid modelling: review, current status and future plans. *Terrestrial, Atmospheric and Oceanic Sciences*, online first. <https://doi.org/10.3319/TAO.2021.08.10.01>
- McCubbine, J.C., Featherstone, W.E., Kirby, J.F., 2017a. Fast-Fourier-based error propagation for the gravimetric terrain correction. *GEOPHYSICS*, 82(4), G71–G76. <https://doi.org/10.1190/geo2016-0627.1>
- McCubbine, J.C., Stagpoole, V., Caratori Tontini, F., Amos, M., Smith, E., Winefield, R., 2017b. Gravity anomaly grids for the New Zealand region. *New Zealand Journal of Geology and Geophysics*, 60(4), 381–391. <https://doi.org/10.1080/00288306.2017.1346692>
- Mehramuz, M., Zomorrodian, H., Ardalan, A.A., 2011. On geophysical application of the separation between the geoid and the quasigeoid case study: four regions in Iran. *Australian Journal of Basic and Applied Sciences*, 5(12), 127-135.
- Meissl, P., 1971. Preparations for the numerical evaluation of second-order Molodensky-type formulas. Department of Geodetic Science and Surveying Report No. 163. The Ohio State University, Columbus, USA. <https://apps.dtic.mil/sti/pdfs/AD0737800.pdf>
- Melchior, P., 1974. Earth tides. *Geophysical Surveys*, 1(3), 275–303. <https://doi.org/10.1007/BF01449116>
- Melchior, P., 1978. The tides of the planet Earth. Pergamon Press, New York.

- Melchior, P., 1983. The tides of the planet Earth 2nd edition. Pergamon Press, New York.
- Melchior, P.J., 1958. Earth Tides. *Advances in Geophysics*, 4, 391–443. [https://doi.org/10.1016/S0065-2687\(08\)60488-4](https://doi.org/10.1016/S0065-2687(08)60488-4)
- Meyer, D., Tachikawa, T., Kaku, M., Iwasaki, A., Gesch, D., Oimoen, M., Zhang, Z., Danielson, J., Krieger, T., Curtis, B., Haase, J., Abrams, M., Crippen, R., Carabajal, C., 2011. ASTER global digital elevation model version 2- summary of validation results. https://ssl.jspacesystems.or.jp/ersdac/GDEM/ver2Validation/Summary_GDEM2_validation_report_final.pdf
- Mishra, U.N., 2018. A comparative evaluation of methods for development of Indian geoid model. Ph.D. Thesis, Indian Institute of Technology Roorkee, India.
- Mishra, U.N., Ghosh, J.K., 2016. Development of a gravimetric geoid model and a comparative study. *Geodesy and Cartography*, 42(3), 75–84. <https://doi.org/10.3846/20296991.2016.1226368>
- Miyahara, B., Kodama, T., Kuroishi, Y., 2014. Development of new hybrid geoid model for Japan, “GSIGEO2011”. *Bulletin of the Geospatial Information Authority of Japan*, 62, 11-20. <https://www.gsi.go.jp/common/000099005.pdf>
- Molodensky, M.S., 1945. Fundamental problems of geodetic gravimetry (in Russian). TRUDY Ts NIIGAİK, 42, Geodezizdat. Moscow, Russia.
- Molodensky, M.S., Eremeev, V.F., Yurkina, M.I., 1962. Methods for study of the external gravity field and figure of the Earth. Israel Program for Scientific Translations, Jerusalem, Israel.
- Morelli, C., Gantar, C., Honkasalo, T., McConnell, R., Szabo, B., Tanner, T., Uotila, U., Whalen, C., 1972. The International Gravity Standardization Net 1971 (I.G.S.N.71). International Association of Geodesy Publication Speciale No. 4. <https://apps.dtic.mil/sti/pdfs/ADA006203.pdf>
- Moritz, H., 1968. On the use of the terrain correction in solving Molodensky’s problem. Department of Geodetic Science Report No. 108. The Ohio State University, Columbus, USA.
- Moritz, H., 1971. Series solutions of Molodensky's problem. Deutsche Geodaetische Kommission Bayer. Akad. Wiss., 70.
- Moritz, H., 1974. Precise gravimetric geodesy. Department of Geodetic Science and Surveying Report No. 219. The Ohio State University, Columbus, USA.
- Moritz, H., 1980. Advanced physical geodesy. *Advances in Planetary Geology*, Abacus Press, Tunbridge, England.
- Moritz, H., 2000. Geodetic Reference System 1980. *Journal of Geodesy*, 74(1), 128–133. <https://doi.org/10.1007/s001900050278>
- Moritz, H., 2011. A contemporary perspective of geoid structure. *Journal of Geodetic Science*, 1(1), 82–87. <https://doi.org/10.2478/v10156-010-0010-7>
- Moritz, H., Sünkel, H., 1978. *Approximation Methods in Geodesy*. Herbert Wichmann Verlag, Karlsruhe.
- Mueller, I.I., 1980. The Geodesist’s Handbook. *Bulletin Géodésique*, 54(3).

- Nagy, D., 1966. The prism method for terrain corrections using digital computers. *Pure and Applied Geophysics*, 63(1), 31–39. <https://doi.org/10.1007/BF00875156>
- Nahavandchi, H., 1998. Precise gravimetric-GPS geoid determination with improved topographic corrections applied over Sweden. Ph.D. Thesis, Royal Institute of Technology (KTH), Stockholm, Sweden.
- Nahavandchi, H., Sjöberg, L.E., 2001. Precise geoid determination over Sweden using the Stokes-Helmert method and improved topographic corrections. *Journal of Geodesy*, 75(2–3), 74–88. <https://doi.org/10.1007/s001900000154>
- Najafi-Alamdari, M., 2004. Technical report of the KNT university geoid model. Department of research, National Cartographic Centre (NCC), TOTAK project. Iran.
- Najafi-Alamdari, M., Emadi, S.R., Moghtased-Azar, K., 2006. The ellipsoidal correction to the Stokes kernel for precise geoid determination. *Journal of Geodesy*, 80(12), 675–689. <https://doi.org/10.1007/s00190-006-0050-z>
- Nardi, F., Annis, A., Di Baldassarre, G., Vivoni, E.R., Grimaldi, S., 2019. GFPLAIN250m, a global high-resolution dataset of Earth's floodplains. *Scientific Data*, 6, 180309. <https://doi.org/10.1038/sdata.2018.309>.
- NCERT, 2006. Fundamentals of physical geography, textbook for class XI. <https://ncert.nic.in/ncerts/l/kegy102.pdf>
- Niethammer, T., 1932. Nivellement und Schwere als Mittel zur Berechnung wahrer Meereshöhen (Levelling and weight as a means for the computation of true sea level heights). Schweizerische Geodätische Kommission, Berne, 76. Zürich, Switzerland.
- NIMA, 2000. World Geodetic System 1984, its definition and relationships with local geodetic systems. Report TR8350.2. Bethesda, MD, USA. <https://earth-info.nga.mil/GandG/publications/tr8350.2/wgs84fin.pdf>
- NOAA, NASA, USAF, 1976. US standard atmosphere. US Government Printing Office, Washington DC, USA.
- Novák, P., 2000. Evaluation of gravity data for the Stokes-Helmert solution to the geodetic boundary-value problem. Ph.D. Thesis, University of New Brunswick, Fredericton, Canada. <http://www2.unb.ca/gge/Pubs/TR207.pdf>
- NRSA, 2006. CARTOSAT-1 data user's handbook. Technical Report CARTOSAT-1/NRSA/NDC/HB-09/06. National Remote Sensing Agency, India.
- O'Loughlin, F.E., Paiva, R.C.D., Durand, M., Alsdorf, D.E., Bates, P.D., 2016. A multi-sensor approach towards a global vegetation corrected SRTM DEM product. *Remote Sensing of Environment*, 182, 49–59. <https://doi.org/10.1016/j.rse.2016.04.018>.
- Olesen, A. V., Andersen, O.B., Tscherning, C.C., 2002. Merging of airborne gravity and gravity derived from satellite altimetry: Test cases along the coast of Greenland. *Studia Geophysica et Geodaetica*, 46(3), 387–394. <https://doi.org/10.1023/A:1019577232253>
- Ophaug, V., Breili, K., Gerlach, C., 2015. A comparative assessment of coastal mean dynamic topography in Norway by geodetic and ocean approaches. *Journal of Geophysical Research: Oceans*, 120(12), 7807–7826. <https://doi.org/10.1002/2015JC011145>

- Pa'suya, M.F., Din, A.H.M., McCubbine, J.C., Omar, A.H., Amin, Z.M., Yahaya, N.A.Z., 2019. Gravimetric geoid modelling over peninsular Malaysia using two different gridding approaches for combining free air anomaly. *ISPRS - International Archives of the Photogrammetry, Remote Sensing and Spatial Information Sciences*, XLII-4/W16, 515–522. <https://doi.org/10.5194/isprs-archives-XLII-4-W16-515-2019>
- Pagiatakis, S.D., Fraser, D., McEwen, K., Goodacre, A.K., Véronneau, M., 1999. Topographic mass density and gravimetric geoid modelling. *Bollettino di Geofisica Teorica ed Applicata*, 40(3–4), 189–194. http://www3.inogs.it/bgo/pdf/bgta40.3.4_PAGIATAKIS.pdf
- Pail, R., Bruinsma, S., Migliaccio, F., Förste, C., Goiginger, H., Schuh, W.-D., Höck, E., Reguzzoni, M., Brockmann, J.M., Abrikosov, O., Veicherts, M., Fecher, T., Mayrhofer, R., Krasbutter, I., Sansò, F., Tscherning, C.C., 2011. First GOCE gravity field models derived by three different approaches. *Journal of Geodesy*, 85(11), 819–843. <https://doi.org/10.1007/s00190-011-0467-x>
- Pail, R., Fecher, T., Barnes, D., Factor, J.F., Holmes, S.A., Gruber, T., Zingerle, P., 2018. Short note: The experimental geopotential model XGM2016. *Journal of Geodesy*, 92(4), 443–451. <https://doi.org/10.1007/s00190-017-1070-6>
- Park, S., Oh, C., Jeon, S., Jung, H., Choi, C., 2011. Soil erosion risk in Korean watersheds, assessed using the revised universal soil loss equation. *Journal of Hydrology*, 399(3–4), 263–273. <https://doi.org/10.1016/j.jhydrol.2011.01.004>.
- Paul, M.K., 1973. A method of evaluating the truncation error coefficients for geoidal height. *Bulletin Géodésique*, 110(1), 413–425. <https://doi.org/10.1007/BF02521951>
- Pavlis, N.K., Holmes, S.A., Kenyon, S.C., Factor, J.K., 2012. The development and evaluation of the Earth Gravitational Model 2008 (EGM2008). *Journal of Geophysical Research: Solid Earth*, 117(B4), B04406. <https://doi.org/10.1029/2011JB008916>
- Pavlis, N.K., Holmes, S.A., Kenyon, S.C., Factor, J.K., 2013. Correction to “The development and evaluation of the Earth Gravitational Model 2008 (EGM2008)”. *Journal of Geophysical Research: Solid Earth*, 118(5), 2633. <https://doi.org/10.1002/jgrb.50167>
- Pellinen, L.P., 1972. On the identity of various solutions of Molodensky's problem with the help of a small parameter. In: *International Symposium on Earth Gravity Models and Related Problems*, August 16-18. Saint-Louis, Missouri.
- Penna, N.T., Featherstone, W.E., Gazeaux, J., Bingham, R.J., 2013. The apparent British sea slope is caused by systematic errors in the levelling-based vertical datum. *Geophysical Journal International*, 194(2), 772–786. <https://doi.org/10.1093/gji/ggt161>
- Petit, G., Luzum, B., 2010. *IERS Conventions (2010)*. IERS Technical Note 36. Verlag des Bundesamtes für Kartographie und Geodäsie, Frankfurt am Main, Germany. <https://www.iers.org/IERS/EN/Publications/TechnicalNotes/tn36.html>
- Popadyev, V.V., 2019. On the Advantage of Normal Heights. In: Novák, P., Crespi, M., Sneeuw, N., Sansò, F., (eds.) *IX Hotine-Marussi Symposium on Mathematical Geodesy*. International Association of Geodesy Symposia, vol. 151, pp. 25-31. Springer. https://doi.org/10.1007/1345_2019_74
- Poutanen, M., Rózsa, S., 2020. The Geodesist's Handbook 2020. *Journal of Geodesy*, 94(11), 109. <https://doi.org/10.1007/s00190-020-01434-z>

- Poutanen, M., Vermeer, M., Mäkinen, J., 1996. The permanent tide in GPS positioning. *Journal of Geodesy*, 70(8), 499–504. <https://doi.org/10.1007/BF00863622>
- Pratt, J.H., 1855. On the attraction of the Himalaya mountains, and of the elevated regions beyond them, upon the plumb-line in India. *Philosophical Transactions of the Royal Society of London*, 145, 53–100. <https://doi.org/10.1098/rstl.1855.0002>
- QPS- Quality Positioning Services, 2020. Permanent tide systems. In: Qinsy documentation, version 9.4. <https://confluence.gps.nl/qinsy/9.4/en/permanent-tide-systems-238783753.html> [Accessed on 28-01-2022].
- Qureshy, M.N., 1971. Relation of gravity to elevation and rejuvenation of blocks in India. *Journal of Geophysical Research*, 76(2), 545–557. <https://doi.org/10.1029/JB076i002p00545>
- Rabehi, N., Belhadj, A., Terbeche, M., 2012. Stokes's kernel modifications. In: FIG working week 2012, Rome, Italy. https://www.fig.net/resources/proceedings/fig_proceedings/fig2012/papers/ts04b/TS04B_rabehi_battaouia_et_al_6132.pdf
- Rapp, R.H., 1961. The orthometric height. M.Sc. Thesis, The Ohio State University, Columbus, USA. http://rave.ohiolink.edu/etdc/view?acc_num=osu1392906622.
- Rapp, R.H., 1968. Gravitational potential of the Earth determined from a combination of satellite, observed, and model anomalies. *Journal of Geophysical Research*, 73(20), 6555–6562. <https://doi.org/10.1029/JB073i020p06555>
- Rapp, R.H., 1974. Current estimates of mean Earth ellipsoid parameters. *Geophysical Research Letters*, 1(1), 35–38. <https://doi.org/10.1029/GL001i001p00035>
- Rapp, R.H., 1977. Potential coefficient determination from 5° terrestrial gravity data. Department of Geodetic Science and Surveying Report No. 251. The Ohio State University, Columbus, USA.
- Rapp, R.H., 1997. Use of potential coefficient models for geoid undulation determinations using a spherical harmonic representation of the height anomaly/geoid undulation difference. *Journal of Geodesy*, 71(5), 282–289. <https://doi.org/10.1007/s001900050096>
- Rapp, R.H., 1998. Past and future developments in geopotential modeling. In: Forsberg, R., Feissel, M., Dietrich, R., (eds.) *Geodesy on the Move*. International Association of Geodesy Symposia, vol. 119, pp. 58-78. Springer. https://doi.org/10.1007/978-3-642-72245-5_9
- Rapp, R.H., Pavlis, N.K., 1990. The development and analysis of geopotential coefficient models to spherical harmonic degree 360. *Journal of Geophysical Research*, 95(B13), 21885. <https://doi.org/10.1029/JB095iB13p21885>
- Rapp, R.H., Steven Nerem, R., Shum, C.K., Klosko, S.M., Williamson, R.G., 1991. Consideration of permanent tidal deformation in the orbit determination and data analysis for the Topex/Poseidon mission. NASA Technical Memorandum 100775. Goddard Space Flight Center, Greenbelt, MD, USA. <https://ntrs.nasa.gov/api/citations/19910021305/downloads/19910021305.pdf>
- Reid, J.L., 1961. On the temperature, salinity, and density differences between the Atlantic and Pacific oceans in the upper kilometre. *Deep Sea Research*, 7(4), 265–275. [https://doi.org/10.1016/0146-6313\(61\)90044-2](https://doi.org/10.1016/0146-6313(61)90044-2)

- Ricardi, L.J., Burrows, M.L., 1972. A recurrence technique for expanding a function in spherical harmonics. *IEEE Transactions on Computers*, C-21(6), 583–585. <https://doi.org/10.1109/TC.1972.5009011>
- Ries, J.C., Eanes, R.J., Shum, C.K., Watkins, M.M., 1992. Progress in the determination of the gravitational coefficient of the Earth. *Geophysical Research Letters*, 19(6), 529–531. <https://doi.org/10.1029/92GL00259>
- Robin, C., Nudds, S., MacAulay, P., Godin, A., de Lange Boom, B., Bartlett, J., 2016. Hydrographic Vertical Separation Surfaces (HyVSEPs) for the tidal waters of Canada. *Marine Geodesy*, 39(2), 195–222. <https://doi.org/10.1080/01490419.2016.1160011>
- Coblentz, D., Chase, C.G., Karlstrom, K.E., van Wijk, J., 2011. Topography, the geoid, and compensation mechanisms for the southern Rocky Mountains. *Geochemistry, Geophysics, Geosystems*, 12(4), Q04002. <https://doi.org/10.1029/2010GC003459>
- Rodriguez, E., Morris, C.S., Belz, J.E., Chapin, E.C., Martin, J.M., Daffer, W., Hensley, S., 2005. An assessment of the SRTM topographic products. Report No. JPL D-31639. Jet Propulsion Laboratory, Pasadena, Technical https://www2.jpl.nasa.gov/srtm/SRTM_D31639.pdf
- Roman, D., Ahlgren, K., 2019. GEOID18: Last U.S. hybrid geoid prior to NAPGD2022. In: FIG working week 2019, Geospatial information for a smarter life and environmental resilience. 22-26 April, Hanoi, Vietnam. https://www.fig.net/resources/proceedings/fig_proceedings/fig2019/papers/ts03e/TSO3E_roman_ahlgren_9933.pdf
- Rummel, R., Teunissen, P., 1988. Height datum definition, height datum connection and the role of the geodetic boundary value problem. *Bulletin Géodésique*, 62(4), 477–498. <https://doi.org/10.1007/BF02520239>
- Sacher, M., Ihde, J., Liebsch, G., Mäkinen, J., 2009. EVRF2007 as the realization of the European vertical reference system. *Bollettino di Geodesia e Scienze Affini*, LXVIII(1), 35–50.
- Sadiq, M., Ahmad, Z., Akhter, G., 2009. A study on the evaluation of the geoid-quasigeoid separation term over Pakistan with a solution of first and second order height terms. *Earth, Planets and Space*, 61(7), 815–823. <https://doi.org/10.1186/BF03353192>
- Sampietro, D., Capponi, M., Triglione, D., Mansi, A.H., Marchetti, P., Sansò, F., 2016. GTE: a new software for gravitational terrain effect computation: theory and performances. *Pure and Applied Geophysics*, 173(7), 2435–2453. <https://doi.org/10.1007/s00024-016-1265-4>
- Sánchez, L., Ågren, J., Huang, J., Wang, Y.M., Mäkinen, J., Pail, R., Barzaghi, R., Vergos, G.S., Ahlgren, K., Liu, Q., 2021. Strategy for the realisation of the International Height Reference System (IHRs). *Journal of Geodesy*, 95(3), 33. <https://doi.org/10.1007/s00190-021-01481-0>
- Sánchez, L., Čunderlík, R., Dayoub, N., Mikula, K., Minarechová, Z., Šíma, Z., Vatrt, V., Vojtíšková, M., 2016. A conventional value for the geoid reference potential W_0 . *Journal of Geodesy*, 90(9), 815–835. <https://doi.org/10.1007/s00190-016-0913-x>
- Sandwell, D.T., Harper, H., Tozer, B., Smith, W.H.F., 2021. Gravity field recovery from geodetic altimeter missions. *Advances in Space Research*, 68(2), 1059–1072. <https://doi.org/10.1016/j.asr.2019.09.011>
- Sansò, F., Rummel, R., 1997. Geodetic boundary value problems in view of the centimeter geoid. pp. 596. Springer. <https://doi.org/10.1007/BFb0011699>

- Santos, M., Kingdon, R., Vaníček, P., Martinec, Z., Foroughi, I., 2021. An oral rebuttal to “the shape of the quasigeoid”. In: International Association of Geodesy Scientific Assembly 2021, Beijing, China.
- Santos, M.C., Vaníček, P., Featherstone, W.E., Kingdon, R., Ellmann, A., Martin, B.-A., Kuhn, M., Tenzer, R., 2006. The relation between rigorous and Helmert’s definitions of orthometric heights. *Journal of Geodesy*, 80(12), 691–704. <https://doi.org/10.1007/s00190-006-0086-0>
- Schettino, A., 2015. Gravity field of the Earth. In: *Quantitative Plate Tectonics*, pp. 363-378. Springer. https://doi.org/10.1007/978-3-319-09135-8_14
- Schwabe, J., Horwath, M., Scheinert, M., 2016. The evaluation of the geoid–quasigeoid separation and consequences for its implementation. *Acta Geodaetica et Geophysica*, 51(3), 451–466. <https://doi.org/10.1007/s40328-015-0136-2>
- Schwarz, G., 1978. Estimating the dimension of a model. *The Annals of Statistics*, 6(2), 461-464. <http://dx.doi.org/10.1214/aos/1176344136>
- Schwarz, K.P., Sideris, M.G., Forsberg, R., 1990. The use of FFT techniques in physical geodesy. *Geophysical Journal International*, 100(3), 485–514. <https://doi.org/10.1111/j.1365-246X.1990.tb00701.x>
- Shankar, D., Shetye, S.R., 2001. Why is mean sea level along the Indian coast higher in the Bay of Bengal than in the Arabian Sea? *Geophysical Research Letters*, 28(4), 563–565. <https://doi.org/10.1029/2000GL012001>
- Shao, J., 1993. Linear model selection by cross-validation. *Journal of the American Statistical Association*, 88(422), 486–494. <https://doi.org/10.2307/2290328>
- Sheng, M.B., Shaw, C., Vaníček, P., Kingdon, R.W., Santos, M., Foroughi, I., 2019. Formulation and validation of a global laterally varying topographical density model. *Tectonophysics*, 762, 45–60. <https://doi.org/10.1016/j.tecto.2019.04.005>
- Sideris, M.G., 1984. Computation of gravimetric terrain corrections using fast Fourier transform techniques. M.Sc. Thesis, University of Calgary, Alberta, Canada. <http://dx.doi.org/10.11575/PRISM/14395>
- Sideris, M.G., 1985. A fast Fourier transform method for computing terrain corrections. *manuscripta geodaetica*, 10, 66-73.
- Sideris, M.G., Li, Y.C., 1993. Gravity field convolutions without windowing and edge effects. *Bulletin Géodésique*, 67(2), 107–118. <https://doi.org/10.1007/BF01371374>
- Singh, S.K., 2007. Development of high-resolution gravimetric geoid model for central India. Ph.D. Thesis, Indian Institute of Technology Roorkee, India.
- Singh, S.K., Balasubramanian, N., Garg, P.K., 2007. Determination of local gravimetric geoid. <https://mycoordinates.org/determination-of-local-gravimetric-geoid/all/1/>
- Singh, S.K., Srivastava, R., 2018. Development of geoid model-A case study on western India. In: *FIG Congress 2018, Embracing our smart world where the continents connect: enhancing the geospatial maturity of societies*. 6-11 May, Istanbul, Turkey. https://fig.net/resources/proceedings/fig_proceedings/fig2018/papers/ts06e/TS06E_singh_sri_vastava_9496.pdf

- Sjöberg, L.E., 1980. Least squares combination of satellite harmonics and integral formulas in physical geodesy. *Gerlands Beiträge zur Geophysik*, 89(5), 371-377.
- Sjöberg, L.E., 1981. Least squares combination of satellite and terrestrial data in physical geodesy. *Annales Geophysicae*, 37(1), 25-30.
- Sjöberg, L.E., 1984a. Least squares modification of Stokes and Venning Meinesz formulas by accounting for errors of truncation, potential coefficients and gravity data. Department of Geodesy, Institute of Geophysics, Technical Report 27. University of Uppsala, Uppsala, Sweden.
- Sjöberg, L.E., 1984b. Least-squares modification of Stokes' and Vening-Meinez' formula by accounting for truncation and potential coefficients errors. *manuscripta geodaetica*, 9, 209–229.
- Sjöberg, L.E., 1986. Comparison of some methods of modifying Stokes' formula. *Bollettino di Geodesia e Scienze Affini*, 45(3), 229–248.
- Sjöberg, L.E., 1990. Contributions to the problem of modifying Stokes' formula. Division of Geodesy, Report No. 24. Royal Institute of Technology, Stockholm, Sweden.
- Sjöberg, L.E., 1991. Refined least squares modification of Stokes' formula. *manuscripta geodaetica*, 16, 367–375.
- Sjöberg, L.E., 1999. The IAG approach to the atmospheric geoid correction in Stokes' formula and a new strategy. *Journal of Geodesy*, 73(7), 362–366. <https://doi.org/10.1007/s001900050254>
- Sjöberg, L.E., 2000. Topographic effects by the Stokes–Helmert method of geoid and quasi-geoid determinations. *Journal of Geodesy*, 74(2), 255–268. <https://doi.org/10.1007/s001900050284>
- Sjöberg, L.E., 2001. Topographic and atmospheric corrections of gravimetric geoid determination with special emphasis on the effects of harmonics of degrees zero and one. *Journal of Geodesy*, 75(5), 283–290. <https://doi.org/10.1007/s001900100174>
- Sjöberg, L.E., 2003a. A computational scheme to model the geoid by the modified Stokes formula without gravity reductions. *Journal of Geodesy*, 77(7–8), 423–432. <https://doi.org/10.1007/s00190-003-0338-1>
- Sjöberg, L.E., 2003b. A solution to the downward continuation effect on the geoid determined by Stokes' formula. *Journal of Geodesy*, 77(1–2), 94–100. <https://doi.org/10.1007/s00190-002-0306-1>
- Sjöberg, L.E., 2003c. Ellipsoidal corrections to order e^2 of geopotential coefficients and Stokes' Formula. *Journal of Geodesy*, 77(3–4), 139–147. <https://doi.org/10.1007/s00190-003-0321-x>
- Sjöberg, L.E., 2003d. A general model for modifying Stokes formula and its least-squares solution. *Journal of Geodesy*, 77(7–8), 459–464. <https://doi.org/10.1007/s00190-003-0346-1>
- Sjöberg, L.E., 2004. A spherical harmonic representation of the ellipsoidal correction to the modified Stokes' formula. *Journal of Geodesy*, 78(3), 180–186. <https://doi.org/10.1007/s00190-004-0378-1>
- Sjöberg, L.E., 2005. A local least-squares modification of Stokes' formula. *Studia Geophysica et Geodaetica*, 49(1), 23–30. <https://doi.org/10.1007/s11200-005-1623-7>

- Sjöberg, L.E., 2010. A strict formula for geoid-to-quasigeoid separation. *Journal of Geodesy*, 84(11), 699–702. <https://doi.org/10.1007/s00190-010-0407-1>
- Sjöberg, L.E., 2013. The geoid or quasigeoid – which reference surface should be preferred for a national height system? *Journal of Geodetic Science*, 3(2), 103–109. <https://doi.org/10.2478/jogs-2013-0013>
- Sjöberg, L.E., 2014. On the topographic effects by Stokes' formula. *Journal of Geodetic Science*, 4(1), 130–135. <https://doi.org/10.2478/jogs-2014-0014>
- Sjöberg, L.E., 2015. The secondary indirect topographic effect in physical geodesy. *Studia Geophysica et Geodaetica*, 59(2), 173–187. <https://doi.org/10.1007/s11200-014-1003-2>
- Sjöberg, L.E., 2018. On the geoid and orthometric height vs. quasigeoid and normal height. *Journal of Geodetic Science*, 8(1), 115–120. <https://doi.org/10.1515/jogs-2018-0011>
- Sjöberg, L.E., Bagherbandi, M., 2017. Gravity inversion and integration. Springer. <https://doi.org/10.1007/978-3-319-50298-4>
- Sjöberg, L.E., Hunegnaw, A., 2000. Some modifications of Stokes' formula that account for truncation and potential coefficient errors. *Journal of Geodesy*, 74(2), 232–238. <https://doi.org/10.1007/s001900050281>
- Sjöberg, L.E., Nahavandchi, H., 2000. The atmospheric geoid effects in Stokes' formula. *Geophysical Journal International*, 140(1), 95–100. <https://doi.org/10.1046/j.1365-246x.2000.00995.x>
- Smith, D.A., 1998. There is no such thing as “The” EGM96 geoid: Subtle points on the use of a global geopotential model. *International Geoid Service Bulletin*, 8, 17–28. https://www.ngs.noaa.gov/PUBS_LIB/EGM96_GEOID_PAPER/egm96_geoid_paper.html
- Sneeuw, N., 1994. Global spherical harmonic analysis by least-squares and numerical quadrature methods in historical perspective. *Geophysical Journal International*, 118(3), 707–716. <https://doi.org/10.1111/j.1365-246X.1994.tb03995.x>
- Šprlák, M., 2010. Generalized geoidal estimators for deterministic modifications of spherical Stokes' function. *Contributions to Geophysics and Geodesy*, 40(1), 45–64. <https://doi.org/10.2478/v10126-010-0003-7>
- Srinivas, N., Tiwari, V.M., Tarial, J.S., Prajapati, S., Meshram, A.E., Singh, B., Nagarajan, B., 2012. Gravimetric geoid of a part of south India and its comparison with global geopotential models and GPS-levelling data. *Journal of Earth System Science*, 121(4), 1025–1032. <https://doi.org/10.1007/s12040-012-0205-7>
- Srivastava, A.M.C., 1985. Indian geoid on GRS 67 from geopotential coefficients. *Bulletin Géodésique*, 59(3), 289–295. <https://doi.org/10.1007/BF02520332>
- Ssengendo, R., 2015. A height datum for Uganda based on a gravimetric quasigeoid model and GNSS/levelling. Ph.D. Thesis, Royal Institute of Technology (KTH), Stockholm, Sweden. <http://kth.diva-portal.org/smash/get/diva2:848931/FULLTEXT01.pdf>
- Stokes, G.G., 1849. On the variation of gravity and the surface of the Earth. Cambridge Philosophical Society, *Transactions*, 8, 672–695.

- Stone, M., 1974. Cross-validators choice and assessment of statistical predictions. *Journal of the Royal Statistical Society, Series B (Methodological)*, 36(2), 111–147. <http://www.jstor.org/stable/2984809>
- Stone, M., 1977. An asymptotic equivalence of choice of model by cross-validation and Akaike's criterion. *Journal of the Royal Statistical Society, Series B (Methodological)*, 39(1), 44–47. <http://www.jstor.org/stable/2984877>
- Strang van Hees, G., 1990. Stokes' formulae using fast Fourier techniques. *manuscripta geodaetica*, 15, 235-239.
- Strykowski, G., Forsberg, R., 1998. Operational merging of satellite, airborne and surface gravity data by draping techniques. In: Forsberg, R., Feissel, M., Dietrich, R., (eds.) *Geodesy on the Move. International Association of Geodesy Symposia*, vol. 119, pp. 243-248. Springer. https://doi.org/10.1007/978-3-642-72245-5_35
- Sturges, W., 1967. Slope of sea level along the Pacific coast of the United States. *Journal of Geophysical Research*, 72(14), 3627–3637. <https://doi.org/10.1029/JZ072i014p03627>
- Sturges, W., 1974. Sea level slope along continental boundaries. *Journal of Geophysical Research*, 79(6), 825–830. <https://doi.org/10.1029/JC079i006p00825>
- Subrahmanyam, C., Verma, R.K., 1980. The nature of free-air, Bouguer and isostatic anomalies in southern peninsular India. *Tectonophysics*, 20(1-2), 147-162. [https://doi.org/10.1016/0040-1951\(80\)90131-6](https://doi.org/10.1016/0040-1951(80)90131-6)
- Sun, W., Vaniček, P., 1998. On some problems of the downward continuation of the 5'×5' mean Helmert gravity disturbance. *Journal of Geodesy*, 72(7), 411–420. <https://doi.org/10.1007/s001900050180>
- Sundaram, R.M., Surendranath, M., Reddy, U.S.N., 2009. Revised gravity maps of India (2006 series) – A cartographic perspective. <https://www.geospatialworld.net/article/revised-gravity-maps-of-india-2006-series-a-cartographic-perspective/>
- SoI – Survey of India, 1930. Geodetic report vol V. The geodetic branch office, Survey of India, Dehradun, India
- SoI – Survey of India, 1950. Technical report 1948-49, Part III-Geodetic work. The office of the geodetic and training circle, Survey of India, Dehradun, India.
- SoI – Survey of India, 1951. Technical report 1950, Part III-Geodetic work. The office of the geodetic and training circle, Survey of India, Dehradun, India.
- Takin, M., 1966. An interpretation of the positive gravity anomaly over Bombay on the west coast of India. *Geophysical Journal International*, 11(5), 527–537. <https://doi.org/10.1111/j.1365-246X.1966.tb03164.x>
- Tapley, B.D., Bettadpur, S., Watkins, M., Reigber, C., 2004. The gravity recovery and climate experiment: Mission overview and early results. *Geophysical Research Letters*, 31(9), L09607. <https://doi.org/10.1029/2004GL019920>
- Tapley, B.D., Ries, J., Bettadpur, S., Chambers, D., Cheng, M., Condi, F., Poole, S., 2007. The GGM03 mean earth gravity model from GRACE. In: *American Geophysical Union Fall Meeting, December 10-14, San Francisco, USA*. http://download.csr.utexas.edu/pub/grace/GGM03/GGM03_Tapley_2007_AGU.pdf

- Tarekegn, T.H., Sayama, T., 2013. Correction of SRTM DEM artefacts by Fourier transform for flood inundation modeling. *Journal of Japan Society of Civil Engineers, Ser. B1 (Hydraulic Engineering)*, 69(4), I_193-I_198. https://doi.org/10.2208/jscejhe.69.I_193.
- Tenzer, R., Hirt, C., Claessens, S., Novák, P., 2015. Spatial and spectral representations of the geoid-to-quasigeoid correction. *Surveys in Geophysics*, 36(5), 627–658. <https://doi.org/10.1007/s10712-015-9337-z>
- Tenzer, R., Janák, J., 2002. Stokes-Helmert's scheme for precise geoid determination. *Revista Cartografica*, 74-75, 135-145.
- Tenzer, R., Novák, P., Janák, J., Huang, J., Najafi-Alamdari, M., Vajda, P., Santos, M., 2003. A review of the UNB approach for precise geoid determination based on the Stokes–Helmert method. In: Santos, M., (ed.) *Honoring the academic life of Petr Vaníček*. Report of Department of Geodesy and Geomatics Engineering, No. 218, pp. 132-178. University of New Brunswick (UNB), Fredericton, Canada.
- Tenzer, R., Novák, P., Moore, P., Kuhn, M., Vaníček, P., 2006. Explicit formula for the geoid-quasigeoid separation. *Studia Geophysica et Geodaetica*, 50(4), 607–618. <https://doi.org/10.1007/s11200-006-0038-4>
- Tenzer, R., Vaníček, P., Santos, M., Featherstone, W.E., Kuhn, M., 2005. The rigorous determination of orthometric heights. *Journal of Geodesy*, 79(1–3), 82–92. <https://doi.org/10.1007/s00190-005-0445-2>
- Tenzer, R., Vatrt, V., Amos, M., 2012. Realization of the world height system in New Zealand: Preliminary study. In: Kenyon, S., Pacino, M., Marti, U., (eds.) *Geodesy for Planet Earth*. International Association of Geodesy Symposia, vol. 136, pp. 343-349. Springer. https://doi.org/10.1007/978-3-642-20338-1_41
- Tiwari, V.M., Veenadhari, B., Gahalaut, V.K., Mukherjee, S., Dimri, V.P., 2014. Gravity, GPS and geomagnetic data in India. *Proceedings of the Indian National Science Academy*, 80(3), 705-712. <https://doi.org/10.16943/ptinsa/2014/v80i3/55145>
- Tóth, G., Rózsa, S., Andritsanos, V.D., Ádám, J., Tziavos, I.N., 2000. Towards a cm-geoid for Hungary: Recent efforts and results. *Physics and Chemistry of the Earth, Part A: Solid Earth and Geodesy*, 25(1), 47–52. [https://doi.org/10.1016/S1464-1895\(00\)00008-9](https://doi.org/10.1016/S1464-1895(00)00008-9)
- Truhetz, H., 2010. High resolution wind field modelling over complex topography analysis and future scenarios. Ph.D. Thesis, The University of Graz, Austria. <https://wegcwww.uni-graz.at/publ/wegcreports/2010/WCV-SciRep-No32-HTruhetz-Apr2010.pdf>
- Tscherning, C.C., 1977. A note on the choice of norm when using collocation for the computation of approximations to the anomalous potential. *Bulletin Géodésique*, 51(2), 137–147. <https://doi.org/10.1007/BF02522283>
- Tscherning, C.C., Rapp, R.H., 1974. Closed covariance expressions for gravity anomalies, geoid undulations, and deflections of the vertical implied by anomaly degree variance models. Department of Geodetic Science Reports No. 208. The Ohio State University, Columbus, USA. <https://earthsciences.osu.edu/sites/earthsciences.osu.edu/files/report-208.pdf>
- Tscherning, C.C., Rapp, R.H., Goad, C., 1983. A comparison of methods for computing gravimetric quantities from high degree spherical harmonic expansions. *manuscripta geodaetica*, 8, 249-272.

- Tsen, A., 1992. Determination of geoidal height difference using ring integration method. M.Sc. Thesis, University of Brunswick, Fredericton, Canada. <http://www2.unb.ca/gge/Pubs/TR158.pdf>
- Tsoulis, D., 2001. Terrain correction computations for a densely sampled DTM in the Bavarian Alps. *Journal of Geodesy*, 75(5-6), 291–307. <https://doi.org/10.1007/s001900100176>
- Tsoulis, D., Novák, P., Kadlec, M., 2009. Evaluation of precise terrain effects using high-resolution digital elevation models. *Journal of Geophysical Research*, 114(B2), B02404. <https://doi.org/10.1029/2008JB005639>
- Tsoulis, D.V., 1998. A combination method for computing terrain corrections. *Physics and Chemistry of the Earth*, 23(1), 53–58. [https://doi.org/10.1016/S0079-1946\(97\)00241-3](https://doi.org/10.1016/S0079-1946(97)00241-3)
- Tziavos, I.N., 1996. Comparisons of spectral techniques for geoid computations over large regions. *Journal of Geodesy*, 70(6), 357–373. <https://doi.org/10.1007/BF00868188>
- Ulotu, P., 2009. Geoid model of Tanzania from space and varying gravity data density by the KTH method. Ph.D. Thesis, Royal Institute of Technology (KTH), Stockholm, Sweden. <http://www.diva-portal.org/smash/get/diva2:213740/FULLTEXT01.pdf>
- UNB – University of New Brunswick, 2009. SHGEO software package. University of New Brunswick, Fredericton, Canada. <http://www2.unb.ca/gge/Research/GRL/GeodesyGroup/SHGeo.html>
- Uotila, U.A., 1980. Note to the users of International Gravity Standardization Net 1971. *Bulletin Géodésique*, 54(3), 407–408. <https://doi.org/10.1007/BF02521481>
- Valty, P., Duquenne, H., Panet, I., 2012. Auvergne dataset: testing several geoid computation methods. In: Kenyon, S., Pacino, M., Marti, U., (eds.) *Geodesy for Planet Earth*. International Association of Geodesy Symposia, vol. 136, pp. 465-472. Springer. https://doi.org/10.1007/978-3-642-20338-1_56
- Vaniček, P., 1973. The Earth tides. *Geodesy and Geomatics Engineering, Lecture Notes No. 36*. University of New Brunswick, Fredericton, Canada. <http://www2.unb.ca/gge/Pubs/LN36.pdf>
- Vaniček, P., 1974. Brief outline of the Molodenskij theory (the determination of the figure of the Earth). *Geodesy and Geomatics Engineering, Lecture Notes No. 23*. University of New Brunswick, Fredericton, Canada. <http://www2.unb.ca/gge/Pubs/LN23.pdf>
- Vaniček, P., Christou, N.T., 1993. *Geoid and its geophysical interpretations*. CRC Press, Boca Raton, FL, USA. <https://doi.org/10.1201/9781003068068>
- Vaniček, P., Featherstone, W.E., 1998. Performance of three types of Stokes's kernel in the combined solution for the geoid. *Journal of Geodesy*, 72(12), 684–697. <https://doi.org/10.1007/s001900050209>
- Vaniček P., Santos, M.C., 2010. Can mean values of Helmert's gravity anomalies be continued downward directly? *Geomatica*, 64(2), 245-251.
- Vaniček, P., Huang, J., Novák, P., Pagiatakis, S., Véronneau, M., Martinec, Z., Featherstone, W.E., 1999. Determination of the boundary values for the Stokes-Helmert problem. *Journal of Geodesy*, 73(4), 180–192. <https://doi.org/10.1007/s001900050235>

- Vaniček, P., Janák, J., Véronneau, M., n.d. Impact of digital elevation models on geoid modelling. <http://www2.unb.ca/gge/Personnel/Vanicsek/ImpactOfDEM.pdf>
- Vaniček, P., Kingdon, R., Kuhn, M., Ellmann, A., Featherstone, W.E., Santos, M.C., Martinec, Z., Hirt, C., Avalos-Naranjo, D., 2013. Testing Stokes-Helmert geoid model computation on a synthetic gravity field: experiences and shortcomings. *Studia Geophysica et Geodaetica*, 57(3), 369–400. <https://doi.org/10.1007/s11200-012-0270-z>
- Vaniček, P., Kingdon, R., Santos, M., 2012. Geoid versus quasigeoid: A case of physics versus geometry. *Contributions to Geophysics and Geodesy*, 42(1), 101–118. <https://doi.org/10.2478/v10126-012-0004-9>
- Vaniček, P., Kleusberg, A., 1987. The Canadian geoid – Stokesian approach. *manuscripta geodaetica*, 12, 86-98.
- Vaniček, P., Kleusberg, A., Martinec, Z., Sun, W., Ong, P., Najafi, M., Vajda, P., Harrie, L., Tomasek, P., ter Horst, B., 1995. Compilation of a precise regional geoid. DSS Contract 23244-1-4405/01-SS, Report for Geodetic Survey Division, Ottawa, Canada. http://www2.unb.ca/gge/Research/GRL/GeodesyGroup/SHGeo/1_Stokes-Helmert_Technique/1995_Vanicsek_et_al.pdf
- Vaniček, P., Martinec, Z., 1994. The Stokes-Helmert scheme for the evaluation of a precise geoid. *manuscripta geodaetica*, 19, 119-128.
- Vaniček, P., Sjöberg, L.E., 1991. Reformulation of Stokes's theory for higher than second-degree reference field and modification of integration kernels. *Journal of Geophysical Research: Solid Earth*, 96(B4), 6529–6539. <https://doi.org/10.1029/90JB02782>
- Varga, M., Bašić, T., 2018. Numerical investigation on the importance of digital elevation models in regional geoid modelling. In: IX Hotine-Marussi Symposium, June 18-22. Rome, Italy.
- Varga, M., Grgić, M., Bjelotomić Oršulić, O., Bašić, T., 2019. Influence of digital elevation model resolution on gravimetric terrain correction over a study-area of Croatia. *Geofizika*, 36(1), 17–32. <https://doi.org/10.15233/gfz.2019.36.1>
- Vatrt, V., 1999. Methodology of testing geopotential models specified in different tide systems. *Studia Geophysica et Geodaetica*, 43(1), 73–77. <https://doi.org/10.1023/A:1023362109108>
- Verma, R.K., 1985. Gravity field, seismicity and tectonics of the Indian peninsula and the Himalayas. Springer, Netherlands. <https://doi.org/10.1007/978-94-009-5259-1>
- Vermeer, M., Poutanen, M., 1997. A modified GRS-80 normal field including permanent tide and atmosphere. In: Segawa, J., Fujimoto, H., Okubo, S., (eds.) Gravity, Geoid and Marine Geodesy. International Association of Geodesy Symposia, vol. 117, pp. 515-522. Springer. https://doi.org/10.1007/978-3-662-03482-8_69
- Walker, J.T., 1863. The trigonometrical survey of India, pp. 17. Survey of India, Dehradun, India.
- Walker, J.T., 1870. On the Indian pendulum observations, pp. 9. Survey of India, Dehradun, India.
- Wang, Y.M., Forsberg, R., 2019. Report of the Joint Working Group 2.2.2: The 1 cm geoid experiment, Reports 2015-2019 of the International Association of Geodesy Travaux vol. 41, pp. 56-58.

- Wang, Y.M., Forsberg, R., Sánchez, L., Ågren, J., Huang, J.L., 2018. Report on Colorado geoid comparisons. In: International Symposium on Gravity, Geoid and Height Systems, September 17-21. Copenhagen, Denmark. https://ihrs.dgfi.tum.de/fileadmin/JWG_2015/Wang_report_GGHS2018ColoradoGeoidReportMod.pdf
- Wang, Y.M., Li, X., Ahlgren, K., Krcmaric, J., 2020. Colorado geoid modeling at the US National Geodetic Survey. *Journal of Geodesy*, 94(10), 106. <https://doi.org/10.1007/s00190-020-01429-w>
- Wang, Y.M., Sánchez, L., Ågren, J., Huang, J., Forsberg, R., Abd-Elmotaal, H.A., Ahlgren, K., Barzaghi, R., Bašić, T., Carrion, D., Claessens, S., Erol, B., Erol, S., Filmer, M., Grigoriadis, V.N., Işık, M.S., Jiang, T., Koç, Ö., Krcmaric, J., ... Zingerle, P. (2021). Colorado geoid computation experiment: Overview and summary. *Journal of Geodesy*, 95(12), 127. <https://doi.org/10.1007/s00190-021-01567-9>
- Wang, Y.M., Rapp, R.H., 1990. Terrain effects on geoid undulation computations. *manuscripta geodaetica*, 15, 23-29.
- Wenzel, H., 1985. Hochauflösende Kugelfunktionsmodelle für das Gravitationspotential der Erde (High-resolution spherical function models for the earth's gravitational potential). *Wissenschaftliche Arbeiten der Fachrichtung Vermessungswesen der Universität Hannover*, 137, 1-155.
- Wenzel, H.-G., 1981. Zur Geoidbestimmung durch Kombination von Schwereanomalien und einem Kugelfunktionsmodell mit Hilfe von Integralformeln. *Zeitschrift für Vermessungswesen*, 106, 102–111.
- Wenzel, H.-G., 1983. Geoid computation by least squares spectral combination using integral kernels. In: *Proceedings of the International Association of Geodesy General Meeting*, pp. 438–453. Tokyo, Japan.
- Wessel, P., Smith, W.H.F., 1996. A global, self-consistent, hierarchical, high-resolution shoreline database. *Journal of Geophysical Research: Solid Earth*, 101(B4), 8741–8743. <https://doi.org/10.1029/96JB00104>
- Wichiencharoen, C., 1982. The indirect effects on the computation of geoid undulations. Department of Geodetic Science Report No. 336. The Ohio State University, Columbus, USA. <https://ntrs.nasa.gov/api/citations/19830016735/downloads/19830016735.pdf>
- Winefield, R.L., 2016. Investigating the optimal integration of airborne, ship-borne, satellite and terrestrial gravity data for use in geoid determination. M.Sc. Thesis, Victoria University of Wellington, New Zealand. <https://doi.org/10.26686/wgtn.17018738.v1>
- Wong, J.C.F., 2001. On Picard criterion and the well-posed nature of harmonic downward continuation. M.Sc. Thesis, University of New Brunswick, Fredericton, Canada. <http://www2.unb.ca/gge/Pubs/TR213.pdf>
- Wong, L., Gore, R., 1969. Accuracy of geoid heights from modified Stokes kernels. *Geophysical Journal International*, 18(1), 81–91. <https://doi.org/10.1111/j.1365-246X.1969.tb00264.x>
- Wu, Q., Wang, H., Wang, B., Chen, S., Li, H., 2020. Performance comparison of geoid refinement between XGM2016 and EGM2008 based on the KTH and RCR Methods: Jilin Province, China. *Remote Sensing*, 12(2), 324. <https://doi.org/10.3390/rs12020324>

- Yamazaki, D., Ikeshima, D., Tawatari, R., Yamaguchi, T., O'Loughlin, F., Neal, J.C., Sampson, C.C., Kanae, S., Bates, P.D., 2017. A high-accuracy map of global terrain elevations. *Geophysical Research Letters*, 44(11), 5844–5853. <https://doi.org/10.1002/2017GL072874>.
- Yang, M., Hirt, C., Rexer, M., Pail, R., Yamazaki, D., 2019. The tree-canopy effect in gravity forward modelling. *Geophysical Journal International*, 219(1), 271-289. <https://doi.org/10.1093/gji/ggz264>.
- Yildiz, H., Forsberg, R., Ågren, J., Tscherning, C., Sjöberg, L., 2012. Comparison of remove-compute-restore and least squares modification of Stokes' formula techniques to quasi-geoid determination over the Auvergne test area. *Journal of Geodetic Science*, 2(1), 53–64. <https://doi.org/10.2478/v10156-011-0024-9>
- Yildiz, H., Simav, M., Sezen, E., Akpınar, I., Akdoğan, Y.A., Cingöz, A., Akabali, O.A., 2020. Determination and validation of the Turkish geoid model-2020 (TG-20). *Bollettino di Geofisica Teorica ed Applicata*. <https://doi.org/10.4430/bgta0346>
- Zhang, K., 1997. An evaluation of FFT geoid determination techniques and their application to height determination using GPS in Australia. Ph.D. Thesis, Curtin University of Technology, Perth, Australia. <https://espace.curtin.edu.au/handle/20.500.11937/910?show=full>
- Zhao, Y., Wu, P., Li, J., Lin, Q., Lu, Y., 2019. A new algorithm for the automatic extraction of valley floor width. *Geomorphology*, 335, 37–47. <https://doi.org/10.1016/j.geomorph.2019.03.015>.

Appendix A: Excerpts of- Survey of India, 1950: Part III - Geodetic work

146

TECHNICAL REPORT [PART III, 1948-49

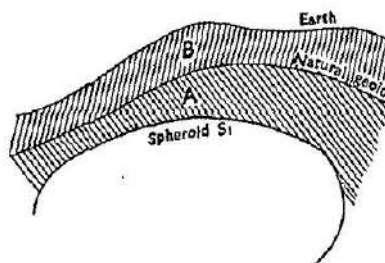
SECTION III—GEOIDS

1. The study of deflections in India on some sort of a systematic basis started in the beginning of this century (see Professional Paper No. 5, Survey of India 1901). In those days, the data was sparse and the plumb-line deflections were plotted and shown vectorially by arrows. Certain important characteristics about their distribution were noticed, such as their being deflected away from the Himalayas in Central India and pointing towards a line in the plains. As more and more data accumulated it was considered that to make a detailed study of the hidden mass anomalies in the earth's crust, it was better to study the rise of the geoid which can be regarded as a synthesis of the deflections rather than individual values of deflections.

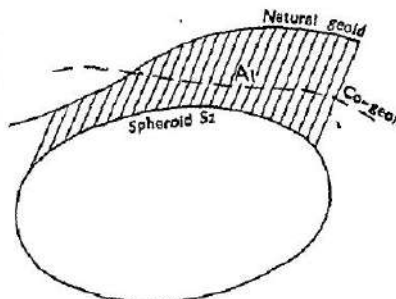
Reliable charts showing the different types of geoids were started in the Survey of India in about 1928 (see Geodetic Report Vol. V, Charts IX, X, XI and XII). These geoidal charts have provided a broad framework for the study of deep seated effects well below the limit of geophysical prospecting. The next step is to narrow down this framework further and further till true knowledge of superficial effects is gained.

Unfortunately the definitions of geoids given on page 57 of Geodetic Report Vol. V are all incorrect. They are accordingly set down in the next para. It is important to put them down clearly as there is no uniformity about their nomenclature and different countries are apt to designate them differently.

2. Natural geoid or Geoid : This is simply the sea-level equipotential surface of the matter comprising the whole earth. It may be reckoned as equipotential of a reference spheroid S_1 + matter A between this spheroid and the geoid + matter B between the geoid and the earth.

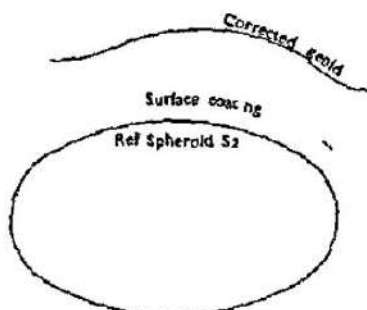


Compensated geoid or Co-geoid : If the topographic masses B between the geoid and the earth be removed together with their compensation, the level surface of the new mass system is called the co-geoid. The new system of masses of which co-geoid is the level surface may be represented by reference spheroid S_2 + matter A_1 .



Obviously all the attracting masses are not external to the co geoid as some parts of A_1 lie above it

Corrected Geoid For many purposes, it is necessary to have a level surface which has no masses external to it. This can be achieved by further modifying the topography by condensing it on reference spheroid S_2 . The equipotential of the new mass system having the same potential as the spheroid S_2 is called the corrected geoid.



Isostatic Geoid This is the theoretical geoid obtained by assuming isostasy to be perfect in all detail. Its height above its reference spheroid can be computed theoretically by calculating the warping produced by the topography and its compensation.

If earth were in isostatic equilibrium, compensated geoid would be a perfect spheroid but not so the isostatic geoid. This will coincide with the natural geoid.

If however as is the actual case isostasy is not perfect then deviation of compensated geoid from its reference spheroid gives a measure of the non fulfilment of isostasy. Some countries particularly the U.S.A. call Co geoid as Isostatic geoid so it is necessary to be clear about the definitions.

Chart XXIV of this Report shows the compensated geoid in India.

3 Normally the observed gravity is reduced to co geoid and is compared against γ_0 the value on the reference spheroid computed theoretically. The conventional isostatic anomaly $(\gamma_c - \gamma_0) = \Delta\gamma_c$ is due to three causes:

- (a) Distance N between co geoid and spheroid
- (b) Matter N between these surfaces
- (c) Anomalous masses

In India the natural geoid has been derived from observed plumb line deflections and not from gravity data. Compensated geoid can be derived by integrating Hayford deflection anomalies but since these are laborious to compute it was derived from the natural geoid by subtracting the height of the isostatic geoid from it. Elevation u of the isostatic geoid above its spheroid was calculated theoretically by considering the effect of topography and its compensation. There is a little irregularity involved here as the conditions under which u is calculated are that masses of geoid and spheroid are the same. This condition is not necessarily satisfied for the geoids determined from plumb line deflections and their reference spheroids but the method has been checked by integrating directly some Hayford deflection anomalies. The results agree to within 1 foot.

Appendix B

Table B.1: Ellipsoidal parameters following Moritz (2000)

Symbol	Name	Dimension
<i>Defining parameters</i>		
a	Semi major axis length	[L]
GM	Geocentric gravitational constant	[L ³][T ²]
J_2	Dynamical form factor	--
ω	Mean angular velocity of Earth's rotation	[T ⁻¹]
<i>Derived geometrical parameters</i>		
b	Semi minor axis length	[L]
c	Polar radius of curvature	[L]
E	Linear eccentricity	[L]
e^2	First numerical eccentricity squared	--
e'^2	First numerical eccentricity squared	--
f	Polar flattening	--
$1/f$	Reciprocal polar flattening	--
Q	Meridian quadrant arc from equator to pole	[L]
R_0	Scale factor for length	[L]
R_1	Mean spherical radius	[L]
R_2	Radius of sphere with same surface area as the ellipsoid	[L]
R_3	Radius of sphere with same volume as the ellipsoid	[L]
<i>Derived physical parameters</i>		
U_0	Normal gravity equipotential on surface of ellipsoid	[L ²][T ²]
J_4	Degree-four even zonal harmonic	--
J_6	Degree-six even zonal harmonic	--
J_8	Degree-eight even zonal harmonic	--
m	Clairaut parameter	--
γ_a	Normal gravity on the ellipsoid surface at the equator	[L][T ⁻²]
γ_b	Normal gravity on the ellipsoid surface at the poles	[L][T ⁻²]
f^*	Normal gravity flattening	--
k	Unnamed (we called it constant in normal gravity formula)	--

Table B.2: Parameters of GRS80 in all the three tide-systems. [ZT= zero-tide; TF=tide-free; MT=mean-tide]

	ZT	TF	MT
GM [m^3s^{-2}]	3.986005000000000E+14	3.986005000000000E+14	3.986005000000000E+14
ω [$rad.s^{-1}$]	7.292115000000000E-05	7.292115000000000E-05	7.292115000000000E-05
J_2	1.08263939308000E-03	1.08263000000000E-03	1.08267050630000E-03
a [m]	6.37813703015779E+06	6.37813700000000E+06	6.37813713005113E+06
b [m]	6.35675225407345E+06	6.35675231414037E+06	6.35675205511047E+06
c [m]	6.39959374685424E+06	6.39959362586401E+06	6.39959414761693E+06
E	5.21855109970296E+05	5.21854009700068E+05	5.21858754440011E+05
e^2	6.69440818830765E-03	6.69438002289616E-03	6.69450148216269E-03
e'^2	6.73952532180726E-03	6.73949677547427E-03	6.73961987742130E-03
f	3.35282481126133E-03	3.35281068118000E-03	3.35287161511507E-03
$1/f$	2.98255965131623E+02	2.98257222101206E+02	2.98251801677077E+02
Q [m]	1.00019657058919E+07	1.00019657293230E+07	1.00019656282799E+07
R_0 [m]	6.36367248889098E+06	6.36367248889098E+06	6.36367248889098E+06
R_1 [m]	6.37100877146301E+06	6.37100877138012E+06	6.37100877173757E+06
R_2 [m]	6.37100718099471E+06	6.37100718092522E+06	6.37100718122489E+06
R_3 [m]	6.37100078998965E+06	6.37100078997414E+06	6.37100079004105E+06
U_0 [m^2s^{-2}]	6.26368658500000E+07	6.26368658500000E+07	6.26368658500000E+07
J_4	-2.37095993044382E-06	-2.37091221865110E-06	-2.37111797112972E-06
J_6	6.08370228569990E-09	6.08347062840596E-09	6.08446964023618E-09
J_8	-1.42692604082946E-11	-1.42681405972791E-11	-1.42729698006965E-11
m	3.44978600310289E-03	3.44978600307769E-03	3.44978600318637E-03
γ_a [ms^{-2}]	9.78032681750099E+00	9.78032677153479E+00	9.78032696975566E+00
γ_b [ms^{-2}]	9.83218627595210E+00	9.83218636851971E+00	9.83218596933875E+00
f^*	5.30242592285509E-03	5.30244011231431E-03	5.30237892285718E-03
k	1.93182300639977E-03	1.93185135328947E-03	1.93172911195904E-03

Table B.3: Parameters of WGS84 in all the three tide-systems. [ZT= zero-tide; TF=tide-free; MT=mean-tide]

	ZT	TF	MT
GM [m^3s^{-2}]	3.98600441800000E+14	3.98600441800000E+14	3.98600441800000E+14
ω [$rad.s^{-1}$]	7.29211500000000E-05	7.29211500000000E-05	7.29211500000000E-05
J_2	1.08263839308000E-03	1.08262900000000E-03	1.08266950630000E-03
a [m]	6.37813703015780E+06	6.37813700000000E+06	6.37813713005113E+06
b [m]	6.35675225417827E+06	6.35675231424520E+06	6.35675205521529E+06
c [m]	6.39959374674872E+06	6.39959362575848E+06	6.39959414751141E+06
E	5.21855108693540E+05	5.21854008423183E+05	5.21858753163265E+05
e^2	6.69440815555109E-03	6.69437999013625E-03	6.69450144940612E-03
e'^2	6.73952528860769E-03	6.73949674227130E-03	6.73961984422171E-03
f	3.35282479482795E-03	3.35281066474494E-03	3.35287159868168E-03
$1/f$	2.98255966593481E+02	2.98257223563226E+02	2.98251803138895E+02
Q [m]	1.00019657059742E+07	1.00019657294052E+07	1.00019656283622E+07
R_0 [m]	6.36367299582987E+06	6.36367299582987E+06	6.36367299582987E+06
R_1 [m]	6.37100877149795E+06	6.37100877141507E+06	6.37100877177252E+06
R_2 [m]	6.37100718102967E+06	6.37100718096018E+06	6.37100718125984E+06
R_3 [m]	6.37100079002467E+06	6.37100079000917E+06	6.37100079007607E+06
U_0 [m^2s^{-2}]	6.26368517146000E+07	6.26368517146000E+07	6.26368517146000E+07
J_4	-2.37095419957422E-06	-2.37090648780648E-06	-2.37111224017979E-06
J_6	6.08367035518563E-09	6.08343869817010E-09	6.08443770882693E-09
J_8	-1.42690792676325E-11	-1.42679594589861E-11	-1.42727886524185E-11
m	3.44978650686606E-03	3.44978650684085E-03	3.44978650694954E-03
γ_a [ms^{-2}]	9.78032538186934E+00	9.78032533590377E+00	9.78032553412478E+00
γ_b [ms^{-2}]	9.83218484529723E+00	9.83218493786360E+00	9.83218453868235E+00
f^*	5.30242721004218E-03	5.30244139931135E-03	5.30238020980227E-03
k	1.93182430579164E-03	1.93185265249369E-03	1.93173041110989E-03

Table B.4: Parameters of IHRS implied possibly new normal ellipsoid (*NOT OFFICIAL*) in all the three tide-systems. [ZT= zero-tide; TF=tide-free; MT=mean-tide]


	ZT	TF	MT
GM [m^3s^{-2}]	3.98600441500000E+14	3.98600441500000E+14	3.98600441500000E+14
ω [$rad.s^{-1}$]	7.29211500000000E-05	7.29211500000000E-05	7.29211500000000E-05
J_2	1.08263559308000E-03	1.08262620000000E-03	1.08266670630000E-03
a [m]	6.37813684115779E+06	6.37813681100000E+06	6.37813694105113E+06
b [m]	6.35675210171768E+06	6.35675216178461E+06	6.35675190275470E+06
c [m]	6.39959352096519E+06	6.39959339997495E+06	6.39959392172786E+06
E	5.21854655859408E+05	5.21853555588155E+05	5.21858300332047E+05
e^2	6.69439693429806E-03	6.69436876888322E-03	6.69449022815310E-03
e'^2	6.73951391559327E-03	6.73948536925753E-03	6.73960847120516E-03
f	3.35281916532672E-03	3.35280503524379E-03	3.35286596918019E-03
$1/f$	2.98256467375733E+02	2.98257724349692E+02	2.98252303907188E+02
Q [m]	1.00019654377677E+07	1.00019654611988E+07	1.00019653601557E+07
R_0 [m]	6.36367281980994E+06	6.36367281980994E+06	6.36367281980994E+06
R_1 [m]	6.37100859467776E+06	6.37100859459487E+06	6.37100859495232E+06
R_2 [m]	6.37100700421486E+06	6.37100700414537E+06	6.37100700444503E+06
R_3 [m]	6.37100061323154E+06	6.37100061321604E+06	6.37100061328295E+06
U_0 [m^2s^{-2}]	6.26368534000000E+07	6.26368534000000E+07	6.26368534000000E+07
J_4	-2.37094059761382E-06	-2.37089288594984E-06	-2.37109863787570E-06
J_6	6.08360822357266E-09	6.08337656759914E-09	6.08437557376241E-09
J_8	-1.42688044508384E-11	-1.42676846500843E-11	-1.42725138094815E-11
m	3.44978622227124E-03	3.44978622224603E-03	3.44978622235472E-03
γ_a [ms^{-2}]	9.78032590317898E+00	9.78032585721398E+00	9.78032605543385E+00
γ_b [ms^{-2}]	9.83218541763973E+00	9.83218551020495E+00	9.83218511102597E+00
f^*	5.30243214532321E-03	5.30244633441570E-03	5.30238514525858E-03
k	1.93183488387683E-03	1.93186323040286E-03	1.93174098936943E-03

Appendix C: Published research papers that provide supporting information.

C.1: Paper on evaluation of global geopotential models.

Note: There is a typographical error in Eq. 9 of paper in C.1 that is the denominator should read r^2 instead of γr .

Evaluation of global geopotential models: a case study for India

Ropesh Goyal ^{*}, Onkar Dikshit and Nagarajan Balasubramania

This paper aims to identify most suitable global geopotential model (GGM) for India, by comparing 15 GGMs developed through 1996 to 2017. The GGM derived geoid undulation values are compared with the geometrical undulation values obtained from GNSS/levelling data on Indian vertical datum. A correction term is added to the computed GGM derived geoid undulation value after fitting three-, four-, five- and seven-parameter models to account for bias and tilt between local geometric Indian vertical datum and global gravimetric vertical datum. The results indicate that EGM2008 model is the best GGM available for India with root-mean-square error (RMSE) of 0.28 m, without model fitting. However, after considering the systematic errors in the two datums with seven-parameter model, GECO GGM has shown significantly better results with RMSE of 0.19 m for India.

Keywords: GGM, Geoid undulation, Accuracy, Bias and tilt, Parameter models, India

Introduction

The mathematical approximation, in terms of coefficients of spherical harmonics, of the Earth's external gravitational potential is termed as global geopotential model (GGM) which have numerous applications (Pavlis 2006, Wenzel 2008). In the past, geodesists have developed certain GGMs for particular applications only. For example, orbit determination of a particular satellite or computing geoid heights for a specific region. However, development of an application independent unique GGM has been one of the important goals of geodesists. GGM development involves combination of a variety of datasets (terrestrial, airborne, satellite, marine). Therefore, accuracy and resolution of such data plays an important role in dictating the overall accuracy and resolution of developed GGMs.

Amos and Featherstone (2003) emphasised on the benefit of selecting a GGM for computation of regional gravimetric geoid model. A proper choice of GGM is one of the important steps in geoid computation. Researchers have tried to make an optimal choice of a GGM that best fits to the local geometric vertical datum of a country/area of interest and with gravity field data (Amos and Featherstone 2003, Benahmed Daho 2010, Ellmann 2010, Kotsakis *et al.* 2010, Strykowski and Forsberg 2010, Doganalp 2016, Yilmaz *et al.* 2017, Saari and Bilker-Koivula 2017).

There are three motivations for conducting the present study for India. First, we need to investigate suitability of any GGM for India in the light of argument by Featherstone (1998) who questions the very need of either a gravimetric geoid or a model of the local vertical datum to transform GNSS heights in India. Secondly, Lambeck

and Coleman (1983) commented that the various GGMs are not as good as they are said to be, because the differences between them are large, which should not have been the case otherwise. And thirdly, Satishkumar *et al.* (2013) derived geoid undulation values for two river basins in India using GOCE level-2 data product (EGM_GOC_2), which contains geoid undulations at an interval of $30' \times 30'$. Geoid undulation values at 148 benchmarks were calculated using interpolation in GOCE user toolbox (GUT) provided by European Space Agency. The authors concluded that after algebraic removal of 1.5 m bias in geoid undulation for GOCE level-2 data product, it is feasible to derive a geoid with an accuracy of 10–15 cm. The GOCE level-2 data comprise spherical harmonic coefficients from satellite data alone and is a lower maximum degree GGM. Generally, lower maximum degree GGMs (low-resolution) have applications in studying plate shifting, satellite orbits, earth rotation variation, etc. and higher maximum degree GGMs (high-resolution) are generally used for computing geoid undulations (Wenzel 2008). It is known that omission errors in the low resolution GGMs are significantly higher than high-resolution GGMs (Tscherning and Rapp 1974). However, as Survey of India (SoI; the competent authority to archive the gravity data in India) has not shared any terrestrial gravity data for the development of high resolution GGMs, it is possible that commission error of high resolution GGMs are more than the omission error of low resolution GGMs. Hence, presently for India, the resolution of GGM does not matter much as long as it fits the control data. Therefore, this study evaluates various lower and higher maximum degree GGMs.

For choosing a GGM for gravimetric geoid computation by combining it with terrestrial data in the modified Stokes formula, it is important to compare the GGM with

Civil Engineering Department, IIT Kanpur, Kanpur, India.

^{*}Corresponding author, email rupeshg@iitk.ac.in

© 2018 Survey Review Ltd
Received 17 January 2018; accepted 16 April 2018
DOI 10.1080/00396265.2018.1468537

402

Survey Review 2019 VOL 51 NO 368

respect to observed gravity anomaly data and GNSS/levelling geometric geoid undulation values. Since gravity data is not available for India, this study is focused on application based comparison of GGM. India neither possess a precise geoid model nor a precise digital elevation model (DEM). Presently, the Indian scientific community for whom heights are an important input in their respective research, make use of SRTM, ASTER, Cartosat DEMs or digitised contours from SoI topographic maps, without mentioning or analysing the accuracy needed (Kumar *et al.* 2007, Ramakrishnan *et al.* 2009, Sreedevi *et al.* 2009, Ahmed *et al.* 2010, Singh and Dowerah 2010, Selvan *et al.* 2011). The claimed accuracy of SRTM30 m for Eurasia is 8.7 m at 90% confidence (Rodríguez *et al.* n.d.) and 10.36 m at 90% confidence with ASTER (Meyer 2011). An alternative to the use of aforementioned sources of height information is to analyse GGMs for the computation of geoid undulations to convert the GNSS derived ellipsoidal heights to orthometric heights.

This paper has two objectives. First, to find the most suitable GGM for the computation of precise geoid undulation values for India, via height anomalies calculated at ellipsoid and continued to Earth's surface utilising the first-order Taylor series which is described in detail in the methodology section. Second, to find a suitable parametric model (from three-, four-, five- and seven-parameter models) to account for the effect of biases, tilts and/or systematic errors in the two datums, the Indian local geometric vertical datum (defined by tide gauge observations) and the global gravimetric vertical datum (defined by GGMs) as suggested by Sjöberg and Bagherbandi (2017). This approach is also further explained in the methodology section. Finally, it is also evaluated whether the aforementioned approaches can replace the need of a precise gravimetric geoid to convert ellipsoidal heights to the orthometric heights with desired accuracy.

In the following sections, first a brief review on different types of GGMs available is presented which is followed by an overview on the data used. The detailed methodology is given in the subsequent section, followed by results and discussions. Finally, the paper ends with the conclusion and suggestions on the scope of future research.

Global geopotential models

GGMs are usually divided into two groups, namely, satellite-only models and combined models. Satellite only models are computed using data from one or more satellites. Amos and Featherstone (2003) explained the limitations on the precision of these models as a factor of the power decay of the gravitational field with altitude, errors in tracking satellite orbits from ground based stations, inaccurate modelling of atmospheric drag, non-gravitational perturbations and incomplete sampling of the global gravity field. Several aforementioned limitations addressed above are reduced significantly by introduction of dedicated satellite gravimetry missions, such as CHAMP, GRACE, and GOCE. Since the damping of the shorter wavelengths of the gravity field is directly proportional to the increasing distance from the Earth, satellite only GGMs have a lower spatial resolution (Barthelmes 2014).

On the other hand, combined models are computed using terrestrial, airborne, shipborne and altimetric gravity data in addition to the satellite data (Rapp 1998) and

therefore, these have higher harmonic degrees. However, there are limitations on the precision of these models as well. These are due to the spatial coverage and quality of the additional data, and merging these data that have different vertical geodetic datums (Heck 1990, Amos and Featherstone 2003). Presently, combined geopotential model is available with the highest degree and order of 2190 and a spatial resolution of about 10 km. However, in practice this spatial resolution only exists in those regions where dense and accurate terrestrial measurements are included in the model (Barthelmes 2014).

GGMs, either satellite only or combined, are truncated at a maximum degree. This truncation of the coefficients above maximum degree produces omission error (Wang 2012). It should be noted that the omission error is due to the fact that a geopotential model can have a finite resolution and therefore a portion is omitted from the Earth's true gravity field spectrum (which extends to infinity). Detailed explanation on omission errors can be found as Kaula's rule in Sansó and Sideris (2013, chapter 3).

Data resources

Table 1 summarises 15 GGMs used in the study whose spherical coefficients were downloaded from ICGEM website (http://icgem.gfz-potsdam.de/tom_longtime) (Barthelmes and Köhler 2016). These GGMs cover a wide range of satellite only (GOCE and/or GRACE) and combined geopotential models with maximum degree varying from 180 to 2190. GNSS/levelling data of 145 ground control points (GCPs) from different parts of India, namely, Hyderabad, Bangalore, Kanpur, Dehradun and Saharanpur were used. These 145 GNSS/levelling data points comprise latitude, longitude, ellipsoidal height and orthometric height. The orthometric height in the dataset varies from 125 to 2000 m reflecting wide variations in the topography of the India. Though the data covers a wide set of topography of India, but is from four regions only and thus the dataset is not sufficient to be a true representative of complete India. However, this dataset can be used for preliminary study for checking the suitability of GGMs in India as the first approximation.

Methodology

In this section, first, a mathematical background on the computation of geoid undulation using GGMs is summarised which is followed by implementation of a two-step methodology.

The equation (1) can be used to compute geoid undulation (N) from height anomaly (ζ) as given by Heiskanen and Moritz (1993, equation 8-100).

$$N(\theta, \lambda) = \zeta(\theta, \lambda, r) + \frac{(\Delta g_B)}{\bar{\gamma}} H, \quad (1)$$

where (θ, λ, r) are the spherical coordinates (co-latitude, longitude, geo-centric radius) of the computation point. Δg_B is the Bouguer anomaly, H is the orthometric height of point P and $\bar{\gamma}$ is an average normal gravity between a point Q' on the ellipsoid and point Q on telluroid (refer Fig. 1).

The equation (1) was modified by Rapp (1997) and rewritten as equation (2) to improve computing efficiency.

$$N(\theta, \lambda) = \zeta_0(\theta, \lambda, r) + C_1(\theta, \lambda) + C_2(\theta, \lambda), \quad (2)$$

Table 1 GGMs used in the study (Barthelmes and Kohler 2016)

Sr. no.	Model name	Degree	Data
1.	EGM96	360	A, EGM96S, G
2.	EGM2008	2190	A, G, S (GRACE)
3.	EIGEN-6C4	2190	A, G, S (GOCE), S (GRACE), S (LAGEOS)
4.	GACO2012	360	A, G, S (GOCE), S (GRACE)
5.	GECO	2190	EGM2008, S (GOCE)
6.	GGM05C	360	A, G, S (GOCE), S (GRACE)
7.	GGM05G	240	S (GOCE), S (GRACE)
8.	GGM05S	180	S (GRACE)
9.	GO_CONS_GCF_2_SPW_R4	280	S (GOCE)
10.	GO_CONS_GCF_2_SPW_R5	330	S (GOCE)
11.	HUST-Grace2016s	160	S (GRACE)
12.	ITU_GGC16	280	S (GOCE), S (GRACE)
13.	ITU_GRACE16	180	S (GRACE)
14.	NULP-02s	250	S (GOCE)
15.	XGM2016	719	A, G, S (GOCC005s)

Notes: Data: S = Satellite tracking data, G = Gravity data, A = Altimetry data.

where ζ_0 is the height anomaly on ellipsoid. This value is corrected by using correction term C_1 to get ζ value at P . C_2 is the correction term to convert height anomaly to geoid undulation.

ζ_0 can be computed by using equation (3) as described by Heiskanen and Moritz (1993).

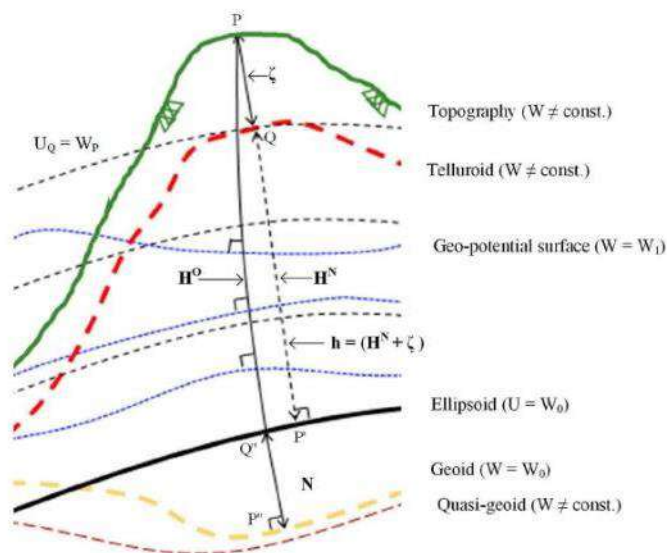
$$\zeta_0(\theta, \lambda, r) = \frac{GM}{\gamma_0 r} \left[\sum_{n=2}^{N_{max}} \left(\frac{a}{r}\right)^n \sum_{m=0}^n (\bar{C}_{nm} \cos m\lambda + \bar{S}_{nm} \sin m\lambda) \times \bar{P}_{nm}(\cos \theta) \right] \quad (3)$$

In this equation, it has been assumed that the ellipsoid has the same mass and the spin rate as the actual

Earth, and that the centre of mass of both the ellipsoid and the Earth are coincident. \bar{C}_{nm} and \bar{S}_{nm} are the fully normalised potential coefficients of degree n and order m , respectively referenced to the normal potential field coefficients of reference ellipsoid. \bar{P}_{nm} are the fully normalised associated Legendre function of the first kind. γ_0 is the normal gravity on the ellipsoid, calculated using Somigliana formula (Somigliana 1929 as cited in Heiskanen and Moritz 1993) for normal gravity.

The correction terms, C_1 and C_2 are given by equations (4) and (5), respectively (Rapp 1997).

$$C_1(\theta, \lambda) = \frac{\partial \zeta}{\partial r} H + \frac{\partial \zeta}{\partial \gamma} \frac{\partial \gamma}{\partial h} H, \quad (4)$$



$H^O \rightarrow$ Orthometric height (PP^*) $H^N \rightarrow$ Normal height (QP')
 $N \rightarrow$ Geoid undulation (P^*Q'') $\zeta \rightarrow$ Height anomaly (QP) $h \rightarrow$ Ellipsoidal height (PP)

1 Various surfaces and heights

$$C_2 = \frac{\Delta g_B}{\gamma} H, \quad (5)$$

where H is the orthometric height, and gradient terms are calculated using equation (6) (Rapp 1997) and equation (7) (derived from Heiskanen and Moritz 1993 equation (2-79)), respectively,

$$\frac{\partial \zeta}{\partial r} = \frac{-GM}{\gamma_0 r^2} \left[\sum_{n=2}^{N_{max}} (n+1) \left(\frac{a}{r}\right)^n \sum_{m=0}^n (\bar{C}_{nm} \cos m\lambda + \bar{S}_{nm} \sin m\lambda) \times \bar{P}_{nm}(\cos \theta) \right]. \quad (6)$$

And

$$\frac{\partial \zeta}{\partial \gamma} \frac{\partial \gamma}{\partial h} = \left[\frac{GM}{\gamma_0^2} \sum_{n=2}^{N_{max}} \left(\frac{a}{r}\right)^n \sum_{m=0}^n (\bar{C}_{nm} \cos m\lambda + \bar{S}_{nm} \sin m\lambda) \times \bar{P}_{nm}(\cos \theta) \right] \times \left[\frac{\gamma_e (1 + k \sin^2 \phi) (2 - e^2 (1 + \sin^2 \phi))}{a(1 - e^2)} + 2\omega^2 \right]. \quad (7)$$

where a, k, e, ω and γ_e are the constants with their defined values and meaning, as mentioned by Moritz (1980) for GRS80.

Δg_B in equation (5) is computed according to Heiskanen and Moritz (1993, equations (3-15) and (3-18)), which is given by equation (8).

$$\Delta g_B = \Delta g_{FA} - 0.01119H. \quad (8)$$

Free-air gravity anomaly (Δg_{FA}) using GGM is computed using equation (9), which is derived from the relationship among equations (2-152), (2-153) and (2-154) in Heiskanen and Moritz (1993)

$$\Delta g_{FA}(\theta, \lambda, r) = \frac{GM}{\gamma r} \left[\sum_{n=2}^{N_{max}} (n-1) \left(\frac{a}{r}\right)^n \sum_{m=0}^n (\bar{C}_{nm} \cos m\lambda + \bar{S}_{nm} \sin m\lambda) \times \bar{P}_{nm}(\cos \theta) \right]. \quad (9)$$

Rapp (1997) suggested that the evaluation of (9) should have been done on Earth's surface. Since a small correction term is computed, it seems reasonable to evaluate (9) on the ellipsoid, i.e. $\gamma = \gamma_0$ and $r = r_E$.

The aforementioned strategy was programmed in MATLAB software and was implemented as the first step given in the flowchart (Fig. 2). First, the geodetic coordinates of all the 145 GCPs were read in the software and transformed to spherical coordinates. Then the spherical harmonic coefficients ($\bar{C}_{nm}, \bar{S}_{nm}$) of all 15 GGMs were read from the respective files with '.gfc' extension available from ICGEM. The degree $n = 2, 4, 6$ and 8 zonal coefficients have been referenced to the field implied by an equipotential reference ellipsoid using equation (10) (Losch and Seuffer 2003)

$$\bar{C}_{n0} = \bar{C}_{n0} + \left(\frac{GM_{ref}}{GM_{GGM}} \right) \times \left(\frac{a_{ref}}{a_{GGM}} \right)^{(n/2)} \left(\frac{J_n}{\sqrt{4(n/2) + 1}} \right), \quad (10)$$

where GM_{ref} and GM_{GGM} are the Earth's gravity constant for reference ellipsoid (GRS80) and the GGM being used, respectively. a_{ref} is the equipotential radius of reference ellipsoid (GRS80) and a_{GGM} is the equipotential scale

factor for GGM. J_2 is the dynamical form factor and J_4, J_6 and J_8 are the derived physical constants for GRS80 reference ellipsoid.

Fully normalised associated Legendre polynomials of the first kind were calculated as proposed by Moazezi and Zomorrodian (2012). The geoid undulation values were computed using equation (2) by developing subroutines for equations (3-5). For the computations in equations (4) and (5), H value has been extracted from SRTM30 m DEM for the given geodetic coordinates of points.

Basic statistical analysis, by calculating mean, standard deviation, mean absolute error (MAE) and root-mean-square error (RMSE) was done to check the suitability of the GGMs for India by comparing the observed and calculated geoid undulation values using equation (11).

$$\Delta N_{GGM} = N_{GNSS/levelling} - N_{GGM} = h - H - N_{GGM}. \quad (11)$$

In equation (11),

$$N_{GNSS/levelling} = h(\text{ellipsoidal height}) - H(\text{levelling height}).$$

MAE and RMSE are calculated by using equations (12) and (13), respectively.

$$\text{MAE} = \frac{\sum_{i=1}^n |h_i - H_i - N_i^{GGM}|}{n}, \quad (12)$$

$$\text{RMSE} = \sqrt{\frac{\sum_{i=1}^n (h_i - H_i - N_i^{GGM})^2}{n}}, \quad (13)$$

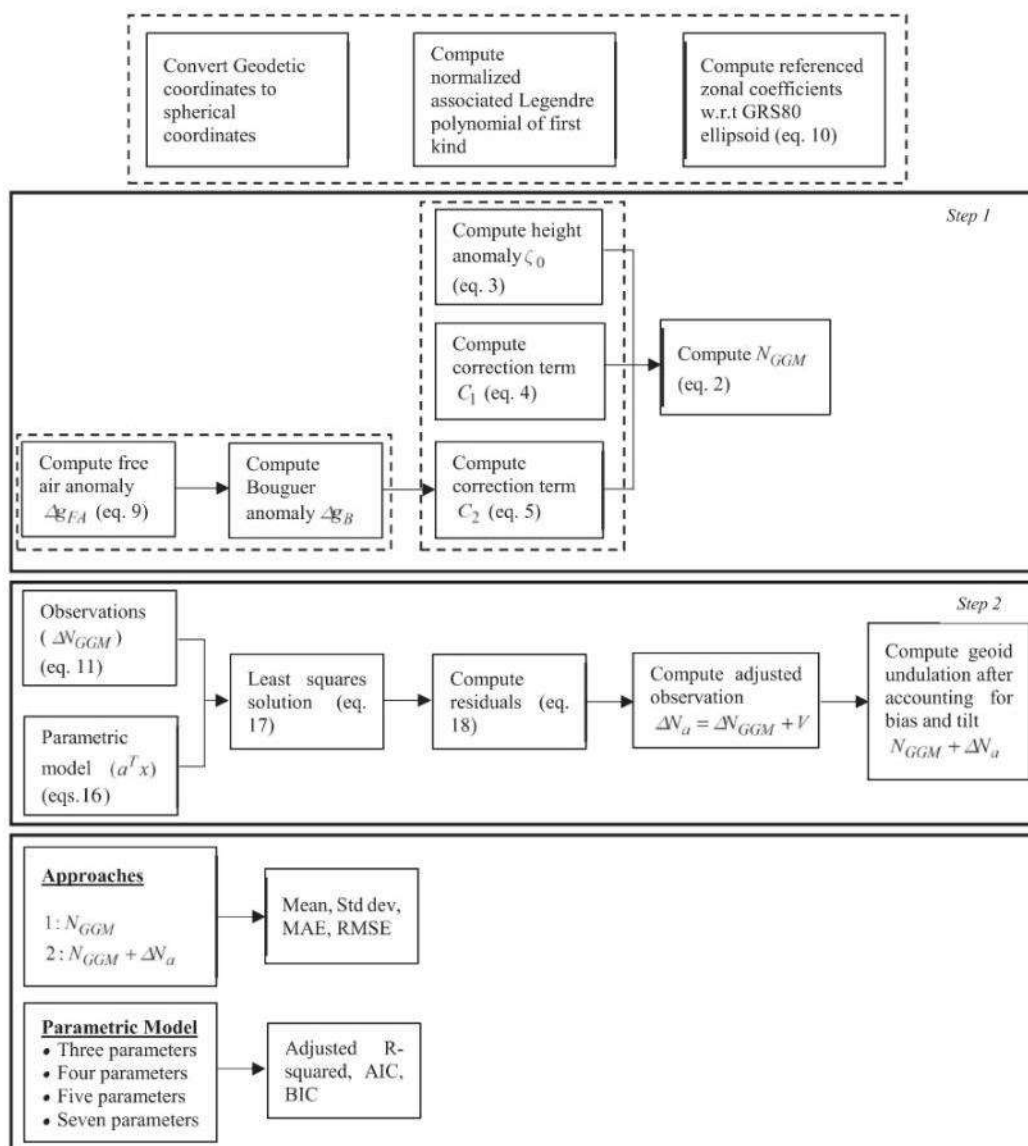
Datum inconsistencies influence the comparison results between geoid undulations derived from GNSS/levelling and GGMs. In the second step (Fig. 2), therefore, various parametric models (with three-, four-, five- and seven-parametric model) are used to minimise the effect of datum inconsistencies (Kotsakis et al. 2010, Yilmaz et al. 2010, Sjöberg and Bagherbandi 2017).

The basic model to study comparisons of geoid evaluations from GGM and GNSS/levelling is given by equation (14) (Kotsakis and Sideris 1999)

$$\Delta N = N_{GNSS/levelling} - N_{GGM} = h - H - N_{GGM} = a^T X + V, \quad (14)$$

where X is an $m \times 1$ vector of unknown parameters in the parametric model, a is an $m \times n$ vector of known coefficients and V is an $n \times 1$ vector of residuals, n is the number of observations and m is the number of parameters in the model. All the possible datum inconsistencies and systematic bias in the data are described by the parametric part $a^T X$. As an example, for a five-parameter model and one observation ($h - H - N_{GGM}$), matrices a and X are given by equation (15). The three-, four-, five- and seven-parameter transformation models as given in equation (16), were implemented in this study to analyse the removal of biases.

$$a = \begin{pmatrix} \cos \phi \cos \lambda \\ \cos \phi \sin \lambda \\ \sin \phi \\ \sin^2 \phi \\ 1 \end{pmatrix} \text{ and } X = \begin{pmatrix} x_1 \\ x_2 \\ x_3 \\ x_4 \\ x_5 \end{pmatrix}. \quad (15)$$



2 Flowchart of the methodology

$$\left. \begin{aligned}
 \text{Three-parameter: } \Delta N &= (\cos \phi \cos \lambda)x_1 + (\cos \phi \sin \lambda)x_2 + (\sin \phi)x_3 + V \\
 \text{Four-parameter: } \Delta N &= (\cos \phi \cos \lambda)x_1 + (\cos \phi \sin \lambda)x_2 + (\sin \phi)x_3 + x_4 + V \\
 \text{Five-parameter: } \Delta N &= (\cos \phi \cos \lambda)x_1 + (\cos \phi \sin \lambda)x_2 + (\sin \phi)x_3 + (\sin^2 \phi)x_4 + x_5 + V \\
 \text{Seven-parameter: } \Delta N &= (\cos \phi \cos \lambda)x_1 + (\cos \phi \sin \lambda)x_2 + (\sin \phi)x_3 + \left(\frac{\cos \phi \sin \phi \sin \lambda}{W}\right)x_4 + \\
 &\quad \left(\frac{\cos \phi \sin \phi \cos \lambda}{W}\right)x_5 + \left(\frac{1 - f^2 \sin^2 \phi}{W}\right)x_6 + \left(\frac{\sin^2 \phi}{W}\right)x_7 + V
 \end{aligned} \right\} \quad (16)$$

where (ϕ, λ) are the geodetic coordinates of the points, f is the flattening of the reference ellipsoid and W is given by $\sqrt{1 - e^2 \sin^2 \phi}$.

There is no information regarding the accuracy of the GNSS/levelling and GGM driven geoid undulations. Therefore, the solution is achieved by the unweighted least squares adjustment technique (Ghilani

Table 2 Statistical results of ΔN_{GGM} for 15 GGMs (all values in m)

Sr. no.	Model name	Nmax	Mean	S.D.	MAE	RMSE
1.	EGM96	360	-0.02	0.76	0.53	0.76
2.	EGM2008	2190	-0.06	0.28	0.22	0.29
3.	EIGEN-6C4	2190	-0.11	0.32	0.27	0.34
4.	GAO2012	360	-0.11	0.49	0.39	0.50
5.	GECO	2190	-0.11	0.31	0.27	0.33
6.	GGM05C	360	-0.13	0.37	0.33	0.39
7.	GGM05G	240	-0.04	0.47	0.36	0.47
8.	GGM05S	180	-0.45	0.58	0.65	0.74
9.	GO_CONS_GCF_2_SPW_R4	280	-0.05	0.48	0.39	0.48
10.	GO_CONS_GCF_2_SPW_R5	330	-0.08	0.48	0.40	0.48
11.	HUST-Grace2016s	160	-0.44	0.52	0.57	0.68
12.	ITU_GGC16	280	-0.05	0.47	0.38	0.47
13.	ITU_GRACE16	180	-0.02	2.34	2.16	2.33
14.	NULP-02s	250	-0.16	0.46	0.41	0.49
15.	XGM2016	719	-0.14	0.32	0.28	0.35

2010) as given by equation (17). If the above information was known, it could have led to a better estimate of the parameters of the parametric model being investigated to account for the datum inconsistencies.

$$X = (A^T A)^{-1} (A^T L), \quad (17)$$

where A is the design matrix of size $n \times m$ and A^T is the transpose of matrix A . L is an $n \times 1$ matrix of the observations obtained using equation (11). Residuals are calculated by equation (18) and are added to matrix L to obtain adjusted ΔN (ΔN_a).

$$V = AX - L. \quad (18)$$

These ΔN_a value represents the biases, tilts or any other type of systematic differences between the two data sets (N_{GGM} and $N_{GNSS/levelling}$). ΔN_a values are added to N_{GGM} to obtain a solution of geoid undulation, which accounts for the datum inconsistencies between the global gravimetric and local geometric vertical datums. The geoid undulation values obtained after the transformation between the two datums are also statistically compared with the $N_{GNSS/levelling}$ values. The complete methodology is depicted in Fig. 2.

A test statistic of goodness of fit of a regression model, known as coefficient of determination (R^2) or R -squared is generally implemented to assess how well a model fits the observation points. A general expression of R -squared is given by equation (19) (Rao et al. 2008).

$$R^2 = 1 - \frac{SS(\text{res})}{SS(\text{tot})}, \quad (19)$$

where $SS(\text{tot}) = \sum_i (y_i - Y)^2$ is total sum of squares and $SS(\text{res}) = \sum_i (\hat{y}_i - y_i)^2$ is sum of squares of residuals. y_i are the individual observations ($h_i - H_i - N_i^{GGM}$ in the present case), Y is the mean value for the set of observations and \hat{y}_i are the adjusted observations ($h_i - H_i - (N_i^{GGM} + \Delta N_i^a)$). However, it is known that R -squared value always increases with the addition of every new parameter to a model, i.e. it is not adjusted for the degrees of freedom. Hence, an ever-increasing value with the addition of parameter can be misleading while estimating the better fit of a model. Therefore, three tests are performed to check the better fit of a model. Firstly, the adjusted coefficient of determination

or adjusted R -squared which is given by equation (20) (Heumann et al. 2016). In a regression model, it may appear reasonable to add more variables to get a good R -squared value. However, some of the variables may be insignificant. The adjusted R -squared penalises for such extra variables and therefore, is a better check than the R -squared value (Rao et al. 2008).

$$R_{adj}^2 = 1 - (1 - R^2) \left(\frac{n-1}{n-k-1} \right). \quad (20)$$

In the above equation, n is the sample size and k is the number of parameters in the transformation model.

The second approach is based on the relationship between likelihood and information theory and is known as Akaike's information criterion (AIC) (Akaike 1998). It is used to select a better model from a set of models (Rao et al. 2008) and is given by equation (21).

$$AIC = n \ln(SS(\text{res})) + 2k - n \ln(n). \quad (21)$$

The AIC is known to be a better model selection criterion in terms that the adjusted R -squared considers only fit to the data via $SS(\text{res})$, while AIC, in addition to what adjusted R -squared do, considers the parsimony of the model via the term $2k$ (Heumann et al. 2016).

Finally, the Bayesian information criterion (BIC) developed by Schwarz (1978, as cited in Rao et al. 2008) was used to assess the model choice. The BIC is given by equation (22).

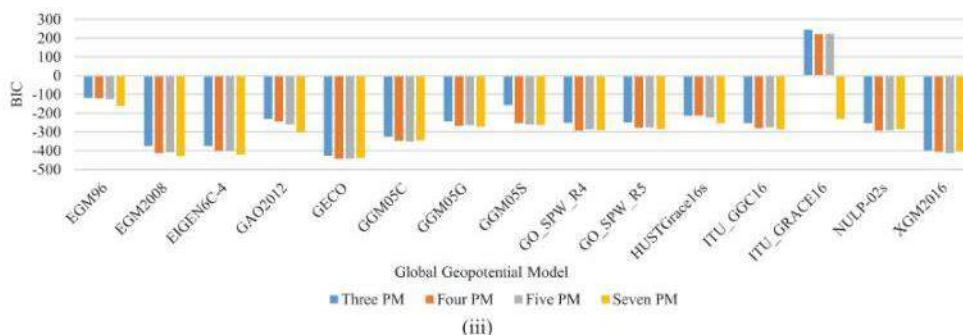
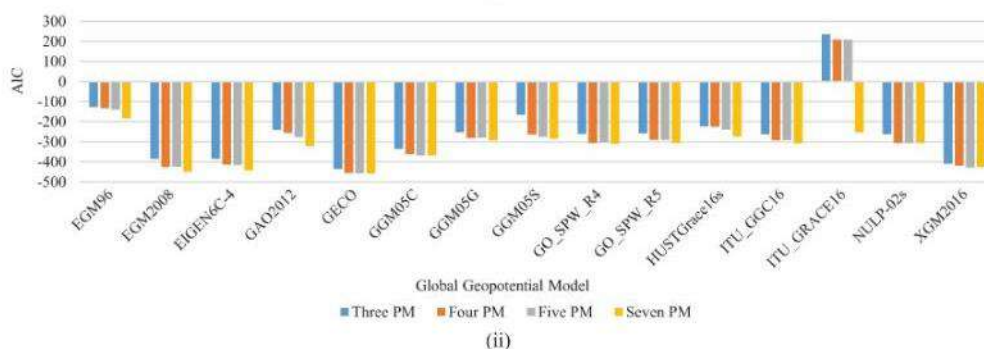
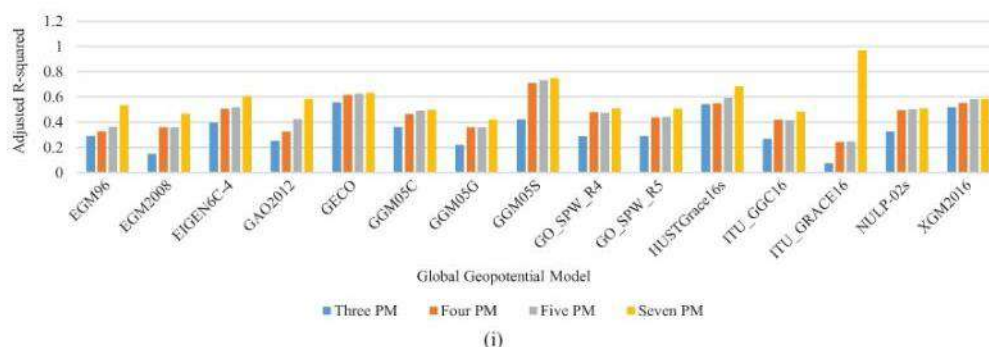
$$BIC = n \ln(SS(\text{res})) + k \ln(n) - n \ln(n). \quad (22)$$

Suitability of a model is inversely proportional to the AIC and BIC values and is directly proportional to the R_{adj}^2 value.

The seven-parameter model was fitted 10 times to a set of randomly selected 100 points from the dataset of 145 points. The remaining 45 points were used for validating the computed parameters.

Results and discussion

Table 2 presents the basic statistical results of ΔN_{GGM} ($= h_i - H_i - N_{GGM}$) for all the 15 GGMs with varying maximum degree. It is observed from Table 2 that the



PM → Parametric model

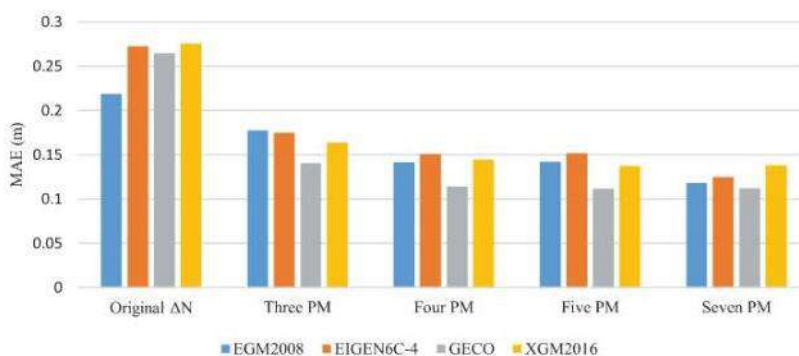
3 Model selection criteria results for all GGMs (i) Adjusted R-squared (ii) AIC (iii) BIC

GGMs with higher maximum degrees have shown better results as compared to the GGMs with relatively lower maximum degrees. It is evident from the fact that the omission errors of a GGM reduces with an increase in the resolution or the maximum degree of a GGM (Wenzel 2008). Among the high degree GGMs (EGM2008, EIGEN-6C4 & GECO), EGM2008 can be considered as the best model with least standard deviation, MAE and RMSE of 0.28, 0.22 and 0.29 m, respectively. However, along with EIGEN-6C4 and GECO, XGM2016 (maximum degree 719) can also be considered as a suitable GGM with the test statistic only marginally different from EGM2008.

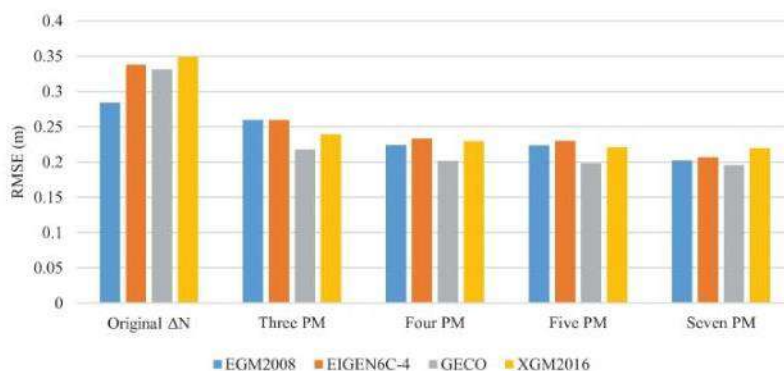
Among the low degree GGMs, it is observed that the GGM05C (maximum degree 360) has shown the best results with standard deviation, MAE and RMSE of 0.37, 0.33 and 0.39 m, respectively. The RMSE of other low maximum degree GGMs fall in the range of 0.47–

2.33 m with ITU_GRACE16 (maximum degree 180) having the poorest results.

Figure 3 shows the results for different criteria (adjusted R-squared, AIC and BIC) applied to check the suitability of the parametric models used to combine global gravimetric and local geometric vertical datums. As mentioned earlier, the higher values of adjusted R-squared and lower values of AIC and BIC support the choice of a model. It is observed from Fig. 3 that the adjusted R-squared values are higher for the seven-parameter model as compared to other models. Also, AIC and BIC values are lower for the seven-parameter model as compared to other models for all GGMs, except GECO, GGM05C, GO_CONS_GCF_2_SPW_R4, NULP-02S and XGM2016, for which the BIC values of seven-parameter model are marginally higher as compared to either four- or five-parameter models. However, adjusted R-squared values are higher and AIC values are



(i)



(ii)

PM → Parametric model

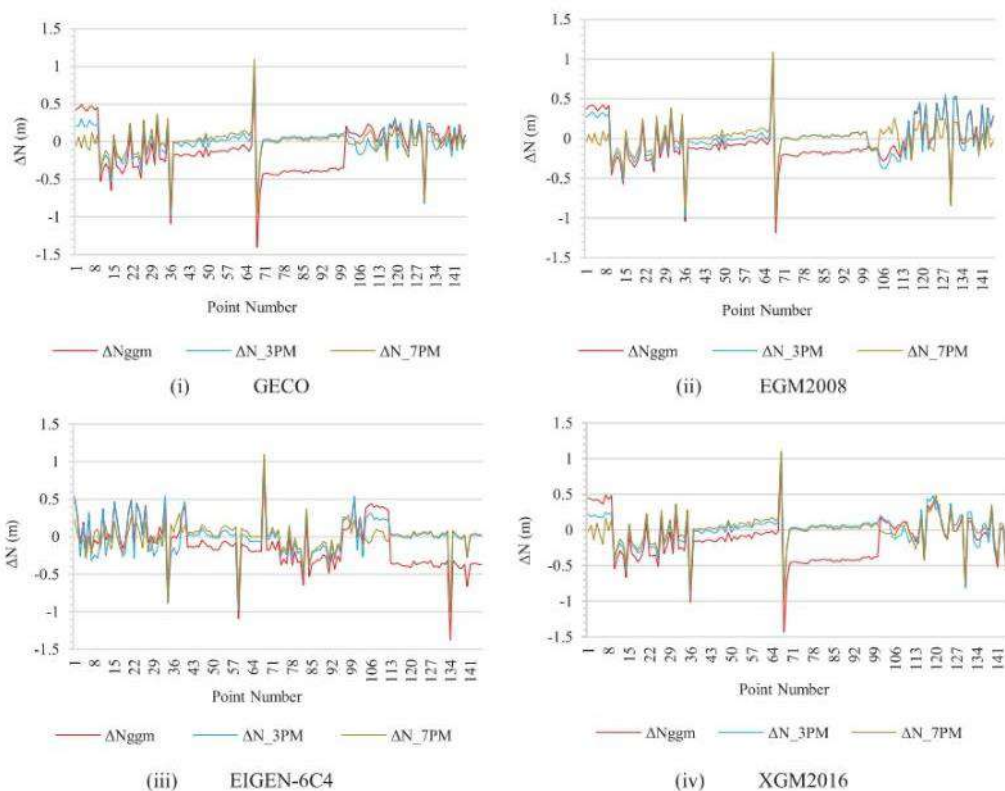
4 MAE and RMSE of ΔN_{GGM} and ΔN after fitting various parametric models to the higher maximum degree GGMs

Table 3 Parameters of seven-parameter model for high degree GGMs

Parameters of seven-parameter model							
GGMs	x_1	x_2	x_3	x_4	x_5	x_6	x_7
EGM2008	251.35689	1314.4632	548.46074	-133.7303	-133.7303	557.86106	-1333.8827
GECO	179.86129	1326.3552	-244.5312	205.94775	54.93856	955.29621	-1314.1874
EIGEN-6C4	383.48266	2021.9521	477.67652	-86.16844	-518.97706	1019.15	-2047.8806
XGM2016	299.90849	1852.0572	-303.65079	196.38916	92.05152	1292.8664	-1850.8774

Table 4 Statistical results of ΔN for 15 GGMs post fitting seven-parameter model (all values in m)

Sr. no.	Model name	Nmax	Mean	S.D.	MAE	RMSE
1.	EGM96	360	0	0.51	0.30	0.51
2.	EGM2008	2190	0	0.20	0.12	0.20
3.	EIGEN-6C4	2190	0	0.21	0.13	0.21
4.	GAO2012	360	0	0.31	0.21	0.31
5.	GECO	2190	0	0.20	0.12	0.20
6.	GGM05C	360	0	0.27	0.18	0.27
7.	GGM05G	240	0	0.35	0.22	0.35
8.	GGM05S	180	0	0.36	0.24	0.36
9.	GO_CONS_GCF_2_SPW_R4	280	0	0.33	0.21	0.33
10.	GO_CONS_GCF_2_SPW_R5	330	0	0.33	0.21	0.33
11.	HUST-Grace2016s	160	0	0.37	0.24	0.37
12.	ITU_GGC16	280	0	0.33	0.22	0.33
13.	ITU_GRACE16	180	0	0.40	0.26	0.40
14.	NULP-02s	250	0	0.33	0.21	0.33
15.	XGM2016	719	0	0.22	0.14	0.22



5 Plot of ΔN_{ggm} and ΔN after three- (delta N_3PM) and seven-parameter (delta N_7PM) fitting for four GGMs on all 145 data points

lower of these GGMs for seven-parameter model as compared to other GGMs. Therefore, it is observed that the seven-parameter model is statistically the best parametric model to account for the inconsistencies between the two vertical datums.

The improvement in the MAE and RMSE of the four high degree GGMs after accounting for the bias and tilts by various parametric model fitting is depicted in Fig. 4.

Figure 4 shows an improvement in the geoid undulation values, based on MAE and RMSE of $\Delta N(=h_i - H_i - (N_{GGM} + \Delta N_i))$, after considering the datum inconsistencies using different parametric models as compared to gravimetric geoid undulation values obtained from GGM alone. There is not significant deviation in the results of geoid undulation among three-, four-, five- or seven-parameter models for any GGM.

Table 5 Statistical results of ΔN for four GGMs on 10 different samples of 100 random data points and remaining 45 test points (all values in m)

GGM name	Statistic	S ^a 1	S 2	S 3	S 4	S 5	S 6	S 7	S 8	S 9	S 10	Average
GECO	Mean	0.08	0.02	0.01	0.02	-0.06	0.02	-0.03	-0.05	-0.03	-0.03	-0.01
	S.D.	0.20	0.13	0.14	0.24	0.20	0.12	0.20	0.20	0.19	0.22	0.18
	MAE	0.12	0.10	0.10	0.13	0.13	0.09	0.11	0.10	0.11	0.12	0.11
	RMSE	0.21	0.13	0.13	0.24	0.21	0.12	0.20	0.20	0.19	0.22	0.19
EGM2008	Mean	0.08	0.02	0.01	0.02	-0.06	0.04	-0.04	-0.06	-0.03	-0.04	-0.01
	S.D.	0.20	0.13	0.14	0.24	0.21	0.15	0.21	0.21	0.21	0.22	0.19
	MAE	0.12	0.10	0.10	0.13	0.14	0.11	0.13	0.10	0.12	0.12	0.12
	RMSE	0.21	0.13	0.14	0.24	0.22	0.15	0.21	0.21	0.20	0.22	0.19
EIGEN-6C4	Mean	0.08	0.01	0.01	0.01	-0.06	0.04	-0.04	-0.06	-0.04	-0.03	-0.01
	S.D.	0.20	0.13	0.15	0.25	0.21	0.16	0.22	0.21	0.21	0.23	0.20
	MAE	0.13	0.10	0.11	0.13	0.14	0.12	0.13	0.11	0.12	0.13	0.12
	RMSE	0.21	0.13	0.15	0.25	0.22	0.16	0.22	0.21	0.21	0.23	0.20
XGM2016	Mean	0.10	0.02	-0.02	0.03	-0.08	0.02	-0.03	-0.06	0.01	-0.07	-0.01
	S.D.	0.20	0.17	0.16	0.26	0.23	0.15	0.25	0.20	0.22	0.26	0.21
	MAE	0.13	0.13	0.12	0.16	0.16	0.11	0.16	0.11	0.15	0.17	0.14
	RMSE	0.22	0.17	0.16	0.26	0.24	0.15	0.25	0.21	0.22	0.26	0.21

^aSample.

However, only a marginal improvement is observed in the geoid undulation values from GGM accounted for datum inconsistencies with seven-parameter model as compared to other parametric models. The parameters calculated for seven-parameter model for the four high degree GGMs are listed in Table 3. The results of basic statistics after correcting for biases, tilts or systematic errors in the two datums using seven-parameter model is listed in Table 4. The greatest improvement can be seen from the MAE and RMSE values of ΔN_{GGM} from ITU-GRACE16, which were 2.16 and 2.33 m, respectively. After accounting for bias and tilts with seven-parameter model, the values of MAE and RMSE of ΔN are 0.26 and 0.39 m, respectively. Considering the systematic errors by fitting the seven-parameter model, it is observed that EGM2008 has performance improvement with MAE and RMSE of 0.12 and 0.2 m, respectively. However, GECO proved a marginally more suitable GGM with a 0.004 m lower value of RMSE and 0.006 m lower value of MAE, as compared to EGM2008.

A comparison in datum inconsistencies for four GGMs, before and after accounting for the biases, tilts and systematic errors using three- and seven-parameter model is shown in Fig. 5. The Figure 5 shows that the biases and tilts in the two datums are significantly minimised after fitting the seven-parameter model as compared to the three-parameter model.

The statistical results of ΔN for multiple test conducted with 10 different sets of 100 random model points and 45 remaining test points using seven-parameter model on four GGMs, i.e. GECO, EGM2008, EIGEN-6C4 and XGM2016, are summarised in Table 5. It is observed from the table, that it is possible to obtain geoid undulation values accurate up to 19 cm by using GGMs and the transformation parameters obtained for seven-parameter model. Table 5 also depicts that it is possible that GGMs can do better with a set of data points (samples 2, 3 and 6) and may not with some other set of data points.

Conclusion

The present study shows that high degree GGMs provide better results as compared to low degree GGMs. For India, with the available data, EGM2008 provides initially better results as compared to other high degree GGMs. However, after accounting for datum inconsistencies, GECO and EGM2008 show almost similar results. EIGEN-6C4 and XGM2016 also proved suitable GGMs with deviations limited to ± 2 cm. To choose a suitable GGM, multiple tests with random sample dataset demonstrates that if a well spread data points are chosen for computing the parameters of seven-parameter model, GECO can provide undulation values that can be used to calculate orthometric heights with an estimated accuracy of ± 19 cm. With the availability of only limited data points for India, the study can be considered as preliminary. However, it provides an alternative to use more meaningful heights than which are being presently used in India. It can also be inferred that a precise gravimetric geoid is needed for India and cannot be replaced by a formulated transformation model to convert the ellipsoidal heights to the orthometric heights as per the need of present scientific community. For India, in the absence of a precise geoid model or precise DEM, the present study

can be replicated by the competent authority (SoI) with the complete GNSS/levelling dataset to compute the parameters of the seven-parameter model which will define a precise conversion surface. The geoid undulation value (obtained using GGM and parameters of conversion surface) with ellipsoidal height can provide orthometric height which is an important input for various practical and research applications.

Future scope

Although, the study was carried out using ground data selected from different topography of the India, the size of the dataset is quite small for a large country like India. Therefore, it is possible that using a dense and well spread data may result in better calculation of parameters to account for datum inconsistencies. Also, the error variances are not available for the GNSS/levelling data. If the data were available, a corrector surface incorporating the random noise effects could be developed and may yield an improvement in the transformation model to convert ellipsoidal heights to orthometric heights. It is observed from the present study that the combined GGMs with high degree presented themselves to be the suitable candidates, it is suggested that a spectral combination of the two or more GGMs from GECO, EGM2008, EIGEN-6C4 and XGM2016, will be helpful to calculate precise geoid undulation values.

Acknowledgement

The authors would like to thank Dr Christopher Jekeli and Dr Siamak Moazezi for providing conceptual help in developing the MATLAB based software for the computation of geoid undulation.

ORCID

Ropesh Goyal  <http://orcid.org/0000-0002-2178-3265>

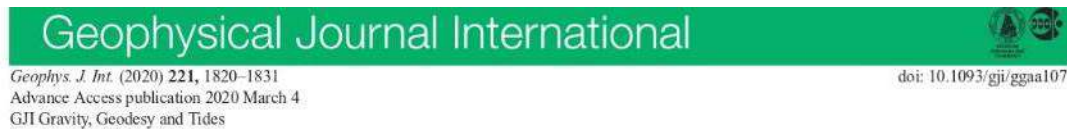
References

- Ahmed, S.A., et al., 2010. Evaluation of morphometric parameters derived from ASTER and SRTM DEM – a study on Bandihole sub-watershed Basin in Karnataka. *Journal of the Indian society of remote sensing*, 38 (2), 227–238.
- Akaike, H., 1998. Information theory and an extension of the maximum likelihood principle. In: E. Parzen, K. Tanabe, and G. Kitagawa, eds. *Selected papers of Hirotugu Akaike*. New York: Springer New York, 199–213.
- Amos, M. and Featherstone, W., 2003. Comparisons of recent global geopotential models with terrestrial gravity field observations over New Zealand and Australia. *Geomatics research Australasia*, 79, 1–20.
- Barthelmes, F., 2014. Global models. In: E. Grafarend, ed. *Encyclopedia of geodesy*. Cham: Springer International Publishing, 1–9.
- Barthelmes, F. and Köhler, W., 2016. International centre for global earth models (ICGEM). In: H. Drewes et al., eds. *The geodesists handbook 2016*. *Journal of Geodesy* (2016), 90(10), pp 907–1205, doi: 10.1007/s00190-016-0948-z.
- Benahmed Daho, S.A., 2010. Assessment of the EGM2008 gravity field in Algeria using gravity and GPS/levelling data. In: S.P. Mertikas, ed. *Gravity, geoid and earth observation: IAG Commission 2: gravity field, Chania, Crete, Greece, 23–27 June 2008*. Berlin, Heidelberg: Springer Berlin Heidelberg, 459–466.
- Doganalp, S., 2016. An evaluation of recent global geopotential models for strip area project in Turkey. *Earth sciences research journal*, 20 (3), 1.
- Ellmann, A., 2010. Validation of the new earth gravitational model EGM2008 over the alitic countries. In: S.P. Mertikas, ed. *Gravity, geoid and earth observation: IAG commission 2: gravity field*.

- Chania, Crete, Greece, 23–27 June 2008. Berlin, Heidelberg: Springer Berlin Heidelberg, 489–496.
- Featherstone, W., 1998. Do we need a gravimetric geoid or a model of the Australian height datum to transform GPS heights in Australia? *Australian surveyor*, 43 (4), 273–280.
- Ghilani, C.D., 2010. *Adjustment computations: spatial data analysis*, 5th ed. Hoboken, NJ: John Wiley & Sons.
- Heck, B., 1990. An evaluation of some systematic error sources affecting terrestrial gravity anomalies. *Bulletin géodésique*, 64 (1), 88–108.
- Heiskanen, W.A. and Moritz, H., 1993. *Physical geodesy, re-print*. New York: Springer-Wien.
- Heumann, C., Schomaker, M., and Shalabh, 2016. *Introduction to statistics and data analysis with exercises, solutions and applications in R*. Switzerland: Springer-Cham.
- Kotsakis, C. and Sideris, M.G., 1999. On the adjustment of combined GPS/levelling/geoid networks. *Journal of geodesy*, 73 (8), 412–421.
- Kotsakis, C., et al., 2010. Evaluation of EGM2008 using GPS and levelling heights in Greece. In: S.P. Mertikas, ed. *Gravity, geoid and earth observation: IAG commission 2: gravity field, Chania, Crete, Greece, 23–27 June 2008*. Berlin: Springer Berlin Heidelberg, 481–488.
- Kumar, A., Chingkhel, R.K., and Dolendro, T., 2007. Tsunami damage assessment: a case study in Car Nicobar Island, India. *International journal of remote sensing*, 28 (13–14), 2937–2959.
- Lambeck, K. and Coleman, R., 1983. The earth's shape and gravity field: a report of progress from 1958 to 1982. *Geophysical journal of the royal astronomical society*, 74, 25–54.
- Losch, M. and Seuffer, V. 2003. *How to compute geoid undulations (geoid height relative to a given reference ellipsoid) from spherical harmonic coefficients for satellite altimetry applications*. Available from: <http://citeseerx.ist.psu.edu/viewdoc/download?doi=10.1.1.508.185&rep=rep1&type=pdf> [Accessed 28 September 2018].
- Meyer, D. 2011. *ASTER global digital elevation model version 2 – summary of validation results*. Joint Japan-US ASTER Science Team. Available from: http://www.jspacesystems.or.jp/ersdac/GDEM/ver2/Validation/Summary_GDEM2_validation_report_final.pdf [Accessed 20 October 2017].
- Moazezi, S. and Zomorrodian, H., 2012. GGMCalc a software for calculation of the geoid undulation and the height anomaly using the iteration method, and classical gravity anomaly. *Earth science informatics*, 5 (2), 123–136.
- Moritz, H., 1980. Geodetic reference system 1980. *Bulletin géodésique*, 54 (3), 395–405.
- Pavlis, N.K., 2006. An overview considering current and future dedicated gravity mapping missions: prepared for IGeS geoid school 2006. *Proc. Lecture Notes International school for the determination and use of the geoid*. Como, Italy, 15–19 September 2008.
- Ramakrishnan, D., Bandyopadhyay, A., and Kusuma, K.N., 2009. SCS-CN and GIS-based approach for identifying potential water harvesting sites in the Kali Watershed, Mahi River Basin, India. *Journal of earth system science*, 118 (4), 355–368.
- Rao, C.R., Toutenburg, H., and Shalabh, H.C., 2008. *Linear models and generalizations*. Berlin: Springer-Verlag.
- Rapp, R.H., 1997. Use of potential coefficient models for geoid undulation determinations using a spherical harmonic representation of the height anomaly/geoid undulation difference. *Journal of geodesy*, 71 (5), 282–289.
- Rapp, R.H., 1998. Past and future developments in geopotential modeling. In *Geodesy on the move*. Rio de Janeiro, Brazil: Springer, 58–78.
- Rodriguez, E., et al. n.d. An assessment of the SRTM topographic products. Jet Propulsion Laboratory D-31639. Available from: https://www2.jpl.nasa.gov/srtm/SRTM_D31639.pdf. [Accessed 20 October 2017].
- Saari, T. and Bilker-Koivula, M., 2017. Applying the GOCE-based GGMs for the quasi-geoid modelling of Finland. *Journal of applied geodesy*, 12 (1), 15–27.
- Sansó, F. and Sideris, M.G., 2013. *Geoid determination: theory and methods*. Berlin: Springer Verlag.
- Satishkumar, B., et al., 2013. Bias-corrected GOCE geoid for the generation of high-resolution digital terrain model. *Current science*, 104 (7), 940–943.
- Selvan, M.T., Ahmad, S., and Rashid, S.M., 2011. Analysis of the geomorphometric parameters in high altitude glacierised terrain using SRTM DEM data in Central Himalaya, India. *ARPN journal of science and technology*, 1 (1), 22–27.
- Singh, B. and Dowerah, J., 2010. ASTER DEM based studies for geological investigation around Singhbhum Shear Zone (SSZ) in Jharkhand, India. *Journal of geographic information system*, 02 (01), 11–14.
- Sjöberg, L. and Bagherbandi, M., 2017. *Gravity inversion and integration: theory and applications in geodesy and geophysics*. Switzerland: Springer-Cham.
- Sreedevi, P.D., et al., 2009. Morphometric analysis of a watershed of South India using SRTM data and GIS. *Journal of the geological society of India*, 73 (4), 543–552.
- Strykowski, G. and Forsberg, R., 2010. Testing EGM2008 on leveling data from Scandinavia, adjacent Baltic areas, and Greenland. In: S.P. Mertikas, ed. *Gravity, geoid and earth observation: IAG commission 2: gravity field, Chania, Crete, Greece, 23–27 June 2008*. Berlin: Springer Berlin Heidelberg, 505–509.
- Tscherning, C.C. and Rapp, R.H. 1974. *Closed covariance expressions for gravity anomalies, geoid undulations, and deflections of the vertical implied by anomaly degree variances*. Report no. 208. Columbus: Dept. of Geodetic Science and Surveying, The Ohio State University.
- Wang, Y.M., 2012. On the omission errors due to limited grid size in geoid computations. In: N. Sneeuw et al., eds. *VII Hotine-Marussi symposium on mathematical geodesy*. International Association of Geodesy Symposia, Vol 137. Berlin: Springer Berlin Heidelberg, 221–226.
- Wenzel, G. 2008. Global models of the gravity field of high and ultra-high resolution. *Proc., Lecture Notes, International school for the determination and use of the geoid*. Como, Italy, 15–19 September.
- Yilmaz, I., Yilmaz, M., and Turgut, B., 2010. Evaluation of recent global geopotential models based on GPS/levelling data over Afyonkarahisar (Turkey). *Scientific research and essays*, 5 (5), 484–493.
- Yilmaz, M., et al., 2017. The evaluation of high-degree geopotential models for regional geoid determination in Turkey. *Afyon Kocatepe University journal of sciences and engineering*, 17 (1), 147–153.

C.2: Paper on local planar gravimetric terrain corrections

Note: There is a typographical error in Table 4 of paper in C.2 that is HSR value of TC4 should read -1.69×10^{-1} instead of -1.69×10^{-6} . Also, in the last line of pg. 1820 “eight-fold” should read “nine-fold”.



Efficient spatial-spectral computation of local planar gravimetric terrain corrections from high-resolution digital elevation models

R. Goyal^{1,2}, W.E. Featherstone^{1,2}, D. Tsoulis³ and O. Dikshit¹

¹Department of Civil Engineering, Indian Institute of Technology Kanpur, Kanpur 208016, India. E-mail: rupeshg@iitk.ac.in

²School of Earth and Planetary Sciences, Curtin University of Technology, GPO Box U1987, Perth, WA 6845, Australia

³Department of Geodesy and Surveying, Aristotle University of Thessaloniki, Univ Box 440, 54124 Thessaloniki, Greece

Accepted 2020 March 3. Received 2020 February 28; in original form 2019 October 15

SUMMARY

Computation of gravimetric terrain corrections (TCs) is a numerical challenge, especially when using very high-resolution (say, ~ 30 m or less) digital elevation models (DEMs). TC computations can use spatial or/and spectral techniques: Spatial domain methods are more exact but can be very time-consuming; the discrete/fast Fourier transform (D/FFT) implementation of a binomial expansion is efficient, but fails to achieve a convergent solution for terrain slopes $>45^\circ$. We show that this condition must be satisfied for each and every computation-point pair in the whole integration domain, not just at or near the computation points. A combination of spatial and spectral methods has been advocated by some through dividing the integration domain into inner and outer zones, where the TC is computed from the superposition of analytical mass-prism integration and the D/FFT. However, there remain two unresolved issues with this combined approach: (1) deciding upon a radius that best separates the inner and outer zones and (2) analytical mass-prism integration in the inner zone remains time-consuming, particularly for high-resolution DEMs. This paper provides a solution by proposing: (1) three methods to define the radius separating the inner and outer zones and (2) a numerical solution for near-zone TC computations based on the trapezoidal and Simpson's rules that is sufficiently accurate w.r.t. the exact analytical solution, but which can reduce the computation time by almost 50 per cent.

Key words: Gravity anomalies and Earth structure; Fourier analysis; Numerical approximations and analysis; Numerical solutions.

1 INTRODUCTION

The gravimetric terrain correction (TC) is computed to account for the gravitational effect of deviations of the Earth's topography from some simplified model for which an exact analytical solution for the gravitational acceleration exists. Arguably the most common simplified model is the Bouguer Plate of thickness equal to the height of the terrain, either relative to some arbitrary height or the geoid depending whether the application is geophysical or geodetic, respectively (*cf.* Nowell 1999). There are several other geometries that can be used (e.g. Bouguer shell or cap), but which will not be reviewed here. Instead, we only work with planar TCs as these are still efficient for local geodetic (e.g. Majkrakova *et al.* 2016; Benedek *et al.* 2018; Dransfield & Chen 2019; McCubbin *et al.* 2019; Sobh *et al.* 2019) and geophysical applications (e.g. Pasteka *et al.* 2017; Saragih & Brotopuspito 2018; Zahorec *et al.* 2019; Ariane Darolle Fofie *et al.* 2019; Fauzi *et al.* 2019).

Although, in this paper, we only consider the simplest case of the Bouguer plate by considering the planar TC for localized computations (out to ~ 100 km), but our proposed methods can be adapted and extended to more complicated geometries for the earth model. Our motivation is to seek simultaneously accurate and numerically efficient algorithms for the computation of local TCs for very high-resolution digital height models, such as those derived from the Shuttle Radar Topography Mission (SRTM; Farr *et al.* 2007), the Advanced Spaceborne Thermal Emission and Reflection Radiometer (ASTER; Meyer *et al.* 2011) or Multi-Error-Removed Improved-Terrain (MERIT; Yamazaki *et al.* 2017). We acknowledge that SRTM and ASTER are strictly digital surface models, not digital elevation models (DEMs) like MERIT, but we have used the $1'' \times 1''$ SRTM as if it is a DEM in our numerical experiments. The term DEM will be used throughout this paper for simplicity.

With the generally free availability of high-resolution ($1'' \times 1''$) near-global DEMs, the time to compute TCs with space-domain methods can be prohibitive, even using supercomputers. For example, in an area of just $1^\circ \times 1^\circ$, the number of computation points for a $1'' \times 1''$ DEM (12 960 000) is increased eight-fold compared to a $3'' \times 3''$ DEM (1 440 000). Therefore, the use of spectral methods becomes attractive.

Despite the computational efficiency offered by spectral methods, there are two principal restrictions attached to the use of discrete or fast Fourier transforms (D/FFTs). First, a convergence criterion due to the use of a binomial expansion (e.g. Huang 2012; sect 2.3v) restricts the use of D/FFTs when terrain gradients are $>45^\circ$ (e.g. Sideris 1984; Forsberg 1985; Martinec *et al.* 1996; Sampietro *et al.* 2016). Secondly, a decision is needed on the truncation limit of the binomial expansion to obtain a convergent TC solution. Some existing strategies to address these restrictions are summarized in the Appendix A1.

From previous TC computations (e.g. Nagy 1966; Forsberg 1984; Tsoulis 1998, 2001; Heck & Seitz 2007; Tsoulis *et al.* 2009) the right-rectangular prism is the most commonly recommended elementary mass body for TC computations. The mass-point and mass-line approximations of the mass-prism, while computationally faster, are not sufficiently accurate (Li & Sideris 1994; Heck & Seitz 2007). Thus, we only use the mass-prism herein.

All the derivations and computations in this paper follow the planar approximation, which is sufficient for local TCs. Tsoulis *et al.* (2009) show that by simulating the spherical approximation using ‘super-elevation’ (Forsberg 1984), the change in the horizontal distance between the computation and roving point at a distance of 100 km is only -4 m, so can be neglected. The effect of laterally and radially varying topographic bulk density on TC is also an important aspect. A constant difference of 100 kg m^{-3} in the density can result in an approximate error of $0.037 \times \text{TC}$ (with $\rho = 2670 \text{ kg m}^{-3}$) mGal in TC computation and a ~ 3.5 mGal error in the Bouguer gravity anomaly for an elevation of 840 m (Hinze 2003). Since the focus of this study is on the use of high-resolution DEMs, we work only with the constant density assumption. However, it is suggested that for either a precise geodetic application (e.g. Tziavos & Featherstone 2001; Caratori Tontini *et al.* 2007; Janák *et al.* 2017; Yang *et al.* 2018) or an unambiguous geophysical interpretation (e.g. Uwiduhaye *et al.* 2018; Saibi *et al.* 2019; Tschirhart *et al.* 2019; Rathnayake *et al.* 2020), a topographic bulk density model (e.g. Blom *et al.* 2017; Tenzer *et al.* 2018; Sheng *et al.* 2019) should be used as an input with the presented methodology and following the formulation provided by Tziavos *et al.* (1996) and Tziavos & Sideris (2013).

Subject to the above conditions, we propose a modification to the combined spatial-spectral approach for local planar TC computation under the assumption of a constant topographic density, in which the FFT is applied in the outer zone and mass-prism integration used in the inner zone. We also propose a strategy to divide the inner and outer zones and choose the truncation limit of the binomial expansion in such ways that the D/FFT-driven convergence criterion is satisfied. Additionally, a new faster numerical mass-prism solution is presented based on the trapezoidal and Simpson’s rules. Our numerical experiments are conducted in the Himalayas, which hosts among some of the most rugged topographies on Earth.

2 D/FFT OUTER ZONE TC COMPUTATION

2.1 Limitations of existing solutions

TC computation using the D/FFT was first presented by Parker (1973), but had geodetic limitations in that the computation points must lie above the topography; a case complying more with aeromagnetic and oceanographic than geodetic applications. Sideris (1984) proposed a revised formulation of Parker (1973) to provide TCs on the topographic surface that is more suited to geodetic application. However, a convergence criterion is attached to this method; also see Forsberg (1984, 1985), Sideris (1985), Martinec *et al.* (1996) and Tsoulis (1998).

The spatial form of the integral for computation of the planar TC that can be expressed as a convolution is (e.g. Sideris 1984)

$$TC = G\rho \iint_E \left(\frac{1}{l} \left[1 - \left[1 + \left(\frac{\Delta z}{l} \right)^2 \right]^{-1/2} \right] \right) dy dx, \quad (1)$$

where G is the universal gravitational constant, ρ is topographic bulk density (herein assumed constant), $l = \sqrt{(x_p - x_i)^2 + (y_p - y_i)^2}$ is the planar Euclidean distance, $\Delta z = h_p - h_i$, and (x_p, y_p, h_p) and (x_i, y_i, h_i) are the coordinates of computation point and running point, respectively.

Making use of the binomial expansion of $(1+x)^{-1/2}$ according to

$$(1+x)^{-1/2} = 1 - \frac{1}{2}x + \frac{1.3}{2.4}x^2 - \frac{1.3.5}{2.4.6}x^3 + \frac{1.3.5.7}{2.4.6.8}x^4 - \frac{1.3.5.7.9}{2.4.6.8.10}x^5 + \frac{1.3.5.7.9.11}{2.4.6.8.10.12}x^6 - \dots \quad (2)$$

one can series-expand $(1 + (\frac{\Delta z}{l})^2)^{-1/2}$ in eq. (1) and rearrange terms to give

$$TC \approx G\rho \int_{x_1}^{x_2} \int_{y_1}^{y_2} \left[\frac{\Delta z^2}{2l^3} - \frac{3\Delta z^4}{8l^5} + \frac{5\Delta z^6}{16l^7} - \frac{35\Delta z^8}{128l^9} + \frac{63\Delta z^{10}}{256l^{11}} - \frac{231\Delta z^{12}}{1024l^{13}} + \dots \right] dx dy \quad (3)$$

where we abbreviate each as

$$TC \approx TC_1 + TC_2 + TC_3 + TC_4 + TC_5 + TC_6 + \dots$$

with each term retains the appropriate sign according to eq. (3). This formulation is a convolution, so can be solved numerically efficiently using the D/FFT (e.g. Schwarz *et al.* 1990).

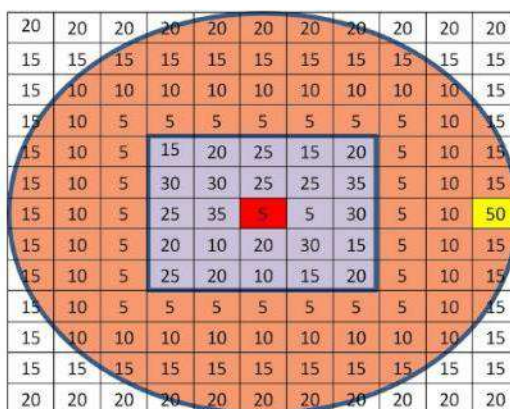


Figure 1. Hypothetical DEM with 5 m resolution. The numbers in the cells represent height. The red cell is the computation point. The yellow cell is one that violates the <45° slope condition.

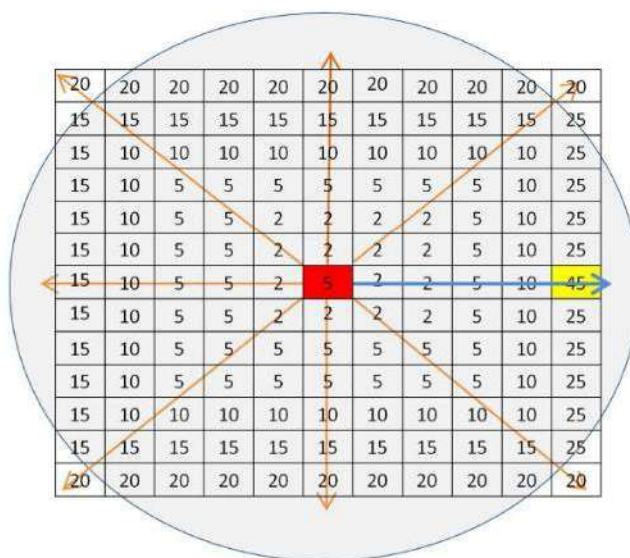


Figure 2. The terrain slope has to be computed in all to identify computation-roving point pairs that are steeper than 45°, otherwise violating the convergence criterion for TC computation.

The convergence criterion for using the binomial expansion in eq. (2) is $-1 < x \leq 1$. Therefore, if using eq. (3), the TC can only be computed when the condition

$$-1 < \left(\frac{\Delta z}{l}\right)^2 \leq 1 \Rightarrow \left|\frac{\Delta z}{l}\right| \leq 1 \quad \forall i \tag{4}$$

is met. This limitation is often referred to as the convergence criterion, which restricts the implementation of eq. (3) to domains having terrain slopes of <45°. The condition $\forall i$ in eq. (4) must be satisfied for each and every combination of computation and roving points in the whole integration domain. However, in some literature, this condition has been misinterpreted as a requirement that only the slope of the terrain at or immediately surrounding the computation point should not exceed 45° (e.g. Forsberg 1985; Sideris 1985; Klose & Ilk 1993; McCubbine et al. 2017; among others).

To exemplify this, consider a hypothetical DEM with a 5 m spatial resolution, as shown in Fig. 1, where the yellow roving cell is distant from the red computation point but which violates the <45° slope condition. Therefore, unless the slope is computed for each and every computation-roving point pair (a time-consuming process as depicted in Fig. 2), and before/during TC computation, numerical convergence

Table 1. TC values (in μGal) after deliberately violating the $<45^\circ$ convergence criterion at only one DEM cell. While the effect may appear small here, we could make it arbitrary larger by increasing the cell height by more or by including more cells that violate the $<45^\circ$ convergence criterion.

TC term	Unchanged SRTM DEM	Single cell height changed to 6731 m
TC_1	331.2	332.7
TC_2	-2.3	-3.7
TC_3	3×10^{-2}	1.3
TC_4	-5×10^{-4}	-1.3
TC_5	1×10^{-5}	1.4
TC_6	-2×10^{-7}	-1.5
TC_7	5×10^{-9}	1.6
TC_8	-1×10^{-10}	-1.7
$TC =$	328.9	327.9
$\Sigma TC_1 \dots TC_8$		

will not be assured. However, we do acknowledge that it is plausible that the presence of only a few such roving points may not always provide noticeably divergent TC results.

To quantify the above statements, TCs were computed up to the eighth order binomial term (TC_8) at the central red cell for a region bounded by 20°N – 21°N latitude and 81°E – 82°E longitude using the SRTM V3.0 $1'' \times 1''$ DEM (Farr *et al.* 2007), with height of the central cell being 531 m. TC values (only from the outer zone beyond an arbitrarily selected 1 km) were computed for two scenarios: (1) the unchanged DEM for which all cells satisfy the convergence criterion and (2) after changing the height of only one DEM cell at $l \approx 6$ km (200 grid cells) from 495 m to 6731 m in order to deliberately violate the convergence criterion ($|\Delta z| \leq l$) at a single point. The results in Table 1 reveal that the presence of even a single point violating the converging criterion causes the solution to diverge.

2.2 Radius separating the inner and outer zones

This and the next subsection provide our proposed solutions to satisfy the convergence criterion in the D/FFT method when used in the combined spatial-spectral approach to local planar TC computation. Recall that the D/FFT method is to be used in our so-called outer zone and the mass-prism method is to be used in our so-called inner zone. The motivation behind this combined approach is to achieve computational efficiency while not compromising accuracy. This raises the question of how best to select the integration radius that separates the inner and outer zones.

There is, however, one further choice of integration radius, which we term the bounding radius (BR) that encloses the outer zone [as we define it here]. In the following, we will assume that the BR of the outer zone is sufficiently large so as to capture the entire planar TC, but we do not consider Earth curvature. A common empirical approach is to increment the BR to a distance beyond which the change to the planar TC becomes negligible. We acknowledge that for non-planar geometries, the far/remote zones beyond the BR may not be negligible (*cf.* Kuhn *et al.* 2009).

We consider three scenarios to select the radius separating inner and outer zones for the planar TC (Fig. 3). We term them: height-defined separating radius (HSR), exact separating radius (ESR) and optimal separating radius (OSR), as follows.

(i) HSR follows directly from eq. (4), which is a radius that is equal to the magnitude of the maximum height difference in the study area, that is

$$HSR = |\Delta z_{\max}| \quad (5)$$

(ii) ESR is calculated from the magnitude of the maximum height difference among all the pairs of computation (P) and rover (R) points in the area bounded by a circle of radius equal to the HSR. This gives the ESR, beyond which the solution will always diverge. Computation of the ESR is time-consuming, especially when the maximum height difference is large, the size of the study area is large, and for a high-resolution DEM. We thus define the ESR as

$$ESR = |\max(\Delta z_{P,R})| \forall \left\{ \begin{array}{l} P(x_P, y_P) \subseteq (x_{\min} \leq x_P \leq x_{\max}, y_{\min} \leq y_P \leq y_{\max}) \\ \& R(x, y) : ((x - x_P)^2 + (y - y_P)^2 - \Delta z_{\max}^2 \leq 0) \end{array} \right\} \quad (6)$$

(iii) OSR is the upper range in the study area. The range is computed by taking the difference between the maximum and the minimum height values in an area around each cell, bounded by a circle of radius equal to the HSR. The upper range is the maximum of these range values in the entire study area. OSR can be computed faster than the ESR because

$$OSR = \max(\text{range}_N); \text{range}_N = (\max(z)_N - \min(z)_N) \forall N \equiv P(x_P, y_P) \rightarrow R(x, y) \quad (7)$$

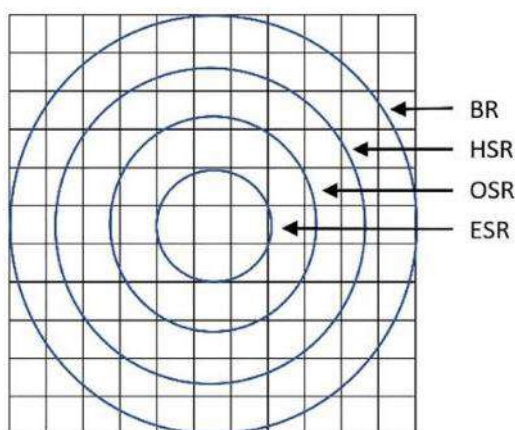


Figure 3. The four integration domains. BR is the bounding radius of the whole integration area. HSR, OSR and ESR are the height-dependent, optimal and exact separating radii, respectively.

Table 2. Details of the five study areas (SA) from SRTM 1" v3.0 (SA5 includes Mount Everest).

Study area	Latitude bounds	Longitude bounds	Heights (m)			
			Min	Max	Mean	STD
SA1	29°N–30°N	86°E–87°E	4111	6399	5161.7	371.5
SA2	28°N–29°N	86°E–87°E	2535	8291	5067.4	545.3
SA3	27°N–28°N	88°E–89°E	182	8314	3389.0	1673.8
SA4	27°N–28°N	87°E–88°E	176	8250	2830.4	1586.7
SA5	27°N–28°N	86°E–87°E	190	8748	2572.1	1605.9

Table 3. Empirically determined choices of separating radii (in metres).

Study area	HSR	ESR	OSR
SA1	2288	1642	1977
SA2	5756	3071	3354
SA3	8132	4290	5381
SA4	8074	3637	4724
SA5	8558	4261	5456

2.3 Numerical choice of separating integration radius

To test the convergence of the TC solution using the proposed choices of separating radii (HSR, ESR and OSR), computations were carried out in five rugged topographies in the Himalayas (Table 2). Table 3 lists the values of the three computed radii for the five study areas using the SRTM 1" V3.0 DEM. A MATLAB™ subroutine was written to compute the ESR. The *focal statistics* tool in ArcGIS™ was used to compute the OSR. Table 3 confirms the relative sizes of the separating radii depicted in Table 3.

2.4 Effect of separation radius on TC convergence

To analyse the effect of truncating the binomial expansion of the D/FFT (eq. 3) at different orders, the TC terms are computed up to the tenth order for SA5 (Table 4) using the three different choices of separating radius (Table 3). All computations were performed for outer zones defined by subtracting the three different separating radii (HSR, ESR and OSR) from the BR, arbitrarily selected to be 111 320 m which was driven solely by the size of the data area. No optimization of the BR was attempted because this is only an illustrative example of the convergence.

Recalling from Fig. 3 and Table 3, $HSR > OSR > ESR$. From Table 4, fewer TC terms are needed to achieve convergence (to $<0.1 \mu\text{Gal}$) with the HSR. However, the HSR makes the inner zone larger, which will increase the computation time for the mass-prism integration (Section 3). Conversely, the ESR makes inner zone smallest but needs the largest number of TC terms which will require more computer memory. Also, it takes a longer time to compute the ESR value, especially for a high-resolution DEM.

The OSR offers a compromise that balances the computation of its radius, the number of TC terms required to achieve numerical convergence, and computation time of the inner zone by mass-prisms. Not presented here, this also holds true for the other four study areas in

Table 4. Descriptive statistics of planar TC values (mGal) in the outer zone up to the tenth order for SA5 with the separating radii of HSR = 8558 m, ESR = 4261 m and OSR = 5456 m and BR = 111 320 m.

TC term	Separating radius	Min	Max	Mean	STD
TC_1	HSR	1.237	76.047	9.195	5.393
	ESR	1.299	124.770	12.648	7.717
	OSR	1.278	107.603	11.361	6.865
TC_2	HSR	-2.45	-8.71×10^{-4}	-7.07×10^{-2}	1.00×10^{-1}
	ESR	-11.399	-8.95×10^{-4}	-2.01×10^{-1}	3.19×10^{-1}
	OSR	-7.402	-8.8×10^{-4}	-1.40×10^{-1}	2.16×10^{-1}
TC_3	HSR	1.10×10^{-6}	1.73×10^{-1}	1.74×10^{-3}	4.30×10^{-3}
	ESR	1.11×10^{-6}	2.299	1.19×10^{-2}	3.58×10^{-2}
	OSR	1.10×10^{-6}	1.128	6.15×10^{-3}	1.75×10^{-2}
TC_4	HSR	-1.69×10^{-6}	-1.84×10^{-9}	-7.84×10^{-5}	2.89×10^{-4}
	ESR	-6.50×10^{-1}	-1.85×10^{-9}	-1.32×10^{-3}	6.66×10^{-3}
	OSR	-2.27×10^{-1}	-1.84×10^{-9}	-5.00×10^{-4}	2.31×10^{-3}
TC_5	HSR	3.61×10^{-12}	1.92×10^{-3}	4.95×10^{-6}	2.54×10^{-5}
	ESR	3.58×10^{-12}	2.30×10^{-1}	2.11×10^{-4}	1.67×10^{-3}
	OSR	3.60×10^{-12}	5.32×10^{-2}	5.78×10^{-5}	4.00×10^{-4}
TC_6	HSR	-2.40×10^{-4}	-7.88×10^{-15}	-3.90×10^{-7}	2.66×10^{-6}
	ESR	-8.97×10^{-2}	1.51×10^{-13}	-4.34×10^{-5}	5.06×10^{-4}
	OSR	-1.36×10^{-2}	-4.70×10^{-15}	-8.45×10^{-6}	8.27×10^{-5}
TC_7	HSR	-7.23×10^{-18}	3.48×10^{-5}	3.60×10^{-8}	3.15×10^{-7}
	ESR	-2.52×10^{-9}	3.71×10^{-2}	1.07×10^{-5}	1.74×10^{-4}
	OSR	-5.5×10^{-11}	3.76×10^{-3}	1.46×10^{-6}	1.92×10^{-5}
TC_8	HSR	-5.31×10^{-6}	7.60×10^{-13}	-3.74×10^{-9}	4.08×10^{-8}
	ESR	-1.61×10^{-6}	9.71×10^{-8}	-3.05×10^{-6}	6.60×10^{-5}
	OSR	-1.08×10^{-3}	1.70×10^{-9}	-2.86×10^{-7}	4.88×10^{-6}
TC_9	HSR	-2.97×10^{-12}	8.45×10^{-7}	4.26×10^{-10}	5.67×10^{-9}
	ESR	-1.96×10^{-6}	7.24×10^{-3}	9.71×10^{-7}	2.66×10^{-5}
	OSR	-1.51×10^{-8}	3.28×10^{-4}	6.17×10^{-8}	1.31×10^{-6}
TC_{10}	HSR	-1.39×10^{-7}	1.19×10^{-11}	-5.24×10^{-11}	8.32×10^{-10}
	ESR	-3.33×10^{-3}	3.50×10^{-6}	-3.37×10^{-7}	1.13×10^{-5}
	OSR	-1.02×10^{-4}	1.67×10^{-7}	-1.44×10^{-8}	3.74×10^{-7}

Table 2. We acknowledge that the exact number of TC terms required will vary depending on the study area, but we have deliberately chosen the extreme example of a 30 m DEM over Mount Everest, where convergence is achieved using six terms with HSR and nine terms with OSR. Also not presented here, we used the D/FFT to compute TCs from the outer zone for $198 2^\circ \times 2^\circ$ tiles covering parts of India, Pakistan, Sri Lanka, Nepal and China. Convergence was achieved in all cases with the same number of terms.

3 ANALYTICAL AND NUMERICAL INNER ZONE TC COMPUTATION

In this section, we begin by stating the formula for analytical mass-prism integration (*cf.* Banerjee & Gupta 1977). This is followed by derivation of our proposed numerical integration techniques utilizing the trapezoidal and Simpson's rules for linear integration extended to double integrals. The analytical mass-prism integral of the TC is a volumetric integral solution. The approach suggested here utilises numerical surface integration of the analytical linear solution of TC integral with respect to the z-direction (height).

3.1 Mass-prism integration

This method assumes that the cells in the DEM grid define right-rectangular prisms with length and width given by the resolution of the DEM in the x and y directions, respectively. The height of the prism is defined by the height difference of the computation and rover points (Δz).

According to Forsberg (1984), the planar TC can be represented as

$$TC = G\rho \int_{x_1}^{x_2} \int_{y_1}^{y_2} \int_{z_1}^{z_2} \frac{z}{r^3} dx dy dz, \quad (8)$$

where $r = \sqrt{x^2 + y^2 + z^2}$ is Euclidean distance (see below). The analytical solution of eq. (8) is

$$TC = \left[\left[\left[x(\log(y+r) + y \log(x+r) - z \tan^{-1} \frac{xy}{zr}) \right]_{x_1}^{x_2} \right]_{y_1}^{y_2} \right]_{z_1}^{z_2} \quad (9)$$

which is a simplified, efficient and accurate version (Banerjee & Gupta 1977; Forsberg 1984) of the solution given by Nagy (1966). Expanding eq. (9) with respect to its limits, gives

$$TC = \left. \begin{aligned} &x_2 \log(y_2 + r_{222}) - x_2 \log(y_2 + r_{221}) - x_2 \log(y_1 + r_{212}) + x_2 \log(y_1 + r_{211}) \\ &- x_1 \log(y_2 + r_{122}) - x_1 \log(y_2 + r_{121}) - x_1 \log(y_1 + r_{112}) + x_1 \log(y_1 + r_{111}) \\ &+ y_2 \log(x_2 + r_{222}) - y_2 \log(x_2 + r_{221}) - y_2 \log(x_1 + r_{122}) + y_2 \log(x_1 + r_{121}) \\ &- y_1 \log(x_2 + r_{212}) + y_1 \log(x_2 + r_{211}) + y_1 \log(x_1 + r_{112}) - y_1 \log(x_1 + r_{111}) \\ &- z_2 \tan^{-1} \left(\frac{z_2 y_2}{z_2^2 r_{222}} \right) + z_2 \tan^{-1} \left(\frac{z_2 y_1}{z_2^2 r_{212}} \right) + z_2 \tan^{-1} \left(\frac{z_1 y_2}{z_1^2 r_{122}} \right) - z_2 \tan^{-1} \left(\frac{z_1 y_1}{z_1^2 r_{112}} \right) \\ &+ z_1 \tan^{-1} \left(\frac{z_2 y_2}{z_1^2 r_{221}} \right) - z_1 \tan^{-1} \left(\frac{z_2 y_1}{z_1^2 r_{211}} \right) - z_1 \tan^{-1} \left(\frac{z_1 y_2}{z_1^2 r_{121}} \right) + z_1 \tan^{-1} \left(\frac{z_1 y_1}{z_1^2 r_{111}} \right) \end{aligned} \right\} \quad (10)$$

where $z_1 = 0; z_2 = h_p - h_i$; h_p is the height of the computation point and h_i the height of the roving point. x_1, x_2, y_1, y_2 are the planar coordinates of a prism assuming the computation point to be at the origin of the planar coordinate system. The order of subscripts of $r = \sqrt{x^2 + y^2 + z^2}$ represents the order of coordinates (x, y, z) and the subscript value represents the lower or upper bound of that coordinate.

For example, r_{122} represents $\sqrt{x_1^2 + y_2^2 + z_2^2}$, etc.

Rearranging the terms in eq. (10), the analytical formula for the TC using right-rectangular mass prisms (TCM) is

$$TCM = \left. \begin{aligned} &x_2 \left[\log \left(\frac{(y_2+r_{222})(y_1+r_{211})}{(y_2+r_{221})(y_1+r_{212})} \right) \right] - x_1 \left[\log \left(\frac{(y_2+r_{122})(y_1+r_{111})}{(y_2+r_{121})(y_1+r_{112})} \right) \right] \\ &+ y_2 \left[\log \left(\frac{(x_2+r_{222})(x_1+r_{121})}{(x_2+r_{221})(x_1+r_{122})} \right) \right] - y_1 \left[\log \left(\frac{(x_2+r_{122})(x_1+r_{111})}{(x_2+r_{121})(x_1+r_{112})} \right) \right] \\ &- z_2 \left[\tan^{-1} \left(\frac{z_2 y_2}{z_2^2 r_{222}} \right) - \tan^{-1} \left(\frac{z_2 y_1}{z_2^2 r_{212}} \right) - \tan^{-1} \left(\frac{z_1 y_2}{z_1^2 r_{122}} \right) + \tan^{-1} \left(\frac{z_1 y_1}{z_1^2 r_{112}} \right) \right] \\ &+ z_1 \left[\tan^{-1} \left(\frac{z_2 y_2}{z_1^2 r_{221}} \right) - \tan^{-1} \left(\frac{z_2 y_1}{z_1^2 r_{211}} \right) - \tan^{-1} \left(\frac{z_1 y_2}{z_1^2 r_{121}} \right) + \tan^{-1} \left(\frac{z_1 y_1}{z_1^2 r_{111}} \right) \right] \end{aligned} \right\} \quad (11)$$

3.2 Trapezoidal rule integration

Solving the TC integral (eq. 8) with respect to 'z' is convenient compared to 'x' and 'y'. Therefore, in this method, the trapezoidal rule for single integration is extended to double integration for solving the surface integral achieved after analytical linear integration of eq. (8) with respect to 'z'. According to the trapezoidal rule for single integration with $n = 2$ subintervals (refer to the end of Section 3.4 for further discussion), we have

$$\int_a^b f(x)dx \approx \frac{g}{2} \left[f(a) + 2f \left(\frac{a+b}{2} \right) + f(b) \right], g = \frac{b-a}{n} \quad (12)$$

Extending eq. (12) to solve double integration gives

$$\left. \begin{aligned} &\int_a^b \left(\int_c^d f(x, y)dy \right) dx \approx \int_a^b \left(\frac{d-c}{4} [f(x, c) + 2f \left(x, \frac{c+d}{2} \right) + f(x, d)] \right) dx \\ &= \int_a^b \left(\frac{d-c}{4} \right) f(x, c)dx + \int_a^b 2 \left(\frac{d-c}{4} \right) f \left(x, \frac{c+d}{2} \right) dx + \int_a^b \left(\frac{d-c}{4} \right) f(x, d)dx \\ &= TT1 + TT2 + TT3 \end{aligned} \right\} \quad (13)$$

where $TT1, TT2, TT3$ represent the three integral terms in eq. (13). By applying the trapezoidal rule for $n = 2$ to these three terms individually, we get

$$\left. \begin{aligned} &TT1 = \left(\frac{b-a}{4} \right) \left(\frac{d-c}{4} \right) [f(a, c) + 2f \left(a, \frac{c+d}{2} \right) + f(a, d)] \\ &TT2 = 2 \left(\frac{b-a}{4} \right) \left(\frac{d-c}{4} \right) [f \left(\frac{a+b}{2}, c \right) + 2f \left(\frac{a+b}{2}, \frac{c+d}{2} \right) + f \left(\frac{a+b}{2}, d \right)] \\ &TT3 = \left(\frac{b-a}{4} \right) \left(\frac{d-c}{4} \right) [f(b, c) + 2f \left(b, \frac{c+d}{2} \right) + f(b, d)] \end{aligned} \right\} \quad (14)$$

The analytical linear integral solution of the TC with respect to 'z' can be written as

$$\left. \begin{aligned} &TC = G\rho \left[\iint_E \int_{z_1=0}^{z_2=h_p-h_i} \frac{z}{r^3} dz dy dx \right] \\ &= G\rho \left[\int_{x_1}^{x_2} \int_{y_1}^{y_2} \left(\frac{1}{r(x, y, z_1)} - \frac{1}{r(x, y, z_2)} \right) dy dx \right] \end{aligned} \right\} \quad (15)$$

Table 5. Geographical bounds of the study areas and their respective height statistics.

Study area	Latitude bound	Longitude bound	SRTM heights (m)			
			Min	Max	Mean	STD
SAA	19.25°N–19.75°N	73.25°E–73.75°E	2	1537	299	264
SAB	26.25°N–26.75°N	80.25°E–80.75°E	94	155	123	5
SAC	28.25°N–28.75°N	83.25°E–83.75°E	723	8141	2976	1334

Using the following substitutions in eq. (14)

$$\left. \begin{aligned} a &= x_1, b = x_2, c = y_1, d = y_2 \\ b - a &= x_2 - x_1 = \Delta x, c - d = y_2 - y_1 = \Delta y \\ z_1 &= 0, z_2 = h_p - h_i = \Delta z \\ \frac{a+b}{2} &= \frac{x_1+x_2}{2} = \bar{x}, \frac{c+d}{2} = \frac{y_1+y_2}{2} = \bar{y} \end{aligned} \right\} \quad (16)$$

and rearranging terms, the TC with the trapezoidal rule (TCT) can be calculated as

$$\left. \begin{aligned} TCT &= G\rho \left\{ \left(\frac{\Delta x}{4} \right) \left(\frac{\Delta y}{4} \right) \left[\left(\frac{1}{r(x_1, y_1)} - \frac{1}{r(x_1, y_1, \Delta z)} \right) + 2 \left(\frac{1}{r(x_1, \bar{y})} - \frac{1}{r(x_1, \bar{y}, \Delta z)} \right) + \left(\frac{1}{r(x_1, y_2)} - \frac{1}{r(x_1, y_2, \Delta z)} \right) \right] \right. \\ &\quad + 2 \left(\frac{\Delta x}{4} \right) \left(\frac{\Delta y}{4} \right) \left[\left(\frac{1}{r(\bar{x}, y_1)} - \frac{1}{r(\bar{x}, y_1, \Delta z)} \right) + 2 \left(\frac{1}{r(\bar{x}, \bar{y})} - \frac{1}{r(\bar{x}, \bar{y}, \Delta z)} \right) + \left(\frac{1}{r(\bar{x}, y_2)} - \frac{1}{r(\bar{x}, y_2, \Delta z)} \right) \right] \\ &\quad \left. + \left(\frac{\Delta x}{4} \right) \left(\frac{\Delta y}{4} \right) \left[\left(\frac{1}{r(x_2, y_1)} - \frac{1}{r(x_2, y_1, \Delta z)} \right) + 2 \left(\frac{1}{r(x_2, \bar{y})} - \frac{1}{r(x_2, \bar{y}, \Delta z)} \right) + \left(\frac{1}{r(x_2, y_2)} - \frac{1}{r(x_2, y_2, \Delta z)} \right) \right] \right\}. \end{aligned} \right\} \quad (17)$$

3.3 Simpson's rule integration

According to Simpson's rule for single integration, again with $n = 2$ subintervals (again refer to the end of Section 3.4), we have

$$\int_a^b f(x) dx \approx \frac{t}{3} \left[f(a) + 4f\left(\frac{a+b}{2}\right) + f(b) \right], t = \frac{b-a}{n}. \quad (18)$$

For double integration, eq. (17) takes the form

$$\left. \begin{aligned} \int_a^b \int_c^d f(x, y) dy dx &\approx \int_a^b \left(\frac{d-c}{6} \left[f(x, c) + 4f\left(x, \frac{c+d}{2}\right) + f(x, d) \right] \right) dx \\ &= \int_a^b \left(\frac{d-c}{6} \right) f(x, c) dx + \int_a^b 4 \left(\frac{d-c}{6} \right) f\left(x, \frac{c+d}{2}\right) dx + \int_a^b \left(\frac{d-c}{6} \right) f(x, d) dx \\ &= ST1 + ST2 + ST3 \end{aligned} \right\} \quad (19)$$

where $ST1$, $ST2$, $ST3$ represent the three integral terms in eq. (19). By applying Simpson's rule to the three terms individually, we get

$$\left. \begin{aligned} ST1 &= \left(\frac{b-a}{6} \right) \left(\frac{d-c}{6} \right) \left[f(a, c) + 4f\left(a, \frac{c+d}{2}\right) + f(a, d) \right] \\ ST2 &= 4 \left(\frac{b-a}{6} \right) \left(\frac{d-c}{6} \right) \left[f\left(\frac{a+b}{2}, c\right) + 4f\left(\frac{a+b}{2}, \frac{c+d}{2}\right) + f\left(\frac{a+b}{2}, d\right) \right] \\ ST3 &= \left(\frac{b-a}{6} \right) \left(\frac{d-c}{6} \right) \left[f(b, c) + 4f\left(b, \frac{c+d}{2}\right) + f(b, d) \right] \end{aligned} \right\} \quad (20)$$

The numerical solution of TC using Simpson's rule (TCS) is obtained using the substitutions from eq. (16) in eq. (20) to yield

$$\left. \begin{aligned} TCS &= G\rho \left\{ \left(\frac{\Delta x}{6} \right) \left(\frac{\Delta y}{6} \right) \left[\left(\frac{1}{r(x_1, y_1)} - \frac{1}{r(x_1, y_1, \Delta z)} \right) + 4 \left(\frac{1}{r(x_1, \bar{y})} - \frac{1}{r(x_1, \bar{y}, \Delta z)} \right) + \left(\frac{1}{r(x_1, y_2)} - \frac{1}{r(x_1, y_2, \Delta z)} \right) \right] \right. \\ &\quad + 4 \left(\frac{\Delta x}{6} \right) \left(\frac{\Delta y}{6} \right) \left[\left(\frac{1}{r(\bar{x}, y_1)} - \frac{1}{r(\bar{x}, y_1, \Delta z)} \right) + 4 \left(\frac{1}{r(\bar{x}, \bar{y})} - \frac{1}{r(\bar{x}, \bar{y}, \Delta z)} \right) + \left(\frac{1}{r(\bar{x}, y_2)} - \frac{1}{r(\bar{x}, y_2, \Delta z)} \right) \right] \\ &\quad \left. + \left(\frac{\Delta x}{6} \right) \left(\frac{\Delta y}{6} \right) \left[\left(\frac{1}{r(x_2, y_1)} - \frac{1}{r(x_2, y_1, \Delta z)} \right) + 4 \left(\frac{1}{r(x_2, \bar{y})} - \frac{1}{r(x_2, \bar{y}, \Delta z)} \right) + \left(\frac{1}{r(x_2, y_2)} - \frac{1}{r(x_2, y_2, \Delta z)} \right) \right] \right\}. \end{aligned} \right\} \quad (21)$$

3.4 Numerical analyses

The proposed numerical methods for mass-prism integration are tested on three different smaller study areas (that exhibit varying terrain roughness) again using the SRTM 1" v3.0 DEM (Table 5). Mass-prism TC values were computed with the separating radius defined by the OSR computed individually for each study area (Table 6). Computations were performed using MATLAB™ parallelization on 18 cores of an Intel® Xeon® E7-8870 v3 @2.10 GHz CPU having 251 GB of RAM. The statistics and time required for TC computation using the analytical (TCM) and numerical (TCT and TCS) methods for the three study areas are given in Table 6. The statistics of the difference between the TC values computed using analytical and numerical methods are given in Table 7.

Although there is no significant variation among the overall TC statistics (Table 6) using the three different methods, TCT provides comparatively better results compared to the TCM than TCS (Table 7). An important observation from Table 6 is that the time required for

Table 6. Statistics of 1''x1'' TC values computed using the three methods (equations 11, 17 and 21) for three different study areas [TCs are in mGal and CPU time is rounded to the nearest second].

	SAA, OSR = 1141 m			SAB, OSR = 46 m			SAC, OSR = 6078 m		
	TCM	TCT	TCS	TCM	TCT	TCS	TCM	TCT	TCS
Min	0.000	0.000	0.000	0.000	0.000	0.000	4.542	4.546	4.531
Max	22.779	22.713	22.627	1.032	0.897	0.839	126.646	126.623	126.563
Mean	0.722	0.720	0.711	0.003	0.003	0.002	22.180	22.162	22.110
STD	1.487	1.483	1.472	0.005	0.004	0.004	11.898	11.892	11.882
RMS	1.653	1.649	1.635	0.006	0.005	0.005	25.170	25.151	25.101
Time	428	201	199	38	12	12	37746	17539	17481

Table 7. Statistics of the difference between TC values computed using analytical (TCM) and numerical (TCS and TCT) methods [units in mGal].

	SAA		SAB		SAC	
	TCM-TCT	TCM-TCS	TCM-TCT	TCM-TCS	TCM-TCT	TCM-TCS
Min	-0.031	0.000	-0.006	0.000	-0.036	0.000
Max	0.136	0.246	0.135	0.192	0.144	0.248
Mean	0.002	0.011	0.001	0.001	0.017	0.070
STD	0.006	0.019	0.001	0.001	0.022	0.040
RMS	0.007	0.022	0.001	0.002	0.028	0.080

TC computation using our proposed methods (both TCT and TCS) is almost half of what is required for analytical TCM. Table 7 confirms that the TCT and TCS are consistent with respect to (i) the ruggedness of topography (*cf.* Table 5) and (ii) the size of the OSR (*cf.* Table 6).

In the trapezoidal and Simpson's rules of integration (TCT and TCS), the numerical results can be improved by increasing the number of subintervals, but at some computational cost. TCT and TCS were rederived using a combination of $n = 2$ subintervals for the inner limit and $n = 4$ for the outer limit. This was done because only an even number of subintervals can be used in Simpson's rule. The derived formulas were tested on SAC. Not significant, but an improvement was observed in the results versus TCM. However, time taken for the computations became equivalent to the TCM.

4 CONCLUDING REMARKS

The free availability of high-resolution (~ 30 m or less) near-global digital elevation models poses a substantial challenge for the numerical computation of gravimetric TCs. One computationally attractive option is to divide the integration domain into inner and outer zones, where spectral methods are used in the outer zone and analytical or discretized numerical mass-prism integration is used in the inner zone. However, this spatial-spectral combination suffers from a few unresolved issues: (1) the need to ascertain that the D/FFT implementation of the binomial expansion of the TC formula (eq. 3) provides a numerically convergent solution, (2) the appropriate separation radius between the inner and outer zones is selected so as to achieve an accurate and convergent result while profiting computationally from a smaller inner zone and (3) the analytical mass-prism integration method (eq. 11) is very time consuming, even on supercomputers.

Our principal conclusions are:

(i) The D/FFT implementation of the binomial expansion of the TC integral is only convergent *iff* the terrain gradients are $<45^\circ$ for each and every computation-rovng point pair in the integration domain. This condition appears to have been overlooked in some previous implementations of the D/FFT method, where it is only considered at or near the computation point.

(ii) The radius separating the inner zone, where mass-prism integration is conducted, and the outer zone, where D/FFT integration is conducted, can be selected so as to achieve a balance among numerical convergence, accuracy and efficient computation time. Our so-called optimal separation radius (OSR) is given by eq. (7) and depends on the range of height differences in the whole integration domain. When using the binomial expansion of the TC (eq. 3) in areas of very rugged terrain and for high-resolution DEMs, higher order terms cannot be neglected (*cf.* Tables 1 and 4).

(iii) The analytical solution to the gravitational attraction of a right-rectangular prism in the inner zone can be replaced by numerical integration based on the trapezoidal and Simpson's rules extended to double integrals. Numerical experiments over Mount Everest on a 1''x1'' grid show all the mass-prism TC solutions to be commensurate but can be achieved in roughly half the computation time when two integration steps are used in the trapezoidal and Simpson's methods.

ACKNOWLEDGEMENTS

We would like to thank Dr Jack McCubbine, Geoscience Australia, for publicly sharing his FFTC.m MATLABTM routine (<https://uk.mathworks.com/matlabcentral/profile/authors/4329165-jack>). Dr Sten Claessens, Curtin University of Technology and Prof Balasubramania Nagarajan, Indian Institute of Technology Kanpur, are also thanked for providing helpful discussions. Will Featherstone thanks the Indian

Scheme for Promotion of Academic and Research Collaboration (SPARC) programme for funding his visit to India. We thank the editor (Prof Bert Vermeersen) and two reviewers (Dr Robert Tenzer and one anonymous) for their extraordinarily prompt and very constructive reviews of this paper.

REFERENCES

- Banerjee, B. & Gupta, S.P.D., 1977. Gravitational attraction of a rectangular parallelepiped, *Geophysics*, **42**(5), 1053–1055.
- Benedek, J., Papp, G. & Kalmár, J., 2018. Generalization techniques to reduce the number of volume elements for terrain effect calculations in fully analytical gravitational modelling, *J. Geod.*, **92**, 361–381.
- Blom, N., Boehm, C. & Fichtner, A., 2017. Synthetic inversions for density using seismic and gravity data, *Geophys. J. Int.*, **209**(2), 1204–1220.
- Capponi, M., Mansi, A.H. & Sampietro, D., 2018. Improving the computation of the gravitational terrain effect close to ground stations in the GTE software, *Stud. Geophys. Geod.*, **62**(2), 206–222.
- Caratori Tontini, F., Graziano, F., Cocchi, L., Carmisciano, C. & Stefanelli, P., 2007. Determining the optimal Bouguer density for a gravity data set: implications for the isostatic setting of the Mediterranean Sea, *Geophys. J. Int.*, **169**(2), 380–388.
- Dransfield, M.H. & Chen, T., 2019. Heli-borne gravity gradiometry in rugged terrain, *Geophys. Prospect.*, **67**(6), 1626–1636.
- Farr, T.G. *et al.*, 2007. The shuttle radar topography mission, *Rev. Geophys.*, **45**(2), RG2004. doi:10.1029/2005RG000183
- Fauzi, F.A., Arifin, M.H., Basori, M.B.I., Mohd Noh, K.A. & Umor, M.R., 2019. Application of gravity survey for tin exploration at bongsu granite, Kulim, Kedah, Malaysia, *Sains Malaysiana*, **48**(11), 2503–2509.
- Fofie, K.A.D., Koumetio, F., Kenfack, J.V. & Yemele, D., 2019. Lineament characteristics using gravity data in the Garoua Zone, North Cameroon: natural risks implications, *Earth planet. Phys.*, **3**(1), 33–44.
- Forsberg, R., 1984. Study of terrain reductions, density anomalies and geophysical inversion methods in gravity field modelling. Report 355, Department of Geodetic Science and Surveying, The Ohio State University, Columbus, USA.
- Forsberg, R., 1985. Gravity field terrain effect computations by FFT, *Bulletin Géodésique*, **59**(4), 342–360.
- Gomez, M.E., Bagu, D.R., Del Cogliano, D. & Perdomo, R.A., 2013. Evaluation of terrain corrections through FFT and classical integration in two selected areas of the Andes and their impact on geoidal heights, *Boletim de Ciências Geodésicas*, **19**(3), 407–419.
- Harrison, J.C. & Dickinson, M., 1991. Practical considerations in the use of FFT methods for computing terrain effects, in *Determination of the Geoid. International Association of Geodesy, Sympasia*, Vol 106, pp. 119–128, eds Rapp, R.H. & Sansò, F., Springer. https://doi.org/10.1007/978-1-4612-3104-2_14
- Heck, B. & Seitz, K., 2007. A comparison of the tesseroid, prism and point-mass approaches for mass reductions in gravity field modelling, *J. Geod.*, **81**(2), 121–136.
- Hinze, W.J., 2003. Bouguer reduction density, why 2.67?, *Geophysics*, **68**(5), 1559–1560.
- Huang, O., 2012. Terrain corrections for gravity gradiometry. Report 500, Department of Geodetic Science and Surveying, The Ohio State University, Columbus, USA.
- Janák, J., Vaniček, P., Foroughi, I., Kingdon, R., Sheng, M.B. & Santos, M.C., 2017. Computation of precise geoid model of Auvergne using current UNB Stokes-Helmert's approach, *Contrib. Geophys. Geod.*, **47**(3), 201–229.
- Kirby, J. & Featherstone, W., 2002. High-resolution grids of gravimetric terrain correction and complete Bouguer corrections over Australia, *Explor. Geophys.*, **33**(4), 161–165.
- Kirby, J.F. & Featherstone, W.E., 1999. Terrain correcting Australian gravity observations using the national digital elevation model and the fast Fourier transform, *Aust. J. Earth Sci.*, **46**(4), 555–562.
- Kirby, J.F. & Featherstone, W.E., 2001. Anomalously large gradients in version 1 of the “GEODATA 9 SECOND” Digital Elevation Model of Australia, and their effects on gravimetric terrain corrections, *Cartography*, **30**(1), 1–10.
- Klose, U. & Ilk, K., 1993. A solution to the singularity problem occurring in the terrain correction formula, *Mamscripta Geodaetica*, **18**(5), 263–279.
- Kuhn, M., Featherstone, W.E. & Kirby, J.F., 2009. Complete spherical Bouguer gravity anomalies over Australia, *Aust. J. Earth Sci.*, **56**(2), 213–223.
- Li, Y.C. & Sideris, M.G., 1994. Improved gravimetric terrain corrections, *Geophys. J. Int.*, **119**(3), 740–752.
- Majkráková, M., Papčo, J., Zahorec, P., Droščák, B., Mikuška, J. & Marušíak, I., 2016. An analysis of methods for gravity determination and their utilization for the calculation of geopotential numbers in the Slovak national levelling network, *Contrib. Geophys. Geod.*, **46**, 179–202.
- Martinec, Z., Vaniček, P., Mainville, A. & Véronneau, M., 1996. Evaluation of topographical effects in precise geoid computation from densely sampled heights, *J. Geod.*, **70**(11), 746–754.
- McCubbine, J.C., Featherstone, W.E. & Brown, N.J., 2019. Error propagation for the Molodensky G1 term, *J. Geod.*, **93**, 889–898.
- McCubbine, J.C., Featherstone, W.E. & Kirby, J.F., 2017. Fast-Fourier-based error propagation for the gravimetric terrain correction, *Geophysics*, **82**(4), G71–G76.
- Meyer, D. *et al.*, 2011. *ASTER Global Digital Elevation Model Version 2- Summary of Validation Results*. Available at: <https://ssl.jspacesystems.or.jp/ersdac/GDEM/ver2Validation/Summary.GDEM2.validation.report.final.pdf>.
- Nagy, D., 1966. The prism method for terrain corrections using digital computers, *Pure appl. Geophys.*, **63**(1), 31–39.
- Nowell, D.A., 1999. Gravity terrain corrections — an overview, *J. appl. Geophys.*, **42**(2), 117–134.
- Parker, R.L., 1973. The rapid calculation of potential anomalies, *Geophys. J. Int.*, **31**(4), 447–455.
- Pašteka, R. *et al.*, 2017. High resolution Slovak Bouguer gravity anomaly map and its enhanced derivative transformations: new possibilities for interpretation of anomalous gravity fields, *Contrib. Geophys. Geod.*, **47**(2), 81–94.
- Rathnayake, S., Tenzer, R., Pitoňák, M. & Novák, P., 2020. Effect of the lateral topographic density distribution on interpretational properties of Bouguer gravity maps, *Geophys. J. Int.*, **220**(2), 892–909.
- Saibi, H., Gabr, A. & Mohamed, F.S., 2019. Subsurface structural mapping using gravity data of Al-Ain region, Abu Dhabi Emirate, United Arab Emirates, *Geophys. J. Int.*, **216**(2), 1201–1213.
- Sampietro, D., Capponi, M., Triglione, D., Mansi, A.H., Marchetti, P. & Sansò, F., 2016. GTE: a new software for gravitational terrain effect computation: theory and performances, *Pure appl. Geophys.*, **173**(7), 2435–2453.
- Saragih, R.D. & Brotopuspito, K.S., 2018. Delineation of the Sumatra fault in the central part of west sumatra based on gravity method, *J. Phys. Conf. Ser.*, **1011**, 012024 doi:10.1088/1742-6596/1011/1/012024.
- Schwarz, K.-P., Sideris, M.G. & Forsberg, R., 1990. The use of FFT techniques in physical geodesy, *Geophys. J. Int.*, **100**(3), 485–514.
- Sheng, M.B., Shaw, C., Vaniček, P., Kingdon, R.W., Santos, M. & Foroughi, I., 2019. Formulation and validation of a global laterally varying topographical density model, *Tectonophysics*, **762**, 45–60.
- Sideris, M.G., 1984. Computation of gravimetric terrain corrections using fast Fourier transform techniques, UCSE Report 20007, University of Calgary, Canada.
- Sideris, M.G., 1985. A fast Fourier transform method for computing terrain corrections, *Mamscripta Geodaetica*, **10**, 66–73.
- Sobh, M., Mansi, A.H., Campbell, S. & Ebbing, J., 2019. Regional gravity field model of Egypt based on satellite and terrestrial data, *Pure appl. Geophys.*, **176**(2), 767–786.
- Tenzer, R., Chen, W., Baranov, A. & Bagherbandi, M., 2018. Gravity maps of antarctic lithospheric structure from remote-sensing and seismic data, *Pure appl. Geophys.*, **175**(6), 2181–2203.

- Tschirhart, P., Morris, W.A., Mims, J. & Ugalde, H., 2019. Applying laterally varying density corrections to ground gravity and airborne gravity gradiometry data: a case study from the Bathurst Mining Camp, *Can. J. Earth Sci.*, **56**(5), 493–503.
- Tsoulis, D., 2001. Terrain correction computations for a densely sampled DTM in the Bavarian Alps, *J. Geod.*, **75**(5-6), 291–307.
- Tsoulis, D., Novák, P. & Kadlec, M., 2009. Evaluation of precise terrain effects using high-resolution digital elevation models, *J. geophys. Res.*, **114**(B2), B02404, doi:10.1029/2008JB005639
- Tsoulis, D.V., 1998. A combination method for computing terrain corrections, *Phys. Chem. Earth*, **23**(1), 53–58.
- Tziavos, I.N. & Featherstone, W.E. (2001) First results of using digital density data in gravimetric geoid computation in Australia. in *Gravity, Geoid and Geodynamics 2000. International Association of Geodesy Symposia*, Vol **123**, pp. 335–340, ed. Sideris, M.G., Springer, doi:10.1007/978-3-662-04827-6_56.
- Tziavos, I.N. & Sideris, M.G., 2013. Topographic reductions in gravity and geoid modelling. in *Geoid Determination. Lecture Notes in Earth System Sciences*, Vol **110**, pp. 337–400, eds Sansò, F. & Sideris, M.G., Springer, https://doi.org/10.1007/978-3-540-74700-0_8
- Tziavos, I.N., Sideris, M.G. & Suenkel, H., 1996. The effect of surface density variations on terrain modelling—A case study in Austria. in *Techniques for Local Geoid Determination*, Report 96(2), pp 99–110, eds Tziavos, I.N. & Vermeer, M., Finnish Geodetic Institute, Masala.
- Uwiduhaye, J.d'A, Mizunaga, H. & Saibi, H., 2018. Geophysical investigation using gravity data in Kinigi geothermal field, northwest Rwanda, *J. Afr. Earth Sci.*, **139**, 184–192.
- Yamazaki, D. et al., 2017. A high-accuracy map of global terrain elevations, *Geophys. Res. Lett.*, **44**(11), 5844–5853.
- Yang, M., Hirt, C., Tenzer, R. & Pail, R., 2018. Experiences with the use of mass-density maps in residual gravity forward modelling, *Stud. Geophys. Geod.*, **62**(4), 596–623.
- Zahorec, P., Papčo, J., Vajda, P. & Szabó, S., 2019. High-precision local gravity survey along planned motorway tunnel in the Slovak Karst, *Contrib. Geophys. Geod.*, **49**(2), 207–227.

APPENDIX

Table A1. TC computation using FFT and strategies used to account for convergence and truncation.

Reference	Order of TC	Remarks / Critique	Area / DEM resolution / max ΔH
FFT alone			
Forsberg (1985)	1	Terrain slopes near the computation point are assumed to be small. No discussion on the convergence of the series.	9 km × 9 km / 100 m × 100 m / 608 m 1° × 1° / 0.5' × 0.5' / 700 m
Sideris (1985)	1	Slope considered are much smaller than 45°. Discussed more on the edge effect and windowing. No discussion on the convergence of the series.	28 km × 36 km / 1 km × 1 km / 2079 m
Harrison & Dickinson (1991)	4	Discussed importance of the <i>generally neglected</i> 4 th order term in the FFT solution of TC. The study area is perhaps not rugged enough.	6' × 6' / 6" × 6" / 1200 m
Li & Sideris (1994)	3	FFT method for mass-line and mass-prism models is derived. Introduced a regularization parameter 'α' for fast convergence of the TC solution. However, convergence still cannot be promised.	5° × 10° / 0.5' × 1' / 3573 m
Kirby & Featherstone (1999)	1	On obtaining spikes in the computed TC using 9" DEM (due to anomalous gradients (Kirby & Featherstone 2001)), the averaged DEM with 27" resolution was used for re-computation of the TC. Convergence is not discussed.	Australia / 9" × 9" / 2217.18 m Australia / 27" × 27" / 2162.26 m
Kirby & Featherstone (2002)	1	TC computed with a refined national DEM. No discussion on convergence.	Australia / 9" × 9" / 2244 m
McCubbine et al. (2017)	1	TC values were removed for the computation points where gradient exceeds 45°. Gradient computed in specific directions only. Cannot guarantee convergence at all points.	Australia / 1" × 1" / 2291.3 m
Space-FFT combined			
Tsoulis (1998)	3	To check the violation of convergence criterion, slopes were computed only in N-S and E-W directions. Also, the convergence of the FFT method was analysed by varying the inner radius (brute-force method). Use of the brute-force method may not guarantee convergence.	15 km × 20 km / 50 m × 50 m / 1450 m
Tsoulis (2001)	3	Extended Tsoulis (1998) with different methods for the inner zone TC computation. Brute-force method applied to check the convergence criterion and to analyse the effect of inner zone.	15 km × 20 km / 50 m × 50 m / 1450 m

Table A1. Continued

Reference	Order of TC	Remarks / Critique	Area / DEM resolution / max ΔH
Huang (2012)	1	Defined the inner zone with a grid of 3×3 cells around the computation point. The inner zone being 1.5 times greater than maximum height difference, convergence is guaranteed. But, the truncation limit for the FFT solution is not discussed. The study area is very plain.	$0.346^\circ \times 0.316^\circ / 3'' \times 3'' / 80 \text{ m}$
Gomez <i>et al.</i> (2013)	1	Inner zone computations are done with 3'' DEM. For outer zone, 3'' DEM was averaged to 30''. Lower resolution DEM was used to circumvent the converging criterion (cf. Kirby & Featherstone 1999).	$\sim 2.5^\circ \times 3.5^\circ / 3'' \times 3'' / 2500 \text{ m}$
Capponi <i>et al.</i> (2018)	2	The study focused on the inner zone TC computation. Suggested to define the inner zone with a distance of a few kilometres from the computation point. May not guarantee convergence.	$2^\circ \times 2^\circ / 3'' \times 3'' / 6500 \text{ m}$ $0.83^\circ \times 0.83^\circ / 3'' \times 3'' / 2887 \text{ m}$
Others			
Martinec <i>et al.</i> (1996)	5	The main conclusion was that the solution will diverge if the height difference of the points is larger than the distance between them and if the height difference is smaller than the distance between the points, the solution will converge. The truncation limit to be used in order to secure a convergent solution is not generalized.	Considered two points with hypothetical heights and distances between them.

C.3: Paper on evaluation of Digital Surface/Elevation Models

Journal of the Indian Society of Remote Sensing (April 2021) 49(4):971–986
<https://doi.org/10.1007/s12524-020-01273-7>



RESEARCH ARTICLE



Comparison and Validation of Satellite-Derived Digital Surface/Elevation Models over India

R. Goyal^{1,2} · W. E. Featherstone^{2,1} · O. Dikshit¹ · N. Balasubramania¹

Received: 28 August 2020 / Accepted: 12 November 2020 / Published online: 4 December 2020
 © Indian Society of Remote Sensing 2020

Abstract

India presents among the world's most topographically complex geomorphologies, with land elevations ranging from -2 m to $+8586$ m and terrain gradients sometimes exceeding 45° . Here, we present an evaluation of four freely available digital surface models (DSMs) on a model-to-model basis, as well as a validation using independent ground-truth data from levelled benchmarks in India. The DSMs tested comprise SRTM1", SRTM3", ASTER1" and Cartodem1" [an India-only model]. Along with these four DSMs, the MERIT3" digital elevation model (DEM) is also tested with the ground-truth data. Our results for India indicate some mismatch of these DEMs/DSMs from their claimed accuracies/precisions. All DSMs/DEMs (except for ASTER) have $> 90\%$ of pixels satisfying ± 16 m at the one-sigma level, but only in the low-lying (< 500 m) parts of India, i.e. the Gangetic plains and the Thar desert.

Keywords Vertical accuracy/precision assessment · Digital surface models · Digital elevation models · India

Introduction

A digital surface model (DSM) is a representation of the shape of the Earth's surface. Several near-global DSMs have been produced from satellite-borne platforms from either radar, e.g. SRTM (Farr et al. 2007) or stereoscopic optical imagery, e.g. ASTER (Meyer et al. 2011). We deliberately distinguish between a DSM and a digital elevation model (DEM) also sometimes known as a digital terrain model (DTM), where a DEM/DTM represents the solid topographic surface, whereas a DSM represents the surface sensed, which includes the height of vegetation

canopy and man-made structures (cf. Hirt 2014). A satellite-derived DSM should be treated for speckle noise (Gallant 2011) and stripe noise (Tarekegn and Sayama 2013), and then, it can be converted to a DEM by accounting for absolute biases (Crippen et al. 2016) and tree height biases (O'Loughlin et al. 2016). Yamazaki et al. (2017) have treated the SRTM v 2.1 DSM for all these four sources to produce the MERIT3" DEM. DEMs and DSMs should also be checked for other artefacts such as spikes, pits and line defects (e.g. Hirt 2018).

DEMs and DSMs are used synonymously in several applications such as mapping soil and vegetation (e.g. Dobos and Hengl 2009; Cavazzi et al. 2013), studying natural hazards (e.g. Gruber et al. 2009; Demirkesen 2012), catchment geomorphology and hydrology (e.g. Barnes et al. 2014; Zhao et al. 2019), watershed modelling (e.g. Park et al. 2011; Li et al. 2019), floodplain mapping (e.g. Jafarzadegan and Merwade 2017; Nardi et al. 2019), weather and flood forecasting (e.g. Truhetz 2010) and gravity field forward modelling (e.g. Banerjee and Gupta 1977; Forsberg 1984). The exemplar citations made above are not exhaustive because the literature on applications is so vast. However, researchers have started analysing the effect of using a DSM and not the "required" DEM for their respective applications, such as done by Yang et al.

✉ R. Goyal
 rupeshg@iitk.ac.in; ropeshgoyal2809@gmail.com

W. E. Featherstone
 w.featherstone@curtin.edu.au

O. Dikshit
 onkar@iitk.ac.in

N. Balasubramania
 nagaraj@iitk.ac.in

¹ Department of Civil Engineering, Indian Institute of Technology Kanpur, Kanpur 208016, India

² School of Earth and Planetary Sciences, Curtin University of Technology, GPO Box U1987, Perth, WA 6845, Australia

(2019) for gravity forward modelling. In this paper, we have used the terms DEM or DSM separately in many instances so as to reinforce the difference between the two.

Since the procedures for generating DSMs vary due to the different types of datasets or sensors involved (Gesch 2012), one should not generally rely on freely available DSMs without appreciating the accuracy/precision required for the application at hand. Rodriguez et al. (2005) and Farr et al. (2007) provide global accuracy analyses of the SRTM DSMs. Meyer et al. (2011) conduct a global accuracy assessment for ASTER. DEM/DSM assessments have also been made on regional scales (e.g. Nikolakopoulos et al. 2006; Racoviteanu et al. 2007; Hayakawa et al. 2008; Chirico et al. 2012; Gesch et al. 2012; Suwandana et al. 2012; Li et al. 2013; Jing et al. 2014; Purinton and Bookhagen 2017; Elkhachy 2018; Zhang et al. 2019; Hawker et al. 2019) and countrywide scales (e.g. Hilton et al. 2003; Denker 2005; Hirt et al. 2010; Athmania and Achour 2014; Gesch et al. 2014; Ioannidis et al. 2014; Rexer and Hirt 2014; Varga and Bašić 2015). We attempt to add to this body of literature by providing results from the whole country of India, where the topographic morphology is quite diverse: heights range from -2 m to $+8586$ m and terrain gradients sometimes exceed 45° (2.4% of the total cells at $1'' \times 1''$ resolution, i.e. 3,748,582,709 cells). While studies have been conducted on the comparison and validation of different DEMs/DSMs in smaller regions of India (see Table 1), none are countrywide as we attempt in this investigation.

India hosts part of the Himalaya Mountain Ranges in the north, the Gangetic Plain in the centre, the Aravalli and Vindhya Mountain ranges, the Western and Eastern Ghats, the Deccan Plateau, the Thar desert and a long peninsular coastline (Fig. 1). Thus, accuracy/precision assessment of DEMs/DSMs for India is of utility, especially when researchers are already using freely available DSMs for applications in India such as geology and geomorphometric analysis (e.g. Selvan et al. 2011; Gayen et al. 2013), watershed delineation (e.g. Sreedevi et al. 2009; Ahmed et al. 2010; Gopinath et al. 2014), identifying potential water harvesting sites near rivers (e.g. Ramakrishnan et al. 2009), assessment of tsunami risk (e.g. Kumar et al. 2007), hydrographic modelling (e.g. Patro et al. 2009) and estimating glacial mass balance (e.g. Berthier et al. 2007).

Unlike some of the previous studies in India (Table 1), and indeed elsewhere, we have deliberately preserved the respective meanings of DEM versus DSM throughout our analyses. Strictly, DEMs and DSMs should never be compared until one is transformed to the other (Yamazaki et al. 2017). In the study presented here, four freely available DSMs for India (SRTM1'', SRTM3'', ASTER1'' and Cartodem1'' [an India-only model; see below]) are inter-compared on a model-to-model basis. They are also

“validated” with independent ground-truth height data provided by the Survey of India (SoI) to which National Aeronautics and Space Administration (NASA) canopy height information (Simard et al. 2011) has been added to give point DSM heights (Sect. 4). Along with these four DSMs, the MERIT3'' DEM is also validated with the same ground-truth data, without canopy heights applied. MERIT3'' was not included in the model-to-model DSM comparison. In India only, the national Cartodem DSM, derived from the Cartosat mission using stereoscopic optical imagery (NRSA 2006), is also used in regional applications (Bera et al. 2014; Das et al. 2015, 2018; Kumar and Gupta 2016), so we include this DSM in our assessments. The DSMs and DEMs evaluated are summarised in Table 2.

Due to the land height range in India (-2 m to $+8586$ m), our analysis is divided into three sub-parts based on classification of the heights into three intervals, with an implicit assumption that these may correlate with the broader morphology, namely $H \leq 500$ m, $500 \text{ m} < H \leq 1500$ m and $H > 1500$ m (Fig. 2b). The rationale behind the chosen three intervals is: regions of the Gangetic plains, the Thar desert and the peninsular coastline are all below 500 m; the whole of the Aravalli range (except a few peaks), the Vindhya range, majority of the Eastern Ghats and half of the Western Ghats are between 500 and 1500 m, while the other half of Western Ghats, a small extent of Eastern Ghats and almost whole of the Himalayan belt are above 1500 m. The claimed accuracies/precisions for all the DEMs/DSMs (Table 2) are also cross-checked on whole of India and height-range-wise bases. This is of utility because the accuracy statistics defined from global assessments may not be applicable to India, which certainly appears to be the case for high-elevation areas.

Subtleties of Indian Height Data

The nominal vertical datum of the Cartodem DSM is WGS84 and it thus provides ellipsoidal heights of the Earth's surface. To achieve a consistent vertical datum among the DSMs (cf. Table 2), the Cartodem was also referenced to EGM96 (Lemoine et al. 1998) by subtracting EGM96 geoid undulation values and rounding to the nearest metre as was done when computing SRTM physical heights (cf. Farr et al. 2007, p. 19). EGM96 is an older spherical harmonic degree-360 geopotential model, and comparatively better high-degree geopotential models are now available, such as EGM2008 to degree 2190 (Pavlis et al. 2012, 2013). To show the effect of using EGM2008 instead of EGM96, a difference map was prepared and truncated to the nearest metre. Figure 3 shows that DEMs/DSMs derived from each geoid model can differ by up to

Table 1 Previous DEM/DSM assessment studies in India

Citation	Data used	Remark
Muralikrishnan et al. (2013)	SRTM1", ASTER1", Cartodem1", three different regions in India	Absolute and relative evaluation of Cartodem was done w.r.t to ground control points (GCPs) and SRTM/ASTER, respectively. It was concluded that in a flat region, height accuracy of Cartodem is better than ± 4 m, and for the hilly regions, the error reaches around ± 8 m. Also, it was established that more than 90% of the SRTM and Cartodem difference points are within 8 m. The absolute and relative vertical accuracies of Cartodem were stated to be 8 m at 90% confidence and 5 m at 68% confidence
Srivastava and Mondal (2012)	SRTM3", ASTER1" and Survey of India (SoI) 1:50,000 topographic map, $3' \times 3'$ area, elevation range: 82 m to 100 m	Only three points in the study area were extracted from the topographic maps with the height values of 82 m, 90 m and 100 m. DEMs/DSMs were evaluated based on these three points. No statistical information was provided. ASTER was concluded to be more precise compared to SRTM, but this has to be heavily qualified because of the small sample size used
Bothale and Pandey (2013)	SRTM3", ASTER1", Cartodem (10 m, 20 m, 30 m, 40 m, 50 m, 90 m), $0.45^\circ \times 0.3^\circ$ area, SoI 1:50,000 topographic map	This DSM evaluation methodology mentioned all the heights relative to WGS84 ellipsoid. However, the ground-truth was extracted from SoI maps which provide heights above local mean sea level (MSL). No information on the conversion of ellipsoidal heights to physical heights or vice versa was provided. RMSEs of ASTER and SRTM were reported to be significantly high compared to the Cartodem (all resolutions). 90% of Cartodem and SRTM difference points were reported to be within ± 8 m as also claimed by Muralikrishnan et al. (2013)
Thomas et al. (2015)	SRTM3", ASTER1", GMTED250m, DEM generated using SoI 1:50,000 topographic map, $0.22^\circ \times 0.42^\circ$ area, 55 spot heights	The study involved evaluation based on spot heights extracted from the topographic map. The comparison concluded that SRTM (RMSE = 17.05 m) is more precise than ASTER (RMSE = 24.09 m) and GMTED (RMSE = 32.85 m). The RMSE of the topographic map-derived DEM was 3.17 m
Krishnan et al. (2016)	SRTM, ASTER, Cartodem and DEM generated using Cartosat imagery, $0.33^\circ \times 0.25^\circ$ area, 25 DGPS surveyed GCPs	The analysis reported the RMSEs for ASTER and SRTM to be 8.13 m and 8.98 m, respectively. RMSE for Cartodem was 60.94 m, while for the generated DEM the value was 36.79 m. Though the study discussed the generation of DSM using Cartosat imagery, we note some complications in the conversion of ellipsoidal heights to physical heights. This might be a reason for the large RMSE observed for Cartodem
Yadav and Indu (2016)	SRTM1", ASTER1", Cartodem, SoI 1:250,000 topographic map, $4^\circ \times 2^\circ$ area, elevation range: 800 m to 2000 m	Reported RMSEs for ASTER, SRTM and Cartodem were 74.78 m, 69.18 m and 69.38 m, respectively. An explanation was missing for using a topographic map of 1:250,000 scale, wherein plotting error is 62.5 m, i.e. the extracted point derived from a map can indicate any point lying in an area of $62.5 \text{ m} \times 62.5 \text{ m}$
Mukul et al. (2017)	SRTM1" X and C band, SRTM3" C band, 221 GPS points	An investigation involving only SRTM DSMs was done, wherein the claimed accuracy of 16 m at 90% confidence was also cross-verified. The C band SRTM data were reduced to WGS84 datum by using geoid values from EGM96 (Lemoine et al. 1996). The study concluded that without any filtering of the DSMs, only X band SRTM1" has an RMSE of 9.18 m. The 1" and 3" C band DSMs have RMSE of 23.53 m and 47.24 m, respectively. Outlier and void filtering techniques were also discussed, after which the RMSEs of 1" X band, 1" C band and 3" C band reduced to 8.00 m, 10.14 m and 14.38 m, respectively
Rawat et al. (2019)	SRTM3", ASTER1", Cartodem1", 20 DGPS surveyed GCPs, Shahjahanpur district	For the 20 points, heights were extracted from the three DSMs and were compared against each other. RMSE values for Cartodem-ASTER = 137.65 m, Cartodem-SRTM = 186.65 m and ASTER-SRTM = 50.87 m



Fig. 1 Physical features of Indian topography. (Source: <https://www.nationonline.org/oneworld/map/India-Administrative-map.htm>)

12 m in magnitude, particularly in the Indian Himalaya (cf. Fig. 1). The effect of the different geoid models will be assessed later in Sect. 3.3.

As well as model-to-model comparisons, the DEMs/DSMs are “validated” with independent ground-truth data, comprising 3842 differentially levelled benchmarks and 145 ground control points (GCPs).

- The 3842 benchmarks (Fig. 4) consist of latitude, longitude and levelled heights above local mean sea level (MSL). They come from the database archived by the Bureau Gravimetric International (BGI) and were originally sourced from the SoI and the Indian National Geophysical Research Institute (NGRI). Though the horizontal and vertical precisions are not known, all the relevant infrastructure and research projects in India are based on benchmarks established by SoI. These are the heights that we have used in our analysis. Vertical precisions are important to be confident that we are not validating the DEM/DSM heights with erroneous ground control. Horizontal precision is important to be confident that we are not interpolating the DEM/DSM height to the wrong location, which can be a substantial problem in areas of steep terrain gradients.
- The 145 GCPs consist of GNSS-determined latitude, longitude and ellipsoidal height. Geoid undulation values from EGM96 were subtracted from these ellipsoidal heights to determine physical heights that are compatible with the DEMs/DSMs (cf. Table 2), but not rounded to the nearest metre. The GCPs are concentrated in five different regions of the country: Hyderabad, Bangalore, Kanpur, Dehradun and Saharanpur (Fig. 5). The GCPs in Kanpur were observed

Table 2 DEMs used in the study (adapted from Rexer and Hirt 2014)

	SRTM V3.0 (S1)	SRTM V4.1 (S3)	ASTER GDEM V2 (AS)	Cartodem V2 (CA)	MERIT (ME)
Model type	DSM	DSM	DSM	DSM	DEM
Satellite mission	Shuttle Radar Topography Mission (SRTM)	SRTM	Terra	Cartosat-1 (NRSA 2006)	SRTM and Advanced Land Observing Satellite (ALOS)
Institution	NASA	CGIAR-CSI	METI, NASA	NRSC-ISRO	Yamazaki et al. (2017)
Resolution (in arc seconds)	One	Three	One	One	Three
Release year	2015	2011	2011	2014	2018
Vertical datum	EGM96	EGM96	EGM96	WGS84	EGM96
Height type	Physical ¹	Physical	Physical	Ellipsoidal	Physical
Claimed accuracy	16 m at 90% confidence, near-global	16 m at 90% confidence, near-global	17 m at 95% confidence, near-global	8 m at 90% confidence, India-only	12 m at 90% confidence, near-global
URL	https://gdex.cr.usgs.gov/gdex/	http://srtm.csi.cgiar.org/	https://search.earthdata.nasa.gov/	https://bhuvan-app3.nrsc.gov.in/data/download/index.php	http://hydro.iis.u-tokyo.ac.jp/~yamada/MERIT_DEM/

¹By physical, we mean that the geometric ellipsoidal/geodetic height (h) has been transformed to a physically meaningful orthometric height (H) using a global geoid (N) model ($H \approx h - N$)

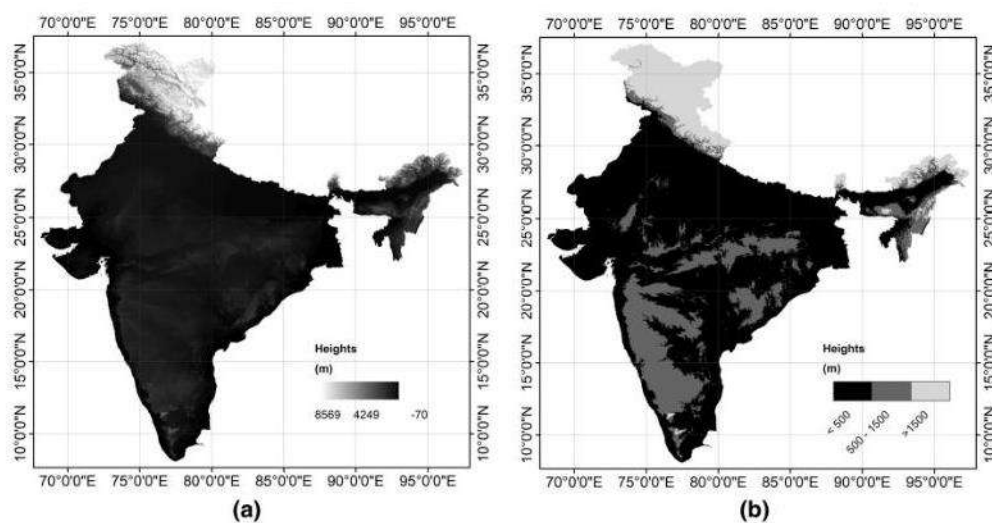


Fig. 2 Terrain of India **a** and the three height ranges tested **b** (equi-rectangular projection)

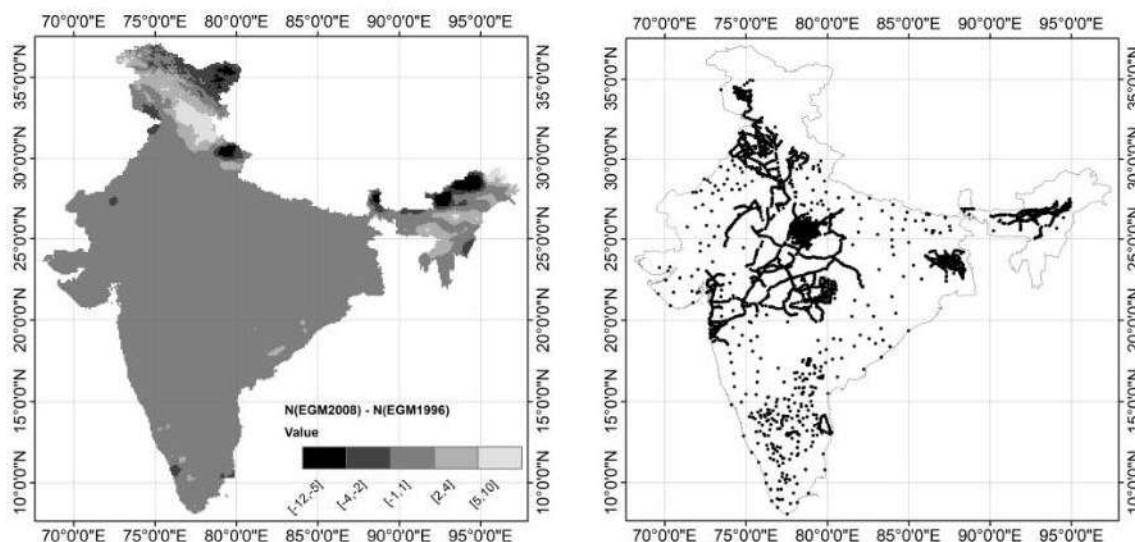


Fig. 3 Geoid differences between EGM2008 and EGM96, truncated to the nearest metre (equi-rectangular projection)

using dual frequency GNSS, while GCPs at other locations were obtained from the SoI archive. The horizontal and vertical precision of these data lies within 12 to 26 mm and 31 to 53 mm, respectively (Mishra 2017).

We return to the caveat in the first paragraph of Introduction, qualifying that a DEM is distinctly different from a DSM. The benchmarks and GCPs give the physical (MSL-based) heights of the solid ground, so are compatible

Fig. 4 Spatial distribution of the 3842 levelled benchmarks (equi-rectangular projection)

with DEMs, but not with DSMs. Therefore, in the later analysis (Sect. 4), canopy height (CH) information is added to the ground-truth data for comparison with DSMs in order to achieve compatibility. We have not conducted an analysis of the veracity of the CH model over India, instead taking the published values “at face value”. We also acknowledge that other corrections are needed, as outlined in Introduction.

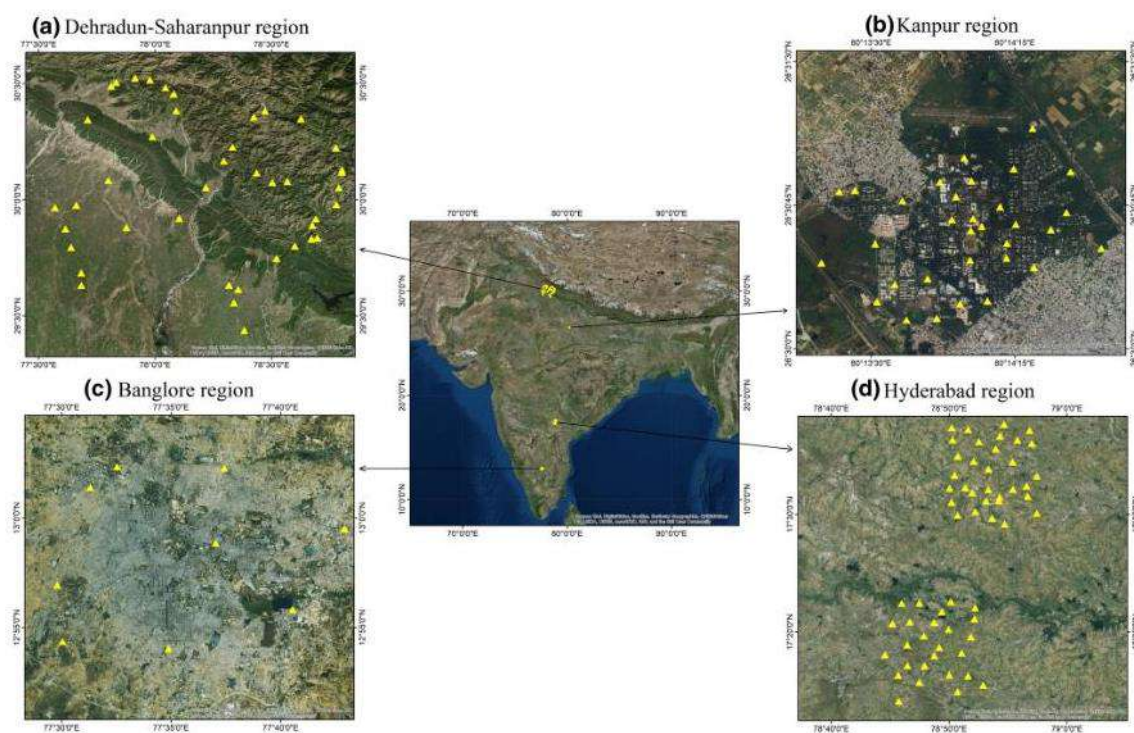


Fig. 5 Spatial distribution of the 145 GCPs (source: Google Earth)

Table 3 Statistics of inter-comparison among DSMs. Units in metres. The abbreviations for the DSM names are given in the first row of Table 2

	S1–S3	S1–AS	S1–CA	S3–AS	S3–CA	AS–CA
Min	– 4287	– 5815	– 4801	– 4363	– 5152	– 5859
Max	5197	3109	3235	5792	4846	4295
Mean	1.4	1.9	– 2.1	– 0.5	0.8	– 0.2
STD	32.4	20.4	35.8	39.3	45.8	39.5

Inter-Comparison Among DSMs

The SRTM v4.1 DSM was first bicubically interpolated from $3'' \times 3''$ to $1'' \times 1''$ resolution to make it spatially consistent with the other three DSMs (SRTM v3.0, ASTER GDEM2 and Cartodem; Table 2). The DSMs were compared according to three criteria:

1. For the whole country of India, producing a total of 3,748,582,709 $1'' \times 1''$ DSM differences
2. For DSM heights divided into three ranges, namely $H \leq 500$ m, $500 \text{ m} < H \leq 1500$ m and $H > 1500$ m (Fig. 2b)
3. For four intervals that are defined according to the claimed accuracies/precisions of the DSMs (Table 6 later).

Finally, we replace EGM96 with EGM2008 for all the DSMs to gauge the effect of using a higher-degree geoid model to obtain physical heights from a DSM.

Nationwide Inter-Comparison

Possibly the most alarming observation from Table 3 is that the DSMs can differ by several kilometres, though the percentage of such pixels is proportionally small (Table 4). These large height differences among the DSMs are most probably due to geolocation errors (Rodriguez et al. 2005), i.e. horizontal shifts among the DSMs are caused by incorrect co-registration (Denker 2005). These shifts result in comparing DEM/DSM cells of two different locations, hence producing substantial height differences, especially in areas of steep terrain gradients. Also, from Table 4, the

Table 4 Distribution of “large” differences among the DSMs over India. The abbreviations for the DSM names are given in the first row of Table 2

Comparison	Frequency of differences (ΔH) as a percentage							Percentage of total number of pixels
	$100\text{ m} < \Delta H \leq 500\text{ m}$	$500\text{ m} < \Delta H \leq 1000\text{ m}$	$\Delta H > 1000\text{ m}$	$-100\text{ m} > \Delta H \geq -500\text{ m}$	$-500\text{ m} > \Delta H \geq -1000\text{ m}$	$\Delta H < -1000\text{ m}$	$\Delta H < -10000\text{ m}$	
S1-S3	0.354	0.126	0.001	0.210	0.003	0.000	0.695	
S1-AS	0.023	0.001	0.000	0.035	0.012	0.009	0.080	
S1-CA	0.313	0.059	0.013	0.473	0.036	0.007	0.901	
S3-AS	0.560	0.138	0.011	0.298	0.004	0.001	1.012	
S3-CA	0.574	0.037	0.007	0.532	0.164	0.016	1.330	
AS-CA	0.292	0.054	0.012	0.504	0.004	0.014	0.880	

number of pixels in different ranges for S1-AS individually and S1-AS and AS-CA collectively show that SRTM1" and ASTER are more consistent with one other than the other model pairs. [The abbreviations for the DSM names are given in the first row of Table 2.] This consistency is also backed up by only 0.1% of the difference pixels for S1-AS lie beyond the range $[-100\text{ m}, 100\text{ m}]$. Also, on analysing the three pairs i.e. S1-AS, S3-CA and AS-CA, it is observed that the Cartodem, compared to SRTM3", has more congruency with SRTM1" and ASTER. This is probably only because SRTM3" was bicubically resampled to a $1'' \times 1''$ spatial resolution. The total number of pixels in each $1'' \times 1''$ DSM is 3,748,582,709, and ΔH represents the difference among various pairs of DSMs (e.g. S1-S3, S1-AS, S1-CA, S3-AS, S3-CA and AS-CA).

Figure 6 shows the striping effects among the DSMs. Striping in ASTER was also observed by Hirt et al. (2010) over Australia. Considering the fact that SRTM have stripe effects with a different pattern compared to ASTER (cf. Gallant and Read 2009), and on comparing (i) Figs. 6b,c and (ii) Fig. 6d, e, it can be claimed that Cartodem also has the stripe effects that are nearly in the same direction as ASTER (Fig. 6c, e). Stripes are also shown in Fig. 6f (AS-CA), indicating the non-negligible difference in the magnitude of the stripes in ASTER and Cartodem. Hirt et al. (2010) pointed out that the stripe effects in ASTER occur on scales of several thousand kilometres; Fig. 6 shows the similarity of this phenomenon for Cartodem in India.

Height-Range-Wise Inter-Comparison

Table 5 shows that, despite the lowest standard deviations (STDs) of ΔH for the height range $H \leq 500\text{ m}$, large differences exist among DSMs (cf. Table 4). The significant differences between S1-S3 (both derived from the same satellite mission) are possibly due to systematic errors between the two DSMs, primarily found in the mountainous regions. This is possibly because SRTM1", a high-resolution DSM, provides a better topographic representation compared to SRTM3", especially along ridges and valleys. Other discrepancies among Cartodem and other DSMs are also observed at the locations of large lakes and active open-pit mine sites (Fig. 7). This is due to the different epochs of the observations and re/processing involved in the development of each DSM, which is [partly] reflected by the release dates in Table 2. A similar observation has been reported by Long et al. (2020) over open-pit mines in Quang Ninh Province in Vietnam.

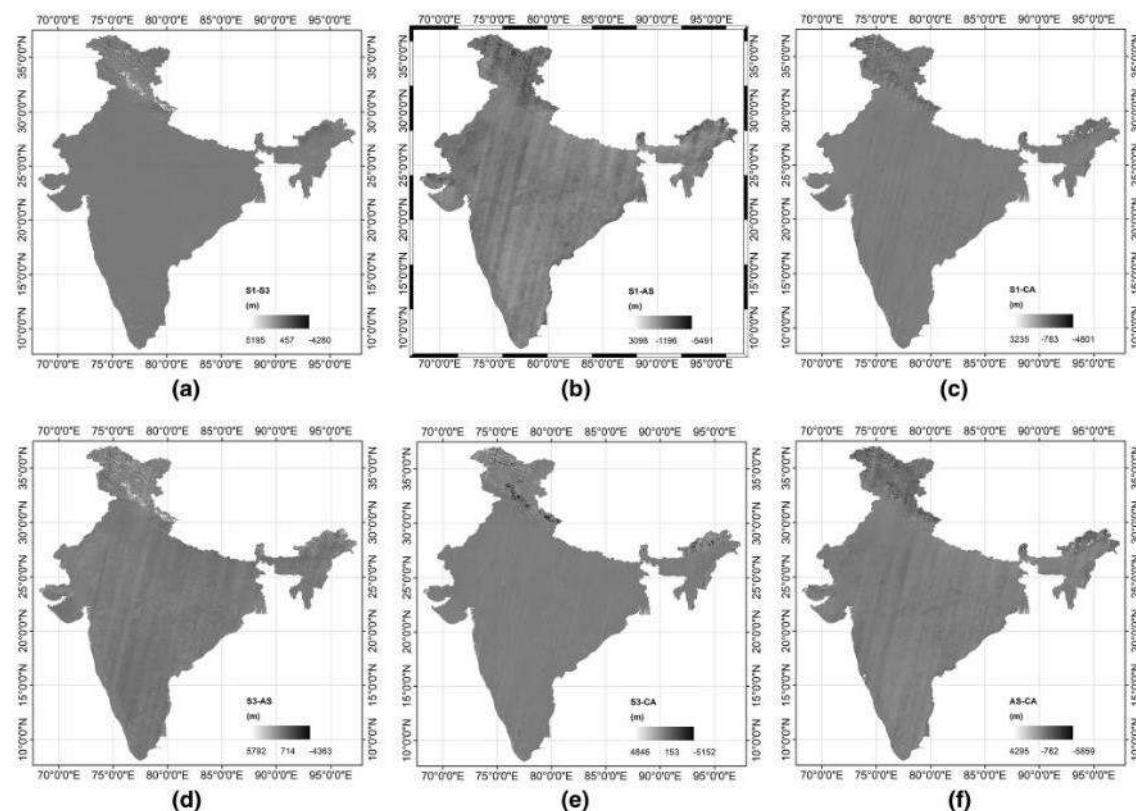


Fig. 6 Visual representation of the differences between DSM pairs over India, showing stripes. [a S1-S3; b S1-AS; c S1-CA; d S3-AS; e S3-CA; f AS-CA]. The abbreviations for the DSM names are given in the first row of Table 2

Table 5 Statistics of the DSM inter-comparison based on a range-wise classification. Units in metres. The abbreviations for the DSM names are given in the first row of Table 2

		S1-S3	S1-AS	S1-CA	S3-AS	S3-CA	AS-CA
Min	$H \leq 500$ m	-301	-389	-1026	-326	-5152	-1180
	$500 \text{ m} < H \leq 1500$ m	-930	-2490	-685	-969	-2400	-2390
	$H > 1500$ m	-4287	-5815	-4801	-4363	-5098	-4295
Max	$H \leq 500$ m	5197	266	1189	5208	1034	1031
	$500 \text{ m} < H \leq 1500$ m	1444	352	2397	2525	773	2578
	$H > 1500$ m	5163	3109	3235	5792	4846	5859
Mean	$H \leq 500$ m	0.1	2.9	-1.5	-2.8	1.5	-1.4
	$500 \text{ m} < H \leq 1500$ m	0.3	3.1	-1.5	-2.8	1.2	-1.6
	$H > 1500$ m	11.0	-5.8	-6.7	16.9	-4.3	12.5
STD	$H \leq 500$ m	5.7	6.9	6.9	9.5	8.2	10.11
	$500 \text{ m} < H \leq 1500$ m	20.5	9.8	17.6	24.8	26.0	19.5
	$H > 1500$ m	90.3	55.7	101.9	107.5	129.3	111.0

Inter-Comparison According to DSM Claimed Precision

We deduce four accuracy/precision intervals according to the claimed accuracies/precisions of the DSMs (Table 6).

The percentages of points lying in these different intervals are shown in Table 7.

From Table 7, the percentages of pixels in intervals In1 and In2 for S1-AS, S3-AS and AS-CA show that ASTER contains more error compared to the other three DSMs. The

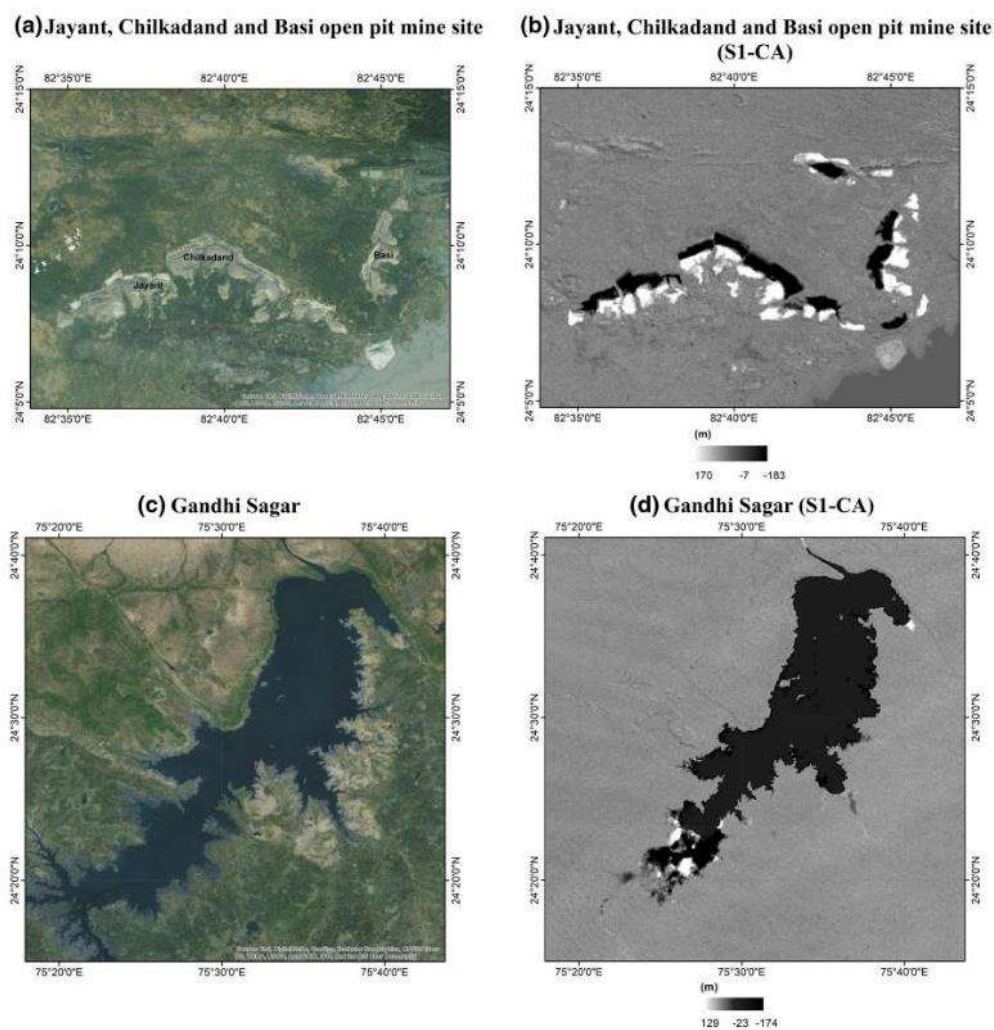


Fig. 7 Differences between SRTM1'' and Cartodem (greyscale panels) at the locations of large lakes and active open-pit mine sites (background images from Google Earth)

Table 6 Accuracy/precision intervals as deduced from other investigations

Interval	One-sigma range (m)	Remarks
In1	[- 3.768, 3.768]	Rodriguez et al. (2005) computed an absolute height error of 6.2 m at 90% (1.645σ for 1D) confidence in SRTM for Eurasia. Therefore, the first interval is taken as bounded within $6.2/1.645 = 3.768$ m
In2	[- 9.726, 9.726]	One of the objectives of the SRTM mission was to obtain the absolute height error within 16 m at 90% confidence (Farr et al. 2007). Therefore, the second interval is taken as bounded within $16/1.645 = 9.726$ m This bound also covers the accuracy estimate of Cartodem (7.6 m at 90% confidence, i.e. 4.62 m (Rao et al. 2014)) and MERIT3'' (12 m at 90% confidence, i.e. 7.29 m (Yamazaki et al. 2017))
In3	[- 16, 16]	This bound is chosen by hypothetically considering 16 m to be the 1σ error bound in the DSMs
In4] - 16, 16[This bound is to check the number of pixels that exceed the above hypothetical 1σ error bound in the DSMs

Table 7 Percentage of pixels (from model-to-model comparison) lying in the intervals set in Table 6

		S1–S3 (%)	S1–AS (%)	S1–CA (%)	S3–AS (%)	S3–CA (%)	AS–CA (%)
In1	Overall	69	34	62	30	56	37
	H ≤ 500 m	83	38	70	35	67	41
	500 m < H ≤ 1500 m	56	32	57	24	46	33
	H > 1500 m	14	16	23	8	11	12
In2	Overall	84	75	91	67	83	76
	H ≤ 500 m	95	82	98	78	94	84
	500 m < H ≤ 1500 m	76	72	91	56	78	72
	H > 1500 m	29	42	52	20	27	32
In3	Overall	89	92	95	83	89	90
	H ≤ 500 m	98	97	97	94	98	97
	500 m < H ≤ 1500 m	85	92	97	76	87	90
	H > 1500 m	43	64	69	33	42	51
In4	Overall	11	8	4	17	11	10
	H ≤ 500 m	2	3	< 1	6	2	3
	500 m < H ≤ 1500 m	15	8	3	24	13	10
	H > 1500 m	57	35	31	67	58	50

Table 8 Statistics (cf. Table 3) and percentage of points in different intervals (cf. Table 6) after replacing EGM96 by EGM2008 geoid values. Units in metres

	S1–S3	S1–AS	S1–CA	S3–AS	S3–CA	AS–CA
Min	– 4280	– 5810	– 4795	– 4356	– 5154	– 5864
Max	5195	3116	3234	5797	4852	4288
Mean	1.4	2.0	– 2.1	– 0.5	0.8	0.1
STD	32.6	20.4	35.7	39.5	45.7	39.7
In1	69%	34%	61%	29%	56%	36%
In2	84%	75%	91%	66%	83%	76%
In3	89%	92%	95%	83%	89%	90%
In4	11%	8%	5%	17%	11%	10%

claimed accuracies/precisions are only valid if 90% of the data satisfy the given accuracy requirements (cf. Rodriguez et al. 2005). In the lowland range (< 500 m), more than 90% of the differences for S1–S3, S1–CA and S3–CA lie in the interval In2. This indicates that the three DSMs (i.e. S1, S3, CA) are congruous with their claimed accuracies, but only in this height range. It is found that 90% of the total S1–CA difference pixels (without any height-banded classification) fall within ± 8 m, which resembles the observations of 90% by Muralikrishnan et al. (2013) and Bothale and Pandey (2013).

Finally, the overall statistics and the percentage of pixels in different accuracy/precision intervals after replacing EGM96 by EGM2008 for all the DSMs are summarised in Table 8. This shows no significant change either in the overall statistics (cf. Table 3) or the distribution of differences (cf. Table 7) after transforming the DSMs to physical heights using EGM2008. Therefore, it appears immaterial

as to which geoid model is used to transform the geometric ellipsoidal heights to physical heights given the former's intrinsic accuracy/precision (cf. Figure 3), but this only applies to India and might not be the case in the countries with relatively lower topographical elevations.

Validating DEMs with Ground-Truth Physical Heights

The DEMs are now “validated” with two sets of independent ground-truth data: 3842 levelled benchmarks and 145 GPS-based GCPs. Recalling from Sect. 2, the ellipsoidal heights of GCPs were converted to physical heights by subtracting the EGM96 geoid model. Since SRTM1”, SRTM3”, ASTER and Cartodem are all DSMs, canopy height (CH) data from NASA (Simard et al. 2011) were added to the ground-truth point heights. The CH data were

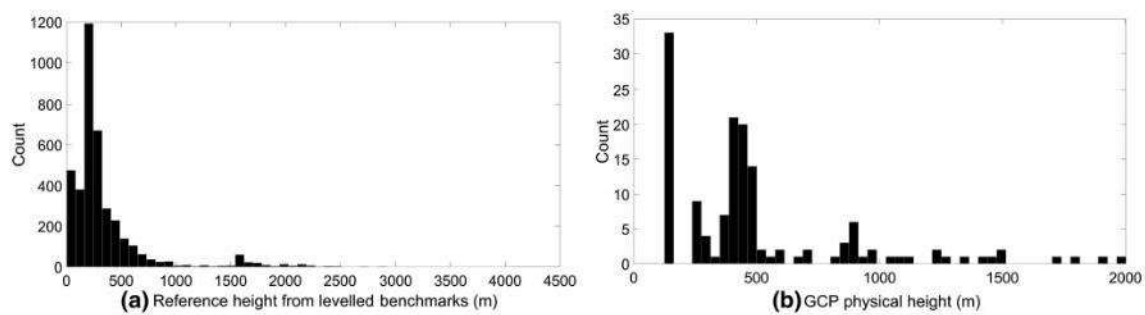


Fig. 8 Distribution of the **a** levelled benchmark heights: max 4057.2 m, min 1.5 m, and **b** GCP heights: max 2002.7 m, min 124.8 m

Table 9 Statistics of comparison between ground-truth heights and the DEMs/DSMs. Units in metres. The abbreviations for the DSM names are given in the first row of Table 2

	3842 benchmarks						145 GCPs					
	Min	Max	Mean	MAE	STD	RMSE	Min	Max	Mean	MAE	STD	RMSE
S1	− 215.9	270.9	1.8	8.1	17.7	17.8	− 13.9	38.4	1.3	5.9	9.8	9.8
S3	− 220.9	257.5	1.9	8.0	17.2	17.3	− 49.3	102.4	2.1	8.1	17.5	17.6
AS	− 212.9	243.9	4.4	10.5	18.8	19.3	− 21.2	43.9	5.4	8.2	10.0	11.4
CA	− 336.7	270.2	1.0	8.5	19.7	19.7	− 11.4	50.2	1.9	5.7	9.4	9.6
ME	− 256.3	249.9	− 0.4	7.1	17.3	17.3	− 33.4	24.3	0.7	4.5	7.1	7.1

not subtracted from the entire DSMs pixel by pixel because the conversion of a DSM to a DEM also involves extra filtering techniques as summarised in Introduction. Thus, just removing the CHs does not necessarily provide a true DEM, but we believe it to be better than using a DSM alone. We did not conduct an analysis of the veracity of the CH data, instead taking the NASA model at face value.

Figure 8 shows the distribution of the heights of the 3842 benchmarks and 145 GCPs. They reflect the difficult logistics of collecting surveying data at inaccessible altitudes. As such, this validation only really holds for elevations less than, say, ~ 500 m (cf. Fig. 8a). In addition, the only sample geographically limited parts of India. Table 9 shows the statistics of comparisons between the DSMs/DEMs and these two ground-truth datasets, where the CH has been added when assessing the DSMs. For the heights extracted from Cartodem, there are two points with unexpectedly large height differences (i.e. -191 m and -186 m). These points are not removed from the analyses because the overall statistics of the comparison after removing them does not change significantly (min = -336.7 m, max = 270.2 m, mean = 0.9 m, MAE = 8.4 m, STD = 19.2 m and RMSE = 19.2 m).

The statistics in Table 9, when viewed collectively and more so by the mean absolute error (MAE) and root mean square error (RMSE), indicate that MERIT3'' compares relatively closer with respect to the ground-truth heights as

compared to the DSMs. This is most probably because other error sources (mentioned in Introduction) were removed in the construction of MERIT3'' (Yamazaki et al. 2017), whereas we have only applied the CHs to the ground-truth in this study. The better results for MERIT3'' with respect to the GCPs can also be attributed to GPS data generally being collected in open areas (away from buildings/trees) for satellite visibility. Therefore, there is less probability of CH error due to the presence of man-made features or vegetation (cf. Denker 2005; Hirt et al. 2010).

We next repeat the analyses conducted among the DSMs, but now with the ground-truth data, including the MERIT3'' DEM, and after CHs have been added to the ground-truth when DSMs are assessed. We restrict the presentation here to only the levelled benchmarks because of the larger sample size with broader spatial (Fig. 3) and vertical (Fig. 8) distributions versus the GCPs (cf. Figs. 4, 8). Our analyses with the GCPs do not contradict the findings presented below. The DEM/DSM comparisons with height-range-wise and accuracy/precision-wise classification are given in Tables 10, 11, respectively.

First, however, it is important to acknowledge that the number of benchmarks with MSL-based land elevations greater than 500 m is relatively few (Fig. 8 and Table 10). As such, while all results are presented for the sake of completeness, lesser emphasis on the interpretation is made from them when $H > 500$ m. This is also demonstrated in

Table 10 Statistics of the comparison with benchmarks based on range-wise classification. The model with the least MAE and RMSE values is the most preferred. Units in metres

		#data	Min	Max	Mean	MAE	STD	RMSE
$H \leq 500$ m	S1	3263	-114.9	206.4	1.6	6.4	12.2	12.3
	S3	3263	-118.6	206.4	1.6	6.3	12.0	12.1
	AS	3263	-107.9	210.4	4.5	8.8	13.6	14.3
	CA	3263	-336.7	204.5	0.6	6.7	14.5	14.5
	ME	3273	-128.6	207.4	0.0	5.5	11.7	11.7
$500 \text{ m} < H \leq 1500$ m	S1	403	-215.9	243.5	2.6	14.1	28.8	28.9
	S3	403	-220.9	257.5	2.1	14.9	30.0	30.1
	AS	403	-212.9	233.5	5.2	16.4	29.4	29.8
	CA	403	-216.5	246.5	2.5	14.6	30.4	30.4
	ME	395	-223.9	229.5	-2.2	12.8	27.9	28.0
$H > 1500$ m	S1	176	-209.3	270.9	3.7	25.9	47.1	47.1
	S3	176	-119.4	181.9	7.2	24.4	41.0	41.5
	AS	176	-209.3	243.9	1.8	27.8	47.8	47.6
	CA	176	-290.7	270.2	5.9	27.3	49.1	49.3
	ME	174	-256.3	249.9	-2.7	24.8	47.3	47.2

Table 11 Percentage of points lying in different accuracy/precision intervals (cf. Table 6). The model with the highest percentage in intervals In1, In2, In3 and the lowest percentage in interval In4 is the most preferred

		S1 (%)	S3 (%)	AS (%)	CA (%)	ME (%)
In1	Overall	44	45	29	43	54
	$H \leq 500$ m	48	48	31	47	58
	$500 \text{ m} < H \leq 1500$ m	27	28	23	29	37
	$H > 1500$ m	24	24	17	15	27
	Overall	80	81	67	80	85
In2	$H \leq 500$ m	84	86	70	84	89
	$500 \text{ m} < H \leq 1500$ m	65	63	50	63	72
	$H > 1500$ m	46	47	37	37	48
	Overall	91	90	85	90	92
	$H \leq 500$ m	94	94	89	94	95
In3	$500 \text{ m} < H \leq 1500$ m	80	80	71	78	81
	$H > 1500$ m	57	60	51	56	60
	Overall	9	9	15	10	8
	$H \leq 500$ m	6	6	11	6	5
	$500 \text{ m} < H \leq 1500$ m	20	22	29	22	18
In4	$H > 1500$ m	43	40	49	44	40

Fig. 9b-d, where the differences become more scattered for the higher-elevation intervals. Figure 9a shows that all the differences are near-normally [Gaussian] distributed, hence justifying our use of descriptive statistics throughout this manuscript.

With the data available to us, focussing on the < 500 m band in Table 10 shows that, despite the presence of large maximum and minimum differences, MERIT3'' is more reliable, while Cartodem is less preferred among all the compared DEM/DSMs. The principal metrics used from Table 10 to make this inference are the MAE and RMSE. From the percentages in Table 11, no DEMs/DSMs have more than 90% points falling in the In1 or In2 intervals,

which are defined based on the claimed DEM/DSM accuracies/precisions (cf. Table 6). In the < 500 m range only, however, all the DEMs/DSMs (except ASTER) have more than 90% of the points in the In3 interval. ASTER provides the smallest percentage in the interval In1 and the highest in In4, indicating it to be the least preferred DSM with respect to the ground-truth data in India. Thus, for the $1'' \times 1''$ DSMs, SRTM1'' and Cartodem appear more reliable as compared to ASTER over India. The MERIT3'' DEM has the highest percentage of points in intervals In1, In2 and In3 and the lowest in In4, indicating to be most preferred among all the five models compared to the ground-truth benchmarks in India.

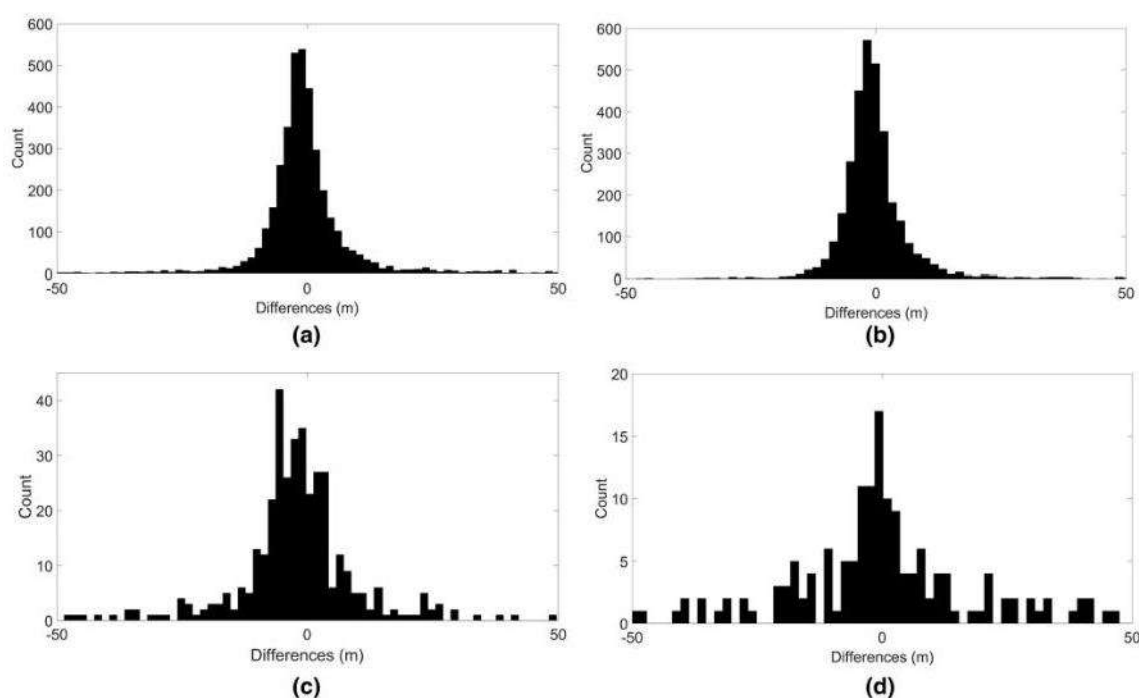


Fig. 9 Distributions of differences among benchmarks and the MERIT3'' DEM for different intervals. **a** All 3842 data points, **b** 3273 points below 500 m, **c** 395 points between 500 and 1500 m, and **d** 174 points above 1500 m. Note the different y-axis scales

Conclusions

In this study, four freely available DSMs (SRTM1'', SRTM3'', ASTER1'' and Cartodem1'') along with the MERIT DEM developed by removing multiple error components from SRTM3 v2.1 are investigated based on a model-to-model comparison over the whole of India and a "validation" using ground-truth benchmark height data over some regions of India. Since India has varying topography (land heights range from -2 m to $+8586$ m), the heights were divided into three ranges, namely $H \leq 500$ m, $500 \text{ m} < H \leq 1500$ m and $H > 1500$ m. The percentage of points lying in the claimed accuracy/precision limits for different DEMs/DSMs were also analysed.

The model-to-model comparison among DSMs shows that SRTM1'', SRTM3'' and Cartodem are congruous with their claimed accuracy/precision, but only for heights less than 500 m. Cartodem has the least discrepancies with SRTM1'' compared to ASTER and SRTM3'' in all three height ranges tested. There are artefacts between Cartodem and other DSMs due to time-varying heights in lakes and open-pit mining sites. Visual representation of the DSM differences confirmed that stripe effects are present in SRTM, ASTER and Cartodem over India, which appear to have been eliminated/reduced following the procedures

involved in the production of MERIT3'' (Yamazaki et al. 2017).

The validation with the only ground-truth data available to us shows that no DEMs/DSMs satisfy their claimed accuracies (intervals In1 and In2 in Table 6) in any height range. However, for elevations less than 500 m only, DEMs/DSMs (except ASTER) satisfy interval In3, but which is still beyond their claimed accuracies/precisions. The MERIT3'' DEM is observed to be more reliable compared to the other DEMs/DSMs based on overall, range-wise and accuracy-wise analyses. However, this needs to be qualified by our use of only canopy heights to convert the ground-truth data to DSM-compatible heights.

Acknowledgements The Bureau Gravimetric International, Survey of India and National Geophysical Research Institute are thanked for providing the ground-truth data. We would like to thank Professor Yamazaki (University of Tokyo) for granting us access to the MERIT3'' DEM. We also thank the providers of DSMs for making them so freely available. Finally, thanks go to the two anonymous reviewers and editor for their prompt and constructive critiques on an earlier version of this manuscript.

Compliance with Ethical Standards

Conflicts of interest The authors declare that they have no known conflicts of interest.

References

- Ahmed, S. A., Chandrashekarappa, K. N., Raj, S. K., Nischitha, V., & Kavitha, G. (2010). Evaluation of morphometric parameters derived from ASTER and SRTM DEM—a study on Bandihole sub-watershed basin in Karnataka. *Journal of the Indian Society of Remote Sensing*, 38(2), 227–238. <https://doi.org/10.1007/s12524-010-0029-3>.
- Athmania, D., & Achour, H. (2014). External validation of the ASTER GDEM2, GMTED2010 and CGIAR-CSI- SRTM v4.1 free access Digital Elevation Models (DEMs) in Tunisia and Algeria. *Remote Sensing*, 6(5), 4600–4620. <https://doi.org/10.3390/rs6054600>.
- Banerjee, B., & Gupta, S. P. D. (1977). Gravitational attraction of a rectangular parallelepiped. *Geophysics*, 42(5), 1053–1055. <https://doi.org/10.1190/1.1440766>.
- Barnes, R., Lehman, C., & Mulla, D. (2014). An efficient assignment of drainage direction over flat surfaces in raster digital elevation models. *Computers & Geosciences*, 62, 128–135. <https://doi.org/10.1016/j.cageo.2013.01.009>.
- Bera, A. K., Singh, V., Bankar, N., Salunkhe, S. S., & Sharma, J. R. (2014). Watershed delineation in flat terrain of Thar desert region in North West India—A semi automated approach using DEM. *Journal of the Indian Society of Remote Sensing*, 42(1), 187–199. <https://doi.org/10.1007/s12524-013-0308-x>.
- Berthier, E., Arnaud, Y., Kumar, R., Ahmad, S., Wagnon, P., & Chevallier, P. (2007). Remote sensing estimates of glacier mass balances in the Himachal Pradesh (Western Himalaya, India). *Remote Sensing of Environment*, 108(3), 327–338. <https://doi.org/10.1016/j.rse.2006.11.017>.
- Bothale, R. V., & Pandey, B. (2013). Evaluation and comparison of multi resolution DEM derived through Cartosat-1 stereo pair—a case study of Damanganga basin. *Journal of the Indian Society of Remote Sensing*, 41(3), 497–507. <https://doi.org/10.1007/s12524-012-0243-2>.
- Cavazzi, S., Corstanje, R., Mayr, T., Hannam, J., & Fealy, R. (2013). Are fine resolution digital elevation models always the best choice in digital soil mapping? *Geoderma*, 195–196, 111–121. <https://doi.org/10.1016/j.geoderma.2012.11.020>.
- Chirico, P. G., Malpeli, K. C., & Trimble, S. M. (2012). Accuracy evaluation of an ASTER-derived global digital elevation model (GDEM) version 1 and version 2 for two sites in Western Africa. *GIScience & Remote Sensing*, 49(6), 775–801. <https://doi.org/10.2747/1548-1603.49.6.775>.
- Crippen, R., Buckley, S., Agram, P., Belz, E., Gurrola, E., Hensley, S., et al. (2016). NASADEM global elevation model: methods and progress. *ISPRS - International Archives of the Photogrammetry, Remote Sensing and Spatial Information Sciences*, XLI-B4, 125–128. <https://doi.org/10.5194/isprsarchives-XLI-B4-125-2016>.
- Das, S., Kar, N. S., & Bandyopadhyay, S. (2015). Glacial lake outburst flood at Kedarnath, Indian Himalaya: a study using digital elevation models and satellite images. *Natural Hazards*, 77(2), 769–786. <https://doi.org/10.1007/s11069-015-1629-6>.
- Das, S., Pardeshi, S. D., Kulkarni, P. P., & Doke, A. (2018). Extraction of lineaments from different azimuth angles using geospatial techniques: a case study of Pravara basin, Maharashtra. *India. Arabian Journal of Geosciences*, 11(8), 160. <https://doi.org/10.1007/s12517-018-3522-6>.
- Demirkesen, A. C. (2012). Multi-risk interpretation of natural hazards for settlements of the Hatay province in the east Mediterranean region, Turkey using SRTM DEM. *Environmental Earth Sciences*, 65(6), 1895–1907. <https://doi.org/10.1007/s12665-011-1171-0>.
- Denker, H. (2005). Evaluation of SRTM3 and GTOPO30 terrain data in Germany. In C. Jekeli, L. Bastos, & J. Fernandes (Eds.), *Gravity, geoid and space missions. IAG international symposium*. Heidelberg: Springer.
- Dobos, E., & Hengl, T. (2009). Soil mapping applications. In T. Hengl & H. I. Reuter (Eds.), *Geomorphometry: Concepts, software, applications, developments in soil science*. Amsterdam: Elsevier.
- Elkhrachy, I. (2018). Vertical accuracy assessment for SRTM and ASTER digital elevation models: A case study of Najran city, Saudi Arabia. *Ain Shams Engineering Journal*, 9(4), 1807–1817. <https://doi.org/10.1016/j.asej.2017.01.007>.
- Farr, T. G., Rosen, P. A., Caro, E., Crippen, R., Duren, R., Hensley, S., et al. (2007). The shuttle radar topography mission. *Reviews of Geophysics*, 45(2), RG2004. <https://doi.org/10.1029/2005RG000183>.
- Forsberg, R., 1984. Study of terrain reductions, density anomalies and geophysical inversion methods in gravity field modelling. Report 355, Department of geodetic science and surveying, The Ohio State University, Columbus, USA.
- Gallant, J. (2011). Adaptive smoothing for noise DEMs. In T. Hengl (Ed.), *Proceedings of Geomorphometry*. California: Redlands.
- Gallant, J. C., & Read, A. (2009). Enhancing the SRTM data for Australia. *Proceedings of Geomorphometry*, 31, 149–154.
- Gayen, S., Bhunia, S. G., & Shit, P. V. (2013). Morphometric analysis of Kangshabati-Darakeswar interfluvial area in West Bengal, India using ASTER DEM and GIS techniques. *Journal of Geology & Geosciences*, 02(04), 1000133. <https://doi.org/10.4172/2329-6755.1000133>.
- Gesch, D. B. (2012). Global digital elevation model development from satellite remote-sensing data. In X. Yang & Li, J. (Eds.), *Advances in mapping from remote sensor imagery: Techniques and applications*. Boca Raton, Florida: CRC Press.
- Gesch, D.B., Oimoen, M.J., Evans, G.A., 2014. Accuracy assessment of the U.S. geological survey national elevation dataset, and comparison with other large-area elevation datasets-SRTM and ASTER. Open file report 2014–1008. U.S. Geological Survey, Reston, Virginia.
- Gesch, D., Oimoen, M., Zhang, Z., Meyer, D., & Danielson, J. (2012). Validation of the aster global digital elevation model version 2 over the conterminous United States. *International Archives of the Photogrammetry, Remote Sensing and Spatial Information Sciences*, XXXIX-B4, 281–286. <https://doi.org/10.5194/isprsarchives-XXXIX-B4-281-2012>.
- Gopinath, G., Swetha, T. V., & Ashitha, M. K. (2014). Automated extraction of watershed boundary and drainage network from SRTM and comparison with survey of India toposheet. *Arabian Journal of Geosciences*. <https://doi.org/10.1007/s12517-013-0919-0>.
- Gruber, S., Huggel, C., & Pike, R. (2009). Modelling mass movements and landslide susceptibility. In T. Hengl & H. I. Reuter (Eds.), *Geomorphometry: concepts, software, applications*. Amsterdam: Developments in soil science Elsevier.
- Hawker, L., Neal, J., & Bates, P. (2019). Accuracy assessment of the TanDEM-X 90 digital elevation model for selected floodplain sites. *Remote Sensing of Environment*, 232, 111319. <https://doi.org/10.1016/j.rse.2019.111319>.
- Hayakawa, Y. S., Oguchi, T., & Lin, Z. (2008). Comparison of new and existing global digital elevation models: ASTER G-DEM and SRTM-3. *Geophysical Research Letters*, 35(17), L17404. <https://doi.org/10.1029/2008GL035036>.
- Hilton, R. D., Featherstone, W. E., Berry, P. A. M., Johnston, C. P. D., & Kirby, J. F. (2003). Comparison of digital elevation models over Australia and external validation using ERS-1 satellite radar altimetry. *Australian Journal of Earth Sciences*, 50, 157–168. <https://doi.org/10.1046/j.1440-0952.2003.00982.x>.

- Hirt, C. (2014). Digital Terrain Models. In E. Grafarend (Ed.), *Encyclopedia of Geodesy* (pp. 1–6). Berlin: Springer. https://doi.org/10.1007/978-3-319-02370-0_31-1.
- Hirt, C. (2018). Artefact detection in global digital elevation models (DEMs): The maximum slope approach and its application for complete screening of the SRTM v4.1 and MERIT DEMs. *Remote Sensing of Environment*, 207, 27–41. <https://doi.org/10.1016/j.rse.2017.12.037>.
- Hirt, C., Filmer, M. S., & Featherstone, W. E. (2010). Comparison and validation of the recent freely available ASTER-GDEM ver1, SRTM ver4.1 and GEODATA DEM-9S ver3 digital elevation models over Australia. *Australian Journal of Earth Sciences*, 57(3), 337–347. <https://doi.org/10.1080/08120091003677553>.
- Ioannidis, C., Xinogalas, E., & Soile, S. (2014). Assessment of the global digital elevation models ASTER and SRTM in Greece. *Survey Review*, 46(338), 342–354. <https://doi.org/10.1179/1752270614Y.0000000114>.
- Jafarzadegan, K., & Merwade, V. (2017). A DEM-based approach for large-scale floodplain mapping in ungauged watersheds. *Journal of Hydrology*, 550, 650–662. <https://doi.org/10.1016/j.jhydrol.2017.04.053>.
- Jing, C., Shortridge, A., Lin, S., & Wu, J. (2014). Comparison and validation of SRTM and ASTER GDEM for a subtropical landscape in Southeastern China. *International Journal of Digital Earth*, 7(12), 969–992. <https://doi.org/10.1080/17538947.2013.807307>.
- Krishnan, S., Sajikumar, N., & Sumam, K. S. (2016). DEM generation using Cartosat-1 stereo data and its comparison with publicly available DEM. *Procedia Technology*, 24, 295–302. <https://doi.org/10.1016/j.protcy.2016.05.039>.
- Kumar, A., Chingkhei, R. K., & Dolendro, T. (2007). Tsunami damage assessment: a case study in Car Nicobar Island. *India. International Journal of Remote Sensing*, 28(13–14), 2937–2959. <https://doi.org/10.1080/01431160601091852>.
- Kumar, S., & Gupta, S. (2016). Geospatial approach in mapping soil erodibility using CartoDEM – a case study in hilly watershed of lower Himalayan range. *Journal of Earth System Science*, 125(7), 1463–1472. <https://doi.org/10.1007/s12040-016-0738-2>.
- Lemoine, F. G., Kenyon, S. C., Factor, J. K., Trimmer, R. G., Pavlis, N. K., Chinn, D. S., et al. (1998). *The development of the joint NASA GSFC and the National Imagery and Mapping Agency (NIMA) Geopotential Model EGM96, NASA/TP-1998-206861*. Greenbelt: National Aeronautics and Space Administration.
- Li, C., Wang, Y., Ye, C., Wei, W., Zheng, B., & Xu, B. (2019). A proposed delineation method for lake buffer zones in watersheds dominated by non-point source pollution. *Science of The Total Environment*, 660, 32–39. <https://doi.org/10.1016/j.scitotenv.2018.12.468>.
- Li, P., Shi, C., Li, Z., Muller, J.-P., Drummond, J., Li, X., et al. (2013). Evaluation of ASTER GDEM using GPS benchmarks and SRTM in China. *International Journal of Remote Sensing*, 34(5), 1744–1771. <https://doi.org/10.1080/01431161.2012.726752>.
- Long, N. Q., Goyal, R., Bui, L. K., & Bui, X. N. (2020). Assessment of Global Digital Height Models over Quang Ninh Province, Vietnam. In X. N. Bui, C. Lee, & C. Drebenstedt (Eds.), *Proceedings of the International Conference on Innovations for Sustainable and Responsible Mining*. Cham: Lecture Notes in Civil Engineering, Springer.
- Meyer, D., Tachikawa, T., Kaku, M., Iwasaki, A., Gesch, D., Oimoen, M., Zhang, Z., Danielson, J., Krieger, T., Curtis, B., Haase, J., Abrams, M., Crippen, R., Carabajal, C., 2011. ASTER global digital elevation model version 2- summary of validation results. Retrieved from https://ssl.jspacesystems.or.jp/ersdac/GDEM/ver2Validation/Summary_GDEM2_validation_report_final.pdf.
- Mishra, U. N., 2017. A comparative evaluation of methods for development of Indian geoid model. PhD Thesis. Indian Institute of Technology Roorkee, India.
- Mukul, M., Srivastava, V., Jade, S., & Mukul, M. (2017). Uncertainties in the shuttle radar topography mission (SRTM) heights: insights from the Indian Himalaya and Peninsula. *Scientific Reports*, 7(1), 41672. <https://doi.org/10.1038/srep41672>.
- Muralikrishnan, S., Pillai, A., Narender, B., Reddy, S., Venkataraman, V. R., & Dadhwal, V. K. (2013). Validation of Indian national DEM from Cartosat-1 data. *Journal of the Indian Society of Remote Sensing*, 41(1), 1–13. <https://doi.org/10.1007/s12524-012-0212-9>.
- Nardi, F., Annis, A., Di Baldassarre, G., Vivoni, E. R., & Grimaldi, S. (2019). GFPLAIN250m, a global high-resolution dataset of Earth's floodplains. *Scientific Data*, 6, 180309. <https://doi.org/10.1038/sdata.2018.309>.
- Nikolakopoulos, K. G., Kamaratakis, E. K., & Chrysoulakis, N. (2006). SRTM vs ASTER elevation products. Comparison for two regions in Crete, Greece. *International Journal of Remote Sensing*, 27(21), 4819–4838. <https://doi.org/10.1080/01431160600835853>.
- NRSA, 2006. CARTOSAT-1 data user's handbook. National Remote Sensing Agency, India, Technical Report CARTOSAT-1/NRSA/NDC/HB-09/06.
- O'Loughlin, F. E., Paiva, R. C. D., Durand, M., Alsdorf, D. E., & Bates, P. D. (2016). A multi-sensor approach towards a global vegetation corrected SRTM DEM product. *Remote Sensing of Environment*, 182, 49–59. <https://doi.org/10.1016/j.rse.2016.04.018>.
- Park, S., Oh, C., Jeon, S., Jung, H., & Choi, C. (2011). Soil erosion risk in Korean watersheds, assessed using the revised universal soil loss equation. *Journal of Hydrology*, 399(3–4), 263–273. <https://doi.org/10.1016/j.jhydrol.2011.01.004>.
- Patro, S., Chatterjee, C., Singh, R., & Raghuvanshi, N. S. (2009). Hydrodynamic modelling of a large flood-prone river system in India with limited data. *Hydrological Processes*, 23(19), 2774–2791. <https://doi.org/10.1002/hyp.7375>.
- Pavlis, N. K., Holmes, S. A., Kenyon, S. C., & Factor, J. K. (2012). The development and evaluation of the earth gravitational model 2008 (EGM2008). *Journal of Geophysical Research: Solid Earth*, 118(5), 2633–2633. <https://doi.org/10.1002/jgrb.50167>.
- Pavlis, N. K., Holmes, S. A., Kenyon, S. C., & Factor, J. K. (2013). Correction to “the development and evaluation of the Earth Gravitational Model 2008 (EGM2008).” *Journal of Geophysical Research: Solid Earth*, 117(B4), B04406. <https://doi.org/10.1029/2011JB008916>.
- Purinton, B., & Bookhagen, B. (2017). Validation of digital elevation models (DEMs) and comparison of geomorphic metrics on the southern Central Andean Plateau. *Earth Surface Dynamics*, 5(2), 211–237. <https://doi.org/10.5194/esurf-5-211-2017>.
- Racoviteanu, A. E., Manley, W. F., Arnaud, Y., & Williams, M. W. (2007). Evaluating digital elevation models for glaciologic applications: an example from Nevado Coropuna. *Peruvian Andes. Global and Planetary Change*, 59(1–4), 110–125. <https://doi.org/10.1016/j.gloplacha.2006.11.036>.
- Ramakrishnan, D., Bandyopadhyay, A., & Kusuma, K. N. (2009). SCS-CN and GIS-based approach for identifying potential water harvesting sites in the Kali Watershed, Mahi River Basin. *India. Journal of Earth System Science*, 118(4), 355–368. <https://doi.org/10.1007/s12040-009-0034-5>.
- Rao, S.P., Murthy, K.S., Kumar, P.A., 2014. Evaluation of Indian national DEM (Version-2) from Cartosat-1 data. National Remote Sensing Center, Indian Space Research Organisation, Hyderabad India, Technical Report NRSC-SDAPSA-Dec 2014-TR-697.

- Rawat, K. S., Singh, S. K., Singh, M. I., & Garg, B. L. (2019). Comparative evaluation of vertical accuracy of elevated points with ground control points from ASTERDEM and SRTMDEM with respect to CARTOSAT-IDEM. *Remote Sensing Applications: Society and Environment*, 13, 289–297. <https://doi.org/10.1016/j.rsase.2018.11.005>.
- Rexer, M., & Hirt, C. (2014). Comparison of free high resolution digital elevation data sets (ASTER GDEM2, SRTM v2.1/v4.1) and validation against accurate heights from the Australian National Gravity Database. *Australian Journal of Earth Sciences*, 61(2), 213–226. <https://doi.org/10.1080/08120099.2014.884983>.
- Rodriguez, E., Morris, C.S., Belz, J.E., Chapin, E.C., Martin, J.M., Daffer, W., Hensley, S., 2005. An assessment of the SRTM topographic products. Jet Propulsion Laboratory, Pasadena, Technical Report JPL D-31639.
- Selvan, M. T., Ahmad, S., & Rashid, S. M. (2011). Analysis of the geomorphometric parameters in high altitude glacierised terrain using SRTM DEM data in Central Himalaya, India. *ARPN Journal of Science and Technology*, 1(1), 22–27.
- Simard, M., Pinto, N., Fisher, J. B., & Baccini, A. (2011). Mapping forest canopy height globally with spaceborne lidar. *Journal of Geophysical Research*, 116(G4), G04021. <https://doi.org/10.1029/2011JG001708>.
- Sreedevi, P. D., Owais, S., Khan, H. H., & Ahmed, S. (2009). Morphometric analysis of a watershed of south India using SRTM data and GIS. *Journal of the Geological Society of India*, 73(4), 543–552. <https://doi.org/10.1007/s12594-009-0038-4>.
- Srivastava, V.K., Mondal, K., 2012. Evaluation of Digital Elevation Models (DEMs) generated from ASTER and SRTM data: a case study of flat alluvium terrain of Bakreshwar-Dubrajpur (W.B.), India. In: Proceedings of 1st international conference on recent advances in information technology, Dhanbad, India.
- Suwandana, E., Kawamura, K., Sakuno, Y., Kustiyanto, E., & Raharjo, B. (2012). Evaluation of ASTER GDEM2 in comparison with GDEM1, SRTM DEM and topographic-map-derived DEM using inundation area analysis and RTK-DGPS data. *Remote Sensing*, 4(8), 2419–2431. <https://doi.org/10.3390/rs4082419>.
- Tarekegn, T. H., & Sayama, T. (2013). Correction of SRTM dem artefacts by fourier transform for flood inundation modeling. *Journal of Japan Society of Civil Engineers, Ser BI Hydraulic Engineering*, 69(4), 193–198. https://doi.org/10.2208/jscejhe.69.1_193.
- Thomas, J., Prasannakumar, V., & Vineetha, P. (2015). Suitability of spaceborne digital elevation models of different scales in topographic analysis: an example from Kerala, India. *Environmental Earth Sciences*, 73(3), 1245–1263. <https://doi.org/10.1007/s12665-014-3478-0>.
- Truhetz, H., 2010. High resolution wind field modelling over complex topography analysis and future scenarios. PhD Thesis, Wegener Center for Climate and Global Change, University of Graz, Graz, Austria.
- Varga, M., & Bašić, T. (2015). Accuracy validation and comparison of global digital elevation models over Croatia. *International Journal of Remote Sensing*, 36(1), 170–189. <https://doi.org/10.1080/01431161.2014.994720>.
- Yadav, S., Indu, J., 2016. Estimation of vertical accuracy of Digital Elevation Models over complex terrains of Indian subcontinent. In: 2016 IEEE International Geoscience and Remote Sensing Symposium, pp. 6036–6039. <https://doi.org/10.1109/IGARSS.2016.7730577>.
- Yamazaki, D., Ikeshima, D., Tawatari, R., Yamaguchi, T., O'Loughlin, F., Neal, J. C., et al. (2017). A high-accuracy map of global terrain elevations. *Geophysical Research Letters*, 44(11), 5844–5853. <https://doi.org/10.1002/2017GL072874>.
- Yang, M., Hirt, C., Rexer, M., Pail, R., & Yamazaki, D. (2019). The tree-canopy effect in gravity forward modelling. *Geophysical Journal International*, 219(1), 271–289. <https://doi.org/10.1093/gji/ggz264>.
- Zhang, K., Gann, D., Ross, M., Robertson, Q., Sarmiento, J., Santana, S., et al. (2019). Accuracy assessment of ASTER, SRTM, ALOS, and TDX DEMs for Hispaniola and implications for mapping vulnerability to coastal flooding. *Remote Sensing of Environment*, 225, 290–306. <https://doi.org/10.1016/j.rse.2019.02.028>.
- Zhao, Y., Wu, P., Li, J., Lin, Q., & Lu, Y. (2019). A new algorithm for the automatic extraction of valley floor width. *Geomorphology*, 335, 37–47. <https://doi.org/10.1016/j.geomorph.2019.03.015>.

Publisher's Note Springer Nature remains neutral with regard to jurisdictional claims in published maps and institutional affiliations.

C.4: Paper on Auvergne quasigeoid.

Empirical comparison between stochastic and deterministic modifiers over the French Auvergne geoid computation test-bed

R. Goyal *^{1,2}, J. Ågren ^{3,4}, W.E. Featherstone ^{2,1}, L.E. Sjöberg ⁵,
O. Dikshit ¹ and N. Balasubramanian¹

Since 2006, several different groups have computed geoid and/or quasigeoid (quasi/geoid) models for the Auvergne test area in central France using various approaches. In this contribution, we compute and compare quasigeoid models for Auvergne using Curtin University of Technology's and the Swedish Royal Institute of Technology's approaches. These approaches differ in many ways, such as their treatment of the input data, choice of type of spherical harmonic model (combined or satellite-only), form and sequence of correction terms applied, and different modified Stokes's kernels (deterministic or stochastic). We have also compared our results with most of the previously reported studies over Auvergne in order to seek any improvements with respect to time [exceptions are when different subsets of data have been used]. All studies considered here compare the computed quasigeoid models with the same 75 GPS-levelling heights over Auvergne. The standard deviation for almost all of the computations (without any fitting) is of the order of 30–40 mm, so there is not yet any clear indication whether any approach is necessarily better than any other nor improving over time. We also recommend more standardisation on the presentation of quasi/geoid comparisons with GPS-levelling data so that results from different approaches over the same areas can be compared more objectively.

Keywords: Regional quasigeoid computation, Auvergne (France), technique comparison

1. Introduction

It is now over 170 years since George Gabriel Stokes published his seminal formula for geoid determination from gravity anomalies (Stokes 1849); over 55 years since the English translation of Mikhail Sergeevich Molodensky's book was published including the formula for quasigeoid determination from gravity anomalies (Molodensky *et al.* 1962); and over 50 years since Martin Hotine's monograph was published including the formula for geoid determination from gravity disturbances (Hotine 1969).

Despite this long-elapsed time, determination of a cm-level-precise geoid and/or quasigeoid (quasi/geoid)

remains an ongoing quest and, hence, comparison studies among the different computational techniques are still required. Arguably, different approaches are necessary in different parts of the world due to, for instance, peculiarities of the data holdings. However, there appears to be some slight subjectivity in the selection of the computation strategy.

As just one example, the third author of this article admits preference for his deterministically modified kernel (Featherstone *et al.* 1998) for the computation of Australian and New Zealand national gravimetric quasigeoid models (Featherstone *et al.* 2001, 2011, 2018a; Amos and Featherstone 2009; Claessens *et al.* 2011). In his defence though, he has compared his kernel with other deterministic modifiers and some simplistic stochastic modifiers (e.g. Featherstone *et al.* 2004), hence the inclusion of the more sophisticated stochastic modifier embedded in the Swedish Royal Institute of Technology's (KTH) approach in the comparisons presented herein.

In attempts to reach some sort of consensus on quasi/geoid computation, two principal approaches have been endorsed historically by the International Association of Geodesy (IAG): synthetic and empirical. The creation

¹Department of Civil Engineering, Indian Institute of Technology Kanpur, Kanpur 208016, India

²School of Earth and Planetary Sciences, Curtin University of Technology, GPO Box U1987, Perth, WA 6845, Australia

³Department of Computer and Geospatial Sciences, University of Gävle, Gävle SE-80176, Sweden

⁴Geodetic Research Division, Lantmäteriet (Swedish Mapping, Cadastre and Registry Authority), Gävle SE-80182, Sweden

⁵Division of Geodesy and Satellite Positioning, Royal Institute of Technology (KTH), Stockholm SE-10044, Sweden

*Corresponding author, email rupeshg@iitk.ac.in Department of Civil Engineering, Indian Institute of Technology Kanpur, Kanpur 208016, India

and use of synthetic gravity fields further comprise two variants. The first is to assume spherical harmonic coefficients of a high-degree Earth Gravitational Model (EGM) are error-free and use them to generate [assumed] self-consistent sets of gravity anomalies and quasi/geoid heights (e.g. Tziavos 1996; Novák *et al.* 2001; Featherstone 2002). The second synthetic approach is to use forward modelling of gravity anomalies and quasi/geoid heights from digital elevation models (DEMs) (e.g. Haagmans 2000; Kuhn and Featherstone 2003a, 2003b, 2005; Ågren 2004; Baran *et al.* 2006; Fellner *et al.* 2012; Vaniček *et al.* 2013).

Empirical study areas have been proposed in regions with reasonably good coverage and free availability of gravity, topographic and GPS-levelling data, most notably Auvergne in central France (Duquenne 2006; Valtý *et al.* 2012) and Colorado in the U.S.A. (e.g. Claessens and Filmer 2020; Liu *et al.* 2020); Australia has been suggested (Featherstone *et al.* 2018b) but not yet used by others. In 2006, the French Institut Géographique National (IGN) provided a dataset of ~240,000 land gravity observations and 75 GPS-levelling points over a region surrounding Auvergne in central France along with two DEMs (Duquenne 2006). These two DEMs were later replaced by the SRTM 3" DEM. The Auvergne point gravity observation data are freely available from the Bureau Gravimétrique International (BGI).

Since 2006, several published studies have presented quasi/geoid computations for Auvergne using several different techniques, which are summarised in Appendix A. We emphasise that the amount of information published on the agreements with the 75 GPS-levelling data is rather inconsistent and we discuss this further in Section 3. In particular, we observe that the reporting of descriptive statistics of the comparison with GPS-levelling data can be inconsistent, which arguably prevents an objective comparison among the different quasi/geoid computation techniques. As such, we present in the Electronic Supplementary Material (ESM) a spreadsheet that others may wish to adopt for a more standardised comparison.

Curtin University of Technology's (CUT) approach to compute the quasigeoid has not been used before for the Auvergne test-bed. In this study, therefore, we compare the CUT and KTH's techniques for quasigeoid modelling so as to add another 'data point' to the Auvergne test-bed with a view to determining how well or not the CUT technique performs with respect to some other methods when using the same input and test data. We choose only these two approaches because they are so substantially different to one another, particularly regarding the use of deterministic versus stochastic modifications to Stokes's formula.

2. Comparing and contrasting the CUT and KTH approaches

Both the CUT and KTH approaches have evolved over time, so we only report on their current status, but with some historical context. We then describe their particular application to the Auvergne test-bed in this study.

2.1. The CUT approach

The CUT approach has evolved over around 25 years with particular focus on computing Australian models,

though it has also been used in New Zealand, Colorado in the U.S.A. and the British mainland (the latter is unpublished). Probably the most Australia-specific aspect is the treatment of the terrestrial gravity data. Usually, refined Bouguer or isostatic gravity anomalies are recommended for gridding as they are smoother and thus more suited to interpolation. In Australia, however, the mean elevation is only ~330 m (max 2228 m) so topographic/isostatic corrections are small and planar simple Bouguer anomalies appear sufficient for interpolation and gridding (Goos *et al.* 2003; Zhang and Featherstone 2004). There is a side-benefit to this approach because it allows for the so-called reconstruction of Faye anomalies on the topography (Featherstone and Kirby 2000).

In short, point planar simple Bouguer anomalies [including the atmospheric correction from Moritz (1980, 2000)] are computed using a constant topographic bulk density of $2,670 \text{ kg m}^{-3}$. They are then interpolated to the $1'' \times 1''$ resolution of the Australian DEM using the tensioned spline algorithm (*surface* with $T=0.25$) embedded in the Generic Mapping Tools (GMT; Wessel *et al.* 2013). Molodensky free air anomalies are 'reconstructed' on the topography by applying a reverse (negative sign) planar simple Bouguer correction with the height of each DEM element. Faye gravity anomalies are then computed by adding the planar terrain correction from the same DEM as an approximation of the Molodensky G_1 term, recently including error propagation (McCubbine *et al.* 2017, 2019). These are then block-averaged (GMT routine *blockmean*) to determine surface-mean Faye gravity anomalies as approximations of Molodensky anomalies for subsequent quasigeoid computation.

The CUT approach has consistently used the highest-available degree of EGM, which is generally a combined model that has merged terrestrial and satellite-only Stokes coefficients (e.g. Pavlis *et al.* 2012, 2013). This is in contrast to the KTH approach that uses a satellite-only EGM so as to avoid correlations in the terrestrial data when used twice (e.g. Vaniček and Sjöberg 1991). The [implicit] rationale for the CUT approach is that, while being fully subject to the undesirable correlation of largely the same terrestrial data being used (most Australian gravity data are in the public domain and have been for decades), the use of a high-degree EGM makes the residual quasigeoid smaller in magnitude and thus less subject to approximation errors in the residual quasigeoid computation. A recent refinement to the CUT treatment of the EGM is to compute ellipsoidal area-mean gravity anomalies on the topography (Featherstone *et al.* 2018a, Section 2.3.2).

The CUT approach to computing the residual quasigeoid from the residual area-mean gravity anomalies is based on the 1D-FFT (Haagmans *et al.* 1993) using F77 code that originated from the University of Calgary, Canada, but which has been adapted to include deterministically modified kernels (Featherstone and Sideris 1998; Featherstone 2003). It also now uses Gauss-Legendre quadrature to better-determine area-means for the deterministically modified kernels in the discretised numerical integration (Hirt *et al.* 2011). The Australian models use the deterministic Featherstone *et al.* (1998) kernel that is a combination of the Vaniček and Kleusberg (1987) and Meissl (1971) modifiers. This

combined modifier aims to simultaneously reduce the truncation error and improve the rate of convergence to zero of the series expansion of the truncation error.

The integer degrees of kernel modification and integration cap radius are chosen empirically through comparisons with GPS-levelling after parameter sweeps. The ellipsoidal correction is handled by using the geocentric radius to the surface of the GRS80 ellipsoid in Stokes's integral along each parallel of latitude of the computation grid in the 1D-FFT (Claessens 2006, Chapter 6).

2.2. The KTH approach

The stochastically modified kernel used in the KTH method comprises a least-squares combination of satellite and terrestrial data (Sjöberg 1981). Since then, the KTH method has been continuously developed and refined (e.g. Sjöberg 1984, 1991, 2003c; Ågren 2004 and the references therein). The KTH method follows remove-interpolate-restore-compute strategy for geoid computations, which contrasts with CUT method that follows an interpolate-remove-compute-restore strategy.

The primary uniqueness of the KTH method lies in the stochastic modification of Stokes's kernel and additive corrections to the gravity data. Unlike other methods, the direct and indirect effects needed to make the observations accordant with the geodetic boundary value problem are added as separate combined corrections to the approximate geoid estimates obtained using the Stokes integration with un-reduced gridded terrestrial gravity data.

The KTH method has been used to compute the Swedish national quasigeoid (Ågren *et al.* 2009b), the Nordic Geodetic Commission 2015 quasigeoid (Ågren *et al.* 2016). The KTH approach has received much wider geographical application than the CUT approach, with quasi/geoid models computed for the Baltic countries (Ellmann 2004), Iran (Kiamehr 2006), Tanzania (Ulotu 2009), Greece (Daras *et al.* 2010), Kazakhstan (Inerbayeva 2010), Sudan (Abdalla and Fairhead 2011), New Zealand (Abdalla and Tenzer 2011), central Turkey (Abbak *et al.* 2012), Moldova (Danila 2012), Saudia Arabia (Abdalla and Mogren 2015), Uganda (Ssendendo 2015), Poland (Kuczynska-Siehien *et al.* 2016), peninsular Malaysia (Pa'suya *et al.* 2019), Estonia (Ellmann *et al.* 2019) and Jilin province in China (Wu *et al.* 2020).

In the KTH treatment of the terrestrial gravity data, point free-air gravity anomalies are computed from the observed gravity values on the Earth's surface. These are then reduced point-wise by subtracting the long wavelength gravity anomalies from synthesising a satellite-only EGM, the high-frequency part of the topography is removed using Residual Terrain Modelling (RTM; Forsberg 1985), and the atmospheric effect applied to obtain residual point free-air gravity anomalies. These are then interpolated using Least Squares Collocation (LSC), in the *geogrid.f* module of the GRAVSOF package (Tscherning *et al.* 1992), to the resolution of the desired model to obtain a regular grid of residual gravity anomalies. Since the KTH method uses un-reduced gravity anomalies for gridding, the contributions of the EGM, RTM and atmospheric effect are all computed at the nodes of the grid and subsequently restored to the interpolated point-wise residual gravity anomalies.

Following Sjöberg (1991, 2003c), approximate values of geoid undulations are computed from the un-reduced gridded gravity anomalies and EGM using the unbiased least squares geoid estimator. This makes use of a stochastic Stokes's modified kernel that simultaneously reduces the errors due to the truncation bias, satellite-only EGM coefficients and the terrestrial gravity data (Sjöberg 1984). Besides the choice of an integration cap radius, the most important step in the computation of approximate geoid in the KTH method is the determination of *a priori* estimates of signal and error degree variances. These are necessary for the computation of a *better choice* of modification parameters to be used in the least-squares modification method. Similar to the CUT approach, the integration cap radius is chosen empirically based on parameter sweeps versus GPS-levelling data.

The Tscherning and Rapp (1974) model is generally preferred by the KTH team to compute the gravity signal degree variance. The error degree variance of the EGM gravity is computed from the published error estimates that accompany the EGM coefficients. The error degree variance of terrestrial gravity anomalies is assumed to be a combination of white noise and a reciprocal distance covariance model (Ågren 2004; Ågren and Sjöberg, 2014). The signal and the EGM error degree variances are further rescaled by an empirically determined factor to best depict the 'reality' of the study area. The stochastically modified Stokes's integral in the geoid estimator is evaluated using the 1D-FFT method (Haagmans *et al.* 1993), but it has not been modified to include Gauss-Legendre quadrature (cf. Hirt *et al.* 2011).

Next are the so-called additive corrections from the combined topographic effect (Sjöberg 2000, 2001), atmospheric effect (Sjöberg 1999; Sjöberg and Nahanvandchi 2000), ellipsoidal shape of the Earth (Sjöberg 2003b; Sjöberg 2004) and downward continuation (Sjöberg 2003a; Ågren 2004), which are added to the approximate geoid to achieve the final geoid.

The KTH method has been designed primarily to compute a gravimetric geoid, which is then converted to quasigeoid by adding the geoid-quasigeoid separation term (Sjöberg 1995, 2010). However, Sjöberg (2000) and Ågren *et al.* (2009b) show that if the combined topographic effects are not applied in the computations using the KTH method and if the downward continuation is also adjusted accordingly, the result will be a quasigeoid. This eliminates the need for computing the topographic effects and further correction terms to convert the geoid to quasigeoid. The latter is the approach that was taken in the computations reported in the following section.

3. Results and discussion

Four separate quasigeoid models over Auvergne were computed at a grid resolution of $0.02^\circ \times 0.02^\circ$ using the CUT and KTH approaches. The computation area encompasses all 75 GPS-levelling points publicly available for validation. The KTH technique was used with the satellite-only DIR_R5 EGM (Bruinsma *et al.* 2013) up to spherical harmonic degree and order (d/o) 240. The CUT method was used with DIR_R5 to d/o 240 (so as to compare the results between the two methods), EGM2008 to d/o 360 (to compare the results from CUT

method with previously published results using some other methods; see Appendix A), and EGM2008 to d/0 2190 (to show the CUT method as it has been used in Australia, New Zealand and the U.S.A.). The SRTM 3" × 3" DEM (Farr et al. 2007) is used in all models.

In this study, we have used the CUT gravity-gridding method as used for Australia and New Zealand, despite the fact that the topography varies between the two study areas (Australia: mean ~330 m, max 2228 m; Auvergne: ~380 m, max 4751 m). As such, other gravity-gridding techniques may also be tested as was done by Goos et al. (2003) and Zhang and Featherstone (2004) in the Australian context. Furthermore, Claessens and Filmer (2020) have compared two gridding techniques over Colorado (one being the same as used in this study) and with the available 'ground-truth' data, they found sub-millimetre difference in the standard deviation of the computed quasigeoids.

In previous studies over Auvergne (Appendix A), the results are presented either with and/or without applying some form of localised fitting surface. These comprise one-parameter (removal of a constant bias) and four-parameters (constant bias plus tilted plane). These are commonly termed hybrid quasigeoid models, where the gravimetric-only model is fitted to GPS-levelling (and hence the local vertical datum) using some parametric or non-parametric surface. To be consistent with these other studies, we have therefore provided our results with and without such surface fitting, which are appended in Table A1.

In addition to simple descriptive statistics (minimum, maximum, mean and standard deviation) that are commonly used in most evaluations of gravimetric quasi/geoid models, we include the mean absolute error (MAE) and skewness, which are given in Table 1. We believe that these additional statistics are informative because the mean and standard deviation alone do not necessarily provide sufficient information to compare two or more methods, as shown later in this section. In other non-quasi/geoid-related literature, the MAE and skewness can be more informative metrics (e.g. Beedles and Simkowitz 1978; Bogner and Pappenberger 2011; Kosek et al. 2011; Mugume et al. 2016).

The standard deviation alone gives the magnitude of the variation of differences but not the direction, which is better quantified by the skewness. The MAE measures the mean magnitude of differences that is not available in case of arithmetic mean values. Thus, MAE and skewness are necessary along with mean and standard deviation to have an overall estimate of the magnitude and direction of the differences and their distribution. In Table 1, we also provide the coefficient of determination (R-squared) values for our four quasigeoid models after-fitting as a measure of how well the four-parameter regression model explains the total variation of gravimetric quasi/geoid with respect to the GPS-levelling points. The closer the R-squared value is to one, the better the regression model is.

Moreover, uncertainty in quasi/geoid computation can be obtained by removing the effect of ellipsoidal and levelling height errors from the overall error estimate computed with respect to the GPS-levelling data. The observed ellipsoidal heights are not correlated with the computed quasi/geoid, but the levelling will have [unknown] correlations if the land gravity observations

have been observed at differentially levelled benchmarks. Therefore, the quasi/geoid uncertainty (σ_N) before any fitting can be obtained using equation 1.

$$\sigma_N = \sqrt{(\sigma_{\text{overall}})^2 - (\sigma_h)^2 - (\sigma_H)^2} \quad (1)$$

where σ_h and σ_H are the uncertainties of ellipsoidal and levelling heights, respectively, and σ_{overall} is the standard deviation obtained on comparison wrt the ground data (e.g. Table A1).

A parametric-fitted quasi/geoid is correlated with the ellipsoidal and levelling heights (see equations for the four-parameter fit in the Electronic Supplementary Material). However, due to the unavailability of the corresponding covariance terms, the quasi/geoid uncertainty of the fitted model can also be computed using equation 1 (cf. Ågren and Sjöberg 2014; Sjöberg and Bagherbandi 2017; Ellmann et al. 2019). Equation 1 is valid iff

σ_{overall} is greater than $\sigma_{\text{GPS/lev}} (= \sqrt{\sigma_h^2 + \sigma_H^2})$. This condition may not always be met. In this regard, the internally propagated errors from GPS data processing software can be 2–10 times overly optimistic, i.e. too small (Rothacher 2002). Therefore, one solution is to scale up the formally propagated ellipsoidal height errors, e.g. as has been done for the Australian data (Featherstone et al. 2019).

For the Auvergne GPS-levelling data, Duquenne (2006) provided an approximate and 'blanket' (i.e. not point by point) error estimate of ~20–30 mm for the ellipsoidal heights and 20 mm for the differentially levelled heights. Therefore, the uncertainty of the four quasigeoids (before and after fit) in our study can only be computed (using equation 1) if the corresponding σ_{overall} is greater than 32 mm ($\sigma_{\text{GPS/lev}} = \sqrt{25^2 + 20^2}$). From Table A1, this condition is true for all the quasigeoid models with no fit but not for any after a parametric fit. Thus, we computed the uncertainties of the quasigeoid with no fit only using equation (1), and these are provided in Table 1.

We also provide results of the relative fit of our quasigeoid models (Table 2) with respect to the tolerances for differential levelling (cf. Featherstone 2001). Testing for the relative fit of quasigeoids can be an analysis tool to investigate quasi/geoid gradients. This type of analysis is of more interest to land surveyors who use relative GNSS baselines and a quasi/geoid gradients as a replacement for the more time-consuming differential levelling. Moreover, like the parameter-fitting, it also cancels the effect of almost constant zero-degree term (discussed later) irrespective of the choice of reference geopotential (W0) value.

Figures 1 and 2 show scatter-plots of the relative difference (magnitude) of the four quasigeoid models before and after parametric fitting, respectively. The curved lines in each figure depict the maximum allowable misclose for first order (lower curve) and third order levelling (upper curve) for all 2775 baselines computed using equation 2 with c equal to 4 and 12, respectively.

$$r = c\sqrt{d} \quad (2)$$

where, r = standard uncertainty, in mm; c = empirically derived factor for a given 'order' of levelling; d = distance between stations, in km. The values adopted for c may

Table 1. Extended analysis of the computed quasigeoid models with respect to 75 GPS/levelling data around Auvergne. L is the degree of kernel modification and Ψ_0 is the integration cap radius.

	L	Ψ_0		MAE (m)	Skewness	R-squared	Quasigeoid uncertainty (m)
KTH (DIR_R5)	240	1°	No Fit	0.819	-0.312	-	0.016
			4P Fit	0.020	0.712	0.448	NA ^b
CUT (DIR_R5)	240	1°	No Fit	0.871	-0.358	-	0.012
			4P Fit	0.021	0.152	0.362	NA
CUT (EGM08 d/o 360)	360	1°	No Fit	0.982	-0.377	-	0.016
			4P Fit	0.020	0.151	0.445	NA
CUT (EGM08 d/o 2190) ^a	360	0.1°	No Fit	0.872	-0.413	-	0.018
			4P Fit	0.020	-0.017	0.481	NA

^aThis solution is almost independent of the modification degree parameter sweeps analysed ($L = 20, 40, 60, 80, 120, 140, 180, 240, 360$).

^bNot applicable because σ_{overall} (after fit) is less than $\sigma_{\text{GPS/lev}}$ (cf. equation 1 and the discussion thereafter).

Table 2. Relative fit of quasigeoid models over (75° 74' 0.5") 2775 possible GPS-levelling baselines around Auvergne.

	L	Ψ_0		Min (m)	Max (m)	Mean (m)	STD (m)	MAE (m)	Skew-ness	Average ppm
KTH (DIR_R5)	240	1°	No Fit	-0.166	0.189	-0.002	0.051	0.040	0.008	0.440
			4P Fit	-0.166	0.170	0.001	0.038	0.029	-0.282	0.354
CUT (DIR_R5)	240	1°	No Fit	-0.152	0.170	0.010	0.048	0.039	-0.114	0.440
			4P Fit	-0.138	0.155	0.002	0.039	0.031	-0.108	0.380
CUT (EGM08 d/o 360)	360	1°	No Fit	-0.150	0.177	0.014	0.049	0.041	-0.122	0.457
			4P Fit	-0.139	0.154	0.002	0.038	0.030	-0.048	0.374
CUT (EGM08 d/o 2190)	360	0.1°	No Fit	-0.159	0.181	0.014	0.050	0.042	-0.121	0.463
			4P Fit	-0.122	0.145	0.002	0.038	0.030	0.011	0.369

vary among countries, and the levelling tolerances for different order levelling in France is unavailable to us, so we have used the c values of 4 and 12 from the Australian perspective (ICSM, 2007).

Following are our key observations from Tables 1 and 2 and A1, coupled with some further discussion:

a) For the solutions without any parametric fitting of the computed quasi/geoid and the GPS-levelling data, the mean differences of approximately -133 mm and -184 mm by the UNB group and Duquenne (2006), respectively, are attributed to a vertical datum offset for France (Rülke *et al.*

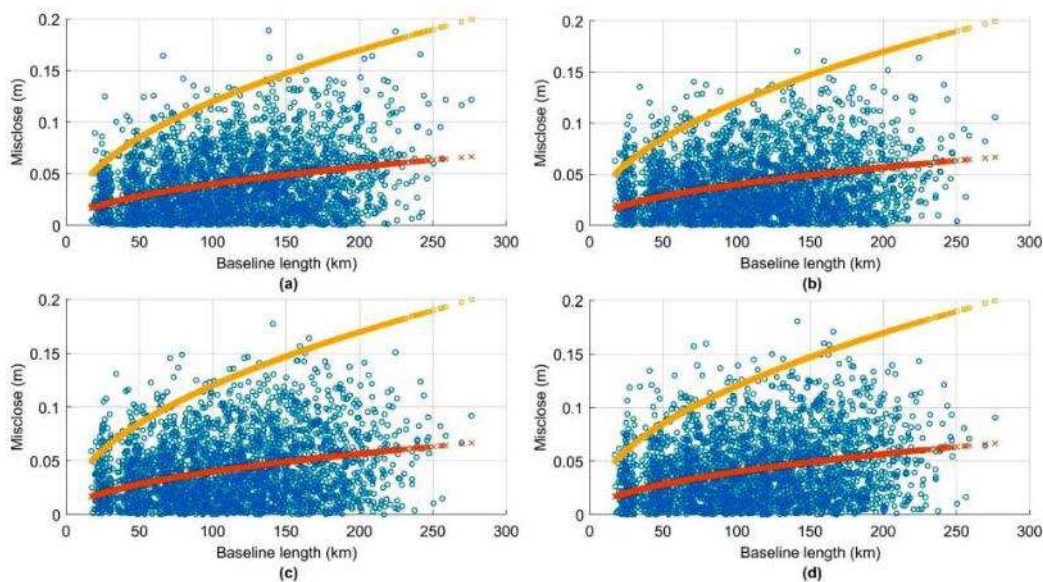


Figure 1. Magnitude of relative differences (circles) for the four quasigeoid models without fitting (a. KTH-DIR_R5, b. CUT-DIR_R5, c. CUT-EGM08_360, d. CUT-EGM08_2190) over 2775 GPS-levelling baselines. Crosses and squares represent the maximum permissible in-field misclose for Australian first order ($c = 4$) and third order ($c = 12$) levelling for each baseline, respectively.

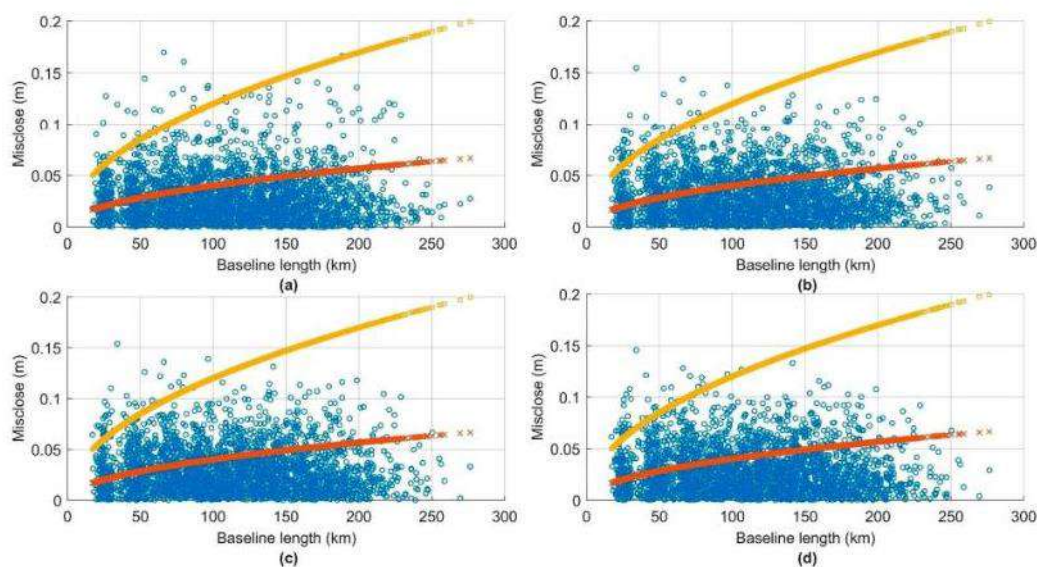


Figure 2. Magnitude of relative error (circles) for the four quasigeoid models after four-parameter fitting (a. KTH-DIR_R5, b. CUT-DIR_R5, c. CUT-EGM08_360, d. CUT-EGM08_2190) over 2775 GPS-leveilling baselines. Crosses and squares represent the maximum permissible in-field misclose for Australian first order ($c = 4$) and third order ($c = 12$) leveling for each baseline, respectively.

2012). However, for the computations using both the methods here (KTH and CUT) and the KTH method in Yildiz *et al.* (2012), the mean difference between quasigeoid and GNSS/levelling is, on average, -863 mm. This is almost 730 mm greater in magnitude as compared to the other reported studies. This large difference is due to the inconsistency in the application of the zero-degree term (cf. Smith 1998) by different groups. While this will cancel when the quasi/geoid is used relatively over baselines (cf. Featherstone 2001), it will not if used with single point positioning techniques (such as PPP). A practical solution if one does not choose to use a parametric fit, a one parameter fit can be used (i.e. a constant term) to simultaneously absorb the zero-degree term and any constant offset in the local vertical datum.

- b) There are differences among the results computed using the KTH method by Ågren *et al.* (2009a), Yildiz *et al.* (2012) and our current study. These differences can be attributed to one, some or all of three plausible reasons: i) the use of different EGMs to different degrees of expansion (and different degrees of modification); ii) different spatial resolutions of the computed quasigeoid models (i.e. yielding a combination of discretisation and interpolation errors); and iii) inconsistent or lack of reporting on the treatment of the zero-degree term. Ågren *et al.* (2009a) use EIGEN_GL04C (d/o360) to compute a quasigeoid at a resolution of $1' \times 1'$ with no zero-degree term applied. Yildiz *et al.* (2012) use EGM2008 (d/o360) and compute a quasigeoid at resolution of $0.02^\circ \times 0.025^\circ$ with a zero-degree term applied. However, their results are presented after removing a mean value, so we

are unable to distinguish what proportion is due to their value of the zero degree term and any constant offset in the French vertical datum over Auvergne. In this study, we use DIR_R5 (d/o 240) with a resolution of $0.02^\circ \times 0.02^\circ$. Our zero-degree term was applied using the W_0 value used in the International Height Reference System (Sánchez *et al.* 2016). We also used the GRS80 ellipsoid and scaled the even degree harmonics as per, e.g. Smith (1998).

- c) From Table A1, we observe that for any method (KTH, UNB or GRAVSOFT), since 2006, there is no clear trend of improvement in the results without a corrector surface. Of all the studies in Table A1 with no surface fitting, the smallest standard deviation of 29 mm is obtained using the Radial Basis Function (RBF) method (Lin *et al.* 2019), while the Finite Element Method (FEM) method (Janák *et al.* 2014) provided the largest standard deviation of 97 mm. The KTH method provided the smallest standard deviations of 24 mm (Yildiz *et al.* 2012), 25 mm (Abbak and Ustun 2015) and 26 mm (this study) after four-parameter, seven-parameter and four-parameter surface fitting, respectively. Utilising the full expansion of EGM2008 (d/o 2190/2159), the CUT method (this study) also provided a standard deviation of 26 mm after four-parameter fitting.
- d) Different geoid modellers have had different views on whether more than a one-parameter model should be used during the GPS-leveilling evaluation or not. One argument for this is that different permanent tide systems are used for the GPS ellipsoidal heights, levelled heights and terrestrial gravity data (cf. Poutanen *et al.* 1996; Ekman 1989). It is not

mentioned in Duquenne (2006) whether the corresponding datasets have been transformed to a common tide system, which means that they most likely are in their default tide systems (e.g. non-tidal for RGF93-ETRS89, unknown for NGF-IGN69 and mean-tide for IGSN71). This will result in a systematic tilt in the north-south direction with the magnitude of a few centimetres (Ekman 1989), which will be absorbed by a four-parameter surface. Based on this and the comments in part (a), we recommend that both one- and four-parameter fits are used in future Auvergne evaluations.

- e) Based on the standard deviations from Table A1 with DIR_R5 EGM, the CUT method ($\sigma = 34$ mm) appears marginally 'better' than the KTH method ($\sigma = 36$ mm) without any surface fitting, whereas the KTH method ($\sigma = 26$ mm) is marginally 'better' than the CUT method ($\sigma = 27$ mm) after four-parameter surface fitting. We use the term marginal because of the blanket error budget used for the GPS-levelling (32 mm) and we are not at the ability to compute millimetre-precise quasigeoid models. Hence, these statements of being 'marginally better' are not statistically significant when accounting for the error budget of the control data (cf. Featherstone *et al.* 2019), but are based solely on numerical values of the standard deviations.
- f) However, for the same EGM (DIR_R5), Table 1 shows that after surface fitting, the KTH method provides results which are significantly (~ 4.5 times) more positively skewed compared to the CUT method. Larger positive skewness represents asymmetrical distribution of the differences, with more values being clustered on the left tail of the distribution and therefore, a larger positive difference. The same pattern of results is also observed for the relative fit of the quasigeoid models computed using the CUT and KTH methods (Table 2). We believe this is why the skewness is an additional and useful metric of quasi/geoids versus GPS-levelling.
- g) Figures 1 and 2(A and B) show that the KTH method (with DIR_R5 EGM d/o 240) provides a larger number of baselines beyond 150 km that have misclosures greater than 150 mm and 100 mm, respectively, as compared to the CUT method. Moreover, the CUT method with EGM2008 (d/o 2190/2159) after a four-parameter fit (Figure 2(D)) results in a misclosure of less than 100 mm for all baselines greater than 200 km. Hence, with the available data, the CUT method (as used for Australia and New Zealand) can be regarded as a 'better' method for longer baselines compared to the KTH method, but we acknowledge that this may be because the French gravity data have been used in the construction of EGM2008 (Pavlis *et al.* 2012, 2013). Another plausible explanation is that the use of a d/o 240 EGM coupled with the data extent of the Auvergne gravity data omits some of the medium frequency content of the KTH-modelled quasigeoid.

4. Conclusions and recommendations

In this study, quasigeoid models of Auvergne were computed using the CUT and KTH techniques and

compared. These results were also compared with respect to previously published studies on quasi/geoid determination over Auvergne. The mean differences of ~ 730 mm among different techniques (e.g. CUT, KTH, UNB, GRAVSOF/LSC) are due mainly to different treatments of the zero-degree term, but offsets in the French vertical datum cannot be eliminated as a candidate. The NGF-IGN69 French vertical datum may have an offset from classical geoid. This is possibly because the mean sea level that is held fixed at Marseille may be subjected to the effects of the ocean's mean dynamic topography, but which is challenging to model in the coastal zone.

Small differences among standard deviations can be due to, one some or all of, the choice of different EGMs, kernel modification degree, cap radii, DEMs, terrain corrections, quasi/geoid resolution and the gridding of the point anomaly data. However, all these terms are inseparable, so we are unable to point to any particular candidates. We, through our analysis, suggest that the practice of commenting on the pre-eminence of one method over other based on only standard deviation is not completely justified, especially if one takes into account the error budget of the GPS-levelling data.

It is therefore recommended to establish some commonly adopted guidelines to define a statistical table for reporting the results of quasi/geoid computations when different methods are compared over the same region. A tentative list of statistical parameters can be adapted from Tables 1 and 2 and A1. These will be important to (1) have an improved understanding of the 'accuracy' of the method in use, and (2) more objectively compare the results with other computation approaches over the same region. This recommendation perhaps may be further taken up by either Sub-Commission 2.2 or 2.4 of the International Association of Geodesy.

Acknowledgements

We wish to thank the French IGN for publicly releasing dense gravity and GPS-levelling data in and around Auvergne for testing quasi/geoid computation techniques. Ropesh Goyal is thankful to the National Centre for Geodesy at IIT Kanpur, India, for supporting his travel to the Universities of Gävle and KTH, Sweden. Will Featherstone thanks and acknowledges many years of research funding from the Australian Research Council, Western Australian State Government, Curtin University and the Cooperative Research Centre for Spatial Information.

Disclosure statement

No potential conflict of interest was reported by the author(s).

Notes on contributors

R. Goyal is currently a jointly enrolled PhD student at IIT Kanpur, India, and Curtin University, Australia, who is working towards the development of gravimetric geoid model for India. His interest is examining the approximations and assumptions made in the geoid modelling techniques that may no longer be assumed negligible from the view-point of the ongoing quest for cm-level

precise geoid, especially over the diverse range of heights and geoid undulations across India.

J. Ågren is a Lecturer at University of Gävle/Sandviken, Sweden, and also works at the Geodetic Research Division of Lantmäteriet (the Swedish Mapping, Cadastre and Registry Authority). He has computed the most recent national quasigeoid model for Sweden.

W. E. Featherstone is Professor of Geodesy at Curtin University, Australia, and distinguished Visiting Professor at IIT Kanpur, India. Will and colleagues have computed the past three national standard quasigeoid models for Australia.

L. E. Sjöberg is Emeritus Professor of Geodesy at Royal Institute of Technology (KTH), Sweden. Since the 1980s, he has developed the KTH method for geoid computation with additive corrections using least squares by spectral weighting of observables.




O. Dikshit is Full Professor at IIT Kanpur. He has been instrumental in bringing geodesy and geospatial education programs to IIT Kanpur, and also developing state-of-the-art facilities under the umbrella of the Indian National Centre for Geodesy.

N. Balasubramanian is Visiting Professor at IIT Kanpur. His PhD at Ohio State University, USA, was on vertical datum unification, and he has served as Additional Surveyor General, Survey of India (now retired).

Data availability statement

The data sets used in this study are all open-source data. The data sets generated in the current study are available from the corresponding author on reasonable request.

ORCID

R. Goyal  <http://orcid.org/0000-0002-2178-3265>
 J. Ågren  <http://orcid.org/0000-0003-0602-142X>
 W.E. Featherstone  <http://orcid.org/0000-0001-9644-4535>
 L.E. Sjöberg  <http://orcid.org/0000-0001-7810-8829>
 O. Dikshit  <http://orcid.org/0000-0003-3213-8218>

References

- Abbak, R.A., et al., 2012. A precise gravimetric geoid model in a mountainous area with scarce gravity data: a case study in central Turkey. *Studia geophysica et geodaetica*, 56, 909–927. doi:10.1007/s11200-011-9001-0.
- Abbak, R.A., 2014. Effect of ASTER DEM on the prediction of mean gravity anomalies: a case study over the Auvergne test region. *Acta geodaetica et geophysica*, 49, 491–502. doi:10.1007/s40328-014-0062-8.
- Abbak, R.A. and Ustun, A., 2015. A software package for computing a regional gravimetric geoid model by the KTH method. *Earth science informatics*, 8, 255–265. doi:10.1007/s12145-014-0149-3.
- Abdalla, A. and Fairhead, D., 2011. A new gravimetric geoid model for Sudan using the KTH method. *Journal of African earth sciences*, 60, 213–221. doi:10.1016/j.jafrearsci.2011.02.012.
- Abdalla, A. and Mogren, S., 2015. Implementation of a rigorous least-squares modification of Stokes' formula to compute a gravimetric geoid model over Saudi Arabia (SAGEO13). *Canadian journal of earth sciences*, 52, 823–832. doi:10.1139/cjes-2014-0192.
- Abdalla, A. and Tenzer, R., 2011. The evaluation of the New Zealand's geoid model using the KTH method. *Geodesy and cartography*, 37, 5–14. doi:10.3846/13921541.2011.558326.
- Ågren, J., 2004. *Regional geoid determination methods for the era of satellite gravimetry: numerical investigations using synthetic Earth gravity models*. Dissertation, Royal Institute of Technology (KTH), Stockholm, Sweden. Available from: <http://www.diva-portal.org/smash/get/diva2:14396/FULLTEXT01.pdf>.
- Ågren, J., et al., 2009a. Different geoid computation methods applied on a test dataset: results and considerations. In: *Poster presented at VII Hotine-Marussi symposium on mathematical geodesy*, Rome, Italy.
- Ågren, J., et al., 2016. The NKG2015 gravimetric geoid model for the Nordic-Baltic region. In: *Presented at the 1st Joint Commission 2 and IGFS Meeting*, 19–23 September 2016, Thessaloniki, Greece.
- Ågren, J. and Sjöberg, L.E., 2014. Investigation of gravity data requirements for a 5 mm-quasigeoid model over Sweden. In: U. Marti, ed. *Gravity, geoid and height systems. International association of geodesy symposia*, vol. 141. Cham: Springer, 143–150. doi:10.1007/978-3-319-10837-7_18.
- Ågren, J., Sjöberg, L.E., and Kiamehr, R., 2009b. The new gravimetric quasigeoid model KTH08 over Sweden. *Journal of applied geodesy*, 3, 143–153. doi:10.1515/JAG.2009.015.
- Amos, M.J. and Featherstone, W.E., 2009. Unification of New Zealand's local vertical datums: iterative gravimetric quasigeoid computations. *Journal of geodesy*, 83, 57–68. doi:10.1007/s00190-008-0232-y.
- Baran, I., et al., 2006. A synthetic Earth gravity model designed specifically for testing regional gravimetric geoid determination algorithms. *Journal of geodesy*, 80, 1–16. doi:10.1007/s00190-005-0002-z.
- Beedles, W.I. and Simkowitz, M.A., 1978. A note on skewness and data errors. *The journal of finance*, 33, 288–292.
- Bogner, K. and Pappenberger, F., 2011. Multiscale error analysis, correction, and predictive uncertainty estimation in a flood forecasting system. *Water resources research*, 47, W07524. doi:10.1029/2010WR009137.
- Bruinsma, S.L., et al., 2013. The new ESA satellite-only gravity field model via the direct approach. *Geophysical research letters*, 40, 3607–3612. doi:10.1002/grl.50716.
- Claessens, S.J., 2006. *Solutions to ellipsoidal boundary value problems for gravity field modelling*. Dissertation, Curtin University of Technology, Perth, Australia. Available from: https://espace.curtin.edu.au/bitstream/handle/20.500.11937/1637/16850_Claessens%20S%202006%20full.pdf?sequence=2&isAllowed=y.
- Claessens, S.J., et al., 2011. The NZGeoid09 model of New Zealand. *Survey review*, 43, 2–15. doi:10.1179/003962610X12747001420780.
- Claessens, S.J. and Filmer, M.S., 2020. Towards an International Height Reference System: insights from the Colorado geoid experiment using AUSGeoid computation methods. *Journal of geodesy*, 94, 52. doi:10.1007/s00190-020-01379-3.
- Danila, U., 2012. *Mold2012-a new gravimetric quasigeoid model over Moldova*. Dissertation, Royal Institute of Technology (KTH), Stockholm, Sweden. Available from: <http://kth.diva-portal.org/smash/get/diva2:572006/FULLTEXT01.pdf>.
- Daras, I., et al., 2010. Determination of a gravimetric geoid model of Greece using the method of KTH. In: S.P. Mertikas, ed. *Gravity, geoid and earth observation. International association of geodesy symposia*, vol. 135. Berlin Heidelberg: Springer, 407–413. doi:10.1007/978-3-642-10634-7_54.
- Duquenne, H., 2006. A data set to test geoid computation methods. In: *Proceedings of the 1st International symposium of the International gravity field service*, Harita Dergisi, Istanbul, Turkey, 61–65.
- Ekman, M., 1989. Impacts of geodynamic phenomena on systems for height and gravity. *Bulletin Géodésique*, 63, 281–296. doi:10.1007/BF02520477.
- Ellmann, A., 2004. *The geoid for the Baltic countries determined by the least squares modification of Stokes' formula*. Dissertation, Royal Institute of Technology (KTH), Stockholm, Sweden. Available from: <http://kth.diva-portal.org/smash/get/diva2:9592/FULLTEXT01.pdf>.
- Ellmann, A., Mårdla, S., and Oja, T., 2019. The 5 mm geoid model for Estonia computed by the least squares modified Stokes's formula. *Survey review*, 52, 352–372. doi:10.1080/00396265.2019.1583848.
- Farr, T.G., et al., 2007. The shuttle radar topography mission. *Reviews of geophysics*, 45, RG2004. doi:10.1029/2005RG000183.
- Featherstone, W.E., 2001. Absolute and relative testing of gravimetric geoid models using global positioning system and orthometric height data. *Computers & geosciences*, 27, 807–814. doi:10.1016/S0098-3004(00)00169-2.
- Featherstone, W.E., et al., 2001. The AUSGeoid98 geoid model of Australia: data treatment, computations and comparisons with GPS-levelling data. *Journal of geodesy*, 75, 313–330. doi:10.1007/s001900100177.
- Featherstone, W.E., 2002. Tests of two forms of Stokes's integral using a synthetic gravity field based on spherical harmonics. In: E.W.

- Grafarend, F.W. Krumm, and V.S. Schwarze, eds. *Geodesy – the challenge for the third millennium*. Berlin Heidelberg: Springer, 163–171. doi:10.1007/978-3-662-05296-9_17.
- Featherstone, W.E., 2003. Software for computing five existing types of deterministically modified integration kernel for gravimetric geoid determination. *Computers & geosciences*, 29, 183–193. doi:10.1016/S0098-3004(02)00074-2.
- Featherstone, W.E., et al., 2004. Comparison of remove-compute-restore and University of New Brunswick techniques to geoid determination over Australia, and inclusion of Wiener-type filters in reference field contribution. *Journal of surveying engineering*, 130, 40–47. doi:10.1061/(ASCE)0733-9453(2004)130:1(40).
- Featherstone, W.E., et al., 2011. The AUSGeoid09 model of the Australian Height Datum. *Journal of geodesy*, 85, 133–150. doi:10.1007/s00190-010-0422-2.
- Featherstone, W.E., et al., 2018a. The first Australian gravimetric quasi-geoid model with location-specific uncertainty estimates. *Journal of geodesy*, 92, 149–168. doi:10.1007/s00190-017-1053-7.
- Featherstone, W.E., et al., 2018b. Description and release of Australian gravity field model testing data. *Australian journal of earth sciences*, 65, 1–7. doi:10.1080/08120099.2018.1412353.
- Featherstone, W., Evans, J., and Olliver, J., 1998. A Meissl-modified Vaníček and Kleusberg kernel to reduce the truncation error in gravimetric geoid computations. *Journal of geodesy*, 72, 154–160. doi:10.1007/s001900005017.
- Featherstone, W.E. and Kirby, J.F., 2000. The reduction of aliasing in gravity anomalies and geoid heights using digital terrain data. *Geophysical journal international*, 141, 204–212. doi:10.1046/j.1365-246X.2000.00082.x.
- Featherstone, W.E., Lyon, T.J., and McCubbine, J.C., 2019. Potentially misleading GPS-leveling-based assessment of gravimetric geoid/quasigeoid models due to vertical land motion and different GPS processing software. *Journal of surveying engineering*, 145, 04019015. doi:10.1061/(ASCE)SU.1943-5428.0000293.
- Featherstone, W.E. and Sideris, M.G., 1998. Modified kernels in spectral geoid determination: first results from Western Australia. In: R. Forsberg, M. Feissl, and R. Dietrich, eds. *Geodesy on the move. International association of geodesy symposia*, vol 119. Berlin, Germany: Springer, 188–193. doi:10.1007/978-3-642-72245-5_26.
- Felner, J.J., Kuhn, M., and Featherstone, W.E., 2012. Development of a synthetic earth gravity model by 3D mass optimisation based on forward modelling. *Earth planets and space*, 64, 5–12. doi:10.5047/eps.2011.07.012.
- Foroughi, I., et al., 2017a. Optimal combination of satellite and terrestrial gravity data for regional geoid determination using Stokes-Helmert's method, the Auvergne test case. In: G. Vergos, R. Pail, and R. Barzaghi, eds. *Gravity, geoid and height systems 2016. International association of geodesy symposia*, vol 148. Berlin Heidelberg: Springer, 37–43. doi:10.1007/1345_2017_22.
- Foroughi, I., et al., 2017b. In defense of the classical height system. *Geophysical journal international*, 211, 1154–1161. doi:10.1093/GJI/GGX366.
- Foroughi, I., et al., 2019. Sub-centimetre geoid. *Journal of geodesy*, 93, 849–868. doi:10.1007/s00190-018-1208-1.
- Forsberg, R., 1985. Gravity field terrain effect computations by FFT. *Bulletin géodésique*, 59, 342–360. doi:10.1007/BF02521068.
- Forsberg, R., et al., 2010. Geoid determination in the mountains using ultrahigh resolution spherical harmonic models – the Auvergne case. In: Contadakis, N. Arabelos, and Z. Editions, eds. *The apple of the knowledge, in Honor of Professor Emeritus Demetrius*. Thessaloniki, 101–111. ISBN: 978-960-243-674-5. Available from: https://www.topo.auth.gr/greek/ORG_DOMI/EMERITUS/TOMOS_ARABELOS/The_apple%20pdf/1-07%20Forsberg.pdf.
- Goli, M., Foroughi, I., and Novák, P., 2019. Application of the one-step integration method for determination of the regional gravimetric geoid. *Journal of geodesy*, 93, 1631–1644. doi:10.1007/s00190-019-01272-8.
- Goos, J.M., et al., 2003. Experiments with two different approaches to gridding terrestrial gravity anomalies and their effect on regional geoid computation. *Survey review*, 37, 92–112. doi:10.1179/sre.2003.37.288.92.
- Haagmans, R.R.N., 2000. A synthetic earth model for use in geodesy. *Journal of geodesy*, 74, 503–511. doi:10.1007/s001900000112.
- Haagmans, R.R.N., de Min, E., and van Geldren, M., 1993. Fast evaluation of convolution integrals on the sphere using IDFFT, and a comparison with existing methods for Stokes's integral. *Manuscripta Geodaetica*, 18, 227–241.
- Hirt, C., Featherstone, W.E., and Claessens, S.J., 2011. On the accurate numerical evaluation of geodetic convolution integrals. *Journal of geodesy*, 85, 519–538. doi:10.1007/s00190-011-0451-5.
- Hotine, M., 1969. *Mathematical Geodesy*. ESSA Monograph 2, Department of Commerce, Washington.
- ICSM, 2007. *Standards and practices for control surveys SPI* (version 1.7). Inter-governmental Committee of Surveying and Mapping, Canberra, Australia.
- Inerbayeva, D., 2010. *Determination of a gravimetric geoid model of Kazakhstan using the KTH-method*. Dissertation. Royal Institute of Technology (KTH), Stockholm, Sweden. Available from: <http://kth.diva-portal.org/smash/get/diva2:465930/FULLTEXT01.pdf>.
- Janák, J., et al., 2017. Computation of precise geoid model of Auvergne using current UNB Stokes-Helmert's approach. *Contributions to geophysics and geodesy*, 47, 201–229. doi:10.1515/congeo-2017-0011.
- Janák, J., Pitoňák, M., and Minařechová, Z., 2014. Regional quasigeoid from GOCE and terrestrial measurements. *Studia Geophysica et Geodaetica*, 58, 626–649. doi:10.1007/s11200-013-0543-1.
- Kiamehr, R., 2006. *Precise gravimetric geoid model for Iran based on GRACE and SRTM data and the least-squares modification of Stokes' formula: with some geodynamic interpretations*. Dissertation. Royal Institute of Technology (KTH), Stockholm, Sweden. Available from: <http://www.diva-portal.org/smash/get/diva2:10840/FULLTEXT01.pdf>.
- Kosek, W., et al., 2011. Analysis of pole coordinate data predictions in the earth orientation parameters combination of prediction pilot project. *Artificial satellites*, 46, 139–150. doi:10.2478/v10018-012-0006-x.
- Kuczynska-Sieghien, J., Lyszkwicz, A., and Birylo, M., 2016. Geoid determination for the area of Poland by the least squares modification of Stokes' formula. *Acta Geodynamica et Geomaterialia*, 13, 19–26. doi:10.13168/AGG.2015.0041.
- Kuhn, M. and Featherstone, W.E., 2003a. On the construction of a synthetic Earth gravity model (SEGM). In: I.N. Tziavos, ed. *Gravity and geoid 2002, Department of surveying and geodesy*. Thessaloniki, Greece: Aristotle University of Thessaloniki, 189–194.
- Kuhn, M. and Featherstone, W.E., 2003b. On the optimal spatial resolution of crustal mass distributions for forward gravity field modelling. In: I.N. Tziavos, ed. *Gravity and geoid 2002, Department of surveying and geodesy*. Thessaloniki, Greece: Aristotle University of Thessaloniki, 195–200.
- Kuhn, M. and Featherstone, W.E., 2005. Construction of a synthetic Earth gravity model by forward gravity modelling. In: F. Sansó, ed. *A window on the future of geodesy. International association of geodesy symposia*, vol 128. Berlin Heidelberg: Springer, 350–355. doi:10.1007/3-540-27432-4_60.
- Lin, M., Denker, H., and Müller, J., 2019. A comparison of fixed- and free-positioned point mass methods for regional gravity field modelling. *Journal of geodynamics*, 125, 32–47. doi:10.1016/j.jog.2019.01.001.
- Liu, Q., et al., 2020. Regional gravity field refinement for (quasi-)geoid determination based on spherical radial basis functions in Colorado. *Journal of geodesy*, 94 (2020), 99. doi:10.1007/s00190-020-01431-2.
- McCubbine, J.C., Featherstone, W.E., and Brown, N.J., 2019. Error propagation for the Molodensky G1 term. *Journal of geodesy*, 93, 889–898. doi:10.1007/s00190-018-1211-6.
- McCubbine, J.C., Featherstone, W.E., and Kirby, J.F., 2017. Fast Fourier-based error propagation for the gravimetric terrain correction. *Geophysics*, 82, G71–G76. doi:10.1190/GEO2016-0627.1.
- Meissl, P., 1971. *Preparations for the numerical evaluation of second-order Molodensky-type formulas*. OSU Report 163, Department of Geodetic Science, Ohio State University, Columbus.
- Molodensky, M.S., Eremeev, V.F., and Yurkina, M.I., 1962. *Methods for study of the external gravitational field and figure of the Earth*. Translated from the 1960 original by the Israeli Programme for the Translation of Scientific Publications, Jerusalem.
- Moritz, H., 1980. Geodetic reference system 1980. *Bulletin Géodésique*, 54, 395–405. doi:10.1007/BF02521480.
- Moritz, H., 2000. Geodetic reference system 1980. *Journal of geodesy*, 74, 128–162. doi:10.1007/S0019000050278.
- Mugume, I., et al., 2016. Comparison of parametric and nonparametric methods for analyzing the bias of a numerical model. *Modelling and simulation in engineering*, 7530759. doi:10.1155/2016/7530759.
- Novák, P., et al., 2001. On the accuracy of modified Stokes's integration in high-frequency gravimetric geoid determination. *Journal of geodesy*, 74, 644–654. doi:10.1007/s001900000126.

- Novák, P., 2003. Geoid determination using one-step integration. *Journal of Geodesy*, 77 (3-4), 193–206. doi:10.1007/s00190-003-0314-9.
- Pa'suya, M.F., et al., 2019. Gravimetric geoid modelling over peninsular Malaysia using two different gridding approaches for combining free air anomaly. *International archives of the photogrammetry, remote sensing and spatial information sciences*, XLII-4/W16, 515–522. doi:10.5194/isprs-archives-XLII-4-W16-515-2019.
- Pavlis, N.K., et al., 2012. The development and evaluation of the Earth Gravitational Model 2008 (EGM2008). *Journal of geophysical research – solid earth*, 117 (B4), B04406. doi:10.1029/2011JB008916.
- Pavlis, N.K., et al., 2013. Correction to 'The development and evaluation of the Earth Gravitational Model 2008 (EGM2008)'. *Journal of geophysical research – solid earth*, 118, 2633. doi:10.1029/jgrb.50167.
- Poutanen, M., Vermeer, M., and Mäkinen, J., 1996. The permanent tide in GPS positioning. *Journal of geodesy*, 70, 499–504. doi:10.1007/BF00863622.
- Rothacher, M., 2002. Estimation of station heights with GPS. In: H. Drewes, A.H. Dodson, L.P.S. Fortes, L. Sánchez, and P. Sandoval, eds. *Vertical reference systems*. International association of geodesy symposia, vol 124. Berlin, Heidelberg: Springer. doi:10.1007/978-3-662-04683-8_17.
- Rülke, A., et al., 2012. Unification of European height system realizations. *Journal of geodetic science*, 2, 343–354. doi:10.2478/v10156-011-0048-1.
- Sánchez, L., et al., 2016. A conventional value for the geoid reference potential W_0 . *Journal of geodesy*, 90, 815–835. doi:10.1007/s00190-016-0913-x.
- Sjöberg, L.E., 1981. Least squares combination of satellite and terrestrial data in physical geodesy. *Annales de Géophysique*, 37, 25–30.
- Sjöberg, L.E., 1984. *Least squares modification of Stokes and Venning Meinesz formulas by accounting for errors of truncation, potential coefficients and gravity data*. Technical Report 27, Department of Geodesy, Institute of Geophysics, University of Uppsala, Uppsala, Sweden.
- Sjöberg, L.E., 1991. Refined least squares modification of Stokes' formula. *Manuscripta Geodetica*, 16, 367–375.
- Sjöberg, L.E., 1995. On the quasigeoid to geoid separation. *Manuscripta Geodetica*, 20, 182–192.
- Sjöberg, L.E., 1999. The IAG approach to the atmospheric geoid correction in Stokes' formula and a new strategy. *Journal of geodesy*, 73, 362–366. doi:10.1007/s001900050254.
- Sjöberg, L.E., 2000. On the topographic effects by the Stokes-Helmert method of geoid and quasi-geoid determinations. *Journal of geodesy*, 74, 255–268. doi:10.1007/s001900050284.
- Sjöberg, L.E., 2001. Topographic and atmospheric corrections of the gravimetric geoid determination with special emphasis of the effects of degrees zero and one. *Journal of geodesy*, 75, 283–290. doi:10.1007/s001900100174.
- Sjöberg, L.E., 2003a. A solution to the downward continuation effect on the geoid determined by Stokes' formula. *Journal of geodesy*, 77, 94–100. doi:10.1007/s00190-002-0306-1.
- Sjöberg, L.E., 2003b. The ellipsoidal corrections to order e^2 of geopotential coefficients and Stokes' formula. *Journal of geodesy*, 77, 139–147. doi:10.1007/s00190-003-0321-x.
- Sjöberg, L.E., 2003c. A computational scheme to model the geoid by the modified Stokes formula without gravity reductions. *Journal of geodesy*, 77, 423–432. doi:10.1007/s00190-003-0338-1.
- Sjöberg, L.E., 2004. A spherical harmonic representation of the ellipsoidal correction to the modified Stokes formula. *Journal of geodesy*, 78, 180–186. doi:10.1007/s00190-004-0378-1.
- Sjöberg, L.E., 2010. A strict formula for geoid-to-quasigeoid separation. *Journal of geodesy*, 84, 699–702. doi:10.1007/s00190-010-0407-1.
- Sjöberg, L.E. and Bagherbandi, M., 2017. *Gravity inversion and integration: theory and application in geodesy and geophysics*. Berlin: Springer. doi:10.1007/978-3-319-50298-4.
- Sjöberg, L.E. and Nahavandchi, H., 2000. The atmospheric geoid effects in Stokes' formula. *Geophysical journal international*, 140, 95–100. doi:10.1046/j.1365-246x.2000.00995.x.
- Smith, D.A., 1998. There is no such thing as 'The' EGM96 geoid: subtle points on the use of a global geopotential model. *International geoid service bulletin*, 8, 17–28. Available from: https://www.ngs.noaa.gov/PUBS_LIB/EGM96_GEOID_PAPER/egm96_geoid_paper.html.
- Ssengendo, R., 2015. *A height datum for Uganda based on a gravimetric quasigeoid model and GNSS/levelling*. Dissertation. Royal Institute of Technology (KTH), Stockholm, Sweden. Available from: <http://kth.diva-portal.org/smash/get/diva2:848931/FULLTEXT01.pdf>.
- Stokes, G.G., 1849. On the variation of gravity on the surface of the Earth. *Transactions of the Cambridge philosophical society*, 8, 672–695.
- Tscherning, C.C., Forsberg, R., and Knudsen, P., 1992. The GRAVSOFTE package for geoid determination. In: *Proceedings of first continental workshop on the geoid in Europe*, Prague, May 1992, pp. 327–334. Research Institute of Geodesy, Topography and Cartography, Prague.
- Tscherning, C.C. and Rapp, R.H., 1974. *Closed covariance expressions for gravity anomalies, geoid undulations, and deflections of the vertical implied by anomaly degree variance models*. Technical report 208. Columbus, USA: The Ohio State University.
- Tziavos, I.N., 1996. Comparisons of spectral techniques for geoid computations over large regions. *Journal of geodesy*, 70, 357–373. doi:10.1007/s001900050027.
- Ulotu, P., 2009. *Geoid model of Tanzania from sparse and varying gravity data density by the KTH method*. Dissertation. Royal Institute of Technology (KTH), Stockholm, Sweden. Available from: <http://kth.diva-portal.org/smash/get/diva2:213740/FULLTEXT01.pdf>.
- Valty, P., Duquenne, H., and Panet, I., 2012. Auvergne dataset: testing several geoid computation methods. In: S. Kenyon, M. Pacino, and U. Marti, ed. *Geodesy for planet earth*. International association of geodesy symposia, vol 136. Berlin, Heidelberg: Springer, 465–472. doi:10.1007/978-3-642-20338-1_56.
- Vaniček, P., et al., 2013. Testing Stokes-Helmert geoid model computation on a synthetic gravity field: experiences and shortcomings. *Studia Geodetica et Geophysica*, 57, 369–400. doi:10.1007/s11200-012-0270-z.
- Vaniček, P. and Kleusberg, A., 1987. The Canadian geoid – Stokesian approach. *Manuscripta geodetica*, 12, 86–98.
- Vaniček, P. and Sjöberg, L.E., 1991. Reformulation of Stokes's theory for higher than second-degree reference field and modification of integration kernels. *Journal of geophysical research – solid earth*, 96, 6529–6539. doi:10.1029/90JB02782.
- Wessel, P., et al., 2013. Generic mapping tools: improved version released. *EOS – transactions of the AGU*, 94, 409–410. doi:10.1002/2013EO450001.
- Wong, L. and Gore, R., 1969. Accuracy of geoid heights from modified Stokes kernels. *Geophysical journal international*, 18, 81–91. doi:10.1111/j.1365-246X.1969.tb00264.x.
- Wu, Q., et al., 2020. Performance comparison of geoid refinement between XGM2016 and EGM2008 based on the KTH and RCR methods: Jilin Province, China. *Remote Sensing*, 12, 324. doi:10.3390/rs12020324.
- Yildiz, H., et al., 2012. Comparison of remove-compute-restore and least squares modification of Stokes' formula techniques to quasigeoid determination over the Auvergne test area. *Journal of Geodetic Science*, 2, 53–64. doi:10.2478/v10156-011-0024-9.
- Zhang, K.F. and Featherstone, W.E., 2004. Investigation of the roughness of the Australian gravity field using statistical, graphical, fractal and Fourier power spectrum techniques. *Survey review*, 37, 520–530. doi:10.1179/003962604791482388.

Appendix A

Table A1. Results from previous and present study for geoid/quasigeoid of Auvergne

Reference	Approach	Type	Software	EGM (degrees)	Odeg	Integration radius	Kernel	Terrain treatment	DEM/ density used	Atmos	Ellip	Fit type	Min	Max	Mean	STD	
Duquenne (2006)	RCR	quasigeoid	GRAVSOFIT	GGM02S (2-100) EGM96 (110-360)	NA	Whole area	WG	RTM	IGN height data base	no	no	none	-0.292	-0.117	-0.184	0.038	
Ágren et al. (2009a)	KTH Fast LSC	quasigeoid	Geolab	EIGEN_GLO4C (360)	No	NA	LSM	Not required	SRTM 3" x 3"	yes	yes	3P	-0.094	0.053	0.000	0.029	
		quasigeoid	NA	EIGEN_GLO4C (360)	NA	NA	NA	NA	SRTM 3" x 3"	NA	NA	3P	-0.117	0.099	0.000	0.042	
		quasigeoid	NA	EIGEN_GLO4C (360)	NA	NA	NA	NA	RTM	SRTM 3" x 3"	NA	NA	3P	-0.085	0.079	0.000	0.035
		quasigeoid	GEOCOL	EIGEN_GLO4C (360)	NA	NA	NA	NA	NA	SRTM 3" x 3"	NA	NA	3P	-0.196	0.161	0.000	0.067
		quasigeoid	NA	EIGEN_GLO4C (360)	NA	NA	NA	NA	NA	SRTM 3" x 3"	NA	NA	3P	-0.066	0.092	0.000	0.035
Forsberg (2010)	RCR	quasigeoid	GRAVSOFIT	EGM2008 (360)	NA	NA	WG	RTM	SRTM 3" x 3"	NA	NA	none	-	-	-0.128	0.030	
	RCR	geoid	GRAVSOFIT	EGM2008 (2190) EGM 2008 (360)	NA	3°	WG	RTM	IGN height data base	no	no	none	-	-	-0.138	0.029	
Vaitý et al. (2012)	KTH	geoid	NA (may be Geolab)	EGM 2008 (360)	NA	3°	LSM	Combined topographic effect	IGN height data base	no	no	none	-	-	-0.336	0.038	
	RCR	quasigeoid	GEOCOL	EGM 2008 (360)	NA	1°	WG	RTM	SRTM 3" x 3"	NA	NA	1P	-0.209	-0.075	-0.133	0.030	
Yildiz et al. (2012)	KTH	quasigeoid	Geolab	EGM 2008 (360)	NA	1°	LSM	Combined topographic effect	SRTM 3" x 3"	no	no	4P	-0.067	0.058	0.000	0.029	
	RCR	quasigeoid	Geolab	EGM 2008 (360)	NA	1°	LSM	Combined topographic effect	SRTM 3" x 3"	no	no	1P	-1.118	-0.961	-1.040	0.035	
Janák et al. (2014)	FEM	quasigeoid	ANSYS	GOCE SGG/ TIM-R1 (224)	NA	NA	NA	NA	SRTM 1" x 1"	NA	NA	4P	-0.051	0.095	0.000	0.024	
	KTH	geoid	NA	GGM05S (180)	NA	NA	LSM	Combined topographic effect	SRTM 3" x 3"	yes	yes	4P	-0.068	0.073	-0.0004	0.028 (RMS)	

(Continued)

Table A1. Continued.

Reference	Approach	Type	Software	EGM (degrees)	0deg	Integration radius	Kernel	Terrain treatment	DEM/ density used	Atmos	Ellip	Fit type	Min	Max	Mean	STD
Abbak & Ustun (2015)	KTH	geoid	LSMSSOFT	ITG-GRACE2010S (120)	NA	1°	LSM	Combined topographic effect	ASTER 1" x 1" / SRTM 3" x 3"	yes	yes	4P	-0.065	0.072	-0.0003	0.028 (RMS) / 0.099
Foroughi et al. (2017a)	UNB	geoid	NA (may be SHGeo)	DIR_R5 (140)	NA	0.75°	VK	DTE, PITE, SITE	NA (may be SRTM 3" x 3")	yes	NA (may be yes)	7P none	-0.064 range	0.047 / 0.163	0.0005	0.025
Foroughi et al. (2017b)	UNB	geoid	NA (may be SHGeo)	DIR_R5 (160) / DIR_R5 (160)	NA	0.75° / 0.75°	VK / VK	DTE, PITE, SITE	SRTM 3" x 3" / density model	yes	yes	none / none	-	-	-	0.033 / 0.033
Janák et al. (2017)	UNB	geoid	NA (may be SHGeo)	DIR_R5 (160)	NA	0.75°	VK	DTE, PITE, SITE	SRTM 3" x 3" / ACE2; JGP95; JGP95; density model	yes	yes	none	0.028	0.207	0.124	0.034
Foroughi et al. (2019)	UNB	geoid	NA (may be SHGeo)	DIR_R5 (140)	NA	1°	VK	DTE, PITE, SITE	ACE2; density model	yes	yes	none	-0.030	-0.190	-0.130	0.033
Goli et al. (2019)	UNB	geoid	NA (may be SHGeo)	GOCO05S (280)	NA	1.5°	VK	DTE, PITE, SITE	SRTM 3" x 3" / SRTM 30" x 30"	NA	NA	none	0.043	0.206	0.124	0.034
Lin et al. (2019)	RBF (Free positioned point mass) / RCR / RBF (Fixed positioned point mass) / RCR	quasigeoid	GRAVSOF	EGM 2008 (360)	NA	NA	Modified VK / NA	RTM	SRTM 3" x 3"	NA	NA	none	0.046	0.205	0.124	0.033
This Study	KTH	quasigeoid	Geolab	DIR_R5 (240)	yes	1°	LSM	Not required	SRTM 3" x 3"	yes	yes	none	-0.922	-0.734	-0.819	0.036
												4P	-0.061	0.108	0.000	0.026

(Continued)

Table A1. Continued.

Reference	Approach	Type	Software	EGM (degrees)	Odeg	Integration radius	Kernel	Terrain treatment	DEM/density used	Atmos	Ellip	Fit type	Min	Max	Mean	STD
	CUT	quasigeoid	FFT1Dmod	DIR_R5 (240)	yes	1°	FEO	Terrain correction	SRTM 3" x 3"	yes	yes	none	-0.958	-0.788	-0.871	0.034
	CUT	quasigeoid	FFT1Dmod	EGM 2008 (360)	yes	1°	FEO	Terrain correction	SRTM 3" x 3"	yes	yes	4P none	-0.067	0.086	0.000	0.027
	CUT	quasigeoid	FFT1Dmod	EGM 2008 (2190)	yes	0.1°	FEO	Terrain correction	SRTM 3" x 3"	yes	yes	4P none	-0.070	0.083	0.000	0.027

Approach:

RCR = Remove-Compute-Restore

LSC = Least Squares Collocation

KTH = Royal Institute of Technology's method

UNB = University of New Brunswick's method

RBF = Radial Basis Function

FEM = Finite Element Method

CUT = Curtin University of Technology's method

Kernel modification:

WG = Wong-Gore (Wong and Gore 1969)

VK = Vaníček-Kleusberg (Vaníček and Kleusberg 1987)

Modified VK = Modified Vaníček-Kleusberg (Novak 2003)

LSM = Least-squares modification (Sjöberg 1984, 1991)

FEO = Featherstone-Evans-Oliver (Featherstone et al. 1998)

C.5: Preprint of the paper on Indian vertical deflections

Digitisation and analysis of historical deflections of the vertical in India

W.E. Featherstone^{1,2,*}, R. Goyal^{2,1}

1) School of Earth and Planetary Sciences, Curtin University of Technology, GPO Box U1987, Perth WA 6845, Australia; w.featherstone@curtin.edu.au

2) Department of Civil Engineering, Indian Institute of Technology Kanpur, Kanpur 208016, India; rupeshg@iitk.ac.in

Abstract

We describe the [somewhat tedious] process of digitising from a 1955 report that lists over 1500 vertical deflections in India and some surrounding countries. It turned out to involve detective work, not only for error-checking with closed-loop tests, but also some ambiguity surrounding the meridional vertical deflection at the Kalianpur origin of the datum. We transformed these Kalianpur coordinates to geocentric geodetic coordinates to compute absolute vertical deflections for future assessment of gravimetric geoid models. However, due to the many adjustments to the Everest spheroid and Kalianpur datum, we were restricted to abridged Molodensky transformation parameters for the 1975 Kalianpur datum and Everest 1956 spheroid based on only seven common points from the WGS84 technical manual. We compared these transformed absolute vertical deflections with EGM2008 and GGMplus (meridional standard deviation: $\pm 2''$; prime vertical standard deviation: $\pm 3''$), showing that digitisation of historical data is worthwhile.

Keywords: vertical deflections, India, Kalianpur datums, Everest spheroids, datum transformations

1. Introduction

The deflection (or deviation) of the vertical is the angular difference between the local gravity vector (direction of the plumbline at a point) and the surface normal of a reference ellipsoid. From Jekeli (1999), these are termed absolute deflections if a geocentric ellipsoid is used and relative deflections if a regional non-geocentric ellipsoid is used. Also, since the plumbline is curved and torsioned, the deflection varies as a function of position and height, leading to subtler definitions such as the Pizzetti deflection at the geoid, the Helmert deflection at the Earth's surface, or the Molodensky deflection with respect to the normal plumbline, all of which are described and explained in Jekeli (1999).

The vertical deflection is usually decomposed into north-south (ξ) and east-west (η) components, principally because how they are observed by comparing geodetic and astronomical coordinates (Eqs 1 and 2). The north-south component is also termed the meridional deflection (ξ) and the east-west component is termed the prime vertical deflection (η). The equations for astronomical observations are:

$$\xi = \Phi - \phi \quad (\text{north-south or meridional deflection}) \quad (1)$$

$$\eta = (\Lambda - \lambda) \cos \phi \quad (\text{east-west or prime vertical deflection}) \quad (2)$$

where Φ and Λ are the astronomical latitude and longitude determined with respect to the local gravity vector from precisely timed stellar observations, and ϕ and λ are the geodetic latitude and longitude from, in this case, the Great Arc triangulations conducted in India (Cook 1990; Keay 2001), as well as some astronomical observations of azimuth for Laplace stations.

The younger generation can be dismissive of historical reports, perhaps because they are not readily available in machine-readable portable document (PDF) format. However, reports can prove to be rich sources of data because of the meticulous attention to detail paid by geodetic surveyors at that time. In this short note, we describe the process of digitising and checking a Survey of India report by Gulatee (1955), which was typeset and produced using a printing press. Examples of similar compilations of historical vertical deflections are Featherstone and Olliver (2013), Featherstone et al. (2018) and Hirt and Wildermann (2018).

2. Digitisation and closed-loop checking

The only copy of Gulatee (1955) that we have access to for electronic sharing is a scanned image-only PDF. We provide this document as a supplement to this manuscript as the copyright will have expired. We have only digitised Table 1 because the other tables are brought into question of their accuracy by Gulatee (1955). This document is not of the highest quality. The paper has yellowed over time, probably due to the use of acids in paper production in the 1950s. The paper is also thin, meaning that the text on the overleaf page comes through in the scan as a silhouette (Figure 1). This makes automated optical character recognition (OCR) challenging as the silhouettes can be interpreted incorrectly as characters on the page subject to OCR.

Year	Geographic		Prime Vertical Deflection		Remarks
	Longitude	Latitude	Everest Spheroid	International Spheroid	
1929	77 43 27.27	17 52	+ 4.4	+ 4.5	431
1925	77 28 47.4	18.4	+ 3.4	+ 3.9	432
1929	77 28 29.4	18.5	+ 3.5	+ 3.8	433
1925	77 28 34.2	18.4	+ 0.8	+ 0.6	434
1926	77 28 33.2	17.3	+ 1.9	+ 1.9	435
..	77 41	18.52	437
..	77 32	18.29	438
..	77 28	18.21	439
..	77 44	17.50	440
..	77 42	18.21	441
..	77 38	17.52	442
1929	77 38 17.07	17.52	+ 2.89	+ 2.71	443
..	77 38 27.38	17.52	+ 2.89	+ 2.72	444
..	77 38	18.52	445
..	77 32	18.52	446
..	77 32	18.52	447
..	77 32	18.52	448
..	77 32	18.52	449
..	77 32	18.52	450
..	77 32	18.52	451
..	77 32	18.52	452
..	77 32	18.52	453
..	77 32	18.52	454
..	77 32	18.52	455
..	77 32	18.52	456
..	77 32	18.52	457
..	77 32	18.52	458
..	77 32	18.52	459
..	77 32	18.52	460
..	77 32	18.52	461
..	77 32	18.52	462
..	77 32	18.52	463
..	77 32	18.52	464
..	77 32	18.52	465
..	77 32	18.52	466
..	77 32	18.52	467
..	77 32	18.52	468
..	77 32	18.52	469
..	77 32	18.52	470
..	77 32	18.52	471
..	77 32	18.52	472
..	77 32	18.52	473
..	77 32	18.52	474
..	77 32	18.52	475
..	77 32	18.52	476
..	77 32	18.52	477
..	77 32	18.52	478
..	77 32	18.52	479
..	77 32	18.52	480
..	77 32	18.52	481
..	77 32	18.52	482
..	77 32	18.52	483
..	77 32	18.52	484
..	77 32	18.52	485
..	77 32	18.52	486
..	77 32	18.52	487
..	77 32	18.52	488
..	77 32	18.52	489
..	77 32	18.52	490
..	77 32	18.52	491
..	77 32	18.52	492
..	77 32	18.52	493
..	77 32	18.52	494
..	77 32	18.52	495
..	77 32	18.52	496
..	77 32	18.52	497
..	77 32	18.52	498
..	77 32	18.52	499
..	77 32	18.52	500

Figure 1: Title page and data page of the Survey of India report by Gulatee (1955) showing the relative transparency of the paper that caused problems for the OCR process.

We first attempted the OCR embedded in Adobe™ Acrobat Pro™, but this was unsuccessful as many parts of the tables were interpreted as smaller sub-images, so not fully digitised as text and numerical values. Therefore, we had to resort to brute-force manual digitisation. As this is imperfect, we had to devise some closed-loop tests to not only verify our manual digitisation, but also to check for typographical errors in Gulatee (1955). Some glaring errors were easy to detect, usually due to mis-registration of a row in a column. These were corrected manually by visual comparison with Gulatee's report.

The closed loop testing involved calculating the meridional and prime vertical deflections for the Everest 1830 spheroid (semi-minor axis 6,377,276 m, inverse flattening 300.8017) from the geodetic and astrogeodetic coordinates provided by Gulatee. Not all stations had both deflection components. Out of the 1071 stations listed, 707 points are in India of which 701 have meridional deflections and 280 have prime vertical deflections.

We compared our computed deflections with the digitised deflections from Gulatee (1955). The first striking observation was a systematic difference of $\sim 3''$ in the prime vertical deflections. This is where the detective work began. Reading Gulatee's introductory text of only nine pages is particularly telling. He identifies the source of this discrepancy to a sequence of blunders which, because they are so small, went unnoticed. In short, the astronomical azimuth used to determine the prime vertical deflection at the Kalianpur origin station was not applied, leading to an error in longitudes of $2.89''$ (cf. Malys et al. 2015). After subtracting this value, there was much closer agreement between the computed and tabulated prime vertical deflections.

The next stage was to search for extrema, which was done through plotting the differences and identifying "outlying" points. This was done in Microsoft™ Excel™, which identifies the row number when

the mouse cursor is hovered over the point in question. This served two purposes. The rouge points were first checked for manual digitisation errors, which located only about 20 errors, showing the first-run to have been proportionally successful (98% success rate).

Once these large errors were identified and corrected, the more interesting detective work could begin. Again using plots, we could concentrate on smaller spurious values. This identified what seems to be just one typographical error in the original report (point 190, Reban HS), where the meridional deflection should be -8.0" not +8.0". This was detected by changing the sign and re-inspecting the closed loop. We acknowledge that given the large amount of numbers that had to be typeset, this is testament to the fastidiousness of the people at that time.

During this closed loop testing, a few other points appeared anomalous but not by a substantial amount (using an arbitrarily chosen threshold of 0.5" difference between the digitised and computed values). We visually cross-checked against Gulatee (1955) and could not find any transcription errors for any of them, so they could simply be surveying errors. We have no proof either way. As such, we have left them in the dataset, but flag them as "questionable" using red font in the spreadsheet provided with this article as electronic supplementary material.

- For the meridional deflections, they are: 750 Majurguda; 766 Hathhena; 792 Ramnagar TS.
- For the prime vertical deflections, they are: 222 Rirana TS; 391 Nojli; 393 Kaliana; 394 Titaora; 395 Saini; 427 Lut; 837 Takht Sindhu Resec; 871 Tilabani; 1067 Kandaw.

Figure 2 shows the coverage of the digitised data.

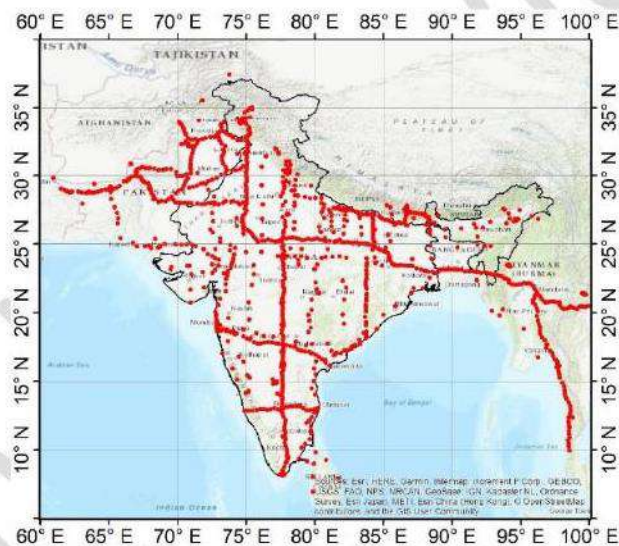


Figure 2: Coverage of the vertical deflections digitised from Gulatee (1955)

3. Transformation from relative to absolute deflections

Not unlike many other countries, modern geodetic data in India is restricted from public/open access. As such, we do not have observed geodetic coordinates in a geocentric datum for any of the 1071 astrogeodetic stations listed by Gulatee. Therefore, we had to rely on a datum transformation based on published parameters. We interrogated several publications and databases, principally the WGS84 technical manual (NIMA 2004 page b3-2) and the EPSG (<https://epsg.org/home.html>), which led to the need for further detective work.

Firstly, there have been many readjustments of the Everest spheroid and the Kalianpur datum (e.g., Anon 1919; Bomford 1939; Mugnier 2014). Probably the most significant is the change of the semi-major axis of the Everest spheroid because of a disparity between the conversion from Indian definition of the imperial foot to metres and the British definition. Secondly, while there have been other estimations of transformation parameters, they have not been published, only their evaluation (e.g., Singh 2002; Ramalingam and Srivastava 2003; Sunehra 2013).

As such, we had to make some assumptions, not only about the datum, but also about the semi-major axis of the Everest spheroid, which we will discuss further in section 4. While there are other ways to transform gravity field functionals between ellipsoids (e.g., Kotsakis 2008), the abridged Molodensky transformation parameters that we have access to are only for the Kalianpur 1975 datum and Everest 1956 spheroid, so we simply took these as a proxy.

The abridged Molodensky transformation parameters for Kalianpur 1975 in the WGS84 technical manual and EPSG database (code #1156) are identical (Table 1). Notably, the parameters are determined from only seven common stations, hence the uncertainty is rather high. This translates to about 18 m on the ground, which equates to approximately half an arc-second in the vertical deflections. We used the trial version of Blue Marble Geographics™ Geographic Calculator™, which uses the same parameters as in Table 1.

Table 1: Molodensky transformation parameters from Kalianpur 1975 to WGS84 for the Everest 1956 spheroid

Δa	$\Delta f \times 10^4$	ΔX	ΔY	ΔZ	a	$1/f$
835.757 m	0.28361368	295±12 m	736±10 m	257±15 m	6,377,301.243 m	300.8017

4. Comparison with EGM2008 and GGMplus

We used the transformed WGS84 geocentric coordinates and heights provided in Gulatee (1955) converted from Indian feet to metres (using 3.280857187 derived from Gulatee's page 1), but noting that many of the heights are approximate, to synthesise EGM2008 Helmert vertical deflections at the Earth's surface using the ICGEM calculation service (<http://icgem.gfz-potsdam.de/calcpoints>). At these locations, we also extracted the values of north-south and east-west components of vertical deflections from the GGMplus dataset (Hirt et al., 2013). GGMplus provides the Helmert's vertical deflection components by taking the latitudinal and longitudinal derivative of the quasigeoid. For Pizzetti's vertical deflection, the derivatives are taken on the geoid. Table 2 shows descriptive statistics of the differences (absolute astrogeodetic deflections minus EGM2008 and GGMplus) and Figure 3 shows the differences versus latitude, longitude and height.

From Figure 3, there are no discernible trends, showing that the use of the Kalianpur 1975 datum transformation parameters and Everest 1956 spheroid have not introduced a bias or tilt between the deflections datasets. This is expected as the change in semi-minor axis only affects scale and not angles. From Table 2, there is no bias (mean zero for each deflection component). The maxima and minima may appear large, but the astronomical deflections were observed many decades ago when chronology was not so accurate and star catalogues were less mature. In addition, EGM2008 (Pavlis et al. 2012, 2013) uses proprietary data over India to spherical harmonic degree and order 900, supplemented by residual terrain modelling of the topographical gravitational attraction. As such, there are two compounding contributors to the descriptive statistics: historical data and modelled instead of observed high-frequency gravity data.

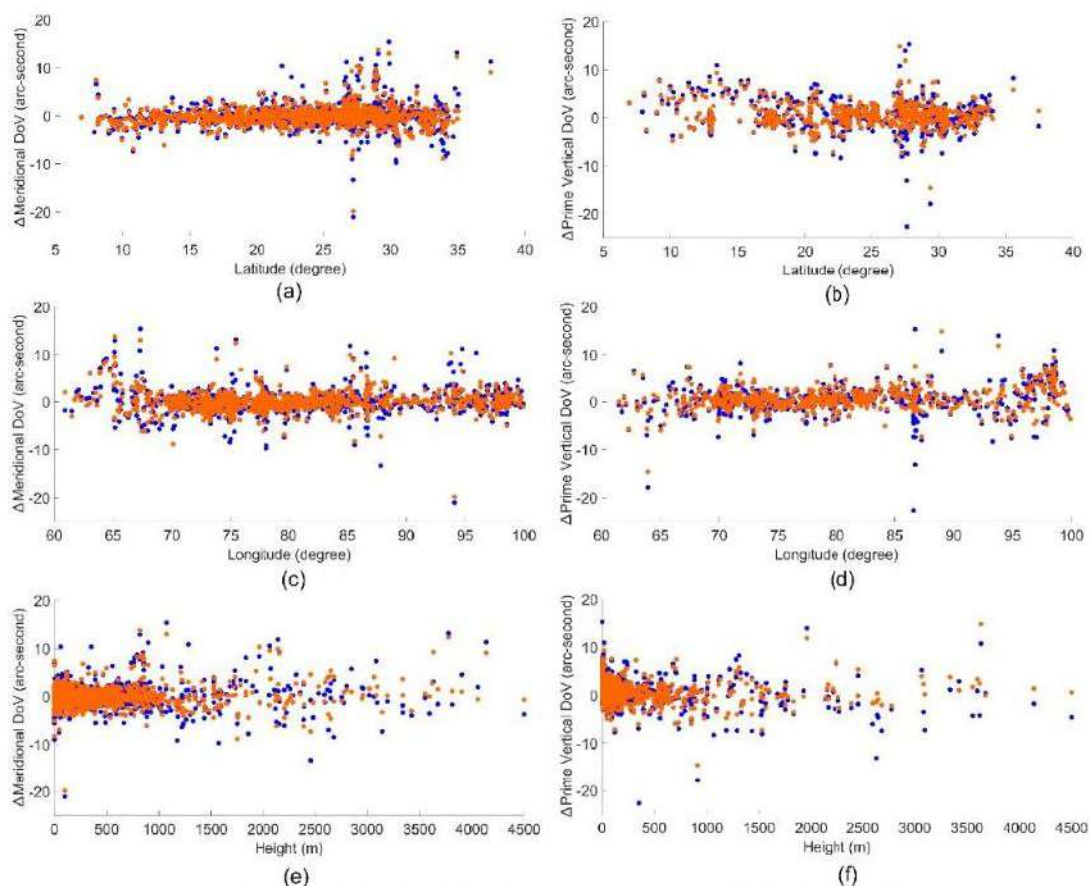


Figure 3: Differences between absolute vertical deflections and EGM2008 (blue circles) and GGMplus (orange circles) versus: a-b) latitude, c-d) longitude and e-f) height in metres.

Table 2: Descriptive statistics of the differences between absolute vertical deflections and EGM2008 and GGMplus in arc-seconds, both on WGS84. Though we provide two decimal places in parentheses, they should be neglected as the precision of the astronomical observations is probably around one arc-second and the transformation introduces around one-half of an arc-second.

		Max	Min	Mean	STD
EGM2008	Meridional deflections	15(.39)''	-21(.02)''	-0(.12)''	±2(.50)''
	Prime vertical deflections*	15(.32)''	-22(.69)''	0(.47)''	±3(.18)''
GGMplus [#]	Meridional deflections	13(.75)''	-19(.87)''	-0(.08)''	±2(.15)''
	Prime vertical deflections*	14(.86)''	-14(.60)''	0(.60)''	±2(.56)''

* Two points (Point nos. 292 and 518) having Prime vertical deflection value of -29'' and -41'' are not considered in calculating the descriptive statistics.

[#] GGMplus does not cover Point no. 790. It is ~30 m northwards or ~105 m eastwards from the closest area covered by GGMplus. This may be possibly due to the limitations of our transformation of coordinates.

5. Concluding remarks

We have: (i) manually digitised a scanned hardcopy report from the Survey of India by Gulatee (1955) of vertical deflections, (ii) devised some closed-loop checks to identify our and other errors, (iii) transformed the relative deflections from the Kalianpur datum to absolute deflections on WGS84 (albeit using a less-than-ideal approach), and then compared (iv) these absolute deflections to those synthesised from EGM2008 and GGMplus.

Though this was quite a tedious process, we feel that our effort was worthwhile to share such a “geodetic commodity”. Given the vintage of the astrogeodetic data in India, our use of an inexact datum transformation, and the use of proprietary and modelled gravity data in EGM2008 and GGMplus, there appear to be no biases. The standard deviations of $\pm 2''$ and $\pm 3''$ could be considered, by some, as quite remarkable given the ranges of topography and vertical deflections in India.

Acknowledgements

We would like to thank (i) Librarians at Curtin University and the National Library of Australia in Canberra for providing the scanned copy of Gulatee’s report, (ii) Don Abbey for assistance with interrogating the PEGS Microsoft™ Access™ database to locate transformation parameters, (iii) the EPSG for its comprehensive data compilation, (iv) Blue Marble Geographics™ for providing a gratis demonstration licence to use Geographic Calculator™, and (v) ICGEM for providing its online facility for synthesising gravity field functionals.

Data availability statement

All data used during this study are now in the public domain through our provision of electronic supplementary materials attached to this article.

Disclosure statement

No potential conflict of interest is reported by the authors.

Notes on contributors

Will Featherstone is Professor of Geodesy at Curtin University, with diverse interests in many aspects of geodesy.

Ropesh Goyal is a jointly enrolled PhD candidate at IIT-Kanpur and Curtin University studying geoid computations for the entire Indian subcontinent.

ORCID

Will Featherstone <http://orcid.org/0000-0001-9644-4535>

Ropesh Goyal <http://orcid.org/0000-0002-2178-3265>

References

- Anon (1919) The figure of the Earth, *Nature*, 2594(103): 381. <https://doi.org/10.1038/103381a0>
- Bomford G (1939) The readjustment of the Indian triangulation, Professional Paper 28, Survey of India, Dehradun, 136pp.
- Cook A (1990) The achievements of Sir George Everest in geodesy, *Survey Review*, 30(238), 368-374, <https://doi.org/10.1179/sre.1990.30.238.368>
- Featherstone WE, Brown NJ, McCubbine JC, Filmer MS (2018) Description and release of Australian gravity field model testing data, *Australian Journal of Earth Sciences* 65(1), 1-7, <https://doi.org/10.1080/08120099.2018.1412353>.
- Featherstone WE, Olliver JG (2013) Assessment of EGM2008 over Britain using vertical deflections, and problems with historical data, *Survey Review* 45(332): 319-324, <https://doi.org/10.1179/1752270613Y.0000000048>.
- Gulatee BL (1955) Deviation of the vertical in India, Technical Paper 9, Survey of India, Dehradun, 147pp.
- Hirt C, Claessens S, Fecher T, Kuhn M, Pail R, Rexer M (2013). New ultrahigh-resolution picture of Earth’s gravity field, *Geophysical Research Letters* 40(16), 4279–4283. <https://doi.org/10.1002/grl.50838>
- Hirt C, Wildermann E (2018) Reactivation of the Venezuelan vertical deflection data set from classical astrogeodetic observations, *Journal of South American Earth Sciences* 85, 97-107, <https://doi.org/10.1016/j.jsames.2018.05.003>.
- Jekeli C (1999) An analysis of vertical deflections derived from high-degree spherical harmonic models, *Journal of Geodesy* 73(1), 10-22, <https://doi.org/10.1007/s001900050213>.
- Keay J (2001) *The Great Arc: The dramatic tale of how India was mapped and Everest was named*, Harper Perennial, 224pp.

- Kotsakis C (2008) Transforming ellipsoidal heights and geoid undulations between different geodetic reference frames, *Journal of Geodesy* 82(4-5), 249-260, <https://doi.org/10.1007/s00190-007-0174-9>.
- Malys S, Seago JH, Pavlis NK, Seidelmann PK, Kaplan GH (2015) Why the Greenwich meridian moved, *Journal of Geodesy* 89(12): 1263-1272, <https://doi.org/10.1007/s00190-015-0844-y>.
- Mugnier CJ (2014) Grids & Datums: Republic of India, *Photogrammetric Engineering and Remote Sensing* 80: 209-211.
- NIMA - National Imagery and Mapping Agency (2004) Department of Defense World Geodetic System 1984, its definition and relationships with local geodetic systems, Technical Report 8350.2, Washington, USA.
- Pavlis NK, Holmes SA, Kenyon SC, Factor JK (2012) The development and evaluation of the Earth Gravitational Model 2008 (EGM2008). *Journal of Geophysical Research – Solid Earth* 117(B4), B04406, <https://doi.org/10.1029/2011JB008916>.
- Pavlis NK, Holmes SA, Kenyon SC, Factor JK (2013) Correction to the development and evaluation of the Earth gravitational model 2008 (EGM2008). *Journal of Geophysical Research – Solid Earth* 118(B5), 2633–2633, <https://doi.org/10.1002/jgrb.50167>.
- Ramalingam K, Srivastava BK (2003) Error estimates for WGS-84 and Everest (India-1956) transformation, *Map Asia Conference 2003*
- Singh SK (2002) Coordinate transformation between Everest and WGS-84 datums - A parametric approach, *Proceedings of Asian GPS*,
- Sunehra D (2013) Validation of algorithms for datum transformations and map projections, *International Journal of Scientific & Engineering Research* 4(6), 376-381.

C.6: Proof-read version of the paper on Indian gravimetric geoid model

Terr. Atmos. Ocean. Sci., Accepted Manuscript

doi: 10.3319/TAO.2021.08.10.02

An experimental Indian gravimetric geoid model using Curtin University's approach

Ropesh Goyal^{1,2,*}, Will E. Featherstone^{1,2}, Sten J. Claessens², Onkar Dikshit¹, and Nagarajan Balasubramanian¹

¹Department of Civil Engineering, Indian Institute of Technology Kanpur, Kanpur, India

²School of Earth and Planetary Sciences, Curtin University of Technology, Perth, Australia

Article history:

Received 05 May 2021

Revised 5 August 2021

Accepted 10 August 2021

Keywords:

Geoid, Quasigeoid, India, Curtin University's approach

Citation:

Goyal, R., W. E. Featherstone, S. J. Claessens, O. Dikshit, and N. Balasubramanian, 2021: An experimental Indian gravimetric geoid model using Curtin University's approach. *Terr. Atmos. Ocean. Sci.*, 32, 1-15, doi: 10.3319/TAO.2021.08.10.02

ABSTRACT

Over the past decade, numerous advantages of a gravimetric geoid model and its possible suitability for the Indian national vertical datum have been discussed and advocated by the Indian scientific community and national geodetic agencies. However, despite several regional efforts, a state-of-the-art gravimetric geoid model for the whole of India remains elusive due to a multitude of reasons. India encompasses one of the most diverse topographies on the planet, which includes the Gangetic plains, the Himalayas, the Thar desert, and a long peninsular coastline, among other topographic features. In the present study, we have developed the first national geoid and quasigeoid models for India using Curtin University's approach. Terrain corrections were found to reach an extreme of 187 mGal, Faye gravity anomalies 617 mGal, and the geoid-quasigeoid separation 4.002 m. We have computed both geoid and quasigeoid models to analyse their representativeness of the Indian normal-orthometric heights from the 119 GNSS-levelling points that are available to us. A geoid model for India has been computed with an overall standard deviation of ± 0.396 m but varying from ± 0.03 to ± 0.158 m in four test regions with GNSS-levelling data. The greatest challenge in developing a precise gravimetric geoid for the whole of India is data availability and its preparation. More densely surveyed precise gravity data and a larger number of GNSS/levelling data are required to further improve the models and their testing.

1. INTRODUCTION

Ideally, Stokes's (1849) integral should be implemented over the entire Earth with continuous gravity anomalies on the geoid and with the condition that there must not be any gravitating masses above it. However, in practice, the availability of gravity observations is limited to a specific area, so the integration domain has to be truncated. Also, the gravity anomalies usually exist discontinuously on or above the Earth's surface so various types of downward continuation and regularisation have been proposed. The gaps between theoretical and practical aspects induce several kinds of errors, which geodesists have tried to reduce, but usually requiring assumptions and approximations.

Based on various ideas, philosophies and numerical

approaches, what we consider the four most commonly used approaches/techniques are adopted for geoid computation experiments in India. (1) Geoid/quasigeoid computation methodology developed at the University of Copenhagen, Denmark (Forsberg 1984, 1985; Forsberg and Tscherning 2008) implemented in the public-domain GRAVSOFT package, (2) the Stokes-Helmert method developed at the University of New Brunswick (UNB), Canada (Vaníček and Kleusberg 1987; Vaníček and Martinec 1994; Vaníček et al. 1999; UNB 2002; Ellmann and Vaníček 2007), (3) the Least Squares Modification of Stokes formula with Additive Corrections (LSMSAC) method developed at the Royal Institute of Technology (KTH), Sweden (Sjöberg 1984, 1991, 2003; Ågren 2004), and (4) geoid/quasigeoid computation methodology developed at Curtin University of Technology (CUT), Australia (Featherstone 2000, 2003; Featherstone et

* Corresponding author
E-mail: ropeshg@iitk.ac.in

al. 1998, 2001, 2011, 2018). There are of course other approaches, such as radial basis functions (e.g., Li 2018; Liu et al. 2020), but perhaps not yet applied as widely. The application areas of the above four approaches are listed in Goyal et al. (2021b).

For India, the first geoid map was developed more than five decades ago. It was based on astrogeodetic observations (Fischer 1961) and with respect to the Everest 1956 ellipsoid (cf. Singh and Srivastava 2018). No more information is available on this geoid, apart from distorted hardcopy contour maps that are difficult to digitise reliably. The levelled height information presently available in India is more than a century old. When these heights were observed, neither the concept of foresight and backsight levelling nor the use of invar staves were considered. Observed gravity values were not available as this was before the development of the low-cost portable relative gravimeter. The Indian vertical datum defined in 1909 was based on constraining the levelling to nine tide-gauges along the Indian coast to zero height (Burrard 1910). We will show later that this approach may have caused a north-south tilt (cf. Fischer 1975, 1977), most probably due to the ocean's time-mean dynamic topography (cf. Featherstone and Filmer 2012).

Frequent seismic activity in various parts of the Indian sub-continent and so-caused crustal movement also necessitate the introduction of a new height system, probably to be based on geopotential numbers and Helmert's orthometric heights (or 'rigorous' orthometric heights as formulated by Santos et al. 2006). The Survey of India (SoI) carried out a re-levelling program (2007 – 2017) with gravity observations at fundamental benchmarks to provide a densified network of Helmert's orthometric heights as a part of the Redefined Indian Vertical Datum 2009 (G&RB 2018; Singh 2018). However, these data are not yet in the public domain, so we are unable to use them to validate our geoid and quasigeoid models. In addition, the national geodetic agencies have proposed to compute a precise national geoid model to serve as the new vertical datum for the country. This can be viewed as following the suit of New Zealand (LINZ 2016), Canada (Véronneau and Huang 2016), and the USA (NGS 2017, 2019). Such an approach is being considered in many other countries too.

Researchers and government organisations have made some efforts to develop local gravimetric geoid models for regions in India (Singh 2007; Carrion et al. 2009; Srinivas et al. 2012; Mishra and Ghosh 2016; Singh and Srivastava 2018), but only using the GRAVSOFTE package with residual terrain modelling (Forsberg 1985). Despite these efforts, a state-of-the-art national gravimetric geoid model for the whole India remains elusive (Goyal et al. 2017). Therefore, in this study, we present the first-ever nationwide geoid and quasigeoid computation results over India with the available data sets using the CUT method implemented using our own computation package developed in MATLAB™.

2. DATASETS

2.1 Terrestrial Gravity

Pointwise observed gravity data is confidential in India. Therefore, with this predicament, we obtained a grid of Indian terrestrial gravity data from GETECH (<https://getech.com/>) that is claimed to come from the Gravity Map Series of India (GMSI), a joint project of five Indian organisations, viz., SoI, Geological Survey of India (GSI), Oil and Natural Gas Corporation (ONGC), National Geophysical Research Institute (NGRI), and Oil India Limited (cf. Tiwari et al. 2014). The GETECH gravity data comprises a $0.02^\circ \times 0.02^\circ$ grid of simple Bouguer gravity anomalies over India (except a for few regions in northern India), with an overall estimated precision of ± 1.5 mGal (GETECH 2006). According to the GETECH manual for Indian gravity data, they used (1) the normal gravity formula from WGS84 (Macomber 1984)

$$\gamma_{0, \text{WGS84}} = 978032.67714 \left(\frac{1 + 0.00193185438639 \sin^2 \phi}{\sqrt{1 - 0.00669437999013 \sin^2 \phi}} \right) \text{ mGal} \quad (1)$$

(2) a second-order free-air correction given by

$$\delta g_{\text{FAC}}^{\text{GETECH}} = (0.3083293357 + 0.0004397732 \cos^2 \phi) h - 7.2125 \times 10^{-8} h^2 \text{ mGal} \quad (2)$$

(3) the following atmospheric correction (Ecker and Mittermayer 1969)

$$\delta g_{\text{atm}}^{\text{GETECH}} = \begin{cases} 0.87 e^{-0.116H^{\text{at}}} \text{ mGal}, & H > 0 \text{ km} \\ 0.87 \text{ mGal}, & H \leq 0 \text{ km} \end{cases} \quad (3)$$

and (4) the simple planar Bouguer correction

$$\delta g_{\text{BC}}^{\text{GETECH}} = -0.04191 \rho H \text{ mGal} \approx -0.1119 H \text{ mGal} \quad (4)$$

where $\gamma_{0, \text{WGS84}}$ is normal gravity on the WGS84 level ellipsoid, $\delta g_{\text{FAC}}^{\text{GETECH}}$ is the free-air correction, ϕ is the geodetic latitude, h is the ellipsoidal height (in m), H is the elevation [in km for Eq. (3) and m for Eq. (4)], $\delta g_{\text{atm}}^{\text{GETECH}}$ is the atmospheric correction, $\delta g_{\text{BC}}^{\text{GETECH}}$ is the planar Bouguer correction and ρ is the constant topographical density of 2670 kg m^{-3} . We re-computed the free-air gravity anomalies (Δg) from the GETECH data so as to be more compatible with the CUT approach by using

$$\Delta g = \Delta g_{SSA}^{GETECH} + 0.1119H + \gamma_{0, WGS84} - \delta g_{FAC}^{GETECH} - \delta g_{alm}^{GETECH} - \gamma_{0, GRS80} + \delta g_{FAC}^{CUT} + \delta g_{alm}^{CUT} \quad (5)$$

where, Δg_{SSA}^{GETECH} are simple Bouguer anomalies from GETECH and

$$\delta g_{FAC}^{CUT} = \gamma_{0, GRS80} \left[\frac{2}{a} (1 + f + m - 2f \sin^2 \phi) H - \frac{3}{a^2} H^2 \right] \quad (6)$$

$$\gamma_{0, GRS80} = \gamma_{\sigma} \left(\frac{1 + k \sin^2 \phi}{\sqrt{1 - e^2 \sin^2 \phi}} \right) \quad (7)$$

$$\delta g_{alm}^{CUT} = 0.871 - 1.0298 \times 10^{-4} H + 5.3105 \times 10^{-9} H^2 - 2.1642 \times 10^{-13} H^3 + 9.5246 \times 10^{-18} H^4 - 2.2411 \times 10^{-22} H^5 \quad (8)$$

For GRS80, $a = 6378137$ m, $e^2 = 0.0066943800229$, $m = 0.0034478600308$, $f = 1/298.257222101$ and $\gamma_{\sigma} = 978032.67715$ mGal, $k = 0.001931851353$ (Moritz 2000). The descriptive statistics of the differences between the free-air anomalies from the GETECH data and re-computed free-air anomalies are (in mGal): min = -0.001, max = 0.188, mean = 0.002, STD = ± 0.007 . It should be noted that we have used H instead of h (ellipsoidal heights) in Eq. (2) because we believe that there might be a typographical error in the GETECH manual. The rationale being that with the

use of h we would obtain gravity disturbances and not gravity anomalies (cf. Hackney and Featherstone 2003). A blanket accuracy estimate of the reconstructed free-air anomalies from the GETECH Bouguer anomalies is ± 2.4 mGal, calculated using the DEM error in the CUT reconstruction technique as per $\sigma_{FA} = \sqrt{(1.5 \times 10^{-5})^2 + (2\pi G \rho \times 17.3)^2}$.

For the oceanic regions surrounding India, we used free-air gravity anomalies (Version 28.1) from the Scripps Institute of Oceanography (SCRIPPS, https://topex.ucsd.edu/marine_grav/mar_grav.html) which has an overall root mean square error of ± 1.23 mGal (Sandwell et al. 2021). The SCRIPPS data is also accompanied with an error grid that we have shown, for our study area, in Fig. 1. The data contains a $1' \times 1'$ grid that also covers the land, but we used the SCRIPPS data only for the oceanic region because the land data, in the SCRIPPS dataset, is from EGM2008 to avoid aliasing (Gibbs fringing) at the coasts.

We do not have gravity data from the countries neighbouring India and a well distributed sufficient data coverage is not available in the Bureau Gravimetric International (<https://bgi.obs-mip.fr/>) archives either (Country: no. of gravity data points - Pakistan: 1270, Bangladesh: 25, Sri Lanka: 48, Myanmar: 71, Afghanistan: 1649, China: 446, Nepal: 617, and Bhutan: 0). Therefore, we constructed a $0.02^\circ \times 0.02^\circ$ grid of free air anomalies over land using EGM2008 (Pavlis et al. 2012, 2013) up to degree and order (d/o) 900 to fill-in the land gravity anomaly data in and around India where the GETECH data is not available, including Nepal, China, Pakistan, Sri Lanka, Bangladesh, Bhutan, Afghanistan, and Myanmar. The specific d/o 900

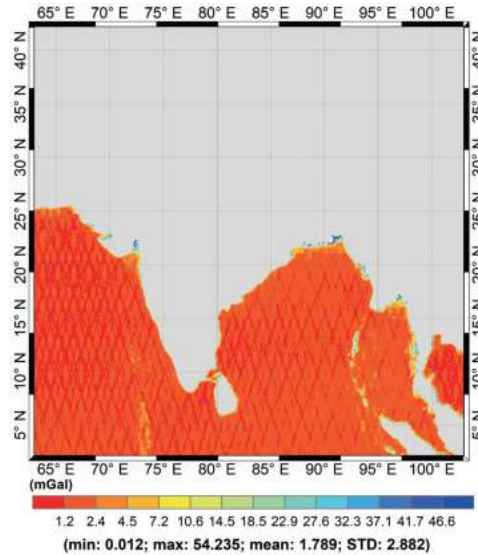


Fig. 1. Error map of the SCRIPPSv28.1 marine gravity-anomaly data (units in mGal).

was chosen because EGM2008 uses proprietary data up to d/o 900 (Pavlis et al. 2013).

As discussed next, we merged these three datasets to get a complete free-air gravity anomaly grid of $0.02^\circ \times 0.02^\circ$, avoiding aliasing or the contamination of land data (both GETECH and EGM2008 individually) with the marine data or vice-versa.

There exist numerous sophisticated space-domain and frequency-domain methods for merging heterogeneous gravity anomaly datasets (e.g., Strykowski and Forsberg 1998; Olesen et al. 2002; Catalao 2006; McCubbine et al. 2017). However, we chose to work with the comparatively straightforward CUT space-domain method (cf. Featherstone et al. 2011, 2018). This choice is somewhat arbitrary because we are working with the land gravity of unknown quality, and the strategy that we use has already been implemented in the computation of the Australian quasigeoid, which is an island nation and approximately 2.3 times larger than India. Other methods can also be tested, but it is left for the time when sufficient marine and airborne gravity data along with reliable terrestrial gravity data will be available over India.

In the adopted method, the GETECH-derived free-air anomaly grid is superimposed over the EGM2008 (d/o 900) derived gravity anomalies. The gravity anomalies of the latter dataset at the overlapping grid nodes are replaced by the gravity anomalies from the former dataset. As a result, a $0.02^\circ \times 0.02^\circ$ grid of gravity anomalies on the land is obtained.

To concatenate the land and marine gravity anomaly data, $1' \times 1'$ gravity anomalies in the ocean are clipped (or separated) from the complete SCRIPPS dataset, i.e., on both ocean and land. It is then block averaged to the $0.02^\circ \times 0.02^\circ$ grid and is superimposed with the land gravity anomaly grid. The former values were replaced by the latter at overlapping nodes to obtain the $0.02^\circ \times 0.02^\circ$ grid of the merged gravity anomalies. Figure 2 shows the merged free-air gravity anomaly map. To check for any discontinuities at the edges of the merged datasets, we computed and plotted the arctangent (Fig. 3a) and logarithmic (Fig. 3b) values of the gradients of the merged data. We observe no clear visual indication of any discontinuities at the boundaries of the merged data, but also partially due to the ruggedness of the dataset in our study area that can be obscuring.

2.2 Digital Elevation Model

The Digital Elevation Model (DEM) is another important input in geoid computation. It is mainly used to compute the topographical effects (e.g., Forsberg 1984). Thus, a precise high-resolution DEM should be used. We would like to mention here that DEM is generally used synonymously with a Digital Surface Model (DSM) (e.g., SRTM, ASTER), but this should be avoided. Quantification of the differences in the topographical effect with the use of DEM

and DSM has been investigated by Yang et al. (2019). Since India does not have a national DEM, therefore, after a DEM/DSM analysis (Goyal et al. 2021a), it was decided to work with the best available DEM over India, i.e., the MERIT $3'' \times 3''$ DEM (Yamazaki et al. 2017), for our computations. Though the accuracy of the MERIT DEM varies considerably (± 11.7 to ± 47.3 m) over different landforms in India, an overall estimate for the whole of India is ± 17.3 m (Goyal et al. 2021a).

2.3 GNSS-Levelling

India has different horizontal and vertical control networks. Therefore, presently there are only a limited number of ground control points where we have the geodetic coordinates (latitude, longitude, ellipsoidal heights) and levelled heights. Moreover, due to several restrictions on the datasets, only a few of these available data points were available to us (Fig. 4). The datasets in the Uttar Pradesh west (UP west) and Uttar Pradesh east (UP east) regions were procured from SoI, while the datasets over Hyderabad and Bangalore have been retrieved from Mishra (2018), who also used the SoI dataset. According to Mishra (2018), horizontal and vertical precisions of GNSS data are within ± 12 to ± 26 mm and ± 31 to ± 53 mm, respectively. The vertical precision of the levelling heights is not known to us, but they are from the high precision first level net of India. These heights are from the Indian Vertical Datum 1909 (Burrard 1910) and are based on the normal-orthometric height system, while those on Indian Vertical Datum 2009 (G&RB 2018) are based on Helmert's orthometric height system. We have not been provided with a clear indication on which heights have been provided to us, and therefore, due to this anonymity of the height system, we consider the levelling heights to be in the normal-orthometric height system (Jekeli 2000; Featherstone and Kuhn 2006).

3. METHODOLOGY AND RESULTS

An overview of the CUT methodology for computing the geoid undulations is shown by a flowchart in Fig. 5. The CUT method primarily computes the quasigeoid using the analytical continuation solution (Moritz 1971, 1980) of Molodensky's problem (Molodensky et al. 1962). Moritz (1971) showed that Molodensky's G_1 term can be approximated by the planar terrain correction (TC), which also needs an additional term that is equal to the first-order indirect effect (FOIE). We could not adopt the full CUT method-based reconstruction of Faye anomalies (Featherstone and Kirby 2000) because we already have gridded data, whereas CUT grids point Bouguer anomalies. Instead, we added the block averaged $0.02^\circ \times 0.02^\circ$ grid of TCs (Fig. 6a) to the free-air gravity anomaly grid to calculate area-mean Faye anomalies (Fig. 6b). The block-averaged $0.02^\circ \times 0.02^\circ$

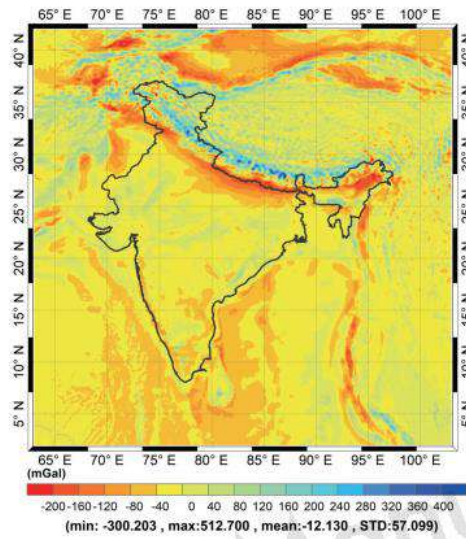


Fig. 2. Merged gravity anomaly data from GETECH, EGM2008 (d/o 900), and SCRIPPS (units in mGal).

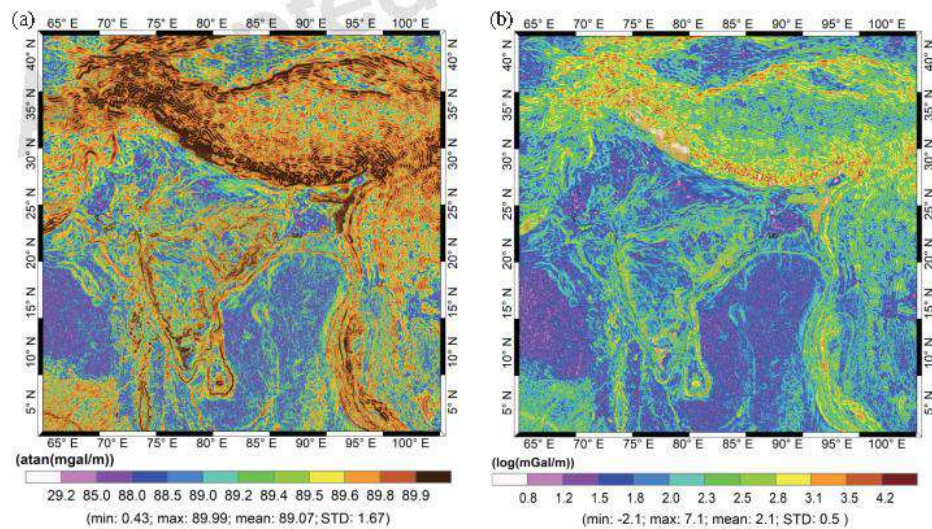


Fig. 3. Aretangent (a) and logarithmic (b) plot of gradients of merged gravity anomaly data to attempt to identify discontinuities at the edges of the merged grids.

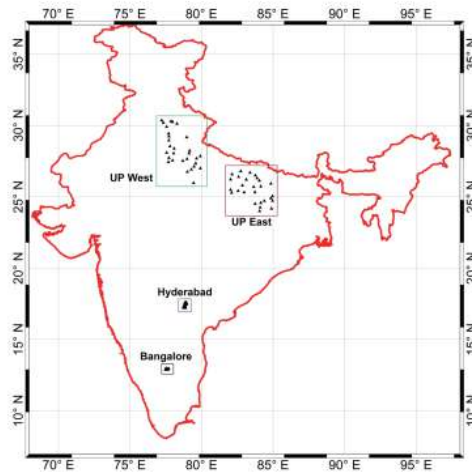


Fig. 4. Spatial coverage of the available 119 GNSS/levelling data points

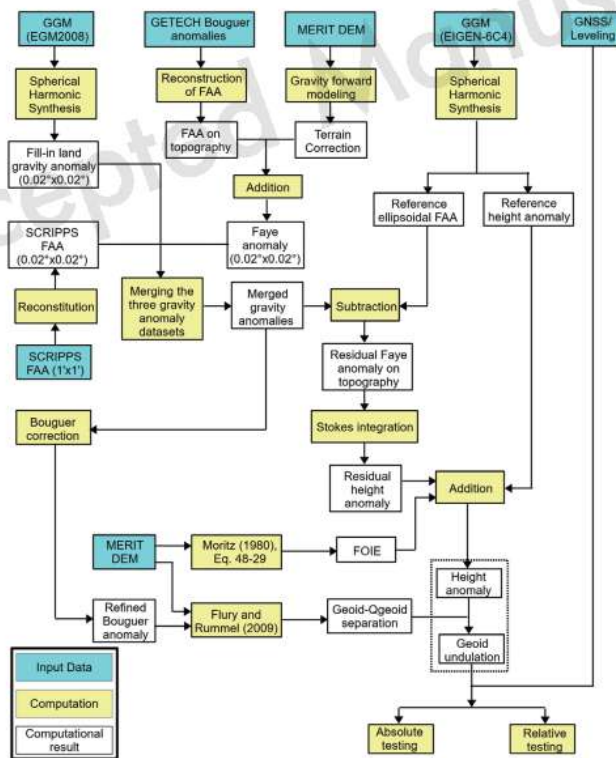


Fig. 5. Flowchart of the CUT methodology of geoid/quasigeoid computation as applied in India for these experiments.

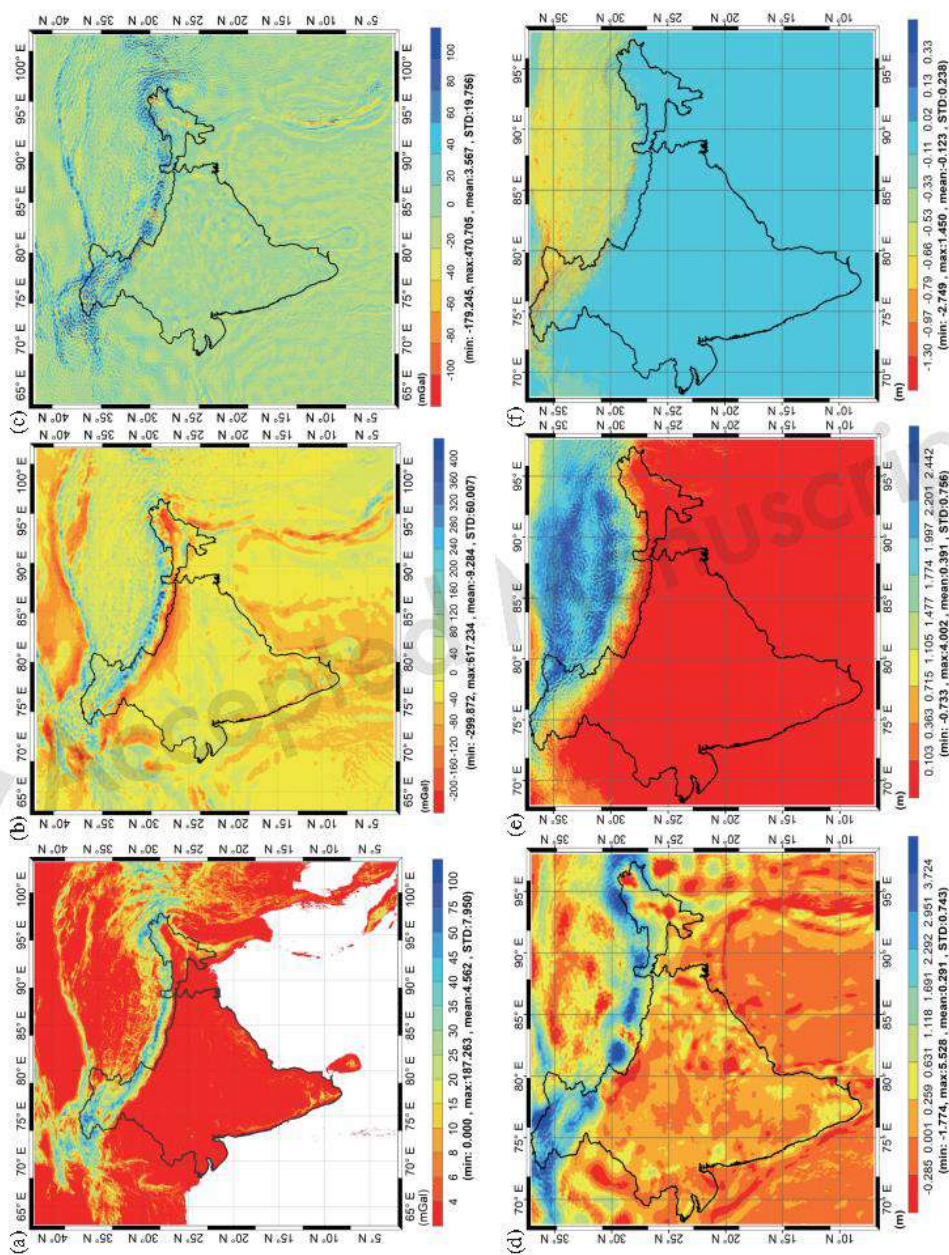


Fig. 6. (a) Block averaged planar TC, (b) Flury anomaly, (c) residual Flury anomaly, (d) residual quasigeoid ($M = 80$ and $\psi = 1.5^\circ$), (e) quasigeoid-geoid separation term (Flury and Rummel 2009), (f) difference in quasigeoid-geoid separation term (Heiskanen and Moritz 1967; Flury and Rummel 2009) (all on a $0.02^\circ \times 0.02^\circ$ grid), units of (a), (b), (c) in mGal and (d), (e), (f) in m).

TC grid was constructed from the $3'' \times 3''$ TC grid computed with the MERIT DEM using the Optimal Separating Radius (OSR) in the spatial-spectral combined method suggested by Goyal et al. (2020). This method of TC guarantees the full convergence of the TC solution, i.e., down to $< 1 \mu\text{Gal}$.

A different approach is used in the CUT method to apply ellipsoidal correction. Unlike other geoid computation strategies considered (UNB or KTH; cf. Huang et al. 2003; Ellmann 2005), the CUT method computes ellipsoidal area-mean free-air gravity anomalies on the topography using a Global Geopotential Model (GGM) (Featherstone et al. 2018). These are subtracted from the mean Faye gravity anomalies to obtain residual gravity anomalies (Fig. 6c), which are then Stokes-integrated with the Featherstone-Evans-Olliver (FEO) modified kernel (Featherstone et al. 1998) to obtain the residual height anomalies. The FEO kernel, a deterministic modifier, is the combination of the Meissl (1971) and Vaníček and Kleusberg (1987) modifiers that simultaneously reduces the truncation error and improves the rate of convergence to zero of the series expansion of the truncation error (cf. Featherstone et al. 1998; Featherstone 2003). Additionally, the spherical reference radius in the Stokes integration is set equal to the geocentric ellipsoidal radius of the computation point, and this negates the need for further ellipsoidal corrections to Stokes's integral (Claessens 2006).

The residual height anomalies were computed using the following parameter-sweeps of the modification degree (M): 0, 40, 80, 120, 160, 200, 240, 280, 300, and integration cap radius (ψ): 0.2° , 0.5° , 0.75° , 1° , 1.5° , 2° (e.g., Fig. 6d for $M = 80$, $\psi = 1.5^\circ$). The reference height anomalies on the topography are computed using GGMs with a zero-degree term (N_0) from the generalised Bruns's formula [Eq. (9)] (Heiskanen and Moritz 1967) calculated for each latitude parallel, which are added to the residual height anomalies to obtain the required height anomalies. An inconsistent use of Eq. (9) can cause an error of ~ 1 m in the computed geoid undulations/height anomalies. We used normal potential U_0 ($= 62636860.85 \text{ m}^2 \text{ s}^{-2}$) from GRS80 (Moritz 2000) and the geopotential W_0 ($= 62636853.4 \text{ m}^2 \text{ s}^{-2}$) from IHR5 (Sánchez et al. 2016).

$$N_0 = \frac{GM_G - GM_E}{r\gamma_0} - \frac{W_0 - U_0}{\gamma_0} \quad (9)$$

As a small modification to the original CUT method, we added the FOIE $= \frac{\kappa G \rho H^2}{\gamma}$ [Moritz 1980, Eqs. (48) – (29); Heiskanen and Moritz 1967, chapter 8] to the computed height anomalies. We note that the negative sign is sometimes omitted (e.g., Sjöberg 2000; Hwang et al. 2020).

The geoid undulations are calculated by adding the quasigeoid-geoid separation term (Fig. 6e; Flury and Rummel 2009) to the height anomalies. The more rigorous quasi-

geoid-geoid separation term from Flury and Rummel (2009) differs quite considerably from the approximate formula given in Heiskanen and Moritz (1967, p 328). The difference in the quasigeoid-geoid separation term from the two methods is shown in Fig. 6f. Acknowledging that the number and distribution of the GNSS/levelling data points are not sufficient for reliable fitting (Kotsakis and Sideris 1999; Fotopoulos 2003), we have not presented hybrid geoid and hybrid quasigeoid models for this experiment over India.

The geoid should be validated with orthometric [Helmert or rigorous (Santos et al. 2006)] heights and the quasigeoid validated with normal heights. A more rigorous validation approach would be to convert the normal-orthometric heights to Helmert's orthometric height and normal heights for validating geoid and quasigeoid, respectively. Examples of this are Foroughi et al. (2017) and Janák et al. (2017) over Auvergne, France, where normal heights were converted to rigorous heights for validation of their developed geoid models. However, Indian levelled heights are based on the normal-orthometric height system for which there is no specific choice of reference surface, i.e., either geoid or quasigeoid. Therefore, we are only able to "validate" the developed geoid and quasigeoid models with the Indian normal-orthometric heights on an uncertain vertical datum (section 2.3).

Absolute and relative testing (Featherstone 2001) of both height anomalies and geoid undulations are done in this study. The absolute testing is realised through point-wise subtraction of gravimetric geoid undulations obtained using Stokesian integration (N) and the geometrical geoid undulation ($h - H$) obtained using GNSS/levelling data [Eq. (10)].

$$\epsilon_i^{abs} = N_i - (h_i - H_i) \quad \forall i = 1, 2, 3, \dots, n \quad (10)$$

where n is the total number of discrete GNSS/levelling data points. It is important to acknowledge that absolute accuracy is only an assumption. This is principally because the levelled heights that refer to the local vertical datum are not necessarily coincident with the geoid. This has been discussed in detail by Featherstone (2001). The descriptive statistics of ϵ_i^{abs} are in Table 1.

The relative testing of geoid and quasigeoid [Eq. (11)] is an analysis tool to investigate their gradients. This type of analysis is of more interest to land surveyors who use relative GNSS baselines and a geoid/quasigeoid gradients as a replacement for the more time-consuming differential levelling.

$$\epsilon_j^{rel} = \Delta N_j - (\Delta h_j - \Delta H_j) \quad \forall i, j = 1, 2, 3, \dots, n; i \neq j \quad (11)$$

The descriptive statistics of ϵ_j^{rel} , and the ratio of mean differences to the mean baseline length in parts per million

Table 1. Statistics for the region-wise geoid/quasigeoid (for $M = 80$ and $\psi = 1.5^\circ$) absolute testing (units in m).

Region (no. of points)	Geoid				Quasigeoid			
	min	max	mean	STD	Min	Max	Mean	STD
India (119)	-0.897	0.788	-0.171	± 0.396	-0.906	0.726	-0.185	± 0.389
UP west (29)	-0.897	-0.154	-0.532	± 0.138	-0.906	-0.164	-0.548	± 0.142
UP east (27)	-0.712	-0.338	-0.521	± 0.114	-0.711	-0.340	-0.523	± 0.114
Hyderabad (56)	-0.385	0.501	0.070	± 0.158	-0.400	0.488	0.057	± 0.158
Bangalore (7)	0.709	0.788	0.751	± 0.030	0.645	0.726	0.690	± 0.032

(average ppm in mm km^{-1}) for the geoid and quasigeoid are in Table 2.

The variation of standard deviation in the Indian geoid and quasigeoid models, on testing with GNSS/levelling data, for different combinations of modification degree and integration cap are shown in Figs. 7a and b, respectively. Table 1 depicts the region-wise (UP west, UP east, Hyderabad, Bangalore, and all together) descriptive statistics for the geoid and quasigeoid for the combination of $M = 80$ and $\psi = 1.5^\circ$. Though the standard deviation for the whole of India is smaller with the combination of $M = 40$ and $\psi = 1.5^\circ$ compared to $M = 80$ and $\psi = 1.5^\circ$ (cf. Fig. 7), standard deviations for the four individual regions are less than or equal to the combination of $M = 80$ and $\psi = 1.5^\circ$ compared to $M = 40$ and $\psi = 1.5^\circ$. Therefore, $M = 80$ and $\psi = 1.5^\circ$ was chosen to present our results. The results of the relative testing are shown in Figs. 8a and b, and Table 2. The computed Indian gravimetric geoid (IndGG-CUT2021) and corresponding contours (at a 2-m contour interval) are shown in Figs. 9a and b, respectively.

4. DISCUSSION, RECOMMENDATIONS AND CONCLUSIONS

Though the number (119) and the distribution (Fig. 4) of the GNSS/levelling data points are insufficient to draw concrete conclusions about the quality of the computed gravimetric geoid and quasigeoid models, the following are some major observations from our experimental results:

- (1) Since the study area comprises the most complex topography varying from the Himalayas to the Gangetic plains and a long peninsular coastline, Fig. 6 possibly depicts the extreme (maximum and minimum) values of planar TC, Faye gravity anomaly, and quasigeoid-geoid separation on the planet.
- (2) From the viewpoint of the “cm-level accurate” geoid, Fig. 6f suggests that a more rigorous method (e.g., Flury and Rummel 2009) should be preferred for calculating the quasigeoid-geoid separation over a simple approximate formula (e.g., Heiskanen and Moritz 1967). There exist other formulas for the quasigeoid-geoid separation

term (e.g., Sjöberg 2010; Foroughi and Tenzer 2017), but they are not tested here.

- (3) Figure 7 suggests that the FEO kernel (Featherstone et al. 1998) is not numerically unstable for higher modification degrees, as shown in Featherstone (2003), Li and Wang (2011), Featherstone et al. (2018), and Claessens and Filmer (2020). However, this observation can also result from our choice of parameter sweeps and limited datasets for validation, thus requiring further investigation.
- (4) Generally, standard deviations versus GNSS/levelling are large for lower modification degrees and larger integration radii (Featherstone et al. 2018; Claessens and Filmer 2020). However, Fig. 7 shows an opposite trend in India, with smaller standard deviations for lower modification degrees and larger integration radii. This is primarily attributable to the north-south tilt in the India height datum (cf. Table 1). However, the smaller number of GNSS/levelling data and their poor distribution are also likely to contribute to this observation.
- (5) Figure 7 shows that the Indian levelling heights are marginally better referred to the quasigeoid ($\text{std} = \pm 0.389$ m) than the geoid ($\text{std} = \pm 0.396$ m). However, Table 1 shows that the geoid has an equal or better precision estimate than the quasigeoid (in terms of standard deviation) in each of the four regions individually. The difference in the standard deviations of the quasigeoid and geoid comparison for the whole of India seems to be a consequence, mostly, of the smaller mean of the quasigeoid (0.690 m) than the geoid (0.751 m) comparison over Bangalore. Also, with the given precision estimate of the data points, there can yet be no preferred choice between geoid or quasigeoid for the Indian vertical datum. Hence, a larger set of data points are needed for any possible claim of reference surface for India. Though the overall standard deviation of the computed geoid/quasigeoid (Table 1) is $\sim \pm 0.40$ m, it varies from $\sim \pm 0.03$ to $\sim \pm 0.16$ m if only evaluated individually in the four small test regions.
- (6) Table 2 indicates that the largest misclosures in Fig. 8 are probably due to the tilt in the Indian height datum and the relative closeness of data points in Hyderabad and Bangalore, which also explains the larger ppm

Table 2. Statistics for the region-wise geoid/quasigeoid (for $M = 80$ and $\psi = 1.5^\circ$) relative testing.

Region (Mean distance)	Geoid					Quasigeoid				
	min (m)	max (m)	mean (m)	STD (m)	Average ppm	min (m)	max (m)	mean (m)	STD (m)	Average ppm
India (713.46 km)	-0.620	1.684	0.373	± 0.418	3.371	-0.625	1.632	0.368	± 0.408	3.362
UP west (197.28 km)	-0.605	0.743	0.040	± 0.191	1.111	-0.602	0.742	0.057	± 0.193	1.118
UP east (169.33 km)	-0.374	0.367	0.015	± 0.161	1.048	-0.372	0.367	0.018	± 0.161	1.052
Hyderabad (18.67 km)	-0.620	0.886	-0.031	± 0.221	13.032	-0.625	0.888	-0.032	± 0.221	13.025
Bangalore (14.08 km)	-0.074	0.079	-0.005	± 0.044	3.113	-0.077	0.081	-0.008	± 0.046	3.281

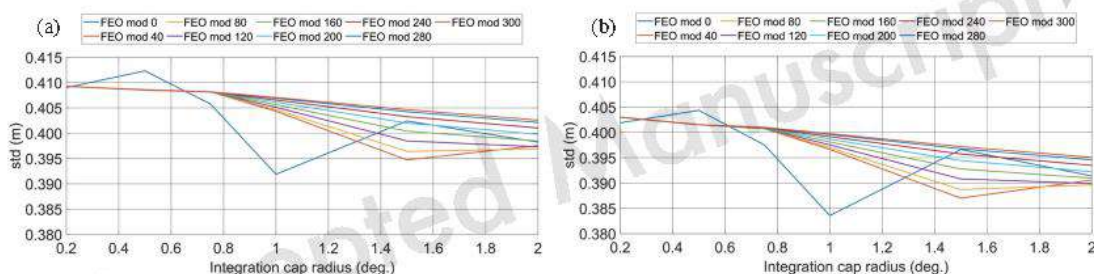
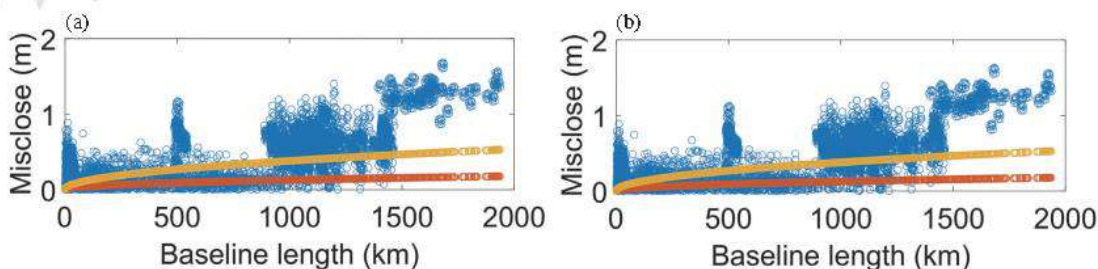


Fig. 7. Standard deviation of (a) geoid and (b) quasigeoid of India for different combinations of modification degree and integration cap (units in m).

Fig. 8. Magnitude of relative differences (blue circles) for the (a) geoid and (b) quasigeoid. Orange and yellow circles represent the maximum permissible in-field misclose for Indian high-precision ($k = 3$) and double tertiary ($k = 12$) levelling for each baseline, respectively (units in m).

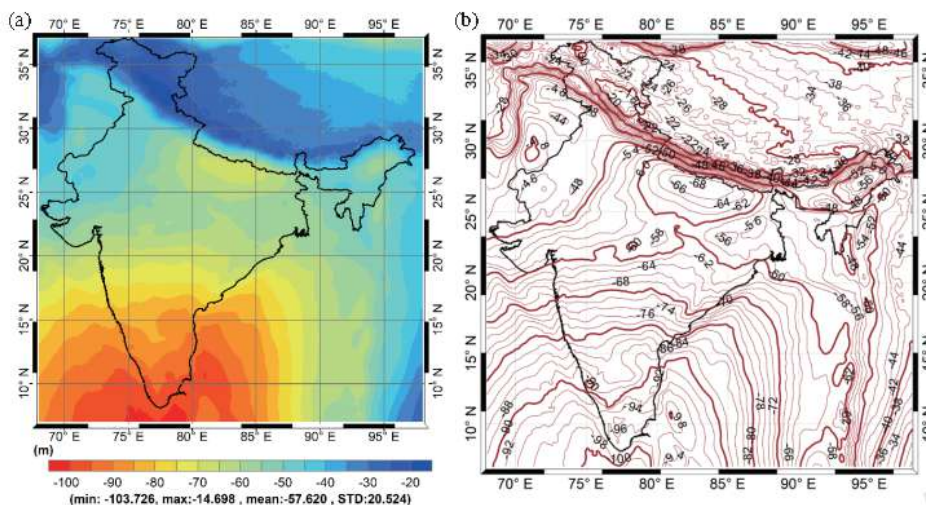


Fig. 9. (a) Indian gravimetric geoid computed using the CUT method (units in m), and (b) corresponding 2 m geoid contours.

values found in those regions. Spikes in Figs. 8a and b at distances of approximately (0 – 50), (450 – 550), (900 – 1200), and (1200 – 1900) km are due to the errors and differences (north-south tilt) in the baselines for (Bangalore and Hyderabad, individually), (Bangalore to Hyderabad), (UP west, UP east to Hyderabad), and (UP west, UP east to Bangalore), respectively.

- (7) On comparison of validations of the Indian gravimetric geoid with the CUT method and the GGM (Table 3), it is observed that though the overall mean values are improved for all regions except Bangalore, an improvement in the standard deviation beyond ± 0.01 m is observed only for UP east. However, the standard deviation of gravimetric geoid in UP west is degraded by ± 0.03 m as compared to the EIGEN-6C4. A degradation in the standard deviation of the gravimetric geoid is also observed in Featherstone and Sideris (1998). This was, and similarly is, attributed to errors in either one or more of terrestrial gravity data, GGMs and the GNSS/levelling data.

There is little to no improvement with the inclusion of the terrestrial gravity data with the CUT method because it makes use of the highest available degree-order GGMs. Also, the GETECH data is possibly already included in the high degree-order GGM (e.g., EGM2008, Pavlis et al. 2012, 2013).

- (8) The Faye gravity anomaly (Fig. 6b), geoid (Fig. 9a), and contour map (Fig. 9b) somewhat depict the separation line of the Indian and the Eurasian plate. Thus, the results presented in this study could be important for geophysical studies. The contour pattern around the location of 24°N and 82°E seems intriguing for some gravimetric

studies in that region. It should also be noted that the area comprises one of the largest coalfields of India with the thickest and different varieties of coal seams.

As a final remark, first experimental geoid and quasigeoid models for India have been computed with a standard deviation of ± 0.396 and ± 0.389 m, respectively, with respect to a small number of test regions. However, for the four regions individually, the standard deviation varies from ± 0.030 to ± 0.158 m for the geoid and ± 0.032 to ± 0.158 m for the quasigeoid. Though all the results presented herein are the first from India, the geoid/quasigeoid must be improved with dense, precise gravity data. Moreover, a larger number of GNSS/levelling data points must become available for more rigorous validation of the gravimetric geoid/quasigeoid. For the re-computation of the Indian geoid/quasigeoid with the CUT method and additional gravity data, the TC and the quasigeoid-geoid separation term need not be computed again unless a high-resolution and more precise DEM is available. Further, due to the complexities of the Indian topography and geomorphic characteristics, other geoid/quasigeoid computation strategies should also be tested over India.

Acknowledgements We are thankful to the GETECH Pty. Ltd. and the Survey of India for providing the gravity data and GNSS/levelling data, respectively. The Indian SPARC scheme is thanked for providing partial funding to procure the GETECH gravity data. The National Centre for Geodesy, established at Indian Institute of Technology Kanpur, is duly thanked for partial funding to procure the GETECH gravity data, and full funding for (a) procurement of the

Table 3. Comparison of EIGEN-6C4 and IndGG-CUT2021 validated with GNSS/levelling data (units in m).

		min	max	mean	STD
India	EIGEN-6C4	-1.203	0.463	-0.428	±0.410
	IndGG-CUT2021	-0.897	0.788	-0.171	±0.396
UP west	EIGEN-6C4	-1.203	-0.643	-0.870	±0.105
	IndGG-CUT2021	-0.897	-0.154	-0.532	±0.138
UP east	EIGEN-6C4	-1.034	-0.361	-0.742	±0.144
	IndGG-CUT2021	-0.712	-0.338	-0.521	±0.114
Hyderabad	EIGEN-6C4	-0.612	0.258	-0.154	±0.157
	IndGG-CUT2021	-0.385	0.501	0.070	±0.158
Bangalore	EIGEN-6C4	0.379	0.463	0.422	±0.029
	IndGG-CUT2021	0.709	0.788	0.751	±0.030

GNSS/levelling data and (b) the additional page charges for this article. We are also thankful to the three anonymous reviewers and the editor (X. Li) for their prompt and constructive comments on an earlier version of this manuscript.

REFERENCES

- Ågren, J., 2004: Regional geoid determination methods for the era of satellite gravimetry: Numerical investigations using synthetic earth gravity models. Ph.D. Thesis, Department of Infrastructure, Royal Institute of Technology (KTH), Stockholm, Sweden, 246 pp.
- Burrard, S., 1910: Levelling of precision in India. The Great Trigonometrical Survey of India, Vol. XIX, Survey of India, Dehradun, India.
- Carrion, D., N. Kumar, R. Barzaghi, A. P. Singh, and B. Singh, 2009: Gravity and geoid estimate in south India and their comparison with EGM2008. *Newton's Bulletin*, **4**, 275-283.
- Catalao, J., 2006: Iberia-Azores Gravity Model (IAGRM) using multi-source gravity data. *Earth Planets Space*, **58**, 277-286, doi: 10.1186/BF03351924. [\[Link\]](#)
- Claessens, S. J., 2006: Solutions to ellipsoidal boundary value problems for gravity field modelling. Ph.D. Thesis, Department of Spatial Sciences, Curtin University of Technology, Perth, Australia, 220 pp.
- Claessens, S. J. and M. S. Filmer, 2020: Towards an International Height Reference System: Insights from the Colorado geoid experiment using AUSGeoid computation methods. *J. Geod.*, **94**, 52, doi: 10.1007/s00190-020-01379-3. [\[Link\]](#)
- Ecker, E. and E. Mittermayer, 1969: Gravity corrections for the influence of the atmosphere. *Boll. Geofis. Teor. Appl.*, **11**, 70-80.
- Ellmann, A., 2005: A Numerical Comparison of Different Ellipsoidal Corrections to Stokes' Formula. In: Sansò, F. (Ed.), *A Window on the Future of Geodesy*, International Association of Geodesy Symposia, Vol. 128, Springer, Berlin, Heidelberg, 409-414, doi: 10.1007/3-540-27432-4_70. [\[Link\]](#)
- Ellmann, A. and P. Vaníček, 2007: UNB application of Stokes-Helmert's approach to geoid computation. *J. Geodyn.*, **43**, 200-213, doi: 10.1016/j.jog.2006.09.019. [\[Link\]](#)
- Featherstone, W. E., 2000: Refinement of gravimetric geoid using GPS and leveling data. *J. Surv. Eng.*, **126**, 27-56, doi: 10.1061/(ASCE)0733-9453(2000)126:2(27). [\[Link\]](#)
- Featherstone, W. E., 2001: Absolute and relative testing of gravimetric geoid models using Global Positioning System and orthometric height data. *Comput. Geosci.*, **27**, 807-814, doi: 10.1016/S0098-3004(00)00169-2. [\[Link\]](#)
- Featherstone, W. E., 2003: Software for computing five existing types of deterministically modified integration kernel for gravimetric geoid determination. *Comput. Geosci.*, **29**, 183-193, doi: 10.1016/S0098-3004(02)00074-2. [\[Link\]](#)
- Featherstone, W. E. and M. S. Filmer, 2012: The north-south tilt in the Australian Height Datum is explained by the ocean's mean dynamic topography. *J. Geophys. Res.*, **117**, C08035, doi: 10.1029/2012JC007974. [\[Link\]](#)
- Featherstone, W. E. and J. F. Kirby, 2000: The reduction of aliasing in gravity anomalies and geoid heights using digital terrain data. *Geophys. J. Int.*, **141**, 204-212, doi: 10.1046/j.1365-246X.2000.00082.x. [\[Link\]](#)
- Featherstone, W. E. and M. Kuhn, 2006: Height systems and vertical datums: A review in the Australian context. *J. Spat. Sci.*, **51**, 21-41, doi: 10.1080/14498596.2006.9635062. [\[Link\]](#)
- Featherstone, W. E. and M. G. Sideris, 1998: Modified kernels in spectral geoid determination: First results from Western Australia. In: Forsberg, R., M. Feissel, and R. Dietrich (Eds.), *Geodesy on the Move*, International

- Association of Geodesy Symposia, Vol. 119, Springer, Berlin, Heidelberg, 188-193, doi: 10.1007/978-3-642-72245-5_26. [[Link](#)]
- Featherstone, W. E., J. D. Evans, and J. G. Olliver, 1998: A Meissl-modified Vaníček and Kleusberg kernel to reduce the truncation error in gravimetric geoid computations. *J. Geod.*, **72**, 154-160, doi: 10.1007/s001900050157. [[Link](#)]
- Featherstone, W. E., J. F. Kirby, A. H. W. Kearsley, J. R. Gilliland, G. M. Johnston, J. Steed, R. Forsberg, and M. G. Sideris, 2001: The AUSGeoid98 geoid model of Australia: Data treatment, computations and comparisons with GPS-levelling data. *J. Geod.*, **75**, 313-330, doi: 10.1007/s001900100177. [[Link](#)]
- Featherstone, W. E., J. F. Kirby, C. Hirt, M. S. Filmer, S. J. Claessens, N. J. Brown, G. Hu, and G. M. Johnston, 2011: The AUSGeoid09 model of the Australian height datum. *J. Geod.*, **85**, 133-150, doi: 10.1007/s00190-010-0422-2. [[Link](#)]
- Featherstone, W. E., J. C. McCubbine, N. J. Brown, S. J. Claessens, M. S. Filmer, and J. F. Kirby, 2018: The first Australian gravimetric quasigeoid model with location-specific uncertainty estimates. *J. Geod.*, **92**, 149-168, doi: 10.1007/s00190-017-1053-7. [[Link](#)]
- Fischer, I., 1961: The present extent of the astro-geodetic geoid and the geodetic world datum derived from it. *Bull. Géodésique*, **61**, 245-264, doi: 10.1007/BF02854151. [[Link](#)]
- Fischer, I., 1975: Does mean sea level slope up or down toward north? *Bull. Géodésique*, **115**, 17-26, doi: 10.1007/BF02523939. [[Link](#)]
- Fischer, I., 1977: Mean sea level and the marine geoid—an analysis of concepts. *Mar. Geod.*, **1**, 37-59, doi: 10.1080/01490417709387950. [[Link](#)]
- Flury, J. and R. Rummel, 2009: On the geoid-quasigeoid separation in mountain areas. *J. Geod.*, **83**, 829-847, doi: 10.1007/s00190-009-0302-9. [[Link](#)]
- Foroughi, I. and R. Tenzer, 2017: Comparison of different methods for estimating the geoid-to-quasi-geoid separation. *Geophys. J. Int.*, **210**, 1001-1020, doi: 10.1093/gji/ggx221. [[Link](#)]
- Foroughi, I., P. Vaníček, M. Sheng, R. W. Kingdon, and M. C. Santos, 2017: In defense of the classical height system. *Geophys. J. Int.*, **211**, 1154-1161, doi: 10.1093/gji/ggx366. [[Link](#)]
- Forsberg, R., 1984: A study of terrain reductions, density anomalies and geophysical inversion methods in gravity field modelling. Reports of the Department of Geodetic Science and Surveying, No. 355, Department of Geodetic Science and Surveying, The Ohio State University, Columbus, Ohio, 129 pp.
- Forsberg, R., 1985: Gravity field terrain effect computations by FFT. *Bull. Géodésique*, **59**, 342-360, doi: 10.1007/BF02521068. [[Link](#)]
- Forsberg, R., 1998: The use of spectral techniques in gravity field modelling: Trends and perspectives. *Phys. Chem. Earth*, **23**, 31-39, doi: 10.1016/S0079-1946(97)00238-3. [[Link](#)] --Not cited!!!
- Forsberg, R. and C. C. Tscherning, 2008: An overview manual for the GRAVSOFTE Geodetic Gravity Field Modelling Programs. DTU Space, 75 pp.
- Fotopoulos, G., 2003: An analysis on the optimal combination of geoid, orthometric and ellipsoidal height data. Ph.D. Thesis, University of Calgary, Calgary, Canada, doi: 10.11575/PRISM/10883. [[Link](#)]
- GETECH, 2006: Gravity data compilation of India. Report No. G0610, University of Leeds, United Kingdom.
- Goyal, R., B. Nagarajan, and O. Dikshit, 2017: Status of precise geoid modelling in India: A review. Proceedings of 37th Indian National Cartographic Association International Congress on Geoinformatics for Carto-Diversity and Its Management, Indian Cartographer, 308-313.
- Goyal, R., W. E. Featherstone, D. Tsoulis, and O. Dikshit, 2020: Efficient spatial-spectral computation of local planar gravimetric terrain corrections from high-resolution digital elevation models. *Geophys. J. Int.*, **221**, 1820-1831, doi: 10.1093/gji/ggaa107. [[Link](#)]
- Goyal, R., W. E. Featherstone, O. Dikshit, and N. Balasubramania, 2021a: Comparison and Validation of Satellite-Derived Digital Surface/Elevation Models over India. *J. Indian Soc. Remote Sens.*, **49**, 971-986, doi: 10.1007/s12524-020-01273-7. [[Link](#)]
- Goyal, R., J. Ågren, W. E. Featherstone, L. E. Sjöberg, O. Dikshit, and N. Balasubramanian, 2021b: Empirical comparison between stochastic and deterministic modifiers over the French Auvergne geoid computation test-bed. *Surv. Rev.*, doi: 10.1080/00396265.2021.1871821. [[Link](#)]
- G&RB, 2018: Report on Redefinition of Indian Vertical Datum IVD2009, Geodetic and Research Branch, Survey of India, Dehradun, India.
- Hackney, R. I. and W. E. Featherstone, 2003: Geodetic versus geophysical perspectives of the 'gravity anomaly'. *Geophys. J. Int.*, **154**, 35-43, doi: 10.1046/j.1365-246X.2003.01941.x. [[Link](#)]
- Heiskanen, W. A. and H. Moritz, 1967: Physical Geodesy, W. H. Freeman and Company, San Francisco, USA, 364 pp.
- Huang, J., M. Véronneau, and S. D. Pagiatakis, 2003: On the ellipsoidal correction to the spherical Stokes solution of the gravimetric geoid. *J. Geod.*, **77**, 171-181, doi: 10.1007/s00190-003-0317-6. [[Link](#)]
- Hwang, C., H.-J. Hsu, W. E. Featherstone, C.-C. Cheng, M. Yang, W. Huang, C.-Y. Wang, J.-F. Huang, K.-H. Chen, C.-H. Huang, H. Chen, and W.-Y. Su, 2020: New gravimetric-only and hybrid geoid models of Taiwan for height modernisation, cross-island datum con-

- nection and airborne LiDAR mapping. *J. Geod.*, **94**, 83, doi: 10.1007/s00190-020-01412-5. [Link]
- Janák, J., P. Vaníček, I. Foroughi, R. Kingdon, M. B. Sheng, and M. C. Santos, 2017: Computation of precise geoid model of Auvergne using current UNB Stokes-Helmert's approach. *Contrib. Geophys. Geod.*, **47**, 201-229, doi: 10.1515/congeo-2017-0011. [Link]
- Jekeli, C., 2000: Heights, the Geopotential, and Vertical Datums. Report No. 459, Geodetic Science and Surveying, Department of Civil and Environmental Engineering and Geodetic Science, The Ohio State University, Columbus, Ohio, USA, 34 pp.
- Kotsakis, C. and M. G. Sideris, 1999: On the adjustment of combined GPS/levelling/geoid networks. *J. Geod.*, **73**, 412-421, doi: 10.1007/s001900050261. [Link]
- Li, X., 2018: Using radial basis functions in airborne gravimetry for local geoid improvement. *J. Geod.*, **92**, 471-485, doi: 10.1007/s00190-017-1074-2. [Link]
- Li, X. and Y. Wang, 2011: Comparisons of geoid models over Alaska computed with different Stokes' kernel modifications. *J. Geod. Sci.*, **1**, 136-142, doi: 10.2478/v10156-010-0016-1. [Link]
- LINZ, 2016: New Zealand Quasigeoid 2016 (NZGeoid2016). Available at <https://www.linz.govt.nz/data/geodetic-system/datums-projections-and-heights/vertical-datums/new-zealand-quasigeoid-2016-nzgeoid2016>. (Accessed on 21 April 2021)
- Liu, Q., M. Schmidt, L. Sánchez, and M. Willberg, 2020: Regional gravity field refinement for (quasi-) geoid determination based on spherical radial basis functions in Colorado. *J. Geod.*, **94**, 99, doi: 10.1007/s00190-020-01431-2. [Link]
- Macomber, M. M., 1984: World Geodetic System 1984. Defense Mapping Agency, Washington D.C., United States of America. Available at https://ia800108.us.archive.org/20/items/DTIC_ADA147409/DTIC_ADA147409.pdf.
- McCubbine, J. C., V. Stagpoole, F. C. Tontini, M. Amos, E. Smith, and R. Winefield, 2017: Gravity anomaly grids for the New Zealand region. *N. Z. J. Geol. Geophys.*, **60**, 381-391, doi: 10.1080/00288306.2017.1346692. [Link]
- Meissl, P., 1971: Preparations for the numerical evaluation of second order Molodensky-type formulas. Reports of Department of Geodetic Science, Report No. 163, Department of Geodetic Science, The Ohio State University Research Foundation, Columbus, Ohio, USA.
- Mishra, U. N., 2018: A comparative evaluation of methods for development of Indian geoid model. Ph.D. Thesis, IIT Roorkee, India.
- Mishra, U. N. and J. K. Ghosh, 2016: Development of a gravimetric geoid model and a comparative study. *Geod. Cartogr.*, **42**, 75-84, doi: 10.3846/20296991.2016.1226368. [Link]
- Molodensky, M. S., V. F. Yeremeev, and M. I. Yurkina, 1962: Methods for study of the external gravitational field and figure of the Earth. Israel Program for Scientific Translations, Jerusalem, Israel.
- Moritz, H., 1971: Series solutions of Molodensky's problem. *Deutsche Geodaetische Kommission Bayer. Akad. Wiss.*, **70**.
- Moritz, H., 1980: Advanced Physical Geodesy, Abacus Press, Tunbridge, England, 500 pp.
- Moritz, H., 2000: Geodetic Reference System 1980. *J. Geod.*, **74**, 128-133, doi: 10.1007/s001900050278. [Link]
- NGS, 2017: Blueprint for 2022, Part 2: Geopotential coordinates. NOAA Technical Report NOS NGS 64, NOAA, 41 pp. Available at https://geodesy.noaa.gov/PUBS_LJB/NOAA_TR_NOS_NGS_0064.pdf.
- NGS, 2019: Blueprint for the modernized NSRS, Part 3: Working in the modernized NSRS. NOAA Technical Report NOS NGS 67, NOAA, 125 pp. https://www.ngs.noaa.gov/PUBS_LJB/NOAA_TR_NOS_NGS_0067.pdf.
- Olesen, A. V., O. B. Andersen, and C. C. Tscherning, 2002: Merging of Airborne Gravity and Gravity Derived from Satellite Altimetry: Test Cases Along the Coast of Greenland. *Stud. Geophys. Geod.*, **46**, 387-394, doi: 10.1023/A:1019577232253. [Link]
- Pavlis, N. K., S. A. Holmes, S. C. Kenyon, and J. K. Factor, 2012: The development and evaluation of the Earth Gravitational Model 2008 (EGM2008). *J. Geophys. Res.*, **117**, B04406, doi: 10.1029/2011JB008916. [Link]
- Pavlis, N. K., S. A. Holmes, S. C. Kenyon, and J. K. Factor, 2013: Correction to "The development and evaluation of the Earth Gravitational Model 2008 (EGM2008)". *J. Geophys. Res.*, **118**, 2633, doi: 10.1002/jgrb.50167. [Link]
- Sánchez, L., R. Čunderlík, N. Dayoub, K. Mikula, Z. Minarechová, Z. Šíma, V. Vátr, and M. Vojtíšková, 2016: A conventional value for the geoid reference potential W_0 . *J. Geod.*, **90**, 815-835, doi: 10.1007/s00190-016-0913-x. [Link]
- Sandwell, D. T., H. Harper, B. Tozer, and W. H. F. Smith, 2021: Gravity field recovery from geodetic altimeter missions. *Adv. Space Res.*, **68**, 1059-1072, doi: 10.1016/j.asr.2019.09.011. [Link]
- Santos, M. C., P. Vaníček, W. E. Featherstone, R. Kingdon, A. Ellmann, B.-A. Martin, M. Kuhn, and R. Tenzer, 2006: The relation between rigorous and Helmert's definitions of orthometric heights. *J. Geod.*, **80**, 691-704, doi: 10.1007/s00190-006-0086-0. [Link]
- Singh, S. K., 2007: Development of a high resolution gravimetric geoid for central India. Ph.D. Thesis, Indian Institute of Technology Roorkee, India, 191 pp.
- Singh, S. K., 2018: Towards a new vertical datum for In-

- dia. FIG Congress 2018, Istanbul, Turkey. Available at https://fig.net/resources/proceedings/fig_proceedings/fig2018/papers/ts06e/TS06E_singh_9497.pdf.
- Singh, S. K. and R. K. Srivastava, 2018: Development of geoid model - A case study on western India. FIG Congress 2018, Istanbul, Turkey. Available at https://fig.net/resources/proceedings/fig_proceedings/fig2018/papers/ts06e/TS06E_singh_srivastava_9496.pdf.
- Sjöberg, L. E., 1984: Least squares modification of Stokes and Venning Meinesz formulas by accounting for errors of truncation, potential coefficients and gravity data. Technical Report 27, Department of Geodesy, Institute of Geophysics, University of Uppsala, Uppsala, Sweden.
- Sjöberg, L. E., 1991: Refined least squares modification of Stokes' formula. *Manuscr. Geod.*, **16**, 367-375.
- Sjöberg, L. E., 2000: Topographic effects by the Stokes-Helmert method of geoid and quasi-geoid determinations. *J. Geod.*, **74**, 255-268, doi: 10.1007/s001900050284. [[Link](#)]
- Sjöberg, L. E., 2003: A computational scheme to model the geoid by the modified Stokes formula without gravity reductions. *J. Geod.*, **77**, 423-432, doi: 10.1007/s00190-003-0338-1. [[Link](#)]
- Sjöberg, L. E., 2010: A strict formula for geoid-to-quasi-geoid separation. *J. Geod.*, **84**, 699-702, doi: 10.1007/s00190-010-0407-1. [[Link](#)]
- Srinivas, N., V. M. Tiwari, J. S. Tarial, S. Prajapti, A. E. Meshram, B. Singh, and B. Nagarajan, 2012: Gravimetric geoid of a part of south India and its comparison with global geopotential models and GPS-levelling data. *J. Earth Syst. Sci.*, **121**, 1025-1032, doi: 10.1007/s12040-012-0205-7. [[Link](#)]
- Stokes, G. G., 1849: On the variation of gravity at the surface of the Earth. *Trans. Camb. Phil. Soc.*, **8**, 672-695.
- Strykowski, G. and R. Forsberg, 1998: Operational Merging of Satellite, Airborne and Surface Gravity Data by Draping Techniques. In: Forsberg, R., M. Feissel, and R. Dietrich (Eds.), *Geodesy on the Move. International Association of Geodesy Symposia*, Vol. 119, Springer, Berlin, Heidelberg, 243-248, doi: 10.1007/978-3-642-72245-5_35. [[Link](#)]
- UNB, 2002: *Theory of Stokes-Helmert's Method of Geoid Determination. SHGEO Software Package, The UNB Application to Stokes-Helmert Approach for Precise Geoid Computation, Reference Manual I. Department of Geodesy and Geomatics Engineering, University of New Brunswick, Fredericton, Canada.* http://www2.unb.ca/gge/Research/GRI/GeodesyGroup/SHGeo/Manual/SHGeo_manual_I_2009.pdf. ---2002? 2009?
- Vaníček, P. and A. Kleusberg, 1987: The Canadian geoid - Stokesian approach. *manuscripta geodeatica*, **12**, 86-98.
- Vaníček, P. and Z. Martinec, 1994: The Stokes-Helmert scheme for the evaluation of a precise geoid. *manuscripta geodeatica*, **19**, 119-128.
- Vaníček, P., J. Huang, P. Novák, S. Pagiatakis, M. Véronneau, Z. Martinec, and W. E. Featherstone, 1999: Determination of the boundary values for the Stokes-Helmert problem. *J. Geod.*, **73**, 180-192, doi: 10.1007/s001900050235. [[Link](#)]
- Véronneau, M. and J. Huang, 2016: The Canadian Geodetic Vertical Datum of 2013 (CGVD2013). *Geomatica*, **70**, 9-19, doi: 10.5623/cig2016-101. [[Link](#)]
- Yamazaki, D., D. Ikeshima, R. Tawatari, T. Yamaguchi, F. O'Loughlin, J. C. Neal, C. C. Sampson, S. Kanae, and P. D. Bates, 2017: A high-accuracy map of global terrain elevations. *Geophys. Res. Lett.*, **44**, 5844-5853, doi: 10.1002/2017GL072874. [[Link](#)]
- Yang, M., C. Hirt, M. Rexer, R. Pail, and D. Yamazaki, 2019: The tree-canopy effect in gravity forward modelling. *Geophys. J. Int.*, **219**, 271-289, doi: 10.1093/gji/ggz264. [[Link](#)]